TÉCNICO LISBOA

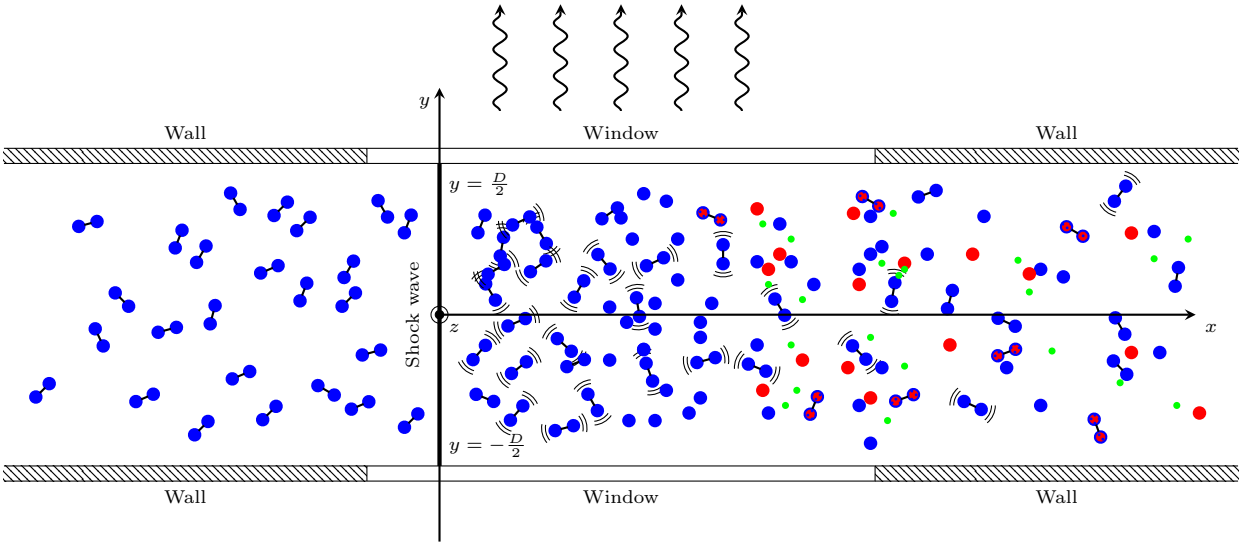

High-temperature kinetic and thermodynamic models for nitrogen plasmas

Élio Cordeiro Pereira

Thesis to obtain the Master of Science Degree in

Aerospace Engineering

Supervisor: Prof. Mário António Prazeres Lino da Silva

Examination Committee

Chairperson: Prof. Full Name

Supervisor: Prof. Mário António Prazeres Lino da Silva

Member of the Committee: Prof. Full Name 3

Month Year

Aos meus pais e irmãos,
que estiveram sempre ao meu lado.

Acknowledgments

I definitely would like to express gratitude to my supervisor Prof. Mário Lino da Silva, for giving me the opportunity of grasping one of the most beautiful and interesting topics of Aerospace Engineering that is currently in development. The area of Aerothermodynamics isn't for sure a common subject to be heard about in the quotidian. Probably, it will take many years to be absorbed by our culture, and I feel lucky to still find in this country some people who try doing something about it. I also have to thank him for granting me an investigation scholarship when money and motivation were lacking.

I do need to thank the help of Prof. Jorge Loureiro from IPFN group for introducing me to the Landau-Zener and Rosen-Zener-Demkov models. I did also enjoy and found myself fortunate to have the opportunity of hearing his remarkable thoughts on some of the philosophical aspects about the scientific research which was done in the old days and the one which is being done in the new days. The acknowledgement extends itself to Prof. Vasco Guerra from the same group, for enlighten me about some particular aspects of the Schrödinger equation, and suggesting me some of Donald Rapp articles which were crucial for my understanding about vibrational transitions of heavy particles in collisions.

With respect to the process of putting thoughts into practice, I cannot forget the aid of the students under the APPLAuSE PhD program Duarte Gonçalves, João Vargas and Ricardo Ferreira, as well as the help of Dr. Bruno Lopez at the University of Illinois, Urbana-Champaign, who provided me technical support for the IPFN in-house SPARK code. Their patience and serenity were overwhelming.

I also want to thank Dr. Annarita Laricchiuta from the National Research Council of Italy, for her clarifications and providing me her values for the branching ratios associated to the process of non-dissociative ionisation of nitrogen molecules by electron impact, as well as the used database for the vibrational energies of the nitrogen molecule in its ground electronic state. I thank Dr. Steven Guberman from the Institute for Scientific Research for his noteworthy discussion about the valid temperature range for which his numerical data may be used in the modelling of rates of dissociative recombination of molecular nitrogen ions. I thank the courtesy of Dr. Brett A. Cruden and Dr. Aaron Brandis from the NASA Ames Research Center, who shared with me their obtained data regarding the test 62 of the EAST shock tube. I acknowledge the clarifications provided by Dr. Julien Annaloro from the National Centre for Space Studies about the lumping procedure with respect to the electronic levels and Einstein coefficients for spontaneous emission issued by NIST (which he had recently done in one of his works). I thank Dr. Dan Potter from CSIRO in Australia for sharing with me his knowledge about the line-broadening mechanisms regarded in his PhD thesis.

I thank all my friends that supported me and made my free time much more pleasant, in lunches, dinners, day and night outs. Their camaraderie will never be forgotten. A special acknowledgement should be attributed to my lab colleagues Luís Fernandes and Marília Matos who shared with me an important part of this challenging adventure in a very humble and honest manner.

Finally, to be fair, I want to give the most of the gratitude to my family, who always cared and loved me. I value them more and more each day goes by, and I should apologise to them for the time I could not reciprocate. The least I can do is to dedicate this work to them.

Resumo

As condições de não-equilíbrio térmico, químico e radiativo que se obtêm ao sujeitar-se um gás de N_2 puro a uma forte onda de choque foram quantificadas usando modelos estado-para-estado específicos quanto aos níveis de energia vibrónica. O modelo do Oscilador Harmónico Forçado (FHO) foi implementado no cálculo de taxas de transição vibracional e dissociação de N_2 e N_2^+ por impacto com espécies pesadas. Taxas de dissociação termal de $N_2(X^1\Sigma_g^+)$ por impacto com N_2 e N foram obtidas e comparadas com os mais recentes resultados experimentais, mostrando uma concordância entre -59.9 e $8.9\,\%$, e entre -80.9 e $-36.1\,\%$ para os dois casos, respetivamente. Constatou-se impraticável uma extensão dos modelos de Landau-Zener e Rosen-Zener-Demkov para transições vibrónicas de partículas moleculares por impacto com espécies pesadas, preferindo-se uma lei do tipo "exponencial de hiato energético". Ajustando-se a curva que representa esta lei aos valores obtidos experimentalmente para as taxas de várias transições vibrónicas de N_2, foram obtidas discrepâncias de até uma ordem de grandeza, revelando alguma ineficácia do modelo. Os disparos 19, 20 e 40 da campanha nº 62 do Tubo de Choque de Arco Eléctrico em Ames (EAST), foram simulados numericamente usando o código SPARK. Constatou-se que os valores de pico da intensidade radiativa obtidos através de uma simulação de escoamento unidimensional do tipo Euler corresponderam entre o dobro e o quintúplo daqueles obtidos através de uma simulação de relaxação temporal, mostrando-se inválida a hipótese de transferência de momento ser negligenciável (sendo esta considerada na última). Os valores obtidos experimentalmente para as variáveis que descrevem a radiação foram subestimados por uma a duas ordens de grandeza. Testes de sensibilidade quanto às taxas cinéticas simuladas mostraram ser ineficazes na obtenção de uma concordância razoável entre os resultados numéricos e os experimentais. As simulações permitiram descrever corretamente a forma dos perfis de intensidade radiativa obtidos no disparo de reduzida velocidade, mas não a dos obtidos nos de moderada e elevada velocidades, pois estes revelaram patamares procedendo ou coalescendo com picos que não foram reproduzidos numericamente. Encontrou-se uma forte evidência das discrepâncias terem resultado da não modelação da transferência de calor por radiação no interior do gás-teste, e possivelmente, entre o gás de alta pressão (assim como o arco eléctrico do tubo de choque) e o gás-teste.

Palavras-chave: Entrada atmosférica, Aerotermodinâmica, Plasma de azoto, Estado-para-estado, Radiação, Tubo de choque

Abstract

The conditions of thermal, chemical and radiative non-equilibrium attained in a pure N_2 gas subjected to a strong shock wave were quantified using vibronic-specific state-to-state models. The Forced-Harmonic-Oscillator model (FHO) was employed in the computation of rate coefficients for vibrational transition and dissociation of N_2 and N_2^+ by heavy particle impact. Thermal dissociation rate coefficients of $N_2(X^1\Sigma_g^+)$ by collisions with N_2 and N were obtained and compared with state-of-the-art experimental results, showing an agreeability between -59.9 and $8.9\,\%$, and between -80.9 and $-36.1\,\%$ for the former and latter interactions, respectively. An extension of the Landau-Zener and Rosen-Zener-Demkov models to vibronic transitions of molecular particles by heavy particle impact was found to be impractical, and an exponential gap law was ultimately preferred. By fitting the curve that represents the law to experimentally obtained values for rate coefficients values of several vibronic transitions of N_2 reported in the literature, discrepancies of as much as one order magnitude were obtained, showing some crudeness of the model. Shots 19, 20 and 40 of the test 62 of the Ames Electric Arc Shock Tube (EAST) were simulated using the SPARK code. The peak values of radiative intensity obtained from a Euler one-dimensional simulation were found to be between the double and the quintuple of the ones obtained from a zero-dimensional simulation, showing the hypothesis of the momentum transfer being negligible (which is taken by the latter) to be invalid. The experimental radiation variables were underestimated by one to two orders of magnitude, and sensibility tests performed on the rate coefficients weren't successful in getting a reasonable agreeability. The shape of the radiative intensities profiles of the low speed shot was correctly predicted, but not the ones of the medium and high speed shots which revealed non-null plateaus proceeding or coalescing with peaks. These plateaus weren't predicted at all. Strong evidence was found for such discrepancies resulting from the non-modelling of heat transfer by radiation within the test gas, and possibly, between the driver gas (as well as the driver arc of the shock tube) and the test gas.

Keywords: Atmospheric entry, Aerothermodynamics, Nitrogen plasma, State-to-state, Radiation, Shock tube

Contents

List of Tables

List of Figures

Nomenclature

Physical constants

Å	Angstrom.	1×10^{-10} m
a_0	Bohr radius.	$\varepsilon_0 h^2/(\pi m_\mathrm{e} \mathrm{e}^2) = 0.529\,177\,210\,67 \times 10^{-10}$ m
atm	Standard atmosphere.	101 325 Pa
c	Speed of light.	299 792 458 m/s
"cm^{-1}"	Reciprocal "centimeter".	$\mathrm{cm}^{-1} \cdot (h \cdot c) = 1.986\,445\,824 \times 10^{-23}$ J
e	Elementary charge.	$1.602\,176\,620\,8 \times 10^{-19}$ C
h	Plank constant.	$6.626\,070\,040 \times 10^{-34}$ J·s
$\hbar$	Reduced Plank constant.	$h/(2\pi) = 1.054\,571\,800 \times 10^{-34}$ J·s
k_B	Boltzmann constant.	$1.380\,648\,52 \times 10^{-23}$ J/K
m_e	Electron mass.	$9.109\,383\,56 \times 10^{-31}$ kg
$\mathscr{N}_A$	Avogadro constant.	$(\mathrm{g/u}) \cdot \mathrm{mol}^{-1} = 6.022\,140\,857 \times 10^{23}$ mol^{-1}
Ry	Rydberg unit of energy.	$m_\mathrm{e}\mathrm{e}^4/(8\varepsilon_0^2 h^2) = 2.179\,872\,325 \times 10^{-18}$ J
$\mathscr{R}$	Molar gas constant.	$k_B \mathscr{N}_A = 8.314\,459\,8$ J/(mol · K)
Torr	Torricelli unit of pressure.	1/760 atm= 133.322 368 4 Pa
u	Atomic mass unit.	$1.660\,539\,040 \times 10^{-27}$ kg
ε_0	Vacuum permittivity.	$8.854\,187\,817 \times 10^{-12}$ F/m
π	Pi number.	3.141 592 653 589 793 ...

Roman symbols

A	Chemical symbol of the first collision partner (regarding binary collisions); or nucleus A (regarding the FHO model).
AB	Molecular particle AB (regarding the FHO model).

A Pre-exponential factor of the repulsive exponential potential (regarding the FHO model); or pre-exponential factor considered considered on the model for H_{12} (regarding the Rosen-Zener-Demkov model).

$A_{s,e,v}^{e',v'}$ Level-specific Einstein coefficient associated to spontaneous emission.

a Mixture speed of sound; or value of H_{12} at the pseudo-crossing or crossing point (regarding the Landau-Zener model).

a_n n-Th coefficient of the expansion of the electronic wave function Φ with respect to the adiabatic basis $\{\phi_n\}$ (regarding the semiclassical approximation).

a_1 First coefficient of the expansion of the electronic wave function Φ with respect to the adiabatic basis $\{\phi_1, \phi_2\}$ (regarding the two-states approximation).

a_2 Second coefficient of the expansion of the electronic wave function Φ with respect to the adiabatic basis $\{\phi_1, \phi_2\}$ (regarding the two-states approximation).

B Chemical symbol of the second collision partner (regarding binary collisions); or nucleus B (regarding the FHO model).

B_v Spectroscopic rotational function associated to the v-th vibrational and e-th electronic levels.

B_e Spectroscopic rotational constant associated to the e-th electronic level.

$B_{s,e,v}^{e',v'}$ Level-specific Einstein coefficient associated to induced emission, if $T_{e'v'} < T_{ev}$ or absorption if $T_{e'v'} > T_{ev}$.

b_n n-Th coefficient of the expansion of the electronic wave function Φ with respect to the diabatic basis $\{\phi_n^0\}$ (regarding the semiclassical approximation).

b_1 First coefficient of the expansion of the electronic wave function Φ with respect to the diabatic basis $\{\phi_1^0, \phi_2^0\}$ (regarding the two-states approximation).

b_2 Second coefficient of the expansion of the electronic wave function Φ with respect to the diabatic basis $\{\phi_1^0, \phi_2^0\}$ (regarding the two-states approximation).

C Nucleus C (regarding the FHO model).

CD Molecular particle CD (regarding the FHO model).

C_V Mixture specific heat at constant volume.

$C_{V,s}$ s-Th species specific heat at constant volume.

$C_{V,s,i}$ s-Th species specific heat at constant volume associated to the i-th energy mode.

C_p Mixture specific heat at constant pressure.

$C_{p,s}$ s-Th species specific heat at constant pressure.

$C_{p,s,i}$ s-Th species specific heat at constant pressure associated to the i-th energy mode.

$C_{kj}^{(n)}$ V-V-T transition probability parameter: (k,j)-th entry of the transformation matrix considered in the V-V-T transitions probabilities (regarding the FHO model).

$\hat{C}_{nm}$ Coupling operator with respect to the n-th and m-th adiabatic electronic wave functions (regarding the adiabatic approximation).

c_s Mass fraction of the s-th species.

c_{nm} m-Th coefficient of the expansion of the n-th adiabatic wave function ϕ_n with respect to the diabatic basis $\{\phi_m^0\}$ (regarding the semiclassical approximation).

c_{11} First coefficient of the expansion of the first adiabatic wave function ϕ_1 with respect to the diabatic basis $\{\phi_1^0, \phi_2^0\}$ (regarding the two-states approximation).

c_{12} Second coefficient of the expansion of the first adiabatic wave function ϕ_1 with respect to the diabatic basis $\{\phi_1^0, \phi_2^0\}$ (regarding the two-states approximation).

c_{21} First coefficient of the expansion of the second adiabatic wave function ϕ_2 with respect to the diabatic basis $\{\phi_1^0, \phi_2^0\}$ (regarding the two-states approximation).

c_{22} Second coefficient of the expansion of the second adiabatic wave function ϕ_2 with respect to the diabatic basis $\{\phi_1^0, \phi_2^0\}$ (regarding the two-states approximation).

D Nucleus D (regarding the FHO model).

Da Damköhler number.

D_0 Dissociation energy.

D_e Potential well depth.

d_{AB} Distance between the centres of two collision partners when in contact with each other (regarding the billiard balls model).

d_{tri} Base length of the triangular function.

d_{rect} Base length of the rectangular function.

$d_{\mathrm{trap},1}$ Lower base length of the trapezoidal function.

$d_{\mathrm{trap},2}$ Upper base length of the trapezoidal function.

E Relative kinetic energy (regarding binary collisions); or energy of the system (regarding the adiabatic approximation).

E_a Activation energy.

E' Energy of the system relatively to its centre of mass (regarding the adiabatic approximation).

E'' Energy of the system relatively to its centre of mass disregarding the centrifugal energy (regarding the Landau-Zener and the Rosen-Zener-Demkov models).

E_0 Initial relative kinetic energy of the collision partners (regarding the FHO model); or arithmetic mean of the asymptotic values of U_1 and U_2 (regarding the Rosen-Zener-Demkov model); or characteristic energy (regarding the energy gap law).

E_M Morse potential well (regarding the FHO model).

E_n n-Th eigenenergy of the quantum free harmonic oscillator (regarding the FHO model).

e e-Th electronic energy level; or initial electronic level; or higher electronic level; or mass-specific internal energy of the flow associated to the mixture.

e' Final electronic level; or lower electronic level.

$e^\dagger$ $e^\dagger$-Th electronic level which regards fine structure.

e_s Mass-specific internal energy of the flow associated to the s-th species.

$e_{s,\mathrm{tr}}$ Contribution of the translation energy mode to the mass-specific internal energy of the flow associated to the s-th species.

$e_{s,\mathrm{tr_h}}$ Contribution of the heavy particle translation energy mode to the mass-specific internal energy of the flow associated to the s-th species.

$e_{s,\mathrm{tr_e}}$ Contribution of the free electron translation energy mode to the mass-specific internal energy of the flow associated to the s-th species.

$e_{s,\mathrm{rot}}$ Contribution of the rotational energy mode to the mass-specific internal energy of the flow associated to the s-th species.

$e_{s,\mathrm{vib}}$ Contribution of the vibrational energy mode to the mass-specific internal energy of the flow associated to the s-th species.

$e_{s,\mathrm{el}}$ Contribution of the electronic energy mode to the mass-specific internal energy of the flow associated to the s-th species.

$e_{s,0}$ Contribution of the ground level energy to the mass-specific internal energy of the flow associated to the s-th species.

$e_{s,0_\mathrm{h}}$ Contribution of the ground level heavy particle energy to the mass-specific internal energy of the flow associated to the s-th species.

$e_{s,0_\mathrm{e}}$ Contribution of the ground level free electron energy to the mass-specific internal energy of the flow associated to the s-th species.

F_1 Slope of H_{11} at the pseudo-crossing or crossing point (regarding the Landau-Zener model).

F_2 Slope of H_{22} at the pseudo-crossing or crossing point (regarding the Landau-Zener model).

F_{vJ} Particle rotational energy associated to the v-th vibrational, J-th rotational and e-th electronic levels.

f Distribution of relative speeds (regarding binary collisions); or force constant of the quantum harmonic oscillator that represents the molecular particle (regarding the FHO model).

$\tilde{f}$ Normalised distribution of relative speeds (regarding binary collisions).

f_s Mass-specific Helmholtz free energy associated to the mixture.

$\vec{f_s}$ Mass-specific external body force vector applied to the s-th species particles.

G Gaussian function.

G_v Particle vibrational energy associated to the v-th vibrational and e-th electronic levels.

g Degree of degeneracy of the energy level.

g_s Mass-specific Gibbs free energy associated to the s-th species.

$g_{s,\mathrm{ref}}$ Mass-specific Gibbs free energy associated to s-th species, at a partial pressure $p_s = p_{\mathrm{ref}}$.

$\mathscr{H}_n$ n-Th order physicists' Hermite polynomial (regarding the FHO model).

H_n n-Th eigenfunction of the quantum free harmonic oscillator (regarding the FHO model).

$\hat{H}$ Global Hamiltonian operator (regarding the adiabatic approximation).

$\hat{H}_e$ Electronic Hamiltonian operator (regarding the adiabatic approximation).

$\hat{H}_e^0$ Diabatic Hamiltonian operator (regarding the semiclassical approximation).

H_{nm} (n, m)-Th entry of the electronic Hamiltonian matrix written with respect to the diabatic basis $\{\phi^0\}$ (regarding the semiclassical approximation).

H_{11} $(1, 1)$-Th entry of the electronic Hamiltonian matrix written with respect to the diabatic basis $\{\phi_1^0, \phi_2^0\}$ (regarding the two-states approximation).

H_{12} $(1, 2)$-Th entry of the electronic Hamiltonian matrix written with respect to the diabatic basis $\{\phi_1^0, \phi_2^0\}$ (regarding the two-states approximation).

H_{21} $(2, 1)$-Th entry of the electronic Hamiltonian matrix written with respect to the diabatic basis $\{\phi_1^0, \phi_2^0\}$ (regarding the two-states approximation).

H_{22} $(2, 2)$-Th entry of the electronic Hamiltonian matrix written with respect to the diabatic basis $\{\phi_1^0, \phi_2^0\}$ (regarding the two-states approximation).

h_0 Mass-specific stagnation enthalpy associated to the mixture.

h_s Mass-specific enthalpy associated to the s-th species.

I_λ Specific radiant intensity.

$\hat{I}$ Instrumentally resolved radiative intensity.

$\hat{I}_\lambda$ Instrumentally resolved specific radiative intensity.

$\hat{I}_\lambda^{\mathrm{ne}}$ instrumentally resolved non-equilibrium metric.

J Rotational quantum number.

$\vec{J}_s$ s-Th species mass diffusion flux vector.

j_λ Emission coefficient.

Kn Knudsen number.

K_c Concentration-wise equilibrium constant.

k Rate coefficient; mixture thermal conductivity coefficient.

k_λ Absorption coefficient.

k_i i-Th thermal conductivity coefficient.

k_f Forward process rate coefficient.

k_b Backward process rate coefficient.

$k_{v_1,v_2}^{v_1',v_2'}$ V-V-T rate coefficient associated to a transition from the vibrational quantum numbers v_1 and v_2 to v_1' and v_2' (regarding the FHO model).

$k_v^{v'}$ V-T rate coefficient associated to a transition from the vibrational quantum number v to v'; or V-V-T rate coefficient associated to a transition of a molecular particle from the vibrational quantum number v to v' which accounts all possible transitions of the other molecular particle (regarding the FHO model).

k_v^D V-D rate coefficient associated to dissociation from the vibrational quantum number v; or V-D rate coefficient associated to dissociation of a molecular particle from the vibrational quantum number v which accounts all possible transitions of the other molecular particle (regarding the FHO model).

L Lorentzian function.

$\hat{l}^2$ Squared angular momentum operator (regarding the adiabatic approximation).

M Chemical symbol of a collision partner (regarding binary collisions).

Ma Mach number.

M Mass of the mixture particles inside a space in the fluid.

$\tilde{M}$ Sum of the collision partners masses (regarding the FHO model).

M_s Mass of s-th species particles inside a space in the fluid.

M_i Mass of the i-th nucleus (regarding the adiabatic approximation).

M_1 Mass of the first nucleus of the diatomic particle (regarding the adiabatic approximation).

M_2 Mass of the second nucleus of the diatomic particle (regarding the adiabatic approximation).

$\tilde{m}$ Reduced mass of the collision partners (regarding the FHO model).

m_s Mass of a s-th species particle.

m_A Mass of the first collision partner (regarding binary collisions); or mass of nucleus A (regarding the FHO model).

m_B Mass of the second collision partner (regarding binary collisions); or mass of nucleus B (regarding the FHO model).

m_C Mass of nucleus C (regarding the FHO model).

m_D Mass of nucleus D (regarding the FHO model).

N Number of particles.

N_S Number of species.

N_R Number of processes.

N_T Number of assigned temperatures.

N_s Number of s-th species particles.

$N_{s,j}$ Number of s-th species particles in the j-th total energy level.

n Number density of the mixture particles inside a space in the fluid.

n_s Number density of s-th species particles inside a space in the fluid.

P Process probability.

$P_{v_1,v_2}^{v_1',v_2'}$ V-V-T transition probability from the vibrational quantum numbers v_1 and v_2 to v_1' and v_2' (regarding the FHO model).

$P_v^{v'}$ V-T transition probability from the vibrational quantum number v to v' (regarding the FHO model).

P_v^D Dissociation probability from the vibrational quantum number v (regarding the FHO model).

$P_{1,2}$ Probability of transition from the first electronic adiabatic state to the second electronic adiabatic state in the approaching motion or in the departing motion of the collision partners (regarding the Landau-Zener and Rosen-Zener-Demkov models).

$\bar{P}_{1,2}$ Probability of transition from the first electronic adiabatic state to the second electronic adiabatic state in the full motion of the collision partners (regarding the Landau-Zener and Rosen-Zener-Demkov models).

p Pressure.

p_{ref} Reference pressure.

p_s s-Th species partial pressure.

Q Partition function.

$\vec{q}$ Mixture heat flux vector.

$\vec{q}_s$ s-Th species heat flux vector.

$\vec{q}_i$ Contribution of the i-th energy mode to the mixture heat flux vector.

$\vec{q}_{\text{c}}$ Contribution of conduction to the mixture heat flux vector.

$\vec{q}_{\text{c},i}$ Contribution of the i-th energy mode, under the form of conduction, to the mixture heat flux vector.

$\vec{q}_{\text{rad}}$ Contribution of radiation to the mixture heat flux vector.

$\vec{q}_{\text{rad},i}$ Contribution of the i-th energy mode, under the form of radiation, to the mixture heat flux vector.

Re Reynolds number.

$\{\vec{R}\}$ Set of nuclei position vectors (regarding the adiabatic approximation).

$\vec{R}_i$ Position vector of the i-th nucleus (regarding the adiabatic approximation).

$\vec{R}_j$ Position vector of the j-th nucleus (regarding the adiabatic approximation).

$\vec{R}_1$ Position vector of the first nucleus of the diatomic particle (regarding the adiabatic approximation).

$\vec{R}_2$ Position vector of the second nucleus of the diatomic particle (regarding the adiabatic approximation).

$\vec{\bar{R}}$ Position vector of the nuclei centre of mass (regarding the adiabatic approximation).

$\vec{R}$ Difference between the position vectors of the diatomic particle nuclei $\vec{R}_2 - \vec{R}_1$ (regarding the adiabatic approximation).

R Internuclear distance of the diatomic particle (regarding the adiabatic approximation).

R_p Internuclear distance of the diatomic particle at which a pseudo-crossing of the adiabatic electronic terms occurs (regarding the Landau-Zener model).

R_c Internuclear distance of the diatomic particle at which a crossing occurs of the adiabatic electronic terms (regarding the Landau-Zener model).

R_s Mass-specific gas constant associated to the s-th species.

$\{\vec{r}\}$ Set of electrons position vectors (regarding the adiabatic approximation).

$\vec{r}_\alpha$ Position vector of the α-th electron (regarding the adiabatic approximation).

$\vec{r}_\beta$ Position vector of the β-th electron (regarding the adiabatic approximation).

r_A Radius of the first collision partner (regarding the billiard balls model).

r_B Radius of the second collision partner(regarding the billiard balls model).

r Internuclear distance (regarding the RKR method).

r_e Equilibrium internuclear distance.

rect Rectangular function.

S Quantum number for the total electronic spin of the diatomic molecular particle.

$S_\text{V-T}$ V-T steric factor (regarding the FHO model) introduced in the transition probability parameter η_0.

$S_\text{V-V}$ V-V steric factor (regarding the FHO model) introduced in the transition probability parameter ρ.

s_s Mass-specific entropy associated to the s-th species.

T Thermal equilibrium temperature; or temporal wave function (regarding the adiabatic approximation).

T_e Particle electronic energy associated to the e-th electronic level.

T_{ev} Particle vibronic energy associated to the e-th electronic and v-th vibrational levels.

T_{vJ} Particle rovibrational energy associated to the v-th vibrational and J-th rotational levels.

T_{evJ} Particle rovibronic energy associated to the e-th electronic, v-th vibrational and J-th rotational levels.

T_0 Stagnation heavy particle translational temperature.

T_w Temperature of the forefront wall of the entry body

T_i i-Th energy mode temperature.

$T_{\mathrm{tr_h}}$ Heavy particle translational temperature.

T_rot Rotational temperature.

T_vib Vibrational temperature.

T_el Electronic temperature.

$T_{\mathrm{tr_e}}$ Free electron translational temperature.

$T_{\mathrm{tr_h\text{-}rot}}$ Heavy particle translational-rotational temperature.

$T_{\mathrm{el\text{-}tr_e}}$ Electronic-free electron translational temperature.

$T_{\mathrm{vib\text{-}el\text{-}tr_e}}$ Vibrational-electronic-free electron translational temperature.

T_{c} Controlling temperature.

$\hat{T}_i$ Kinetic energy operator associated to the i-th nucleus (regarding the adiabatic approximation).

$\hat{T}_\alpha$ Kinetic energy operator associated to the α-th electron (regarding the adiabatic approximation).

t Instant of time.

tri Triangular function.

trap Trapezoidal function.

U_n n-Th adiabatic electronic term (regarding the adiabatic approximation).

U_1 First adiabatic electronic term (regarding the two-states approximation).

U_2 Second adiabatic electronic term (regarding the two-states approximation).

U_n^0 n-Th diabatic electronic term (regarding the semiclassical approximation).

$\vec{u}$ Mixture flow velocity vector.

u Mixture flow speed; or x-component of the flow velocity vector.

$\vec{u}_s$ s-Th species flow velocity vector.

u_s s-Th species flow speed.

$\vec{u'}_s$ s-Th species diffusion flow velocity vector.

u'_s s-Th species diffusion flow speed.

$\mathscr{V}$ Space in the fluid.

$\mathscr{V}_s$ Space in the fluid which boundary moves with the s-th species particles.

V Volume of a space in the fluid; or global potential energy of the collision partners (regarding the FHO model); or non-centrifugally corrected internuclear potential (regarding the RKR method); or Voigt function.

V_J Centrifugally corrected internuclear potential curve (regarding the RKR method).

V_{sr} Short-range part of the non-centrifugally corrected internuclear potential.

V_{lr} Long-range part of the non-centrifugally corrected internuclear potential.

V_{RKR} Non-centrifugally corrected internuclear potential obtained through the RKR method.

V_{HH} Hulburt-Hirschfelder potential.

V_{ER} Extended Rydberg potential.

V_{ij} Potential energy associated to the Coulomb electrostatic interaction between the i-th and j-th nuclei (regarding the adiabatic approximation).

$V_{\alpha\beta}$ Potential energy associated to the Coulomb electrostatic interaction between the α-th and β-th electrons (regarding the adiabatic approximation).

$V_{i\alpha}$ Potential energy associated to the Coulomb electrostatic interaction between the i-th nucleus and α-th electron (regarding the adiabatic approximation).

$\hat{V}_{\mathrm{s.o.}}$ Spin-orbit interaction potential (regarding the adiabatic approximation).

V' Interaction potential energy between the collision partners (regarding the FHO model).

V'_{M} Morse potential (regarding the FHO model).

V'_{LJ} Lennard-Jones $(12-6)$ potential (regarding the FHO model).

V'_{HS} Hard-spheres potential (regarding the FHO model).

$\vec{v}$ Relative velocity vector (regarding binary collisions).

v Relative velocity speed (regarding binary collisions); or relative speed of the collision partners at the pseudo-crossing or crossing point (regarding the Landau-Zener model); or initial relative speed of the collision partners (regarding the Rosen-Zener-Demkov model); or v-th vibrational quantum number; or initial vibrational quantum number.

v_0 Initial relative speed of the collision partners (regarding the FHO model).

v_i Initial relative speed of the collision partners (regarding the FHO model).

v_f Final relative speed of the collision partners (regarding the FHO model).

v_1 Initial vibrational quantum number of the molecular particle AB (regarding the FHO model).

v_2 Initial vibrational quantum number of the molecular particle CD (regarding the FHO model).

v_D Vibrational quantum number associated to the dissociation limit (regarding the FHO model).

v_{max} Maximum vibrational quantum number for which the respective Dunham expansion is valid.

v' Final vibrational quantum number.

v'_1 Final vibrational quantum number of the molecular particle AB (regarding the FHO model).

v'_2 Final vibrational quantum number of the molecular particle CD (regarding the FHO model).

w Half-width at half-maximum of the symmetric function.

X_s s-Th species chemical symbol.

$[\mathrm{X}_s]$ s-Th species amount concentration (number of s-th species particles per unit volume).

$\tilde{X}$ Difference between $\tilde{x}$ and $\tilde{x}_t$ (regarding the FHO model).

$\tilde{x}$ Difference between the centres of mass positions of the collision partners (regarding the FHO model).

$\tilde{x}_t$ Classical turning point of the trajectory (regarding the FHO model).

$\tilde{x}_{\mathrm{A}}$ Position of nucleus A (regarding the FHO model).

$\tilde{x}_{\mathrm{B}}$ Position of nucleus B (regarding the FHO model).

$\tilde{x}_{\mathrm{C}}$ Position of nucleus C (regarding the FHO model).

$\tilde{x}_{\mathrm{D}}$ Position of nucleus D (regarding the FHO model).

$\tilde{x}_R$ Centre of mass of the two collision partners (regarding the FHO model).

$x_{n,l,m}$ n-Th radial wave function associated to the rotational quantum number l and quantum number for the z-component of the angular momentum m (regarding the adiabatic approximation).

Y_{ij} (i,j)-Th Dunham parameter.

$Y_{l,m}$ Spherical harmonic function associated to the rotational quantum number l and quantum number for the z-component of the angular momentum m (regarding the adiabatic approximation).

$\tilde{Y}$ Difference between $\tilde{y}$ and $\tilde{y}_0$ (regarding the FHO model).

$\tilde{Y}_1$ Difference between $\tilde{y}_1$ and $\tilde{y}_{0,1}$ (regarding the FHO model).

$\tilde{Y}_2$ Difference between $\tilde{y}_2$ and $\tilde{y}_{0,2}$ (regarding the FHO model).

$\tilde{y}$ Difference between the positions of the molecular particle nuclei (regarding the FHO model).

$\tilde{y}_1$ Difference between the positions of the molecular particle AB nuclei (regarding the FHO model).

$\tilde{y}_2$ Difference between the positions of the molecular particle CD nuclei (regarding the FHO model).

$\tilde{y}_0$ Equilibrium difference between the positions of the molecular particle nuclei (regarding the FHO model).

$\tilde{y}_{0,1}$ Equilibrium difference between the positions of the molecular particle AB nuclei (regarding the FHO model).

$\tilde{y}_{0,2}$ Equilibrium difference between the positions of the molecular particle CD nuclei (regarding the FHO model).

Z Specific collisional frequency (regarding binary collisions).

Z_i Number of protons in the i-th nucleus (regarding the adiabatic approximation).

$\tilde{z}$ Difference between the positions of two interacting particles (regarding the FHO model).

$\tilde{z}_0$ Equilibrium difference between the positions of two interacting particles (regarding the FHO model).

Greek symbols

α Inverse length parameter of the repulsive exponential potential; or inverse length parameter of the Morse potential (regarding the FHO model); or inverse length parameter considered on the model for H_{12} (regarding the Rosen-Zener-Demkov model).

α_e Spectroscopic rotational constant associated to the e-th electronic level.

γ Ratio of specific heats; or mass factor associated to the molecular particle (regarding the FHO model).

γ_1 Mass factor associated to the molecular particle AB (regarding the FHO model).

γ_2 Mass factor associated to the molecular particle CD (regarding the FHO model).

Δ Difference between the asymptotic values of U_2 and U_1 (regarding the Rosen-Zener-Demkov model).

ΔF Difference between F_2 and F_1 (regarding the Landau-Zener model).

$\Delta\epsilon_0$ Difference between the sum of the products ground level energies and the one associated to the reactants of the chemical equation.

ΔE Energy defect (regarding the energy gap law).

ϵ Particle sensible energy.

ϵ' Particle absolute energy.

ϵ_i Particle sensible energy associated to the i-th energy mode.

ϵ_{tr} Particle sensible translational energy.

ϵ_{int} Particle sensible internal energy.

ϵ_{rot} Particle sensible rotational energy.

ϵ_{vib} Particle sensible vibrational energy.

ϵ_{el} Particle sensible electronic energy.

ϵ_{sp} Particle sensible spin energy.

ϵ_s s-Th species particle sensible energy.

ϵ_{m} Molecular particle sensible energy.

ϵ_{a} Atomic particle sensible energy.

ϵ_{e} Free electron sensible energy.

$\epsilon_{i,j}$ Particle sensible energy associated to the j-th level of the i-th energy mode.

$\epsilon_{i,0}$ Particle ground-level energy associated to i-th energy mode.

$\epsilon_{s,j}$ s-Th species particle sensible energy associated to the j-th total energy level.

ϵ_s^+ Ionisation energy of a s-th species particle.

η_0 V-T and V-V-T transition probability parameter: ratio between the energy of a classical free harmonic oscillator and the quantum energy $\hbar\omega$ (regarding the FHO model).

θ Polar angle; or wave function associated to the relative translation of the collision partners as well as the translation of their centre of mass (regarding the FHO model).

$\Lambda_{s,e,v}^{e',v'}$ Escape factor with respect to the vibronic levels (e, v) and (e', v').

Λ Quantum number for the projection of the total electronic orbital angular momentum vector on the internuclear axis of the diatomic molecular particle.

$\hat{\Lambda}$ Label given to the quantum number for the projection of the total electronic orbital angular momentum vector on the internuclear axis of the diatomic molecular particle.

λ Photon wavelength; or mixture bulk viscosity coefficient.

λ_0 Centre of the wavelength-specific symmetric function.

μ Mixture dynamic viscosity coefficient; or reduced mass of collision partners (regarding binary collisions); or reduced mass of the diatomic molecular particle (regarding the FHO model and the the adiabatic approximation).

μ_1 Reduced mass of the molecular particle AB (regarding the FHO model).

μ_2 Reduced mass of the molecular particle CD (regarding the FHO model).

ν Photon frequency.

ν_s s-Th species stoichiometric coefficient in the reactants side of the chemical equation.

ν_s' s-Th species stoichiometric coefficient in the products side of the chemical equation.

ν_0 Centre of the frequency-specific symmetric function.

ξ V-V-T corrective factor introduced in the transition probability parameter ρ, for the case of collisions between molecular particles of different species (regarding the FHO model).

ρ Mass density of the mixture particles inside a space in the fluid; or V-V-T transition probability parameter (regarding the FHO model).

ρ_s Mass density of s-th species particles inside a space in the fluid.

σ Symmetry factor of the diatomic particle nuclei; or collisional cross section.

σ_{av} Average collisional cross section.

σ_p Process cross section.

$\sigma_{p,\mathrm{av}}$ Average process cross section.

σ_0 Characteristic cross section (regarding the energy gap law).

$[\sigma]$ Mixture Cauchy's stress tensor.

$[\sigma_s]$ s-Th species Cauchy's stress tensor.

$[\tau]$ Mixture viscous stress tensor.

$[\tau_s]$ s-Th species viscous stress tensor.

Φ Electronic wave function (regarding the adiabatic approximation).

ϕ_n n-Th adiabatic electronic wave function (regarding the adiabatic approximation).

ϕ_1 First adiabatic electronic wave function (regarding the two-states approximation).

ϕ_2 Second adiabatic electronic wave function (regarding the two-states approximation).

ϕ_n^0 n-Th diabatic electronic wave function (regarding the semiclassical approximation).

ϕ_1^0 First diabatic electronic wave function (regarding the two-states approximation).

ϕ_2^0 Second diabatic electronic wave function (regarding the two-states approximation).

$\phi_{\lambda,s,e,v}^{e',v'}$ Wavelength-specific line-shape factor associated to the set of vibronic levels (e,v) and (e',v') of the s-th species.

$\phi_{\nu,s,e,v}^{e',v'}$ Frequency-specific line-shape factor associated to the set of vibronic levels (e,v) and (e',v') of the s-th species.

$\hat{\phi}^{\mathrm{spe}}$ Instrument line-shape factor.

$\hat{\phi}^{\mathrm{spa}}$ Spatial resolution function.

$\hat{\phi}_{\mathrm{opt}}^{\mathrm{spa}}$ Optics spatial resolution function.

$\hat{\phi}_{\mathrm{cam}}^{\mathrm{spa}}$ Camera spatial resolution function.

$\hat{\phi}_{\mathrm{mot}}^{\mathrm{spa}}$ Motion spatial resolution function.

φ Azimuthal angle.

χ_n n-Th nuclei wave function (regarding the adiabatic approximation).

Ψ Global wave function (regarding the FHO model and the adiabatic approximation).

ψ Wave function associated to the vibration of the collision partners (regarding the FHO model); or global spatial wave function (regarding the adiabatic approximation).

Ω Solid angle.

$\dot{\Omega}_{j,i}$ Rate of energy transfer from the j-th energy mode to the i-th internal energy mode due to collisional processes.

$\dot{\Omega}^{\text{int}}_{s,\text{e}}$ Energy transferred per unit of time per unit of volume from the inner s-th species particles to the inner free electrons.

$\dot{\Omega}_{\text{rad}}$ Variation in time of the mixture energy density due to radiative processes.

ω Natural angular frequency of the quantum harmonic oscillator that represents the molecular particle (regarding the FHO model); Photon angular frequency.

ω_e Spectroscopic vibrational constant associated to the e-th electronic level.

$\dot{\omega}_s$ Variation of mass of the s-th species particles per unit of time and per unit of volume due to chemical reactions.

$\dot{\omega}_{s,v}$ Variation of mass of the s-th species particles at the vibrational level v per unit of time and per unit of volume due to collisional and radiative processes.

$\dot{\omega}_{s,e}$ Variation of mass of the s-th species particles at the electronic level e per unit of time and per unit of volume due to collisional and radiative processes.

$\dot{\omega}_{s,e,v}$ Variation of mass of the s-th species particles at the electronic level e and vibrational level v per unit of time and per unit of volume due to collisional and radiative processes.

Subscripts

0 Ground-level.

∞ Flow upstream of the shock wave.

1 Molecular particle AB (regarding the FHO model); or first nucleus of the diatomic particle (regarding the adiabatic approximation); or first adiabatic or diabatic electronic state(regarding the two-states approximation).

2 Flow immediately downstream of the shock wave; or molecular particle CD (regarding the FHO model); or second nucleus of the diatomic particle (regarding the adiabatic approximation); or second adiabatic or diabatic electronic state (regarding the two-states approximation).

a	Atomic particle.
b	Backward direction of the process.
c	Crossing of adiabatic electronic terms (regarding the Landau-Zener model).
D	Doppler broadening.
e	Free electron.
e	e-Th electronic energy level; or initial electronic level; or electronic level of the higher vibronic level.
el	Electronic energy mode.
el-tr$_\mathrm{e}$	Electronic-free electron translational energy mode.
e'	Electronic level of the lower vibronic level.
f	Forward direction of the process.
G	Gaussian function.
int	Internal energy mode.
i	i-Th energy mode; or i-th nucleus (regarding the adiabatic approximation).
J	Rotational quantum number.
j	j-Th total energy level; or j-th energy level of some energy mode; or j-th nucleus (regarding the adiabatic approximation).
k	k-Th translational energy level.
k_1	Translational quantum number with respect to the x_1 axis.
k_2	Translational quantum number with respect to the x_2 axis.
k_3	Translational quantum number with respect to the x_3 axis.
l	l-Th rotational energy level.
L	Lorentzian function.
m	Molecular particle.
m	m-Th vibrational energy level.
n	n-Th electronic energy level.
p	p-Th spin energy level; or p-th process; or pseudo-crossing of adiabatic electronic terms (regarding the Landau-Zener model).

q q-Th species.

rot Rotational energy mode.

r r-Th reaction.

res Resonance broadening.

S Stark broadening.

sp Spin energy mode.

s s-Th species.

tr Translational energy mode.

$\mathrm{tr_h}$ Heavy particle translational energy mode.

$\mathrm{tr_e}$ Free electron translational energy mode.

tr-rot Heavy particle translational-rotational energy mode.

V Voigt function.

vib Vibrational energy mode.

vib-el-$\mathrm{tr_e}$ Vibrational-electronic-free electron translational energy mode.

v v-Th vibrational quantum number; or initial vibrational quantum number; or vibrational quantum number of the higher vibronic level.

v' Vibrational quantum number of the lower vibronic level.

w Forefront wall of the entry body.

α α-Th electron (regarding the adiabatic approximation).

β β-Th electron (regarding the adiabatic approximation).

Superscripts

0 Diabatic electronic state (regarding the semiclassical approximation).

* Thermodynamic equilibrium condition.

a Absorption.

Blue "Blue" radiation.

D Dissociation.

e Electronic level of the higher vibronic level.

e' Final electronic level; or electronic level of the lower vibronic level.

ie Induced emission.

IR Infra-red radiation.

l l-Th wavelength interval.

Red "Red" radiation.

se Spontaneous emission.

s s-Th species.

VUV Vacuum ultra-violet radiation.

v Vibrational quantum number of the higher vibronic level.

v' Final vibrational quantum number; or vibrational quantum number of the lower vibronic level.

Mathematical entities

$\cdot$ Product; or inner product; or matrix-vector product.

$*$ Convolution.

$\otimes$ Dyadic product.

$\vec{\nabla}$ Gradient.

∇^2 Laplacian.

$[\,]^*$ Complex conjugate (being "[ ]" the operand).

$[\,]^{-1}$ Tensor inverse (being "[ ]" the operand).

$[\,]^{\mathrm{T}}$ Tensor transpose (being "[ ]" the operand).

$[\,]^\dagger$ Tensor conjugate transpose (being "[ ]" the operand).

$\dot{[\,]}$ Time derivative (being "[ ]" the operand).

$\ddot{[\,]}$ Double time derivative (being "[ ]" the operand).

$\|[\,]\|$ Norm (being "[ ]" the operand).

div Divergence.

$\mathrm{H}(x)$ Heaviside function of argument x.

i Unit imaginary number.

$[I]$ Identity tensor.

$\vec{n}$ Outward-pointing normal vector of a closed surface.

δ_{ij} Kronecker delta.

Acronyms

ADV Adaption in respect of the Database for the Vibrational energy levels.

CCD Charge-Coupled Device.

CFD Computational Fluid Dynamics.

EAST Electric Arc Shock Tube.

FGH Fourier Grid Hamiltonian method.

FHO Forced Harmonic Oscillator model.

FOPT First Order Perturbation Theory.

IPFN Instituto de Plasmas e Fusão Nuclear (or in english, Institute for Plasmas and Nuclear Fusion).

IR Infra-Red radiation.

IST Instituto Superior Técnico.

JAXA-HIEST Japan Aerospace Exploration Agency's High-Enthalpy Shock Tunnel.

NASA National Aeronautics and Space Administration.

NIST National Institute of Standards and Technology.

QCT Quasi-Classical Trajectory model.

RKR Rydberg-Klein-Rees method.

SPARK Software Package for Aerothermodynamics, Radiation and Kinetics.

SSH Schwartz-Slawsky-Herzfeld model.

TPS Thermal Protection System.

V-D Vibrational-Dissociation process.

V-T Vibrational-Translational process.

V-V-T Vibrational-Vibrational-Translational process.

VRP Vibrational Redistribution Procedure.

VUV Vacuum Ultra-Violet radiation.

Glossary

Boltzmann distribution	The Boltzmann distribution associated to an energy mode of the particles, corresponds to the population distribution of these particles with respect to the different energy levels of this energy mode, if its self-equilibrium was reached.
CFD	Computational Fluid Dynamics (CFD) is a branch of Fluid Mechanics that uses numerical methods and algorithms to solve problems involving fluid flows.
Chemical equilibrium	Chemical equilibrium with respect to the interior of an element of matter corresponds to a condition in which there's no change of its chemical composition.
Chemical kinetics	The chemical kinetics of a system correspond to the rates of the chemical reactions that occur in them.

Energy mode self-equilibrium An energy mode of particles that compose an element of matter is said to be in self-equilibrium, or in equilibrium with itself, if the energy (associated to that energy mode) transferred between the particles, due to interactions, is such, that no heat transfer (associated to that energy mode) occurs inside the element of matter. For instance, if a body, with a sufficiently higher dimension than the typical one of the particles, was present in the element of matter when the energy mode self-equilibrium was reached, no energy from that energy mode would be transferred to the body. If this condition is satisfied, a temperature specific to that energy mode can be attributed to the element of matter.

Mechanical equilibrium Mechanical equilibrium with respect to the interior of an element of matter corresponds to a condition in which the transfer of momentum between its particles, due to interactions, is such, that the produced internal forces are balanced. For instance, if a body, with a sufficiently higher dimension than the typical one of the particles, was present in the element of matter when the mechanical equilibrium was reached, the sum of all interaction forces that act on it would be null. If this condition is satisfied, a pressure can be attributed to the element of matter.

Multi-temperature model A multi-temperature model is a thermodynamic model which assumes that all energy modes of the particles are in self-equilibrium or even in equilibrium with some other. Multiple temperatures should therefore be assigned to the system, each one associated to a single or combination of energy modes.

Non-chemical kinetics	The non-chemical kinetics of a system correspond to the rates of the non-chemical processes (processes in which there's no change of the involved particles chemical species) that occur in them.
Plasma	Plasma is one of the known four states of the matter, being the other three the solid, liquid and gas. A plasma has charges (ions and free electrons) in its composition, meaning that such matter can conduct electricity, produce magnetic fields, and respond strongly to electromagnetic forces.
Radiative equilibrium	Radiative equilibrium with respect to the interior of an element of matter corresponds to a condition in which the absorption and emission of radiation by the particles is balanced (both in intensity and energy).
SPARK	Software Package for Aerothermodynamics, Radiation and Kinetics (SPARK) is a code for the numerical simulation of hypersonic non-equilibrium flows, developed by Lopez et al. and being maintained at the University of Illinois at Urbana-Champaign (UIUC) and at the research unit Instituto de Plasmas e Fusão Nuclear (IPFN) of Instituto Superior Técnico (IST).
Shock tube	A shock tube is a ground-based test facility used for the study of the chemical and non-chemical kinetics, as well as heat transfer on a post-shock flow. In a shock tube, a shock wave is generated by the rupture of a diaphragm that separates two sections of the tube: one containing a gas at very high pressure and the other containing a gas at low pressure. The low pressure gas is the one being tested, which is subjected to post-shock high temperature phenonema for a very brief period of time.

Single-temperature model	A single-temperature model is a thermodynamic model which assumes thermal equilibrium, i.e. all energy modes of the particles are considered to be in equilibrium with each other. These energy modes are described by a single temperature.
State-to-state model	A state-to-state model is a thermodynamic model which assumes that some energy modes of the particle are not in self-equilibrium, and therefore the respective energy levels need to be dealt one by one.
Thermal equilibrium	Thermal equilibrium with respect to the interior of an element of matter corresponds to a condition in which all their energy modes are in self-equilibrium and the respective temperatures are identical - therefore, a single temperature is enough to describe all of the particles energy modes. One can also say that in thermal equilibrium, the energy modes are in equilibrium with each other, besides themselves.
Thermochemical equilibrium	Thermochemical equilibrium is a condition of both thermal and chemical equilibrium.
Thermochemistry	The thermochemistry of a system corresponds to the heat energy associated to the chemical reactions and physical transformations occurring in them.
Thermodynamic equilibrium	Thermodynamic equilibrium is a condition of both mechanical, thermal, chemical and radiative equilibrium.

Chapter 1

Introduction

> "If you want to learn about nature, to appreciate nature, it is necessary to understand the language that she speaks in."
>
> — Richard P. Feynman

In this chapter a brief introduction to the problems and the state-of-the-art of the possible solutions associated to the study of atmospheric entry flows will be presented with a lot of words and not much of mathematics. Mostly, to acquaint the reader with all the highly technical terms and their meaning, which will suffer overuse from the very beginning to the very end of this thesis. The thorough mathematics will be saved for chapter 2.

1.1 A synopsis on atmospheric entry flows

When a body from the outer space moves towards a planet, it suffers acceleration due to gravity, increasing its speed. Let's assume here that the body is blunt (which is a very common characteristic of entry objects like meteors and the modern spacecrafts). The acceleration will be such that the body enters the atmosphere at a *supersonic speed* (a speed higher than the *sound speed* in the unperturbed flow) producing a detached[1] *shock wave*, which corresponds to a propagating disturbance that causes an abrupt increase in temperature, pressure and density of the gas immediately downstream of the wave. For simplicity reasons, let's assume here that the atmosphere is solely composed by heavy particles[2]. The above-mentioned temperature is associated to the *translational energy mode* of the particles, being called *heavy particle translational temperature*, $T_{\mathrm{tr_h}}$. It's important to warn the reader about the concept of a temperature, which as will be shown later in this work, isn't as evident as may seem (see section §2.2). Immediately downstream of the shock wave, the fast collisions between the gas particles induce a very rapid distribution of their translational energy - such distribution can be proved to be a *Boltzmann distribution* - and

[1] The shock wave is detached from the body, acquiring a bow shape, if the body is blunt. This is one of the main reasons for modern spacecrafts having a blunt nose, since a detached shock wave is stronger than an attached oblique one, heating more the flow and less the body [1]. On the other hand, the bluntness of the nose gives it more volume, requiring more energy to melt. A major drawback is in respect of the heat received by radiation, which increases with the area of the nose.

[2] A heavy particle corresponds to a particle with a mass equal or greater than the mass of the proton. A heavy particle then needs to be an atomic or a molecular particle.

translational equilibrium is said to occur [2]. Only in these conditions a translational temperature can be attributed to the gas. That means that there's a region, however very tiny, downstream of the shock wave and upstream of the translational equilibrium region, where enough collisions didn't occur and a translational temperature can't be defined. To not leave the reader into the void, the Boltzmann distribution and the equilibrium condition will be explored later in this work (see section §2.2).

In the flowfield between the shock wave and the body - termed *shock layer* - a lot of physical phenomena occur besides the abrupt change in the translational mode of the particles. The increase of the translational temperature is associated to an increase of the relative speed between the colliding particles as well as an increase of the number of collisions per unit of time. Collisions in these circumstances induce an excitation of the rotational and vibrational modes of the molecular particles, with the cost of some of the translational energy being transformed into rotational and vibrational energies, which in its turn reduces the translational temperature [2]. Since these physical aspects may be new to the reader, the different *energy modes* that the atomic and molecular particles can assume will be further described in this work (see section §2.1). The rotational excitation occurs almost simultaneously with the translational equilibration (except for cases in which the gas is composed by molecular hydrogen [2]) and therefore a *rotational temperature* T_{rot} being equal to the translational temperature $T_{\mathrm{tr_h}}$ can almost immediately be defined. This equality means that a designation for the combination of both temperatures may be employed: the *heavy particle translational-rotational temperature* $T_{\mathrm{tr_h\text{-}rot}} = T_{\mathrm{tr_h}} = T_{\mathrm{rot}}$. Translational and rotational excitations are much more faster than vibrational excitation (except, again, for cases in which the gas is composed by molecular hydrogen [2]), and translational-rotational equilibrium can be assumed to occur even before the commence of the vibrational excitation.

With the excitation of the rotational and vibrational modes, comes the dissociation of the molecular particles, occurring through overstretching of the vibrational stroke (vibrational dissociation) or centrifugal tearing (rotational dissociation), by collisions with another particles [2]. Such processes produce atomic particles. The higher the rotational or vibrational energy of the molecular particle, the higher the probability of the particle to suffer dissociation (since less energy is required to cause the dissociation). Therefore, the dissociation process is preferential to the highly rotationally and vibrationally excited molecular particles, meaning an aftermath reduction of the number of these particles in the gas. Also, dissociation requires energy, which is supplied by the translational energy of the colliding particles, reducing even more the translational temperature. Since dissociation is preceded by excitation of the molecular particles, an interval of time called *incubation period* can be defined, corresponding to the period in which rotational and vibrational excitation occur without dissociation.

With the presence of atomic particles in the flow, comes the possibility of occurring *associative ionisation reactions* in which the atomic particles associate, creating excited molecular particles, that spontaneously ionise, producing ionic molecular particles and free electrons. The produced ions and free electrons that become part of the flowing fluid may conduct electricity, produce magnetic fields, and respond strongly to electromagnetic forces. Such resultant fluid is termed *plasma* (plasma is one of the known four states of the matter, being the other three the solid, liquid and gas). Collisions between the free electrons and atomic particles will excite and ionise them, freeing even more electrons. Similarly,

collisions between free electrons and molecular particles will excite and ionise them, and may even cause their dissociation. The electronic excitation of heavy particles (i.e. excitation of the bound electrons of heavy particles) by electron impact is much more efficient than the respective excitation by heavy particle impact [2], and therefore, the electronic excitation process has its major importance in the region of the flow where free electrons are present.

Excited particles, may de-excite by a process termed *spontaneous emission*, which consists in the emission of a *photon* without any kind of external stimulus (therefore in a "spontaneous" way), lowering the *particle internal energy*. A *radiation field* is then created, inducing the emission of even more photons (by a process called *induced emission*), causing de-excitation of the particles. Some of the emitted photons may be absorbed by the particles in the plasma and in the body (by a process called *absorption*), causing their excitation. Also, the emitted photons may even dissociate or ionise the particles. Such processes are called *photodissociation* and *photoionisation* [3], respectively. The transfer of radiative energy to the body is termed *radiative heating*. Since the present author doesn't want the reader to feel blank about all these introduced radiative processes, a section in this work will be dedicated to them (see section §2.5).

After a considerable amount of collisions, the plasma begins a process of *relaxation*, i.e. it initiates an evolution to *thermodynamic equilibrium*. However, equilibrium may not be reached since as the flow gets more and more close to the body, new interactions between the two start to occur. The density of the plasma increases due to compressibility effects, and a *boundary layer* is formed, in which the viscosity effects are significant (due to a coexistence of a flow and a stationary wall), decelerating the flow - some of the *flow translational kinetic energy* is converted to *thermal energy* (the energy associated to the energy modes of the particles). Also, due to the temperature of the particles in the boundary layer being much higher than the one of the particles in the surface of the body, there's a transfer of energy, by the name of *convective heating*, from the former to the latter (through collisions between the particles of the two mediums). The plasma temperature therefore decreases in the boundary layer, with the possibility of occurring atomic particles association, and recombination of ionic particles with electrons [4].

The surface of the body may induce chemical reactions, more specifically, between particles of the plasma and particles of the body, as well as between the particles of plasma solely. Such reactions are termed *plasma-surface reactions*. Particles of the plasma are *adsorbed* by the surface (i.e. "stuck" to the surface), due to the interaction forces between these particles and the particles of the body, which after reacting with other adsorbed gas particles or body particles, may or may not *desorb* (i.e. "unstick" the surface) [2]. One example of a plasma-surface reaction is the so-called *surface-catalytic recombination*, in which two adsorbed atomic particles associate forming a molecular particle. The reaction occurs with a transfer of energy to a particle in the body wall, being therefore exothermic (such reaction heats the body). Another two examples of plasma-surface reactions are the oxidation of atomic carbon by a molecular oxygen, and the oxidation of atomic carbon by an atomic oxygen. The former is and endothermic reaction, and the latter is an exothermic one [2]. These details are of capital importance for the design of the spacecraft *thermal protection system* (TPS) - the ideal TPS would be one that catalyses endothermic reactions and inhibits exothermic reactions, since the less the received heat, the higher the chance of the spacecraft to survive the atmospheric entry.

Particles from the body may be transferred to the flow by processes that don't change their chemical composition. *Ablation* is the general designation for such processes, which are twofold: *sublimation* - if the particles are removed one by one, forming a gas - and *spallation* - if fragments (i.e. clusters of particles, still forming a solid material) are ejected as a result of the cracks and slits caused by the gas particles impact and by stress. These processes reduce the heat transferred to the inner part of the body, since a substantial part of the energy is spent in bond breaking and other substantial part is carried away by the removed particles.

Some spacecrafts may use *active cooling* in their thermal protection system, corresponding to an injection of a cooled gas from the body to the boundary layer. If the gas injection is restricted to a limited surface area of the body wall, such as from a slot, the process is called *film cooling*. If the gas injection occurs over a wide surface are, the process is called *transpiration cooling* [4]. Such processes reduce the amount of heat transferred to the body - some of the energy in the boundary layer is transferred to the injected gas instead of the body wall, and some of the energy in the body wall is transferred to the injected gas as it flows through the supply tube to the boundary layer.

The products of the plasma-surface reactions, ablation, and active cooling become part of the boundary layer plasma, meaning that reactions involving the new species in the flow may occur, influencing the physics around the body.

This whole wording is just a small introduction to the relevant phenomenology that occurs in atmosphere entry flows. Such introduction is necessary to properly define *hypersonic flows* - the flow upstream of a shock wave is said to be hypersonic if the herein described physical phenomena (with less or more accentuation) are present in the flow downstream of the wave. The *Mach number*[3] of a hypersonic flow needs to be much greater than unity, i.e $\mathrm{Ma}_\infty \gg 1$. Anderson [1] refers that, as a rule of thumb, a flow can be considered to be hypersonic if the respective Mach number is greater than five, i.e. $\mathrm{Ma}_\infty > 5$. Meanwhile there are other authors, such as Park [2] and Bertin [4], that consider a different value for this lower limit: $\mathrm{Ma}_\infty > 4$. The uncertainty in attributing a threshold value to the Mach number of a hypersonic flow comes mostly from the fact that the transformation of an *supersonic flow* into a hypersonic flow is with respect to an accentuation of the post-shock physical effects which evolve in a non abrupt way, and not to a discontinuity in the physical phenomena. There's actually no threshold, but an interval of Ma_∞ values for which both labels may be subjectivity used to describe the type of flow. Another reason for the difficulty of defining hypersonic flows is with respect to the amount of other parameters beyond the Mach number that the respective post-shock phenomena depend on. Examples of such parameters are the *Knudsen number* Kn - corresponding to the ratio between the particles mean free path (i.e. the average distance travelled by the particles between two consecutive collisions) and a characteristic dimension of the flowfield (for example the body length) - the *Reynolds number* Re - corresponding to the ratio between the inertial and the viscous forces - and the *Damköhler number* Da- corresponding to the ratio between some characteristic flow time and some characteristic chemical reaction time [5].

Some remarkable examples of Earth atmospheric entries are the ones of the Mercury, Gemini and

[3]The Mach number of a flow in a point corresponds to the ratio between the flow and sound speeds evaluated at that same point.

Vostok manned orbital spacecrafts reaching a Mach number of 25 in 1960, the Apollo spacecraft which returned men from the moon in 1969, reaching a Mach number of 36 [1], and the Chelyabinsk meteor that penetrated the atmosphere at an estimated Mach number of 60 over the city Chelyabinsk, Russia in 2013 [6].

1.2 The importance of experiments and numerical simulations for Spacecraft Design

The main objective of Spacecraft Design with respect to atmospheric entries is to devise a vehicle that can sustain the harsh conditions of the flight, descend in a stable and controllable way, and decelerate so that landing can safely happen. Regarding the survival of the spacecraft against the harsh conditions, one should speak about the strong convective and radiative heats received by the vehicle. The distribution of the heat around the body needs to be well predicted for a correct estimation of the thickness of the thermal protection system. A thermal protection system with an underestimated thickness would compromise the integrity of the vehicle due to the removal of a considerable part of the protective material by ablative processes. On the other hand, a thermal protection system with an overestimated thickness would make the spacecraft inevitably heavier. The higher the structural weight, the higher the required rate of ejected fuel to provide the same acceleration, at its launch from the ground and in manoeuvrers at the outer space - a higher structural weight would therefore also mean a higher fuel weight. Note that a thermal protection system may even be required for the spacecraft *base* (the back of the vehicle) besides the nose, due to the considerable amount of radiation emitted by the wake [5].

Regarding the stability and controllability of the spacecraft, one should speak about aerodynamic forces (lift and drag) and moments that act on it. These are a result of the pressure and shear stress distributions around the body. The intensity and direction of the forces will dictate the trajectory of the body, and the intensity and direction of the moments will dictate its attitude. A trimmed descent (i.e. without rotation of the body) is of capital interest to the spacecraft designers, since a rotation would drift the vehicle to undesired angles of attack. Some spacecrafts (as is example the Space Shuttle) require control surfaces to redistribute the pressure and shear stress around the body in way that the designed angle of attack is achieved. The knowledge of the value for the deflection angle of such control surfaces to trim the vehicle would be undoubtedly convenient (and obviously much safer than trying to find it in real time flight). A historic example in which the required body-flap deflection angle wasn't at all correctly predicted, was the case of the Space Shuttle. The actual required value was two times higher than the one predicted from wind-tunnel data [4]. This is an indication of the lack of reliability on some of the experimental tests made at the time.

There is other relevant phenomenology to be concerned with - the free electrons produced in the entry flow will absorb radio-frequency radiation, causing *communications blackout* to and from the vehicle during parts of the entry trajectory. In the modern days, this problem can be alleviated, since the radio-frequency radiations may be sent to a satellite and resent to the spacecraft from a path that doesn't intersect the region of high electrons density. However, it's still of high priority to predict the electron

density distribution around the body, if not at least to know the path through which the radio-frequency radiations should be sent [1].

All of these aspects referred here are with respect to the spacecraft design objectives. To accomplish them, the interaction between the flow and the body, in a microscopic and macroscopic way, needs to be understood. Experiments and *Computational Fluid Dynamics* (CFD) simulations are the two required tools to achieve such understanding. Regarding the experiments, one should speak about the ones that would immediatly tell us all the truth (although only in a macroscopic way) about the atmospheric entry: flight-tests of the full-scale vehicle. These provide an uncompromising representation of the vehicle's environment, but are too expensive and can only be done in the final stage of the design, development and fabrication process. Flight-tests of simpler small-scale models[4] would be more feasible, but still too expensive. The majority of the experiments are therefore made in ground-based test facilities. Not only ground-based tests can be used to estimate aerodynamic forces and moments, the distribution of heat-transfer and another important variables, useful for the design of the spacecraft in a direct way, but they can also provide data for *calibration* and *validation* of CFD codes. These CFD codes, in their turn, may then be put into practice for the spacecraft design. Validation of a code corresponds to the quantification of its predictability with respect to some reliable experimental results. A valid code should, in principle, produce results which are very similar with those obtained through experiment. On the other hand, calibration of a code consists in making its results more agreeable with the experimental ones, by adjusting its numerical parameters. An invalid code can then be transformed into a valid one, if a proper calibration through sufficient reliable experimental results is performed (and if the code had already a good physical and mathemical structure in its basis). The number of ground-based tests for the purpose of benchmarking CFD codes is increasing as much as the reliance on CFD as a design tool [4]. This shows how important is CFD becoming for the spacecraft design.

According to Bertin [4], there are nine parameters that can be simulated in ground based facilities: free stream Mach number M_∞, free stream Reynolds number Re_∞, free stream velocity $\vec{u}_\infty$, free stream static pressure p_∞, specific stagnation enthalpy of the flow h_0, the density ratio across the shock wave ρ_∞/ρ_2 (being ρ_∞ the free stream density and ρ_2 the density immediately downstream of the shock wave), the free stream chemical composition of the gas, the wall-to-stagnation temperature ratio T_w/T_0 (being T_w the temperature of the wall and T_0 the stagnation heavy particle translational temperature of the flow), and the thermochemistry of the flowfield (the heat energy associated with chemical reactions). It's not however possible to simulate simultaneously all of these parameters in a ground-based faciliy (the same can't be said about CFD) [4]. In ground-based facility tests, some parameters are then chosen to be simulated with the expense of the remainder. An experiment is therefore only a "partial simulation" and various different tests need to be performed for a more complete study of the entry flow. Examples of ground-based facilities dedicated to study of hypersonic flows are the *shock tubes*, *arc-heated test facilities*, *hypersonic wind tunnels* and *ballistic free-flight ranges* [4]. Some comments about shock tubes should be made, since experimental data obtained from a test performed on the NASA's EAST shock tube was found useful in this work. Shock tubes are mainly used for the study of the *chemical kinetics* (i.e. the

[4] An historic example of such flight-tests is the so-called Re-entry F Flight Test [4].

rates of chemical reactions), *non-chemical kinetics*[5] (rates of processes which involve transitions in the energy levels of the particles) and heat transfer on a post-shock flow. In particular, the resultant radiative field is of paramount importance for the validation of CFD codes regarding the population distribution of the particles internal energy levels [7]. Note that radiative processes are intimately associated to the degree of excitation of the particles, and therefore, numerical results which agree with experimentally measured radiative fields, should, in priciple, also agree with the population distribution of the internal energy levels. In a shock tube, a shock wave is generated by the rupture of a diaphragm that separates two sections of the tube: one containing a gas at very high pressure (the *driver gas*) and the other containing a gas at low pressure (the *driven gas*). The low pressure gas is the one being tested, which is subjected to post-shock high temperature phenonema for a very brief period of time. Due to the high temperatures of the free stream that these facilities produce, the respective Mach number can't be high enough to match the typical values of an entry flow [4]. Note that the free stream speed of sound is given by $a_\infty = \sqrt{\gamma_\infty R_\infty T_\infty}$ [1], being γ_∞ the free stream ratio of specific heats and R_∞ the free stream mass-specific ideal gas constant. For a fixed free stream speed u_∞, the higher the temperature T_∞, the lower the Mach number $\mathrm{Ma}_\infty = u_\infty/a_\infty$. This is an example that illustrates the above mentioned impossibility of ground-based facilities to perform complete simulations of entry flows in the present days.

In respect of the optimisation of some particular configuration, one should say that CFD can be used for such goal without spending the resources and labour that a full set of equivalent models in an optimisation by experiment would require [4]. A numerical optimisation would therefore make a more effective use of the ground-test facilities, since the resultant numerically optimised model would be firstly tested in those instead of others which, together with all the effort put into them, would be probably disregarded. Another particular advantage of CFD simulations is the fact that they can provide a lot more details about the variables on the flowfield, from the microscopic to the macroscopic ones, not requiring intrusive methods for their extraction.

1.3 Numerical models

The accuracy of the numerical simulations is intimately linked to the accuracy of the considered models for representation of the important physical phenomena which occur in the problem of study. One big difficulty about modelling entry post-shock flows is with respect to the quantification of the *non-equilibrium* effects. It is here that non-equilibrium thermodynamic and kinetic models come into play.

1.3.1 Thermodynamic models

The term "non-equilibrium" may seem too vague when heard for the first time. There are a lot of different types of non-equilibrium that may occur in the flow: *mechanical non-equilibrium*, *chemical non-equilibrium*, *radiative non-equilibrium*, *thermal non-equilibrium* and *energy mode self-non-equilibrium*. And from these five terms, even more complicated ones can be built to represent a simultaneity of

[5] Non-chemical processes are processes that don't involve a chemical change of the species of the particles, and therefore they can't be identified as chemical reactions. They do involve a change in the internal energy levels of the particles.

different types of non-equilibrium, as is example the *thermochemical non-equilibrium*, corresponding to a condition of both thermal and chemical non-equilibria.

A mechanical equilibrium with respect to the interior of an element of fluid corresponds to a condition in which the transfer of momentum between its particles, due to interactions, is such, that the produced internal forces are balanced. For instance, if a body, with a sufficiently higher dimension than the typical one of the particles, was present in the element of fluid when the mechanical equilibrium was reached, the sum of all interaction forces that act on it would be null. If this condition is satisfied, a pressure p can be attributed to the element of fluid.

The interior of an element of fluid is in chemical equilibrium if there's no tendency for a change in its chemical composition. As referred in section §1.1, there is a cascade of physical phenomena in the post-shock flows which changes its chemical composition as an aftermath, and therefore one shouldn't assume that chemical equilibrium is reached in those cases.

Radiative equilibrium with respect to the interior of an element of fluid corresponds to a condition in which the internal absorption and emission of radiation by the particles is balanced (both in intensity and energy). Such condition is not observed in post-shock flows, and therefore, radiative equilibrium shouldn't be assumed [3].

Thermal equilibrium occurs if the energy transferred between the particles, due to interactions, is such, that no heat transfer occurs inside the element of fluid. For instance, if a body, with a sufficiently higher dimension than the typical one of the particles, was present in the element of fluid when the thermal equilibrium was reached, no heat would be transferred to the body. If this condition is satisfied, a temperature T can be attributed to the element of fluid, and the population of the particles energy levels would follow a Boltzmann distribution, with the temperature T as parameter.

An energy mode of the particles that constitute some element of fluid is in self-equilibrium if the conditions said above about thermal equilibrium were true for that energy mode in particular. Therefore, if the i-th energy mode associated to the particles of the s-th species is in self-equilibrium, a temperature $T_{s,i}$ can be assigned. The population of the particles energy levels in that energy mode would follow a Boltzmann distribution, with the temperature $T_{s,i}$ as parameter. The term "self-equilibrium" is used to emphasize the fact the mode may be in equilibrium with itself but not with others. Thermodynamic models which account the possibility of energy modes to be in self-equilibrium correspond to the so-called *multi-temperature models*. Well known examples of multiple-temperature models are the *Lee's three-temperature model* [8] and the *Park's two-temperature model* [9]. In both models it's assumed that all heavy species have the same temperature values for the same type of energy modes. Such proposition comes from the assumption that the particles of the considered heavy species are sufficiently similar to be affected by the physical phenomena in an identical way. Lee and Park consider other two common assumptions. The first one regards the tendency that the rotational mode has to equilibrate very fast with the heavy particles translational mode. Therefore, both authors define a heavy particle translational-rotational temperature, $T_{\mathrm{tr_h\text{-}rot}} = T_{\mathrm{tr_h}} = T_{\mathrm{rot}}$. The second assumption regards the strong dependency that the electronic excitation of particles have on the translation of free electrons - this proposition is particular true for the low laying electronic levels of the particles. Park considers one more assumption

than Lee, corresponding to a fast energy transfer between the translational mode of free electrons and the vibrational mode of molecular particles - which is particular true for the case of molecular nitrogen N_2 [9]. Therefore Lee considers two temperatures besides the heavy particle translational-rotational one - the vibrational temperature T_{vib} and the electronic-free electron translational temperature $T_{\text{el-tr}_\text{e}} = T_{\text{el}} = T_{\text{tr}_\text{e}}$ - and Park considers one - the vibrational-electronic-free electron translational temperature $T_{\text{vib-el-tr}_\text{e}} = T_{\text{vib}} = T_{\text{el}} = T_{\text{tr}_\text{e}}$.

As pointed out by Park [10], numerical results obtained through multi-temperature models are significantly more agreeable with the accurate experimental ones for the post-shock conditions than the *single-temperature models*, which assume thermal equilibrium. Several works such as the ones of Candler [11], Hornung [12] and Lobb [13] evidenced that the single-temperature model predicts the flow to be closer to thermodynamic equilibrium than it actually is. The use of the single-temperature model may then lead for incorrect predictions for the aerodynanamic characteristics of a hypersonic vehicle. And as Park [10] said "[b]ecause of this mistake, most people thought that the flight regime of the most hypersonic vehicles would be in the equilibrium regime, while, in reality, they would be in the nonequilibrium regime. The mistake is caused by using the one-temperature model".

There is the possibilty of the particles vibrational energy mode not being in self-equilibrium in some post-shock flows, as shown by Candler et al. [14], which means that a vibrational temperature T_{vib} can't even be assigned, and that the population of the vibrational energy levels doesn't follow a Boltzmann distribution. Since the distribution of the vibrational energy levels is unknown in such cases, there is no chance to treat all the vibrational levels as a group. Each vibrational energy level does need to be treated individually. The electronic energy mode and even the rotational energy mode may also not be in self-equilibrium, as referred by Munafó et al. [15], and a similar procedure with respect to the rotational and electronic energy levels would be needed. Such procedures require models which are specific to the internal energy levels of the involved particles. Models that treat internal energy levels of the particles individually are the so-called *state-to-state models* (some authors also call them *collisional-radiative models*) [16]. Dealing with internal levels introduces an extensive set of variables to the problem, requiring much more computational resources than for the case of the multi-temperature models. The higher the number of specified internal energy modes the higher the associated computational costs. Therefore, the simultaneous assumption of self-equilibrium with respect to the fastest equilibrating energy modes, such as the rotational one, may be convenient if not necessary. And in fact, this approach is commonly taken: the most part of the existing state-to-state models aren't rotational-specific [16]. In this work a vibronic[6]-specific state-to-state model will be considered.

1.3.2 Kinetic models

Models for the plasma kinetics, i.e. the chemical and non-chemical processes, are required to properly describe the phenomenology in an entry post-shock flow. These models may be purely theoretical, semi-empirical (with a theoretical form, calibrated by experimental results) or purely empirical (solely described by experimental results). Both valid theoretical and semi-empirical models should agree with

[6]The term vibronic is an agglutination of two other terms: **vib**rational and elect**ronic**.

the experimental results. However, a significant part of the experimental data is obtained at room temperature (around 300 K), without specificity of the internal energy levels of the particles. Therefore, the validity of some of the theoretical and semi-empirical models may be only assured for the low temperature regime, and not for each internal energy level but for the overall contribution of the set. When the process isn't reasonably well understood, there's no option but to consider some crude assumptions for the dependencies on the temperature and internal levels. Example of such crude assumptions are the expressions associated to the so-called *vibrational redistribution* procedure, being employed by João Vargas [17], and by Julien Annaloro [18] in their thesis, the latter in a more sophisticated form.

One important non-chemical process that will be further addressed in this work is the vibrational excitation and de-excitation of molecular particles by heavy particle impact. Adamovich et al. [19–21] did a good job reviewing the currently available models that can describe this particular process. One of the simplest models is the *Schwartz—Slawsky—Herzfeld model* (SSH) [22]. This is a *semiclassical model*[7] derived under a *first-order perturbation theory* (FOPT) approach, assuming collinearity of the collision (all nuclei and the collision velocity vector are disposed in a single line), harmonicity of the molecular particles (internuclear forces follow Hooke's law), and an exponential repulsive interaction potential. Due to the first-order perturbation theory approach, only single vibrational energy level jumps are regarded to occur in the excitation or de-excitation process, which is solely true for cases of small collision speeds. The model shouldn't therefore be employed in numerical simulations of entry post-shock flows, due to the very high heavy particle translational temperatures that occur in those conditions. The most precise models include the exact *quantum mechanical models*, like the one suggested by Secrest and Johnson [23], and semiclassical models like the one developed by Billing [24]. The latter, which corresponds to a *Quasi-Classical Trajectory* model (QCT) [25], considers three-dimensional collisions, and a more reallistic interaction potential. Both the model of Secrest and Johnson, and the one of Billing, require a considerable amount of computational resources, limiting their applicability. An alternative model which is much more accurate than the SSH model, and at the same time more practical than the two above mentioned, is the *Forced Harmonic Oscillator model* (FHO) [21]. It was originally conceived by Kerner [26] and Treanor [27], being only applicable for the case of a molecular particle-atomic particle collision. It consisted of a non-perturbative semiclassical model, assuming collinearity of the collision, harmonicity of the molecular particle and an exponential repulsive interaction potential. It was then generalised by Zelechow et al. [28] for the case of molecular particle-molecular particle collisions. At last, Adamovich et al. [19–21] applied corrections in the model to account the anharmonicity of the molecular particles, the attractive long-range part of the interaction potential, the possible non-collinearity of the collision, the case in which the molecular particles are non-identical, and energy conservation. The resultant model was shown to agree considerable well with the results obtained through the state-of-the-art Billing's model [24]. The work of M. Lino da Silva et al. [29], which considers the model of Adamovich et al. additionally regarding a more accurate method for computing the energies of the vibrational levels of the colliding particles, endorses this agreeability.

Another important non-chemical processes that should be accounted for are the vibronic transitions

[7] In semiclassical models both *Quantum Mechanics* and *Classical Mechanics* laws are taken into consideration.

of molecular particles by heavy particle impact. There are two well-known theoretical models which deal with the homologous processes for the case of atomic particles - the electronic transitions of atomic particles by atomic particle impact: the *Landau-Zener model* [30, 31] and *Rosen-Zener-Demkov* model [32, 33]. In this work, the possibility of these models being extended to the case of vibronic transitions of molecular particles by heavy particles will be studied. Empirical models may be used alternatively, such as the *exponential gap law* considered in the works of Bachmann et al. [34, 35], and a different kind of exponential gap law regarded in the works of Katayama et al. [36–38]. In the latter, the so-called *Franck-Condon factors* are employed. Katayama et al. [39] even suggests a different model, which takes into account the intermolecular potential well depth of the interaction.

1.4 The case of Earth atmospheric entries

When considering Earth atmospheric entries, one needs to deal with air. Its chemical composition and thermodynamic properties vary with altitude, due to the Earth and outer space effects. The higher the altitude the lower the gravitational force, and therefore, the higher the probability of an air particle surpassing the so-called *escape speed* - the required speed to escape Earth's attraction. This implies a decrease of the air density with altitude. On the other hand, the higher the altitude the higher the probability of a photon emitted by the sun to reach an air particle causing its excitation, photoionisation or photodissociation. These trigger a cascade of other processes, changing the air chemistry as aftermath. However it is only below the *Kármán line* (~ 100 km) that air is dense enough to interact strongly with an spacecraft or meteor in its entry, being the chemical composition of the air almost constant in that layer of the atmosphere. The air components in such conditions are molecular nitrogen N_2, with a *mole fraction* of $x_{N_2} := N_{N_2}/N = 78.08$ %, molecular oxygen O_2 with $x_{O_2} = 20.95$ %, water H_2O with $x_{H_2O} \sim 2 \times 10^{-6}$ - 3×10^{-2} %, argon Ar with $x_{Ar} = 9.34 \times 10^{-3}$ %, and some other chemical species whose mole fractions are negligible [40]. However, it is important to add that the water mole fraction is only relevant below the *tropopause* (~ 11 km), and since the body already suffered most of the entry effects above that limit, one can disregard the water in the entry environment.

As referred in the section §1.1, the unperturbed flow suffers a lot of physical phenomena downstream of the entry shock wave, causing a change in its chemical composition. By neglecting the small mole fraction of argon and the other trace chemical species, one can expect at least eleven species in the post-shock flow - N, O, N_2, O_2, NO, O^+, N^+, N_2^+, O_2^+, NO^+ and e^- - resultant from the two ones in the unperturbed flow - N_2 and O_2 [2]. There are therefore a lot of chemical species to take into account in an Earth atmospheric entry, which complicates the job of creating a reliable model that replicates all the inherent physical phenomena in the post-shock flow. One smart move is to start by building a less extensive model dedicated to hypothetical entry flows composed by solely one chemical species upstream of the shock wave, i.e. solely by N_2 or by O_2. The only way to validate it is by experimental data taken from ground-based facilities using the one chemical species gas, such as shock tubes.

This work will only deal with pure nitrogen hypersonic flows (i.e. in which the gas upstream of the shock wave is solely composed by molecular nitrogen N_2), and therefore, only five post-shock chemical

species were considered - N, N_2, N^+, N_2^+ and e^-. Also, this work will be restricted to *zero-dimensional* and *one-dimensional* simulations, being these used to describe the physical phenomena obtained in shock tube tests. Figure 1.1 tries to depict such phenomena. Note that the label "n-dimension simulation" is used to describe the simulation in respect of the number of spatial dimensions (the number n), along which, the flowfield variables are allowed to vary. The number n also represents the number of components of the flow velocity vector. Therefore, in a zero-dimensional simulation, all variables are assumed to be constant in space, and no flow occurs (the gas is assumed to be at rest) - the change in the variables values occurs only in time, or in other words, the change occurs simultaneously and identically at all points of the space. For instance, in a one-dimensional simulation, the variables may vary along one direction and the flow velocity vector has only one component, defined by this same direction. A zero-dimensional simulation is particularly useful for a focused study on the chemical and non-chemical kinetics of the plasma from some initial conditions, disregarding fluid flow effects [41]. It runs faster than a one-dimensional simulation since it considers the momentum transfer between elements of fluid to be negligible, solving one less differential equation. The use of a zero-dimensional simulation as an approximation of a one-dimensional flow will turn to be more clear after the reading of section §3.4.

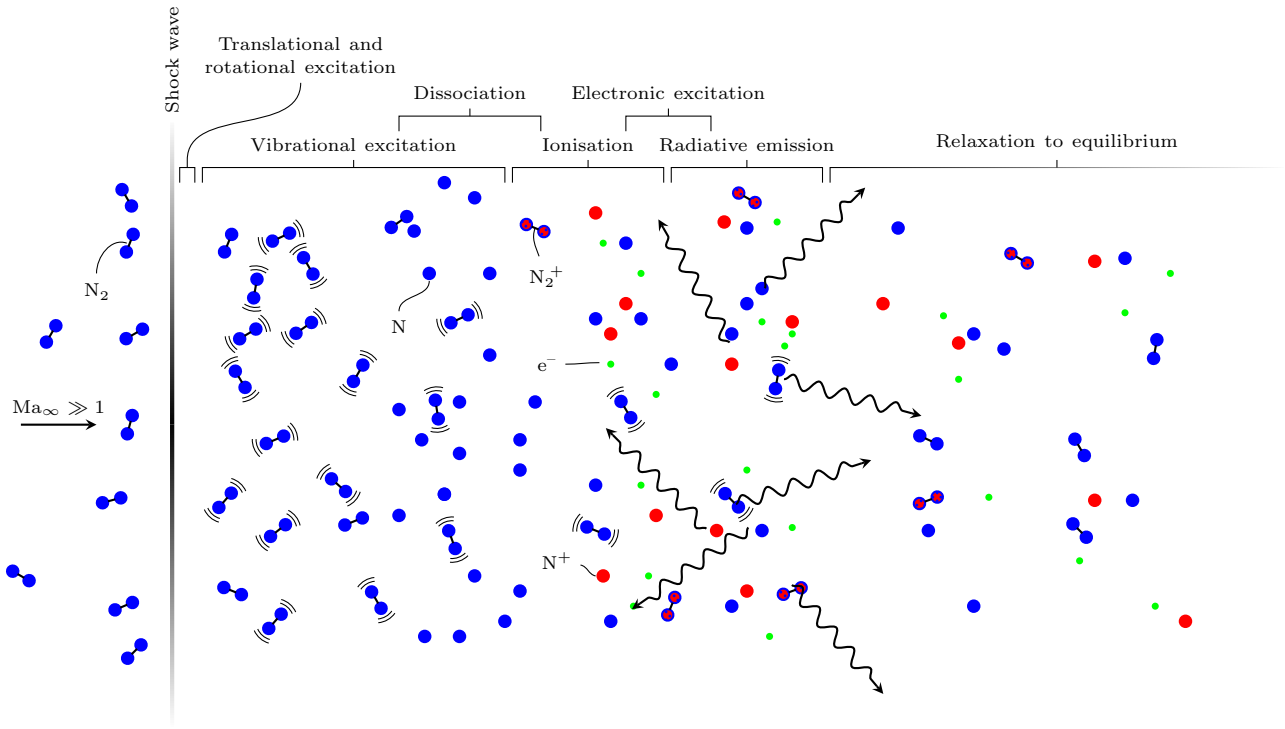

Figure 1.1: Representation of the post-shock physical phenomena that occur in a pure nitrogen hypersonic flow, inside a shock tube.

1.5 Objectives

In this thesis, as said before, a hypothetical pure nitrogen entry flow was studied. Zero and one-dimensional numerical simulations were performed to mimic the high-temperature phenomena of the post-shock flow. The main objective of this study is to create a database of chemical and non-chemical rates, as well as a full set of vibrational and electronic energy levels of the involved species, which together could accurately depict the physical phenomena that occur in a pure nitrogen post-shock flow. This main objective can only be achieved by following a recipe of tasks, each one associated to an accessory smaller objective:

- Computation of the *internuclear potential curves* associated to the molecular particles N_2 and N_2^+, in their ground and electronically excited electronic levels, by employing the *Rydberg–Klein–Rees method* allied with an extrapolation procedure for the short and long-range parts. Computation of the vibrational energy values by applying the *Fourier Grid Hamiltonian method* and using the previously obtained internuclear potential curves. ;

- Computation of rates for vibrational excitation and vibronic-specific dissociation of the molecular particles N_2 and N_2^+ by collisions with the heavy particles (N, N_2, N^+ and N_2^+), using the *Forced Harmonic Oscillator model*. Computation of the respective thermal rates of dissociation (the dissociation rates of the involved molecular particles, at thermal equilibrium) and their comparison with numerically and experimentally determined values taken from the literature;

- Study of the possibility of computation of rate coefficients for transitions between vibronic levels of N_2 by collisions with heavy particles, through the *Landau-Zener model* and the *Rosen-Zener-Demkov model*;

- Zero and one-dimensional numerical simulations, regarding vibronic-specific state-to-state approaches, of the high-temperature phenomena that occur in pure nitrogen post-shock flows, employing the conceived database in the CFD in-house code SPARK (see reference [42] to know more about this numerical code). Calibration and validation of the database by comparison of the radiative field obtained in the simulations with the radiative field measured in the test 62 of the EAST shock tube in 2018 (data taken from reference [43]).

By reaching this milestone, the reader should now be able to decipher the title of the thesis: "High-temperature kinetic and thermodynamic models for nitrogen plasmas". The term "high-temperature" is with respect to the high temperatures that the entry post-shock flows (the object of study of this thesis) can achieve, "kinetic" is with respect to the modelling of chemical kinetics (rates of chemical reactions) as well as the modelling of non-chemical kinetics (the excitation and de-excitation of the internal modes of the particles) that occur in those conditions, "thermodynamic models" is with respect to the modelling of the thermodynamic variables (temperatures, enthalpies, internal energies, etc.), and "nitrogen plasmas" is with respect to the state of the matter in the post-shock flow, which, upstream of the shock wave, corresponds to gaseous nitrogen.

1.6 Thesis Outline

This work is divided into five parts:

- Chapter 1 (the present one), which acquaints the reader to the the post-shock physical phenomena that typically occur in atmospheric entries, the state-of-the-art of the models used in the numerical simulations of such entries, the objectives of this thesis and its outline;
- Chapter 2, that provides the mathematical formulation of the models introduced in Chapter 1, and enunciates relations for the involved physical variables and their dynamics;
- Chapter 3, which presents the application of the theory reported in Chapter 2 to the computation of rate coefficients values of the processes regarded in the kinetic database, and the way that the governing equations were adapted for the simulation of post-shock flows generated by a shock tube;
- Chapter 4, that reports the results of the zero and one-dimensional SPARK simulations of three benchmark shots executed in the EAST 62^{th} campaign, and presents the obtained values for the radiation variables, mole fractions, temperatures and evolution to equilibrium. A discussion on the discrepancies from the experimental results is made, possible causes for them are enunciated, and sensibility tests on the rate coefficients values are reported;
- Chapter 5, which presents the conclusions of this work, its achievements, and modifications that may be tried in a near future in order to achieve better results.

Chapter 2

Background

In this chapter, a detailed physical and mathematical characterisation of the high-temperature phenomena that occur in atmospheric entry flows will be done. To properly guide the reader, such characterisation will firstly address the most microscopic aspects of the problem (the ones associated to the particles). The object of study will then gradually grow in scale, offering a general description about the quantification of the collisional and radiative processes, the thermodynamic variables, as well as the fluid flow governing equations. In the last part of this chapter, emphasis will be given to some particular models for collisional processes.

2.1 Energy modes of a particle

The energy of a particle measured relatively to some point in space is a result of the motion of all its parts: nuclei and electrons. The motion can be described as a combination of two other: the motion of some reference point of the particle and the motion of its parts relatively to that point. For convenience, the reference point is usually defined as the *centre of mass* of the particle. Therefore, the energy of the particle ϵ' is the sum of two contributions: the translational kinetic energy of its centre of mass ϵ'_{tr}, and the so-called particle internal energy ϵ'_{int}, which corresponds to the energy associated to the motion of the nuclei and electrons relatively to the center of mass [3]. One has then $\epsilon' = \epsilon'_{\text{tr}} + \epsilon'_{\text{int}}$.

Due to the fact that electrons have a much lower mass than the nuclei, they move much faster, and therefore the motion of the electrons and the motion of the nuclei can be considered to be independent of each other. This is the so-called *adiabatic approximation* (or *Born–Oppenheimer approximation*) [44]. On the other hand, the motion of the nuclei relatively to the centre of mass corresponds to a combination of rotation, vibration and *spin* (rotation upon themselves). Nuclear spin can be neglected since it doesn't play any role in the chemical and non-chemical processes [3]. Rotation and vibration are in some way coupled, since the rotation causes stretching by centrifugation, which affects the vibration, while the vibration changes the distance between the nuclei, and therefore also the moment of inertia of the molecular particle, which ultimately influences the rotation. Anyway, for most engineering purposes the decoupling of the rotational and vibrational motions can also be assumed [3]. In theses circumstances, the

internal energy of the particle is a sum of the rotational contribution (ϵ'_{rot}, rotational kinetic energy of the molecular particle around its centre of mass), vibrational contribution (ϵ'_{vib}, sum of the nuclei translational kinetic energy relatively to the molecular particle centre of mass, and the respective internuclear potential energy) and electronic contribution (ϵ'_{el}, sum of the translational kinetic energy of the electrons around the nuclei, and the potential energy between themselves as also between them and the nuclei), i.e. $\epsilon'_{\text{int}} = \epsilon'_{\text{rot}} + \epsilon'_{\text{vib}} + \epsilon'_{\text{el}}$.

The above paragraphs assumed that the depicted particle has multiple nuclei and electrons in their internal structure. Some particles can't express some of the stated energy modes. The number of nuclei and electrons in their internal structure will dictate this expression. Molecular particles are constituted by multiple nuclei, and therefore, they may rotate and vibrate. Atomic particles are constituted by a single nucleus, and no rotation and vibration can be associated to them. If electrons aren't present in the internal structure of the molecular or atomic particle, then, obviously there's no electronic contribution to its energy. Free electrons, on the other hand, can translate and spin, being the latter motion associated their only form of internal energy ($\epsilon'_{\text{e,int}} = \epsilon'_{\text{sp}}$). Mathematically, the energy of a molecular particle, atomic particle and free electron is given by

$$\epsilon'_{\text{m}} = \epsilon'_{\text{tr}} + \epsilon'_{\text{rot}} + \epsilon'_{\text{vib}} + \epsilon'_{\text{el}} \ , \quad (2.1) \qquad \epsilon'_{\text{a}} = \epsilon'_{\text{tr}} + \epsilon'_{\text{el}} \ , \quad (2.2) \qquad \epsilon'_{\text{e}} = \epsilon'_{\text{tr}} + \epsilon'_{\text{sp}} \ , \quad (2.3)$$

respectively. The translational, rotational, and vibrational energy modes of a diatomic molecular particle, and the electronic energy mode of an atomic particle are depicted by Figures 2.1, 2.2, 2.3 and 2.4.

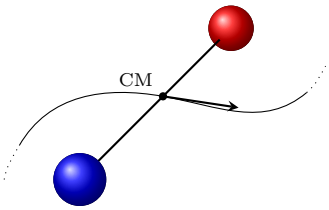

Figure 2.1: Representation of the translational energy mode of a diatomic molecular particle.

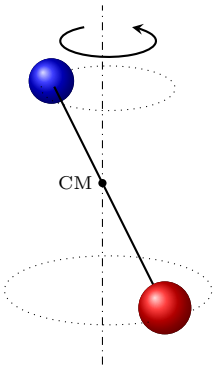

Figure 2.2: Representation of the rotational energy mode of a diatomic molecular particle.

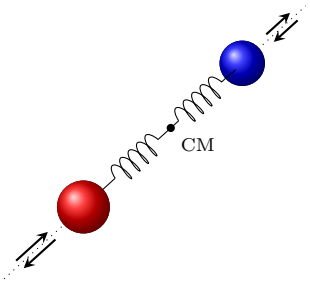

Figure 2.3: Representation of the vibrational energy mode of a diatomic molecular particle.

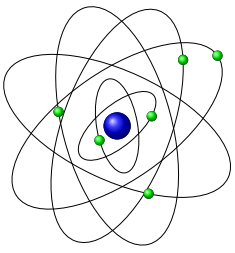

Figure 2.4: Representation of the electronic energy mode of an atomic particle.

It's well known that particles follow the laws of *Quantum Mechanics* (although in some cases, the laws of *Classical Mechanics* may depict considerably well the related physical phenomena). According to the theory of Quantum Mechanics, the movement of the particles and their internal structure agree with restrictedly defined directions and intensities. The restriction is in respect of the distribution of the admissible values: they are discrete, or in other words, *quantised*. These admissible values of directions and intensities, combined, are called *energy states*, or simply *states* of the particle [3]. Due to the fact that movement has an energy associated to it, the quantisation of the former leads to the quantisation of the latter, and therefore, the admissible energy values of a particle are also discrete. These are called *energy levels*. There's the possibility of various different movements associated to some energy mode, having the same energy value. Thus, an energy level may admit different energy states - in this case, the energy level is said to be *degenerate*, being the number of the different admissible states the *degree of degeneracy* of the level, g. In addition to the fact of particle movements and energies values being discrete, it's also known that the energies of each energy mode are lower bounded, i.e. for each energy mode there's an energy level whose value is the lowest of them all. Such energy level is termed *ground energy level*. Let $\epsilon'_{i,j}$ correspond to the energy associated to the j-th level of the i-th mode, and $\epsilon_{i,0}$ the energy of the ground level of that mode. A convenient physical quantity, by the name of *sensible energy* associated to the j-th level of the i-th mode, may be defined as the energy above the ground level energy of that mode [1], that is

$$\epsilon_{i,j} = \epsilon'_{i,j} - \epsilon_{i,0} \ . \tag{2.4}$$

To better differentiate the nomenclature in respect of the energy ϵ' and the sensible energy ϵ of a particle, the former will be for now on termed *absolute energy*.

Since the energies of all modes are quantised, the sum of them is also quantised, which gives the opportunity of defining a *total energy level*. Therefore, the sensible energy of the j-th total energy level of a molecular particle corresponds to the sum of the sensible energies of the respective k-th translational level, l-th rotational level, m-th vibrational level and n-th electronic level, i.e.

$$\epsilon_{\mathrm{m},j} = \epsilon_{\mathrm{m},k,l,m,n} = \epsilon_{\mathrm{tr},k} + \epsilon_{\mathrm{rot},l} + \epsilon_{\mathrm{vib},m} + \epsilon_{\mathrm{el},n} \ . \tag{2.5}$$

And the respective degree of degeneracy is given by the multiplication between the degrees of degeneracy of the respective modes levels, i.e.

$$g_{\mathrm{m},j} = g_{\mathrm{m},k,l,m,n} = g_{\mathrm{tr},k} \cdot g_{\mathrm{rot},l} \cdot g_{\mathrm{vib},m} \cdot g_{\mathrm{el},n} \ . \tag{2.6}$$

Analogous expressions hold for the energy of the j-th total energy level of an atomic particle - $\epsilon_{\mathrm{a},j} = \epsilon_{\mathrm{a},k,n} = \epsilon_{\mathrm{tr},k} + \epsilon_{\mathrm{el},n}$ - and its degree of degeneracy - $g_{\mathrm{a},j} = g_{\mathrm{a},k,n} = g_{\mathrm{tr},k} \cdot g_{\mathrm{el},n}$ - as well as for the j-th total energy level of a free electron - $\epsilon_{\mathrm{e},j} = \epsilon_{\mathrm{e},k,p} = \epsilon_{\mathrm{tr},k} + \epsilon_{\mathrm{sp},p}$ - and the respective degree of degeneracy - $g_{\mathrm{e},j} = g_{\mathrm{e},k,p} = g_{\mathrm{tr},k} \cdot g_{\mathrm{sp},p}$.

Although decoupling of the energy modes was assumed (leading to relations (2.1), (2.2) and (2.3)) it's possible to account, in an approximated way, the coupling of the modes by applying corrections on the

constants that describe each motion [44], has it is usually done in *Spectroscopy* (the scientific area that studies the interaction between matter and electromagnetic radiation). As result, a set of vibrational levels is defined for each electronic level, and a set of rotational levels is defined for each vibrational level (see appendix B to know more about this). In order to express these dependencies, the vibrational sensible energy and its degree of degeneracy should now take into account the label for the respective electronic level, and the rotational sensible energy and its degree of degeneracy should take into account the labels for the respective vibrational and electronic levels. Relations (2.5) and (2.6) are then transformed into

$$\epsilon_{\mathrm{m},j} = \epsilon_{\mathrm{tr},k} + \epsilon_{\mathrm{rot},n,m,l} + \epsilon_{\mathrm{vib},n,m} + \epsilon_{\mathrm{el},n} \ , \qquad (2.7) \qquad\qquad g_{\mathrm{m},j} = g_{\mathrm{tr},k} \cdot g_{\mathrm{rot},n,m,l} \cdot g_{\mathrm{vib},n,m} \cdot g_{\mathrm{el},n} \ . \qquad (2.8)$$

2.2 The Boltzmann distribution

2.2.1 The case of the single-temperature model

Let's consider a system constituted by several different chemical species. There's a set of admissible total energy levels for each species. If the system has reached thermal equilibrium, it's possible to show that the number of particles of the s-th species which is in the j-th total energy level is given by the so-called Boltzmann distribution [3]

$$N_{s,j} = N_s \frac{g_{s,j}\, e^{-\frac{\epsilon_{s,j}}{k_B T}}}{Q_s} \ , \qquad (2.9)$$

in which N_s is the number of particles of the s-th species in the system, $\epsilon_{s,j}$ and $g_{s,j}$ are the sensible energy and the degree of degeneracy of the j-th total energy level of the s-th species, respectively, k_B is the *Boltzmann constant*, T is the temperature of the system, and Q_s is the so-called *partition function* of the s-th species. This last quantity is given by

$$Q_s = \sum_j g_{s,j}\, e^{-\frac{\epsilon_{s,j}}{k_B T}} \ , \qquad (2.10)$$

in which the sum is in respect of all total energy levels of the s-th species.

Let's consider that the particles of the s-th species are molecular. By inserting the identities (2.7) and (2.8) in (2.10), it's possible to obtain [2]

$$Q_s = \sum_k \sum_n \sum_m \sum_l g_{s,\mathrm{tr},k} \cdot g_{s,\mathrm{rot},n,m,l} \cdot g_{s,\mathrm{vib},n,m} \cdot g_{s,\mathrm{el},n}\, e^{-\frac{\epsilon_{s,\mathrm{tr},k} + \epsilon_{s,\mathrm{rot},n,m,l} + \epsilon_{s,\mathrm{vib},n,m} + \epsilon_{s,\mathrm{el},n}}{k_B T}} =$$

$$= \underbrace{\left(\sum_k g_{s,\mathrm{tr},k}\, e^{-\frac{\epsilon_{s,\mathrm{tr},k}}{k_B T}} \right)}_{:= Q_{\mathrm{s,tr}}} \cdot \underbrace{\left\{ \sum_n g_{s,\mathrm{el},n}\, e^{-\frac{\epsilon_{s,\mathrm{el},n}}{k_B T}} \left[\sum_m g_{s,\mathrm{vib},n,m}\, e^{-\frac{\epsilon_{s,\mathrm{vib},n,m}}{k_B T}} \left(\sum_l g_{s,\mathrm{rot},n,m,l}\, e^{-\frac{\epsilon_{s,\mathrm{rot},n,m,l}}{k_B T}} \right) \right] \right\}}_{:= Q_{\mathrm{s,int}}} \ . \qquad (2.11)$$

The partition function of the s-th species is therefore a multiplication between its *translational partition*

function $Q_{s,\mathrm{tr}}$ and its *internal partition function* $Q_{s,\mathrm{int}}$. And this latter quantity can be expressed through

$$Q_{s,\mathrm{int}} = \sum_n g_{s,\mathrm{el},n}\, e^{-\frac{\epsilon_{s,\mathrm{el},n}}{k_B T}} Q_{s,\text{vib-rot},n} = \sum_n g_{s,\mathrm{el},n}\, e^{-\frac{\epsilon_{s,\mathrm{el},n}}{k_B T}} \underbrace{\left(\sum_m g_{s,\mathrm{vib},n,m}\, e^{-\frac{\epsilon_{s,\mathrm{vib},n,m}}{k_B T}} Q_{s,\mathrm{rot},n,m} \right)}_{:=Q_{s,\text{vib-rot},n}} =$$

$$= \sum_n g_{s,\mathrm{el},n}\, e^{-\frac{\epsilon_{s,\mathrm{el},n}}{k_B T}} \left[\sum_m g_{s,\mathrm{vib},n,m}\, e^{-\frac{\epsilon_{s,\mathrm{vib},n,m}}{k_B T}} \underbrace{\left(\sum_l g_{s,\mathrm{rot},n,m,l}\, e^{-\frac{\epsilon_{s,\mathrm{rot},n,m,l}}{k_B T}} \right)}_{:=Q_{s,\mathrm{rot},n,m}} \right] , \tag{2.12}$$

being $Q_{s,\text{vib-rot},n}$ the *vibrational-rotational partition function* associated to the n-th electronic level and $Q_{s,\mathrm{rot},m,n}$ the *rotational partition function* associated to the n-th electronic level and m-th vibrational level of the s-th species. If the rotational, vibrational and electronic energy modes were completely decoupled from each other, the internal partition function would instead correspond to a multiplication between three partition functions, each one associated to a different internal energy mode, i.e. $Q_{s,\mathrm{int}} = Q_{s,\mathrm{el}} \cdot Q_{s,\mathrm{vib}} \cdot Q_{s,\mathrm{rot}}$.

By inserting the identities (2.7) and (2.8) in (2.9), one has

$$N_{s,k,l,m,n} = N_s \frac{g_{s,\mathrm{tr},k} \cdot g_{s,\mathrm{rot},n,m,l} \cdot g_{s,\mathrm{vib},n,m} \cdot g_{s,\mathrm{el},n}\, e^{-\frac{\epsilon_{s,\mathrm{tr},k} + \epsilon_{s,\mathrm{rot},n,m,l} + \epsilon_{s,\mathrm{vib},n,m} + \epsilon_{s,\mathrm{el},n}}{k_B T}}}{Q_s} . \tag{2.13}$$

The reader should be warned about the very particular nomenclature that is being employed in this section. The label j represents a total energy level, being subscripted on the respective symbol. The labels k, l, m and n represent energy levels of the translational, rotational, vibrational and electronic modes, respectively, being also subscripted on the respective symbol. For the case of the number of particles N, the subscripted labels for the energy levels define the specificity of the quantity with respect to the energy modes. For example, $N_{s,k,m,n}$ represents the number of particles of the s-th species that are in the k-th translational, m-th vibrational level and n-th electronic level, and $N_{s,k,m} = \sum_n N_{s,k,m,n}$ represents the number of particles of the s-th species that are in the k-th translational and m-th vibrational level.

2.2.2 The case of the multi-temperature model

Let's assume here the hypothesis of same temperatures for same energy modes of the different heavy species particles, and consider that the s-th species is molecular (since it allows a more general analysis than the atomic and free electron species, although one important comment about free electrons is saved for last). With a particular temperature for each energy mode - $T_{\mathrm{tr_h}}$ for translation, T_{rot} for rotation, T_{vib} for vibration and T_{el} for electronic contribution - the number of particles of the s-th species that is in the k-th translational level, l-th rotational level, m-th vibrational level and n-th electronic levels can be expressed by

$$N_{s,k,l,m,n} = N_s \frac{g_{s,\mathrm{tr},k} \cdot g_{s,\mathrm{rot},n,m,l} \cdot g_{s,\mathrm{vib},n,m} \cdot g_{s,\mathrm{el},n}\, e^{-\frac{\epsilon_{s,\mathrm{tr},k}}{k_B T_{\mathrm{tr_h}}} - \frac{\epsilon_{s,\mathrm{rot},n,m,l}}{k_B T_{\mathrm{rot}}} - \frac{\epsilon_{s,\mathrm{vib},n,m}}{k_B T_{\mathrm{vib}}} - \frac{\epsilon_{s,\mathrm{el},n}}{k_B T_{\mathrm{el}}}}}{Q_s} . \tag{2.14}$$

The expression has then the same structure as the one for the case of thermal equilibrium (2.13). However, it considers a particular temperature for each particular energy mode, instead of a general temperature T. This property extends itself to the total partition function Q_s, and therefore also to the translational partition function $Q_{s,\mathrm{tr}}$, internal partition function $Q_{s,\mathrm{int}}$, vibrational-rotational partition function $Q_{s,\text{vib-rot},n}$ and rotational partition function $Q_{s,\mathrm{rot},n,m}$. These last four quantities are given by

$$Q_{s,\mathrm{tr}} = \sum_n g_{s,\mathrm{tr},k}\, e^{-\frac{\epsilon_{s,\mathrm{tr},k}}{k_B T_{\mathrm{tr_h}}}} \ , \qquad (2.15) \qquad Q_{s,\mathrm{int}} = \sum_n g_{s,\mathrm{el},n}\, e^{-\frac{\epsilon_{s,\mathrm{el},n}}{k_B T_{\mathrm{el}}}} Q_{s,\text{vib-rot},n} \ , \qquad (2.16)$$

$$Q_{s,\text{vib-rot},n} = \sum_m g_{s,\mathrm{vib},n,m}\, e^{-\frac{\epsilon_{s,\mathrm{vib},n,m}}{k_B T_{\mathrm{vib}}}} Q_{s,\mathrm{rot},n,m} \ , \qquad Q_{s,\mathrm{rot},n,m} = \sum_l g_{s,\mathrm{rot},n,m,l}\, e^{-\frac{\epsilon_{s,\mathrm{rot},n,m,l}}{k_B T_{\mathrm{rot}}}} \ , \qquad (2.18)$$

$$(2.17)$$

respectively. Such partition functions can be computed if the sensible energies of the modes levels are known. The absolute energies of the translational levels associated to the s-th species may be obtained by solving the *Schrödinger equation*[1] for a free particle[2] of the s-th species with a mass m_s, inside a rectangular box of dimensions $a_1 \times a_2 \times a_3$ with impenetrable walls [3] (such box may be interpreted as an hypothetical element of fluid). These absolute energies and the respective degrees of degeneracy are given by

$$\begin{cases} \epsilon'_{s,\mathrm{tr},k_1,k_2,k_3} = \dfrac{h^2}{8m_s}\left(\dfrac{k_1^2}{a_1^2} + \dfrac{k_2^2}{a_2^2} + \dfrac{k_3^2}{a_3^2}\right) \ , & (2.19a) \\ g_{s,\mathrm{tr},k_1,k_2,k_3} = 1 \ , & (2.19b) \end{cases}$$

in which k_1, k_2 and $k_3 = 1, 2, 3, ...$ correspond to the *translational quantum numbers* (responsible for the quantisation of the translational energy, since they are natural numbers). There's one quantum number for each dimension of the box. The absolute energy of the ground translational level $\epsilon_{s,\mathrm{tr},0}$ is found to be small enough to be neglected [1], and therefore, the sensible energy of a translational level may be approximated by the respective absolute energy, i.e. $\epsilon_{s,\mathrm{tr},k_1,k_2,k_3} = \epsilon'_{s,\mathrm{tr},k_1,k_2,k_3} - \epsilon_{s,\mathrm{tr},0} \approx \epsilon'_{s,\mathrm{tr},k_1,k_2,k_3}$. From the definition of the translational partition function (2.15), and by adding the fact that one has typically $\frac{h^2}{8m_s k_B T_{\mathrm{tr_h}}} \ll 1$ [3], the involved series may be approximated by an integral (since each term has a very small contribution to the sum), giving

$$Q_{s,\mathrm{tr}} = \sum_{k_1=1}^{\infty}\sum_{k_1=2}^{\infty}\sum_{k_3=1}^{\infty} g_{s,\mathrm{tr},k_1,k_2,k_3}\, e^{-\frac{\epsilon_{s,\mathrm{tr_h},k_1,k_2,k_3}}{k_B T_{\mathrm{tr_h}}}} \approx \int_0^{\infty}\int_0^{\infty}\int_0^{\infty} e^{-\frac{h^2}{8m_s k_B T_{\mathrm{tr_h}}}\left(\frac{k_1^2}{a_1^2}+\frac{k_2^2}{a_2^2}+\frac{k_3^2}{a_3^2}\right)} dk_1\, dk_2\, dk_3 \Leftrightarrow$$

$$\Leftrightarrow Q_{s,\mathrm{tr}}(T_{\mathrm{tr_h}}, V) = V\left(\frac{2\pi m_s k_B T_{\mathrm{tr_h}}}{h^2}\right)^{\frac{3}{2}} \ , \qquad (2.20)$$

in which $V = a_1 \cdot a_2 \cdot a_3$ corresponds to the volume of the box.

[1] The Schrödinger equation is one of the fundamental equations of Quantum Mechanics. From a conceptual perspective of view, one may state that the Schrödinger equation is for Quantum Mechanics what the Newtown's equations are for Classical Mechanics.

[2] A particle is considered to be free if it isn't being subjected to any potential.

For the case of the rotational energy mode, the respective partition function associated to the e-th electronic level and v-th vibrational level may be easily computed if the particle is *diatomic* (with two nuclei) and *heteronuclear* (in which the nuclei are dissimilar). By solving the Schrödinger equation for a *rigid rotor* (or *dumb-bell*) with a constant moment of inertia $I_{s,e,v}$, the absolute energies and respective degrees of degeneracy of the rotational levels associated to the v-th vibrational level and e-th electronic level of the s-th species, assuming that it is diatomic and heteronuclear, may be shown to be [3]

$$\begin{cases} \epsilon'_{s,\mathrm{rot},e,v,J} = \dfrac{h^2}{8\pi^2 I_{s,e,v}} J\,(J+1) \ , & \text{(2.21a)} \\ g_{s,\mathrm{rot},e,v,J} = 2J+1 \ , & \text{(2.21b)} \end{cases}$$

being $J = 0,\ 1,\ 2,\ ...$ the *rotational quantum number*. Note that from (2.21a) one has $\epsilon_{s,\mathrm{rot},0} = 0$, meaning that $\epsilon_{s,\mathrm{rot},e,v,J} = \epsilon'_{s,\mathrm{rot},e,v,J}$. By recalling the expression for the rotational partition function (2.18), and by enunciating that one has usually $\frac{h^2}{8\pi^2 I_{s,e,v} k_B T_{\mathrm{rot}}} \ll 1$ [3], the involved series can be approximated by an integral, giving

$$Q_{s,\mathrm{rot},e,v} = \sum_{J=0}^{\infty} g_{s,\mathrm{rot},e,v,J}\, e^{-\frac{\epsilon_{s,\mathrm{rot},e,v,J}}{k_B T_{\mathrm{rot}}}} \approx \int_0^{\infty} (2J+1)\, e^{-\frac{h^2}{8\pi^2 I_{s,e,v} k_B T_{\mathrm{rot}}} J(J+1)}\, dJ = \frac{8\pi^2 I_{s,e,v} k_B T_{\mathrm{rot}}}{h^2} := \frac{k_B T_{\mathrm{rot}}}{B_{s,e,v}} \ , \tag{2.22}$$

in which $B_{s,e,v} = h^2/8\pi^2 I_{s,e,v}$ corresponds to the rotational energy function B_v associated to the e-th electronic level and v-th vibrational level of the s-th species. This function is introduced in appendix B, being given by (B.8). For the case of a diatomic homonuclear particle, the expression for the degree of degeneracy of a rotational level (2.21b) doesn't hold. The actual one changes in an alternate way with the rotational level [2]. It's possible to show that the expression for the rotational partition function of a diatomic homonuclear particle is one half of the one for the heteronuclear particle (2.23). Therefore, one can define a general expression for the partition function of a diatomic particle, by writing

$$Q_{s,\mathrm{rot},e,v}(T_{\mathrm{rot}}) = \frac{k_B T_{\mathrm{rot}}}{\sigma B_{s,e,v}} \ , \tag{2.23}$$

in which σ corresponds to a *symmetry factor*, giving 1 if the particle is heteronuclear or 2 if the particle is homonuclear.

Let's assume, for instance, that the dependence of the function $B_{s,e,v}$ on the vibrational quantum number v can be neglected, so that $B_{s,e,v} \approx B_{s,e}$. In that case, the vibrational-rotational partition function associated to the e-th electronic level corresponds to a multiplication between a vibrational partition function and the rotational partition function, i.e. $Q_{s,\text{vib-rot},e} = Q_{s,\mathrm{vib},e} \cdot Q_{s,\mathrm{rot},e}$. The vibrational partition function can be easily computed if the particle is diatomic. The absolute energies and the respective degrees of degeneracy of the vibrational levels of the s-th species, assuming that it is diatomic, can be obtained by solving the Schrödinger equation for a *harmonic oscillator*[3] of constant natural

[3] See appendix A for more details about the quantum harmonic oscillator.

angular frequency $\omega_{s,e}$, giving [3]

$$\begin{cases} \epsilon'_{s,\text{vib},e,v} = \hbar\omega_{s,e}\left(v+\dfrac{1}{2}\right) \ , & \text{(2.24a)} \\ g_{s,\text{vib},e,v} = 1 \ , & \text{(2.24b)} \end{cases}$$

in which $v = 0$, 1, 2, ... corresponds to the *vibrational quantum number*. From (2.24a), one has $\epsilon'_{s,\text{vib},0} = \frac{1}{2}\hbar\omega_{s,e}$, and therefore, $\epsilon_{s,\text{vib},e,v} = v\hbar\omega_{s,e}$. The vibrational partition function can be shown to be a sum of a convergent geometric series, resulting in [3]

$$Q_{s,\text{vib},e} = \sum_{v=0}^{\infty} g_{s,\text{vib},e,v}\, e^{-\frac{\epsilon_{s,\text{vib},e,v}}{k_B T_\text{vib}}} = \sum_{v=0}^{\infty} e^{-\frac{v\hbar\omega_{s,e}}{k_B T_\text{vib}}} = \sum_{v=0}^{\infty}\left(e^{-\frac{\hbar\omega_{s,e}}{k_B T_\text{vib}}}\right)^v \Leftrightarrow$$

$$\Leftrightarrow Q_{s,\text{vib},e}(T_\text{vib}) = \frac{1}{1-e^{-\frac{\hbar\omega_{s,e}}{k_B T_\text{vib}}}} \ . \tag{2.25}$$

The natural angular frequency $\omega_{s,e}$ corresponds to the *spectroscopic vibrational constant* ω_e associated to e-th electronic level of the s-th species. This constant is introduced in appendix B, being one of several that describe the vibrational energy function G_v. Such function is given by (B.6).

There's no simple model for an electronic partition function, and therefore, the internal partition function needs to be computed through the expression that exactly defines it (2.16), in which the electronic sensible energy associated to the e-th electronic level $\epsilon_{s,\text{el},e}$ is the same as the spectroscopic constant $T_{s,e} := T_e$ introduced in appendix B

$$Q_{s,\text{int}}(T_\text{rot}, T_\text{vib}, T_\text{el}) = \sum_e g_{s,\text{el},e}\, e^{-\frac{T_{s,e}}{k_B T_\text{el}}} Q_{s,\text{vib-rot},e}(T_\text{rot}, T_\text{vib}) \ . \tag{2.26}$$

One should present here an expression for the partition function of the translational energy mode of free electrons as well as an expression for the partition function of its spin energy mode (*spin partition function*). The expression for the free electron translation partition function corresponds the one for the heavy particle translation partition function (2.20) with T_{tr_h} substituted by T_{tr_e} and m_s by m_e

$$Q_{\text{e,tr}}(T_\text{e}, V) = V\left(\frac{2\pi m_\text{e} k_B T_{\text{tr}_\text{e}}}{h^2}\right)^{\frac{3}{2}} \ . \tag{2.27}$$

The spin energy mode of a free electron has only one energy level, and two possible energy states. Therefore, the sensible energy of the spin level is null, i.e. $\epsilon_{\text{e,sp}} = 0$, and its degree of degeneracy corresponds to $g_{\text{e,sp}} = 2$. The spin partition function of the free electron is then given by

$$Q_{\text{e,sp}} = 2 \ . \tag{2.28}$$

It's worthy to mention that in the case of thermal equilibrium, one has $T := T_{\text{tr}_\text{h}} = T_{\text{tr}_\text{e}} = T_\text{rot} = T_\text{vib} = T_\text{el}$, and it can be easily shown that the expressions for the particles population distribution on their energy levels (2.14) and (2.13) do match with each other.

2.2.3 The case of the vibronic-specific state-to-state model

Let's consider here a three-temperature vibronic-specific state-to-state model: temperatures $T_{\mathrm{tr_h}}$ and T_{rot} are assigned to the translational and rotational energy modes of the heavy particles, respectively, and $T_{\mathrm{tr_e}}$ is assigned to the free electron translational energy mode. Also, let's assume here in similar way to the previous section that the particles of s-th species are molecular. Although such particles may not follow a Boltzmann distribution in the electronic and vibrational levels, they will follow a Boltzmann distribution in the translational and rotational levels. Therefore, the number of particles of the s-th species in the k-th translational level, l-th rotational level, m-th vibrational level and n-th electronic level corresponds to[4]

$$N_{s,k,l,m,n} = N_{s,m,n} \frac{g_{s,\mathrm{tr},k} \cdot g_{s,\mathrm{rot},n,m,l}\, e^{-\frac{\epsilon_{s,\mathrm{tr},k}}{k_B T_{\mathrm{tr_h}}} - \frac{\epsilon_{s,\mathrm{rot},n,m,l}}{k_B T_{\mathrm{rot}}}}}{Q_{s,\mathrm{tr}} \cdot Q_{s,\mathrm{rot},n,m}} , \tag{2.29}$$

in which $N_{s,m,n}$ is the number of particles of the s-th species in the m-th vibrational level and n-th electronic level, $Q_{s,\mathrm{tr}}$ is the translational partition function given by (2.15), and $Q_{s,\mathrm{rot},n,m}$ is the rotational partition function given by (2.23) (if a rigid rotor model is assumed).

2.3 Thermodynamic variables

The thermodynamic variables associated to some system depend on the distribution of the particles on their energy levels. Let this system correspond to an hypothetical element of fluid. The computation of these thermodynamic variables for the cases of the single-temperature, multi-temperature and vibronic-specific state-to-state models will be analysed here.

2.3.1 The case of the single-temperature model

For the case of the single-temperature model, the thermodynamic variables of interest are the mass-specific *internal energy* e_s, *enthalpy* h_s, *entropy* s_s, *Helmholtz free energy* f_s, *Gibbs free energy partial* g_s, as well as the *partial pressure* p_s for some s-th species. It will be assumed that the particles of the s-th species correspond to molecular particles so that the most general case may be analysed. The respective properties for the combination of all species (the mixture) in the element of fluid are also important to be known.

The term "internal" in "internal energy" is with respect to the element of fluid and not to the particles that constitute it, and therefore, this internal energy should not be mistaken for the internal energy of the particles. A less ambiguous designation for this physical quantity would be "internal energy of the flow". When a element of fluid moves, therefore producing a flow, a translational kinetic energy may be attributed to it. Simultaneously, the particles inside the element fluid move relatively to the element of fluid, being the energy associated to that motion the contribution of all particles energy modes which were reported in §2.1. Thus, the internal energy of the flow associated to the s-th species, E_s, is defined

[4] For the case of the multi-temperature model, a relation with the same form as (2.29) may be simply obtained by noticing that $N_{s,m,n}$ corresponds to a sum on k and l of (2.14). However, for the case of the vibronic-specific state-to-state model, relation (2.29) holds but not (2.14).

by the sum of total absolute energy of the particles of s-th species in the element of fluid

$$E_s = \sum_j \epsilon'_{s,j} N_{s,j} \ . \tag{2.30}$$

The specific (in a mass basis) internal energy of the flow associated to the s-th species corresponds to $e_s = E_s/M_s$ where $M_s = N_s m_s$ is the mass of s-th species particles in the element of fluid, and m_s is the mass of a single s-th species particle. In thermal equilibrium, $N_{s,j}$ is given by (2.9), and by invoking the relation (2.10) for the partition function Q_s, and mathematically manipulating expression (2.30), one can obtain

$$e_s = R_s T^2 \left[\frac{\partial \left(\ln Q_s\right)}{\partial T}\right]_V + \frac{\epsilon_{s,0}}{m_s} \ , \tag{2.31}$$

where $R_s = k_B/m_s$ is the *specific (in a mass basis) gas constant* of the s-th species. Note that the subscripted symbol V in (2.31) means that the derivative is taken at constant volume V.

The specific entropy of the element of fluid associated to the s-th species, $s_s = S_s/M_s$, at thermal equilibrium, is given according to *Statistical Mechanics* [3] by

$$s_s = R_s \left[\ln\left(\frac{Q_s}{N_s}\right) + 1\right] + R_s T \left[\frac{\partial \left(\ln Q_s\right)}{\partial T}\right]_V \ . \tag{2.32}$$

The specific Helmholtz free energy associated to the s-th species, at thermal equilibrium, is defined by $f_s = F_s/M_s = e_s - T s_s$, and therefore, from (2.31) and (2.32), one has

$$f_s = \frac{\epsilon_{s,0}}{m_s} - R_s T \left[\ln\left(\frac{Q_s}{N_s}\right) + 1\right] \ . \tag{2.33}$$

Before introducing the definition of partial pressure, it's important to formerly enunciate the *first law of Thermodynamics* for a chemically reactive open system in thermal equilibrium [3]

$$dE_s = T dS_s - p_s dV + \mu_s dN_s \ , \tag{2.34}$$

being μ_s the *chemical potential* associated to the s-th species. According to (2.34) and the definition of the Helmholtz free energy, the differential of this quantity may then be then expressed through

$$dF_s = dE_s - S_s dT - T dS_s = \mu_s dN_s - S_s dT - p_s dV \ . \tag{2.35}$$

From (2.35) one can immediately find, with the help of relation (2.33), that the partial pressure associated to the s-th species, p_s, is given by

$$p_s = -\left(\frac{\partial F_s}{\partial V}\right)_{T,N_s} = N_s k_b T \left[\frac{\partial \left(\ln Q_s\right)}{\partial V}\right]_{T,N_s} \ . \tag{2.36}$$

From (2.11) one has $Q_s(T,V) = Q_{s,\mathrm{tr}}(T,V) \cdot Q_{s,\mathrm{int}}(T)$. Solely the translational partition function $Q_{s,\mathrm{tr}}(T,V)$ depends on the volume V, and therefore, only the translation energy mode of the particles

contributes to the partial pressure p_s, as can be shown through the reasoning:

$$p_s = N_s k_b T \left[\frac{\partial\left(\ln Q_s\right)}{\partial V}\right]_{T,N_s} = N_s k_b T \left(\frac{\partial\left\{\ln\left[Q_{s,\mathrm{tr}}(T,V)\cdot Q_{s,\mathrm{int}}(T)\right]\right\}}{\partial V}\right)_{T,N_s} =$$

$$= N_s k_b T \left[\underbrace{\left(\frac{\partial\left\{\ln\left[Q_{s,\mathrm{tr}}(T,V)\right]\right\}}{\partial V}\right)_{T,N_s}}_{=\frac{1}{V},\text{ from (2.20)}} + \underbrace{\left(\frac{\partial\left\{\ln\left[Q_{s,\mathrm{int}}(T)\right]\right\}}{\partial V}\right)_{T,N_s}}_{=0}\right] = \frac{N_s k_b T}{V} \Leftrightarrow$$

$$\Leftrightarrow p_s = \rho_s R_s T \ , \tag{2.37}$$

being $\rho_s = M_s/V$ the mass density of s-th species particles in the element of fluid. Result (2.37) can be identified as the well-known *ideal gas law*.

The specific enthalpy associated to the s-th species, at thermal equilibrium, is defined by $h_s = e_s + p_s/\rho_s$, and therefore, by invoking (2.31) and (2.37), it's possible to show that

$$h_s = R_s T + R_s T^2 \left[\frac{\partial\left(\ln Q_s\right)}{\partial T}\right]_V + \frac{\epsilon_{s,0}}{m_s} \ . \tag{2.38}$$

The specific Gibbs free energy associated to the s-th species, at thermal equilibrium, is defined by $g_s = e_s + p_s/\rho_s - T s_s$. From (2.31), (2.32) and (2.37) one may then get

$$g_s = \frac{\epsilon_{s,0}}{m_s} - R_s T \ln\left(\frac{Q_s}{N_s}\right) \ . \tag{2.39}$$

For compactness reasons the operations applied on the partition function Q_s shown in the above expressions for the specific thermodynamic variables will not be evaluated in this section.

Now that a way to compute the important specific thermodynamic variables for some s-th species was presented, one may advance to the computation of the specific thermodynamic variables associated the combination of all these species (the mixture) of the element of fluid. Let $\mathcal{Q}_s \in \{E_s, S_s, F_s, H_s, G_s\}$ correspond to a thermodynamic variable associated to the s-th species, and $\mathcal{Q} = \sum_s \mathcal{Q}_s \in \{E, S, F, H, G\}$ the respective thermodynamic variable associated to the mixture. Also, let $q_s = \mathcal{Q}_s/M_s \in \{e_s, s_s, f_s, h_s, g_s\}$ and $q = \mathcal{Q}/M \in \{e, s, f, h, g\}$ be the respective specific quantities, where M corresponds to the mass of the mixture, i.e. $M = \sum_s M_s$. A relation between the mixture variable q and the species variables q_s can be easily found:

$$q = \frac{\mathcal{Q}}{M} = \frac{\sum_s \mathcal{Q}_s}{M} = \sum_s \underbrace{\left(\frac{M_s}{M}\right)}_{:=c_s} \underbrace{\left(\frac{\mathcal{Q}_s}{M_s}\right)}_{=q_s} \Leftrightarrow$$

$$\Leftrightarrow \ q = \sum_s c_s q_s \ , \tag{2.40}$$

being $c_s = M_s/M$ the so-called *mass fraction* of the s-th species. Note that the partial pressure p_s doesn't satisfy (2.128) since it is not a specific thermodynamic variable. Anyway, a pressure associated

to the mixture can be defined:

$$p := \sum_s p_s = \sum_s \rho_s R_s T = \sum_s \frac{M_s}{V} T = \sum_s \underbrace{\left(\frac{M}{V}\right)}_{:=\rho} \underbrace{\left(\frac{M_s}{M}\right)}_{=c_s} R_s T = \underbrace{\rho \left(\sum_s c_s R_s\right)}_{:=R} T \Leftrightarrow$$

$$\Leftrightarrow p = \rho R T \ , \tag{2.41}$$

where $\rho = M/V$ and $R = \sum_s c_s R_s$ are the mass density and the specific (in a mass basis) gas constant of the mixture, respectively. Result (2.41) can be identified as the *Dalton's law of partial pressures.*

2.3.2 The case of the multi-temperature model

For the case of the case of the multi-temperature model, the thermodynamic variables that do matter are the specific internal energy e_s, enthalpy h_s, the partial pressure p_s as well as the respective quantities for the mixture. It will be assumed here that the particles of s-th species are diatomic.

From the definition of the internal energy of the flow associated with the s-th species (2.30), the relation between the total sensible energy of a particle and the contributions of its energy modes (2.7), the definition of partition functions with respect to these energy modes (2.15), (2.16), (2.17) and (2.18), as well as the distribution of particles in their energy levels according to the multi-temperature model (2.14), it's possible to show that

$$E_s = \sum_j \epsilon'_{s,j} N_{s,j} = \left(\sum_j \epsilon_{s,j} N_{s,j}\right) + \epsilon_{s,0} N_s = \left[\sum_{k,l,m,n} \epsilon_{s,k,l,m,n}\, N_{s,k,l,m,n}\right] + \epsilon_{s,0} N_s =$$

$$= \left[\sum_{k,l,m,n} \left(\epsilon_{s,\mathrm{tr},k} + \epsilon_{s,\mathrm{rot},n,m,l} + \epsilon_{s,\mathrm{vib},n,m} + \epsilon_{s,\mathrm{el},n}\right) N_{s,k,l,m,n}\right] + \epsilon_{s,0} N_s \Leftrightarrow$$

$$\Leftrightarrow e_s = \underbrace{R_s T_{\mathrm{tr_h}}^2 \left[\frac{\partial \left(\ln Q_{s,\mathrm{tr}}\right)}{\partial T_{\mathrm{tr_h}}}\right]_V}_{:=e_{s,\mathrm{tr}}} + \underbrace{R_s T_{\mathrm{rot}}^2 \left[\frac{\partial \left(\ln Q_{s,\mathrm{int}}\right)}{\partial T_{\mathrm{rot}}}\right]_V}_{:=e_{s,\mathrm{rot}}} + \underbrace{R_s T_{\mathrm{vib}}^2 \left[\frac{\partial \left(\ln Q_{s,\mathrm{int}}\right)}{\partial T_{\mathrm{vib}}}\right]_V}_{:=e_{s,\mathrm{vib}}} + \underbrace{R_s T_{\mathrm{el}}^2 \left[\frac{\partial \left(\ln Q_{s,\mathrm{int}}\right)}{\partial T_{\mathrm{el}}}\right]_V}_{:=e_{s,\mathrm{el}}} + \underbrace{\frac{\epsilon_{s,0}}{m_s}}_{:=e_{s,0}} \ . \tag{2.42}$$

The internal energy of the flow associated to the s-th species is therefore a sum of five contributions, four associated to each energy mode of the particles regarding solely their sensible energy, and one associated to the ground level energy of the particles, i.e.

$$e_s = e_{s,\mathrm{tr}} + e_{s,\mathrm{rot}} + e_{s,\mathrm{vib}} + e_{s,\mathrm{el}} + e_{s,0} \ . \tag{2.43}$$

The evaluation of the mathematical operations on $Q_{s,\mathrm{int}}$ that occur in (2.42) can be rather cumbersome if the dependence of the internal energy modes on each other is regarded. However, if such dependence is disregarded, and simple models are chosen for each internal energy modes, then e_s can be easily expressed. For instance, if one considers the harmonic oscillator model with an effective natural angular angular frequency $\omega_{s,e} = \omega_s$ that doesn't depend on the electronic level e, and a rigid rotor model with a effective rotational constant $B_{s,e,v} = B_s$ that doesn't depend on the electronic level e neither on the vibrational

level v, the internal partition function will then correspond to the product of three partition functions, each one associated to an internal energy mode, i.e. $Q_{s,\text{int}}(T_\text{rot}, T_\text{vib}, T_\text{el}) = Q_{s,\text{rot}}(T_\text{rot})Q_{s,\text{vib}}(T_\text{vib})Q_{s,\text{el}}(T_\text{el})$, with $Q_{s,\text{rot}}(T_\text{rot})$ and $Q_{s,\text{vib}}(T_\text{vib})$ given by (2.23) and (2.25), respectively. In these conditions the specific internal energy of the flow associated to the s-th species e_s corresponds to

$$e_s = \underbrace{R_s T_{\text{tr}_\text{h}}^2 \left[\frac{\partial\left(\ln Q_{s,\text{tr}}\right)}{\partial T_{\text{tr}_\text{h}}}\right]_V}_{:=e_{s,\text{tr}}} + \underbrace{R_s T_\text{rot}^2 \left[\frac{\partial\left(\ln Q_{s,\text{rot}}\right)}{\partial T_\text{rot}}\right]_V}_{:=e_{s,\text{rot}}} + \underbrace{R_s T_\text{vib}^2 \left[\frac{\partial\left(\ln Q_{s,\text{vib}}\right)}{\partial T_\text{vib}}\right]_V}_{:=e_{s,\text{vib}}} + \underbrace{R_s T_\text{el}^2 \left[\frac{\partial\left(\ln Q_{s,\text{el}}\right)}{\partial T_\text{el}}\right]_V}_{:=e_{s,\text{el}}} + \underbrace{\frac{\epsilon_{s,0}}{m_s}}_{:=e_{s,0}} , \tag{2.44}$$

with $e_{s,\text{tr}}$, $e_{s,\text{rot}}$, $e_{s,\text{vib}}$, $e_{s,\text{el}}$ and $e_{s,0}$ given by

$$e_{s,\text{tr}}(T_{\text{tr}_\text{h}}) = \frac{3}{2} R_s T_{\text{tr}_\text{h}} , \tag{2.45}$$

$$e_{s,\text{rot}}(T_\text{rot}) = R_s T_\text{rot} , \tag{2.46}$$

$$e_{s,\text{vib}}(T_\text{vib}) = \frac{\frac{\hbar\omega_s}{k_B T_\text{vib}}}{e^{\frac{\hbar\omega_s}{k_B T_\text{vib}}} - 1} R_s T_\text{vib} , \tag{2.47}$$

$$e_{s,\text{el}}(T_\text{el}) = \frac{\sum_e g_{s,\text{el},e} \frac{T_{s,e}}{m_s} e^{-\frac{T_{s,e}}{k_B T_\text{el}}}}{\sum_e g_{s,\text{el},e}\, e^{-\frac{T_{s,e}}{k_B T_\text{el}}}} , \tag{2.48}$$

$$e_{s,0} = \frac{\epsilon_{s,0}}{m_s} . \tag{2.49}$$

Relations (2.20), (2.23) and (2.25) were used in order to obtain results (2.45), (2.46) and (2.48), respectively. Because there's no simple model for the electronic energy mode, equation (2.48) expresses the general definition of $e_{s,\text{el}}$.

In respect of the partial pressure of the s-th species, p_s, it was shown in section §2.3.1 that only the translational mode of the particles contributes to this thermodynamic variable. Therefore, p_s is given by (2.37) with T substituted by T_{tr_h}

$$p_s = \rho_s R_s T_{\text{tr}_\text{h}} . \tag{2.50}$$

One may then write $p_{s,\text{tr}} = p_s = \rho_s R_s T_{\text{tr}_\text{h}}$, and $p_{s,\text{rot}} = p_{s,\text{vib}} = p_{s,\text{el}} = p_{s,0} = 0$.

The specific enthalpy associated to the s-th species, h_s, is defined by $h_s = e_s + p_s/\rho_s$, which under the assumption of separability of the internal energy modes of the particles can be shown to have a form similar to (2.43):

$$h_s = h_{s,\text{tr}} + h_{s,\text{rot}} + h_{s,\text{vib}} + h_{s,\text{el}} + h_{s,0} , \tag{2.51}$$

where the contributions $h_{s,\text{tr}}$, $h_{s,\text{rot}}$, $h_{s,\text{vib}}$, $h_{s,\text{el}}$ and $h_{s,0}$ are given by

$$h_{s,\text{tr}}(T_{\text{tr}_\text{h}}) = \frac{5}{2} R_s T_{\text{tr}_\text{h}} , \tag{2.52}$$

$$h_{s,\text{rot}}(T_\text{rot}) = R_s T_\text{rot} , \tag{2.53}$$

$$h_{s,\text{vib}}(T_\text{vib}) = \frac{\frac{\hbar\omega_s}{k_B T_\text{vib}}}{e^{\frac{\hbar\omega_s}{k_B T_\text{vib}}} - 1} R_s T_\text{vib} , \tag{2.54}$$

$$h_{s,\text{el}}(T_\text{el}) = \frac{\sum_e g_{s,\text{el},e} \frac{T_{s,e}}{m_s} e^{-\frac{T_{s,e}}{k_B T_\text{el}}}}{\sum_e g_{s,\text{el},e}\, e^{-\frac{T_{s,e}}{k_B T_\text{el}}}} , \tag{2.55}$$

$$h_{s,0} = \frac{\epsilon_{s,0}}{m_s} . \tag{2.56}$$

The contribution $h_{s,\text{tr}} = e_{s,\text{tr}} + p_{s,\text{tr}}/\rho_s$ is the only one that differs from its specific internal energy counterpart, $e_{s,\text{tr}}$, since all contributions for the partial pressure with the exception of $p_{s,\text{tr}}$ are null.

It's worthy to also treat here the thermodynamic variables associated to free electrons. Free electrons express their energy through two energy modes: translation and spin. However there's only one energy level for spin - as explained in §2.2.2 - and therefore, spin only contributes to the ground state specific internal energy of the flow associated to free electrons $e_{\mathrm{e},0} = \epsilon_{\mathrm{e},0}/m_{\mathrm{e}}$. Thus, one may write $e_{\mathrm{e}} = e_{\mathrm{e,tr}} + e_{\mathrm{e},0}$ as well as $h_{\mathrm{e}} = h_{\mathrm{e,tr}} + h_{\mathrm{e},0}$. The contribution of the translational energy mode to the specific internal energy of the flow associated to free electrons is the same as the one associated to heavy particles (2.45) with $T_{\mathrm{tr_h}}$ substituted by $T_{\mathrm{tr_e}}$. Only translation contributes to the partial pressure and therefore, similarly to what happened with $e_{\mathrm{e,tr}}$, p_{e} is given by (2.50) with $T_{\mathrm{tr_h}}$ substituted by $T_{\mathrm{tr_e}}$. One has ultimately

$$e_{\mathrm{e}}(T_{\mathrm{tr_e}}) = \underbrace{\frac{3}{2}R_{\mathrm{e}}T_{\mathrm{tr_e}}}_{=e_{\mathrm{e,tr}}(T_{\mathrm{tr_e}})} + \underbrace{\frac{\epsilon_{\mathrm{e},0}}{m_{\mathrm{e}}}}_{=e_{\mathrm{e},0}} , \qquad (2.57)$$

$$p_{\mathrm{e}} = \rho_{\mathrm{e}} R_{\mathrm{e}} T_{\mathrm{tr_e}} , \qquad (2.58)$$

$$h_{\mathrm{e}}(T_{\mathrm{tr_e}}) = \underbrace{\frac{5}{2}R_{\mathrm{e}}T_{\mathrm{tr_e}}}_{=h_{\mathrm{e,tr}}(T_{\mathrm{tr_e}})} + \underbrace{\frac{\epsilon_{\mathrm{e},0}}{m_{\mathrm{e}}}}_{=h_{\mathrm{e},0}} . \qquad (2.59)$$

2.3.3 The case of the vibronic-specific state-to-state model

For the case of the vibronic-specific state-to-state model, temperatures for the translational and rotational energy modes can be defined, but not for the vibrational and electronic ones. Let's assume here that particles of the s-th species are diatomic. The distribution of the particles of s-th species in their energy levels follows the law (2.29). Taking this into account, the internal energy of the flow associated to the s-th species is then given by

$$e_s = \underbrace{R_s T_{\mathrm{tr_h}}^2 \left[\frac{\partial\left(\ln Q_{s,\mathrm{tr}}\right)}{\partial T_{\mathrm{tr_h}}}\right]_V}_{:=e_{s,\mathrm{tr}}} + \underbrace{\sum_{m,n} \frac{N_{s,m,n}}{N_s} R_s T_{\mathrm{rot}}^2 \left[\frac{\partial\left(\ln Q_{s,\mathrm{rot},n,m}\right)}{\partial T_{\mathrm{rot}}}\right]_V}_{:=e_{s,\mathrm{rot}}} + \underbrace{\sum_{m,n} \frac{N_{s,m,n}}{N_s} \frac{\epsilon_{s,\mathrm{vib},n,m}}{m_s}}_{:=e_{s,\mathrm{vib}}} + \underbrace{\sum_{n} \frac{N_{s,n}}{N_s} \frac{\epsilon_{s,\mathrm{el},n}}{m_s}}_{:=e_{s,\mathrm{el}}} + \underbrace{\frac{\epsilon_{s,0}}{m_s}}_{:=e_{s,0}} . \qquad (2.60)$$

Result (2.60) expresses e_s as a sum of the contributions of the sensible and ground level energies associated to the energy modes of the particles, i.e. $e_s = e_{s,\mathrm{tr}} + e_{s,\mathrm{rot}} + e_{s,\mathrm{vib}} + e_{s,\mathrm{el}} + e_{s,0}$. The contribution $e_{s,0}$ is the same as the one obtained for the case of the multi-temperature model, (2.49). Moreover, if the free particle in a box and the rigid rotor models are considered for the translational and rotational energy modes, respectively, then $e_{s,\mathrm{tr}}$ and $e_{s,\mathrm{rot}}$ can be shown to be also the same as the ones obtained for the case of the multi-temperature model, (2.45) and (2.46). On the other hand, the contributions $e_{s,\mathrm{vib}}$ and $e_{s,\mathrm{el}}$ are given by

$$e_{s,\mathrm{vib}} = \sum_{m,n} \frac{N_{s,m,n}}{N_s} \frac{\epsilon_{s,\mathrm{vib},n,m}}{m_s} , \qquad (2.61)$$

$$e_{s,\mathrm{el}} = \sum_{n} \frac{N_{s,n}}{N_s} \frac{\epsilon_{s,\mathrm{el},n}}{m_s} . \qquad (2.62)$$

In respect of the partial pressure p_s, since the translation is the only energy mode that contributes to this quantity, and since the vibronic-specific state-to-state model considers the existence of a heavy particle translational temperature $T_{\mathrm{tr_h}}$, p_s is given by (2.50) as happened with the case of the multi-temperature model.

The specific enthalpy associated to the s-th species $h_s = e_s + p_s/\rho_s$ may express itself through the relation $h_s = h_{s,\mathrm{tr}} + h_{s,\mathrm{rot}} + h_{s,\mathrm{vib}} + h_{s,\mathrm{el}} + h_{s,0}$ in a similar manner to what happened with the

specific internal energy e_s. Contribution $h_{s,0} = e_{s,0}$ has a form which is identical to the one for the multi-temperature model (2.56). If the same choices for the models of the translational and rotational energy models are made, the contributions $h_{s,\mathrm{tr}}$ and $h_{s,\mathrm{rot}}$ can be shown to correspond to the same ones obtained for the case of the multi-temperature model, i.e. (2.52) and (2.53), respectively. The contributions $h_{s,\mathrm{vib}} = e_{s,\mathrm{vib}}$ and $h_{s,\mathrm{el}} = e_{s,\mathrm{el}}$ are given by (2.61) and (2.62).

2.4 Collisional processes

In this section, processes initiated by collisions between particles are analysed. Such processes may induce a chemical change of the colliding particles - corresponding to chemical reactions - or may solely cause the excitation or de-excitation of their energy levels - corresponding to non-chemical collisional processes.

2.4.1 The rate coefficient for a collisional process

Rate coefficients for collisional processes by taking and not taking into account the involved energy levels may be defined in an identical way. By treating a particle in some energy level as a chemical species, the mathematical relation for the respective rate coefficient has the same form as the one for a homologous process in which the involved energy levels aren't regarded. To properly define the rate coefficient for any collisional process, the term "species" will be employed here with some ambiguity: it may mean a chemical species - if the energy levels involved in the collisional process aren't regarded - or a chemical species and some energy level associated to it - if the energy levels are indeed regarded.

2.4.1.1 Definition

It's important to know the variation in time of the number of particles of a species in a plasma, so that its composition may be described at each instant. The rate coefficient is not equivalent to this quantity, but it's intimately related to it. Let's consider a collisional process expressed in the general form

$$\nu_1 \mathrm{X}_1 + \nu_2 \mathrm{X}_2 + ... + \nu_{N_S} \mathrm{X}_{N_S} \longrightarrow \nu'_1 \mathrm{X}_1 + \nu'_2 \mathrm{X}_2 + ... + \nu'_{N_S} \mathrm{X}_{N_S} \Leftrightarrow$$

$$\Leftrightarrow \sum_{s=1}^{N_S} \nu_s \mathrm{X}_s \longrightarrow \sum_{s=1}^{N_S} \nu'_s \mathrm{X}_s \ , \tag{2.63}$$

where X_s is the s-th species in the plasma, ν_s and ν'_s are the associated *stoichiometric coefficients*[5] at the reactant and products sides, respectively. The index s goes from 1 to N_S, being N_S the number of species in the plasma. The variation in time of a species amount concentration (number of particles per unit of volume), due to this particular process, should follow some kind of law. History tells us that in many (but not all) collisional processes a well-known law can be observed [3]. If the process is one of

[5] Note that if the s-th species isn't present in one side or the other of the equation (or it isn't at all present in the process) the correspondent value ν_s or (and) ν'_s are zero.

those, then the variation in time of amount concentration of the s-th species is given by

$$\frac{d\left[\mathrm{X}_s\right]}{dt} = \left(\nu'_s - \nu_s\right) k \prod_{q=1}^{N_S} \left[\mathrm{X}_q\right]^{z_q} \ , \tag{2.64}$$

where $[\mathrm{X}_q]$ is the concentration (number of particles per unit volume) of the species X_q, and z_q is some number associated to this species, which value may or may not be related to its stoichiometric coefficient ν_q. It is known that if the process is a simple, single-step one, then $z_q = \nu_q$. For the sake of simplicity, let's from now on assume that the process is indeed a simple, single-step one. Also, it should be borne in mind that the relation (2.64) doesn't take into account the contribution from others processes, which may occur in the plasma. To consider these contributions a summation on all the processes that involve the species would be required.

The quantity k is the important rate coefficient which the current section tries to focus on. This rate coefficient is specific to the process, and it may depend on the several different temperatures that govern the system. One may then write $k = k(\{T_i\})$, being $\{T_i\}$ the set of governing temperatures. When taking into account the fact that a process may be reversible, a better label for the rate coefficient should be used: k_f if the forward (from left to right) process is considered, and k_b if the backward (from right to left) process is considered instead. Each rate is specific to the respective direction. The right pointing arrow in the chemical equation should be replaced by a double harpoon to represent this reversibility:

$$\sum_{s=1}^{N_S} \nu_s \mathrm{X}_s \underset{k_b}{\overset{k_f}{\rightleftharpoons}} \sum_{s=1}^{N_S} \nu'_s \mathrm{X}_s \ . \tag{2.65}$$

By taking into account the equation (2.64), and assuming that the process is a simple, single-step one, it is easy to conclude that the variations in time of the s-th species amount concentration due to the forward and backward processes, separately, are given by

$$\left(\frac{d\left[\mathrm{X}_s\right]}{dt}\right)_f = \left(\nu'_s - \nu_s\right) k_f \prod_{q=1}^{N_S} \left[\mathrm{X}_q\right]^{\nu_q} \ , \tag{2.66}$$

$$\left(\frac{d\left[\mathrm{X}_s\right]}{dt}\right)_b = \left(\nu_s - \nu'_s\right) k_b \prod_{q=1}^{N_S} \left[\mathrm{X}_q\right]^{\nu'_q} \ , \tag{2.67}$$

respectively. The total variation in time of the s-th species amount concentration, due to one single reversible process, is the sum of the two contributions:

$$\frac{d\left[\mathrm{X}_s\right]}{dt} = \left(\frac{d\left[\mathrm{X}_s\right]}{dt}\right)_f + \left(\frac{d\left[\mathrm{X}_s\right]}{dt}\right)_b \Leftrightarrow$$

$$\frac{d\left[\mathrm{X}_s\right]}{dt} = \left(\nu'_s - \nu_s\right) \left\{ k_f \prod_{q=1}^{N_S} \left[\mathrm{X}_q\right]^{\nu_q} - k_b \prod_{q=1}^{N_S} \left[\mathrm{X}_q\right]^{\nu'_q} \right\} \ . \tag{2.68}$$

If the rate coefficients k_f and k_b solely depend on some controlling temperature[6], say T_c, then the so-called *quasi-steady-state condition* (QSS) may be assumed [2], and one rate coefficient can be obtained from the other by analysing the case of thermodynamic equilibrium. When the plasma is in thermodynamic equilibrium, and therefore also in chemical equilibrium, the concentration of each species

[6] This concept of controlling temperature will turn to be more evident with the reading of section §2.4.1.2.

stagnates. By denoting thermodynamic equilibrium conditions by $[\,]^*$, this statement is expressed by $\left(\frac{d[\mathrm{X}_s]}{dt}\right)^* = 0$, for $s = 1$, ..., N_S. And from equation (2.68), one gets

$$0 = (\nu'_s - \nu_s)\left\{k_f(T_\mathrm{c})\prod_{q=1}^{N_S}\left([\mathrm{X}_q]^*\right)^{\nu_q} - k_b(T_\mathrm{c})\prod_{q=1}^{N_S}\left([\mathrm{X}_q]^*\right)^{\nu'_q}\right\} \Leftrightarrow$$

$$\Leftrightarrow \frac{k_f(T_\mathrm{c})}{k_b(T_\mathrm{c})} = \frac{\prod_{q=1}^{N_S}\left([\mathrm{X}_q]^*\right)^{\nu'_q}}{\prod_{q=1}^{N_S}\left([\mathrm{X}_q]^*\right)^{\nu_q}} := K_c(T_\mathrm{c})\ , \tag{2.69}$$

being $K_c(T_\mathrm{c})$ a quantity denominated by *concentration-wise equilibrium constant*[7] of the combined processes (2.65), although it isn't truly a constant, since it depends on the controlling temperature T_c. Equation (2.69) is quite useful: if two of three quantities $k_f(T_\mathrm{c})$, $k_b(T_\mathrm{c})$ and $K_c(T_\mathrm{c})$ are known, then the other would also be known.

It is also possible to express the equilibrium constant through the specific Gibbs free energies of the species involved in the process or even through their partition functions [3]. The respective expressions are

$$K_c(T_\mathrm{c}) = e^{-\sum_{s=1}^{N_S}\left(\nu'_s-\nu_s\right)\frac{g_{s,\mathrm{ref}}(T_\mathrm{c})}{R_s T_\mathrm{c}}}\left(\frac{p_\mathrm{ref}}{\mathscr{R}T_\mathrm{c}}\right)^{\sum_{s=1}^{N_S}\left(\nu'_s-\nu_s\right)} \quad , \quad K_c(T_\mathrm{c}) = e^{-\frac{\Delta\epsilon_0}{k_B T_\mathrm{c}}}\prod_{s=1}^{N_S}\left[\frac{Q_s(T_\mathrm{c},V)}{\mathscr{N}_A V}\right]^{\nu'_s-\nu_s} \quad . \tag{2.71}$$

(2.70)

These two relations contain a lot of physical quantities, which can't be explained in a single sentence. $\mathscr{R}$ is the *molar gas constant* and $\mathscr{N}_A$ is the *Avogadro constant*. The quantity $g_{s,\mathrm{ref}}(T_\mathrm{c}) = g_s(T_\mathrm{c}, p_\mathrm{ref})$ is the specific (in a mass basis) Gibbs free energy associated to the s-th species of the system, at a thermal equilibrium temperature T_c and partial pressure $p_s = p_\mathrm{ref}$, being p_ref some reference value. The quantity $\Delta\epsilon_0$ corresponds to the difference between the sum of the products ground level energies and the one associated to the reactants, i.e.

$$\Delta\epsilon_0 = \sum_{s_=1}^{N_S}\left(\nu'_s - \nu_s\right)\epsilon_{s,0}\ . \tag{2.72}$$

And $Q_s(T_\mathrm{c}, V)$ is the partition function associated to the s-th species at the equilibrium temperature T_c and volume V. Note that $Q_s(T_\mathrm{c}, V)/V$ is independent of the volume V, since one has $Q_s(T_\mathrm{c}, V) = Q_{s,\mathrm{tr}}(T_\mathrm{c}, V)\cdot Q_{s,\mathrm{int}}(T_\mathrm{c})$, and the translational partition function $Q_{s,\mathrm{tr}}(T_\mathrm{c}, V)$, given by (2.20), is proportional to V. Note that expressions (2.70) and (2.71) are stated assuming the number of particles to be regarded in units of mole, hence the presence of $\mathscr{R}$ and $\mathscr{N}_A$. If, conversely, the units of the number of particles are regarded as 1 (unity), then $\mathscr{R}$ and $\mathscr{N}_A$ in the expressions should be substituted by k_B and 1, respectively.

By substituting (2.69) in (2.68), one can get the important result

$$\frac{d\,[\mathrm{X}_s]}{dt} = (\nu'_s - \nu_s)\,k_f(T_\mathrm{c})\left\{\prod_{q=1}^{N_S}[\mathrm{X}_q]^{\nu_q} - \frac{1}{K_c(T_\mathrm{c})}\prod_{q=1}^{N_S}[\mathrm{X}_q]^{\nu'_q}\right\}\ . \tag{2.73}$$

Let's now consider the case when N_R different processes (each one with a forward and backward directions) occur in the plasma. There's a set of $k_f(T_\mathrm{c})$, $k_b(T_\mathrm{c})$, $K_c(T_\mathrm{c})$, ν_s and ν'_s values, with $s =$

[7] This quantity is expressed in terms of the species concentrations, hence the subscripted "c" in K_c.

1, ..., N_S, for each process. A subscripted index $r = 1, ..., N_R$ in each of these quantities symbols will be used to identify the process which they refer to. The variation in time of the s-th species amount concentration due to the full set of forward and backward N_R processes, corresponds to a summation of (2.73) in all r, i.e.

$$\frac{d\left[\mathrm{X}_s\right]}{dt} = \sum_{r=1}^{N_R} \left(\left(\nu'_{s,r} - \nu_{s,r}\right) k_{f,r}(T_\mathrm{c}) \left\{ \prod_{q=1}^{N_S} \left[\mathrm{X}_q\right]^{\nu_{q,r}} - \frac{1}{K_{c,r}(T_\mathrm{c})} \prod_{q=1}^{N_S} \left[\mathrm{X}_q\right]^{\nu'_{q,r}} \right\} \right) . \tag{2.74}$$

And the variation in time of the s-th species mass density due to these processes is simply given by $\dot{\omega}_s := m_s \frac{d[\mathrm{X}_s]}{dt}$.

2.4.1.2 Computation

Now that the definion of rate coefficient for a collisional process was given, a way to compute it should be introduced. The theory in this section will only focus on processes initiated by collisions between two particles (these are therefore called *binary collisions*). Such processes can be identified through the notation "A + B" (being A and B the species of the two colliding particles) in the reactants side of a a chemical equation. A rate coefficient can be computed through a physical quantity denominated by *process cross section* [45], σ_p. Before explaining what is meant by a process cross section, it's necessary to firstly introduce the so-called *collisional cross section* or *scattering cross section*, σ. The two are correlated. The collisional cross section of two colliding particles corresponds to the area of a plane surface transverse to their relative motion within which they must meet in order to scatter from each other. For example, if the particles behave like hard spheres, which can only interact through contact (*billiard balls model*), the collisional cross section is related to their geometric size, corresponding to $\sigma = \pi d_{\mathrm{AB}}^2$, being $d_{\mathrm{AB}} = r_\mathrm{A} + r_\mathrm{B}$ the distance between the spheres centres when their surfaces touch each other (see Figure 2.5). In that case, the cross section area can be visualised as the area of the set of all the possible B points where a collision is said to occur, projected to a plane normal to the relative velocity, $\vec{v}$.

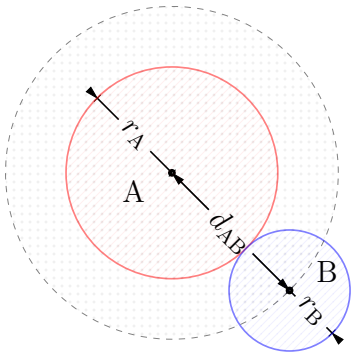

Figure 2.5: Collisional cross section (black circle) for a collision between the particles A (red circle) and B (blue circle) according to the billiard balls model. The figure depicts a very particular case: a tangent collision (where the relative velocity vector is normal to the line that connects the two centres). The plane of view is one perpendicular to the relative velocity vector, $\vec{v}$.

But a collision doesn't necessarily mean contact. Real particles do interact at distance, through electromagnetic forces, being the scattering cross section generally larger than the one that would be obtained if the particles only interacted through contact.

The process cross section σ_p corresponds to a collisional cross section weighted by the probability of the collision to induce the process: $\sigma_p = P \cdot \sigma$, being P the given probability. Note that both collisional cross section and process probability may depend on the relative velocity of the particles, $\vec{v}$, or even solely on its norm v (the relative speed of collision), which in such case, one has $\sigma = \sigma(v)$ and $P = P(v)$. Let's assume here this latter hypothesis.

Now, a helpful function should be introduced. Let $f(v)$ be a function such that $\sigma_p(v) f(v) [\mathrm{A}][\mathrm{B}]\, dv$ is the number of forward processes, per unit of time, per unit of volume, induced by collisions between the particles A and B, with a relative speed $v \in [v,\, v + dv]$. The function $f(v)$ is commonly referred to as the *distribution of relative speeds*. Let C be one of the products of the process, and ν_C and ν'_C its stoichiometric coefficients. Note that there's also the possibility of C being identical to A or B. The respective chemical equation can be expressed through

$$\mathrm{A} + \mathrm{B} \rightleftharpoons \nu'_\mathrm{C}\mathrm{C} + \cdots \,. \tag{2.75}$$

By considering the definition of $f(v)$, and by knowing that each forward process results in $\nu'_\mathrm{C} - \nu_\mathrm{C}$ new C particles, it's easy to find that the change, per unit of time of the amount concentration of the C species, with $v \in [v,\, v + dv]$, is given by

$$d\left(\frac{d\,[\mathrm{C}]}{dt}\right)_f (v) = (\nu'_\mathrm{C} - \nu_\mathrm{C})\, \sigma_p(v) f(v) [\mathrm{A}][\mathrm{B}]\, dv \,. \tag{2.76}$$

And the total change, per unit of time, of the amount concentration of the C species, is obtained by summing all the contributions of each dv (resulting in an integral) along the whole range of relative speed values, $v \in [0, \infty]$:

$$\left(\frac{d\,[\mathrm{C}]}{dt}\right)_f = (\nu'_\mathrm{C} - \nu_\mathrm{C}) \left\{ \int_0^\infty \sigma_p(v) f(v)\, dv \right\} [\mathrm{A}][\mathrm{B}] \,. \tag{2.77}$$

By comparing (2.77) with (2.66), one can find an expression for the forward rate coefficient:

$$k_f = \int_0^\infty \sigma_p(v) f(v)\, dv \,. \tag{2.78}$$

If the species of both collision partners A and B have their translational energy mode in self-equilibrium, a translational temperature $T_{\mathrm{tr,A}}$ and a translational temperature $T_{\mathrm{tr,B}}$ can be respectively assigned to the particles. The distribution of absolute velocities of each particle will correspond to a *Maxwell-Boltzmann distribution*, having the respective translational temperature as parameter [3]. The distribution of relative speeds between the two particles is directly obtained from the distributions of absolute velocities. If A and B are heavy particles and their translational temperatures are the same, i.e. $T_{\mathrm{tr,A}} = T_{\mathrm{tr,B}} = T_{\mathrm{tr_h}}$,

then the relative distribution of relative speeds can be shown to be

$$f(v, T_{\mathrm{tr_h}}) = \frac{4\pi}{1+\delta_{\mathrm{AB}}} \left(\frac{\mu}{2\pi k_B T_{\mathrm{tr_h}}}\right)^{\frac{3}{2}} v^3 e^{-\frac{\mu v^2}{2k_B T_{\mathrm{tr_h}}}} \ , \tag{2.79}$$

being $\mu = m_{\mathrm{A}} \cdot m_{\mathrm{B}} / (m_{\mathrm{A}} + m_{\mathrm{B}})$ the reduced mass of the particles, and δ_{AB} a Kronecker delta (it gives 1 if the particles are identical, i.e. if A=B, and 0 if not). Therefore, by substituting (2.79) in (2.78) one may obtain

$$k_f(T_{\mathrm{tr_h}}) = \frac{1}{1+\delta_{\mathrm{AB}}} \cdot \frac{\sqrt{\frac{8k_B T_{\mathrm{tr_h}}}{\pi\mu}}}{2\left(\frac{k_B T_{\mathrm{tr_h}}}{\mu}\right)^2} \int_0^\infty \sigma_p(v) v^3 e^{-\frac{\mu v^2}{2k_B T_{\mathrm{tr_h}}}} \, dv \ . \tag{2.80}$$

This equation can be rewritten considering the relative kinetic energy of the colliding particles, $E = \frac{1}{2}\mu v^2$, instead of the relative speed, v, by performing a change of variables:

$$k_f(T_{\mathrm{tr_h}}) = \frac{1}{1+\delta_{\mathrm{AB}}} \cdot \frac{\sqrt{\frac{8k_B T_{\mathrm{tr_h}}}{\pi\mu}}}{\left(k_B T_{\mathrm{tr_h}}\right)^2} \int_0^\infty \sigma_p(E) E e^{-\frac{E}{k_B T_{\mathrm{tr_h}}}} \, dE \ . \tag{2.81}$$

And if the adimensional variable $u = \frac{E}{k_B T_{\mathrm{tr_h}}}$ is considered instead, one gets

$$k_f(T_{\mathrm{tr_h}}) = \frac{\sqrt{\frac{8k_B T_{\mathrm{tr_h}}}{\pi\mu}}}{1+\delta_{\mathrm{AB}}} \int_0^\infty \sigma_p(u, T_{\mathrm{tr_h}}) \, u \, e^{-u} \, du \ . \tag{2.82}$$

It may now be opportune to introduce here the concept of *average process cross section* $\sigma_{p,\mathrm{av}}$. This quantity corresponds to the average of the process cross section with respect to the distribution of relative speeds of the collision partners, i.e

$$\sigma_{p,\mathrm{av}}(T_{\mathrm{tr_h}}) = \frac{\int_0^\infty \sigma_p(v) f(v, T_{\mathrm{tr_h}}) \, dv}{\int_0^\infty f(v, T_{\mathrm{tr_h}}) \, dv} = \frac{\int_0^\infty \sigma_p(E) E e^{-\frac{E}{k_B T_{\mathrm{tr_h}}}} \, dE}{\left(k_B T_{\mathrm{tr_h}}\right)^2} \ . \tag{2.83}$$

With this relation taken into account, the rate coefficient of the process given by (2.81) may be expressed in the manner

$$k_f(T_{\mathrm{tr_h}}) = \frac{\sigma_{p,\mathrm{av}}(T_{\mathrm{tr_h}})}{1+\delta_{\mathrm{AB}}} \sqrt{\frac{8k_B T_{\mathrm{tr_h}}}{\pi\mu}} \ . \tag{2.84}$$

The process may require a minimum value of relative kinetic energy of the colliding particles to occur [3] - the so-called *activation energy* E_a. The process probability $P(E)$ and consequently the process cross section $\sigma_p(E) = P(E)\sigma(E)$ would then be null for $E < E_a$. If the process instead occurs for any relative kinetic energy E, the respective activation energy would correspond to $E_a = 0$. The lower limit of integration in the expression (2.81) may be then substituted by E_a without loss of generality, which ultimately gives [2]

$$k_f(T_{\mathrm{tr_h}}) = \frac{1}{1+\delta_{\mathrm{AB}}} \cdot \frac{\sqrt{\frac{8k_B T_{\mathrm{tr_h}}}{\pi\mu}}}{\left(k_B T_{\mathrm{tr_h}}\right)^2} \int_{E_a}^\infty \sigma_p(E) E e^{-\frac{E}{k_B T_{\mathrm{tr_h}}}} \, dE = \frac{\sqrt{\frac{8k_B T_{\mathrm{tr_h}}}{\pi\mu}}}{1+\delta_{\mathrm{AB}}} \int_{\frac{E_a}{k_B T_{\mathrm{tr_h}}}}^\infty \sigma_p(u, T_{\mathrm{tr_h}}) \, u \, e^{-u} \, du \Leftrightarrow$$

$$\Leftrightarrow k_f(T_{\mathrm{tr_h}}) = \frac{\sqrt{\frac{8k_BT_{\mathrm{tr_h}}}{\pi\mu}}}{1+\delta_{\mathrm{AB}}} e^{-\frac{E_a}{k_BT_{\mathrm{tr_h}}}} \int_0^\infty \sigma_p(w, T_{\mathrm{tr_h}}) \left(w + \frac{E_a}{k_BT_{\mathrm{tr_h}}}\right) e^{-w}\, dw \Leftrightarrow$$

$$\Leftrightarrow k_f(T_{\mathrm{tr_h}}) = \frac{\sqrt{\frac{8k_BT_{\mathrm{tr_h}}}{\pi\mu}}}{1+\delta_{\mathrm{AB}}} e^{-\frac{E_a}{k_BT_{\mathrm{tr_h}}}} \left[\left(\int_0^\infty \sigma_p(w, T_{\mathrm{tr_h}})\, w\, e^{-w}\, dw\right) + \left(\int_0^\infty \sigma_p(w, T_{\mathrm{tr_h}})\, e^{-w}\, dw\right) \frac{E_a}{k_BT_{\mathrm{tr_h}}}\right], \tag{2.85}$$

being $w = u - E_a/k_BT_{\mathrm{tr_h}}$.

Also, it's worthy to say that a *specific collisional frequency*, Z, can be simply obtained from (2.80) if one substitutes the process cross section by the collisional cross section, i.e. $\sigma_p \leftrightarrow \sigma$, giving

$$Z(T_{\mathrm{tr_h}}) = \frac{\sigma_{\mathrm{av}}(T_{\mathrm{tr_h}})\sqrt{\frac{8k_BT_{\mathrm{tr_h}}}{\pi\mu}}}{1+\delta_{AB}}\ . \tag{2.86}$$

The quantity σ_{av} corresponds to the *average collisional cross section*, with a definition homologous to the expression (2.83). The quantity Z is such that $Z \cdot [A] \cdot [B]$ corresponds to the frequency of collisions between particles A and B per unit of volume.

If A corresponds to a heavy particle with a translational temperature $T_{\mathrm{tr_h}}$, and B to a free electron with a translational temperature $T_{\mathrm{tr_e}}$, one obtains the distribution of relative speeds by simply assuming the heavy particles to be fixed in space, since the small mass of the free electrons makes them much faster than the heavy particles [2]. In such conditions, the formulae for the rate coefficient have the same structure as the ones above, with the reduced mass μ substituted by the electron mass m_{e}, the relative speed v substituted by the absolute speed of the electrons and the heavy particle temperature $T_{\mathrm{tr_h}}$ substituted by the free electron translational temperature $T_{\mathrm{tr_e}}$. And since the collision partners are different, one has also $\delta_{\mathrm{AB}} = 0$, which ultimately gives

$$k_f(T_{\mathrm{tr_e}}) = \frac{\sqrt{\frac{8k_BT_{\mathrm{tr_e}}}{\pi m_{\mathrm{e}}}}}{2\left(\frac{k_BT_{\mathrm{tr_e}}}{m_{\mathrm{e}}}\right)^2} \int_0^\infty \sigma_p(v) v^3 e^{-\frac{m_{\mathrm{e}}v^2}{2k_BT_{\mathrm{tr_e}}}}\, dv. \tag{2.87}$$

The integrals that appear in the formulae for the process rate coefficients aren't usually analytically solvable. The known process cross section values σ_p are often discrete (being obtained through experiment or even through theory allied with a numerical method) which makes a numerical procedure for the integrals evaluation much more convenient. Even if an analytical process cross section function $\sigma_p(E)$ is known (being obtained through theory or by curve fitting of experimental results) the resultant integrands functions are usually still too complicated to make the respective integrals analitically solvable. The process rate coefficients are then ordinarly obtained through a numerical procedure, resulting in a set of discrete rate values instead of a curve. A praticabillity problem arises with this circumstance: CFD simulations require rate values evaluated at some temperatures that may or may not belong to the set of ones associated to the previously compute rates. Obtaining a rate coefficient function by fitting the discrete set of rate values may solve this problem. However a proper fitting curve is required to model the data. History tells us that the process rate coefficient should approximately follow a law [3]. The

modified Arrhenius equation

$$k_f(T_c) = A{T_c}^n e^{-\frac{E_a}{k_B T_c}}, \tag{2.88}$$

is one possible candidate for that law, being A, n and E_a some constants particular to the process, and T_c the respective controlling temperature. The constant E_a has the physical meaning of an activation energy, and for a matter of fact, relation (2.88) do share a similar structure with the previously derived relation (2.85) for the rate coefficient which takes into account such activation energy. The term "modified" was employed in the designation "modified Arrhenius equation", since in the past, a more simple Arrhenius equation was introduced: $k_f(T_c) = Ae^{-\frac{E_a}{k_B T_c}}$. The modified one is however more adjustable, having one more free parameter (n). A physically coherent function $k_f(T_c)$ can be achieved by fitting the function (2.88) to the previously computed (by equation (2.81)) rate values. If the rate data points don't follow a modified Arrhenius equation, then a function with even more degrees of freedom should be used. An example of such function is

$$\begin{aligned}\frac{k_f(T_c)}{[k_f]} = \exp\Bigg[& a_1 \left(\frac{T_c}{T_{c,\text{ref}}}\right)^{-3} + a_2 \left(\frac{T_c}{T_{c,\text{ref}}}\right)^{-2} + a_3 \left(\frac{T_c}{T_{c,\text{ref}}}\right)^{-1} + a_4 \ln\left(\frac{T_c}{T_{c,\text{ref}}}\right) \\ & + a_5 + a_6 \frac{T_c}{T_{c,\text{ref}}} + a_7 \left(\frac{T_c}{T_{c,\text{ref}}}\right)^{2} + a_8 \left(\frac{T_c}{T_{c,\text{ref}}}\right)^{3} + a_9 \left(\frac{T_c}{T_{c,\text{ref}}}\right)^{4} \Bigg] ,\end{aligned} \tag{2.89}$$

being $\{a_i\}$, with $i = 1, ..., 9$, the set of free parameters, which are adimensional, and $T_{c,\text{ref}} = 1000\text{K}$ a reference temperature. Note that the function is adimensional, hence the division of the rate coefficient by its units $[k_f]$ in the left-hand side of the relation. Function (2.89) can be reduced to the modified Arrhenius function if the constraints

$$\begin{cases} a_3 = -\frac{E_a}{k_B T_{\text{ref}}} , \\ a_4 = n , \\ a_5 = \ln\left(\frac{T_{c,\text{ref}}^n A}{[k_f]}\right) , \\ a_i = 0, \, \forall i \neq 3, 4, 5 . \end{cases} \tag{2.90}$$

are applied to the free parameters. This property is rather useful. A function with a lot of parameters can turn to be unstable when fitting the data. Such function requires good initial estimates to properly converge. By first fitting a modified Arrhenius function (which has less free parameters, and therefore is more stable), applying the transformation (2.90) (and also substituting the null a_i constants by small values), and then performing a second fit with the resultant nine parameters function as initial estimate, convergence is more easily achieved.

2.5 Radiative processes

Radiative processes correspond to transitions between energy levels of atomic particles, molecular particles and free electrons [3], or the assembly and disassembly of components (nuclei and electrons) of the internal structure of the heavy particles, in which the involved energy change is transferred to or received from

photons. The photon is a massless particle corresponding to the *quantum* (the minimum amount) of electromagnetic radiation, having an energy $E = h\nu$ according to the Planck-Einstein relation, being h the Planck constant, and ν the frequency of the electromagnetic wave associated with it. And since the wavelength of the electromagnetic wave λ is related to ν through $\lambda = c/\nu$, being c the *speed of light*, one may also write $E = hc/\lambda$. The law of conservation of energy tells that the net change of energy of the particles involved in the radiative process needs to be equal to the absorbed photon energy (for the case of absorption) or the symmetric of the emitted photon energy (for the case of emission).

The transitions that occur in such processes can be divided into three groups: *bound-bound*, *bound-free* (and *free-bound*) and *free-free transitions*. The nomenclature is built in respect of the state of attachment or detachment of nuclei or/and electrons in the particles internal structure, before and after the transition occurs.

Bound-bound transitions correspond to radiative processes in which all the components (nuclei and electrons) of the internal structure of the particles that were previously attached (bound) still remain attached after the transitions. These particles need to be heavy particles (since they are the ones that may have a multiplicity of components in the internal structure). The transitions are between two internal energy levels, which are by definition quantised. Therefore, in bound-bound transitions of atomic particles, solely changes in their electronic state can happen (atomic particles have only one internal energy mode, the electronic). And in bound-bound transitions of molecular particles, the changes can be in their vibrational, rotational, and electronic states. Such transitions correspond to spontaneous emissions, induced (or stimulated) emissions and absorptions. A spontaneous emission occurs when the particle, without being subjected to any external stimulus, transits to a lower energy level, emitting a photon. The photon energy is equal to the gap between the two levels. An induced emission occurs when the particle after being "hit" by a photon transits to a lower energy level, emitting another photon with same energy, direction, *phase* and *polarisation* as the incident one. Note that the incident photon isn't absorbed, it only interacts with the particle. Also, note that both incident and emitted photons need to have an energy equal to the gap between the initial and final levels. In a photon absorption, as the name says, the incident photon is absorbed by the particle, causing an excitation: an higher energy level is achieved. The incident photon needs therefore to have the same energy as the gap between the two levels[8].

Bound-free transitions imply a detachment of components of the particles. Therefore, these particles also need to be heavy particles. The energy of the incident photon needs to be higher or equal to the binding energy of the components that suffer the detachment. The remnant energy (the difference between the photon energy and the binding energy) will contribute to the translational kinetic energy of the detached components. Since the energy levels associated to the translational kinetic energy mode of the particles are so close together that a continuum of energy values may be assumed, there's no requirement for the incident photon to have some particular discrete energy value. The reverse process is denominated by *free-bound transition*.

[8]One should however to be careful with these statements since in this introductory text the *uncertainty principle* is disregarded, and the heavy particle is considered to be stationary and isolated from other particles. Such conditions do not hold in reality, and the further details treated in section §2.5.2.1 need to be taken into account.

A bound-free transition may correspond to a photoionisation - in which the detached component is an electron - or to a photodissociation - in which the detached component is an atomic or molecular particle. The reverse of these processes, being of the type free-bound, are denominated *radiative recombination* and *radiative association*.

Finally there are the free-free transitions, in which a free electron remains free after the interaction. A free-free transition corresponds to the so-called *bremsstrahlung*[9] process, in which the interaction of two charged particles results in the emission of radiation by them. Typically, bremsstrahlung is observed in free electron-nucleus interactions, or free electron-positive ion interactions.

For simplicity reasons, this work will only address the bound-bound transitions. Furthermore, only bound-bound transitions that involve electronic and vibrational energy modes of the particles will be considered. Anyway, a generalisation that accounts transitions in the rotational levels may be done in a straightforward manner.

2.5.1 The radiation field

The radiation field of a system may be described by the so-called *specific radiant intensity* I_λ. This quantity is defined as the radiant energy at wavelengths $\lambda \in [\lambda,\, \lambda + d\lambda]$, transported by photons propagating at azimuthal angles $\varphi \in [\varphi,\, \varphi + d\varphi]$ and polar angles $\theta \in [\theta,\, \theta + d\theta]$, that cross an infinitesimal surface dS located in $\vec{r}$, normal to the direction of propagation, during the interval of time $[t,\, t + dt]$, per unit of area, time, solid angle and wavelength. A frequency-specific radiant intensity I_ν, which is given per unit of frequency instead of wavelength, can be shown to be related to the wavelength-specific counterpart I_λ simply by[10] $I_\nu = (c/\nu^2) I_\lambda$. It can also be proved that in thermodynamic equilibrium (which also implies radiative equilibrium, ultimately meaning that radiation doesn't contribute to a change in the distribution of the species states populations) the distribution of the photon states population is such that the specific radiant intensity is given by [3]

$$I^*_\lambda(\vec{r}, t, \varphi, \theta, \lambda) = \frac{2hc^2}{\lambda^5 \left(e^{\frac{hc}{\lambda k_B T}} - 1 \right)} := B_\lambda(\lambda, T) \ . \tag{2.91}$$

The resulting quantity $B_\lambda(\lambda, T)$ is the so-called *Planck function*. Equation (2.91) tells that under conditions of thermodynamic equilibrium, the specific radiant intensity I_λ is an isotropic variable, solely depending on the wavelength λ and equilibrium temperature T at point $\vec{r}$ and instant t.

2.5.2 Bound-bound transitions

2.5.2.1 Line broadening and shift

Although one may at first expect the radiation field generated by bound-bound transitions to be completely discrete due to the fact that the internal energy levels of particles are associated to discrete energy values, it is actually continuous. A plot of the specific radiant intensity I_λ versus wavelength λ would in fact show finite-height peaks - the so-called *broadened lines*, instead of infinite-height lines associated to *Dirac*

[9] From the German: "bremsen" means "to brake" and "strahlung" means "radiation".
[10] Note that one has $d\lambda = d(c/\nu) = -c/\nu^2 d\nu$.

delta functions. One contribution to these line broadening and shift corresponds to the *natural line broadening* which is closely related to the *Heisenberg uncertainty principle*: there's an uncertainty on the energy of the heavy particle, resulting in an uncertainty on the energy of the emitted or absorbed photon [3, 46–48]. This contribution is however usually tiny. As Griem [47] says, "[n]atural line broadening is almost always completely negligible in applications of plasma spectroscopy". Collisions between the particles shorten the *lifetimes* of their states ultimately influencing the breadth of the lines [48]. Such contribution - termed *collisional broadening* - may be accounted by considering an *optical collisional frequency per particle* [46]. This quantity is intimately related to the respective collisional frequency per particle. Another contribution is the *Doppler broadening* which occurs with the thermal agitation motion of the particles making the frequency of the radiation observed from some reference point to be different from the one observed by the emitter or absorber [3, 46–48]. Additionally, the electric field produced by the particles in the system may induce a splitting of the particles energy levels and therefore also a splitting of the spectral lines. Since this is a result of interactions between particles of the system, it is generally called *pressure broadening* [47]. The phenomena may be associated to an interaction of a charged particle with another particle - being termed *Stark broadening* - or an interaction between two neutral particles through *van der Waals forces* - hence termed *van der Waals broadening* - or a *resonant* interaction between two particles of the same species - hence termed *resonance broadening* [47–49]. Van der Waals broadening was disregarded in this work since no reasonably practical model for the mechanism was found in the literature. Also, it was assumed that line broadening occurred without shift.

2.5.2.2 The Einstein coefficients

Bound-bound transitions can be described quantitatively through the so-called *Einstein coefficients* [3]. There's an Einstein coefficient for each of the three possible types of bound-bound transitions. The physical meaning of these coefficients will now be presented for the case of molecular particles (since it is more general).

The Einstein coefficient associated to spontaneous emission, $A_{s,e,v}^{e',v'}$, is defined such that the number of transitions of particles of the s-th species from the electronic level e and vibrational level v to the electronic level e' and vibrational level v' [11] per unit of volume, time and solid angle, in $\vec{r} \in [x,\, x+dx] \times [y,\, y+dy] \times [z,\, z+dz]$, during the interval of time $[t,\, t+dt]$, and spontaneously emitting photons at azimuthal angles $\varphi \in [\varphi,\, \varphi+d\varphi]$ and polar angles $\theta \in [\theta,\, \theta+d\theta]$, is given by

$$-\left(\frac{d^2 n_{s,e,v}}{dt\, d\Omega}\right)_{s,e,v}^{e',v',\mathrm{se}}(\vec{r},t,\varphi,\theta) = \frac{A_{s,e,v}^{e',v'}}{4\pi}\, n_{s,e,v}(\vec{r},t)\ , \tag{2.92}$$

where $n_{s,e,v} = dN_{s,e,v}/dV$ corresponds to the number density or amount concentration (number of particles per unit of volume) of s-th species particles in the electronic level e and vibrational level v. The superscript term "se" in (2.92) is a label for spontaneous emission. Because e, e', v and v' represent levels and not states, the Einstein coefficient $A_{s,e,v}^{e',v'}$ is *level-specific* and should be denominated in that way to

[11] Let's assume in this section that the energy associated to the vibronic level $(e,\, v)$ is higher than the one associated to $(e',\, v')$.

avoid ambiguity problems with the *state-specific* counterpart. Note that $A_{s,e,v}^{e',v'}$ corresponds to a constant - thus, $A_{s,e,v}^{e',v'}$ doesn't depend on the emission direction angles φ and θ, and one can say that the law (2.92) assumes that the spontaneous emission is an isotropic process. The variation in time of the number density of s-th species particles in the vibronic level $(e,\, v)$, due to transitions by spontaneous emission from $(e,\, v)$ to $(e',\, v')$ can be obtained by multiplication of (2.92) by $\sin\theta$ (note that $d\Omega = \sin\theta\, d\varphi\, d\theta$), integration in φ and θ and transfer of the minus sign to the right hand side of the equation. The result is

$$\left(\frac{dn_{s,e,v}}{dt}\right)_{s,e,v}^{e',v',\mathrm{se}}(\vec{r},t) = -A_{s,e,v}^{e',v'}\, n_{s,e,v}(\vec{r},t)\ . \tag{2.93}$$

The level-specific Einstein coefficient associated to photon absorption, $B_{s,e',v'}^{e,v}$, is defined such that in a radiation field of specific radiant intensity I_λ, the number of transitions of particles of the s-th species from (e',v') to (e,v), per unit of volume, time and solid angle, by absorbing photons at angles $\varphi \in [\varphi,\, \varphi + d\varphi]$ and $\theta \in [\theta,\, \theta + d\theta]$, is given by

$$\left(\frac{d^2 n_{s,e,v}}{dt\, d\Omega}\right)_{s,e',v'}^{e,v}(\vec{r},t,\varphi,\theta) = \frac{B_{s,e',v'}^{e,v}}{4\pi}\, n_{s,e',v'}(\vec{r},t)\left(\int_0^\infty I_\lambda(\vec{r},t,\varphi,\theta,\lambda)\cdot\phi_{\lambda,s,e,v}^{e',v'}(\vec{r},t,\lambda)\, d\lambda\right)\ , \tag{2.94}$$

in which a superscript term for absorption wasn't added since it is only by absorption that such radiative transition can occur. The function $\phi_{\lambda,s,e,v}^{e',v'}$ corresponds the so-called *line-shape factor* [3] associated to the particular set of vibronic levels (e,v) and (e',v') of the s-th species. In absorption, it may be interpreted as the probability density function of an incident photon of wavelength λ to be absorbed, causing a transition of the s-th species particle from (e',v') to (e,v). By multiplying (2.94) by $\sin\theta$, and integrating it with respect to φ and θ one would get the variation in time of the number density of s-th species particles in $(e,\, v)$, due to transitions by photon absorption from $(e',\, v')$ to $(e,\, v)$:

$$\left(\frac{dn_{s,e,v}}{dt}\right)_{s,e',v'}^{e,v}(\vec{r},t) = \frac{B_{s,e',v'}^{e,v}}{4\pi}\, n_{s,e',v'}(\vec{r},t)\left\{\int_0^\pi\left[\int_0^{2\pi}\left(\int_0^\infty I_\lambda(\vec{r},t,\varphi,\theta,\lambda)\cdot\phi_{\lambda,s,e,v}^{e',v'}(\vec{r},t,\lambda)\, d\lambda\right)\, d\varphi\right]\sin\theta\, d\theta\right\}\ . \tag{2.95}$$

In a similar manner to the absorption, the level-specific Einstein coefficient associated to induced emission $B_{s,e,v}^{e',v'}$ is defined such that in a radiation field of specific radiant intensity I_λ, the number of transitions of particles of the s-th species from (e,v) to (e',v'), per unit of volume, time and solid angle, by induced emission, emitting photons at angles $\varphi \in [\varphi,\, \varphi + d\varphi]$ and $\theta \in [\theta,\, \theta + d\theta]$, is given by

$$-\left(\frac{d^2 n_{s,e,v}}{dt\, d\Omega}\right)_{s,e,v}^{e',v',\mathrm{ie}}(\vec{r},t,\varphi,\theta) = \frac{B_{s,e,v}^{e',v'}}{4\pi}\, n_{s,e,v}(\vec{r},t)\left(\int_0^\infty I_\lambda(\vec{r},t,\varphi,\theta,\lambda)\cdot\phi_{\lambda,s,e,v}^{e',v'}(\vec{r},t,\lambda)\, d\lambda\right)\ , \tag{2.96}$$

where the superscript term "ie" is a label for induced emission. By multiplication of (2.96) by $\sin\theta$, integration in φ and θ, and transfer of the minus sign to the right hand side one would get

$$\left(\frac{dn_{s,e,v}}{dt}\right)_{s,e',v'}^{e,v,\mathrm{ie}}(\vec{r},t) = -\frac{B_{s,e,v}^{e',v'}}{4\pi}\, n_{s,e,v}(\vec{r},t)\left\{\int_0^\pi\left[\int_0^{2\pi}\left(\int_0^\infty I_\lambda(\vec{r},t,\varphi,\theta,\lambda)\cdot\phi_{\lambda,s,e,v}^{e',v'}(\vec{r},t,\lambda)\, d\lambda\right)\, d\varphi\right]\sin\theta\, d\theta\right\}\ . \tag{2.97}$$

The variation in time of the number density of s-th species particles in the vibronic level $(e,\, v)$, due

solely to radiative transitions from $(e,\, v)$ to $(e',\, v')$ is the sum of the contributions from the spontaneous emission (2.93) and induced emission (2.97):

$$\left(\frac{dn_{s,e,v}}{dt}\right)_{s,e,v}^{e',v'}(\vec{r},t) = \left(\frac{dn_{s,e,v}}{dt}\right)_{s,e,v}^{e',v',\mathrm{se}}(\vec{r},t) + \left(\frac{dn_{s,e,v}}{dt}\right)_{s,e,v}^{e',v',\mathrm{ie}}(\vec{r},t) \Leftrightarrow$$

$$\Leftrightarrow \left(\frac{dn_{s,e,v}}{dt}\right)_{s,e,v}^{e',v'}(\vec{r},t) = -n_{s,e,v}(\vec{r},t)\left(A_{s,e,v}^{e',v'} + \frac{B_{s,e,v}^{e',v'}}{4\pi}\left\{\int_0^{\pi}\left[\int_0^{2\pi}\left(\int_0^{\infty} I_\lambda(\vec{r},t,\varphi,\theta,\lambda)\cdot\phi_{\lambda,s,e,v}^{e',v'}(\vec{r},t,\lambda)\,d\lambda\right)d\varphi\right]\sin\theta\,d\theta\right\}\right)\,. \tag{2.98}$$

It can be easily shown that the three Einstein coefficients are correlated. Since these correspond to properties of the particles and not of the macroscopic system, one may extract a relation between them by simply considering a system in thermodynamic equilibrium and where the line broadening phenomena is negligible. In such circumstances the line-shape factor may be approximated by a Dirac delta function, implying

$$\int_0^{\infty} I_\lambda(\vec{r},t,\varphi,\theta,\lambda)\cdot\phi_{\lambda,s,e,v}^{e',v'}(\vec{r},t,\lambda)\,d\lambda \approx \int_0^{\infty} I_\lambda(\vec{r},t,\varphi,\theta,\lambda)\cdot\delta(\lambda-\lambda_{s,e,v}^{e',v'})\,d\lambda = I_\lambda(\vec{r},t,\varphi,\theta,\lambda_{s,e,v}^{e',v'})\,, \tag{2.99}$$

being $\lambda_{s,e,v}^{e',v'}$ the wavelength of a photon with a energy equal to the gap between the involved energy levels. In thermodynamic equilibrium, and therefore also in radiative equilibrium, radiative processes can't contribute to a change in the population of the particles levels. Thus,

$$\left(\frac{dn_{s,e,v}}{dt}\right)^{*}(\vec{r},t) = 0,\ \forall\,(e,\,v)\,. \tag{2.100}$$

A principle should be invoked when speaking about equilibrium: the principle of *detailed balancing*. This principle tells us that equilibrium can only be achieved if each elementary process and his reverse are in equilibrium as well. Note that no reverse process is associated to spontaneous emission, and the above proposition should be taken with care since the term "elementary process" was used with some abuse. Herein an "elementary process" is considered to be the most smallest combination of processes that can be counterbalanced. Therefore, an "elementary process" associated to a transition from an upper to a lower level corresponds to a combination of both spontaneous and induced emission, and an "elementary process" associated to a transition from a lower to an upper level corresponds to absorption. Detailed balancing applied to bound-bound transitions can be expressed mathematically by

$$\left(\frac{dn_{s,e,v}}{dt}\right)_{s,e,v}^{e',v',*}(\vec{r},t) + \left(\frac{dn_{s,e,v}}{dt}\right)_{s,e',v'}^{e,v,*}(\vec{r},t) = 0,\ \forall\,(e,\,v),\,(e',\,v')\,. \tag{2.101}$$

On the other hand, since the population of levels in equilibrium follows a Boltzmann distribution, it can be shown that the ratio between the number densities $n_{s,e',v'}$ and $n_{s,e,v}$ is given by

$$\frac{n_{s,e',v'}^{*}(\vec{r},t)}{n_{s,e,v}^{*}(\vec{r},t)} = \frac{g_{s,e',v'}}{g_{s,e,v}}e^{\frac{hc}{\lambda_{s,e,v}^{e',v'}\cdot k_B T}}\,. \tag{2.102}$$

By substituting (2.91), (2.95), (2.98) and (2.102) in (2.101), neglecting line broadening, one gets

$$\frac{A^{e',v'}_{s,e,v}}{B^{e',v'}_{s,e,v}} = \frac{2hc^2}{\left(\lambda^{e',v'}_{s,e,v}\right)^5} \cdot \frac{\frac{B^{e,v}_{s,e',v'}}{B^{e',v'}_{s,e,v}} \cdot \frac{g_{s,e',v'}}{g_{s,e,v}} \cdot e^{\frac{hc}{\lambda^{e',v'}_{s,e,v} \cdot k_B T}} - 1}{e^{\frac{hc}{\lambda^{e',v'}_{s,e,v} \cdot k_B T}} - 1} \ . \tag{2.103}$$

And since Einstein coefficients don't depend on macroscopic variables, the left hand side of equation (2.103) doesn't depend on T, neither the right hand side (due to the equality relation). By knowing that the derivative of the right hand side in respect of T needs to be null, one can get the result

$$\frac{B^{e,v}_{s,e',v'}}{B^{e',v'}_{s,e,v}} = \frac{g_{s,e,v}}{g_{s,e',v'}} \ . \tag{2.104}$$

And by substitution of (2.104) in (2.103), it's possible to obtain

$$\frac{A^{e',v'}_{s,e,v}}{B^{e',v'}_{s,e,v}} = \frac{2hc^2}{\left(\lambda^{e',v'}_{s,e,v}\right)^5} \ . \tag{2.105}$$

Equations (2.104) and (2.105) allows the computation of two Einstein coefficients from knowledge of the other one.

It's important to mention that some authors consider a different definition for the Einstein coefficients. For instance, Vincenti and Kruger [3] consider an Einstein coefficient for spontaneous emission which is given by the one employed here divided by 4π. And for the induced emission and absorption processes they consider Einstein coefficients which are given by the ones employed here divided by 4π as well as by $\left(\lambda^{e',v'}_{s,e,v}\right)^2/c$. The reason for the second division is due to the fact that Vincenti and Kruger regard a specific radiative intensity in (2.94) and (2.96), which is with respect to frequency instead of wavelength.

2.5.2.3 Emission and absorption coefficients

Each element of matter in a system may emit and absorb photons. The *emission coefficient* j_λ is defined as the radiative energy emitted at wavelengths $\lambda \in [\lambda,\, \lambda + d\lambda]$ and at angles $\varphi \in [\varphi,\, \varphi + d\varphi]$ and $\theta \in [\theta,\, \theta + d\theta]$, per unit of volume, time, solid angle and wavelength, by particles in the element of volume $[x,\, x+dx] \times [y,\, y+dy] \times [z,\, z+dz]$ during the interval of time $[t,\, t+dt]$. On the other hand, the *absorption coefficient* k_λ multiplied by the specific radiative intensity I_λ corresponds to the radiative energy absorbed at wavelengths $\lambda \in [\lambda,\, \lambda+d\lambda]$ and at angles $\varphi \in [\varphi,\, \varphi+d\varphi]$ and $\theta \in [\theta,\, \theta+d\theta]$ by particles in the element of volume $[x,\, x+dx] \times [y,\, y+dy] \times [z,\, z+dz]$ during the interval of time $[t,\, t+dt]$. The variation in time of the volumetric radiative energy in $\vec{r} \in [x,\, x+dx] \times [y,\, y+dy] \times [z,\, z+dz]$ during the interval of time $[t,\, t+dt]$ due to solely emission and absorption of photons with wavelengths $\lambda \in [\lambda,\, \lambda+d\lambda]$ and direction angles $\varphi \in [\varphi,\, \varphi+d\varphi]$ and $\theta \in [\theta,\, \theta,+d\theta]$, per unit of solid angle and wavelength, by particles in this same element of volume is then given by

$$\frac{d^2\dot{\Omega}_{\text{rad}}}{d\Omega d\lambda}(\vec{r},t,\varphi,\theta,\lambda) = j_\lambda(\vec{r},t,\varphi,\theta,\lambda) - k_\lambda(\vec{r},t,\varphi,\theta,\lambda) \cdot I_\lambda(\vec{r},t,\varphi,\theta,\lambda) \tag{2.106}$$

From the definitions of the Einstein coefficients for spontaneous emission (2.92) and induced emission (2.96) it can be shown that, if solely bound-bound transitions occur in the system, the emission coefficient is given by

$$j_\lambda(\vec{r},t,\varphi,\theta,\lambda) = \frac{hc}{\lambda}\left\{\left[\sum_{\text{se}} \frac{A^{e',v'}_{s,e,v}}{4\pi}\,\phi^{e',v'}_{\lambda,s,e,v}(\vec{r},t,\lambda)\,n_{s,e,v}(\vec{r},t)\right] + I_\lambda(\vec{r},t,\varphi,\theta,\lambda)\left[\sum_{\text{ie}} \frac{B^{e',v'}_{s,e,v}}{4\pi}\,\phi^{e',v'}_{\lambda,s,e,v}(\vec{r},t,\lambda)\,n_{s,e,v}(\vec{r},t)\right]\right\}\ , \tag{2.107}$$

where the sums are done in all the spontaneous and induced emission processes of all heavy particles[12]. And similarly, from the definition of the Einstein coefficient for absorption (2.94), it can be shown that the absorption coefficient is given by

$$k_\lambda(\vec{r},t,\varphi,\theta,\lambda) = \frac{hc}{\lambda}\left[\sum_{\text{a}} \frac{B^{e,v}_{s,e',v'}}{4\pi}\,\phi^{e',v'}_{\lambda,s,e,v}(\vec{r},t,\lambda)\,n_{s,e',v'}(\vec{r},t)\right]\ , \tag{2.108}$$

being the sum done in all the absorption processes of all heavy particles.

2.6 Fluid flow governing equations

The formulation of balance equations for mass, linear momentum and energy of a *multicomponent fluid*[13] flow requires the definition of *control volumes* that properly account the presence of several different species. Let $\mathscr{V}(t)$ be some space in the fluid and $\partial\mathscr{V}(t)$ its boundary. The space may vary in time and therefore also its boundary, hence the instant of time t in their arguments. Let $B_s(t)$ correspond to some extensive physical quantity associated to the s-th species in the space $\mathscr{V}(t)$ and $\beta_s(\vec{r},t)$ the respective specific (in a mass basis) quantity. The two quantities are related to each other through

$$B_s(t) = \iiint_{\mathscr{V}(t)} \rho_s(\vec{r},t)\beta_s(\vec{r},t)\,dV\ . \tag{2.109}$$

The variation in time of $B_s(t)$ is given according to the *Reynolds transport theorem*[14] by

$$\frac{dB_s}{dt}(t) = \frac{d}{dt}\left(\iiint_{\mathscr{V}(t)} \rho_s(\vec{r},t)\beta_s(\vec{r},t)\,dV\right) = \iiint_{\mathscr{V}(t)} \frac{\partial\left[\rho_s(\vec{r},t)\beta_s(\vec{r},t)\right]}{\partial t}\,dV + \oiint_{\partial\mathscr{V}(t)} \rho_s(\vec{r},t)\beta_s(\vec{r},t)\,(\vec{v}\cdot\vec{n})\,dS\ , \tag{2.110}$$

being $\vec{v}$ the velocity of a point on the surface that represents the boundary $\partial\mathscr{V}(t)$, and $\vec{n}$ the respective outward-pointing normal vector at that point.

Physical laws may be applied more conveniently if $\mathscr{V}(t)$ is chosen so that the boundary $\partial\mathscr{V}(t)$ moves with the average bulk of particles of the s-th species, implying that $\vec{v} = \vec{u}_s$ in (2.110), being $\vec{u}_s$ the flow velocity[15] of s-th species particles. Let $\mathscr{V}_s(t) = \mathscr{V}(t)$ be the space and $\partial\mathscr{V}_s(t) = \partial\mathscr{V}_s$ its boundary in such

[12] Although the notation employed in (2.107) is solely with respect to the molecular particles, it does as well implicitly refer to the atomic particles (for which the labels v and v' should be supressed).

[13] A multicomponent fluid is one which is constituted by multiple chemical species.

[14] The Reynolds transport theorem is also referred to as the *Leibniz integral rule*.

[15] The flow is considered to be constituted by a continuum of material and therefore the velocity that one needs to regard (the so-called flow velocity) corresponds to an average of the velocities of the individual particles.

circumstances. The Reynolds transport theorem (2.110) would then give

$$\frac{dB_s}{dt}(t) = \frac{d}{dt}\left(\iiint_{\mathscr{V}_s(t)} \rho_s(\vec{r},t)\beta_s(\vec{r},t)\,dV\right) = \iiint_{\mathscr{V}_s(t)} \frac{\partial\left[\rho_s(\vec{r},t)\beta_s(\vec{r},t)\right]}{\partial t}\,dV + \oiint_{\partial\mathscr{V}_s(t)} \rho_s(\vec{r},t)\beta_s(\vec{r},t)\left(\vec{u}_s\cdot\vec{n}\right)\,dS\ . \tag{2.111}$$

Note that the particles of different species may move with different flow velocities $\vec{u}_s$, due to the *mass diffusion* phenomenon [3]. A flow velocity is attributed to the mixture, corresponding to a mass average of the species flow velocities:

$$\vec{u} := \frac{\sum_s M_s\vec{u}_s}{\sum_s M_s} = \sum_s c_s\vec{u}_s\ . \tag{2.112}$$

This quantity corresponds to the so called *mixture flow velocity*. The flow motion of the s-th species relatively to the mixture is described by the respective *diffusion flow velocity* and the *mass diffusion flux vector* - a physical quantity that needs to be modelled. These two quantities are given by

$$\vec{u'}_s := \vec{u}_s - \vec{u}\ , \tag{2.113}$$

$$\vec{J}_s := \rho_s\vec{u'}_s\ , \tag{2.114}$$

respectively. Let $\mathscr{S}$ be some surface and $\vec{n}$ its normal vector. The quantity $\iint_{\mathscr{S}}\left(\vec{J}_s\cdot\vec{n}\right)\,dS$ gives the mass of s-th species particles that escapes from the mixture (in which it was previously in) through the surface $\mathscr{S}$ to the neighbour domain that $\vec{n}$ points to, per unit of time. The diffusive motion of the s-th species occurs with a gradient in the mass fraction of the s-th species c_s or even with a gradient in the temperatures [3]. For the most cases the latter contribution can be disregarded, since it is usually much smaller than the former contribution [1]. It's worthy to mention that the sum of the mass diffusion flux vectors in all species is null, i.e.

$$\sum_s \vec{J}_s = \vec{0}\ , \tag{2.115}$$

which can be shown by simply invoking relations (2.112) and (2.113).

Let's now consider a space $\mathscr{V}(t)$ whose boundary $\partial\mathscr{V}(t)$ moves with the bulk velocity $\vec{u}$. Let's also consider a space $\mathscr{V}_s(t)$ whose boundary $\partial\mathscr{V}_s(t)$ moves with the flow velocity of the s-th species particles. The space $\mathscr{V}_s(t)$ is chosen so that it matches $\mathscr{V}(t)$ in the instant of time t. An illustrative evolution in time of $\mathscr{V}_s(t)$ and $\mathscr{V}_q(t)$ (being q the q-th species) is depicted by Figure 2.6, as well as the respective flow velocities of their centres $\vec{u}_s(t)$ and $\vec{u}_q(t)$. This picture is found to be helpful in the treatment of the following sections.

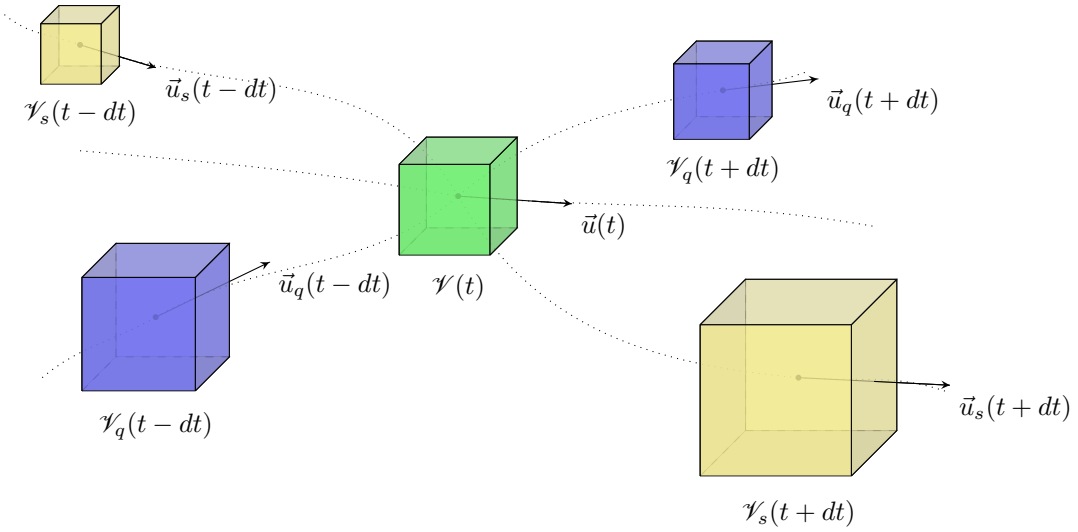

Figure 2.6: Evolution in time of two spaces $\mathscr{V}_s(t)$ and $\mathscr{V}_q(t)$ whose boundaries move with flow velocities associated to the s-th and q-th species, respectively. The two spaces match the mixture space $\mathscr{V}(t)$ at instant t.

2.6.1 The case of the single-temperature model

2.6.1.1 Balance equation for mass

The balance equation for the mass of the s-th species particles may be obtained through (2.111) with $\beta_s = 1$. The variation of mass of the s-th species particles M_s in the space $\mathscr{V}_s$ can only happen through chemical reactions occurring inside it. Let $\dot{\omega}_s$ be the variation of mass of the s-th species particles per unit of time and per unit of volume due to these chemical reactions[16]. One has then $\frac{dB_s}{dt} = \iiint_{\mathscr{V}_s(t)} \dot{\omega}_s \, dV$ on the left side of equation (2.111), which ultimately leads to

$$\iiint_{\mathscr{V}_s(t)} \dot{\omega}_s \, dV = \iiint_{\mathscr{V}_s(t)} \frac{\partial \rho_s}{\partial t} \, dV + \oiint_{\partial \mathscr{V}_s(t)} \rho_s \left(\vec{u}_s \cdot \vec{n} \right) \, dS, \qquad \forall s \ . \tag{2.116}$$

By applying the *divergence theorem* to the surface integral in (2.116), and choosing an elementary space $\mathscr{V}_s$, it's possible to express (2.116) through

$$\dot{\omega}_s \, dV = \frac{\partial \rho_s}{\partial t} \, dV + \operatorname{div}\left(\rho_s \vec{u}_s\right) \, dV \Leftrightarrow \frac{\partial \rho_s}{\partial t} + \operatorname{div}\left(\rho_s \vec{u}_s\right) = \dot{\omega}_s, \qquad \forall s \ . \tag{2.117}$$

And by using relations (2.113) and (2.114), one can obtain the final form of a differential equation for the balance of mass of the s-th species particles [50]:

$$\frac{\partial \rho_s}{\partial t} + \operatorname{div}\left(\rho_s \vec{u}\right) = -\operatorname{div}\left(\vec{J}_s\right) + \dot{\omega}_s, \qquad \forall s \ . \tag{2.118}$$

[16] A way to compute $\dot{\omega}_s$ was described in section §2.4.1.1.

2.6.1.2 Balance equation for momentum

The balance equation for the momentum of the s-th species particles may be obtained through (2.111) with $\beta_s = \vec{u}_s$. According to the *Newton's second law* the variation in time of the momentum of s-th species particles inside the space $\mathscr{V}_s$ is equal to the resultant of all forces applied on them: $\vec{F}_s = \vec{F}^{\text{ext}}_{s,B} + \vec{F}^{\text{ext}}_{s,S} + \sum_q \vec{F}^{\text{int}}_{q,s}$. The contribution $\vec{F}^{\text{ext}}_{s,B} = \iiint_{\mathscr{V}_s(t)} \rho_s \vec{f}_s \, dV$ corresponds to the external *body force* (e.g. gravity) applied to the s-th species particles in the space $\mathscr{V}_s$ (being $\vec{f}_s$ the respective specific (in a mass basis) force). The contribution $\vec{F}^{\text{ext}}_{s,S} = \oiint_{\partial\mathscr{V}_s(t)} ([\sigma_s] \cdot \vec{n}) \, dS = \iiint_{\mathscr{V}_s(t)} \operatorname{div}([\sigma_s]) \, dV$, corresponds to the *surface force* applied by the outer particles to the s-th species inner particles of the space $\mathscr{V}_s$. The tensor $[\sigma_s]$ corresponds to the *Cauchy's stress tensor* associated to the s-th species, which is a sum of two contributions, one due to viscosity and another due to pressure, $[\sigma_s] = [\tau_s] - p_s[I]$, being $[\tau_s]$ the *viscous stress tensor* associated to the s-th species and $[I]$ the *identity tensor*. Lastly, $\sum_q \vec{F}^{\text{int}}_{q,s}$ is the sum of the forces applied by all the inner particles to the s-th species inner particles of the space $\mathscr{V}_s$. One has then $\frac{dB_s}{dt} = \vec{F}_s$ on the left side of equation (2.111), which by invoking the divergence theorem for the surface integral on the right side, ultimately gives

$$\iiint_{\mathscr{V}_s(t)} \rho_s \vec{f}_s \, dV + \iiint_{\mathscr{V}_s(t)} \operatorname{div}([\sigma_s]) \, dV + \sum_q \vec{F}^{\text{int}}_{q,s} = \iiint_{\mathscr{V}_s(t)} \frac{\partial(\rho_s \vec{u}_s)}{\partial t} \, dV + \iiint_{\mathscr{V}_s(t)} \operatorname{div}(\rho_s \vec{u}_s \otimes \vec{u}_s) \, dV, \qquad \forall s \; . \tag{2.119}$$

It's particularly useful to sum (2.119) in all species (i.e. in s). It's difficult to evaluate $\sum_q \vec{F}^{\text{int}}_{q,s}$, but it's trivially easy to evaluate $\sum_{s,q} \vec{F}^{\text{int}}_{q,s}$: this quantity is null due to the *Newton's third law*[17]. Also, by knowing that $\mathscr{V}_s = \mathscr{V}$ for all s at instant t, and by choosing an elementary space $\mathscr{V}$, the sum of (2.119) in s can be shown to give

$$\left(\sum_s \rho_s \vec{f}_s\right) dV + \operatorname{div}\left(\sum_s [\sigma_s]\right) dV = \frac{\partial\left(\sum_s \rho_s \vec{u}_s\right)}{\partial t} dV + \operatorname{div}\left(\sum_s \rho_s \vec{u}_s \otimes \vec{u}_s\right) dV \Leftrightarrow$$

$$\Leftrightarrow \frac{\partial\left(\sum_s \rho_s \vec{u}_s\right)}{\partial t} + \operatorname{div}\left(\sum_s \rho_s \vec{u}_s \otimes \vec{u}_s\right) = \operatorname{div}\left(\sum_s [\sigma_s]\right) + \left(\sum_s \rho_s \vec{f}_s\right) \; . \tag{2.120}$$

One can define a Cauchy's stress tensor for the mixture expressed by

$$[\sigma] := \sum_s [\sigma_s] = [\tau] - p[I] \; , \tag{2.121}$$

being $[\tau] := \sum_s [\tau_s]$ the respective mixture viscous stress tensor. By regarding the mixture as a *Newtonian fluid* and by assuming the *Stokes' hypothesis*[18], it's possible to show that the i,j-th entry of the mixture viscous stress tensor τ_{ij} is given by

$$\tau_{ij} = \mu\left(\frac{\partial u_i}{\partial x_j} + \frac{\partial u_j}{\partial x_i}\right) \underbrace{-\frac{2}{3}\mu}_{=\lambda} \delta_{ij} \sum_i \frac{\partial u_i}{\partial x_i} \; , \tag{2.122}$$

[17] When one body exerts a force on a second body, the second body simultaneously exerts a force equal in magnitude and opposite in direction on the first body.

[18] The Stokes hypothesis considers that the *bulk viscosity* λ and the *dynamic viscosity* μ are related to each other by $\lambda = -\frac{2}{3}\mu$.

being δ_{ij} a Kronecker delta and μ the so-called *mixture dynamic viscosity coefficient* - a physical quantity that needs to be modelled. Let's now evaluate the sums on the left side of (2.120). By invoking relations (2.113), (2.114) and (2.115), and by assuming that all $\vec{J}_s$ vectors are sufficiently small (first-order infinitesimals) such that the products between their components are negligible, it can be shown that the sums are given by

$$\sum_s \rho_s \underbrace{\vec{u}_s}_{=\vec{u}+\vec{u'}_s} = \underbrace{\left(\sum_s \rho_s\right)}_{=\rho} \vec{u} + \underbrace{\sum_s \underbrace{\rho_s \vec{u'}_s}_{=J_s}}_{=\vec{0}} = \rho\vec{u} \ , \tag{2.123}$$

and

$$\sum_s \rho_s \underbrace{\vec{u}_s}_{=\vec{u}+\vec{u'}_s} \otimes \underbrace{\vec{u}_s}_{=\vec{u}+\vec{u'}_s} = \sum_s \rho_s \left(\vec{u}+\vec{u'}_s\right) \otimes \left(\vec{u}+\vec{u'}_s\right) =$$

$$= \underbrace{\left(\sum_s \rho_s\right)}_{=\rho} \vec{u}\otimes\vec{u} + \vec{u}\otimes \underbrace{\left(\sum_s \underbrace{\rho_s \vec{u'}_s}_{\vec{J}_s}\right)}_{=\vec{0}} + \underbrace{\left(\sum_s \underbrace{\rho_s \vec{u'_s}}_{\vec{J}_s}\right)}_{=\vec{0}} \otimes \vec{u} + \underbrace{\sum_s \underbrace{\rho_s \vec{u'}_s}_{=\vec{J}_s} \otimes \underbrace{\vec{u'}_s}_{=\vec{J}_s/\rho_s}}_{\approx[0]} = \rho\vec{u}\otimes\vec{u} \ , \tag{2.124}$$

respectively. By inserting the results (2.121), (2.123) and (2.124) into (2.120), one can obtain the final form of a differential equation for the balance of momentum of the mixture particles [50]:

$$\frac{\partial(\rho\vec{u})}{\partial t} + \operatorname{div}(\rho\vec{u}\otimes\vec{u}) = \operatorname{div}([\tau]) - \vec{\nabla}p + \left(\sum_s \rho_s \vec{f}_s\right) \ . \tag{2.125}$$

2.6.1.3 Balance equation for energy

The balance equation for the energy of the s-th species particles may be obtained through (2.111) with $\beta_s = e_s + \frac{1}{2}u_s^2$, i.e. the sum of the mass-specific internal and kinetic energies of the flow associated to the s-th species. The variation in time of the energy of s-th species particles inside the space $\mathscr{V}_s$ is equal to the sum of the rates of energy transfer through heat and work between the inner s-th species particles and the complementary system: $\dot{\mathscr{E}}_s = \dot{Q}_s^{\text{ext}} + \dot{W}_{s,B}^{\text{ext}} + \dot{W}_{s,S}^{\text{ext}} + \sum_q \dot{\mathscr{E}}_{q,s}^{\text{int}}$. The contribution $\dot{Q}_s^{\text{ext}} = -\oiint_{\partial\mathscr{V}_s(t)} (\vec{q}_s\cdot\vec{n})\, dS = -\iiint_{\mathscr{V}_s(t)} \operatorname{div}(\vec{q}_s)\, dV$, where $\vec{q}_s$ is the *heat flux vector* associated to the s-th species, corresponds to the rate of heat transferred from the outer particles to the s-th species particles inside the space $\mathscr{V}_s$. The contribution $\dot{W}_{s,B}^{\text{ext}} = \iiint_{\mathscr{V}_s(t)} \left(\rho_s\vec{f}_s\cdot\vec{u}_s\right) dV$ corresponds to the rate of work done by the external body forces on the inner s-th species particles. The contribution $\dot{W}_{s,S}^{\text{ext}} = \oiint_{\partial V_s(t)} ([\sigma_s]\cdot\vec{n})\cdot\vec{u}_s\, dS = \iiint_{\mathscr{V}_s(t)} \operatorname{div}([\sigma_s]\cdot\vec{u}_s)\, dV$ corresponds to the rate of work done by the surface forces applied by the outer particles on the inner s-th species ones. And $\sum_q \dot{\mathscr{E}}_{q,s}^{\text{int}}$ is the sum of the rates of energy transfer from all the inner particles to the inner s-th species particles. One has then $\frac{dB_s}{dt} = \dot{\mathscr{E}}_s$ on the left side of equation (2.111), which by invoking the divergence theorem for the surface integral on the right side, gives

$$-\iiint_{\mathscr{V}_s(t)} \operatorname{div}(\vec{q}_s)\, dV + \iiint_{\mathscr{V}_s(t)} \left(\rho_s\vec{f}_s\cdot\vec{u}_s\right) dV + \iiint_{\mathscr{V}_s(t)} \operatorname{div}([\sigma_s]\cdot\vec{u}_s)\, dV + \sum_q \dot{\mathscr{E}}_{q,s}^{\text{int}} =$$

$$= \iiint_{\mathscr{V}_s(t)} \frac{\partial\left[\rho_s\left(e_s+\frac{1}{2}u_s^2\right)\right]}{\partial t} dV + \iiint_{\mathscr{V}_s(t)} \operatorname{div}\left[\rho_s\left(e_s+\frac{1}{2}u_s^2\right)\vec{u}_s\right] dV, \qquad \forall s \ . \tag{2.126}$$

As happened with the balance of momentum, it's of particular interest to sum (2.126) in all species (i.e. in s). It's difficult to evaluate $\sum_q \dot{\mathscr{E}}^{\text{int}}_{q,s}$, but it's trivially easy to evaluate $\sum_{s,q} \dot{\mathscr{E}}^{\text{int}}_{q,s}$: this quantity is null, since the energy transferred from one particle to another is the symmetric of the energy transferred from the latter to the former. By knowing that $\mathscr{V}_s = \mathscr{V}$ for all s at instant t, and by choosing an elementary space $\mathscr{V}$, the sum of (2.126) in s can be shown to give

$$
\begin{aligned}
&-\operatorname{div}\left(\sum_s \vec{q}_s\right) dV + \left(\sum_s \rho_s \vec{f}_s \cdot \vec{u}_s\right) dV + \operatorname{div}\left(\sum_s [\sigma_s] \cdot \vec{u}_s\right) dV = \\
&\qquad = \frac{\partial \left[\sum_s \rho_s \left(e_s + \frac{1}{2}u_s^2\right)\right]}{\partial t} dV + \operatorname{div}\left[\sum_s \rho_s \left(e_s + \frac{1}{2}u_s^2\right) \vec{u}_s\right] dV \Leftrightarrow \\
&\Leftrightarrow \frac{\partial \left[\sum_s \rho_s \left(e_s + \frac{1}{2}u_s^2\right)\right]}{\partial t} + \operatorname{div}\left[\sum_s \rho_s \left(e_s + \frac{1}{2}u_s^2\right) \vec{u}_s\right] = -\operatorname{div}\left(\sum_s \vec{q}_s\right) + \operatorname{div}\left(\sum_s [\sigma_s] \cdot \vec{u}_s\right) + \left(\sum_s \rho_s \vec{f}_s \cdot \vec{u}_s\right) \ .
\end{aligned}
\tag{2.127}
$$

The three sums on the right side of (2.127) require particular attention. Let $\vec{q} = \sum_s \vec{q}_s$ be the mixture heat flux vector. This physical quantity has two contributions, one due to conduction $\vec{q}_{\text{c}}$, and another due to radiation $\vec{q}_{\text{rad}}$. The *Fourier's law* states that heat conduction occurs with a gradient of temperature [1], i.e. $\vec{q}_{\text{c}} = -k\vec{\nabla}T$, being k the mixture *thermal conductivity coefficient* - a physical quantity that needs to be modelled. The radiative heat flux vector corresponds to $\vec{q}_{\text{rad}} = \int_0^{\pi} \left[\int_0^{2\pi} \left(\int_0^{\infty} I_\lambda \vec{e}_s \, d\lambda\right) d\varphi\right] \sin\theta \, d\theta$, being $\vec{e}_s = \cos\varphi \sin\theta \vec{e}_x + \sin\varphi \sin\theta \vec{e}_y + \cos\theta \vec{e}_z$ the unit vector for the direction of propagation of the photons at angles φ and θ. One may then write

$$
\vec{q} = \vec{q}_{\text{c}} + \vec{q}_{\text{rad}} = -k\vec{\nabla}T + \int_0^{\pi} \left[\int_0^{2\pi} \left(\int_0^{\infty} I_\lambda \vec{e}_s \, d\lambda\right) d\varphi\right] \sin\theta \, d\theta \ . \tag{2.128}
$$

By invoking relations (2.113) and (2.114), and by assuming that all $\vec{J}_s$ vectors and all $[\tau_s]$ tensors are sufficiently small (first order infinitesimals) such that products between their components are negligible, the second and third sums on the right side of (2.127) can be shown to give

$$
\begin{aligned}
\sum_s [\sigma_s] \cdot \vec{u}_s &= \sum_s \left([\tau_s] - p_s[I]\right) \cdot \underbrace{\vec{u}_s}_{=\vec{u}+\vec{u'}_s} = \underbrace{\left(\sum_s [\tau_s]\right)}_{=[\tau]} \cdot \vec{u} + \underbrace{\left(\sum_s [\tau_s] \cdot \underbrace{\vec{u'}_s}_{=\vec{J}_s/\rho_s}\right)}_{\approx \vec{0}} - \underbrace{\left(\sum_s p_s\right)}_{=p} \vec{u} - \left(\sum_s p_s \vec{u'}_s\right) = \\
&= [\tau] \cdot \vec{u} - p\vec{u} - \left(\sum_s \frac{p_s}{\rho_s} \underbrace{\rho_s \vec{u'}_s}_{=\vec{J}_s}\right) = [\tau] \cdot \vec{u} - p\vec{u} - \left(\sum_s \frac{p_s}{\rho_s} \vec{J}_s\right) \ ,
\end{aligned}
\tag{2.129}
$$

and

$$
\sum_s \rho_s \vec{f}_s \cdot \underbrace{\vec{u}_s}_{=\vec{u}+\vec{u'}_s} = \left(\sum_s \rho_s \vec{f}_s \cdot \vec{u}\right) + \left(\sum_s \rho_s \vec{f}_s \cdot \underbrace{\vec{u'}_s}_{=\vec{J}_s/\rho_s}\right) = \sum_s \rho_s \vec{f}_s \cdot \left(\vec{u} + \frac{\vec{J}_s}{\rho_s}\right) \ . \tag{2.130}
$$

Let's now evaluate the sums on the left side of (2.127). By invoking relations (2.113), (2.114) and

(2.115), it can be shown that the sums are given by

$$\sum_s \rho_s \left(e_s + \frac{1}{2} u_s^2 \right) = \left(\sum_s \underbrace{\rho_s}_{=\rho c_s} e_s \right) + \left(\sum_s \underbrace{\frac{1}{2} \rho_s u_s^2}_{= \frac{1}{2}\rho_s \left[u^2 + 2\left(\vec{u} \cdot \vec{u'}_s \right) + {u'_s}^2 \right]} \right) =$$

$$= \rho \underbrace{\left(\sum_s c_s e_s \right)}_{=e} + \frac{1}{2} \underbrace{\left(\sum_s \rho_s \right)}_{=\rho} u^2 + \underbrace{\left(\sum_s \underbrace{\rho_s \vec{u'}_s}_{=\vec{J}_s} \right)}_{=\vec{0}} \cdot \vec{u} + \left(\sum_s \frac{1}{2} \underbrace{\rho_s {u'}_s^2}_{=J_s^2/\rho_s \approx 0} \right) = \rho \left(e + \frac{1}{2} u^2 \right) , \qquad (2.131)$$

and

$$\sum_s \rho_s \left(e_s + \frac{1}{2} u_s^2 \right) \underbrace{\vec{u}_s}_{=\vec{u}+\vec{u'}_s} = \underbrace{\left(\sum_s \rho_s e_s \right)}_{=\rho e} \vec{u} + \left(\sum_s e_s \underbrace{\rho_s \vec{u'}_s}_{=\vec{J}_s} \right) + \underbrace{\left(\sum_s \frac{1}{2} \rho_s u_s^2 \right)}_{\approx \frac{1}{2}\rho u^2} \vec{u} + \left(\sum_s \underbrace{\frac{1}{2} \rho_s u_s^2 \vec{u'}_s}_{= \frac{1}{2}\rho_s \left[u^2 + 2\left(\vec{u} \cdot \vec{u'}_s \right) + {u'_s}^2 \right] \vec{u'}_s} \right) =$$

$$= \left[\rho \left(e + \frac{1}{2} u^2 \right) \right] \vec{u} + \left(\sum_s e_s \vec{J}_s \right) + \frac{1}{2} u^2 \underbrace{\left(\sum_s \underbrace{\rho_s \vec{u'}_s}_{=\vec{J}_s} \right)}_{=\vec{0}} + \underbrace{\left[\sum_s \left(\vec{u} \cdot \underbrace{\vec{u'}_s}_{=\vec{J}_s/\rho_s} \right) \underbrace{\rho_s \vec{u'}_s}_{=\vec{J}_s} \right]}_{\approx \vec{0}} + \left(\sum_s \frac{1}{2} \underbrace{\rho_s {u'_s}^2}_{J_s^2/\rho_s \approx 0} \vec{u'}_s \right) =$$

$$= \left[\rho \left(e + \frac{1}{2} u^2 \right) \right] \vec{u} + \left(\sum_s e_s \vec{J}_s \right) . \qquad (2.132)$$

respectively. By inserting the results (2.129), (2.130), (2.131) and (2.132) into (2.127), one can then write the final form of a differential equation for the energy of the mixture particles [50]:

$$\frac{\partial \left[\rho \left(e + \frac{1}{2} u^2 \right) \right]}{\partial t} + \operatorname{div} \left[\rho \left(e + \frac{1}{2} u^2 \right) \vec{u} \right] + \operatorname{div} \left(\sum_s e_s \vec{J}_s \right) =$$

$$= -\operatorname{div} \left(\vec{q} \right) + \operatorname{div} \left([\tau] \cdot \vec{u} \right) - \operatorname{div} \left(p \vec{u} \right) - \operatorname{div} \left(\sum_s \frac{p_s}{\rho_s} \vec{J}_s \right) + \sum_s \rho_s \vec{f}_s \cdot \left(\vec{u} + \frac{\vec{J}_s}{\rho_s} \right) \Leftrightarrow$$

$$\Leftrightarrow \frac{\partial \left[\rho \left(e + \frac{1}{2} u^2 \right) \right]}{\partial t} + \operatorname{div} \left[\rho \left(e + \frac{1}{2} u^2 \right) \vec{u} \right] =$$

$$= \operatorname{div} \left([\tau] \cdot \vec{u} \right) - \operatorname{div} \left(p \vec{u} \right) - \operatorname{div} \left(\vec{q} \right) - \operatorname{div} \left[\sum_s \underbrace{\left(e_s + \frac{p_s}{\rho_s} \right)}_{=h_s} \vec{J}_s \right] + \sum_s \rho_s \vec{f}_s \cdot \left(\vec{u} + \frac{\vec{J}_s}{\rho_s} \right) \Leftrightarrow$$

$$\Leftrightarrow \frac{\partial \left[\rho \left(e + \frac{1}{2} u^2 \right) \right]}{\partial t} + \operatorname{div} \left[\rho \left(e + \frac{1}{2} u^2 \right) \vec{u} \right] =$$

$$= \operatorname{div} \left([\tau] \cdot \vec{u} \right) - \operatorname{div} \left(p \vec{u} \right) - \operatorname{div} \left(\vec{q} \right) - \operatorname{div} \left(\sum_s h_s \vec{J}_s \right) + \sum_s \rho_s \vec{f}_s \cdot \left(\vec{u} + \frac{\vec{J}_s}{\rho_s} \right) . \qquad (2.133)$$

It should be mentioned that the term $\operatorname{div}\left(\sum_s h_s \vec{J}_s\right)$ in (2.133) doesn't usually appears in an explicit form but implicitly through the definition of the heat flux vector $\vec{q}$. However, the author avoided to make such consideration here, since it is a matter of subjectivity.

2.6.1.4 Balance equation for radiative energy

A balance equation for the radiative energy needs to be regarded in order to evaluate $\operatorname{div}(\vec{q}_{\text{rad}})$. It will be considered here that the vibronic-specific bound-bound transitions are the only radiative processes that may occur. Let's consider a space $\mathscr{V}_\gamma(t)$ whose boundary $\partial\mathscr{V}_\gamma(t)$ moves with the velocity of photons with wavelength λ and angles φ and θ. Let $\mathscr{E}_\gamma(t)$ be the radiant energy in $\mathscr{V}_\gamma(t)$ at instant t and $\varepsilon_\gamma(\vec{r},t) = (d\mathscr{E}_\gamma/dV)(\vec{r},t)$ the respective volumetric radiant energy. Note that one may also write $\mathscr{E}_\gamma(t) = \iiint_{\mathscr{V}_\gamma(t)} \varepsilon_\gamma(\vec{r},t)\,dV$. It can be easily shown that [3]

$$\frac{d^2\varepsilon_\gamma}{d\Omega\,d\lambda}(\vec{r},t,\varphi,\theta,\lambda) = \frac{I_\lambda(\vec{r},t,\varphi,\theta,\lambda)}{c}\ . \tag{2.134}$$

Since the boundary $\partial\mathscr{V}_\gamma(t)$ moves with the photons of wavelength λ and angles φ and θ, the variation in time of the respective radiative energy in $\mathscr{V}_\gamma(t)$ is solely due to emission and absorption from particles in this same space. One has then from (2.106)

$$\frac{d}{dt}\left(\frac{d^2\mathscr{E}_\gamma}{d\Omega\,d\lambda}\right) = \iiint_{\mathscr{V}_\gamma(t)} \frac{d^2\dot{\Omega}_{\text{rad}}}{d\Omega\,d\lambda}\,dV = \iiint_{\mathscr{V}_\gamma(t)} \left[j_\lambda - k_\lambda \cdot I_\lambda\right]\,dV\ . \tag{2.135}$$

And by invoking the Reynolds transport theorem (2.111), the results (2.134) and (2.135) as well as the divergence theorem, it's possible to obtain the so-called *equation of radiative transfer*:

$$\frac{d}{dt}\left(\frac{d^2\mathscr{E}_\gamma}{d\Omega\,d\lambda}\right) = \iiint_{\mathscr{V}_\gamma(t)} \frac{\partial}{\partial t}\left(\frac{d^2\varepsilon_\gamma}{d\Omega\,d\lambda}\right)\,dV + \oiint_{\partial\mathscr{V}_\gamma(t)} \frac{d^2\varepsilon_\gamma}{d\Omega\,d\lambda}\,(\vec{c}\cdot\vec{n})\,dS \Leftrightarrow$$

$$\Leftrightarrow \iiint_{\mathscr{V}_\gamma(t)} \left[j_\lambda - k_\lambda \cdot I_\lambda\right]\,dV = \frac{1}{c}\iiint_{\mathscr{V}_\gamma(t)} \frac{\partial I_\lambda}{\partial t}\,dV + \iiint_{\mathscr{V}_\gamma(t)} \left(\vec{\nabla} I_\lambda \cdot \vec{e}_s\right)\,dV \Leftrightarrow$$

$$\frac{1}{c}\frac{\partial I_\lambda}{\partial t} + \left(\vec{\nabla} I_\lambda \cdot \vec{e}_s\right) = j_\lambda - k_\lambda \cdot I_\lambda\ . \tag{2.136}$$

The divergence of the radiative heat flux vector $\vec{q}_{\text{rad}}$ may be further developed using relation (2.136) and the definition of $\vec{q}_{\text{rad}}$ (the second term of (2.128)):

$$\operatorname{div}(\vec{q}_{\text{rad}}) = \int_0^\pi \left\{\int_0^{2\pi}\left[\int_0^\infty \left(\vec{\nabla} I_\lambda \cdot \vec{e}_s\right)\,d\lambda\right]\,d\varphi\right\}\sin\theta\,d\theta = \int_0^\pi \left\{\int_0^{2\pi}\left[\int_0^\infty \left(j_\lambda - k_\lambda \cdot I_\lambda - \frac{1}{c}\frac{\partial I_\lambda}{\partial t}\right)\,d\lambda\right]\,d\varphi\right\}\sin\theta\,d\theta\ . \tag{2.137}$$

And since solely bound-bound transitions are regarded, relations (2.107) and (2.108) for the emission and

absorption coefficients do hold, allowing one to transform (2.137) into

$$\begin{aligned}\operatorname{div}(\vec{q}_{\mathrm{rad}}) = hc\int_0^{\pi}\left\{\int_0^{2\pi}\left[\int_0^{\infty}\frac{1}{\lambda}\left(\sum_{\mathrm{se}}\frac{A_{s,e,v}^{e',v'}}{4\pi}\phi_{\lambda,s,e,v}^{e',v'}\,n_{s,e,v}\right)d\lambda\right]d\varphi\right\}\sin\theta\,d\theta \\ + hc\int_0^{\pi}\left\{\int_0^{2\pi}\left[\int_0^{\infty}\frac{I_\lambda}{\lambda}\left(\sum_{\mathrm{ie}}\frac{B_{s,e,v}^{e',v'}}{4\pi}\phi_{\lambda,s,e,v}^{e',v'}\,n_{s,e,v}\right)d\lambda\right]d\varphi\right\}\sin\theta\,d\theta \\ - hc\int_0^{\pi}\left\{\int_0^{2\pi}\left[\int_0^{\infty}\frac{I_\lambda}{\lambda}\left(\sum_{\mathrm{a}}\frac{B_{s,e',v'}^{e,v}}{4\pi}\phi_{\lambda,s,e,v}^{e',v'}\,n_{s,e',v'}\right)d\lambda\right]d\varphi\right\}\sin\theta\,d\theta \\ - \frac{1}{c}\int_0^{\pi}\left[\int_0^{2\pi}\left(\int_0^{\infty}\frac{\partial I_\lambda}{\partial t}\,d\lambda\right)d\varphi\right]\sin\theta\,d\theta \Leftrightarrow\end{aligned}$$

$$\begin{aligned}\Leftrightarrow \operatorname{div}(\vec{q}_{\mathrm{rad}}) = hc\left(\sum_{\mathrm{se}}A_{s,e,v}^{e',v'}\,n_{s,e,v}\int_0^{\infty}\frac{\phi_{\lambda,s,e,v}^{e',v'}}{\lambda}\,d\lambda\right) \\ + hc\left\{\sum_{\mathrm{ie}}\frac{B_{s,e,v}^{e',v'}}{4\pi}n_{s,e,v}\int_0^{\pi}\left[\int_0^{2\pi}\left(\int_0^{\infty}\frac{I_\lambda\phi_{\lambda,s,e,v}^{e',v'}}{\lambda}\,d\lambda\right)d\varphi\right]\sin\theta\,d\theta\right\} \\ - hc\left\{\sum_{\mathrm{a}}\frac{B_{s,e',v'}^{e,v}}{4\pi}n_{s,e',v'}\int_0^{\pi}\left[\int_0^{2\pi}\left(\int_0^{\infty}\frac{I_\lambda\phi_{\lambda,s,e,v}^{e',v'}}{\lambda}\,d\lambda\right)d\varphi\right]\sin\theta\,d\theta\right\} \\ - \frac{1}{c}\int_0^{\pi}\left[\int_0^{2\pi}\left(\int_0^{\infty}\frac{\partial I_\lambda}{\partial t}\,d\lambda\right)d\varphi\right]\sin\theta\,d\theta\ . \qquad (2.138)\end{aligned}$$

By taking the assumption that the ratio between the local variation in time of the specific radiant intensity divided by the speed of light is negligible (a usually valid hypothesis [3]), the last term in (2.138) may be disregarded, and one has $\operatorname{div}(\vec{q}_{\mathrm{rad}}) = \dot{\Omega}_{\mathrm{rad}}$, i.e. the divergence of the radiative heat flux vector $\operatorname{div}(\vec{q}_{\mathrm{rad}})$ corresponds to the volumetric radiative energy source term $\dot{\Omega}_{\mathrm{rad}}$ referred in (2.135). Therefore,

$$\begin{aligned}\Leftrightarrow \operatorname{div}(\vec{q}_{\mathrm{rad}}) = \dot{\Omega}_{\mathrm{rad}} = hc\left(\sum_{\mathrm{se}}A_{s,e,v}^{e',v'}\,n_{s,e,v}\int_0^{\infty}\frac{\phi_{\lambda,s,e,v}^{e',v'}}{\lambda}\,d\lambda\right) \\ + hc\left\{\sum_{\mathrm{ie}}\frac{B_{s,e,v}^{e',v'}}{4\pi}n_{s,e,v}\int_0^{\pi}\left[\int_0^{2\pi}\left(\int_0^{\infty}\frac{I_\lambda\phi_{\lambda,s,e,v}^{e',v'}}{\lambda}\,d\lambda\right)d\varphi\right]\sin\theta\,d\theta\right\} \\ - hc\left\{\sum_{\mathrm{a}}\frac{B_{s,e',v'}^{e,v}}{4\pi}n_{s,e',v'}\int_0^{\pi}\left[\int_0^{2\pi}\left(\int_0^{\infty}\frac{I_\lambda\phi_{\lambda,s,e,v}^{e',v'}}{\lambda}\,d\lambda\right)d\varphi\right]\sin\theta\,d\theta\right\}\ . \qquad (2.139)\end{aligned}$$

Equation (2.139) may be further simplified, although in a very crude way, by disregarding induced emission and by introducing the concept of a *escape factor* [51]. Let $\Lambda_{s,e,v}^{e',v'}$ be the escape factor associated to bound-bound transitions of the s-th species between the vibronic levels (e, v) and (e', v'). The designation of this quantity is self-explanatory: $\Lambda_{s,e,v}^{e',v'}$ corresponds to the fraction of the emitted photons due to spontaneous emissions from (e, v) to (e', v') which escape from the system, or in other words, that are not absorbed. This factor is limited to the interval [0, 1]. If $\Lambda_{s,e,v}^{e',v'} = 0$, none of the emitted photons escape from the system and the medium is said to be *optically thick*. If, on the other hand $\Lambda_{s,e,v}^{e',v'} = 1$, all of the emitted photons escape from the system and the medium is said to be *optically thin*. One may

then express (2.139) through

$$\mathrm{div}\,(\vec{q}_{\mathrm{rad}}) = \dot{\Omega}_{\mathrm{rad}} = hc\left(\sum_{\mathrm{se}} \Lambda^{e',v'}_{s,e,v} A^{e',v'}_{s,e,v}\, n_{s,e,v} \int_0^{\infty} \frac{\phi^{e',v'}_{\lambda,s,e,v}}{\lambda}\, d\lambda\right) \ . \tag{2.140}$$

Additionally, the net variation in time of the mass density of particles of the s-th species in the vibronic level (e, v), due to spontaneous emission and absorption processes between the vibronic levels (e, v) and (e', v') is according to the definition of the escape factor and the relation (2.93)

$$(\dot{\omega}_{s,e,v})^{e',v',\mathrm{rad}}_{s,e,v} = \left(\frac{d\rho_{s,e,v}}{dt}\right)^{e',v',\mathrm{rad}}_{s,e,v} = \left(\frac{d\rho_{s,e,v}}{dt}\right)^{e',v',\mathrm{se}}_{s,e,v} - \left(\frac{d\rho_{s,e,v}}{dt}\right)^{s,e,v,\mathrm{a}}_{e',v'} = -\Lambda^{e',v'}_{s,e,v} A^{e',v'}_{s,e,v}\, \rho_{s,e,v} \ . \tag{2.141}$$

2.6.1.5 The number of equations and unknowns

There are as many equations as there are unknowns. The equations are the balance equations for the species masses (2.118) (N_S equations, being N_S the number of different species in the mixture), balance equation for the mixture momentum (2.125) (three equations[19]) and balance equation for the mixture energy (2.133) (one equation). There are therefore in total $N_S + 4$ equations. On the other hand, the unknowns are the species mass densities ρ_s (N_S unknowns), mixture flow velocity $\vec{u}$ (three unknowns[20]) and temperature T (one unknown). It should be mentioned that all of these unknowns are necessary and sufficient to define through appropriate models the variables $\dot{\omega}_s$, $\vec{J}_s$, $[\tau]$, p, $\vec{f}_s$, e, $\vec{q}$ and h_s, for all s. There are therefore in total $N_S + 4$ unknowns for the $N_S + 4$ equations.

2.6.2 The case of the multi-temperature model

For the case of the multi-temperature model, all of the balance equations derived for the single-temperature case (2.118), (2.125) and (2.133) do hold. However, there's a slight difference with respect to the heat flux vector $\vec{q}$. One should define mixture thermal conductivity coefficients for each of the energy modes of the particles, k_i, being $i \in \{\mathrm{tr_h}, \mathrm{rot}, \mathrm{vib}, \mathrm{el}, \mathrm{tr_e}\}$ the i-th energy mode. This can be accomplished, for instance, by defining thermal conductivity coefficients for each species and each of their energy modes $k_{s,i}$ through the *Eucken's relation*, and then using these to compute mixture thermal conductivity coefficients for each of the energy modes, k_i, through the *Wilke's rule* [1]. Or alternatively, one may use the relations of Gupta et al. [52] for the same effect. The contribution of the i-th mode to the heat flux vector, $\vec{q}_i$, can be defined in a similar way to (2.128):

$$\vec{q}_i = -k_i \vec{\nabla} T_i + \vec{q}_{i,\mathrm{rad}} \ , \tag{2.142}$$

such that $\vec{q} = \sum_i \vec{q}_i$. Note that if thermal equilibrium is reached, then $\vec{q} = -\left(\sum_i k_i\right) \vec{\nabla} T + \vec{q}_{\mathrm{rad}}$ with $\vec{q}_{\mathrm{rad}} = \sum_i \vec{q}_{i,\mathrm{rad}}$, and therefore by comparison with (2.128), one may conclude that the mixture thermal conductivity coefficient k and the respective coefficients for the energy modes k_i are related with each other through $k = \sum_i k_i$.

[19] Note that a tridimensional vectorial equation contributes with three three scalar equations: one for each dimension.
[20] Note that a tridimensional vectorial unknown contributes with three scalar unknowns: one for each component.

Let N_T be the number of assigned temperatures, and n the n-th energy mode or combined energy modes for which a temperature T_n is considered. For example, if the Park's two temperature model is chosen, a heavy particle translational-rotational temperature $T_{\mathrm{tr_h\text{-}rot}}$ and an vibrational-electronic-free electron translational temperature $T_{\mathrm{vib\text{-}el\text{-}tr_e}}$ are assigned, implying $n \in \{\mathrm{tr_h\text{-}rot},\ \mathrm{el\text{-}tr_e}\}$. With the introduction of these temperatures the number of unknowns increases by $N_T - 1$, being -1 associated to the necessary act of disregarding the single temperature T. Therefore, there are in total $N_S + N_T + 3$ unknowns. For the new $N_T - 1$ unknowns, new $N_T - 1$ equations need to be assigned. The new $N_T - 1$ equations should correspond to mixture energy balance equations associated to each of the regarded temperatures T_n, with the exception of the one associated to the heavy particle translational mode (a common consideration [2]). Note that such exception is totally unequivocal since the mixture total energy balance equation (2.133) - which includes a dependence on this temperature - is regarded. By following a procedure similar to the one considered in the derivation of equation (2.133), it's possible to show that the mixture energy balance equations associated to the i-th internal energy mode corresponds to [2]:

$$\frac{\partial\left(\rho e_i\right)}{\partial t} + \mathrm{div}\left[\left(\rho e_i\right)\vec{u}\right] = -\mathrm{div}\left(\vec{q}_i\right) - \mathrm{div}\left(\sum_s e_{s,i}\vec{J}_s\right) + \sum_j \dot{\Omega}_{ji}, \qquad \forall i \in \{\mathrm{rot},\ \mathrm{vib},\ \mathrm{el}\}\ , \tag{2.143}$$

being $\dot{\Omega}_{ji}$ the rate of energy transfer from the j-th energy mode to the i-th internal energy mode due to collisional processes - a physical quantity that needs to be modelled. Note that equation (2.143) doesn't include the specific kinetic energy of the flow $\frac{1}{2}u^2$, the work done by partial pressures p_s, neither the viscous stress tensors $[\tau_s]$ since these are solely associated to the translational energy mode of the particles (the translational motion relatively to the element of fluid and the translational motion of the element of fluid).

Particular attention should be given to the energy balance equation for the energy of the free electrons. By evaluating equation (2.126) for $s = \mathrm{e}$, and by assuming that $\vec{J}_\mathrm{e}$ and $[\tau_\mathrm{e}]$ are negligible, it can be shown that the energy balance equation for the energy of the free electrons is given by [2]

$$\frac{\partial\left[\rho_\mathrm{e}\left(e_\mathrm{e} + \frac{1}{2}u^2\right)\right]}{\partial t} + \mathrm{div}\left[\rho_\mathrm{e}\left(e_\mathrm{e} + \frac{1}{2}u^2\right)\vec{u}\right] = -\mathrm{div}\left(p_\mathrm{e}\vec{u}\right) - \mathrm{div}\left(\vec{q}_\mathrm{e}\right) + \rho_\mathrm{e}\left(\vec{f}_\mathrm{e}\cdot\vec{u}\right) + \sum_s \dot{\Omega}^{\mathrm{int}}_{s,\mathrm{e}}\ , \tag{2.144}$$

where $\vec{q}_\mathrm{e}$ is an heat flux vector such that $\dot{Q}^{\mathrm{ext}}_\mathrm{e} = -\oiint_{\partial\mathscr{V}(t)}\left(\vec{q}_\mathrm{e}\cdot\vec{n}\right)dS$ corresponds to the rate of heat transfer from the particles that are outside of the space $\mathscr{V}$ to the inner free electrons. This quantity should not be confused with $\vec{q}_{\mathrm{tr_e}}$, which is an heat flux vector such that $\dot{Q}^{\mathrm{ext}}_{\mathrm{tr_e}} = -\oiint_{\partial\mathscr{V}(t)}\left(\vec{q}_{\mathrm{tr_e}}\cdot\vec{n}\right)dS$ corresponds to the rate of heat transfer from the particles outside of the space $\mathscr{V}$ to the inner particles due to the translation energy mode of free electrons. The quantity $\sum_s \dot{\Omega}^{\mathrm{int}}_{s,\mathrm{e}}$ corresponds to the energy transferred per unit of time per unit of volume from the inner particles to the inner free electrons, or in other words, the volumetric quantity associated to $\sum_s \dot{\mathscr{E}}^{\mathrm{int}}_{s,\mathrm{e}}$.

It's worthy to mention that if temperatures are assigned to combinations of energy modes, then the mixture energy balance equation associated to a temperature should correspond to the sum of the energy balance equations for the energy modes that were combined.

2.6.3 The case of the vibronic-specific state-to-state model

All of the balance equations derived for the single-temperature case (2.118), (2.125) and (2.133) do hold for the case of the vibronic-specific state-to-state model, as also happened for the case of the multi-temperature model. However, since the electronic and vibrational levels of the particles need to be dealt one by one, it's necessary to consider mass balance equations that are vibronic-specific beyond species-specific. Following a similar procedure to the one regarded in the derivation of equation (2.118), it can be shown that the mass balance equations for the s-th species particles in their e-th electronic and v-th vibrational levels correspond to

$$\frac{\partial \rho_{s,e,v}}{\partial t} + \operatorname{div}\left(\rho_{s,e,v}\vec{u}\right) = -\operatorname{div}\left(\vec{J}_{s,e,v}\right) + \dot{\omega}_{s,e,v}, \qquad \forall s,\, e \,\text{and}\, v \;. \tag{2.145}$$

In this model, temperatures should be assigned to the heavy particle translational, rotational, and free electrons translational modes (or to combinations of these). And therefore, equations in the form of (2.143) and (2.144) need to be taken into account.

2.6.4 The case of the zero-dimensional vibronic-specific state-to-state model

In this work, the zero-dimensional vibronic-specific state-to-state model was employed assuming an equilibrium between the translational and rotational energy modes of the heavy particles - therefore, allowing the assignment of a heavy particle translational-rotational temperature $T_{\mathrm{tr_h\text{-}rot}} = T_{\mathrm{tr_h}} = T_{\mathrm{rot}}$. No particular energy balance equation for the combination of the two modes needs to be added since it includes the heavy particle translational mode (see §2.6.3 for more details about this proposition).

The equations to be dealt with in the zero-dimensional vibronic-specific state-to-state model correspond to (2.145), (2.133) with $\operatorname{div}\left(\vec{q}_{\mathrm{rad}}\right)$ substituted by $\dot{\Omega}_{\mathrm{rad}}$ as according to (2.140), and (2.144), disregarding all derivatives in space and the flow velocity vectors of the species, i.e.

$$\begin{cases} \dfrac{d\rho_{s,e,v}}{dt} = \dot{\omega}_{s,e,v}, \qquad \forall s,\, e \,\text{and}\, v \;, & \text{(2.146a)} \\ \dfrac{d\left(\rho e\right)}{dt} = -\dot{\Omega}_{\mathrm{rad}} \;, & \text{(2.146b)} \\ \dfrac{d\left(\rho_{\mathrm{e}} e_{\mathrm{e}}\right)}{dt} = \displaystyle\sum_{s} \dot{\Omega}^{\mathrm{int}}_{s,\mathrm{e}} \;. & \text{(2.146c)} \end{cases}$$

Note that the partial derivative $\partial/\partial t$ was substituted by the total derivative d/dt since the variables solely depend on the instant of time t. The equations can be further developed. By summing (2.146a) in s, e and v, one has

$$\frac{d}{dt}\left(\sum_{s,e,v} \underbrace{\rho_{s,e,v}}_{=\rho c_{s,e,v}}\right) = \underbrace{\sum_{s,e,v} \dot{\omega}_{s,e,v}}_{=0} \Leftrightarrow \frac{d}{dt}\left[\rho \underbrace{\left(\sum_{s,e,v} c_{s,e,v}\right)}_{=1}\right] = 0 \Leftrightarrow \frac{d\rho}{dt} = 0 \;, \tag{2.147}$$

where the result $\sum_{s,e,v}\dot{\omega}_{s,e,v}=0$ was used[21]. By inserting (2.147) into (2.146a), it's possible to obtain a final expression for the mass balance of the s-th species particles in their e-th electronic and v-th vibrational levels:

$$\frac{d}{dt}\underbrace{\rho_{s,e,v}}_{=\rho c_{s,e,v}}=\dot{\omega}_{s,e,v}\Leftrightarrow\rho\frac{dc_{s,e,v}}{dt}+c_{s,e,v}\underbrace{\frac{d\rho}{dt}}_{=0}=\dot{\omega}_{s,e,v}\Leftrightarrow\frac{dc_{s,e,v}}{dt}=\frac{\dot{\omega}_{s,e,v}}{\rho},\qquad\forall s,\,e\text{ and }v\;. \tag{2.148}$$

By using the results (2.146c), (2.147) and (2.148), the mixture total energy balance equation (2.146b) can be transformed into

$$\begin{aligned}
&\frac{d}{dt}\underbrace{(\rho e)}_{=\left(\sum_{s\in\{\mathrm{h}\}}\rho_s e_s\right)+\rho_\mathrm{e}e_\mathrm{e}}=-\dot{\Omega}_\mathrm{rad}\Leftrightarrow\frac{d}{dt}\left(\sum_{s\in\{\mathrm{h}\}}\underbrace{\rho_s}_{=\rho c_s}e_s\right)+\underbrace{\frac{d}{dt}\left(\rho_\mathrm{e}e_\mathrm{e}\right)}_{=\sum_s\dot{\Omega}^\mathrm{int}_{s,\mathrm{e}}}=-\dot{\Omega}_\mathrm{rad}\Leftrightarrow\\
&\Leftrightarrow\underbrace{\frac{d\rho}{dt}}_{=0}\left(\sum_{s\in\{\mathrm{h}\}}c_s e_s\right)+\rho\left(\sum_{s\in\{\mathrm{h}\}}\underbrace{\frac{dc_s}{dt}}_{=\frac{\dot{\omega}_s}{\rho}}e_s\right)+\rho\left(\sum_{s\in\{\mathrm{h}\}}c_s\frac{de_s}{dt}\right)=-\dot{\Omega}_\mathrm{rad}-\sum_s\dot{\Omega}^\mathrm{int}_{s,\mathrm{e}}\Leftrightarrow\\
&\Leftrightarrow\sum_{s\in\{\mathrm{h}\}}c_s\frac{de_s}{dt}=-\frac{\dot{\Omega}_\mathrm{rad}+\sum_s\dot{\Omega}^\mathrm{int}_{s,\mathrm{e}}+\left(\sum_{s\in\{\mathrm{h}\}}\dot{\omega}_s e_s\right)}{\rho}\;,
\end{aligned} \tag{2.149}$$

being $\{\mathrm{h}\}$ the set of heavy species in the system.

Let's now evaluate the left side of (2.149). By invoking the results enunciated in §2.3.3, one can write

$$\begin{aligned}
&\sum_{s\in\{\mathrm{h}\}}c_s\frac{de_s}{dt}=\sum_{s\in\{\mathrm{h}\}}c_s\frac{d}{dt}\left[e_{s,\mathrm{tr}}(T_{\mathrm{tr_h}})+e_{s,\mathrm{rot}}(T_{\mathrm{tr_h}})+e_{s,\mathrm{vib}}+e_{s,\mathrm{el}}+e_{s,0}\right]=\\
&=\sum_{s\in\{\mathrm{h}\}}c_s\left[\underbrace{\frac{de_{s,\mathrm{tr}}}{dT_{\mathrm{tr_h}}}}_{:=C_{V,s,\mathrm{tr}}}\frac{dT_{\mathrm{tr_h}}}{dt}+\underbrace{\frac{de_{s,\mathrm{rot}}}{dT_{\mathrm{tr_h}}}}_{:=C_{V,s,\mathrm{rot}}}\frac{dT_{\mathrm{tr_h}}}{dt}+\frac{d}{dt}\left(\sum_{e,v}\frac{c_{s,e,v}}{c_s}\frac{\epsilon_{s,\mathrm{vib},e,v}}{m_s}\right)+\frac{d}{dt}\left(\sum_e\frac{c_{s,e}}{c_s}\frac{\epsilon_{s,\mathrm{el},e}}{m_s}\right)\right]=\\
&=\left[\sum_{s\in\{\mathrm{h}\}}c_s\underbrace{\left(C_{V,s,\mathrm{tr}}+C_{V,s,\mathrm{rot}}\right)}_{:=C_{V,s,\text{tr-rot}}}\right]\frac{dT_{\mathrm{tr_h}}}{dt}+\left[\sum_{s\in\{\mathrm{h}\},e,v}c_s\frac{d}{dt}\left(\frac{c_{s,e,v}}{c_s}\right)\underbrace{\frac{\epsilon_{s,\mathrm{vib},e,v}+\epsilon_{s,\mathrm{el},e}}{m_s}}_{:=\frac{\epsilon_{s,\text{el-vib},e,v}}{m_s}}\right]=\\
&=\left(\sum_{s\in\{\mathrm{h}\}}c_s C_{V,s,\text{tr-rot}}\right)\frac{dT_{\mathrm{tr_h}}}{dt}+\left[\sum_{s\in\{\mathrm{h}\},e,v}\left(\underbrace{\frac{dc_{s,e,v}}{dt}}_{=\frac{\dot{\omega}_{s,e,v}}{\rho}}-\frac{c_{s,e,v}}{c_s}\underbrace{\frac{dc_s}{dt}}_{=\frac{\dot{\omega}_s}{\rho}}\right)\frac{\epsilon_{s,\text{el-vib},e,v}}{m_s}\right]\Leftrightarrow
\end{aligned}$$

[21] Equation $\sum_{s,e,v}\dot{\omega}_{s,e,v}=0$ holds since the contribution of the mass of a species in the increase of the mass of another species due to some process is the symmetric of the contribution of the mass of the later for the decrease of the mass of the former due to the same process.

$$\Leftrightarrow \sum_{s\in\{\mathrm{h}\}} c_s \frac{de_s}{dt} = \left(\sum_{s\in\{\mathrm{h}\}} c_s C_{V,s,\text{tr-rot}}\right)\frac{dT_{\mathrm{tr_h}}}{dt} + \frac{1}{\rho}\left[\sum_{s\in\{\mathrm{h}\},e,v}\left(\dot{\omega}_{s,e,v} - \frac{c_{s,e,v}}{c_s}\dot{\omega}_s\right)\frac{\epsilon_{s,\text{el-vib},e,v}}{m_s}\right] , \tag{2.150}$$

being $C_{V,s,\text{tr-rot}} = de_{s,\mathrm{tr}}/dT_{\mathrm{tr_h}} + de_{s,\mathrm{rot}}/dT_{\mathrm{tr_h}}$ the *translational-rotational specific heat at constant volume* of the s-th species particle, and $\epsilon_{s,\text{el-vib},e,v} = \epsilon_{s,\mathrm{el},e} + \epsilon_{s,\mathrm{vib},e,v}$ the sensible energy associated to the (e,v)-th vibronic level of the s-th species. It can be shown that $C_{V,s,\text{tr-rot}} = \frac{3}{2}R_s$ if the s-th species is atomic or $C_{V,s,\text{tr-rot}} = \frac{5}{2}R_s$ if the s-th species is molecular. By inserting (2.150) in (2.149), an ultimate expression for the heavy particle translation-rotational temperature $T_{\mathrm{tr_h}}$ can be obtained:

$$\frac{dT_{\mathrm{tr_h}}}{dt} = -\frac{\dot{\Omega}_{\mathrm{rad}} + \left(\sum_s \dot{\Omega}^{\mathrm{int}}_{s,\mathrm{e}}\right) + \left(\sum_{s\in\{\mathrm{h}\}}\dot{\omega}_s e_s\right) + \left[\sum_{s\in\{\mathrm{h}\},e,v}\left(\dot{\omega}_{s,e,v} - \frac{c_{s,e,v}}{c_s}\dot{\omega}_s\right)\frac{\epsilon_{s,\text{el-vib},e,v}}{m_s}\right]}{\rho\left(\sum_{s\in\{\mathrm{h}\}} c_s C_{V,s,\text{tr-rot}}\right)} . \tag{2.151}$$

Let's now regard the free electron energy balance equation (2.146c). By invoking relations (2.147), (2.148) and (2.57), one can ultimately write

$$\frac{d}{dt}\left(\underbrace{\rho_{\mathrm{e}}}_{=\rho c_{\mathrm{e}}} e_{\mathrm{e}}\right) = \sum_s \dot{\Omega}^{\mathrm{int}}_{s,\mathrm{e}} \Leftrightarrow \underbrace{\frac{d\rho}{dt}}_{=0} c_{\mathrm{e}} e_{\mathrm{e}} + \rho \underbrace{\frac{dc_{\mathrm{e}}}{dt}}_{=\frac{\dot{\omega}_{\mathrm{e}}}{\rho}} e_{\mathrm{e}} + \rho c_{\mathrm{e}} \underbrace{\frac{de_{\mathrm{e}}}{dT_{\mathrm{tr}_e}}}_{:=C_{V,\mathrm{e}}} \frac{dT_{\mathrm{tr_e}}}{dt} = \sum_s \dot{\Omega}^{\mathrm{int}}_{s,\mathrm{e}} \Leftrightarrow$$

$$\Leftrightarrow \frac{dT_{\mathrm{tr_e}}}{dt} = \frac{\left(\sum_s \dot{\Omega}^{\mathrm{int}}_{s,\mathrm{e}}\right) - \dot{\omega}_{\mathrm{e}} e_{\mathrm{e}}}{\rho c_{\mathrm{e}} C_{V,\mathrm{e}}} , \tag{2.152}$$

being $C_{V,\mathrm{e}} = \frac{3}{2}R_{\mathrm{e}}$ the free electrons specific heat at constant volume.

2.6.5 The case of the Euler one-dimensional vibronic-specific state-to-state model

The equations to be dealt with in the Euler one-dimensional vibronic-specific state-to-state model are (2.145), (2.125), (2.133) with $\mathrm{div}\,(\vec{q}_{\mathrm{rad}})$ substituted by $\dot{\Omega}_{\mathrm{rad}}$ as according to (2.140), and (2.144), disregarding all the derivatives with respect to the y and z variables, the y and z-components of the flow velocity vector $\vec{u}$ - due to the one-dimensional hypothesis - as well as the transport phenomena (heat conduction, diffusion and viscosity) - due to the Euler hypothesis. It was assumed in this work that the external body forces were negligible, the flow was stationary (the derivatives with respect to the instant of time t were null), and the translational and rotational energy modes of the heavy particles were in equilibrium with each other. The resultant fluid flow governing equations were then

$$\begin{cases} \dfrac{d}{dx}\left(\rho_{s,e,v} u\right) = \dot{\omega}_{s,e,v}, \qquad \forall s,\, e \text{ and } v\ , & \text{(2.153a)} \\ \dfrac{d}{dx}\left(\rho u^2\right) = -\dfrac{dp}{dx}\ , & \text{(2.153b)} \\ \dfrac{d}{dx}\left[\rho\left(h + \dfrac{1}{2}u^2\right)u\right] = -\dot{\Omega}_{\mathrm{rad}}\ , & \text{(2.153c)} \\ \dfrac{d}{dx}\left[\rho_{\mathrm{e}}\left(h_{\mathrm{e}} + \dfrac{1}{2}u^2\right)u\right] = \displaystyle\sum_s \dot{\Omega}^{\mathrm{int}}_{s,\mathrm{e}}\ , & \text{(2.153d)} \end{cases}$$

being u the x-component of the flow velocity vector. Note that the partial derivative $\partial/\partial x$ was substituted by the total derivative d/dx since the variables solely depend on the x-position. The equations can be further developed. By summing (2.153a) in s, e and v, one has

$$\frac{d}{dx}\left[\left(\sum_{s,e,v}\underbrace{\rho_{s,e,v}}_{=\rho c_{s,e,v}}\right)u\right]=\underbrace{\sum_{s,e,v}\dot{\omega}_{s,e,v}}_{=0}\Leftrightarrow\frac{d}{dx}\left[\rho u\underbrace{\left(\sum_{s,e,v}c_{s,e,v}\right)}_{=1}\right]=0\Leftrightarrow\frac{d}{dx}\left(\rho u\right)=0\ . \tag{2.154}$$

By inserting (2.154) into (2.153a), it's possible to obtain a final expression for the mass balance of the s-th species particles in their e-th electronic and v-th vibrational levels:

$$\frac{d}{dx}\left(\underbrace{\rho_{s,e,v}}_{=\rho c_{s,e,v}}u\right)=\dot{\omega}_{s,e,v}\Leftrightarrow\rho u\frac{dc_{s,e,v}}{dx}+c_{s,e,v}\underbrace{\frac{d}{dx}\left(\rho u\right)}_{=0}=\dot{\omega}_{s,e,v}\Leftrightarrow\frac{dc_{s,e,v}}{dx}=\frac{\dot{\omega}_{s,e,v}}{\rho u},\qquad\forall s,\,e\,\text{and}\,v\ . \tag{2.155}$$

The balance equation for momentum can be further developed by employing in (2.153b) the result (2.154), the balance equation for mass (2.155), and the definitions of the partial pressures (2.50) and (2.58), giving

$$\frac{d}{dx}\left(\rho u^2\right)=-\frac{dp}{dx}\Leftrightarrow\underbrace{\frac{d}{dx}\left(\rho u\right)}_{=0}u+\rho u\frac{du}{dx}=-\frac{d}{dx}\left[\left(\sum_{s\in\{\mathrm{h}\}}p_s\right)+p_{\mathrm{e}}\right]\Leftrightarrow\rho u\frac{du}{dx}=-\frac{d}{dx}\left[\left(\sum_{s\in\{\mathrm{h}\}}\underbrace{\rho_s}_{=\rho c_s}R_sT_{\mathrm{tr_h}}\right)+\underbrace{\rho_{\mathrm{e}}}_{=\rho c_{\mathrm{e}}}R_{\mathrm{e}}T_{\mathrm{tr_e}}\right]\Leftrightarrow$$

$$\Leftrightarrow\rho u\frac{du}{dx}=-\underbrace{\frac{d\rho}{dx}}_{=-\frac{\rho}{u}\frac{du}{dx}}\underbrace{\left[\left(\sum_{s\in\{\mathrm{h}\}}c_sR_sT_{\mathrm{tr_h}}\right)+c_{\mathrm{e}}R_{\mathrm{e}}T_{\mathrm{tr_e}}\right]}_{=\frac{p}{\rho}}-\rho\left[\left(\sum_{s\in\{\mathrm{h}\}}\underbrace{\frac{dc_{\mathrm{s}}}{dx}}_{=\frac{\dot{\omega}_{\mathrm{s}}}{\rho u}}\underbrace{R_sT_{\mathrm{tr_h}}}_{=\frac{p_s}{\rho c_s}}\right)+\underbrace{\frac{dc_{\mathrm{e}}}{dx}}_{=\frac{\dot{\omega}_{\mathrm{e}}}{\rho u}}\underbrace{R_{\mathrm{e}}T_{\mathrm{tr_e}}}_{=\frac{p_{\mathrm{e}}}{\rho c_{\mathrm{e}}}}\right]$$

$$-\rho\left[\left(\sum_{s\in\{\mathrm{h}\}}\underbrace{c_sR_s}_{=\frac{p_s}{\rho T_{\mathrm{tr_h}}}}\frac{dT_{\mathrm{tr_h}}}{dx}\right)+\underbrace{c_{\mathrm{e}}R_{\mathrm{e}}}_{=\frac{p_{\mathrm{e}}}{\rho T_{\mathrm{tr_e}}}}\frac{dT_{\mathrm{tr_e}}}{dx}\right]\Leftrightarrow\rho u\frac{du}{dx}=\frac{p}{u}\frac{du}{dx}-\frac{1}{\rho u}\left[\left(\sum_{s\in\{\mathrm{h}\}}\frac{\dot{\omega}_sp_s}{c_s}\right)+\frac{\dot{\omega}_{\mathrm{e}}p_{\mathrm{e}}}{c_{\mathrm{e}}}\right]-\left[\left(\sum_{s\in\{\mathrm{h}\}}\frac{p_s}{T_{\mathrm{tr_h}}}\frac{dT_{\mathrm{tr_h}}}{dx}\right)+\frac{p_{\mathrm{e}}}{T_{\mathrm{tr_e}}}\frac{dT_{\mathrm{tr_e}}}{dx}\right]\Leftrightarrow$$

$$\Leftrightarrow\left(\frac{\rho u^2}{p}-1\right)\frac{du}{dx}+\frac{u}{p}\left[\left(\sum_{s\in\{\mathrm{h}\}}\frac{p_s}{T_{\mathrm{tr_h}}}\frac{dT_{\mathrm{tr_h}}}{dx}\right)+\frac{p_{\mathrm{e}}}{T_{\mathrm{tr_e}}}\frac{dT_{\mathrm{tr_e}}}{dx}\right]=-\frac{1}{p\rho}\left[\left(\sum_{s\in\{\mathrm{h}\}}\frac{\dot{\omega}_sp_s}{c_s}\right)+\frac{\dot{\omega}_{\mathrm{e}}p_{\mathrm{e}}}{c_{\mathrm{e}}}\right]\ , \tag{2.156}$$

Similarly, by using the result (2.154), the mass balance equation (2.155), and the free electron energy balance equation (2.153d), one can transform the mixture total energy balance equation (2.153c) into

$$\frac{d}{dx}\left[\rho\left(\underbrace{h}_{=\left(\sum_{s\in\{\mathrm{h}\}}c_sh_s\right)+c_{\mathrm{e}}h_{\mathrm{e}}}+\frac{1}{2}u^2\right)u\right]=-\dot{\Omega}_{\mathrm{rad}}\Leftrightarrow\left\{\sum_{s\in\{\mathrm{h}\}}\frac{d}{dx}\left[\rho c_s\left(h_s+\frac{1}{2}u^2\right)u\right]\right\}+\underbrace{\frac{d}{dx}\left[\rho c_{\mathrm{e}}\left(h_{\mathrm{e}}+\frac{1}{2}u^2\right)u\right]}_{=\sum_s\dot{\Omega}^{\mathrm{int}}_{s,\mathrm{e}}}=-\dot{\Omega}_{\mathrm{rad}}\Leftrightarrow$$

$$\Leftrightarrow \underbrace{\frac{d}{dx}(\rho u)}_{=0}\left[\sum_{s\in\{\mathrm{h}\}} c_s\left(h_s+\frac{1}{2}u^2\right)\right]+\rho u\left\{\left[\sum_{s\in\{\mathrm{h}\}}\underbrace{\frac{dc_s}{dx}}_{=\frac{\dot\omega_s}{\rho u}}\left(h_s+\frac{1}{2}u^2\right)\right]+\left(\sum_{s\in\{\mathrm{h}\}} c_s\frac{dh_s}{dx}\right)+\left(\sum_{s\in\{\mathrm{h}\}} c_s\right)u\frac{du}{dx}\right\}=-\dot\Omega_{\mathrm{rad}}-\left(\sum_s \dot\Omega^{\mathrm{int}}_{s,\mathrm{e}}\right)\Leftrightarrow$$

$$\Leftrightarrow \left(\sum_{s\in\{\mathrm{h}\}} c_s\frac{dh_s}{dx}\right)+\left(\sum_{s\in\{\mathrm{h}\}} c_s\right)u\frac{du}{dx}=-\frac{\dot\Omega_{\mathrm{rad}}+\left(\sum_s \dot\Omega^{\mathrm{int}}_{s,\mathrm{e}}\right)+\left[\sum_{s\in\{\mathrm{h}\}}\dot\omega_s\left(h_s+\frac{1}{2}u^2\right)\right]}{\rho u}\,. \tag{2.157}$$

Let's evaluate the first term at the left side of (2.157). According to the definitions of the specific enthalpies under the vibronic-specific state-to-state model (as stated in §2.3.3), one can write

$$\sum_{s\in\{\mathrm{h}\}} c_s\frac{dh_s}{dx}=\sum_{s\in\{\mathrm{h}\}} c_s\frac{d}{dx}\left[h_{s,\mathrm{tr}}(T_{\mathrm{tr_h}})+h_{s,\mathrm{rot}}(T_{\mathrm{tr_h}})+h_{s,\mathrm{vib}}+h_{s,\mathrm{el}}+h_{s,0}\right]=$$

$$=\sum_{s\in\{\mathrm{h}\}} c_s\left[\underbrace{\frac{dh_{s,\mathrm{tr}}}{dT_{\mathrm{tr_h}}}}_{:=C_{p,s,\mathrm{tr}}}\frac{dT_{\mathrm{tr_h}}}{dx}+\underbrace{\frac{dh_{s,\mathrm{rot}}}{dT_{\mathrm{tr_h}}}}_{:=C_{p,s,\mathrm{rot}}}\frac{dT_{\mathrm{tr_h}}}{dx}+\frac{d}{dx}\left(\sum_{e,v}\frac{c_{s,e,v}}{c_s}\frac{\epsilon_{s,\mathrm{vib},e,v}}{m_s}\right)+\frac{d}{dx}\left(\sum_{e}\frac{c_{s,e}}{c_s}\frac{\epsilon_{s,\mathrm{el},e}}{m_s}\right)\right]=$$

$$=\left[\sum_{s\in\{\mathrm{h}\}} c_s\underbrace{\left(C_{p,s,\mathrm{tr}}+C_{p,s,\mathrm{rot}}\right)}_{:=C_{p,s,\text{tr-rot}}}\right]\frac{dT_{\mathrm{tr_h}}}{dx}+\left[\sum_{s\in\{\mathrm{h}\},e,v} c_s\frac{d}{dx}\left(\frac{c_{s,e,v}}{c_s}\right)\underbrace{\frac{\epsilon_{s,\mathrm{vib},e,v}+\epsilon_{s,\mathrm{el},e}}{m_s}}_{:=\frac{\epsilon_{s,\text{el-vib},e,v}}{m_s}}\right]=$$

$$=\left(\sum_{s\in\{\mathrm{h}\}} c_s C_{p,s,\text{tr-rot}}\right)\frac{dT_{\mathrm{tr_h}}}{dx}+\left[\sum_{s\in\{\mathrm{h}\},e,v}\left(\underbrace{\frac{dc_{s,e,v}}{dx}}_{=\frac{\dot\omega_{s,e,v}}{\rho u}}-\frac{c_{s,e,v}}{c_s}\underbrace{\frac{dc_s}{dx}}_{=\frac{\dot\omega_s}{\rho u}}\right)\frac{\epsilon_{s,\text{el-vib},e,v}}{m_s}\right]\Leftrightarrow$$

$$\Leftrightarrow \sum_{s\in\{\mathrm{h}\}} c_s\frac{dh_s}{dx}=\left(\sum_{s\in\{\mathrm{h}\}} c_s C_{p,s,\text{tr-rot}}\right)\frac{dT_{\mathrm{tr_h}}}{dx}+\frac{1}{\rho u}\left[\sum_{s\in\{\mathrm{h}\},e,v}\left(\dot\omega_{s,e,v}-\frac{c_{s,e,v}}{c_s}\dot\omega_s\right)\frac{\epsilon_{s,\text{el-vib},e,v}}{m_s}\right]\,, \tag{2.158}$$

being $C_{p,s,\text{tr-rot}}=dh_{s,\mathrm{tr}}/dT_{\mathrm{tr_h}}+dh_{s,\mathrm{rot}}/dT_{\mathrm{tr_h}}$ the *translational-rotational specific heat at constant pressure* of the s-th species particle. It can be shown that $C_{p,s,\text{tr-rot}}=\frac{5}{2}R_s$ if the s-th species is atomic or $C_{p,s,\text{tr-rot}}=\frac{7}{2}R_s$ if the s-th species is molecular. By inserting (2.158) in (2.157), one can finally obtain

$$\frac{dT_{\mathrm{tr_h}}}{dx}+\frac{\left(\sum_{s\in\{\mathrm{h}\}} c_s\right)u}{\sum_{s\in\{\mathrm{h}\}} c_s C_{p,s,\text{tr-rot}}}\cdot\frac{du}{dx}=$$
$$=-\frac{\dot\Omega_{\mathrm{rad}}+\left(\sum_s \dot\Omega^{\mathrm{int}}_{s,\mathrm{e}}\right)+\left[\sum_{s\in\{\mathrm{h}\}}\dot\omega_s\left(h_s+\frac{1}{2}u^2\right)\right]+\left[\sum_{s\in\{\mathrm{h}\},e,v}\left(\dot\omega_{s,e,v}-\frac{c_{s,e,v}}{c_s}\dot\omega_s\right)\frac{\epsilon_{s,\text{el-vib},e,v}}{m_s}\right]}{\rho u\left(\sum_{s\in\{\mathrm{h}\}} c_s C_{p,s,\text{tr-rot}}\right)}\,. \tag{2.159}$$

Let's now regard the free electron energy balance equation (2.153d). By invoking relations (2.154),

(2.155) and the definition of specific enthalpy of the free electrons (2.59), one can ultimately write

$$\frac{d}{dx}\left[\underbrace{\rho_{\mathrm{e}}}_{=\rho c_{\mathrm{e}}}\left(h_{\mathrm{e}}+\frac{1}{2}u^2\right)u\right]=\sum_s\dot{\Omega}^{\mathrm{int}}_{s,\mathrm{e}}\Leftrightarrow\underbrace{\frac{d}{dx}\left(\rho u\right)}_{=0}\left[c_{\mathrm{e}}\left(h_{\mathrm{e}}+\frac{1}{2}u^2\right)\right]+\rho u\underbrace{\frac{dc_{\mathrm{e}}}{dx}}_{=\frac{\dot{\omega}_{\mathrm{e}}}{\rho u}}\left(h_{\mathrm{e}}+\frac{1}{2}u^2\right)+\rho uc_{\mathrm{e}}\frac{d}{dx}h_{\mathrm{e}}(T_{\mathrm{tr_e}})+\rho c_{\mathrm{e}}u^2\frac{du}{dx}=\sum_s\dot{\Omega}^{\mathrm{int}}_{s,\mathrm{e}}\Leftrightarrow$$

$$\Leftrightarrow\dot{\omega}_{\mathrm{e}}\left(h_{\mathrm{e}}+\frac{1}{2}u^2\right)+\rho uc_{\mathrm{e}}\underbrace{\frac{dh_{\mathrm{e}}}{dT_{\mathrm{tr_e}}}}_{:=C_{p,\mathrm{e}}}\frac{dT_{\mathrm{tr_e}}}{dx}+\rho c_{\mathrm{e}}u^2\frac{du}{dx}=\sum_s\dot{\Omega}^{\mathrm{int}}_{s,\mathrm{e}}\Leftrightarrow$$

$$\Leftrightarrow\frac{dT_{\mathrm{tr_e}}}{dx}+\frac{u}{C_{p,\mathrm{e}}}\frac{du}{dx}=\frac{\left(\sum_s\dot{\Omega}^{\mathrm{int}}_{s,\mathrm{e}}\right)-\dot{\omega}_{\mathrm{e}}\left(h_{\mathrm{e}}+\frac{1}{2}u^2\right)}{\rho uc_{\mathrm{e}}C_{p,\mathrm{e}}}\,, \tag{2.160}$$

being $C_{p,\mathrm{e}}=\frac{5}{2}R_{\mathrm{e}}$ the free electrons specific heat at constant pressure.

2.7 The Forced Harmonic Oscillator model

2.7.1 Characterisation of the modelled kinetic processes

Before going into the details of the Forced Harmonic Oscillator model (FHO), it's important to describe the kinetic processes that may be modelled by it. These correspond to the so-called *V-T*, *V-V-T* and *V-D processes*.

A V-T process corresponds to a collision between a molecular particle and an atomic particle, in which the former transfers part of its vibrational energy (hence the letter "V" in "V-T") to the latter, in the form of translational kinetic energy (hence the letter "T" in "V-T"). This type of energy transfer results in a quenching or relaxation of the molecular particle vibrational mode. When the direction of energy exchange is inverted there's a gain in vibrational energy (therefore an excitation of the mode), and the T-V label may be used instead. However, the V-T label will be employed in this work to designate both processes, as in accordance to the usual nomenclature found in the literature. A V-T energy transfer between a molecular particle AB and an atomic particle C can be depicted by

$$\mathrm{AB}(v)+\mathrm{C}\longrightarrow\mathrm{AB}(v')+\mathrm{C}\,, \tag{2.161}$$

where v and v' are the initial and final vibrational quantum numbers of the molecular particle, respectively. No labels for the translational kinetic energy of the particles are shown in the above equation, but the their change in the collision is implicit.

A V-V-T process corresponds to a collision between two molecular particles, in which energy transfers involving their vibrational and translational energy modes occur. A V-V-T process associated to a collision between a molecular particle AB and a molecular particle CD may be depicted by

$$\mathrm{AB}(v_1)+\mathrm{CD}(v_2)\longrightarrow\mathrm{AB}(v_1')+\mathrm{CD}(v_2')\,, \tag{2.162}$$

where v_1 and v_1' are the initial and final vibrational quantum numbers of AB, respectively, and v_2' are

the initial and final vibrational quantum numbers of CD, respectively .

A V-D process corresponds to a collision between a molecular particle and another heavy particle (atomic or molecular) which excites the former (or/and the latter, if it is molecular) to a very high vibrational level (hence the letter "V" in the "V-D" label), leading to its dissociation (hence the letter "D" in the "V-D" label). Therefore, a V-D process is a combination of a V-T process, if the second particle is atomic, or V-V-T process, if the second particle is molecular, and dissociation. Representative equations for a V-D process in which the second particle is atomic, and in which the second particle is molecular, are given by

$$\mathrm{AB}(v) + \mathrm{C} \longrightarrow \mathrm{A} + \mathrm{B} + \mathrm{C} \ , \tag{2.163}$$

and the set

$$\begin{cases} \mathrm{AB}(v_1) + \mathrm{CD}(v_2) \longrightarrow \mathrm{A} + \mathrm{B} + \mathrm{CD}(v_2') \ , & \text{(2.164a)} \\ \mathrm{AB}(v_1) + \mathrm{CD}(v_2) \longrightarrow \mathrm{AB}(v_1') + \mathrm{C} + \mathrm{D} \ , & \text{(2.164b)} \\ \mathrm{AB}(v_1) + \mathrm{CD}(v_2) \longrightarrow \mathrm{A} + \mathrm{B} + \mathrm{C} + \mathrm{D} \ , & \text{(2.164c)} \end{cases}$$

respectively. It's important to warn the reader about the multitude of different nomenclatures found in the literature, with respect to some particular processes. For example, a process that derives from a collision between two molecular particles, in which vibrational energy comes from one particle to the other only in translational form may be termed a V-T process, although a process that involves the vibrational and translational modes of two colliding molecular particles is generally denominated a V-V-T process, and the V-T label is usually assigned to the case in which the colliding particles correspond to a molecular particle and an atomic particle. Furthermore, a process that derives from a collision between two molecular particles, in which vibrational energy comes from one particle to the other only in vibrational form may be denominated a V-V process. It is worth mentioning that the label V-V process is even sometimes used when the variation of the vibrational quantum number of one particle is the symmetric of the variation of the other, i.e. $v_1' - v_1 = -(v_2' - v_2)$, regardless if there's also or not some exchange of translational energy. Also, the symmetric variation of the particles vibrational quantum numbers only means a symmetric variation of their vibrational energy if the jumps are are also symmetric in energy. The use of this very particular and sometimes abusive nomenclature was denied in this work to avoid ambiguity problems.

2.7.2 The case of V-T processes

The probability of a molecular particle AB to transit from some vibrational quantum number to another one by collision with an atomic particle C, according to the FHO theory [26, 27, 53], will be herein presented. The collision is assumed to be collinear (all the nuclei are positioned in the same line, and the relative velocity vector is aligned with this line). Such collision is depicted by Figure 2.7.

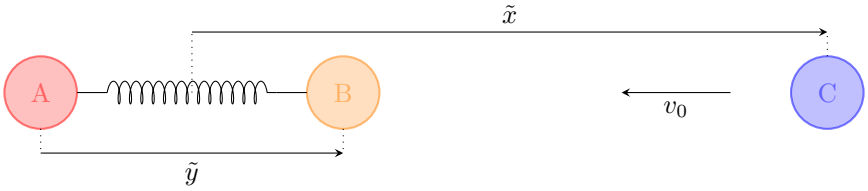

Figure 2.7: Collinear collision between a diatomic molecular particle AB and an atomic particle C.

Let $\tilde{x}_{\mathrm{A}}$, and m_{A} be respectively the position of the nucleus A and its mass. The analogous notation follows for the other two nuclei, B and C. Let $\tilde{x}_R$ be the *centre of mass* of the whole system[22]. The coordinates presented by Figure 2.7 are: the difference between the positions of the nucleus C and the centre of mass of the molecular particle AB, $\tilde{x} = \tilde{x}_{\mathrm{C}} - \tilde{\bar{x}}_{\mathrm{AB}}$, and the difference between the positions of the nuclei B and A, $\tilde{y} = \tilde{x}_{\mathrm{B}} - \tilde{x}_{\mathrm{A}}$. Note that "difference between positions" and not "distances" are mentioned here, to avoid ambiguity problems (distances in a one-dimensional world are by definition the absolute value of the differences between positions). The quantity v_0 corresponds to the approaching relative speed of the particles v when they are sufficiently far away, i.e. when $\tilde{x} = \infty$, such that there's no interaction between them. There are four mass parameters, whose employment will be useful throughout all this section to describe the dynamics of the system: factor γ, the *reduced mass* of the molecular particle μ, the reduced mass of the combination of the molecular particle and the atomic particle $\tilde{m}$, and the sum of all particles masses $\tilde{M}$. These are defined by

$$\gamma = \frac{m_{\mathrm{A}}}{m_{\mathrm{A}} + m_{\mathrm{B}}} \,, \tag{2.165}$$

$$\mu = \frac{m_{\mathrm{A}} m_{\mathrm{B}}}{m_{\mathrm{A}} + m_{\mathrm{B}}} \,, \tag{2.166}$$

$$\tilde{m} = \frac{(m_{\mathrm{A}} + m_{\mathrm{B}})\, m_{\mathrm{C}}}{m_{\mathrm{A}} + m_{\mathrm{B}} + m_{\mathrm{C}}} \,, \tag{2.167}$$

$$\tilde{M} = m_{\mathrm{A}} + m_{\mathrm{B}} + m_{\mathrm{C}} \,, \tag{2.168}$$

respectively. It's assumed that the interaction between the nuclei A and C is negligible when in comparison with the interaction between B and C, since B is much closer to C than A to C. Therefore, the interaction potential energy between the molecular particle and the atomic particle, V', only depends on $\tilde{x}_{\mathrm{C}} - \tilde{x}_{\mathrm{B}}$. The potential is also assumed to be exponentially repulsive, having the form $V'(\tilde{x}_{\mathrm{C}} - \tilde{x}_{\mathrm{B}}) = A\, e^{-\alpha(\tilde{x}_{\mathrm{C}} - \tilde{x}_{\mathrm{B}})}$, where A and α are two positive constants. And by noticing that $\tilde{x}_{\mathrm{C}} - \tilde{x}_{\mathrm{B}} = \tilde{x} - \gamma\tilde{y}$, the potential can expressed through

$$V'(\tilde{x}, \tilde{y}) = A\, e^{-\alpha(\tilde{x} - \gamma\tilde{y})} \,. \tag{2.169}$$

Note, also, that in contrast to the assumed one, the interaction potential is usually repulsive at short distances and attractive at long ones. But as said by Svehla [54]: "(...) *at higher temperatures the colliding molecules approach closely, and repulsive forces become dominant*", which supports the consideration of a purely repulsive potential when dealing with high temperature post-shock flows, and on the other hand, it simplifies the problem.

[22] The centre of mass of a system of particles, with masses $\{m_i\}$ and positions $\{\tilde{x}_i\}$, is defined by: $\tilde{\bar{x}} = \frac{\sum_{i=1} m_i\, \tilde{x}_i}{\sum_{i=1} m_i}$.

It's important to mention that the force that nucleus B imposes on C is given by the symmetric of the derivative of the interaction potential relatively to its dependence variable, i.e. $F_{\mathrm{BC}} = -\frac{dV'}{d(\tilde{x}_{\mathrm{C}} - \tilde{x}_{\mathrm{B}})}$.

Because the molecular particle is assumed to be a harmonic oscillator, the force that A imposes on B follows Hooke's law, and therefore it is given by $F_{\mathrm{AB}} = -f\,(\tilde{y} - \tilde{y}_0)$, being f the force constant and $\tilde{y}_0$ the difference between the positions of the nuclei of the molecular particle at equilibrium. Forces F_{AB} and F_{BC} have a conventional positive signal to the right direction.

The FHO model is semiclassical, i.e. it considers one part of the system dynamics to be described by Classical Mechanics, and the other part to be described by Quantum Mechanics. This model, in particular, considers that the displacement of the atomic particle relatively to the molecular particle, $\tilde{x}$, is in agreement with Classical Mechanics and the molecular particle vibrations are in agreement with Quantum Mechanics. Let's first try to obtain the trajectory $\tilde{x}(t)$. Just for the sake of achieving this classical quantity, it's necessary to initially take the assumption that the whole system behaves classically, i.e. by considering that the Newton's laws are in fact applicable (and to achieve the quantum mechanical solutions for the molecular particle vibrations, a Schrödinger equation for the whole system is instead regarded, in which the previously obtained trajectory $\tilde{x}(t)$ is inserted). Because the physics of a collision is mainly due (and in this model, only) to the relative and to the average properties of the collision partners, it would be rather useful to express the dynamic equations for each of the individual nuclei local positions, in terms of relative positions (differences between local positions) and average positions (centres of mass). According to the Newton's second law, one can write the equations of movement for each nucleus as

$$\begin{cases} m_{\mathrm{A}}\ddot{\tilde{x}}_{\mathrm{A}} = F_{\mathrm{BA}} + F_{\mathrm{CA}} \ , & \text{(2.170a)} \\ m_{\mathrm{B}}\ddot{\tilde{x}}_{\mathrm{B}} = F_{\mathrm{AB}} + F_{\mathrm{CB}} \ , & \text{(2.170b)} \\ m_{\mathrm{C}}\ddot{\tilde{x}}_{\mathrm{C}} = F_{\mathrm{AC}} + F_{\mathrm{BC}} \ , & \text{(2.170c)} \end{cases}$$

where the double dot notation, $\ddot{[\,]}$, corresponds to a double derivative in time. Making a change of variables, and by substituting the already exposed approximations, one can transform the above equations into

$$\begin{cases} \mu\ddot{\tilde{y}} = -f\,(\tilde{y} - \tilde{y}_0) - \gamma\alpha A\, e^{-\alpha(\tilde{x} - \gamma\tilde{y})} \ , & \text{(2.171a)} \\ \tilde{m}\ddot{\tilde{x}} = \alpha A\, e^{-\alpha(\tilde{x} - \gamma\tilde{y})} \ , & \text{(2.171b)} \\ \tilde{M}\ddot{\tilde{x}}_R = 0 \ . & \text{(2.171c)} \end{cases}$$

Equation (2.171c) can be disregarded: it only tells that no external forces are acting in the system corresponding to the combination of the molecular and atomic particles. Conversely, equation (2.171b) tells something useful: since the exponential is a positive function, and α and A are positive constants, the relative acceleration is positive at all instants, i.e. $\ddot{\tilde{x}} > 0$, $\forall t$. On the other hand, it is known that at a sufficiently long time before the collision, say $t = -\infty$, the relative velocity is negative. In fact, $\dot{\tilde{x}}(-\infty) = -v_0$, with $v_0 > 0$. Therefore, from these two propositions, one can infer that a turning point in the trajectory of the particles will for sure occur, at which the relative velocity becomes positive. The

particles will get closer and then depart after reaching the turning point. Since this is a classical result (deriving from the Newton's laws) such point is usually denominated "classical turning point", being denoted by $\tilde{x}_t$. Let's associate the zero value to the instant at which the turning point is reached, i.e. $\tilde{x}(0) = \tilde{x}_t$. Note that, by definition, the relative velocity is null in the turning point, $\dot{\tilde{x}}(0) = 0$. A change of variables will now be performed, to simplify the further work:

$$\tilde{X} = \tilde{x} - \tilde{x}_t \ , \qquad (2.172) \qquad\qquad \tilde{Y} = \tilde{y} - \tilde{y}_0 \ . \qquad (2.173)$$

By substituting the above relations in (2.171a), (2.171b), one gets

$$\begin{cases} \mu\ddot{\tilde{Y}} = -f\tilde{Y} - \gamma\alpha A'' \, e^{-\alpha\left(\tilde{X}-\gamma\tilde{Y}\right)} \ , & (2.174a) \\ \tilde{m}\ddot{\tilde{X}} = \alpha A'' \, e^{-\alpha\left(\tilde{X}-\gamma\tilde{Y}\right)} \ , & (2.174b) \end{cases}$$

with $A'' = A \, e^{-\alpha(\tilde{x}_t - \gamma\tilde{y}_0)}$. Now, there's the objective to obtain the function $\tilde{X}(t)$, so that the relative trajectory of the particles may be described. An approximation is commonly performed: there's the assumption that the vibrational amplitude of the oscillator is not driven at large values during the collision, so that $|\tilde{Y}| \ll L$, being $L = 1/\alpha$ the characteristic length of the molecular particle-atomic particle interaction. And therefore, $e^{\alpha\gamma\tilde{Y}} \approx 1$. This approximation is valid if the relative kinetic energy of the particles is much greater than the transferred vibrational energy. Note also that if there's any exchange between translational and vibrational energies, the final relative speed, v_f, would not be the same as the initial relative speed of the particles, v_0. Anyway, a corrective approach can be performed to reduce the eventual inaccuracies [55]: substitution of the initial relative speed v_0 by a mean value, $v_0 = (v_i + v_f)/2$, being v_i and v_f, the relative speeds of the particles before and after the collision (v_i is the same as the previous defined v_0, and v_f is obtained by an energy balance, taking into account the vibrational and translational energy transfers). In these terms, to obtain the solution $\tilde{X}(t)$, only equation (2.174b) needs to be solved, and it may be transformed into

$$\tilde{m}\ddot{\tilde{X}} = \alpha A'' \, e^{-\alpha\tilde{X}} \ . \qquad (2.175)$$

The solution of this differential equation can be shown to be

$$\tilde{X}(t) = \frac{2}{\alpha} \ln\left[\cosh\left(\sqrt{\frac{A''}{2\tilde{m}}}\alpha t\right)\right] \ . \qquad (2.176)$$

The relative velocity is then given by $\dot{\tilde{X}}(t) = \sqrt{\frac{2A''}{\tilde{m}}} \tanh\left(\sqrt{\frac{A''}{2\tilde{m}}}\alpha t\right)$. By applying the initial condition $\dot{\tilde{X}}(-\infty) = -v_0$, one can find that

$$A'' = \frac{1}{2}\tilde{m}v_0^2 := E_0 \ , \qquad (2.177)$$

being E_0 the relative kinetic energy of the colliding particles at $t = -\infty$. By inserting the solution (2.176) and the relation (2.177) into the interaction potential defined by (2.169), the dependence on $\tilde{X}$

is substituted by a dependence on t, giving

$$V'\left(t,\tilde{Y}\right) = E_0 \operatorname{sech}^2\left(\frac{\alpha v_0}{2}t\right) e^{\alpha\gamma\tilde{Y}} \ . \tag{2.178}$$

The interaction potential in this form is ready to be inserted into the Schrödinger equation of the whole system. Such Schrödinger equation is expressed by

$$\left[-\frac{\hbar^2}{2}\left(\frac{1}{m_{\mathrm{A}}}\frac{\partial^2}{\partial\tilde{x}_{\mathrm{A}}^2}+\frac{1}{m_{\mathrm{B}}}\frac{\partial^2}{\partial\tilde{x}_{\mathrm{B}}^2}+\frac{1}{m_{\mathrm{C}}}\frac{\partial^2}{\partial\tilde{x}_{\mathrm{C}}^2}\right)+V\left(t,\tilde{Y}\right)\right]\Psi = i\hbar\frac{\partial\Psi}{\partial t} \ , \tag{2.179}$$

being $V\left(t,\tilde{Y}\right)$ the sum of the potential energies of all interactions (the interaction between the molecular particle and the atomic particle and the interaction between the nuclei of the molecular particle):

$$V\left(t,\tilde{Y}\right) = V'\left(t,\tilde{Y}\right) + \frac{1}{2}f\tilde{Y}^2 \ . \tag{2.180}$$

By making a change of variables of the local coordinates $\tilde{x}_{\mathrm{A}}$, $\tilde{x}_{\mathrm{B}}$ and $\tilde{x}_{\mathrm{C}}$ to the relative and average ones $\tilde{x}_R$, $\tilde{X}$, $\tilde{Y}$, it's possible to transform equation (2.179) into

$$\left[-\frac{\hbar^2}{2}\left(\frac{1}{\tilde{M}}\frac{\partial^2}{\partial\tilde{x}_R^2}+\frac{1}{\tilde{m}}\frac{\partial^2}{\partial\tilde{X}^2}+\frac{1}{\mu}\frac{\partial^2}{\partial\tilde{Y}^2}\right)+V\left(t,\tilde{Y}\right)\right]\Psi = i\hbar\frac{\partial\Psi}{\partial t} \ . \tag{2.181}$$

Because the potential V doesn't depend on $\tilde{x}_R$ neither on $\tilde{X}$, the separation of variables method can be applied, and the wave function Ψ can be transformed into a multiplication of other two, each one with the respective separated variables as arguments:

$$\Psi\left(t,\tilde{x}_R,\tilde{X},\tilde{Y}\right) = \theta\left(\tilde{x}_R,\tilde{X}\right)\psi\left(t,\tilde{Y}\right) \ . \tag{2.182}$$

By inserting (2.182) into (2.181), and by taking into account the dependence of each side of the resultant equation on the separated variables, two new equations can be obtained:

$$\begin{cases} -\dfrac{\hbar^2}{2}\left(\dfrac{1}{\tilde{M}}\dfrac{\partial^2}{\partial\tilde{x}_R^2}+\dfrac{1}{\tilde{m}}\dfrac{\partial^2}{\partial\tilde{X}^2}\right)\theta = \lambda\theta \ , & \text{(2.183a)} \\ \left[-\dfrac{\hbar^2}{2\mu}\dfrac{\partial^2}{\partial\tilde{Y}^2}+\lambda+V\left(t,\tilde{Y}\right)\right]\psi = i\hbar\dfrac{\partial\psi}{\partial t} \ , & \text{(2.183b)} \end{cases}$$

being λ some constant. Only equation (2.183b) will matter from now on, since it is the one which deals with the vibration of the molecular particle. By invoking again the assumption $|\tilde{Y}| \ll L$ the exponential term in the interaction potential (2.178) can be approximated by its first order Taylor expansion around $\alpha\tilde{Y} = 0$, i.e. $e^{\alpha\gamma\tilde{Y}} \approx 1+\alpha\gamma\tilde{Y}$ giving

$$V'(t,\tilde{Y}) = -F(t)\left(\frac{1}{\alpha\gamma}+\tilde{Y}\right) \ , \tag{2.184}$$

with $F(t) = -\alpha\gamma E_0 \operatorname{sech}^2\left(\frac{\alpha v_0}{2}t\right)$. Note that $F(t)$ has units of force, and it would be equivalent to the quantity $-\gamma F_{BC}(t)$, if $\tilde{Y} = 0\ \forall\, t$. By substituting (2.184) in (2.180), and inserting the result in (2.183b),

one can obtain

$$\left[-\frac{\hbar^2}{2\mu}\frac{\partial^2}{\partial\tilde{Y}^2}+\lambda-F(t)\left(\frac{1}{\alpha\gamma}+\tilde{Y}\right)+\frac{1}{2}f\tilde{Y}^2\right]\psi=i\hbar\frac{\partial\psi}{\partial t}\ . \tag{2.185}$$

Let's now perform a convenient change of variables from ψ to ϕ, where ϕ is given by

$$\phi\left(t,\tilde{Y}\right)=\psi\left(t,\tilde{Y}\right)e^{\frac{i}{\hbar}\int_{-\infty}^{t}\left[\lambda-\frac{F(t')}{\alpha\gamma}\right]dt'}\ . \tag{2.186}$$

By substituting (2.186) in (2.185), an equation which no longer depends on the constant λ and on the term $F(t)/\alpha\gamma$ is obtained:

$$\left[-\frac{\hbar^2}{2\mu}\frac{\partial^2}{\partial\tilde{Y}^2}-F(t)\tilde{Y}+\frac{1}{2}f\tilde{Y}^2\right]\phi=i\hbar\frac{\partial\phi}{\partial t}\ . \tag{2.187}$$

Equation (2.187) it's still too complicated to be solved as it is. Let's perform another convenient change of variables

$$\Phi(t,\xi)=\phi(t,\tilde{Y})e^{-g(t)\tilde{Y}}\ , \tag{2.188}$$

where $\xi\left(t,\tilde{Y}\right)=\tilde{Y}-u(t)$, being $u(t)$ and $g(t)$ some functions of time. By substituting the relation (2.188) in (2.187), one can get

$$\left(-\frac{\hbar^2}{2\mu}\frac{\partial^2}{\partial\xi^2}+\left[i\hbar\dot{u}-\frac{\hbar^2}{\mu}g\right]\frac{\partial}{\partial\xi}+\left\{\left[\frac{1}{2}fu^2-Fu-i\hbar u\dot{g}-\frac{\hbar^2}{2\mu}g^2\right]+\left[fu-F-i\hbar\dot{g}\right]\xi+\frac{1}{2}f\xi^2\right\}\right)\Phi=i\hbar\frac{\partial\Phi}{\partial t}\ . \tag{2.189}$$

Note that no restrictions were imposed to the functions $u(t)$ and $g(t)$. They are arbitrary and can be defined in any useful manner. To simplify equation (2.189), one can choose $u(t)$ and $g(t)$ such that the multiplying coefficients of $\frac{\partial\Phi}{\partial\xi}$ and $\xi\Phi$ become null. These conditions result in two new equations:

$$\begin{cases} i\hbar g(t)=-\mu\dot{u}(t)\ , & \text{(2.190a)}\\ \mu\ddot{u}(t)+fu(t)=F(t)\ . & \text{(2.190b)}\end{cases}$$

Curiously, (2.190b) corresponds to the equation of movement of a classical harmonic oscillator, of mass $m=\mu$, subjected to an applied force $F(t)$, being $u(t)$ the displacement relatively to the equilibrium position. Note that (2.190b) is a second order differential equation, which requires two boundary conditions to be totally defined. These boundary conditions will be chosen to be $u(-\infty)=\dot{u}(-\infty)=0$. The hypothetical classical harmonic oscillator is then considered to be initially at rest and at equilibrium. By substituting (2.190a) and (2.190b) in (2.189), one obtains

$$\left[-\frac{\hbar^2}{2\mu}\frac{\partial^2}{\partial\xi^2}+\delta(t)+\frac{1}{2}f\xi^2\right]\Phi=i\hbar\frac{\partial\Phi}{\partial t}\ , \tag{2.191}$$

being $\delta(t)=\frac{1}{2}\mu\dot{u}^2(t)-\frac{1}{2}fu^2(t)$. As shown before, the change of variables

$$\Theta(t,\xi)=\Phi(t,\xi)e^{\frac{i}{\hbar}\int_{-\infty}^{t}\delta(t')dt'} \tag{2.192}$$

proves to be useful in simplifying equation (2.191). By substituting (2.192) in (2.191), one obtains

$$\left[-\frac{\hbar^2}{2\mu}\frac{\partial^2}{\partial\xi^2}+\frac{1}{2}f\xi^2\right]\Theta = i\hbar\frac{\partial\Theta}{\partial t}\ . \tag{2.193}$$

Equation (2.193) is the well-known equation of the quantum free harmonic oscillator (A.1) with mass $m=\mu$, whose solution according to (A.2) is

$$\Theta(t,\xi)=\sum_{n=0}^{\infty}c_n H_n(\xi)e^{-i\frac{E_n}{\hbar}t}\ . \tag{2.194}$$

And in comparison with (A.3) and (A.4), the eigenfunctions $H_n(\xi)$ and eigenenergies E_n are given by

$$H_n(\xi)=\left(\frac{\mu\omega}{\pi\hbar}\right)^{\frac{1}{4}}(2^n n!)^{-\frac{1}{2}}\mathscr{H}_n\left(\frac{\xi}{\sqrt{\frac{\hbar}{\mu\omega}}}\right)e^{-\frac{\mu\omega}{2\hbar}\xi^2}\ , \qquad E_n=\left(n+\frac{1}{2}\right)\hbar\omega\ , \tag{2.195, 2.196}$$

respectively. By reverting the last two changes of variables, (2.192) and (2.188), and substituting $g(t)$ by the result (2.190a), the solution (2.194) can be written as

$$\phi\left(t,\tilde{Y}\right)=\sum_{n=0}^{\infty}c_n H_n(\xi)e^{\frac{i}{\hbar}\left(-E_n t+\mu\dot{u}(t)\tilde{Y}-\int_{-\infty}^{t}\delta(t')dt'\right)}\ . \tag{2.197}$$

And by reverting one more change of variables, the one represented by (2.186), it's possible to finally obtain a general solution for the vibrational wave function:

$$\psi\left(t,\tilde{Y}\right)=\sum_{n=0}^{\infty}c_n H_n(\xi)e^{\frac{i}{\hbar}\left(-E_n t+\mu\dot{u}(t)\tilde{Y}-\int_{-\infty}^{t}\left[\lambda+\delta(t')-\frac{F(t')}{\alpha\gamma}\right]dt'\right)}\ . \tag{2.198}$$

It can be shown that at sufficiently long time before the collision, say $t=-\infty$, the solution (2.198) is identical to the one of the free harmonic oscillator (A.2), with mass $m=\mu$, and displacement $\tilde{Y}$:

$$\lim_{t\to-\infty}\psi\left(t,\tilde{Y}\right)=\sum_{n=0}^{\infty}c_n H_n(\tilde{Y})e^{-i\frac{E_n}{\hbar}t}\ . \tag{2.199}$$

If the molecular particle was initially in the n-th vibrational level, then only the n-th term of the infinite series is present in the solution (2.199), which means that only the coefficient c_n is non-null. In fact, one has $c_m=\delta_{nm}\ \forall m=0,\ ...,\ \infty$, due to the wave function normalisation condition. Hence, solution (2.198) is simplified to

$$\psi\left(t,\tilde{Y}\right)=H_n(\xi)e^{\frac{i}{\hbar}\left(-E_n t+\mu\dot{u}(t)\tilde{Y}-\int_{-\infty}^{t}\left[\lambda+\delta(t')-\frac{F(t')}{\alpha\gamma}\right]dt'\right)}\ . \tag{2.200}$$

To compute the probability of transition between vibrational levels it's necessary to firstly express function (2.200) in terms of the eigenfunctions $H_n\left(\tilde{Y}\right)$. Since these constitute an orthonormal basis, they can be used to express $\psi\left(t,\tilde{Y}\right)$ through a series expansion:

$$\psi\left(t,\tilde{Y}\right)=\sum_{m=0}^{\infty}b_m(t)H_m\left(\tilde{Y}\right)e^{-i\frac{E_m}{\hbar}t}\ , \tag{2.201}$$

where $b_m(t)$ are some time-dependent functions. According to *Born's rule*, the probability of the molecular particle AB to transit from the vibrational level n to the vibrational level m is given by

$$P_n^m = \left| \int_{-\infty}^{\infty} \psi^* \left(\infty, \tilde{Y}\right) H_m(\tilde{Y}) e^{-i\frac{E_m}{\hbar}t} \, d\tilde{Y} \right|^2 = |b_m(+\infty)|^2 \ . \tag{2.202}$$

From (2.202), (2.201), (2.200) and by considering the properties of the physicists' Hermite polynomials, one may express $P_{n\to m}$ through some already known physical quantities:

$$P_n^m = n!m!\eta_0^{n+m} e^{-\eta_0} \left(\sum_{k=0}^{l} \frac{(-1)^k \eta_0^{-k}}{(n-k)!(m-k)!k!} \right)^2 \ , \tag{2.203}$$

where $l = \min(n, m)$. The quantity η_0 is the energy (sum of kinetic and potential energies) of the classical harmonic oscillator at $t = +\infty$, divided by the quantum energy $\hbar\omega$:

$$\eta_0 = \frac{\frac{1}{2} f u^2(+\infty) + \frac{1}{2}\mu \dot{u}^2(+\infty)}{\hbar\omega} \ . \tag{2.204}$$

By solving the differential equation (2.190b), with the initial conditions $u(-\infty) = \dot{u}(-\infty) = 0$, and force $F(t) = -\alpha\gamma E_0 \operatorname{sech}^2\left(\frac{\alpha v_0}{2} t\right)$, one may show that

$$\eta_0 = \frac{2\pi^2 \omega \tilde{m}^2 \gamma^2}{\mu\hbar\alpha^2} \operatorname{csch}^2\left(\frac{\pi\omega}{\alpha v_0}\right) \ . \tag{2.205}$$

2.7.3 The case of V-V-T processes

Here, the computation of probabilities of transition between vibrational levels due to a collision between two diatomic molecular particles, AB and CD, based on the FHO theory [28, 53] will be presented. The collision model is depicted in Figure 2.8.

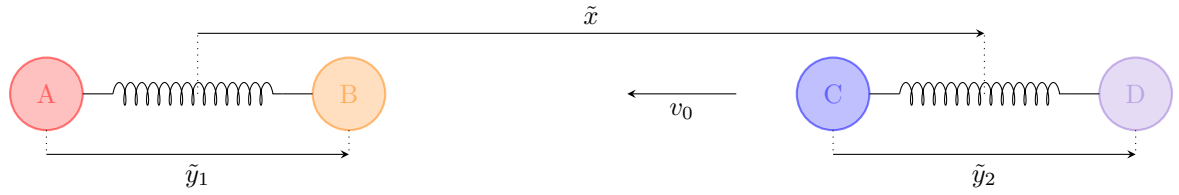

Figure 2.8: Collinear collision between two diatomic molecular particles AB and CD.

Similarly to what was previously defined for the V-T processes case, $\tilde{x}_{\mathrm{A}}$ and m_{A} are the position of the nucleus A and its mass, respectively. The analogous notation follows for the other nuclei, B, C and D. The quantity $\tilde{x}_R$ is the centre of mass of the whole system. The coordinates presented by Figure 2.8 are: the difference between the positions of the molecular particles centres of mass, $\tilde{x} = \tilde{\tilde{x}}_{\mathrm{CD}} - \tilde{\tilde{x}}_{\mathrm{AB}}$, the difference between the positions of the nuclei of the molecular particle AB, $\tilde{y}_1 = \tilde{x}_{\mathrm{B}} - \tilde{x}_{\mathrm{A}}$, and the difference between the positions of the nuclei of the molecular particle CD, $\tilde{y}_2 = \tilde{x}_{\mathrm{D}} - \tilde{x}_{\mathrm{C}}$. There are six mass parameters that will prove to be useful in the upcoming derivations: factors γ_1 and γ_2, the reduced mass of the molecular particle AB μ_1, the reduced mass of the molecular particle CD μ_2, the reduced

mass of the two molecular particles $\tilde{m}$, and the sum of all particles masses $\tilde{M}$. These are defined by

$$\gamma_1 = \frac{m_{\mathrm{A}}}{m_{\mathrm{A}} + m_{\mathrm{B}}} \ , \qquad (2.206) \qquad \gamma_2 = \frac{m_{\mathrm{D}}}{m_{\mathrm{C}} + m_{\mathrm{D}}} \ , \qquad (2.207) \qquad \mu_1 = \frac{m_{\mathrm{A}} m_{\mathrm{B}}}{m_{\mathrm{A}} + m_{\mathrm{B}}} \ , \qquad (2.208)$$

$$\mu_2 = \frac{m_{\mathrm{C}} m_{\mathrm{D}}}{m_{\mathrm{C}} + m_{\mathrm{D}}} \ , \qquad (2.209) \qquad \tilde{m} = \frac{(m_{\mathrm{A}} + m_{\mathrm{B}})\,(m_{\mathrm{C}} + m_{\mathrm{D}})}{m_{\mathrm{A}} + m_{\mathrm{B}} + m_{\mathrm{C}} + m_{\mathrm{D}}} \ , \qquad (2.210)$$

$$\tilde{M} = m_{\mathrm{A}} + m_{\mathrm{B}} + m_{\mathrm{C}} + m_{\mathrm{D}} \ , \qquad (2.211)$$

respectively. As also happened for the V-T processes case, it's assumed that only the interaction between the nearest nuclei, B and C, matters, and therefore, the interaction potential, V', only depends on $\tilde{x}_{\mathrm{C}} - \tilde{x}_{\mathrm{B}}$. It has then the following form: $V'\left(\tilde{x}_{\mathrm{C}} - \tilde{x}_{\mathrm{B}}\right) = A\, e^{-\alpha(\tilde{x}_{\mathrm{C}} - \tilde{x}_{\mathrm{B}})}$, being A and α two positive constants. And by noticing that $\tilde{x}_{\mathrm{C}} - \tilde{x}_{\mathrm{B}} = \tilde{x} - \gamma_1 \tilde{y}_1 - \gamma_2 \tilde{y}_2$, the potential can be expressed through

$$V'\left(\tilde{x}, \tilde{y}_1, \tilde{y}_2\right) = A\, e^{-\alpha(\tilde{x} - \gamma_1 \tilde{y}_1 - \gamma_2 \tilde{y}_2)} \ . \qquad (2.212)$$

Because the molecular particles are assumed to be harmonic oscillators, the force that A imposes in B and the force that C imposes in D follow Hooke's law, and therefore these are given by $F_{\mathrm{AB}} = -f_1\left(\tilde{y}_1 - \tilde{y}_{0,1}\right)$ and $F_{\mathrm{CD}} = -f_2\left(\tilde{y}_2 - \tilde{y}_{0,2}\right)$, respectively, being f_1 and f_2 force constants and $\tilde{y}_{0,1}$ and $\tilde{y}_{0,2}$, the difference between the positions of the nuclei of the respective molecular particles at equilibrium. Forces F_{BC}, F_{AB} and F_{CD} have a conventional positive signal to the right direction.

According to the Newton's second law, one can write

$$\begin{cases} m_{\mathrm{A}} \ddot{\tilde{x}}_{\mathrm{A}} = F_{\mathrm{BA}} + F_{\mathrm{CA}} + F_{\mathrm{DA}} \ , & (2.213a) \\ m_{\mathrm{B}} \ddot{\tilde{x}}_{\mathrm{B}} = F_{\mathrm{AB}} + F_{\mathrm{CB}} + F_{\mathrm{DB}} \ , & (2.213b) \\ m_{\mathrm{C}} \ddot{\tilde{x}}_{\mathrm{C}} = F_{\mathrm{AC}} + F_{\mathrm{BC}} + F_{\mathrm{DC}} \ , & (2.213c) \\ m_{\mathrm{D}} \ddot{\tilde{x}}_{\mathrm{D}} = F_{\mathrm{AD}} + F_{\mathrm{BD}} + F_{\mathrm{CD}} \ . & (2.213d) \end{cases}$$

By making a change of variables, and by substituting the already referred approximations, one can transform the above equations into

$$\begin{cases} \mu_1 \ddot{\tilde{y}}_1 = -f_1\left(\tilde{y}_1 - \tilde{y}_{0,1}\right) - \gamma_1 \alpha A\, e^{-\alpha(\tilde{x} - \gamma_1 \tilde{y}_1 - \gamma_2 \tilde{y}_2)} \ , & (2.214a) \\ \mu_2 \ddot{\tilde{y}}_2 = -f_2\left(\tilde{y}_2 - \tilde{y}_{0,2}\right) - \gamma_2 \alpha A\, e^{-\alpha(\tilde{x} - \gamma_1 \tilde{y}_1 - \gamma_2 \tilde{y}_2)} \ , & (2.214b) \\ \tilde{m} \ddot{\tilde{x}} = \alpha A\, e^{-\alpha(\tilde{x} - \gamma_1 \tilde{y}_1 - \gamma_2 \tilde{y}_2)} \ , & (2.214c) \\ \tilde{M} \ddot{\tilde{x}}_R = 0 \ . & (2.214d) \end{cases}$$

Similarly to the V-T processes case, one can conclude from equation (2.214c) that there's a classical turning point in the trajectory, at $\tilde{x}_t$, at which an inversion in the motion of the particles occurs.

A change of variables will now be performed:

$$\tilde{X} = \tilde{x} - \tilde{x}_t \ , \qquad (2.215) \qquad \tilde{Y}_1 = \tilde{y}_1 - \tilde{y}_{0,1} \ , \qquad (2.216) \qquad \tilde{Y}_2 = \tilde{y}_2 - \tilde{y}_{0,2} \ . \qquad (2.217)$$

By substituting the variables in (2.214a), (2.214b) and (2.214c) for the respective new ones, it's possible to obtain

$$\begin{cases} \mu_1 \ddot{\tilde{Y}}_1 = -f_1 \tilde{Y}_1 - \gamma_1 \alpha A'' \, e^{-\alpha\left(\tilde{X} - \gamma_1 \tilde{Y}_1 - \gamma_2 \tilde{Y}_2\right)} \ , & (2.218a) \\ \mu_2 \ddot{\tilde{Y}}_2 = -f_2 \tilde{Y}_2 - \gamma_2 \alpha A'' \, e^{-\alpha\left(\tilde{X} - \gamma_1 \tilde{Y}_1 - \gamma_2 \tilde{Y}_2\right)} \ , & (2.218b) \\ \tilde{m} \ddot{\tilde{X}} = \alpha A'' \, e^{-\alpha\left(\tilde{X} - \gamma_1 \tilde{Y}_1 - \gamma_2 \tilde{Y}_2\right)} \ , & (2.218c) \end{cases}$$

with $A'' = A \, e^{-\alpha(\tilde{x}_t - \gamma_1 \tilde{y}_{0,1} - \gamma_2 \tilde{y}_{0,2})}$. Under the assumption $|\tilde{Y}_1|, |\tilde{Y}_2| \ll L$, the following approximation $e^{\alpha\left(\gamma_1 \tilde{Y}_1 + \gamma_2 \tilde{Y}_2\right)} \approx 1$ may be performed. In these terms, equation (2.218c) can be transformed into

$$\tilde{m} \ddot{\tilde{X}} = \alpha A'' \, e^{-\alpha \tilde{X}} \ . \tag{2.219}$$

Equation (2.219) has the same form has the one obtained for the V-T processes case, (2.175). And therefore, it has also an identical solution:

$$\tilde{X}(t) = \frac{2}{\alpha} \ln \left[\cosh \left(\sqrt{\frac{A''}{2\tilde{m}}} \alpha t \right) \right] \ . \tag{2.220}$$

And by applying the initial condition $\dot{\tilde{X}}(-\infty) = -v_0$, one can find that

$$A'' = \frac{1}{2} \tilde{m} v_0^2 := E_0 \ , \tag{2.221}$$

being E_0 the relative kinetic energy of the two molecular particles centres of mass at $t = -\infty$. By inserting the solution (2.220) and the relation (2.221) into the interaction potential defined by (2.212), the dependence on $\tilde{X}$ is substituted by a dependence on t, giving

$$V'(t, \tilde{Y}_1, \tilde{Y}_2) = E_0 \, \mathrm{sech}^2 \left(\frac{\alpha v_0}{2} t \right) e^{\alpha\left(\gamma_1 \tilde{Y}_1 + \gamma_2 \tilde{Y}_2\right)} \ . \tag{2.222}$$

The interaction potential in this form is ready to be inserted into the Schrödinger equation of the whole system. Such Schrödinger equation is expressed by

$$\left[-\frac{\hbar^2}{2} \left(\frac{1}{m_\mathrm{A}} \frac{\partial^2}{\partial \tilde{x}_\mathrm{A}^2} + \frac{1}{m_\mathrm{B}} \frac{\partial^2}{\partial \tilde{x}_\mathrm{B}^2} + \frac{1}{m_\mathrm{C}} \frac{\partial^2}{\partial \tilde{x}_\mathrm{C}^2} + \frac{1}{\tilde{m}_\mathrm{D}} \frac{\partial^2}{\partial \tilde{x}_\mathrm{D}^2} \right) + V\left(t, \tilde{Y}_1, \tilde{Y}_2\right) \right] \Psi = i\hbar \frac{\partial \Psi}{\partial t} \ , \tag{2.223}$$

being V the sum of the potential energy of all interactions (the interaction between the molecular particles and the interactions between the nuclei of each molecular particle):

$$V\left(t, \tilde{Y}_1, \tilde{Y}_2\right) = V'\left(t, \tilde{Y}_1, \tilde{Y}_2\right) + \frac{1}{2} f_1 Y_1^2 + \frac{1}{2} f_2 \tilde{Y}_2^2 \ . \tag{2.224}$$

By making a change of variables of the local coordinates $\tilde{x}_A$, $\tilde{x}_B$, $\tilde{x}_C$ and $\tilde{x}_D$ to the relative and average ones $\tilde{x}_R$, $\tilde{X}$, $\tilde{Y}_1$ and $\tilde{Y}_2$, it's possible to transform equation (2.223) into

$$\left[-\frac{\hbar^2}{2} \left(\frac{1}{\tilde{M}} \frac{\partial^2}{\partial \tilde{x}_R^2} + \frac{1}{\tilde{m}} \frac{\partial^2}{\partial \tilde{X}^2} + \frac{1}{\mu_1} \frac{\partial^2}{\partial \tilde{Y}_1^2} + \frac{1}{\mu_2} \frac{\partial^2}{\partial \tilde{Y}_2^2} \right) + V\left(t, \tilde{Y}_1, \tilde{Y}_2\right) \right] \Psi = i\hbar \frac{\partial \Psi}{\partial t} \ . \tag{2.225}$$

Because the potential V doesn't depend on $\tilde{x}_R$ neither on $\tilde{X}$, the separation of variables method can be applied, and the wave function Ψ can be transformed into a multiplication of other two, each one with the respective separated variables:

$$\Psi\left(t, \tilde{x}_R, \tilde{X}, \tilde{Y}_1, \tilde{Y}_2\right) = \theta\left(\tilde{x}_R, \tilde{X}\right)\psi\left(t, \tilde{Y}_1, \tilde{Y}_2\right) \ . \tag{2.226}$$

By making the substitution of (2.226) in (2.225), and by taking into account the dependence of each side of the resultant equation on the separated variables, two new equations can be obtained:

$$\begin{cases} -\dfrac{\hbar^2}{2}\left(\dfrac{1}{\tilde{M}}\dfrac{\partial^2}{\partial\tilde{x}_R^2} + \dfrac{1}{\tilde{m}}\dfrac{\partial^2}{\partial\tilde{X}^2}\right)\theta = \lambda\theta \ , & \text{(2.227a)} \\ \left[-\dfrac{\hbar^2}{2}\left(\dfrac{1}{\mu_1}\dfrac{\partial^2}{\partial\tilde{Y}_1^2} + \dfrac{1}{\mu_2}\dfrac{\partial^2}{\partial\tilde{Y}_2^2}\right) + \lambda + V\left(t, \tilde{Y}_1, \tilde{Y}_2\right)\right]\psi = i\hbar\dfrac{\partial\psi}{\partial t} \ , & \text{(2.227b)} \end{cases}$$

being λ some constant. Only equation (2.227b) will matter from now on, since it is the one which deals with the vibration of the molecular particles.

It's important to refer here that an analytic expression for the transition probabilities between any vibrational levels can only be obtained for the case of a symmetrical collision AB-BA, i.e. in which C = B and D = A, as depicted in Figure 2.9. Therefore, one may derive such analytic expression and then apply a correction that generalises the collision to the asymmetric case (although only in an approximate way). The details associated to the correction are saved for later.

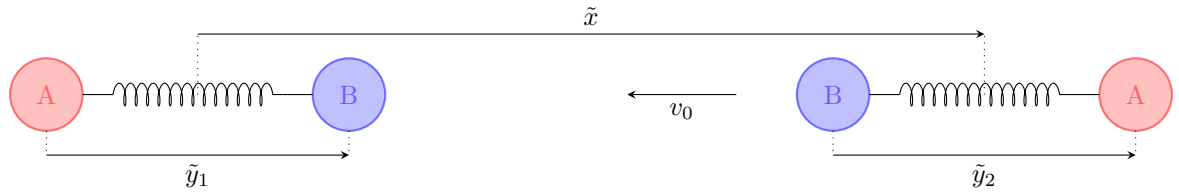

Figure 2.9: Collinear collision between two diatomic molecular particles AB and BA.

Very intuitively, it's possible to show that the parameters associated to each molecular particle in a symmetric collision are equal:

$$\gamma_1 = \gamma_2 = \frac{m_\mathrm{A}}{m_\mathrm{A} + m_\mathrm{B}} := \gamma \ , \tag{2.228}$$

$$\mu_1 = \mu_2 = \frac{m_\mathrm{A} m_\mathrm{B}}{m_\mathrm{A} + m_\mathrm{B}} := \mu \ , \tag{2.229}$$

$$f_1 = f_2 := f \ , \tag{2.230}$$

and because of this, the subscript indices 1 and 2 in the notation of these quantities will be no more necessary. Note that if the molecular particles weren't equal, the above relations would not be satisfied, and even if they were equal, but their orientation was the inverse (i.e. if the collision was AB-AB instead of AB-BA) the relation $\gamma_1 = \gamma_2$ would not hold. Therefore, both constitution and orientation of the molecular particles do matter in the collision. The theory herein presented for the symmetric collinear collision between diatomic molecular particles follows the procedure of Zelechow et al. [28].

By invoking again the assumption $|\tilde{Y}_1|, |\tilde{Y}_2| \ll L$, the exponential in equation (2.222) can be approximated

by its second order Taylor series expansion around $\alpha\left(\tilde{Y}_1+\tilde{Y}_2\right)=0$, resulting in

$$e^{\alpha\gamma\left(\tilde{Y}_1+\tilde{Y}_2\right)} \approx 1+\alpha\gamma\left(\tilde{Y}_1+\tilde{Y}_2\right)+\frac{\alpha^2\gamma^2}{2}\left(\tilde{Y}_1+\tilde{Y}_2\right)^2 \ . \tag{2.231}$$

And by substituting (2.231) in (2.222), one would get

$$V'(t,\tilde{Y}_1,\tilde{Y}_2)=-F(t)\left[\frac{1}{\alpha\gamma}+\tilde{Y}_1+\tilde{Y}_2+\frac{\alpha\gamma}{2}\left(\tilde{Y}_1+\tilde{Y}_2\right)^2\right] \ , \tag{2.232}$$

being $F(t)=-\alpha\gamma E_0\,\mathrm{sech}^2\left(\frac{\alpha v_0}{2}t\right)$. Note that $F(t)$ has units of force, and it would be equivalent to the quantity $-\gamma F_{BC}(t)$, if $\tilde{Y}_1=\tilde{Y}_2=0\,\forall\, t$.

By taking into account relations (2.228), (2.229), (2.230), (2.224), and the interaction potential in its new form (2.232), the Schrödinger equation for the molecular particles vibrations (2.227b) becomes

$$\left\{-\frac{\hbar^2}{2\mu}\left(\frac{\partial^2}{\partial\tilde{Y}_1^2}+\frac{\partial^2}{\partial\tilde{Y}_2^2}\right)+\lambda-F(t)\left[\frac{1}{\alpha\gamma}+\tilde{Y}_1+\tilde{Y}_2+\frac{\alpha\gamma}{2}\left(\tilde{Y}_1+\tilde{Y}_2\right)^2\right]+\frac{1}{2}f\left(\tilde{Y}_1^2+\tilde{Y}_2^2\right)\right\}\psi=i\hbar\frac{\partial\psi}{\partial t} \ . \tag{2.233}$$

The quantity $\lambda-\frac{F(t)}{\alpha\gamma}$ can be removed from (2.233), by performing the substitution

$$\phi\left(t,\tilde{Y}_1,\tilde{Y}_2\right)=\psi\left(t,\tilde{Y}_1,\tilde{Y}_2\right)e^{\frac{i}{\hbar}\int_{-\infty}^{t}\left[\lambda-\frac{F(t')}{\alpha\gamma}\right]dt'} \ , \tag{2.234}$$

resulting in

$$\left\{-\frac{\hbar^2}{2\mu}\left(\frac{\partial^2}{\partial\tilde{Y}_1^2}+\frac{\partial^2}{\partial\tilde{Y}_2^2}\right)-F(t)\left[\tilde{Y}_1+\tilde{Y}_2+\frac{\alpha\gamma}{2}\left(\tilde{Y}_1+\tilde{Y}_2\right)^2\right]+\frac{1}{2}f\left(\tilde{Y}_1^2+\tilde{Y}_2^2\right)\right\}\phi=i\hbar\frac{\partial\phi}{\partial t} \ . \tag{2.235}$$

By performing a change of variables from $\tilde{Y}_1$ and $\tilde{Y}_2$ to $\tilde{Y}_S$ and $\tilde{Y}_A$, where $\tilde{Y}_S=1/\sqrt{2}\left(\tilde{Y}_1+\tilde{Y}_2\right)$ and $\tilde{Y}_A=1/\sqrt{2}\left(\tilde{Y}_1-\tilde{Y}_2\right)$, it's possible to transfrom equation (2.235) into

$$\left\{-\frac{\hbar^2}{2\mu}\left(\frac{\partial^2}{\partial\tilde{Y}_S^2}+\frac{\partial^2}{\partial\tilde{Y}_A^2}\right)-F(t)\left[\sqrt{2}\tilde{Y}_S+\alpha\gamma\tilde{Y}_S^2\right]+\frac{1}{2}f\left(\tilde{Y}_S^2+\tilde{Y}_A^2\right)\right\}\psi=i\hbar\frac{\partial\psi}{\partial t} \ . \tag{2.236}$$

Using the method of separation of variables, one can write

$$\phi\left(t,\tilde{Y}_S,\tilde{Y}_A\right)=\phi_S\left(t,\tilde{Y}_S\right)\phi_A\left(t,\tilde{Y}_A\right) \ . \tag{2.237}$$

By substituting (2.237) in (2.236), and by taking into account the dependence on the variables $\tilde{Y}_S$ and $\tilde{Y}_A$ in each side of the resulting equation one, it's possible to obtain two new equations:

$$\begin{cases}\left\{-\dfrac{\hbar^2}{2\mu}\dfrac{\partial^2}{\partial\tilde{Y}_S^2}-\sqrt{2}F(t)\tilde{Y}_S+\dfrac{1}{2}\left[f-2\alpha\gamma F(t)\right]\tilde{Y}_S^2\right\}\phi_S=i\hbar\dfrac{\partial\phi_S}{\partial t}-g(t)\phi_S \ , & \text{(2.238a)}\\ \left(-\dfrac{\hbar^2}{2\mu}\dfrac{\partial^2}{\partial\tilde{Y}_A^2}+\dfrac{1}{2}f\tilde{Y}_A^2\right)\phi_A=i\hbar\dfrac{\partial\phi_A}{\partial t}+g(t)\phi_A \ , & \text{(2.238b)}\end{cases}$$

where $g(t)$ is some time-dependent function. Let's now perform a convenient change of variables from ϕ_S

and ϕ_A to ψ_S and ψ_A where

$$\psi_S\left(t,\tilde{Y}_S\right)=\phi_S\left(t,\tilde{Y}_S\right)e^{\frac{i}{\hbar}\int_{-\infty}^{t}g(t')\,dt'}\ , \quad (2.239) \qquad \psi_A\left(t,\tilde{Y}_A\right)=\phi_A\left(t,\tilde{Y}_A\right)e^{-\frac{i}{\hbar}\int_{-\infty}^{t}g(t')\,dt'}\ . \quad (2.240)$$

Equations (2.238a) and (2.238b) under such transformations, become:

$$\begin{cases} \left\{-\dfrac{\hbar^2}{2\mu}\dfrac{\partial^2}{\partial\tilde{Y}_S^2}-\sqrt{2}F(t)\tilde{Y}_S+\dfrac{1}{2}\left[f-2\alpha\gamma F(t)\right]\tilde{Y}_S^2\right\}\psi_S=i\hbar\dfrac{\partial\psi_S}{\partial t}\ , & (2.241a)\\ \left(-\dfrac{\hbar^2}{2\mu}\dfrac{\partial^2}{\partial\tilde{Y}_A^2}+\dfrac{1}{2}f\tilde{Y}_A^2\right)\psi_A=i\hbar\dfrac{\partial\psi_A}{\partial t}\ . & (2.241b)\end{cases}$$

If $2\alpha\gamma F(t)\ll f$ (note that this condition may not be valid for too high temperatures) one can assume that $f_S(t):=f-2\alpha\gamma F(t)$ is constant. With this approximation taken into consideration, equation (2.241a) turns to be identical to equation (2.187) with $F(t)$ substituted by $\sqrt{2}F(t)$ and f substituted by $f_S(t)$. Therefore, its solution is in the same manner identical to (2.197), with the referred modifications, i.e.

$$\psi_S\left(t,\tilde{Y}_S\right)=\sum_{n=0}^{\infty}c_{S,n}H_{S,n}(t,\xi)e^{\frac{i}{\hbar}\left(-E_{S,n}(t)t+\mu\dot{u}(t)\tilde{Y}_S-\int_{-\infty}^{t}\delta(t')dt'\right)}\ , \quad (2.242)$$

where:

$$\xi\left(t,\tilde{Y}_S\right)=\tilde{Y}_S-u(t)\ , \quad (2.243) \qquad \omega_S(t)=\sqrt{\frac{f_S(t)}{\mu}}\ , \quad (2.244) \qquad \delta(t)=\frac{1}{2}\mu\dot{u}^2(t)-\frac{1}{2}f_S(t)u^2(t)\ , \quad (2.245)$$

$$H_{S,n}\left(t,\xi\right)=\left[\frac{\mu\omega_S(t)}{\pi\hbar}\right]^{\frac{1}{4}}\left(2^n n!\right)^{-\frac{1}{2}}\mathscr{H}_n\left(\frac{\xi}{\sqrt{\frac{\hbar}{\mu\omega_S(t)}}}\right)e^{-\frac{\mu\omega_S(t)}{2\hbar}\xi^2}\ , \quad (2.246)$$

$$E_{S,n}(t)=\hbar\omega_S(t)\left(n+\frac{1}{2}\right)\ . \quad (2.247)$$

According to (2.190b), the quantity $u(t)$ is the solution of the initial value problem

$$\begin{cases}\mu\ddot{u}(t)+f_S(t)u(t)=\sqrt{2}F(t)\ , & (2.248a)\\ u(-\infty)=\dot{u}(-\infty)=0\ . & (2.248b)\end{cases}$$

Equation (2.241b) is identical to (A.1), which governs a free harmonic oscillator of mass μ and natural frequency $\omega=\sqrt{\frac{f}{\mu}}$. By comparison with (A.2), one can write

$$\psi_A\left(t,\tilde{Y}_A\right)=\sum_{n=0}^{\infty}c_{A,n}H_{A,n}\left(\tilde{Y}_A\right)e^{-\frac{i}{\hbar}E_{A,n}t}\ , \quad (2.249)$$

being $H_{A,n}$ and $E_{A,n}$ the n-th eigenfunction and n-th eigenenergy of the equation, respectively. These are given by

$$H_{A,n}\left(\tilde{Y}_A\right)=\left(\frac{\mu\omega}{\pi\hbar}\right)^{\frac{1}{4}}\left(2^n n!\right)^{-\frac{1}{2}}\mathscr{H}_n\left(\frac{\tilde{Y}_A}{\sqrt{\frac{\hbar}{\mu\omega}}}\right)e^{-\frac{\mu\omega}{2\hbar}\tilde{Y}_A^2}\ , \quad (2.250) \qquad E_{A,n}=\left(n+\frac{1}{2}\right)\hbar\omega\ . \quad (2.251)$$

Therefore, by reverting the changes of variables (2.240), (2.239) and (2.234) the general solution for the vibrational wave function is given by

$$\psi\left(t,\tilde{Y}_1,\tilde{Y}_2\right)=\sum_{n,m=0}^{\infty}c_{nm}H_{S,n}(t,\xi)H_{A,m}\left(\tilde{Y}_A\right)e^{\frac{i}{\hbar}\left(-E_{S,n}(t)t-E_{A,m}t+\mu\dot{u}(t)\tilde{Y}_S-\int_{-\infty}^{t}\left[\lambda+\delta(t')-\frac{F(t')}{\alpha\gamma}\right]dt'\right)}\ . \tag{2.252}$$

It can be shown that if the molecular particles AB and CD were initially in the vibrational levels n and m, respectively, the function ψ evaluated at $t=-\infty$ corresponds to

$$\lim_{t=-\infty}\psi\left(t,\tilde{Y}_1,\tilde{Y}_2\right)=H_n\left(\tilde{Y}_1\right)e^{-\frac{i}{\hbar}E_nt}H_m\left(\tilde{Y}_2\right)e^{-\frac{i}{\hbar}E_mt}\ . \tag{2.253}$$

This is the initial condition to impose in the general solution (2.252). By invoking the properties of the physicists' Hermite polynomials, and the Born's rule, one can show, after some cumbersome algebra, that the probability of the molecular particles AB and CD transiting from the vibrational levels n, m to k, j is given by

$$P_{n,m}^{k,j}=\left|\sum_{g=1}^{q}(-1)^{n+m-g+1}\,C_{g,m+1}^{(n+m)}\,C_{g,j+1}^{(k+j)}\,\eta_0^{\frac{n+m}{2}+\frac{k+j}{2}-g+1}\,e^{-\frac{\eta_0}{2}}\right.$$
$$\left.\times\left[(n+m-g+1)!\,(k+j-g+1)!\right]^{\frac{1}{2}}e^{-i(k+j+g-1)\rho}\sum_{l=0}^{q-g}\frac{(-1)^l\eta_0^{-l}}{(n+m-g+1-l)!\,(k+j-g+1-l)!l!}\right|^2\ , \tag{2.254}$$

where $q=\min\left(n+m,k+j\right)$, and $\rho=\frac{2\tilde{m}\gamma^2\alpha v_0}{\mu\omega}$. The quantity $C_{kj}^{(n)}$ is the (k,j)-th entry of a transformation matrix. It is given by

$$C_{kj}^{(n)}=2^{-\frac{n}{2}}\binom{n}{j-1}^{-\frac{1}{2}}\binom{n}{k-1}^{\frac{1}{2}}\sum_{l=0}^{k-1}(-1)^l\binom{n-k+1}{j-l-1}\binom{k-1}{l}\ . \tag{2.255}$$

In (2.255), the brackets notations represent combinations. Similarly to the V-T processes case, the quantity η_0 is the energy (sum of kinetic and potential energies) of the classical harmonic oscillator at $t=+\infty$, divided by the quantum energy $\hbar\omega$. It can be shown that this quantity is given by

$$\eta_0=\frac{4\pi^2\omega\tilde{m}^2\gamma^2}{\hbar\mu\alpha^2}\,\mathrm{csch}^2\left(\frac{\pi\omega}{\alpha v_0}\right)\ . \tag{2.256}$$

Result (2.256) is equivalent to the one obtained for the V-T processes case (2.205) multiplied by 2.

2.7.4 Consideration of a better interaction potential

In the above sections, when dealing with V-T and V-V-T processes, it was considered a very simple interaction potential between the colliding particles: the repulsive exponential. A more reasonable potential would be one that takes into account the long-range attractive forces, beyond the short-range repulsive ones. The Morse potential V_{M}' depicted in Figure 2.10, is an example.

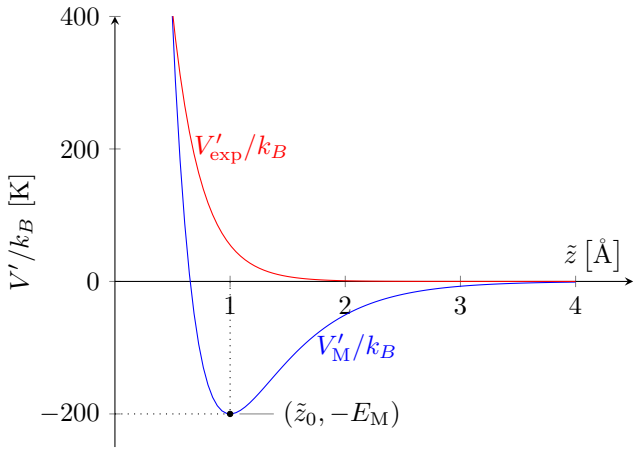

Figure 2.10: The Morse potential V'_{M} and the repulsive exponential potential V'_{exp} divided by the Boltzmann constant k_B, with some illustrative parameters values: $A/k_B = 3000\,\text{K}$, $E_{\text{M}}/k_B = 200\,\text{K}$, $\alpha = 4\,\text{Å}^{-1}$, and $\tilde{z}_0 = 1\,\text{Å}$.

The Morse potential between two particles with difference in positions $\tilde{z}$ is given by

$$V'_{\text{M}}(\tilde{z}) = E_{\text{M}}\left[e^{-\alpha(\tilde{z}-\tilde{z}_0)} - 2e^{-\frac{\alpha}{2}(\tilde{z}-\tilde{z}_0)}\right], \tag{2.257}$$

being E_{M} the potential well (symmetric of the minimum energy value), α an inverse length parameter, and $\tilde{z}_0$ the difference of positions at equilibrium (more specifically, it's the $\tilde{z}$ value for which there's no force between the particles).

Instead of deriving a whole new FHO theory departing from a Morse potential between the B and C nuclei, a different approach is considered [53], in which the interaction potential is simply substituted by

$$V'(\tilde{x}, \tilde{Y}) = E_{\text{M}}\left[e^{-\alpha(\tilde{x}-\tilde{x}_0)} - 2e^{-\frac{\alpha}{2}(\tilde{x}-\tilde{x}_0)}\right] e^{\alpha\gamma\tilde{Y}}\,, \tag{2.258}$$

for the V-T processes case, and

$$V'(\tilde{x}, \tilde{Y}_1, \tilde{Y}_2) = E_{\text{M}}\left[e^{-\alpha(\tilde{x}-\tilde{x}_0)} - 2e^{-\frac{\alpha}{2}(\tilde{x}-\tilde{x}_0)}\right] e^{\alpha\gamma\left(\tilde{Y}_1+\tilde{Y}_2\right)}\,, \tag{2.259}$$

for the V-V-T processes case, being $\tilde{x}_0$ the $\tilde{x}$ equilibrium value. Note that these potentials retain some of the repulsive exponential form, due to the presence of the $\tilde{Y}$ coordinates in an identical way as before. If a full derivation from a pure Morse potential was performed (as done for the repulsive exponential case) different expressions would have been attained for the interaction potential. This isn't then a purist way of deducing a new model, but it is simple and rough as many of the approximations that were taken into account when developing the FHO theory.

By computing $F(t)$ (in which the results of Cottrell and Ream [56] were proven to be useful), and by following the same recipe as before, it's possible to obtain new η_0 and ρ values:

$$\eta_0 = \frac{8\pi^2\omega\tilde{m}^2\gamma^2}{\hbar\mu\alpha^2}\,\text{csch}^2\left(\frac{2\pi\omega}{\alpha v_0}\right)\cosh^2\left[\frac{2\pi\omega}{\alpha v_0}\left(\frac{1}{2}+\frac{\phi}{\pi}\right)\right]\,, \tag{2.260}$$

$$\rho = \frac{4\tilde{m}\gamma^2\alpha v_0}{\mu\omega}\,, \tag{2.261}$$

where $\phi = \arctan\left(\sqrt{E_{\mathrm{M}}/\frac{1}{2}\tilde{m}v_0^2}\right)$. The quantity given by (2.260) is in respect of the V-T processes case. For the V-V-T processes case, η_0 is the double of that one, i.e. $\eta_0^{(\text{V-V-T})} = 2\eta_0^{(\text{V-T})}$.

2.7.5 Approximation that reduces the computational efforts

According to Adamovich et al. [21], if $T_{\mathrm{tr_h}} \gg T_{\mathrm{vib}}$, which usually happens immediately downstream of a strong shock wave, the transition probability of a V-V-T process can be approximated by a multiplication of two uncoupled probabilities with V-T process resemblance:

$$P_{v_1,v_2}^{v_1',v_2'} = P_{v_1}^{v_1'} \cdot P_{v_2}^{v_2'} \ , \tag{2.262}$$

where $P_{v_1}^{v_1'}$ is given by (2.203), and the dependent physical quantities are the ones associated to the first molecular particle, AB. The analogous follows for $P_{v_2}^{v_2'}$. This approximation allows a reduction in the number of rate coefficients that need be computed, as will be later shown.

2.7.6 The case of V-D processes

The FHO theory can be used to build a model for dissociation processes, like the one developed by Macheret and Adamovich [57]. Dissociation happens when the molecular particle achieve sufficiently high vibrational energy levels. But practicability imposes the need of defining a threshold for which it may occur. According to the Macheret and Adamovich, dissociation can be assumed to occur if the energy associated to the final vibrational level is equal or higher than the potential well D_e. The vibrational levels above or at the dissociation limit are called *quasi-bound levels*, and can be obtained through the solution of the Schrödinger equation. Let v_D be the vibrational quantum number associated to a lowest quasi-bound level. The probability of a molecular particle, initially in the v-th vibrational level, to dissociate after a collision with an atomic or molecular particle is then

$$P_v^D = \sum_{v' \geq v_D} P_v^{v'} \ , \tag{2.263}$$

being $P_v^{v'}$ given by (2.203). Note that there was no attempt to discriminate the second collision partner (i.e. the question of being an atomic or a molecular particle), since a decoupling of the V-V-T transition probabilities into two V-T probabilities was assumed. This model has one major drawback: the number of quasi-bound levels involved in the sum in (2.263) is completely arbitrary. One way to overcome this problem is through adjustment, i.e. by choosing this number so that the resultant numerical results are in accordance with experimental data (or more precise theoretical data if the former isn't available).

2.7.7 Computation of the vibrational excitation/de-excitation and dissociation rate coefficients

Vibrational excitation/de-excitation and dissociation rate coefficients can be defined in a similar way as the ones associated to chemical reactions that result from binary collisions. In fact, the processes can be

expressed by a chemical equation with the form of (2.75), as already shown by (2.161), (2.162), (2.163), (2.164a), (2.164b), (2.164c).

The rate of change of the amount concentration of a process product and the associated rate coefficient are given by expressions similar to (2.77) and (2.78), respectively. For example, the rate of change of the amount concentration of molecular particles $\mathrm{AB}(v_1')$ due to collisions between $\mathrm{AB}(v_1)$ with $\mathrm{CD}(v_2)$, in which v_2' may represent a quasi-bound level (hence meaning a dissociation of CD) but not v_1', is according to (2.77)

$$\left(\frac{d\left[\mathrm{AB}(v_1')\right]}{dt}\right)_{v_1,v_2}^{v_1',v_2'} = \left(\nu'_{\mathrm{AB}(v_1')} - \nu_{\mathrm{AB}(v_1')}\right) k_{v_1,v_2}^{v_1',v_2'} \left[\mathrm{AB}(v_1)\right]\left[\mathrm{CD}(v_2)\right] \ . \tag{2.264}$$

It can be shown that $\nu'_{\mathrm{AB}(v_1')} - \nu_{\mathrm{AB}(v_1')} = 1 - \delta_{v_1,v_1'} + \delta_{\mathrm{AB,CD}} \cdot \left(\delta_{v_2',v_1'} - \delta_{v_2,v_1'}\right)$, being δ the Kronecker delta. The respective rate coefficient is then from (2.78):

$$k_{v_1,v_2}^{v_1',v_2'} = \int_0^\infty \sigma_{v_1,v_2}^{v_1',v_2'}(v_0)\, f(v_0)\, dv_0 \ . \tag{2.265}$$

The process cross-section, $\sigma_{v_1,v_2}^{v_1',v_2'}(v_0)$, corresponds to the collisional cross-section, $\sigma(v_0)$, multiplied by the probability of process occurrence in the collision, $P_{v_1,v_2}^{v_1',v_2'}(v_0)$, i.e. $\sigma_{v_1,v_2}^{v_1',v_2'}(v_0) = \sigma(v_0) \cdot P_{v_1,v_2}^{v_1',v_2'}(v_0)$. It's necessary to define a proper distribution function $f(v_0)$ that accounts the restrictive assumptions of the FHO model, more specifically the collinearity of the collisions. Therefore, it may not be right to define v_0 in $f(v_0)$ as the real relative speed of the collision, i.e. the norm of the relative velocity, say v. Adamovich et al. [21], defined the relative speed of collision as the projection of the relative velocity in the line that links the two collision partners centres, $v_0 = v\cos\psi$, being ψ the angle between the relative velocity vector $\vec{v}$, and the line of the centres. On the other hand, because the system is assumed to be in heavy particle translational self-equilibrium, the distribution function $f(v_0) = f(v_0, T_{\mathrm{tr_h}})$ can be shown to be

$$f(v_0, T_{\mathrm{tr_h}}) = \frac{4}{1 + \delta_{\mathrm{AB}(v_1),\mathrm{CD}(v_2)}} \sqrt{\frac{\mu}{2\pi k_B T_{\mathrm{tr_h}}}} v_0 e^{-\frac{\mu v_0^2}{2k_B T_{\mathrm{tr_h}}}} \ , \tag{2.266}$$

being $\delta_{\mathrm{AB}(v_1),\mathrm{CD}(v_2)} = \delta_{\mathrm{AB,CD}} \cdot \delta_{v_1,v_2}$. By substituting (2.266) and the relation for the process cross-section in (2.265), one can obtain

$$k_{v_1,v_2}^{v_1',v_2'}(T_{\mathrm{tr_h}}) = \frac{1}{1 + \delta_{\mathrm{AB,CD}} \cdot \delta_{v_1,v_2}} \frac{\sqrt{\frac{8k_B T_{\mathrm{tr_h}}}{\pi\mu}}}{\frac{k_B T_{\mathrm{tr_h}}}{\mu}} \int_0^\infty \sigma(v_0) P_{v_1,v_2}^{v_1',v_2'}(v_0)\, v_0 e^{-\frac{\mu v_0^2}{2k_B T_{\mathrm{tr_h}}}}\, dv_0 \ . \tag{2.267}$$

One comment should be made about the uncoupling approximation of the transition probabilities for the case of V-V-T processes, given by equation (2.262). This approximation allows one to compute a rate coefficient associated to an excitation/de-excitation of a molecular particle, say $v_1 \to v_1'$, that accounts all the possible excitation/de-excitation transitions as well as dissociation of the other molecular particle, $v_2 \to v_2'$ (including the v_2' quasi-bound levels, meaning dissociation of CD). Let $k_{v_1}^{v_1'}(T_{\mathrm{tr_h}})$ be this rate coefficient. To show the enunciated proposition, one can start by first noticing that the rate of change of

the amount concentration of molecular particles $\mathrm{AB}(v_1')$ due to the transition $v_1, v_2 \to v_1', v_2'$ is given by

$$\left(\frac{d\left[\mathrm{AB}(v_1')\right]}{dt}\right)_{v_1,v_2}^{v_1',v_2'} = \left(\nu'_{\mathrm{AB}(v_1')} - \nu_{\mathrm{AB}(v_1')}\right) k_{v_1,v_2}^{v_1',v_2'}(T_{\mathrm{tr_h}})\left[\mathrm{AB}(v_1)\right]\left[\mathrm{CD}(v_2)\right] . \tag{2.268}$$

And the rate of change of the amount concentration of molecular particles $\mathrm{AB}(v_1')$ due to all transitions $v_1, v_2 \to v_1', v_2'$, with v_1 and v_1' fixed, is given by a sum in v_2 and v_2' (including the v_2' quasi-bound levels) of the contributions (2.268), i.e.

$$\left(\frac{d\left[\mathrm{AB}(v_1')\right]}{dt}\right)_{v_1}^{v_1'} = \sum_{v_2,v_2'}\left(\frac{d\left[\mathrm{AB}(v_1')\right]}{dt}\right)_{v_1,v_2}^{v_1',v_2'} = \sum_{v_2,v_2'}\left(\nu'_{\mathrm{AB}(v_1')} - \nu_{\mathrm{AB}(v_1')}\right) k_{v_1,v_2}^{v_1',v_2'}(T_{\mathrm{tr_h}})\left[\mathrm{AB}(v_1)\right]\left[\mathrm{CD}(v_2)\right] . \tag{2.269}$$

Both the quantities $\nu'_{\mathrm{AB}(v_1')} - \nu_{\mathrm{AB}(v_1')} = 1 - \delta_{v_1,v_1'} + \delta_{\mathrm{AB,CD}} \cdot \left(\delta_{v_2',v_1'} - \delta_{v_2,v_1'}\right)$ and $k_{v_1,v_2}^{v_1',v_2'}(T_{\mathrm{tr_h}})$, that appear in equation (2.269), depend on Kronecker deltas involving the vibrational quantum numbers v_2 and v_2', more precisely $\delta_{\mathrm{AB,CD}} \cdot \delta_{v_2',v_1'}$, $\delta_{\mathrm{AB,CD}} \cdot \delta_{v_2,v_1'}$ and $\delta_{\mathrm{AB,CD}} \cdot \delta_{v_2,v_1}$. If the species AB and CD were different, these Kronecker deltas would be disregarded (since in such case $\delta_{\mathrm{AB,CD}} = 0$). If the species were equal, the combinations $\{v_1, v_2, v_1', v_2'\}$ for which any of the Kronecker deltas that involve v_2 and v_2' correspond to unity would be very few compared to the combinations for which they are null. And, if the rate coefficients associated to the former cases aren't much greater than the rate coefficients for the latter cases, one can approximate equation (2.269) by another disregarding such Kronecker deltas. By taking into account this approximation, the uncoupling relation (2.262), the definition of the rate coefficient (2.265), and the definition of the process cross-section, $\sigma_{v_1,v_2}^{v_1',v_2'}(v_0)$, one can write

$$\sum_{v_2,v_2'} k_{v_1,v_2}^{v_1',v_2'}(T_{\mathrm{tr_h}})\left[\mathrm{CD}(v_2)\right] = \int_0^\infty \sigma(v_0) P_{v_1}^{v_1'}(v_0) \sum_{v_2}\left(\left[\mathrm{CD}(v_2)\right] \underbrace{\sum_{v_2'} P_{v_2}^{v_2'}(v_0)}_{=1,\text{ by definition}}\right) f(v_0, T_{\mathrm{tr_h}})\, dv_0 \Leftrightarrow$$

$$\Leftrightarrow \sum_{v_2,v_2'} k_{v_1,v_2}^{v_1',v_2'}(T_{\mathrm{tr_h}})\left[\mathrm{CD}(v_2)\right] = \underbrace{\int_0^\infty \sigma(v_0) P_{v_1}^{v_1'}(v_0) f(v_0, T_{\mathrm{tr_h}})\, dv_0}_{:=k_{v_1}^{v_1'}(T_{\mathrm{tr_h}})} \underbrace{\sum_{v_2}\left[\mathrm{CD}(v_2)\right]}_{:=[\mathrm{CD}]} = k_{v_1}^{v_1'}(T_{\mathrm{tr_h}})\left[\mathrm{CD}\right] , \tag{2.270}$$

where $k_{v_1}^{v_1'}(T_{\mathrm{tr_h}})$ is the wanted rate: $k_{v_1}^{v_1'}(T_{\mathrm{tr_h}}) = \int_0^\infty \sigma(v_0) P_{v_1}^{v_1'}(v_0) f(v_0, T_{\mathrm{tr_h}})\, dv_0$. By substituting (2.270) in (2.269) one can obtain an expression with a familiar form,

$$\left(\frac{d\left[\mathrm{AB}(v_1')\right]}{dt}\right)_{v_1}^{v_1'} = \left(1 - \delta_{v_1,v_1'}\right) k_{v_1}^{v_1'}(T_{\mathrm{tr_h}})\left[\mathrm{AB}(v_1)\right]\left[\mathrm{CD}\right] . \tag{2.271}$$

Let's now consider the case of dissociation of a molecular particle independently of the fate of the second colliding molecular particle. The variation of the amount concentration of molecular particles $\mathrm{AB}(v_1)$ due to dissociation caused by collisions between $\mathrm{AB}(v_1)$ with $\mathrm{CD}(v_2)$ in which v_2' may represent

a quasi-bound level (hence meaning a dissociation of CD) is given by

$$\left(\frac{d\left[\mathrm{AB}(v_1)\right]}{dt}\right)_{v_1,v_2}^{D,v_2'} = \left(\nu'_{\mathrm{AB}(v_1)} - \nu_{\mathrm{AB}(v_1)}\right) k_{v_1,v_2}^{D,v_2'}(T_{\mathrm{tr_h}})\left[\mathrm{AB}(v_1)\right][\mathrm{CD}(v_2)] \ . \tag{2.272}$$

And similarly to what was done for the case of V-V-T processes, one has

$$\left(\frac{d\left[\mathrm{AB}(v_1)\right]}{dt}\right)_{v_1}^{D} = \sum_{v_2,v_2'}\left(\frac{d\left[\mathrm{AB}(v_1)\right]}{dt}\right)_{v_1,v_2}^{D,v_2'} = \sum_{v_2,v_2'}\left(\nu'_{\mathrm{AB}(v_1)} - \nu_{\mathrm{AB}(v_1)}\right) k_{v_1,v_2}^{D,v_2'}(T_{\mathrm{tr_h}})\left[\mathrm{AB}(v_1)\right][\mathrm{CD}(v_2)] \ . \tag{2.273}$$

Both quantities $\left(\nu'_{\mathrm{AB}(v_1)} - \nu_{\mathrm{AB}(v_1)}\right) = \delta_{\mathrm{AB},CD}\left(\delta_{v_2',v_1} - \delta_{v_2,v_1}\right) - 1$ and $k_{v_1,v_2}^{D,v_2'}$ depend on Kronecker deltas involving the vibrational quantum numbers v_2 and v_2', more precisely $\delta_{\mathrm{AB,CD}} \cdot \delta_{v_2',v_1}$, $\delta_{\mathrm{AB,CD}} \cdot \delta_{v_2,v_1}$ and $\delta_{\mathrm{AB,CD}} \cdot \delta_{v_2,v_1}$. And by disregarding these Kronecker deltas (for the same reasons as before) one gets

$$\left(\frac{d\left[\mathrm{AB}(v_1)\right]}{dt}\right)_{v_1}^{D} = -k_{v_1}^{D}(T_{\mathrm{tr_h}})\left[\mathrm{AB}(v_1)\right][\mathrm{CD}] \ , \tag{2.274}$$

being $k_{v_1}^{D}(T_{\mathrm{tr_h}}) = \int_0^\infty \sigma(v_0) P_{v_1}^{D}(v_0) f(v_0, T_{\mathrm{tr_h}})\, dv_0$ the wanted rate.

2.7.8 Corrections

There are four corrections that may be applied to the FHO model regarding: collisions between molecular particles of different species, anharmonicity of the molecular particles, conservation of energy, and non-collinearity of the collisions.

- About collisions between molecular particles of different species: according to Adamovich et al. [21], it can be taken into account by substituting ρ by

$$\rho \leftrightarrow \frac{\xi}{\sinh(\xi)}\rho \ , \tag{2.275}$$

  being $\xi = 2\frac{|\omega_1 - \omega_2|}{\alpha v_0}$. The result is still an approximation.

  Note that the term "species" employed all through this section doesn't mean the same as chemical species, but the combination of chemical species and electronic level, since the vibrational level of the species is defined in respect of some electronic level, due to the coupling of the vibrational and electronic modes. For instance, particles AB and CD that are of the same chemical chemical species but are at different electronic levels are considered to be of different species here;

- About the anharmonicity of the molecular particles: real molecular particles aren't exactly harmonic oscillators, and therefore, their energy levels may be different from the ones given by equation (A.4). To correct this, the angular frequency ω of a molecular particle may be substituted by an effective angular frequency, so that the absolute value of the difference between the final and initial vibrational energies of the molecular particle is given by the same formula as for the harmonic oscillator case [58]. And because the formula has an indeterminate form when the initial and final vibrational energies are equal, an work around should be performed: for such cases the angular

frequency is substituted by the effective one regarding the transition to the next upper vibrational level. Therefore, the correction can be expressed mathematically through

$$\omega = \begin{cases} \frac{1}{\hbar}\left|\frac{E_{v'}-E_v}{v'-v}\right|, & \text{if } v' \neq v \ , \\ \frac{1}{\hbar}\left|E_{v+1}-E_v\right|, & \text{if } v' = v \ , \end{cases} \tag{2.276}$$

where E_v is the real vibrational energy associated to the quantum number v, being all the quantities associated to one molecular particle. Note that there's an effective angular frequency for each one of the molecular particles that participate in the collision;

- About energy conservation (mentioned before): because the classical dynamics equation for the relative trajectory of the particles was derived under the assumption of negligible energy transfer between the vibrational and translational modes, the law of energy conservation is violated if indeed the transfer happens. If the transfer happens, the initial and final relative speed of the particles would be different, i.e. $v_i \neq v_f$. The speed v_f can be obtaining through an energy balance. To overcome this problem of violation of the law of energy conservation energy, Billing [59] suggested the substitution of the initial relative speed of collision that is argument of the probability of transition $P(v_0)$ by an arithmetic mean: $v_0 = \frac{v_i+v_f}{2}$;

- About noncollinear collisions: according to Adamovich et al. [19] to account the effect of noncollinear collisions, two corrective factors, $S_{\text{V-T}}$ and $S_{\text{V-V}}$, denominated by *steric factors* may be inserted into the transition probabilities formulae by performing the substitutions

$$\eta_0 \leftrightarrow S_{\text{V-T}}\,\eta_0 \ , \tag{2.277}$$

$$\rho \leftrightarrow S_{\text{V-V}}^{\frac{1}{2}}\,\rho \ . \tag{2.278}$$

The subscripts V-T and V-V in $S_{\text{V-T}}$ and $S_{\text{V-V}}$, are associated to the process which they are computed from. Adamovich et al. [19] obtained the $S_{\text{V-T}}$ factor by adjusting this parameter, so that the obtained FHO transition probability $P_{1,0}^{0,0}$ at low v_0 speeds matched the one obtained through the semiclassical three-dimensional trajectory calculations performed by Billing and Fisher [60]. The $S_{\text{V-V}}$ factor was in a similarly way obtained by adjustment of the transition probability $P_{1,0}^{0,1}$. As result, the values of $S_{\text{V-T}} = 4/9$ and $S_{\text{V-V}} = 1/27$ were obtained.

Note, that since the uncoupling of transition of probabilities was assumed, the first correction may be disregarded in this work.

2.8 Heavy particle impact-vibronic transitions

2.8.1 Characterisation of heavy particle impact-vibronic transitions

Let's consider a collision between a molecular particle and a heavy particle that induces a vibronic transition of the former. The term "vibronic transition" was herein employed to emphasise the fact that the transition is with respect to the electronic level of the molecular particle which necessarily also

implies a transition in its vibrational level, since there's a particular set of vibrational levels associated to each electronic level (see section §2.1 for more details), although the change in the vibrational energy may be negligible. The vibronic transition of the molecular particle may come with the cost of the collision particle suffering a transition in its internal energy levels or even dissociation or ionisation. In this work, only transitions of the collision partner in their electronic level, if it corresponds to an atomic particle, or vibrational or vibronic level, if it corresponds to a molecular particle, were considered as a possibility. These processes will be herein termed "VE-m-h processes" - "VE" represents the vibronic transition of the molecular particle with possible outcome of the collision partner suffering an electronic, vibrational or vibronic transition, "m" represents the molecular particle, and "h" represents the type of collision partner: a heavy particle. If the vibronic transition of the molecular particle due to a collision with a heavy particle occurs without excitation/de-excitation of the latter, then the process is said to be "intramolecular" since it only affects the internal energy level of the molecular particle. In this case only translational energy is exchanged between the collision partners. Conversely, if there's an excitation/de-excitation of the heavy particle, the process is said to be "intermolecular" since it affects the internal energies of both collision partners. In this case, an exchange of internal energy beyond the translational one may occur between the particles. A VE-m-h process can be depicted by

$$\mathrm{AB}(e_1, v_1) + \mathrm{C}(e_2) \longrightarrow \mathrm{AB}(e_1', v_1') + \mathrm{C}(e_2') \ , \tag{2.279}$$

$$\mathrm{AB}(e_1, v_1) + \mathrm{CD}(e_2, v_2) \longrightarrow \mathrm{AB}(e_1', v_1') + \mathrm{CD}(e_2', v_2') \ , \tag{2.280}$$

being the employed notation the already familiar one considered for the FHO model in §2.7.

After performing an extensive search on the literature, no well based and simultaneously feasible theoretical models were found for these processes, but very simplistic postulatory models or empirical correlations which can only be shown to be valid for low temperatures (since almost all experiments associated to these processes were done at low temperatures throughout History). However, well based theoretical models were actually found for the case of electronic excitations/de-excitations of atomic particles by collisions with another atomic particles: the Landau-Zener model and the Rosen-Zener-Demkov model. One of the objectives of this thesis was to study the possibility of extending the Landau-Zener and Rosen-Zener-Demkov models to the case of VE-m-h processes. But before that, it is necessary to present here the original models so that the reader can be acquainted with them. Both Landau-Zener and Rosen-Zener-Demkov models consider several crucial approximations, such as the adiabatic approximation (or Born-Oppenheimer approximation), the semiclassical approximation and the so-called *two-states approximation*. Therefore, the introduction of the Landau-Zener and Rosen-Zener-Demkov models needs, in its turn, to be halted, since the above-mentioned approximation should be firstly addressed.

2.8.2 The adiabatic approximation

2.8.2.1 The case of a general isolated system of particles

Let's consider an isolated system of particles that may comprise free electrons, atomic and molecular particles. A set of nuclei and a set electrons can therefore be identified in the system. Let $\{\vec{R}\}$ be the set of nuclei coordinates and $\{\vec{r}\}$ the set of electrons coordinates relatively to some fixed referential. The Schrödinger equation for such system corresponds to

$$i\hbar\frac{\partial\Psi}{\partial t}(\{\vec{R}\},\{\vec{r}\},t)=\hat{H}(\{\vec{R}\},\{\vec{r}\})\,\Psi(\{\vec{R}\},\{\vec{r}\},t)\ , \tag{2.281}$$

being $\hat{H}(\{\vec{R}\},\{\vec{r}\})$ the *Hamiltonian operator*, which is given by [61]

$$\hat{H}(\{\vec{R}\},\{\vec{r}\})=\sum_i\hat{T}_i+\sum_\alpha\hat{T}_\alpha+\sum_{i,\,j>i}V_{ij}(\vec{R}_i,\vec{R}_j)+\sum_{\alpha,\,\beta>\alpha}V_{\alpha\beta}(\vec{r}_\alpha,\vec{r}_\beta)+\sum_{i,\alpha}V_{i\alpha}(\vec{R}_i,\vec{r}_\alpha)+\hat{V}_{\text{s.o.}}\ . \tag{2.282}$$

In the above relation, $\hat{T}_i$ and $\hat{T}_\alpha$ are the kinetic energy operators of the i-th nucleus and α-th electron

$$\hat{T}_i=-\frac{\hbar^2}{2M_i}\nabla^2_{\vec{R}_i}\ , \tag{2.283}$$

$$\hat{T}_\alpha=-\frac{\hbar^2}{2m_{\text{e}}}\nabla^2_{\vec{r}_\alpha}\ , \tag{2.284}$$

respectively, where $\nabla^2_{\vec{R}_i}$ corresponds to the Laplacian operator taken with respect to the coordinates of the $\vec{R}_i$ vector, and the analogous follows for $\nabla^2_{\vec{r}_\alpha}$. The quantity M_i is the mass of the i-th nucleus. The quantities $V_{ij}(\vec{R}_i,\vec{R}_j)$, $V_{\alpha\beta}(\vec{r}_\alpha,\vec{r}_\beta)$ and $V_{i\alpha}(\vec{R}_i,\vec{r}_\alpha)$ are the potential energies associated to the *Coulomb electrostatic interactions* between the i and j-th nuclei, between the α and β-th electrons, and between the i-th nucleus and the α-th electron, i.e.

$$V_{ij}(\vec{R}_i,\vec{R}_j)=\frac{Z_iZ_j\text{e}^2}{4\pi\varepsilon_0\left\|\vec{R}_j-\vec{R}_i\right\|}\ , \tag{2.285}$$

$$V_{\alpha\beta}(\vec{r}_\alpha,\vec{r}_\beta)=\frac{\text{e}^2}{4\pi\varepsilon_0\left\|\vec{r}_\beta-\vec{r}_\alpha\right\|}\ , \tag{2.286}$$

$$V_{i\alpha}(\vec{R}_i,\vec{r}_\alpha)=-\frac{Z_i\text{e}^2}{4\pi\varepsilon_0\left\|\vec{r}_\alpha-\vec{R}_i\right\|}\ , \tag{2.287}$$

respectively, where ε_0 is the *vacuum permittivity*, e is the *elementary charge* (the proton charge, or equivalently, the symmetric of the electron charge), and Z_i is the number of protons in the i-th nucleus. The quantity $\hat{V}_{\text{s.o.}}$ is the so-called *spin-orbit interaction operator* which is usually significantly smaller than the potential energies for the Coulomb electrostatic interactions [61]. By this reason, the operator of the spin-orbit interaction was disregarded.

Because the Hamiltonian $\hat{H}(\{\vec{R}\},\{\vec{r}\})$ doesn't depend on the instant of time t, one can consider a separation of variables and write $\Psi(\{\vec{R}\},\{\vec{r}\},t)=T(t)\,\psi(\{\vec{R}\},\{\vec{r}\})$, being $T(t)$ some function of time and $\psi(\{\vec{R}\},\{\vec{r}\})$ some function of $\{\vec{R}\}$ and $\{\vec{r}\}$. Equation (2.281) will then lead to two new equations:

$$\begin{cases}\dfrac{\frac{\partial T}{\partial t}(t)}{T(t)}=-\dfrac{i}{\hbar}E\ , & \text{(2.288a)}\\[2ex] \hat{H}(\{\vec{R}\},\{\vec{r}\})\,\psi(\{\vec{R}\},\{\vec{r}\})=E\,\psi(\{\vec{R}\},\{\vec{r}\})\ , & \text{(2.288b)}\end{cases}$$

being E the separation constant, physically meaning the energy of the isolated system. By solving

equation (2.288a), one can express the global wave function $\Psi(\{\vec{R}\},\{\vec{r}\},t)$ as

$$\Psi(\{\vec{R}\},\{\vec{r}\},t) = \psi(\{\vec{R}\},\{\vec{r}\})\, e^{-\frac{i}{\hbar}Et} \ . \tag{2.289}$$

One of the principles in which the adiabatic approximation relies on is in the fact that the mass of the electrons is so much smaller than the mass of the nuclei that the velocity of the former achieve much greater values than the velocity of the latter, and therefore, one may describe the electronic motion by assuming the nuclei to be at rest. In other words, one may consider the Hamiltonian for such motion to be the one represented by (2.282), neglecting the kinetic energy operators for the nuclei, and assuming fixed nuclei coordinates $\{\vec{R}\}$. The set of nuclei coordinates $\{\vec{R}\}$ may be then regarded as parameters of the resulting Hamiltonian, which has then the form

$$\hat{H}_{\mathrm{e}}(\{\vec{R}\},\{\vec{r}\}) = \sum_{\alpha}\hat{T}_{\alpha} + \sum_{i,\,j>i} V_{ij}(\vec{R}_i,\vec{R}_j) + \sum_{\alpha,\,\beta>\alpha} V_{\alpha\beta}(\vec{r}_{\alpha},\vec{r}_{\beta}) + \sum_{i,\alpha} V_{i\alpha}(\vec{R}_i,\vec{r}_{\alpha}) + \hat{V}_{\mathrm{s.o.}} \ . \tag{2.290}$$

This Hamiltonian will be for now on called "the electronic Hamiltonian operator". The Schrödinger equation for this hypothetical system can be expressed by

$$i\hbar\frac{\partial\Phi}{\partial t}(\{\vec{R}\},\{\vec{r}\},t) = \hat{H}_{\mathrm{e}}(\{\vec{R}\},\{\vec{r}\})\,\Phi(\{\vec{R}\},\{\vec{r}\},t) \ . \tag{2.291}$$

The quantisation condition implies that there is a set of orthonormal (in respect of the set of variables $\{\vec{r}\}$) electronic wave functions $\Phi_m(\{\vec{R}\},\{\vec{r}\},t)$ representing the different electronic states, and since the Hamiltonian $\hat{H}_{\mathrm{e}}(\{\vec{R}\},\{\vec{r}\})$ doesn't depend on the instant of time t, one can consider a separation of variables and write $\Phi_m(\{\vec{R}\},\{\vec{r}\},t) = T_m(t)\,\phi_m(\{\vec{R}\},\{\vec{r}\})$, being $T_m(t)$ some function of time and $\phi_m(\{\vec{R}\},\{\vec{r}\})$ some function of $\{\vec{r}\}$ having the set $\{\vec{R}\}$ as parameter. Similarly to what happened with the global Schrödinger equation (2.281), the electronic Schrödinger equation (2.291) leads to two new equations:

$$\begin{cases} \dfrac{\frac{\partial T_m}{\partial t}(t)}{T_m(t)} = -\dfrac{i}{\hbar}U_m(\{\vec{R}\}) \ , & \text{(2.292a)} \\ \hat{H}_{\mathrm{e}}(\{\vec{R}\},\{\vec{r}\})\,\phi_m(\{\vec{R}\},\{\vec{r}\}) = U_m(\{\vec{R}\})\,\phi_m(\{\vec{R}\},\{\vec{r}\}) \ , & \text{(2.292b)} \end{cases}$$

being $U_m(\{\vec{R}\})$ the separation "constant" having the set $\{\vec{R}\}$ as parameter. This quantity is referred as the m-th *adiabatic electronic term* (which is an eigenenergy of the electronic system), and $\phi_m(\{\vec{R}\},\{\vec{r}\})$ is the m-th *adiabatic electronic function* (which is an eigenfunction of the electronic system). Being $\{\vec{R}\}$ regarded as parameter, one should emphasise that there's an equation (2.292a) and an equation (2.292b) for each value of $\{\vec{R}\}$.

Since the functions $\phi_m(\{\vec{R}\},\{\vec{r}\})$ constitute an orthonormal basis with respect to the set of variables $\{\vec{r}\}$, one can use them to express the dependence on $\{\vec{r}\}$ of the wave function $\psi(\{\vec{R}\},\{\vec{r}\})$ through an expansion:

$$\psi(\{\vec{R}\},\{\vec{r}\}) = \sum_{m}\chi_m(\{\vec{R}\})\,\phi_m(\{\vec{R}\},\{\vec{r}\}) \ , \tag{2.293}$$

being $\chi_m(\{\vec{R}\})$ some functions of the set of variables $\{\vec{R}\}$. The global wave function will then become

$$\Psi(\{\vec{R}\},\{\vec{r}\},t) = \left[\sum_m \chi_m(\{\vec{R}\})\,\phi_m(\{\vec{R}\},\{\vec{r}\})\right] e^{-\frac{i}{\hbar}Et} \ . \tag{2.294}$$

By substituting (2.293) in the time-independent Schrödinger equation (2.288b), multiplying the equation by $\phi_n^*(\{\vec{R}\},\{\vec{r}\})$ and integrating it over the set of variables $\{\vec{r}\}$, one can obtain the result

$$\left[\left(\sum_i -\frac{\hbar^2}{2M_i}\nabla^2_{\vec{R}_i}\right) + \hat{C}_{nn} + U_n(\{\vec{R}\})\right]\chi_n(\{\vec{R}\}) = E\chi_n(\{\vec{R}\}) - \left[\sum_m \hat{C}_{nm}\,\chi_m(\{\vec{R}\})\right] \ . \tag{2.295}$$

where the orthonormality property of the adiabatic electronic functions, i.e. $\int \phi_m^*\,\phi_n\,d\{\vec{r}\} = \delta_{mn}$, was used. The operator $\hat{C}_{nm}$ corresponds to the so-called *coupling operator* with respect to the n-th and m-th adiabatic electronic wave functions, being given by

$$\hat{C}_{nm} = \sum_i -\frac{\hbar^2}{2M_i}\left[\int \phi_n^*\,\nabla^2_{\vec{R}_i}\phi_m\,d\{\vec{r}\} + 2\left(\int \phi_n^*\,\vec{\nabla}_{\vec{R}_i}\phi_m\,d\{\vec{r}\}\cdot\vec{\nabla}_{\vec{R}_i}\right)\right] \ . \tag{2.296}$$

If the adiabatic electronic terms U_m are not too close to each other - another assumption of the adiabatic approximation - then one can neglect the contribution of the operators $\hat{C}_{nm}$ [61, 62] and write equation (2.295) as

$$\left[\left(\sum_i -\frac{\hbar^2}{2M_i}\nabla^2_{\vec{R}_i}\right) + U_n(\{\vec{R}\})\right]\chi_n(\{\vec{R}\}) = E\chi_n(\{\vec{R}\}) \ . \tag{2.297}$$

Equation (2.297) represents a Schrödinger equation for the motion of nuclei under a potential energy $U_n(\{\vec{R}\})$. Therefore, if the adiabatic approximation does hold, the adiabatic electronic terms correspond to nuclear potential energy functions.

2.8.2.2 The case of an isolated diatomic molecular particle

Let's now consider an isolated system composed by a diatomic molecular particle. To simplify even more the problem let's consider an inertial coordinate system with the origin coinciding with the centre of mass of the diatomic molecular particle. Since the molecular particle is isolated, it isn't subjected to external forces, and therefore, its centre of mass doesn't suffer any acceleration. There's a set of nuclear coordinates composed by two vectors, $\{\vec{R}\} = \{\vec{R}_1,\vec{R}_2\}$, representing the positions of the two nuclei, and a set of electronic coordinates $\{\vec{r}\}$. Doing the same procedure as the one for the case of the general isolated system, the time-independent Schrödinger equation for the isolated diatomic molecular particle can be written in the form

$$\left[-\frac{\hbar^2}{2M_1}\nabla^2_{\vec{R}_1} - \frac{\hbar^2}{2M_2}\nabla^2_{\vec{R}_2} + \hat{H}_{\rm e}(\vec{R}_1,\vec{R}_2,\{\vec{r}\})\right]\psi(\vec{R}_1,\vec{R}_2,\{\vec{r}\}) = E'\,\psi(\vec{R}_1,\vec{R}_2,\{\vec{r}\}) \ , \tag{2.298}$$

being the electronic Hamiltonian $\hat{H}_{\rm e}(\vec{R}_1,\vec{R}_2,\{\vec{r}\})$ given by (2.290). The separation constant E' is the energy of the system relatively to its centre of mass. Transforming the local variables of the nuclei $\vec{R}_1$ and $\vec{R}_2$ into a combination of the centre of mass of the two nuclei $\vec{\vec{R}} = \left(M_1\vec{R}_1 + M_2\vec{R}_2\right)/\left(M_1+M_2\right)$

and the difference between the two coordinates $\vec{R} = \vec{R}_2 - \vec{R}_1$, equation (2.298) can be transformed into

$$\left[-\frac{\hbar^2}{2M}\nabla^2_{\vec{R}} - \frac{\hbar^2}{2\mu}\nabla^2_{\vec{R}} + \hat{H}_{\mathrm{e}}(\vec{\vec{R}}, \vec{R}, \{\vec{r}\})\right] \psi(\vec{\vec{R}}, \vec{R}, \{\vec{r}\}) = E' \, \psi(\vec{\vec{R}}, \vec{R}, \{\vec{r}\}) \ , \tag{2.299}$$

being $M = M_1 + M_2$ the mass of the two nuclei and $\mu = M_1 M_2 / (M_1 + M_2)$ the reduced mass of the two nuclei. The kinetic energy of the centre of mass of the nuclei can be shown to be significantly smaller than the kinetic energy of the electrons, and therefore the operator $-\frac{\hbar^2}{2M}\nabla^2_{\vec{\vec{R}}}$ may be disregarded in equation (2.299) [62]. Due to the much higher mass of the nuclei when in comparison with the one of the electrons, it's correct to approximate the centre of mass of the whole molecular particle by the centre mass of the nuclei, making $\vec{\vec{R}} \approx \vec{0}$. One can therefore remove the $\vec{\vec{R}}$ variable from the argument of the involved functions. Additionally, by invoking the expansion relation (2.293), one may express (2.299) through

$$\left[-\frac{\hbar^2}{2\mu}\nabla^2_{\vec{R}} + \hat{H}_{\mathrm{e}}(\vec{R}, \{\vec{r}\})\right] \sum_m \chi_m(\vec{R})\phi_m(\vec{R}, \{\vec{r}\}) = E' \sum_m \chi_m(\vec{R})\phi_m(\vec{R}, \{\vec{r}\}) \ . \tag{2.300}$$

By multiplying (2.300) by $\phi^*_n(\vec{R}, \{\vec{r}\})$, integrating it over $\{\vec{r}\}$, and by neglecting the resultant $\hat{C}_{nm}$ operator with a form identical to (2.296), one may get:

$$\left[-\frac{\hbar^2}{2\mu}\nabla^2_{\vec{R}} + U_n(R)\right] \chi_n(\vec{R}) = E'\chi_n(\vec{R}) \ , \tag{2.301}$$

where $U_n(R)$ is the n-th adiabatic electronic term which in a diatomic molecular particle only depends on the norm R of the internuclear vector $\vec{R}$ [62]. By using spherical coordinates relatively to the inertial frame - the radius R, the azimuthal angle φ, and the polar angle θ - one may write (2.301) as

$$\left\{-\frac{\hbar^2}{2\mu}\left[\frac{1}{R^2}\frac{\partial}{\partial R}\left(R^2\frac{\partial}{\partial R}\right) - \frac{\hat{l^2}}{R^2}\right] + U_n(R)\right\} \chi_n(R, \varphi, \theta) = E'\chi_n(R, \varphi, \theta) \ , \tag{2.302}$$

being $\hat{l^2}$ the so-called *squared angular momentum operator* [62], given by

$$\hat{l^2} = -\left[\frac{1}{\sin^2\theta}\frac{\partial^2}{\partial\varphi^2} + \frac{1}{\sin\theta}\frac{\partial}{\partial\theta}\left(\sin\theta\frac{\partial}{\partial\theta}\right)\right] \ . \tag{2.303}$$

Since the potential energy $U_n(R)$ only depends on the radius R, a separation of variables can be considered, allowing the writing of $\chi_n(R, \phi, \theta) = X_n(R)Y_n(\varphi, \theta)$, being $X_n(R)$ some function of R and $Y_n(\varphi, \theta)$ some function of φ and θ. Equation (2.302) can then be separated into two:

$$\begin{cases} \left[-\dfrac{\hbar^2}{2\mu}\dfrac{1}{R^2}\dfrac{\partial}{\partial R}\left(R^2\dfrac{\partial}{\partial R}\right) + U_n(R)\right] X_n(R) = \lambda \, X_n(R) \ , & \text{(2.304a)} \\ \dfrac{\hbar^2}{2\mu}\dfrac{\hat{l^2}}{R^2} \, Y_n(\varphi, \theta) = \zeta \, Y_n(\varphi, \theta) \ , & \text{(2.304b)} \end{cases}$$

in which λ and ζ are the respective separation constants, making $E' = \lambda + \zeta$. It can be shown that the eigenfunctions of (2.304b) correspond to $Y_n(\varphi, \theta) = Y_{l,m}(\varphi, \theta)$, the so-called *spherical harmonic functions*, and the eigenenergies are $\zeta = l\,(l+1)$ [62]. The quantities l and m are respectively the so-called *angular momentum quantum number* (or simply the *rotational quantum number*), with $l = 0, 1, 2, ...$, and the

so-called *quantum number for the z-component of the angular momentum*, with $m = -l,\ -l+1,\ ...,\ l-1, l$. The eigenfunctions $Y_{l,m}(\varphi, \theta)$ are orthonormal, satisfying

$$\int_0^{\pi} \left(\int_0^{2\pi} Y^*_{l',m'} Y_{l,m} d\varphi \right) \sin\theta \, d\theta = \delta_{ll'} \cdot \delta_{mm'} \ . \tag{2.305}$$

Since $Y_{l,m}(\varphi, \theta)$ constitute an orthonormal basis in respect of the φ and θ variables, one may express the dependence of the wave function $\chi_n(R, \phi, \theta)$ on these variables through an expansion:

$$\chi_n(R, \phi, \theta) = \sum_{l',m'} X_{n,l',m'}(R) Y_{l',m'}(\varphi, \theta) \ . \tag{2.306}$$

By substituting (2.306) in (2.302), multiplying it by $Y^*_{l,m} \sin\theta$ and integrating it in φ and θ, it's possible to obtain

$$\left[-\frac{\hbar^2}{2\mu} \frac{1}{R^2} \frac{\partial}{\partial R} \left(R^2 \frac{\partial}{\partial R} \right) + U_n(R) + \frac{\hbar^2}{2\mu} \frac{l(l+1)}{R^2} \right] X_{n,l,m}(R) = E' X_{n,l,m}(R) \ . \tag{2.307}$$

And by making the change of variables $x_{n,m,l}(R) = R\, X_{n,m,l}(R)$, equation (2.307) can be transformed into the so-called *radial Schrödinger equation*:

$$\left[-\frac{\hbar^2}{2\mu} + U_{n,l}(R) \right] x_{n,l,m}(R) = E' x_{n,l,m}(R) \ , \tag{2.308}$$

being $U_{n,l}(R)$ the *centrifugally corrected potential energy* given by

$$U_{n,l}(R) = U_n(R) + \frac{\hbar^2}{2\mu} \frac{l(l+1)}{R^2} \tag{2.309}$$

The quantity $\hbar^2 l(l+1) / \left(2\mu R^2\right)$ is commonly called the *centrifugal energy*.

2.8.3 The semiclassical approximation

The adiabatic approximation per se allows one to describe the motion of the nuclei if its electronic state is indeed known. However, the electronic state of the system of particles may change when the adiabatic electronic terms $U_m(\{\vec{R}\})$ get too close to each other [61]. To study the evolution of the system electronic state, a simplifying approximation such as the semiclassical approximation is undoubtedly convenient.

A common assumption when dealing with both nuclei and electrons is to regard the movement of the nuclei according to Classical Mechanics and the movement of the nuclei according to Quantum Mechanics - a semiclassical approximation. Therefore, the set of nuclei coordinates $\{\vec{R}\}$ is obtained through the Newton's second law, being now parametrised by the instant of time t, which allows it to be expressed as $\{\vec{R}(t)\}$. The Schrödinger equation for the electronic system can be written in the same manner as in (2.291), but with $\{\vec{R}\}$ substituted by $\{\vec{R}(t)\}$, and the argument $\{\vec{R}\}$ in the electronic wave function $\Phi(\{\vec{R}\}, \{\vec{r}\}, t)$ suppressed since $\{\vec{R}\}$ now depends on t, and a t-dependence of the wave function already appears in its argument:

$$i\hbar \frac{\partial \Phi}{\partial t}(\{\vec{r}\}, t) = \hat{H}_{\mathrm{e}}(\{\vec{R}(t)\}, \{\vec{r}\})\, \Phi(\{\vec{r}\}, t) \ . \tag{2.310}$$

And by invoking the quantisation condition, there is a set of orthonormal (in respect of the set of

variables $\{\vec{r}\}$) wavefunctions $\Phi_m(\{\vec{R}(t)\},\{\vec{r}\},t)$ which under the adiabatic approximation[23] have the form $\Phi_m(\{\vec{R}(t)\},\{\vec{r}\},t) = T_m(t)\phi_m(\{\vec{R}(t)\},\{\vec{r}\})$. The substitution of $\Phi(\{\vec{r}\},t) = \Phi_m(\{\vec{R}(t)\},\{\vec{r}\},t)$ in (2.310) results in two equations with the same format as (2.292a) and (2.292b):

$$\begin{cases} \dfrac{\frac{\partial T_m}{\partial t}(t)}{T_m(t)} = -\dfrac{i}{\hbar}U_m(\{\vec{R}(t)\}) \ , & \text{(2.311a)} \\ \hat{H}_{\rm e}(\{\vec{R}(t)\},\{\vec{r}\})\,\phi_m(\{\vec{R}(t)\},\{\vec{r}\}) = U_m(\{\vec{R}(t)\})\,\phi_m(\{\vec{R}(t)\},\{\vec{r}\}) \ . & \text{(2.311b)} \end{cases}$$

By solving (2.311a) one may write $\Phi_m(\{\vec{R}(t)\},\{\vec{r}\},t) = \phi_m(\{\vec{R}(t)\},\{\vec{r}\})e^{-\frac{i}{\hbar}\int_{-\infty}^{t}U_m(\{\vec{R}(t')\})dt'}$. Since $\Phi_m(\{\vec{R}(t)\},\{\vec{r}\},t)$ constitute an orthonormal basis in respect of the set of variables $\{\vec{r}\}$, they can be used to express the $\{\vec{r}\}$-dependence of the electronic wave function $\Phi(\{\vec{r}\},t)$ through an expansion:

$$\Phi(\{\vec{r}\},t) = \sum_m a_m(t)\phi_m(\{\vec{R}(t)\},\{\vec{r}\})e^{-\frac{i}{\hbar}\int_{-\infty}^{t}U_m(\{\vec{R}(t')\})dt'} \ , \tag{2.312}$$

being $a_m(t)$ some functions of the instant of time t.

It is sometimes more convenient to express the expansion (2.312) through another orthonormal basis. Such orthonormal basis is the so-called *diabatic basis* and can be obtained through the time-independent Schrödinger equation associated to an hypothetical system with $H^0_{\rm e}(\{\vec{R}(t)\},\{\vec{r}\})$ as Hamiltonian [61]:

$$\hat{H}^0_{\rm e}(\{\vec{R}(t)\},\{\vec{r}\})\,\phi^0_m(\{\vec{R}(t)\},\{\vec{r}\}) = U^0_m(\{\vec{R}(t)\})\,\phi^0_m(\{\vec{R}(t)\},\{\vec{r}\}) \ , \tag{2.313}$$

being $\phi^0_m(\{\vec{R}(t)\},\{\vec{r}\})$ the so-called diabatic electronic functions that constitute the diabatic orthonormal basis. Because these functions constitute a basis in respect of $\{\vec{r}\}$, they can be used to expressed the adiabatic electronic functions ones through an expansion:

$$\phi_n(\{\vec{R}(t)\},\{\vec{r}\}) = \sum_m c_{nm}(\{\vec{R}(t)\})\phi^0_m(\{\vec{R}(t)\},\{\vec{r}\}) \ , \tag{2.314}$$

being $c_{nm}(\{\vec{R}(t)\})$ some functions of $\{\vec{R}(t)\}$. By using the diabatic electronic functions the electronic wave function may be expressed through

$$\Phi(\{\vec{r}\},t) = \sum_m b_m(t)\phi^0_m(\{\vec{R}(t)\},\{\vec{r}\})e^{-\frac{i}{\hbar}\int_{-\infty}^{t}H_{mm}(\{\vec{R}(t')\})dt'} \ , \tag{2.315}$$

being $b_m(t)$ some functions of the instant of time t, and $H_{mm} = \int \left(\phi^0_n\right)^* \hat{H}_{\rm e}\phi^0_m\, d\{\vec{r}\}$.

By substituting the expansion (2.312) in the electronic Schrödinger equation (2.310), multiplying it by ϕ^*_n and integrating it in $\{\vec{r}\}$, an expression for the variation in time of the coefficient $a_n(t)$ is obtained:

$$\dot{a}_n(t) = -\sum_{m\neq n}\left(\int \phi^*_n\frac{\partial\phi_m}{\partial t}\,d\{\vec{r}\}\right)e^{-\frac{i}{\hbar}\int_{-\infty}^{t}(U_m-U_n)dt'}a_m(t) \ . \tag{2.316}$$

A particular property of the adiabatic electronic functions ϕ_m was used in the derivation of (2.316):

[23] Under the adiabatic approximation one may consider $\hat{H}_{\rm e}(\{\vec{R}(t)\},\{\vec{r}\})$ with fixed $\{\vec{R}(t)\}$ coordinates, making a separation of variables of Φ_m in t and $(\{\vec{R}(t)\},\{\vec{r}\})$ possible.

because the spin-orbit interaction operator $\hat{V}_{\text{s.o.}}$ was assumed to be negligible in the Hamiltonian $\hat{H}_{\text{e}}$, it can be shown that the eigenfunctions ϕ_n are real [61] (meaning that $\phi_n^* = \phi_n$), and therefore one has

$$\int \phi_n^* \frac{\partial \phi_m}{\partial t}\, d\{\vec{r}\} = \frac{\partial}{\partial t} \underbrace{\left(\int \phi_n^* \phi_m \, d\{\vec{r}\} \right)}_{=\delta_{nm}} - \underbrace{\int \frac{\partial \phi_n^*}{\partial t} \phi_m \, d\{\vec{r}\}}_{=\int \phi_m^* \frac{\partial \phi_n}{\partial t}\, d\{\vec{r}\}} \Leftrightarrow$$

$$\Leftrightarrow \int \phi_n^* \frac{\partial \phi_m}{\partial t}\, d\{\vec{r}\} = (\delta_{nm} - 1) \int \phi_m^* \frac{\partial \phi_n}{\partial t}\, d\{\vec{r}\} = \begin{cases} 0, & \text{if } n = m \ , \\ -\int \phi_m^* \frac{\partial \phi_n}{\partial t}\, d\{\vec{r}\}, & \text{if } n \neq m \ . \end{cases} \tag{2.317}$$

Equation (2.316) reveals that the evolution of each coefficient a_n does depend on the instantaneous values of the others a_m. This coupling may induce a change of the electronic state of the system. It can be shown that such change is more likely to occur in the regions of $\{\vec{R}(t)\}$ where the adiabatic electronic terms $U_m(\{\vec{R}(t)\})$ get closer to each other [61]. Note that one may write $\partial \phi_m / \partial t = \sum_i \left(\dot{\vec{R}}_i \cdot \vec{\nabla}_{\vec{R}_i} \right) \phi_m$ due to the dependence of ϕ_m on $\vec{R}$ and the dependence of $\vec{R}$ on t. If spherical coordinates are considered - R_i for the radius, φ_i for the azimuthal angle and θ_i the polar angle of $\vec{R}_i$ - one has then $\partial \phi_m / \partial t = \sum_i \left(\dot{R}_i \partial / \partial R_i + \dot{\varphi}_i \partial / \partial \varphi_i + \dot{\theta}_i \partial / \partial \theta_i \right) \phi_m$.

Regarding the expansion (2.315), by substituting it in the electronic Schrödinger equation (2.310), multiplying it by $\left(\phi_n^0\right)^*$, integrating it in $\{\vec{r}\}$ and invoking the property (2.317) with respect to the ϕ_n^0 functions, an expression for the variation in time of the coefficient $b_n(t)$ is obtained:

$$\dot{b}_n(t) = -\sum_{m \neq n} \left(\frac{i}{\hbar} H_{nm} + \int \left(\phi_n^0\right)^* \frac{\partial \phi_m^0}{\partial t}\, d\{\vec{r}\} \right) e^{-\frac{i}{\hbar} \int_{-\infty}^{t} (H_{mm} - H_{nn}) dt'} b_m(t) \ . \tag{2.318}$$

2.8.4 The two-states approximation

Let's consider the case in which only two adiabatic electronic terms $U_1(\{\vec{R}(t)\})$ and $U_2(\{\vec{R}(t)\})$ are significantly close to each other so that the possibility of a transition of the system electronic state from one state to the other during the nuclei motion may be required to be taken into account. In these circumstances, one may retain only the two terms associated to $U_1(\{\vec{R}(t)\})$ and $U_2(\{\vec{R}(t)\})$ in the expansion (2.312), giving

$$\Phi(\{\vec{r}\}, t) = a_1(t) \phi_1(\{\vec{R}(t)\}, \{\vec{r}\}) e^{-\frac{i}{\hbar} \int_{-\infty}^{t} U_1(\{\vec{R}(t')\}) dt'} + a_2(t) \phi_2(\{\vec{R}(t)\}, \{\vec{r}\}) e^{-\frac{i}{\hbar} \int_{-\infty}^{t} U_2(\{\vec{R}(t')\}) dt'} \ . \tag{2.319}$$

Besides that, it will be assumed that two diabatic electronic functions $\phi_1^0(\{\vec{R}(t)\}, \{\vec{r}\})$ and $\phi_2^0(\{\vec{R}(t)\}, \{\vec{r}\})$ are enough to describe the expansion (2.315), giving

$$\Phi(\{\vec{r}\}, t) = b_1(t) \phi_1^0(\{\vec{R}(t)\}, \{\vec{r}\}) e^{-\frac{i}{\hbar} \int_{-\infty}^{t} H_{11}(\{\vec{R}(t')\}) dt'} + b_2(t) \phi_2^0(\{\vec{R}(t)\}, \{\vec{r}\}) e^{-\frac{i}{\hbar} \int_{-\infty}^{t} H_{22}(\{\vec{R}(t')\}) dt'} \ , \tag{2.320}$$

and that a relation between the adiabatic electronic functions $\phi_m(\{\vec{R}(t)\},\{\vec{r}\})$ and the diabatic electronic functions $\phi_m^0(\{\vec{R}(t)\},\{\vec{r}\})$ of the of form of (2.314) is still valid, giving

$$\begin{cases} \phi_1(\{\vec{R}(t)\},\{\vec{r}\}) = c_{11}(\{\vec{R}(t)\})\,\phi_1^0(\{\vec{R}(t)\},\{\vec{r}\}) + c_{12}(\{\vec{R}(t)\})\,\phi_2^0(\{\vec{R}(t)\},\{\vec{r}\}) \ , & \text{(2.321a)} \\ \phi_2(\{\vec{R}(t)\},\{\vec{r}\}) = c_{21}(\{\vec{R}(t)\})\,\phi_1^0(\{\vec{R}(t)\},\{\vec{r}\}) + c_{22}(\{\vec{R}(t)\})\,\phi_2^0(\{\vec{R}(t)\},\{\vec{r}\}) \ . & \text{(2.321b)} \end{cases}$$

The two relations (2.321a) and (2.321b) can be expressed through a matrix representation:

$$\underbrace{\begin{Bmatrix} \phi_1 \\ \phi_2 \end{Bmatrix}}_{:=\{\phi\}} = \underbrace{\begin{bmatrix} c_{11} & c_{12} \\ c_{21} & c_{22} \end{bmatrix}}_{:=[C]} \underbrace{\begin{Bmatrix} \phi_1^0 \\ \phi_2^0 \end{Bmatrix}}_{:=\{\phi^0\}} \ . \tag{2.322}$$

Because both adiabatic electronic functions and diabatic electronic functions are orthonormal with respect to themselves, it can be shown that matrix C is unitary, i.e. its inverse is equal to its conjugate transpose: $[C]^{-1} = [C]^{\dagger}$. With this property taken into account, one can also show that $[C]^{\mathrm{T}}$ is the matrix that diagonalises the so-called *Hamiltonian matrix* written under the $\{\phi_0\}$ basis, $[H]$, producing the Hamiltonian matrix written under the $\{\phi\}$ basis, $[U]$:

$$\underbrace{\begin{bmatrix} U_1 & 0 \\ 0 & U_2 \end{bmatrix}}_{:=[U]} = \underbrace{\left(\begin{bmatrix} c_{11} & c_{12} \\ c_{21} & c_{22} \end{bmatrix}^{\mathrm{T}} \right)^{-1}}_{:=([C]^{\mathrm{T}})^{-1}} \underbrace{\begin{bmatrix} H_{11} & H_{12} \\ H_{21} & H_{22} \end{bmatrix}}_{:=[H]} \underbrace{\begin{bmatrix} c_{11} & c_{12} \\ c_{21} & c_{22} \end{bmatrix}^{\mathrm{T}}}_{:=[C]^{\mathrm{T}}} \ . \tag{2.323}$$

Because Hamiltonian operators are hermitian [62], their matrix representation and the respective conjugate transpose are equal: $[H] = [H]^{\dagger}$. That means that the diagonal elements H_{11} and H_{22} are real and the off-diagonal elements H_{11} and H_{22} are the conjugate of each other: $H_{21} = H_{12}^*$. Also, because the spin-orbit interaction $\hat{V}_{\text{s.o.}}$ of the Hamiltonian operators was disregarded, all elements of the $[H]$ matrix are real, and therefore $H_{21} = H_{12}$ [61].

Equation (2.323) tells that the adiabatic electronic terms U_1 and U_2 are the eigenvalues of the $[H]$ matrix, meaning that

$$\begin{cases} U_1 = \dfrac{1}{2}\left(H_{11} + H_{22}\right) + \dfrac{1}{2}\sqrt{\left(H_{11} - H_{22}\right)^2 + 4H_{12}^2} \ , & \text{(2.324a)} \\ U_1 = \dfrac{1}{2}\left(H_{11} + H_{22}\right) - \dfrac{1}{2}\sqrt{\left(H_{11} - H_{22}\right)^2 + 4H_{12}^2} \ . & \text{(2.324b)} \end{cases}$$

On the other hand, equation (2.323) together with the fact that C is a unitary matrix tells that $(c_{11}, c_{12})^{\mathrm{T}}$ and $(c_{21}, c_{22})^{\mathrm{T}}$ are the normalised eigenvectors of $[H]$, resulting in

$$\begin{bmatrix} c_{11} & c_{12} \\ c_{21} & c_{22} \end{bmatrix} = \begin{bmatrix} \cos(\chi) & \sin(\chi) \\ -\sin(\chi) & \cos(\chi) \end{bmatrix} \ , \tag{2.325}$$

with χ given by:

$$\chi = \frac{1}{2}\arctan\left(\frac{2H_{12}}{H_{11} - H_{22}}\right) \ . \tag{2.326}$$

In respect of the evolution in time of the coefficients $a_1(t)$ and $a_2(t)$ under the two-states approximation, one may obtain from relation (2.316) constrained to the respective two terms the result

$$\begin{cases} \dot{a}_1(t) = -\left(\int \phi_1^* \dfrac{\partial \phi_2}{\partial t}\, d\{\vec{r}\}\right) e^{-\frac{i}{\hbar}\int_{-\infty}^{t}(U_2-U_1)dt'} a_2(t) \ , & \text{(2.327a)} \\ \dot{a}_2(t) = \left(\int \phi_1^* \dfrac{\partial \phi_2}{\partial t}\, d\{\vec{r}\}\right) e^{\frac{i}{\hbar}\int_{-\infty}^{t}(U_2-U_1)dt'} a_1(t) \ , & \text{(2.327b)} \end{cases}$$

where the property (2.317) was used. Also, it's possible to express the above relations through the diabatic electronic functions instead of the adiabatic ones: by using the relation between the adiabatic and diabatic electronic functions (2.322) and the results (2.325) and (2.326), one may write $\int \phi_1^* \frac{\partial \phi_2}{\partial t}\, d\{\vec{r}\} = \int \left(\phi_1^0\right)^* \frac{\partial \phi_2^0}{\partial t}\, d\{\vec{r}\} - \dot{\chi}$.

In respect of the evolution in time of the coefficients $b_1(t)$ and $b_2(t)$ under the two-states approximation, one may obtain in a similar way

$$\begin{cases} \dot{b}_1(t) = \left(-\int \left(\phi_1^0\right)^* \dfrac{\partial \phi_2^0}{\partial t}\, d\{\vec{r}\} - \dfrac{i}{\hbar} H_{12}\right) e^{-\frac{i}{\hbar}\int_{-\infty}^{t}(H_{22}-H_{11})dt'} b_2(t) \ , & \text{(2.328a)} \\ \dot{b}_2(t) = \left(\int \left(\phi_1^0\right)^* \dfrac{\partial \phi_2^0}{\partial t}\, d\{\vec{r}\} - \dfrac{i}{\hbar} H_{12}\right) e^{\frac{i}{\hbar}\int_{-\infty}^{t}(H_{22}-H_{11})dt'} b_1(t) \ . & \text{(2.328b)} \end{cases}$$

2.8.5 The Landau-Zener model

Herein the Landau-Zener model which was independently derived by Landau [30] and Zener [31] in 1932 will be described.

Let's consider the case of two atomic particles approaching each other from infinity. The two particles will start to interact forming a *quasi-molecular particle*[24], whose respective interaction nuclear potential corresponds to the one of an equivalent molecular particle composed by the same two particles. Let this interaction nuclear potential be $U_{l_1,1}(R)$ (the initial electronic wave function is assumed to be $\Phi(\{\vec{r}\},t) = \phi_1(R(t),\{\vec{r}\})$). Also, let's assume that there's another interaction nuclear potential $U_{l_2,2}(R)$, with a dissociation limit higher than the first one but lower than the relative energy of the particles, and that it is sufficiently closer to $U_{l_1,1}(R)$ to make plausible a transition between the two. If such transition occurs, the departed atomic particles will be found in a higher excitation state than the their initial one. Due to the law of conservation of the total angular momentum of the system, and due to the fact that the electrons are highly ineffective in changing the angular momentum of the nuclei [2], the nuclei total angular momentum is conserved in the collision. Therefore, the rotational quantum numbers of the nuclei l_1 and l_2 are identical, i.e. $l_1 = l_2 := l$ [62], and one may work with the non-centrifugally corrected internuclear potentials $U_1(R)$ and $U_2(R)$ and the energy relatively to the centre of mass disregarding the centrifugal energy $E'' = E' - \hbar^2 l\,(l+1)\,/\left(2\mu R^2\right)$. Two particular cases will be considered: one in which the internuclear potential curves $U_1(R)$ and $U_2(R)$ being of identical symmetry get very close at the point $R = R_p$ departing very sharply in the vicinity of that point (see Figure 2.11) - this localised behaviour of the potential curves is often called *pseudo-crossing* or *avoided crossing* [63] - and another in which the

[24] The system composed by the two atomic particles can't be called a molecular particle since the energy relatively to its centre of mass is higher than the dissociation limit associated to the interaction nuclear potential, meaning that after reaching the turning point, if no change in the interaction nuclear potential curve occurs, the particles will depart from each other without returning.

internuclear potential curves $U_1(R)$ and $U_2(R)$ being of different symmetry cross each other at the point $R = R_c$ (see Figure 2.12).

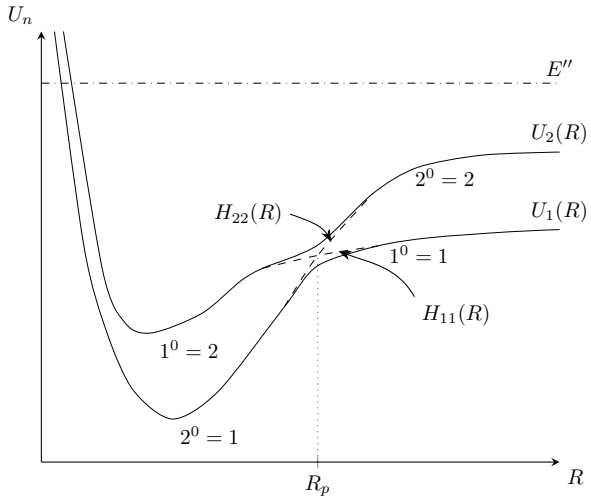

Figure 2.11: Representation of two electronic terms $U_1(R)$ and $U_2(R)$ that perform an avoiding crossing at $R = R_p$, as well as the diagonal elements of the Hamiltonian matrix represented in the diabatic basis H_{11} and H_{22}.

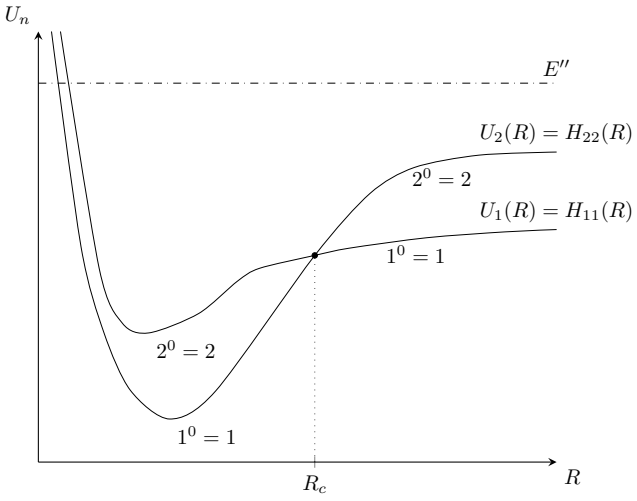

Figure 2.12: Representation of two electronic terms $U_1(R) = H_{11}(R)$ and $U_2(R) = H_{22}(R)$ that cross each other at $R = R_c$. The diabatic electronic functions were chosen to coincide with the adiabatic electronic functions at all points R.

Two electronic terms may only cross each other if they are of a different *symmetry* [62]. One may check if two electronic terms of a diatomic molecular particle are indeed asymmetric just by analysing their *term symbols*. A term symbol has the form

$$^{2S+1}\hat{\Lambda}^{(+/-)}_{(\mathrm{u/g})} ,$$

where $2S+1$ is the so-called *multiplicity* of the term (being S the quantum number for the total electronic spin of the molecular particle), $\hat{\Lambda}$ is a capital Greek letter that represents the quantum number for the projection of the total electronic orbital angular momentum vector on the internuclear axis Λ (for example, for $\Lambda = 0$, 1, 2 one has $\hat{\Lambda} = \Sigma$, Π, Δ). The subscripted letter (u/g) represents the *parity* of the term: u if odd or g if even. The superscripted signal $(+/-)$ only occurs if $\hat{\Lambda} = \Sigma$, and may correspond to $+$ or $-$. For example, the term symbol associated to the ground state of the nitrogen molecule corresponds to $^1\Sigma^+_{\mathrm{g}}$. Two electronic terms are said to be of different symmetry if they have a different $\hat{\Lambda}$ and a different multiplicity or parity, or the same $\hat{\Lambda}$ with $\hat{\Lambda} = \Sigma$, but a different sign [62].

2.8.5.1 The case of a pseudo-crossing

Let's consider the first case, in which the electronic terms perform a pseudo-crossing. The region in the vicinity of the pseudo-crossing point R_p is the one in which the electronic terms get the closest from each other, and therefore, it is also the region where transitions are more probable to occur - this region will be referred to from now on as the "transition region". In this transition region each adiabatic electronic

function depends strongly on both diabatic electronic functions due to the proximity in the values of the two sets of functions. At the left of this region, the diabatic electronic function $\phi_1^0(\vec{R},\{\vec{r}\})$ tends to the adiabatic electronic function $\phi_2(\vec{R},\{\vec{r}\})$ and, similarly, $\phi_2^0(\vec{R},\{\vec{r}\})$ tends to $\phi_1(\vec{R},\{\vec{r}\})$. Conversely, at the right, the diabatic electronic function $\phi_1^0(\vec{R},\{\vec{r}\})$ tends to the adiabatic electronic function $\phi_1(\vec{R},\{\vec{r}\})$ and $\phi_2^0(\vec{R},\{\vec{r}\})$ tends to $\phi_2(\vec{R},\{\vec{r}\})$, as shown by Figure 2.11. The motion of the two atomic particles can be divided into two parts: the approaching motion (before reaching the turning point), and the departing motion (after reaching the turning point). Let's start by studying the first part of the motion, attributing the value $t=-\infty$ to the instant before entering the transition region, $t=0$ to the instant at which the pseudo-crossing point R_p is reached, and $t=+\infty$ to the instant after leaving the transition region. Because the atomic particles are found with an electronic wave function $\Phi(\{\vec{r}\},t)=\phi_1(\vec{R}(t),\{\vec{r}\})$ before reaching the transition region, one has

$$\Phi(\{\vec{r}\},-\infty)=\phi_1(\vec{R}(-\infty),\{\vec{r}\})=\phi_1^0(\vec{R}(-\infty),\{\vec{r}\})\ , \tag{2.329}$$

and therefore, from relation (2.315), one also has

$$\begin{cases} b_1(-\infty)=1\ , & \text{(2.330a)} \\ b_2(-\infty)=0\ . & \text{(2.330b)} \end{cases}$$

These are the initial conditions for the differential equations (2.328a) and (2.328b) that determine the evolution of the coefficients $b_1(t)$ and $b_2(t)$ in time. It will be assumed that the transition region is so small that in that part of the trajectory the elements of the Hamiltonian matrix written under the diabatic basis almost don't change. The elements H_{11} and H_{22} may be expressed through a first order Taylor expansion around $R=R_p$, and H_{12} may be assumed to be constant [31], i.e.

$$\begin{cases} H_{11}(R)\approx H_{11}(R_p)+\underbrace{\dfrac{\partial H_{11}}{\partial R}(R_p)}_{:=F_1}(R-R_p)=H_{11}(R_p)+F_1\,(R-R_p)\ , & \text{(2.331a)} \\ H_{22}(R)\approx H_{22}(R_p)+\underbrace{\dfrac{\partial H_{22}}{\partial R}(R_p)}_{:=F_2}(R-R_p)=H_{22}(R_p)+F_2\,(R-R_p)\ , & \text{(2.331b)} \\ H_{12}(R)\approx H_{12}(R_p):=a\ . & \text{(2.331c)} \end{cases}$$

For the same reasons, the relative speed of the particles in the transition region is assumed to be constant, and therefore, $\dot{R}(t)\approx\dot{R}(0):=-v$, meaning that one may express $R(t)$ through a first order Taylor expansion around $t=0$:

$$R(t)\approx R_p-vt\ . \tag{2.332}$$

The difference between $H_{22}(R(t))$ and $H_{11}(R(t))$ can be obtained through subtraction of (2.331a) from (2.331b). And by knowing that the equality $H_{11}(R_p)=H_{22}(R_p)$ holds - the elements H_{11} and H_{22} intersect at $R=R_p$ (see Figure 2.11) - and using the relation (2.332), it's possible to show that

$$H_{22}(R(t))-H_{11}(R(t))=-\Delta F\,vt\ , \tag{2.333}$$

where $\Delta F = F_2 - F_1$, the difference between the values of the slopes of $H_{22}(R)$ and $H_{11}(R)$ curves in the transition region. Additionally, $\int \left(\phi_1^0\right)^* \frac{\partial \phi_2^0}{\partial t}\, d\{\vec{r}\}$ is assumed to be negligible when in comparison with H_{12} [61].

With all these assumptions taken into account, equations (2.328a) and (2.328b) for the evolution in time of the coefficients $b_1(t)$ and $b_2(t)$, respectively, may be expressed through

$$\begin{cases} \dot{b}_1(t) = -i\dfrac{a}{\hbar} e^{i\frac{\Delta F v}{\hbar}\left(\frac{t^2}{2}+\infty\right)} b_2(t) \ , & \text{(2.334a)} \\ \dot{b}_2(t) = -i\dfrac{a}{\hbar} e^{-i\frac{\Delta F v}{\hbar}\left(\frac{t^2}{2}+\infty\right)} b_1(t) \ . & \text{(2.334b)} \end{cases}$$

By differentiating (2.334a) and applying the results (2.334a) and (2.334b) in it, one can obtain a second-order differential equation:

$$\ddot{b}_1(t) - i\frac{\Delta F v}{\hbar} t \dot{b}_1(t) + \frac{a^2}{\hbar^2} b_1(t) = 0 \ . \tag{2.335}$$

And by performing further manipulations of (2.335) it's possible to express it through a *Weber equation* [31], which by imposing the initial conditions (2.330a) and (2.330b) allows one to obtain the coefficient values after the transition region, $b_1(+\infty)$ and $b_2(+\infty)$. Due to the already mentioned behaviour of the adiabatic and diabatic electronic functions outside of the transition region, the probability of transition of the system from ϕ_1 to ϕ_2 in the approaching motion of the nuclei, i.e. $P_{1,2}$, is equivalent to the probability on non-transition from ϕ_1^0, $P_{1^0,1^0}$. And according to the Born's rule one has $P_{1^0,1^0} = |b_1(+\infty)|^2$, ultimately giving [31]

$$P_{1,2} = P_{1^0,1^0} = e^{-\frac{2\pi a^2}{\hbar v |\Delta F|}} \ . \tag{2.336}$$

By following a similar procedure, it's also possible to show that $P_{2,1} = P_{2^0,2^0} = P_{1,2} = P_{1^0,1^0}$.

Regarding the departing motion of the particles, the same result (2.336) as well as the above-mentioned one hold if the interference caused by the transition from an electronic term to the other in the two motions is sufficiently small to be neglected [61]. By taking such assumption, the probability of transition of the system from ϕ_1 to ϕ_2 in a collision between the atomic particles, let it be $\bar{P}_{1,2}$, is given by the probability of transition from ϕ_1 to ϕ_2 in the approaching motion and non-transition in the the departing motion, i.e. $P_{1,2} \cdot P_{2,2} = P_{1,2}\,(1 - P_{1,2})$, plus the probability of non-transition in the approaching motion and transition from ϕ_1 to ϕ_2 in the departing motion, i.e. $P_{1,1} \cdot P_{1,2} = (1 - P_{1,2})\, P_{1,2}$:

$$\bar{P}_{1,2} = P_{1,2}\,(1 - P_{1,2}) + (1 - P_{1,2})\, P_{1,2} = 2P_{1,2}\,(1 - P_{1,2}) \Leftrightarrow$$

$$\Leftrightarrow \bar{P}_{1,2} = 2e^{-\frac{2\pi a^2}{\hbar v |\Delta F|}} \left(1 - e^{-\frac{2\pi a^2}{\hbar v |\Delta F|}}\right) \ . \tag{2.337}$$

This result is the so-called *Landau-Zener formula* [61].

2.8.5.2 The case of a crossing

Let's now consider the case in which the electronic terms $U_1(R)$ and $U_2(R)$ cross each other at $R = R_c$ as depicted by Figure 2.12. The diabatic electronic functions ϕ_1^0 and ϕ_2^0 are chosen to coincide with the adiabatic electronic functions ϕ_1 and ϕ_2, respectively, implying that $H_{11}(R) = U_1(R)$, $H_{22}(R) = U_2(R)$

and $H_{12}(R) = 0$ for all R. The approximations (2.331a), (2.331b) and (2.332) with R_p substituted by R_c are considered, and because the condition $H_{12}(R) = 0$ holds, one should now regard the contribution of $\int \left(\phi_1^0\right)^* \frac{\partial \phi_2^0}{\partial t}\, d\{\vec{r}\}$ for the equations of evolution in time of the coefficients $b_1(t)$ and $b_2(t)$, (2.328a) and (2.328b), respectively. These are therefore transformed into

$$\begin{cases} \dot{b}_1(t) = -\left(\int \left(\phi_1^0\right)^* \dfrac{\partial \phi_2^0}{\partial t}\, d\{\vec{r}\}\right) e^{i\frac{\Delta F v}{\hbar}\left(\frac{t^2}{2}+\infty\right)} b_2(t)\ , & \text{(2.338a)} \\ \dot{b}_2(t) = \left(\int \left(\phi_1^0\right)^* \dfrac{\partial \phi_2^0}{\partial t}\, d\{\vec{r}\}\right) e^{-i\frac{\Delta F v}{\hbar}\left(\frac{t^2}{2}+\infty\right)} b_1(t)\ . & \text{(2.338b)} \end{cases}$$

Let's also consider that the system is initially with an electronic wave function $\Phi(\{\vec{r}\}, t) = \phi_1(\vec{R}(t), \{\vec{r}\})$, meaning that the initial conditions of the problem in the approaching motion are the same as the ones considered for the pseudo-crossing case, which are expressed by (2.330a) and (2.330b).

Similarly to what was done for the pseudo-crossing case, the two differential equations (2.338a) and (2.338b) can be transformed into a second-order different equation:

$$\ddot{b}_1(t) - i\frac{(-\Delta F)\, v}{\hbar} t \dot{b}_1(t) + \frac{\left(\hbar \int \left(\phi_1^0\right)^* \frac{\partial \phi_2^0}{\partial t}\, d\{\vec{r}\}\right)^2}{\hbar^2} b_1(t) = 0\ . \tag{2.339}$$

By comparing (2.339) with (2.335), one can immediately find that the solution for $P_{1^0,1^0}$ is the same one as for the pseudo-crossing case (2.336) with ΔF substituted by $-\Delta F$ and a substituted by $\hbar \int \left(\phi_1^0\right)^* \frac{\partial \phi_2^0}{\partial t}\, d\{\vec{r}\}$ giving

$$P_{1,1} = P_{1^0,1^0} = e^{-\frac{2\pi\hbar\left(\int \left(\phi_1^0\right)^* \frac{\partial \phi_2^0}{\partial t}\, d\{\vec{r}\}\right)^2}{v|\Delta F|}}\ , \tag{2.340}$$

It is also possible to show that $P_{2,2} = P_{2^0,2^0} = P_{1,1}$.

The probability of transition of the system from ϕ_1 to ϕ_2 in a collision between the atomic particles $\bar{P}_{1,2}$, is given by the probability of transition from ϕ_1 to ϕ_2 in the approaching motion and non-transition in the the departing motion, i.e. $P_{1,2} \cdot P_{2,2} = (1 - P_{1,1}) \cdot P_{2,2}$, plus the probability of non-transition in the approaching motion and transition from ϕ_1 to ϕ_2 in the departing motion, i.e. $P_{1,1} \cdot P_{1,2} = P_{1,1}\,(1 - P_{1,1})$:

$$\begin{aligned} &\bar{P}_{1,2} = (1 - P_{1,1}) \cdot P_{2,2} + P_{1,1}\,(1 - P_{1,1}) = 2P_{1,1}\,(1 - P_{1,1}) \Leftrightarrow \\ &\Leftrightarrow \bar{P}_{1,2} = 2e^{-\frac{2\pi\hbar\left(\int \left(\phi_1^0\right)^* \frac{\partial \phi_2^0}{\partial t}\, d\{\vec{r}\}\right)^2}{v|\Delta F|}} \left[1 - e^{-\frac{2\pi\hbar\left(\int \left(\phi_1^0\right)^* \frac{\partial \phi_2^0}{\partial t}\, d\{\vec{r}\}\right)^2}{v|\Delta F|}}\right]\ . \end{aligned} \tag{2.341}$$

2.8.6 The Rosen-Zener-Demkov model

Herein the Rosen-Zener-Demkov model will be described. Let's consider the case of two atomic particles approaching each other from infinity, colliding, and then departing. The electronic wave function of the system is initially $\Phi(\{\vec{r}\}, t) = \phi_1(\vec{R}(t), \{\vec{r}\})$. The electronic term $U_1(R)$ is the initial non-centrifugally corrected interaction potential between the two nuclei. Another electronic term, let it be called $U_2(R)$, gets very close to $U_1(R)$ for sufficiently large R values, such that their asymptotes have a small separation Δ as depicted by Figure 2.13. It is in this region that electronic transitions may occur. The dissociation

limit of $U_2(R)$ is considered to be higher than the dissociation limit of $U_1(R)$, but lower than the relative energy (disregarding the centrifugal energy) of the colliding atomic particles E''.

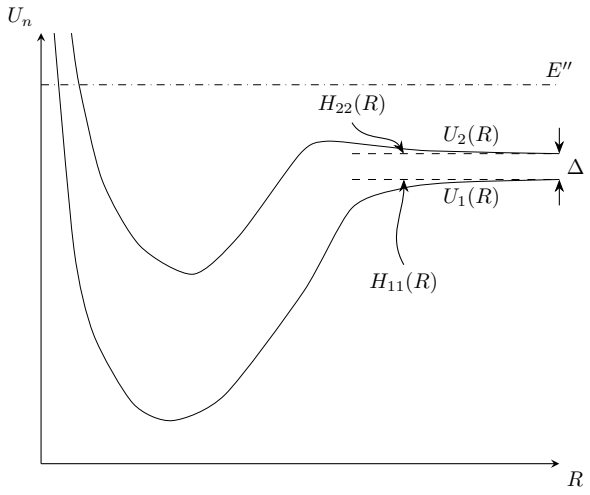

Figure 2.13: Representation of two electronic terms $U_1(R)$ and $U_2(R)$ that get very close to each other for sufficiently large R values, and the diagonal elements of the Hamiltonian matrix represented in the diabatic basis $H_{11}(R)$ and $H_{22}(R)$ which coincide with the asymptotic values of $U_1(R)$ and $U_2(R)$ for those large R values.

Demkov [33] described an electronic transition in a system constituted by two colliding atomic particles as the one mentioned above. The mathematical structure of the problem was found to be the same as the one previously obtained by Rosen and Zener [32], although these two authors studied a completely different phenomena - the physics of the Stern-Gerlach experiment. The two different contributions justify the presence of the three authors' names in the model's designation. Demkov assumed that $H_{11}(R)$ and $H_{22}(R)$ are constant in the transition region, and $H_{12}(R)$ has an exponential decaying form, i.e.

$$H_{11}(R) \approx E_0 - \frac{\Delta}{2} \ , \quad (2.342) \qquad H_{22}(R) \approx E_0 + \frac{\Delta}{2} \ , \quad (2.343) \qquad H_{12}(R) \approx A e^{-\alpha R} \ , \quad (2.344)$$

where E_0 is the arithmetic mean of the asymptotic values of $U_1(R)$ and $U_2(R)$, i.e. $E_0 = [U_1(+\infty) + U_2(+\infty)]/2$, and A and α are some positive constants. Relation (2.344) expresses the way that the diabatic electronic functions $\phi_1^0(R)$ and $\phi_2^0(R)$ tend to $\phi_1(R)$ and $\phi_2(R)$, respectively, as R increases. In the limit $R \to +\infty$, one has $\phi_1^0(R) = \phi_1^0(R)$ and $\phi_2^0(R) = \phi_2(R)$, meaning that $H_{12}(R) = 0$ (as supported by relation (2.344)), due to the fact that the adiabatic electronic functions are orthonormal eigenfunctions of the Hamiltonian operator $\hat{H}$. It is of particular interest to obtain the dependence of R on time, so that the whole problem can be solved through the already mentioned semiclassical approach. Therefore, an equation for the classical motion of the nuclei involving the elements of the Hamiltonian represented in the diabatic basis needs to be obtained. It can be easily shown that if one considers an expansion for the $\psi(\{\vec{R}\},\{\vec{r}\})$ function expressed through the diabatic basis,

$$\psi(\{\vec{R}\},\{\vec{r}\}) = \sum_m \chi_m^0(\{\vec{R}\})\, \phi_m^0(\{\vec{R}\},\{\vec{r}\}) \ , \quad (2.345)$$

instead of the adiabatic basis in the Schrödinger equation (2.299), and following the procedure done in section §2.8.2.2 as well as applying the two-states approximation, two coupled Schrödinger equations for the nuclei motion can be obtained:

$$\begin{cases} \left[-\frac{\hbar^2}{2\mu} + H_{11}(R)\right] x^0_{1,l,m}(R) = E''_{l,m} x^0_{1,l,m}(R) - H_{12}(R) x^0_{2,l,m} \ , & \text{(2.346a)} \\ \left[-\frac{\hbar^2}{2\mu} + H_{22}(R)\right] x^0_{2,l,m}(R) = E''_{l,m} x^0_{2,l,m}(R) - H_{12}(R) x^0_{1,l,m} \ , & \text{(2.346b)} \end{cases}$$

being $x^0_{n,l,m}(R)$ with $n = 1, 2$ some wave functions which are related to $\chi^0_n(\{\vec{R}\})$ in the same way as the wave functions $x_{n,l,m}(R)$ in the Schrödinger equation (2.308) are related to $\chi_n(\{\vec{R}\})$ (see section §2.8.2.2). The energy $E''_{l,m} = E' - \hbar^2 l(l+1)/\left(2\mu R^2\right)$ corresponds to the relative energy of the colliding atomic particles disregarding the rotational contribution. The indices l and m in $x^0_{n,l,m}(R)$ and $E''_{l,m}$ represent the two quantum numbers associated to the rotation of the quasi-molecular particle. They will be omitted henceforth since it is known that the total angular momentum of the nuclei is conserved in the collision, meaning that nuclei rotation doesn't need to be dealt with.

Since the electronic terms $U_1(R)$ and $U_2(R)$ are permanently close to each other from infinity to a sufficiently high R value, the nuclei will pass most of their time in this infinite region in the approaching and departing motions. The physical phenomena that occurs near the turning point may be disregarded and the elements of the Hamiltonian matrix represented in the diabatic basis may be approximated by the ones given by (2.342), (2.343) and (2.344) at all instants of time t, allowing one to transform equations (2.346a) and (2.346b) into

$$\begin{cases} \left[-\frac{\hbar^2}{2\mu}\frac{\partial^2}{\partial R^2} + E_0 - \frac{\Delta}{2}\right] x^0_1(R) = E'' x^0_1(R) - A e^{-\alpha R} x^0_2 \ , & \text{(2.347a)} \\ \left[-\frac{\hbar^2}{2\mu}\frac{\partial^2}{\partial R^2} + E_0 + \frac{\Delta}{2}\right] x^0_2(R) = E'' x^0_2(R) - A e^{-\alpha R} x^0_1 \ . & \text{(2.347b)} \end{cases}$$

By multiplying (2.347a) and (2.347a) by $1/\sqrt{2}$ and summing them, it's possible to obtain

$$\left[-\frac{\hbar^2}{2\mu}\frac{\partial^2}{\partial R^2} + A e^{-\alpha R}\right] \frac{1}{\sqrt{2}}\left[x^0_1(R) + x^0_2(R)\right] = (E'' - E_0)\frac{1}{\sqrt{2}}\left[x^0_1(R) + x^0_2(R)\right] + \frac{\Delta}{2}\frac{1}{\sqrt{2}}\left[x^0_2(R) - x^0_1(R)\right] \ . \tag{2.348}$$

In near resonance, i.e. if $\Delta \approx 0$ holds, the last left term in (2.348) may be neglected, and the equation may be transformed into

$$\left[-\frac{\hbar^2}{2\mu}\frac{\partial^2}{\partial R^2} + A e^{-\alpha R}\right] x^0(R) = E''' x^0(R) \ , \tag{2.349}$$

with $x^0(R) = 1/\sqrt{2}\left[x^0_1(R) + x^0_2(R)\right]$ and $E''' = E'' - E_0$. The classical counterpart of equation (2.349) corresponds to

$$\frac{1}{2}\mu\dot{R}^2 + A e^{-\alpha R} = E''' \ . \tag{2.350}$$

And by differentiating (2.351) with respect to time the classical equation that governs the relative radial motion of the nuclei can be finally obtained:

$$\mu\ddot{R} = \alpha A e^{-\alpha R} \ , \tag{2.351}$$

which has the same form as (2.175), and therefore its solution is given according to (2.176) by

$$R(t) = \frac{2}{\alpha} \ln \left[\cosh \left(\sqrt{\frac{A}{2\mu}} \alpha t \right) \right] \ . \tag{2.352}$$

It's important to mention that the result (2.352) assumes that the classical turning point occurs at $t = 0$. By applying the initial condition $\dot{R}(-\infty) = -v$, being v the initial relative radial speed of the colliding atomic particles, one may find that

$$A = \frac{1}{2} \mu v^2 \ , \tag{2.353}$$

and (2.352) may be transformed into

$$R(t) = \frac{2}{\alpha} \ln \left(\cosh \left(\frac{\alpha v}{2} t \right) \right) \ . \tag{2.354}$$

Solution (2.354) corresponds to the relative radial trajectory of the nuclei that needs to be inserted into (2.344), which by taking into account (2.353), ultimately gives

$$H_{12}(t) = \frac{\frac{1}{2}\mu v^2}{\cosh^2 \left(\frac{\alpha v}{2} t \right)} = \frac{\mu v^2}{\cosh \left(\frac{\alpha v}{2} t \right) + 1} \approx \frac{\mu v^2}{\cosh \left(\frac{\alpha v}{2} t \right)} \ , \tag{2.355}$$

where in the last step the previous assumption that only the transition region matters for the problem was taken. The transition region is accessed for instants of time t such that $|t| \gg 1$ (note that the turning point occurs at $t = 0$), implying that $\cosh \left(\frac{\alpha v}{2} t \right) \gg 1$ [64].

To determine the probability of an electronic transition due to the described collision, one needs to solve the equations for the evolution in time of the coefficients $b_1(t)$ and $b_2(t)$, given by (2.328a) and (2.328b) respectively. It will be assumed that $\int \left(\phi_1^0 \right)^* \frac{\partial \phi_2^0}{\partial t} \, d\{\vec{r}\}$ is negligible when in comparison with $H_{12}(t)$. By substituting (2.342), (2.343) and (2.355) in the evolution equations (2.328a) and (2.328b), one may write

$$\begin{cases} \dot{b}_1(t) = -i \dfrac{\mu v^2}{\hbar \cosh \left(\frac{\alpha v}{2} t \right)} e^{-i \frac{\Delta}{\hbar} (t + \infty)} b_2(t) \ , & \text{(2.356a)} \\ \dot{b}_2(t) = -i \dfrac{\mu v^2}{\hbar \cosh \left(\frac{\alpha v}{2} t \right)} e^{i \frac{\Delta}{\hbar} (t + \infty)} b_1(t) \ . & \text{(2.356b)} \end{cases}$$

These two equations have the same mathematical structure as the ones treated by Rosen and Zener [32]. By differentiating (2.356a) with respect to time, and inserting the relations (2.356a) and (2.356b) in the result, it's possible to obtain a second-order differential equation:

$$\ddot{b}_1(t) + \left[\frac{\alpha v}{2} \tanh \left(\frac{\alpha v}{2} t \right) + i \frac{\Delta}{\hbar} \right] \dot{b}_1(t) + \left[\frac{\mu v^2}{\hbar^2 \cosh \left(\frac{\alpha v}{2} t \right)} \right]^2 b_1(t) = 0 \ . \tag{2.357}$$

The differential equation (2.357), can then be tranformed into a *hypergeometrical differential equation* through a change of variables [32]. By taking account the initial conditions (2.330a) and (2.330b), a

solution for this differential equation $b_1(t)$ may be obtained. By invoking the Born's rule, the probability of transition from the electronic wave function $\Phi(\{\vec{r}\},t) = \phi_1(\vec{R}(t),\{\vec{r}\})$ at $t = -\infty$ to $\Phi(\{\vec{r}\},t) = \phi_2(\vec{R}(t),\{\vec{r}\})$ at $t = +\infty$ in a collision can then be shown to be [32, 65]

$$\bar{P}_{1,2} = \frac{\sin^2\left(\frac{\pi\mu v}{\hbar\alpha}\right)}{\cosh^2\left(\frac{\pi\Delta}{2\hbar\alpha v}\right)} \ . \tag{2.358}$$

Although no mathematical demonstration will be given (for compactness reasons), it can be shown that the probability of transition from the electronic wave function $\Phi(\{\vec{r}\},t) = \phi_1(\vec{R}(t),\{\vec{r}\})$ to $\Phi(\{\vec{r}\},t) = \phi_2(\vec{R}(t),\{\vec{r}\})$ in a single approaching or departing motion corresponds to $P_{1,2}$, such that [66]

$$\frac{1}{\cosh^2\left(\frac{\pi\Delta}{2\hbar\alpha v}\right)} = 4P_{1,2}\left(1 - P_{1,2}\right) \Leftrightarrow$$

$$P_{1,2} = \frac{1}{1 + e^{\frac{\pi\Delta}{\hbar\alpha v}}} \ . \tag{2.359}$$

2.8.7 A study of the possibility of extension of the Landau-Zener and Rosen-Zener-Demkov models to the case of VE-m-h processes

Let's consider a collision between a molecular particle and a heavy particle. The presence of the heavy particle would perturb the internuclear potential associated to the molecular particle. The nuclei of the molecular particle would then be subjected to an internuclear potential curve which changes parametrically with the position of the heavy particle. If another potential curve is sufficiently close to the current one for some particular internuclear distance values, a vibronic transition may occur [61]. Vibration of the molecular particle means that the nuclei may match the particular internuclear distance values several times during the collision, and therefore, successive vibronic transitions may happen. If the coupling is due to a crossing or an avoided crossing of the potential curves, then the Landau-Zener model may be applied. It's worthy to mention that unperturbed electronic terms which are of different symmetry due to different parities are transformed into terms of same symmetry when perturbed, since the presence of the collision partner would destroy the parity symmetry of the electronic terms [67]. That means that if a crossing of the respective unperturbed internuclear potential curves occurs, this will be transformed into a pseudo-crossing, implying a strong coupling between the two terms. One example of such transformation is the one that occurs for the electronic terms $A^3\Sigma_u^+$ and $B^3\Pi_g$ of molecular nitrogen N_2 (see Figure (B.3)). The unperturbed potential curves associated to $A^3\Sigma_u^+$ and $B^3\Pi_g$ would be regarded as crossing diabatic terms, and the respective perturbed ones would be regarded as adiabatic terms that perform an avoiding crossing.

The Rosen-Zener-Demkov model can't be applied in any circumstance since the coupling described by this model only occurs for internuclear distance values associated to the dissociation of the molecular particle.

It's important to note that if the collision partner also corresponds to a molecular particle and there's an internuclear potential curve which is close enough to the current one, then it is also necessary to take into account the possibility of this particle suffering a vibronic transition in the collision.

One way of determining the probability of heavy particle-impact vibronic transition is by solving the classical equations of motion of the nuclei and applying the Landau-Zener model at the internuclear distances associated to the crossing or pseudo-crossing of the potential curves - the so-called *Trajectory Surface Hopping Approach* (TSHA) [68]. However, this approach requires the knowledge of the perturbation induced by the collision partner on the potential curves. No data for the parameters that define this perturbation were found in the literature for the case of the heavy particle-impact vibronic transition of N_2 and N_2^+. An overall lack of such data is indeed acknowledged by the scientific community, as underlined by Capitelli et al. [69], who say "[...] it is practically impossible to carry out reliable theoretical calculations of the corresponding transition probabilities owing to the lack of accurate information on the structure and intersections of the colliding particles' electronic terms".

There has been a recent attempt, done by Kirillov [70, 71], to account both Landau-Zener and Rosen-Zener-Demkov models through a general analytic expression using experimental results to calibrate the values of the involved parameters. However, not only the derivation of the analytic expression is somewhat puzzling, but the approach per se lacks physical coherency, since Kirillov applied both models assuming that the respective original formulae are directly valid for vibronic transitions of colliding molecular and heavy particles beyond electronic transitions of colliding atomic particles. The relative speed between the nuclei v which appears in expressions (2.336), (2.340) and (2.359) should be the one associated to the nuclei of the same molecular particle, due to the fact that the considered vibronic transitions are the ones between electronic terms of the this molecular particle. Kirillov erroneously regarded v as the relative speed of the collision partners, and used the above-mentioned expressions to obtain rate coefficients considering a distribution of relative speeds $f(v, T_{\mathrm{tr_h}})$.

Curiously, the expression proposed by Kirillov for the average process cross section $\sigma_{p,\mathrm{av}}$ resembles some well-known semi-empiric relations for VE-m-h transitions. The Kirillov expression [70] written under the nomenclature presented by the chemical equations (2.279) and (2.280) corresponds to

$$\sigma_{p,\mathrm{av}}(T_{\mathrm{tr_h}}) = \begin{cases} \sigma_{\mathrm{el}}\left(T_{\mathrm{tr_h}}, |\Delta E|\right)\ \mathrm{FC}_1\, e^{-\frac{|\Delta E|}{2k_B T_{\mathrm{tr_h}}}}, & \text{if M} = \mathrm{C}(e_2)\ , \\ \sigma_{\mathrm{el}}\left(T_{\mathrm{tr_h}}, |\Delta E|\right)\ \mathrm{FC}_1\, \mathrm{FC}_2\, e^{-\frac{|\Delta E|}{2k_B T_{\mathrm{tr_h}}}}, & \text{if M} = \mathrm{CD}(e_2, v_2)\ , \end{cases} \tag{2.360}$$

where σ_{el} is the so-called *intrinsic electronic cross section* [36], being associated to the initial and final electronic levels of the collision partners e_1, e_2, e_1' and e_2'. In the case of the Kirillov approach, σ_{el} corresponds to the average cross section obtained from the application of the Landau-Zener or the Rosen-Zener-Demkov models. The quantities FC_1 and FC_2 are the so-called *Franck-Condon factors* [36] which are associated to the overlapping between the vibrational wave functions of the initial and final vibronic levels of the molecular particle AB, i.e. (e_1, v_1) and (e_1', v_1'), and of the initial and final vibronic levels of the collision partner CD, i.e. (e_2, v_2) and (e_2', v_2'), respectively. Finally, ΔE is the *energy defect*, i.e. the difference between the initial and final internal energies of the collision partners. Since the transition of the molecular particle AB is vibronic, and the transition of the collision partner is electronic if it

corresponds to an atomic particle, or vibronic if it is a molecular particle, ΔE is given by

$$\Delta E = \begin{cases} (T_{e_1 v_1} + T_{e_2}) - \left(T_{e'_1 v'_1} + T_{e'_2}\right), & \text{if M} = \text{C}(e_2)\ , \\ (T_{e_1 v_1} + T_{e_2 v_2}) - \left(T_{e'_1 v'_1} + T_{e'_2 v'_2}\right), & \text{if M} = \text{CD}(e_2, v_2)\ . \end{cases} \tag{2.361}$$

Relation (2.360) for the case M = C(e_2) differs just slightly from a most common model originally postulated by Katayama et al. [36]:

$$\sigma_{p,\text{av}}\left(T_{\text{tr}_\text{h}}\right) = \sigma_{\text{el}}\, \text{FC}_1\, e^{-\frac{|\Delta E|}{k_B T_{\text{tr}_\text{h}}}}\ . \tag{2.362}$$

The difference is on the factor of 1/2 that appears in the argument of the exponential function in (2.360) but not in the argument of the exponential function in (2.362). These particular exponential functions express a type of "exponential gap law": they tell that the average process cross section would decrease with the absolute value of the energy defect ΔE, and increase with the temperature T_{tr_h}.

Since relation (2.362) is a simplistic postulatory model it may lack some physical coherence. Conclusions reached by several researchers rose concern and doubt about its application. Bachmann et al. reported that the results of his works [34, 35] had no obvious correlation with the Franck-Condon factors, and that their use would be questionable since factors associated to the overlap of wave functions for the whole collision system should be regarded instead of Franck-Condon factors associated to isolated molecular particles. Bachmann et al. also added that in some works, such as the one of Bondybey et al. [72], the ones of and Katayama et al. [36–38] and the one of Dentamaro et al. [73], the dependence on the Franck-Condon factors is in qualitative agreement with the observations, but for others, such as the one of Jihua et al. [74], no correlation with the Franck-Condon factors was reported. In the latter, the authors referred that their results were "clearly inconsistent" with relation (2.362). Also, Piper [75] reported that, according to his results, the model fails to predict the energy level distributions of the species involved in the various studied energy transfer processes even qualitatively. Bachmann et al. [34, 35] considered the possibility, that for a constant temperature T_{ref}, the average cross section may be expressed by a exponential gap law of the form

$$\sigma_{p,\text{av}} = \sigma_0\, e^{-\frac{|\Delta E|}{E_0}}\ , \tag{2.363}$$

being σ_0 a characteristic cross section and E_0 a characteristic energy. If the VE-m-h process is *resonant*, i.e. if $\Delta E = 0$ does hold, then one would have $\sigma_{p,\text{av}} = \sigma_0$, and therefore, σ_0 can be interpreted as the average cross section value for the case of energy resonance. The results of Bachmann et al. [34] agree considerable well with the relation (2.363). However, a more detailed work [35] showed some evidences of the behaviour of the average cross sections for VE-m-h endothermic processes departing from the one associated to the exothermic VE-m-h processes, being the latter favoured over the former.

The exponential function which appears in (2.362) expressing the respective exponential gap law has been found to be incorrect. In a work of Katayama et al. [37] a decrease of the average process cross section with a decrease of the temperature was observed when the inverse was expected. Katayama et al. [39] said that the regarded exponential factor is characteristic of a repulsive interaction and that an

attractive interaction would be more appropriate. They then suggested a substitution of the symmetric of the energy defect absolute value, $-|\Delta E|$, in the argument of the exponential function by the well depth of the interaction potential, ε. Such substitution is complacent with the results of the works of Parmenter et al. [76, 77].

By taking this analysis into account, it was decided to employ in this work an expression for VE-m-h average cross sections with the vibronic dependence suggested by Bachmann et al. [34, 35] and the thermal dependence suggested by Katayama et al. [39]:

$$\sigma_{p,\mathrm{av}}\left(T_{\mathrm{tr_h}}\right) = \sigma_0' \, e^{-\frac{|\Delta E|}{E_0} + \frac{\varepsilon}{k_B T_{\mathrm{tr_h}}}} \ , \tag{2.364}$$

being $\sigma_0' = \sigma_0 e^{-\frac{\varepsilon}{k_B T_{\mathrm{ref}}}}$ (implying that at $T_{\mathrm{tr_h}} = T_{\mathrm{ref}}$ one has $\sigma_{p,\mathrm{av}}$ given by (2.363), i.e. $\sigma_{p,\mathrm{av}} = \sigma_0 \, e^{-\frac{|\Delta E|}{E_0}}$) and ε the well depth of the potential energy curve associated to interaction between the collision partners. And from (2.84), the respective rate coefficient is given by

$$k_f(T_{\mathrm{tr_h}}) = \frac{\sigma_0' \, e^{-\frac{|\Delta E|}{E_0}}}{1 + \delta_{\mathrm{AB}(e_1,v_1),\mathrm{M}}} \sqrt{\frac{8 k_B T_{\mathrm{tr_h}}}{\pi \mu}} e^{\frac{\varepsilon}{k_B T_{\mathrm{tr_h}}}} \ . \tag{2.365}$$

which may be conveniently expressed through a modified Arrhenius function (2.88).

2.9 A vibrational redistribution procedure

Let's consider some important process involving the vibrational energy mode, which isn't reasonably well understood, yet, its rate coefficient can be measured for some particular vibrational quantum number or for the overall contribution of the full set of vibrational quantum numbers. In order to apply these rate coefficients on vibronic-specific state-to-state simulations it's firstly necessary to obtain vibronic-specific ones from them. Being proper theoretical models unavailable, it's necessary to rely on some general semi-empirical rules which may or may not describe reasonably well the vibrational dependence. In this section an approach to compute a full set of vibronic-specific rate coefficients from an overall rate coefficient or from a single vibronic-specific rate coefficient is described. Such approach is based on the *vibrational redistribution procedure* (VRP) considered by Julien Annaloro in his PhD thesis [18].

2.9.1 VRP on the final vibrational quantum number, from an overall rate coefficient

Let's consider a vibronic-specific process described by the chemical equation

$$\cdots \longrightarrow \mathrm{X}(e', v') + \cdots \ , \tag{2.366}$$

where the ellipses represent reactants and the other products. Vibronic-specific rate coefficients of the form $k^{v'}(T_{\mathrm{c}})$ are to be computed from an overall rate coefficient $k(T_{\mathrm{c}})$ being the latter with respect to

the electronic-specific counterpart process of (2.366), i.e.:

$$\cdots \longrightarrow \mathrm{X}(e') + \cdots \,. \tag{2.367}$$

Note that T_c corresponds to the controlling temperature of the process. By invoking the arguments perpetrated on §2.7.7, one may show that the two types of rate coefficients are related to each other through

$$k(T_\mathrm{c}) = \sum_{v'} k^{v'}(T_\mathrm{c}) \,. \tag{2.368}$$

Now, let's take the assumption that both rate coefficients may be described by modified Arrhenius functions (2.88):

$$\begin{cases} k(T_\mathrm{c}) = A\, {T_\mathrm{c}}^{n} e^{-\frac{E_a}{k_B T_\mathrm{c}}} \,, & \text{(2.369a)} \\ k^{v'}(T_\mathrm{c}) = A^{v'}(T_\mathrm{c})\, {T_\mathrm{c}}^{n^{v'}} e^{-\frac{E_a^{v'}}{k_B T_\mathrm{c}}} \,. & \text{(2.369b)} \end{cases}$$

being the pre-exponential factor of the vibronic-specific rate $A^{v'}$ allowed to be dependent on the controlling temperature T_c (hence the presence of the respective symbol on its argument). The parameters A, n and E_a of the overall rate coefficient are all known. Annaloro [18] assumes that the power on the temperature of the vibronic-specific rate is the same as the one of the overall rate:

$$n^{v'} = n \,. \tag{2.370}$$

And the activation energy of vibronic-specific rate is defined as the difference between the internal energy of the products and the internal energy of the reactants, if non-negative, or as zero, if negative. One may express this in terms of the previously introduced energy defect[25] ΔE as

$$E_a^{v'} = -\Delta E^{v'} \cdot \mathrm{H}(-\Delta E^{v'}), \tag{2.371}$$

being $\mathrm{H}(-\Delta E^{v'})$ the *Heaviside function*, which gives 0 if $-\Delta E^{v'} < 0$ and 1 if $-\Delta E^{v'} \geq 0$. Regarding the pre-exponential factor $A^{v'}(T_\mathrm{c})$, Annaloro assumed that it increases linearly with $|\Delta E^{v'}|$ if $\Delta E^{v'} < 0$ or with the inverse of $|\Delta E^{v'}|$ if $\Delta E^{v'} > 0$. The proportionality coefficients for each cases are defined through a common coefficient, say $B(T_\mathrm{c})$, and the minimum values of $|\Delta E^{v'}|$ associated to the respective signals, $|\Delta E^{-}|_\mathrm{min}$ and $|\Delta E^{+}|_\mathrm{min}$. The case $|\Delta E^{v'}| = 0$ isn't regarded, being assumed to not occur. One has

$$A^{v'}(T_\mathrm{c}) = B(T_\mathrm{c}) \left[\frac{|\Delta E^{v'}|}{|\Delta E^{-}|_\mathrm{min}} \mathrm{H}(-\Delta E^{v'}) + \frac{|\Delta E^{+}|_\mathrm{min}}{|\Delta E^{v'}|} \mathrm{H}(\Delta E^{v'}) \right]. \tag{2.372}$$

The common coefficient $B(T_\mathrm{c})$ is determined from condition (2.368), which gives

$$B(T_\mathrm{c}) = \frac{A\, e^{-\frac{E_a}{k_B T_\mathrm{c}}}}{\sum_{v'} \left[\frac{|\Delta E^{v'}|}{|\Delta E^{-}|_\mathrm{min}} e^{\frac{\Delta E^{v'}}{k_B T_\mathrm{c}}} \mathrm{H}(-\Delta E^{v'}) + \frac{|\Delta E^{+}|_\mathrm{min}}{|\Delta E^{v'}|} \mathrm{H}(\Delta E^{v'}) \right]}. \tag{2.373}$$

[25] The energy defect ΔE was defined as the difference between the internal energy of the reactants and the internal energy of the products, precisely the symmetric of the difference of energies mentioned in the text.

2.9.2 VRP on the final vibrational quantum number, from a single vibronic-specific rate coefficient

Let's consider the case in which solely a rate coefficient of (2.366) for a particular vibrational quantum number $v' = v'_{\text{ref}}$ is known, being given by a modified Arrhenius function:

$$k^{v'_{\text{ref}}}(T_{\text{c}}) = A\,{T_{\text{c}}}^{n} e^{-\frac{E_a}{k_B T_{\text{c}}}} \ . \tag{2.374}$$

By assuming that the vibronic-specific rate coefficients $k^{v'}(T_{\text{c}})$ follow the law (2.369b), with $n^{v'} = n$, $E_a^{v'}$ given by (2.371), and $A^{v'}(T_{\text{c}})$ by (2.372) one can easily show from (2.374) that

$$B(T_{\text{c}}) = \frac{A\, e^{-\frac{E_a}{k_B T_{\text{c}}}}}{\frac{|\Delta E^{v'_{\text{ref}}}|}{|\Delta E^-|_{\text{min}}}\, e^{\frac{\Delta E^{v'_{\text{ref}}}}{k_B T_{\text{c}}}}\, \text{H}(-\Delta E^{v'_{\text{ref}}}) + \frac{|\Delta E^+|_{\text{min}}}{|\Delta E^{v'_{\text{ref}}}|}\, \text{H}(\Delta E^{v'_{\text{ref}}})}. \tag{2.375}$$

2.9.3 VRP on the initial vibrational quantum number, from a single vibronic-specific rate coefficient

If one instead deals with a vibronic-specific process of the form

$$\text{X}(e, v) + \cdots \longrightarrow \cdots \ , \tag{2.376}$$

and knows the rate coefficient for a particular vibrational quantum number $v = v_{\text{ref}}$, it is possible the obtain the rate coefficients for all the other if the model (2.369b) (constrained by (2.370) and (2.372)) with v' simply substituted by v is regarded. The parameters are then the ones obtained in §2.9.2, also with v' substituted by v.

Chapter 3

Implementation

3.1 Considered species and their energy levels

The considered species were the molecular nitrogen N_2, molecular nitrogen ion N_2^+, atomic nitrogen N, atomic nitrogen ion N^+ and free electron e^-.

The electronic energies of the molecular nitrogen N_2 and molecular nitrogen ion N_2^+ were taken from the literature. The respective vibrational energies of each of the considered electronic levels, were obtained using the *Fourier Grid Hamiltonian method* [78]. The required potential curves were generated by implementation of the *Rydberg* [79, 80]–*Klein* [81]–*Rees* [82] *method* allied with extrapolation. To familiarise the reader with such methods and the way that they were implemented in this work, a detailed description is made in appendix B.

Electronic energies ϵ_{el} of the atomic nitrogen N and atomic nitrogen ion N^+ can be obtained from the National Institute of Standards and Technology (NIST) database [83]. The NIST database takes into account the *fine structure* of the electronic levels. This fine structure comes into play when relativistic effects which depend on the spin of the electrons of the particle are regarded [62]. When taking account relativistic effects, electronic levels that ignored them should now be "split" into a distinct (though very close) levels that differ in the value of the quantum number for the total angular momentum of the electrons in the particle, J. The NIST database issues this set of split electronic levels. Due to the small difference in the sensible energy of the split electronic levels, some studied collisional and radiative processes that are found in the literature consider the non-split electronic levels instead of the split ones. Therefore, the applicability of the compiled data for such processes in this work also requires the author to make this assumption, and single representative levels for each set of split electronic levels need to be obtained. Herein, the sensible energy of the representative electronic level associated to a set of split electronic levels was defined as the mean sensible energy that a state belonging to that set may have. Let the representative electronic level and the set be denoted by e and $\left\{e^\dagger\right\}$, respectively. Mathematically, the definition of the sensible energy of the representative electronic level ϵ_e, is given by

$$\epsilon_e := \sum_{e^\dagger} P_{e^\dagger} \epsilon_{e^\dagger} = \sum_{e^\dagger} \frac{g_{e^\dagger}}{g_e} \epsilon_{e^\dagger} \ , \tag{3.1}$$

being $\epsilon_{e^\dagger}$ the sensible energy of the $e^\dagger$ electronic level that belongs to the set of split ones $\{e^\dagger\}$. The quantity $P_{e^\dagger}$ corresponds to the probability of a state of the set belonging to the electronic level $e^\dagger$. The sum in the expression is made in all the electronic levels $e^\dagger$ of the set. By taking the assumption that all states of the set are equiprobable, this probability is simply given by the ratio between the number of different states that the electronic level $e^\dagger$ allows[1] ($g_{e^\dagger}$) and the number of different states that the set allows[2] ($g_e := \sum_{e^\dagger} g_{e^\dagger}$). This operation will be denominated from now on as "lumping" of the electronic levels.

All considered species and their energy levels are reported in Table (3.1).

Table 3.1: Considered species and respective energy levels. The interval that appears between parenthesis immediately after the molecular term symbols of the electronic levels of N_2 and N_2^+ correspond to the set of values of vibrational quantum numbers for which bound vibrational levels were computed.

Type	Species	Energy levels	Reference
Molecule	N_2	$X^1\Sigma_g^+$ ([0, 61]), $A^3\Sigma_u^+$ ([0, 31]), $B^3\Pi_g$ ([0, 32]), $W^3\Delta_u$ ([0, 44]), $B'^3\Sigma_u^-$ ([0, 47]), $a'^1\Sigma_u^-$ ([0, 57]), $a^1\Pi_g$ ([0, 52]), $w^1\Delta_u$ ([0, 49]), $A'^5\Sigma_g^+$ ([0, 5]), $C^3\Pi_u$ ([0, 4]), $b^1\Pi_u$ ([0, 28]), $c_3{}^1\Pi_u$ ([0, 4]), $c_4'^1\Sigma_u^+$ ([0, 8]), $b'^1\Sigma_u^+$ ([0, 54]) and $o_3{}^1\Pi_u$ ([0, 4])	This work
Molecular ion	N_2^+	$X^2\Sigma_g^+$ ([0, 65]), $A^2\Pi_u$ ([0, 66]), $B^2\Sigma_u^+$ ([0, 38]), $D^2\Pi_g$ ([0, 38]) and $C^2\Sigma_u^+$ ([0, 13])	This work
Atom	N	^4S_u, ^2D_u, ^2P_u, ^4P, ^2P, ... (131 levels) ([a])	NIST[83]
Atomic ion	N^+	^3P, ^1D, ^1S, ^5S_u, ^3D_u, ... (81 levels) ([a])	NIST[83]
Free electron	e^-	—	—

[a] As a reminder to the reader: the electronic levels were obtained through a lumping procedure applied on the ones issued by NIST.

3.2 Collisional processes

Forward rate constants k_f for processes that involve collisions between particles were computed through theoretical models (as is example of the Forced Harmonic Oscilator model), empirical correlations (as is example of the exponential gap law), or by relying on process cross sections σ_p and average process cross sections $\sigma_{p,\mathrm{av}}$ found in the literature. Also, whenever cross sections weren't found but forward rate constants k_f were, the latter were taken and a curve fitting procedure was performed. All collisional processes considered in this work are resultant from binary collisions (therefore involving only two particles) being one of the collision partners necessarily a heavy species particle. The determination of forward rate constants through the different methods will be described for some particular processes. Section §3.2.1 illustrates the way that the Forced Harmonic Oscilator model was implemented on the determination of forward rates k_f for the vibrational transition and dissociation of N_2 and N_2^+ by collisions with heavy particles. In sections 3.2.2 to 3.2.6, processes of vibronic transition of N_2 by heavy particle impact are studied, and average process sections $\sigma_{p,\mathrm{av}}$ are used to compute the respective forward rate coefficients k_f through empirical correlations. Section §3.2.7 describes the procedure involved in

[1] Which is the same as the degree of degeneracy of the electronic level $e^\dagger$.

[2] Which is the same as the degree of degeneracy of the representative electronic level e, under the assumption of equiprobability of the set states.

the computation of forward rates k_f through process cross sections values σ_p with respect to the non-dissociative ionisation of N_2 by electron impact. Section §3.2.8 illustrates an extrapolation of forward rate values k_f evaluated at low free electron translational temperatures $T_{\mathrm{tr_e}}$ for the case of the dissociative recombination of N_2^+ with electrons. Section §3.2.9 describes the application of adapted *Drawin formulae* to the case of electronic excitation and ionisation of N and N^+ by electron impact. And section §3.2.10 presents the way that the formula obtained by Annaloro et al. [84] was regarded in this work to compute rate coefficients for the electronic excitation and ionisation of N and N^+ by heavy particle impact.

Table 3.2 makes a synopsis on the regarded collisional processes due to heavy particle impact. And Table 3.3 makes a synopsis on the regarded collisional processes due to electron impact. The two tables present the type of process, chemical equation, and reference from which data was taken to compute the forward rate k_f. If the chemical equation is expressed in a general form involving variables which may represent different possible species, electronic, or vibrational levels, a description of those variables is made in the column "Remarks" of the table. Some processes reported in the literature which involve the vibrational levels of $N_2\left(X^1\Sigma_g^+\right)$ consider a database for these energy levels that is different from the one employed in this work. Therefore, to make such results applicable, it was determined to linearly (or bi-linearly if two vibrational levels are involved) interpolate the issued rates in respect of the vibrational energies if the issued energies are comprised to the in-work database, or to linearly (or bi-linearly) extrapolate if they aren't. The application of this procedure will be identified by the acronym ADV (from "Adaption in respect of the Database for the Vibrational energy levels") in the respective entry of the "Remarks" column. By implementing the vibrational redistribution procedure (VRP) described in §2.9, it's possible to compute rate coefficients for a full set of vibrational quantum numbers from the knowledge of a rate coefficient for a particular vibrational quantum number or for the contribution of all of them. This procedure will be identified by the acronym VRP in the "Remarks" column. A codename for the type of process, taking into account only the initial and final states of the collision partners, was defined to simplify the description of the process. It consists of three terms separated by hyphens. If the process corresponds solely to a transition in the internal energy modes of the collision partners, the first term of the codename will correspond to a set of capital letters each one representing the involved internal energy modes ("V" from "vibrational" or/and "E" from "electronic"). Note that since every collisional process may involve transitions in the translational energies of the collision partners the respective capital letter "T" was disregarded. If the process corresponds to a bond breaking or/and forming of the internal structure, the first term will be defined by a set of capital letters, each one representing a type of bond breaking or forming ("I" from "ionisation", "R" from "recombination", "D" from "dissociation" or "A" from "association"). The second and third terms correspond to labels of minuscule letters representing the type of the collision partners ("h" from "heavy species", "m" from "molecular particle" (neutral or ionic), "a" from "atomic particle" (neutral or ionic), or "e" from "electron"). For example, the non-dissociative ionisation of a nitrogen molecule by electron impact may be represented by the codename I-m-e.

Table 3.2: Collisional processes due to heavy particle impact for which forward rate constants were obtained. The symbol after the reference in the column "Reference" represents the physical quantity which was extracted from it: process cross section (if σ_p), average process cross section (if $\sigma_{p,\mathrm{av}}$) or forward rate constant (if k_f).

Type	Chemical equation	Remarks	Reference
V-m-h	$\mathrm{N_2}\,(e,v) + \mathrm{M} \rightleftharpoons \mathrm{N_2}\,(e,v') + \mathrm{M}$	$e \in \{\mathrm{X},\mathrm{A},\mathrm{B},\mathrm{W},\mathrm{B}',\mathrm{a}',\mathrm{a},\mathrm{w},\mathrm{A}',\mathrm{C},\mathrm{b},\mathrm{c}_3,\mathrm{c}_4',\mathrm{b}',\mathrm{o}_3\}$, $\forall\, v$, $\forall\, v' > v$ and $\mathrm{M} \in \{\mathrm{N_2},\mathrm{N_2^+},\mathrm{N},\mathrm{N^+}\}$	This work [a]
V-m-h	$\mathrm{N_2^+}\,(e,v) + \mathrm{M} \rightleftharpoons \mathrm{N_2^+}\,(e,v') + \mathrm{M}$	$e \in \{\mathrm{X},\mathrm{A},\mathrm{B},\mathrm{D},\mathrm{C}\}$, $\forall\, v$, $\forall\, v' > v$ and $\mathrm{M} \in \{\mathrm{N_2},\mathrm{N_2^+},\mathrm{N},\mathrm{N^+}\}$	This work [a]
VE-m-a	$\mathrm{N_2}\,(\mathrm{A},v) + \mathrm{N}(^4\mathrm{S_u}) \rightleftharpoons \mathrm{N_2}\,(\mathrm{X},v') + \mathrm{N}(^2\mathrm{P_u})$	$\forall\, v$, and $\forall\, v'$	[85]-k_f
VE-m-a	$\mathrm{N_2}\,(\mathrm{A},v) + \mathrm{N}(^4\mathrm{S_u}) \rightleftharpoons \mathrm{N_2}\,(\mathrm{B},v') + \mathrm{N}(^4\mathrm{S_u})$	$\forall\, v$, and $\forall\, v'$	[35]-$\sigma_{p,\mathrm{av}}$
VE-m-a	$\mathrm{N_2}\,(\mathrm{W},v) + \mathrm{N}(^4\mathrm{S_u}) \rightleftharpoons \mathrm{N_2}\,(\mathrm{B},v') + \mathrm{N}(^4\mathrm{S_u})$	$\forall\, v$, and $\forall\, v'$	[35]-$\sigma_{p,\mathrm{av}}$
VE-m-a	$\mathrm{N_2}\,(\mathrm{A}',0) + \mathrm{N}(^4\mathrm{S_u}) \rightleftharpoons \mathrm{N_2}\,(\mathrm{B},10) + \mathrm{N}(^4\mathrm{S_u})$	—	[86]-$\sigma_{p,\mathrm{av}}$
VE-m-m	$\mathrm{N_2}\,(\mathrm{A},v_1) + \mathrm{N_2}\,(\mathrm{X},v_2) \rightleftharpoons \mathrm{N_2}\,(\mathrm{X},v_1') + \mathrm{N_2}\,(\mathrm{X},v_2')$	$\forall\, v_1$, $\forall\, v_2$, $\forall\, v_1'$ and $\forall\ v_2'$	[87]-k_f
VE-m-m	$\mathrm{N_2}\,(\mathrm{A},v_1) + \mathrm{N_2}\,(\mathrm{X},v_2) \rightleftharpoons \mathrm{N_2}\,(\mathrm{B},v_1') + \mathrm{N_2}\,(\mathrm{X},v_2')$	$\forall\, v_1$, $\forall\, v_2$, $\forall\, v_1'$ and $\forall\ v_2'$	[35]-$\sigma_{p,\mathrm{av}}$
VE-m-m	$\mathrm{N_2}\,(\mathrm{A},v_1) + \mathrm{N_2}\,(\mathrm{A},v_2) \rightleftharpoons \mathrm{N_2}\,(\mathrm{B},v_1') + \mathrm{N_2}\,(\mathrm{X},v_2')$	$\forall\, v_1$, $\forall\, v_2$, $\forall\, v_1'$ and $\forall\ v_2'$	[88]-k_f
VE-m-m	$\mathrm{N_2}\,(\mathrm{A},v_1) + \mathrm{N_2}\,(\mathrm{A},v_2) \rightleftharpoons \mathrm{N_2}\,(\mathrm{C},v_1') + \mathrm{N_2}\,(\mathrm{X},v_2')$	$\forall\, v_1$, $\forall\, v_2$, $\forall\, v_1'$ and $\forall\ v_2'$	[89]-k_f
VE-m-m	$\mathrm{N_2}\,(\mathrm{W},v_1) + \mathrm{N_2}\,(\mathrm{X},v_2) \rightleftharpoons \mathrm{N_2}\,(\mathrm{B},v_1') + \mathrm{N_2}\,(\mathrm{X},v_2')$	$\forall\, v_1$, $\forall\, v_2$, $\forall\, v_1'$ and $\forall\ v_2'$	[35]-$\sigma_{p,\mathrm{av}}$
VE-m-m	$\mathrm{N_2}\,(\mathrm{A}',0) + \mathrm{N_2}\,(\mathrm{X},0) \rightleftharpoons \mathrm{N_2}\,(\mathrm{B},10) + \mathrm{N_2}\,(\mathrm{X},0)$	—	[86]-$\sigma_{p,\mathrm{av}}$
E-a-h	$\mathrm{N}\,(e) + \mathrm{M} \rightleftharpoons \mathrm{N}\,(e') + \mathrm{M}$	$\forall e$, $\forall e' > e$ and $\mathrm{M} \in \{\mathrm{N},\mathrm{N_2}\}$	[41]-k_f
E-a-h	$\mathrm{N^+}\,(e) + \mathrm{M} \rightleftharpoons \mathrm{N^+}\,(e') + \mathrm{M}$	$\forall e$, $\forall e' > e$ and $\mathrm{M} \in \{\mathrm{N},\mathrm{N_2}\}$	[41]-k_f
D-m-h	$\mathrm{N_2}\,(e,v) + \mathrm{M} \rightleftharpoons \mathrm{N}\,(e_1') + \mathrm{N}\,(e_2') + \mathrm{M}$	$e \in \{\mathrm{X},\mathrm{A},\mathrm{B},\mathrm{W},\mathrm{B}',\mathrm{a}',\mathrm{a},\mathrm{w},\mathrm{A}',\mathrm{C},\mathrm{b},\mathrm{b}'\}$, $\forall\, v$ and $\mathrm{M} \in \{\mathrm{N_2},\mathrm{N_2^+},\mathrm{N},\mathrm{N^+}\}$	This work [a]
D-m-h	$\mathrm{N_2^+}\,(e,v) + \mathrm{M} \rightleftharpoons \mathrm{N}\,(e_1') + \mathrm{N^+}\,(e_2') + \mathrm{M}$	$e \in \{\mathrm{X},\mathrm{A},\mathrm{B},\mathrm{D},\mathrm{C}\}$, $\forall\, v$ and $\mathrm{M} \in \{\mathrm{N_2},\mathrm{N_2^+},\mathrm{N},\mathrm{N^+}\}$	This work [a]
I-a-h	$\mathrm{N}\,(e) + \mathrm{M} \rightleftharpoons \mathrm{N^+}\,(^3\mathrm{P}) + \mathrm{M} + \mathrm{e^-}$	$\forall e$ and $\mathrm{M} \in \{\mathrm{N},\mathrm{N_2}\}$	[41]-k_f
IR-m-a	$\mathrm{N_2}\,(\mathrm{X},v) + \mathrm{N^+}(^3\mathrm{P}) \rightleftharpoons \mathrm{N_2^+}\,(\mathrm{X},v') + \mathrm{N}(^4\mathrm{S_u})$	VRP on v and v' from case $v = 0$ and $\sum_{v'}$	[90]-σ_p

[a] Note that although the respective chemical equation doesn't show any possible transition in the vibrational level (or even dissociation) of the second collision partner (for the case of this one being molecular), such consideration is implicit. The chemical equation is written in a way that illustrates the probabilities uncoupling assumption that was described in the section §2.7.7.

Table 3.3: Collisional processes due to electron impact for which forward rate constants were obtained. The symbol after the reference in the column "Reference" represents the physical quantity which was extracted from it: process cross section (if σ_p), average process cross section (if $\sigma_{p,\mathrm{av}}$) or forward rate constant (if k_f).

Type	Chemical equation	Remarks	Reference
V-m-e	$\mathrm{N_2}\left(\mathrm{X}^1\Sigma_\mathrm{g}^+,\, v\right) + \mathrm{e}^- \rightleftharpoons \mathrm{N_2}\left(\mathrm{X}^1\Sigma_\mathrm{g}^+,\, v'\right) + \mathrm{e}^-$	$\forall v$ and $\forall\, v' > v$, ADV	[91]-σ_p (from [92])
VE-m-e	$\mathrm{N_2}\left(\mathrm{X}, v\right) + \mathrm{e}^- \rightleftharpoons \mathrm{N_2}\left(e', v'\right) + \mathrm{e}^-$	$e' \in \{\mathrm{A}, \mathrm{B}, \mathrm{W}, \mathrm{B}', \mathrm{a}', \mathrm{a}, \mathrm{w}, \mathrm{C}\}$, VRP on v and v' from case $v = 0$ and $\sum_{v'}$	[93]-σ_p
		$e' \in \{\mathrm{c}_3, \mathrm{o}_3\}$, VRP on v and v' from case $v = 0$ and $\sum_{v'}$	[94]-σ_p
		$e' \in \{\mathrm{b}, \mathrm{c}_4', \mathrm{b}'\}$, VRP on v and v' from case $v = 0$ and $\sum_{v'}$	[95]-σ_p
		$e' = \mathrm{A}'$, Assumption of same reference values as for $e' = \mathrm{A}$, VRP on v and v' from case $v = 0$ and $\sum_{v'}$	—
VE-m-e	$\mathrm{N_2^+}\left(\mathrm{X}, v\right) + \mathrm{e}^- \rightleftharpoons \mathrm{N_2^+}\left(e', v'\right) + \mathrm{e}^-$	$e' = \mathrm{B}$, $v = 0$ and $v' = 0$, Remainder of v and v': VRP from case $v = 0$ and $v' = 0$	[96]-σ_p
		$e' \in \{\mathrm{A}, \mathrm{D}, \mathrm{C}\}$, Assumption of same reference values as for $e' = \mathrm{B}$, $v = 0$ and $v' = 0$, Remainder of v and v': VRP from case $v = 0$ and $v' = 0$	—
E-a-e	$\mathrm{N}\left(e\right) + \mathrm{e}^- \rightleftharpoons \mathrm{N}\left(e'\right) + \mathrm{e}^-$	$(e, e') \in \{(^4\mathrm{S_u}, {}^2\mathrm{D_u}), (^4\mathrm{S_u}, {}^2\mathrm{P_u}), (^2\mathrm{D_u}, {}^2\mathrm{P_u})\}$	[97]-σ_p
		Remainder of (e, e'), with $e' > e$	[98]-k_f
E-a-e	$\mathrm{N^+}\left(e\right) + \mathrm{e}^- \rightleftharpoons \mathrm{N^+}\left(e'\right) + \mathrm{e}^-$	$\forall e$ and $\forall e' > e$	[98]-k_f
D-m-e	$\mathrm{N_2}\left(\mathrm{X}^1\Sigma_\mathrm{g}^+,\, v\right) + \mathrm{e}^- \rightleftharpoons \mathrm{N}\left(e_1'\right) + \mathrm{N}\left(e_2'\right) + \mathrm{e}^-$	$\forall\, v$, $(e_1', e_2') = (^4\mathrm{S_u}, {}^4\mathrm{S_u})$, ADV	[91]-σ_p (from [92])
		$\forall\, v$, $(e_1', e_2') = (^4\mathrm{S_u}, {}^2\mathrm{D_u})$, ADV	[99]-σ_p (from [92])
DR-m-e	$\mathrm{N_2^+}\left(\mathrm{X}^2\Sigma_\mathrm{g}^+,\, v\right) + \mathrm{e}^- \rightleftharpoons \mathrm{N}\left(e_1'\right) + \mathrm{N}\left(e_2'\right)$	$v \in \{0, 2\}$ and $(e_1', e_2') \in \{(^4\mathrm{S_u}, {}^2\mathrm{D_u}), (^4\mathrm{S_u}, {}^2\mathrm{P_u}), (^2\mathrm{D_u}, {}^2\mathrm{P_u})\}$	[100]-k_f
		$v \in \{1, 3, 4\}$ and $(e_1', e_2') \in \{(^4\mathrm{S_u}, {}^2\mathrm{D_u}), (^4\mathrm{S_u}, {}^2\mathrm{P_u}), (^2\mathrm{D_u}, {}^2\mathrm{D_u}), (^2\mathrm{D_u}, {}^2\mathrm{P_u})\}$	
		Remainder of v with $(e_1', e_2') \in \{(^4\mathrm{S_u}, {}^2\mathrm{D_u}), (^4\mathrm{S_u}, {}^2\mathrm{P_u}), (^2\mathrm{D_u}, {}^2\mathrm{D_u}), (^2\mathrm{D_u}, {}^2\mathrm{P_u})\}$: VRP from case $v = 4$	
I-m-e	$\mathrm{N_2}\left(\mathrm{X}^1\Sigma_\mathrm{g}^+,\, v\right) + \mathrm{e}^- \rightleftharpoons \mathrm{N_2^+}\left(e', v'\right) + 2\,\mathrm{e}^-$	$\forall\, v$ and $e' \in \{\mathrm{X}, \mathrm{A}, \mathrm{B}\}$, ADV, VRP on v' from case $\sum_{v'}$	[101]-σ_p (from [92])
I-a-e	$\mathrm{N}\left(e\right) + \mathrm{e}^- \rightleftharpoons \mathrm{N^+}\left(^3\mathrm{P}\right) + 2\,\mathrm{e}^-$	$e = {}^4\mathrm{S_u}$	[102]-σ_p
		$e \in \{^2\mathrm{D_u}, {}^2\mathrm{P_u}\}$	[103]-σ_p
		Remainder of e	[98]-k_f

3.2.1 Vibrational transition and dissociation of N_2 and N_2^+ by heavy particle impact

By recalling the previously introduced theory that supports the Forced Harmonic Oscillator (FHO) model (in section §2.7), one can compute rates for the vibrational transition and dissociation of molecular particles by collision with heavy species. Since in this work the considered heavy species were the atomic nitrogen N, atomic nitrogen ion N^+, molecular nitrogen N_2 and molecular nitrogen ion N_2^+, it's necessary to compute rates for seven different interactions: N_2 - N, N_2 - N^+, N_2 - N_2, N_2 - N_2^+, N_2^+ - N, N_2^+ - N^+ and N_2^+ - N_2^+. Note that one needs to consider the electronic and vibrational levels of the collision partners, and therefore, from each one of these species-specific interactions there is a fullset of vibronic-specific interactions to be accounted for. To compute rates of vibrational transition and dissociation, the knowledge of some parameters that describe the interactions is necessary. These parameters are: collisional cross section σ, reciprocal characteristic length α, and potential well depth E_{M} of the Morse interaction potential given by (2.257). Regarding the Morse parameters α and E_{M}, only values for the interaction N_2 - N_2 were found in the literature, being the collision partners in the ground electronic level. These were defined by Adamovich et al. [21], who also employed the same values for two other cases: N_2 - O_2 and O_2 - O_2. It was then decided to extrapolate this assumption for all the Morse parameters of the seven interactions, independently of the electronic levels of the collision partners. Regarding the collisional cross section σ, only a value for the case N_2 - N_2 was obtained, being this value estimated from another one found in the literature (Svehla's technical report [54]). The raw value from which the collisional cross section was obtained from, corresponds to the parameter d of the *Lennard-Jones (12-6) potential*, called *collision diameter*, for the interaction N_2 - N_2. In the technical report it is assumed that both collision partners are in the ground vibrational and electronic level. The estimation of the collisional cross section will now be explained. The Lennard-Jones (12-6) potential, $V'_{\mathrm{LJ}}(r)$ is given by the expression

$$V'_{\mathrm{LJ}}(r) = 4E_{\mathrm{LJ}}\left[\left(\frac{d}{r}\right)^{12} - \left(\frac{d}{r}\right)^{6}\right] , \tag{3.2}$$

being E_{LJ} the potential well depth, and r the internuclear distance. The collision diameter can be easily interpreted and its designation justified when one compares the Lennard-Jones potential with a *hard-spheres potential*[3]. Hard spheres can only interact by contact and in a total rigid way, which means that the collision is instantaneous and an infinite repulsive force is applied in that single instant of the collision (giving a finite momentum transfer). Let d_{AB} be the distance between centres of hypothetical collision partners A and B, as represented by Figure 2.5. The hard-spheres potential can be represented by a constant finite value for $r \geq d_{\mathrm{AB}}$, and an infinite value for $r < d_{\mathrm{AB}}$. Let the constant finite value be zero. Note that the value of the interaction potential doesn't matter, but the gradient, since it is the symmetric of the gradient that has physical meaning (corresponding to the interaction force), and

[3]The hard-spheres potential is the interaction potential between two particles under the assumption of the billiard balls model.

therefore, a reference value can be arbitrated. The hard-spheres potential V'_{HS} is given by

$$V'_{\mathrm{HS}}(r) = \begin{cases} \infty, & \text{if } r < d_{\mathrm{AB}} \ , \\ 0, & \text{if } r \geq d_{\mathrm{AB}} \ . \end{cases} \tag{3.3}$$

Figure 3.1 makes a comparison between the Lennard-Jones (12-6) potential for the interaction N_2 - N_2 provided by Svehla, and a hard-spheres potential with $d_{\mathrm{AB}} = d$.

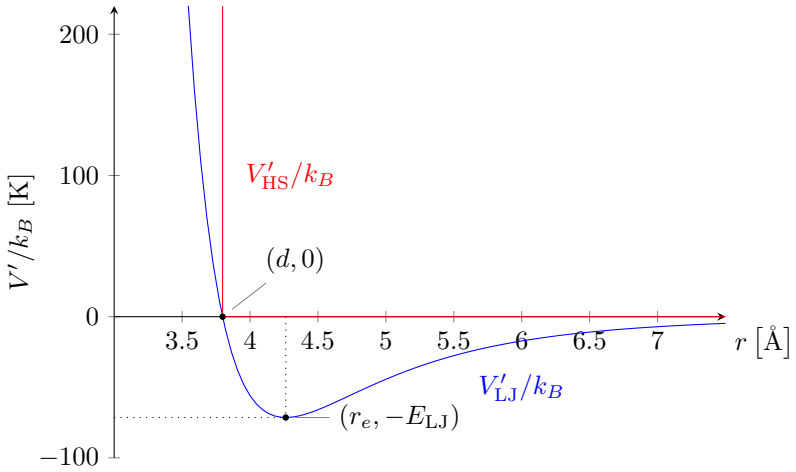

Figure 3.1: The Lennard-Jones (12-6) interaction potential divided by the Boltzmann constant, V'_{LJ}/k_B, for the case N_2 - N_2, provided by Svehla [54], and a hard-spheres potential divided by the Boltzmann constant, V'_{HS}/k_B, with $d_{\mathrm{AB}} = d$.

The collision diameter parameter of the Lennard-Jones (12-6) potential corresponds to the r coordinate of the intersection point of the short-range part with the r axis. For internuclear distances lower than this value, the potential curve becomes very steep, meaning a strong repulsive force. Therefore, in the short-range domain, one may approximate the Lennard-Jones (12-6) potential by a hard-spheres potential with $d = d_{\mathrm{AB}}$. If one also neglects the long-range part of the Lennard-Jones (12-6) potential (which is justifiable for high relative speeds of the particles) the collision diameter designation makes sense, corresponding to the distance between the centres of the two hard spheres that represent the collision partners, i.e. $d = d_{\mathrm{AB}}$. According to the definition of the collisional cross section for hard spheres given in the section **??**, one has $\sigma = \pi d_{\mathrm{AB}}^2 = \pi d^2$. And using particular notation for the N_2 - N_2 case, the formula translates itself to $\sigma_{\mathrm{N_2\text{ - }N_2}} = \pi d_{\mathrm{N_2\text{ - }N_2}}^2$, being $d_{\mathrm{N_2\text{ - }N_2}}$ the respective collision diameter. Svehla's technical report also provides a collision parameter value for the N - N case. This value in combination with the one associated to the N_2 - N_2 case can be used to estimate the collisional cross section for the N_2 - N interaction. By recalling the billiard balls model again and invoking the approximation of the Lennard-Jones potential by a hard-spheres potential, one has

$$\sigma_{\mathrm{N_2\text{ - }N}} = \pi d_{\mathrm{N_2\text{ - }N}}^2 = \pi \left(r_{\mathrm{N_2}} + r_{\mathrm{N}}\right)^2 = \pi \left(\frac{d_{\mathrm{N_2\text{ - }N_2}}}{2} + \frac{d_{\mathrm{N\text{ - }N}}}{2}\right)^2 \Leftrightarrow \tag{3.4}$$

$$\Leftrightarrow \sigma_{\mathrm{N_2\text{ - }N}} = \frac{\pi}{4}\left(d_{\mathrm{N_2\text{ - }N_2}} + d_{\mathrm{N\text{ - }N}}\right)^2 \ , \tag{3.5}$$

being $r_{\mathrm{N_2}}$ and r_{N} the radii of the hard-spheres representing the $\mathrm{N_2}$ and N species, respectively. Since data for the interactions that involve the ions $\mathrm{N^+}$ or $\mathrm{N_2^+}$ wasn't found in the literature, it was assumed that the respective collisional cross sections values were the same as the ones that involve the counterpart neutral species. Therefore, one has $\sigma_{\mathrm{N_2}-\mathrm{N^+}} = \sigma_{\mathrm{N_2\text{ - }N}} = \sigma_{\mathrm{N_2^+\text{ - }N}} = \sigma_{\mathrm{N_2^+\text{ - }N^+}}$ and $\sigma_{\mathrm{N_2\text{ - }N_2^+}} = \sigma_{\mathrm{N_2\text{ - }N_2}} = \sigma_{\mathrm{N_2^+\text{ - }N_2}} = \sigma_{\mathrm{N_2^+\text{ - }N_2^+}}$. Note that this approximation is quite rough since a positive ion has one less bounded electron than the respective counterpart neutral species, which influences the electromagnetic force acting in the collision partner, and in its turn influences the collisional cross section value. Table 3.4 makes a synopsis of collisional cross sections σ and Morse parameters α and E_{M} considered for the seven different interactions.

Table 3.4: Collisional cross sections σ, and Morse parameters α and E_{M} for the collisions m - a and m - m, in which a $\in \left\{\mathrm{N}, \mathrm{N^+}\right\}$ represents an atomic particle, and m $\in \left\{\mathrm{N_2}, \mathrm{N_2^+}\right\}$ represents a molecular particle.

Collision	$\sigma[\mathrm{Å}^2]$	$\alpha[\mathrm{Å}^{-1}]$	$E_{\mathrm{M}}/k_B[\mathrm{K}]$
m - a	39.547	4.0	200.0
m - m	45.317		

Rate coefficients for vibrational transition $k_v^{v'}(T_{\mathrm{tr_h}})$ and dissociation $k_v^D(T_{\mathrm{tr_h}})$ of $\mathrm{N_2}$ and $\mathrm{N_2^+}$ in their electronic levels, due to collisions with $\mathrm{N_2}$, $\mathrm{N_2^+}$, N and $\mathrm{N^+}$, were computed. To illustrate one of those results, Figures 3.2 and 3.3 depict the rate coefficients for vibrational transition of $\mathrm{N_2}(\mathrm{X}^1\Sigma_{\mathrm{g}}^+)$ by collision with N, at a heavy particle translational temperature $T_{\mathrm{tr_h}} = 20,000$ K.

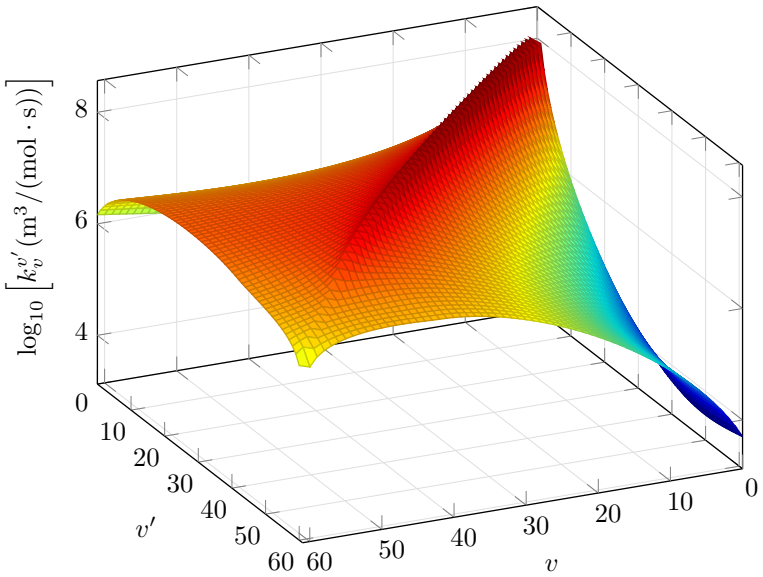

Figure 3.2: Surface plot of rate coefficient values for vibrational transition of $\mathrm{N_2}(\mathrm{X}^1\Sigma_{\mathrm{g}}^+)$ by collision with N, at a heavy particle translational temperature $T_{\mathrm{tr_h}} = 20,000$ K.

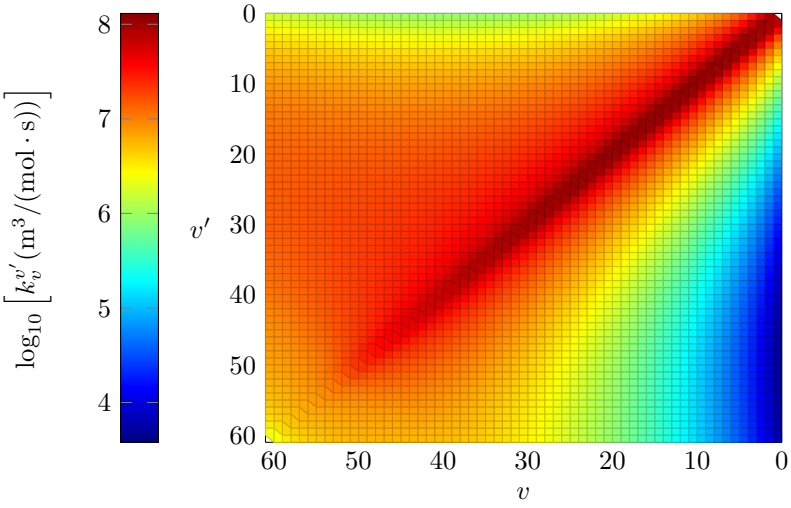

Figure 3.3: Contour plot of rate coefficient values for vibrational transition of $N_2(X^1\Sigma_g^+)$ by collision with N, at a heavy particle translational temperature $T_{\mathrm{tr_h}} = 20,000$ K.

It can be concluded that the vibrational transition process is more effective if the transition is between two adjacent levels, and even more effective if the two adjacent levels are of low energy. For the case of transitions between non-adjacent levels, it is observed that rate coefficient values for de-excitation are in general greater than the ones for excitation. Excitation from the lowest energy levels to the highest ones, are the less effective.

It's of paramount importance to validate the computed rates of vibrational transition $k_v^{v'}$ as well as the rates of dissociation k_v^D, for all the considered interactions. Unfortunately, experimental results expressed in the exact same form as these obtained numerically weren't found in the literature. What was found were experimental results for the dissociation of N_2 in its ground electronic level $e = X^1\Sigma_g^+$ by impact with N and with N_2, in thermal equilibrium conditions. Note that the numerical computation of dissociation rates using the FHO model implies the assignment of a value for a free parameter that can't be a priori computed. That parameter is the number of quasi-bound levels for the sum involved in the dissociation rate formula (2.263), as presented in section §2.7.6. Instead of the number of quasi-bound levels, one can define a quantity corresponding to the difference between the upper bound value for the vibrational energy of the quasi-bound levels[4] $G_{v'_u}$ and the potential well D_e, i.e. $G_{v'_u}^{D_e} := G_{v'_u} - D_e$. Therefore, the considered quasi-bound levels are the ones with a vibrational energy $G_{v'}$ higher than the potential well depth D_e and lower or equal to the upper bound vibrational energy $G_{v'_u}$, i.e. $D_e < G_{v'} \leq G_{v'_u}$. Such free parameter gives opportunity for calibration of the model by comparison with the aforementioned experimental results, increasing the reliability on the numerical dissociation rates, and at the same, on the numerical vibrational transition rates, since the former uses the later for its computation. However, vibrational transition and dissociation rates of N_2 in its ground electronic level, due to impact with N^+ and N_2^+ can't be calibrated since there is no experimental data for them. And the same happens for the vibrational transition and dissociation rates of N_2^+ and the electronically excited N_2, due to impact with N, N_2, N^+ and N_2^+. In the former case, it was decided to set the differences between the upper bound

[4]The notation used for the upper bound vibrational energy is analogous to the one used for the vibrational energy function G_v in appendix B.

vibrational energy and the potential well for the interactions with N^+ and N_2^+ as the ones obtained from calibration of the interactions $N_2(X^1\Sigma_g^+)$ - N and $N_2(X^1\Sigma_g^+)$ - N_2, respectively. In the latter case, it was decide to solely account the first quasi-bound level.

A numerical rate coefficient for thermal dissociation in respect of the interactions $N_2(X^1\Sigma_g^+)$ - N_2 and $N_2(X^1\Sigma_g^+)$ - N can be computed from the obtained vibronic-specific rate coefficients for the interactions $N_2(X^1\Sigma_g^+, v)$ - N_2 and $N_2(X^1\Sigma_g^+, v)$ - N, respectively. The reasoning presented in the paragraphs below should be followed.

The rate coefficient for the dissociation of particles of the X species in the e_1-th electronic level and v_1-th vibrational level due to collisions with particles of the M species in the e_2-th electronic level, corresponds to $k^D_{\mathrm{X}(e_1,v_1)\text{ - }\mathrm{M}(e_2)}$, such that the variation of the amount concentration of the first particles due to that process is given by (2.274):

$$\left(\frac{d[\mathrm{X}(e_1,v_1)]}{dt}\right)^D_{\mathrm{X}(e_1,v_1)\text{ - }\mathrm{M}(e_2)} = -k^D_{\mathrm{X}(e_1,v_1)\text{ - }\mathrm{M}(e_2)}[\mathrm{X}(e_1,v_1)][\mathrm{M}(e_2)] \ . \tag{3.6}$$

Due to the assumption of uncoupling of the transition probabilities for the V-V-T processes (detailed in section §2.7.5) one can show that the rate coefficient $k^D_{\mathrm{X}(e_1,v_1)\text{ - }\mathrm{M}(e_2)}$ doesn't depend on the electronic level e_2, and simply write $k^D_{\mathrm{X}(e_1,v_1)\text{ - }\mathrm{M}(e_2)} = k^D_{\mathrm{X}(e_1,v_1)\text{ - }\mathrm{M}}$. The variation of the amount concentration of the X species in the e_1-th electronic level due to the above-mentioned dissociative process regardless of the vibrational level v_1 and electronic level e_2 corresponds to a sum on all vibrational levels v_1 and electronic levels e_2 of the vibronic-specific contributions given by (3.6):

$$\begin{aligned}\left(\frac{d[\mathrm{X}(e_1)]}{dt}\right)^D_{\mathrm{X}(e_1)\text{ - }\mathrm{M}} &= \sum_{v_1,e_2}\left(\frac{d[\mathrm{X}(e_1,v_1)]}{dt}\right)^D_{\mathrm{X}(e_1,v_1)\text{ - }\mathrm{M}(e_2)} = -\left\{\sum_{v_1} k^D_{\mathrm{X}(e_1,v_1)\text{ - }\mathrm{M}}[\mathrm{X}(e_1,v_1)]\right\}\underbrace{\left(\sum_{e_2}[\mathrm{M}(e_2)]\right)}_{=[\mathrm{M}]} \Leftrightarrow \\ \Leftrightarrow \left(\frac{d[\mathrm{X}(e_1)]}{dt}\right)^D_{\mathrm{X}(e_1)\text{ - }\mathrm{M}} &= -\left\{\sum_{v_1} k^D_{\mathrm{X}(e_1,v_1)\text{ - }\mathrm{M}}[\mathrm{X}(e_1,v_1)]\right\}[\mathrm{M}] \ .\end{aligned} \tag{3.7}$$

If the rotational constants don't depend on the vibrational level, the rotational and vibrational energy modes are decoupled from each other, and it can be easily proved from relations (2.13) and (2.11) that the amount concentration of particles of the X species in the e_1-th electronic level and v_1-th vibrational level at thermal equilibrium corresponds to

$$[\mathrm{X}(e_1,v_1)](T) = [\mathrm{X}(e_1)]\frac{g_{\mathrm{X,vib},e_1,v_1}e^{-\frac{\epsilon_{\mathrm{X,vib},e_1,v_1}}{k_B T}}}{Q_{\mathrm{X,vib},e_1}} \ , \tag{3.8}$$

being $[\mathrm{X}_{e_1}]$ the amount concentration of particles of the X species in the e_1-th electronic level. The degree of degeneracy of the vibrational level is according to (2.24b) $g_{\mathrm{X,vib},e_1,v_1} = 1$. By substituting (3.8) in (3.7), one can identify the rate coefficient of thermal dissociation for the interaction $\mathrm{X}(e_1)$ - M, i.e.

$k^D_{\mathrm{X}(e_1)\text{ - M}}(\mathrm{T})$:

$$\left(\frac{d[\mathrm{X}(e_1)]}{dt}\right)^D_{\mathrm{X}(e_1)\text{ - M}}(T) = -\underbrace{\left\{\sum_{v_1}\frac{e^{-\frac{\epsilon_{\mathrm{X,vib},e_1,v_1}}{k_B T}}}{Q_{\mathrm{X,vib},e_1}}k^D_{\mathrm{X}(e_1,v_1)\text{ - M}}\right\}}_{:=k^D_{\mathrm{X}(e_1)\text{ - M}}(T)}[\mathrm{X}(e_1)][\mathrm{M}]\ , \tag{3.9}$$

being $k^D_{\mathrm{X}(e_1)\text{ - M}}(T)$ therefore given by

$$k^D_{\mathrm{X}(e_1)\text{ - M}}(T) = \sum_{v_1}\frac{e^{-\frac{\epsilon_{X,\mathrm{vib},e_1,v_1}}{k_B T}}}{Q_{X,\mathrm{vib},e_1}}k^D_{\mathrm{X}(e_1,v_1)\text{ - M}}\ . \tag{3.10}$$

The addressed experimentally obtained thermal dissociation rates are listed in Table 3.5.

Table 3.5: Coefficients A, n and E_a/k_B of the modified Arrhenius function (2.88) for experimentally obtained rates for the thermal dissociation of $\mathrm{N_2}(\mathrm{X}^1\Sigma^+_\mathrm{g})$ by collision with N and $\mathrm{N_2}$, as well as the respective interval of temperatures $T \in [T_{\min},\, T_{\max}]$ in which they are valid.

Experiment	Interaction	$A\,[\mathrm{cm^3\cdot K^{-\eta}/(mol\cdot s)}]$	n	E_a/k_B [K]	$[T_{\min},\, T_{\max}]$ [K]
Cary (1965) [104]	$\mathrm{N_2}(\mathrm{X}^1\Sigma^+_\mathrm{g})$ - N	7.1×10^{19}	-1.0	113,310	[6,000; 10,000]
	$\mathrm{N_2}(\mathrm{X}^1\Sigma^+_\mathrm{g})$ - $\mathrm{N_2}$	5.6×10^{22}	-1.7		
Byron (1966) [105]	$\mathrm{N_2}(\mathrm{X}^1\Sigma^+_\mathrm{g})$ - N	4.3×10^{22}	-1.5	113,200	[6,000; 9,000]
	$\mathrm{N_2}(\mathrm{X}^1\Sigma^+_\mathrm{g})$ - $\mathrm{N_2}$	4.8×10^{17}	-0.5		
Appleton et al. (1968) [106]	$\mathrm{N_2}(\mathrm{X}^1\Sigma^+_\mathrm{g})$ - N	1.6×10^{22}	-1.6	113,200	[8,000; 15,000]
	$\mathrm{N_2}(\mathrm{X}^1\Sigma^+_\mathrm{g})$ - $\mathrm{N_2}$	3.7×10^{21}	-1.6		
Hanson and Baganoff (1972) [107]	$\mathrm{N_2}(\mathrm{X}^1\Sigma^+_\mathrm{g})$ - N	2.2×10^{26}	-2.5	113,000	[5,700; 12,000]
	$\mathrm{N_2}(\mathrm{X}^1\Sigma^+_\mathrm{g})$ - $\mathrm{N_2}$	3.9×10^{33}	-4.5		
Kewley and Hornung (1974) [108]	$\mathrm{N_2}(\mathrm{X}^1\Sigma^+_\mathrm{g})$ - N	8.5×10^{25}	-2.5	113,200	[6,000; 14,000]
	$\mathrm{N_2}(\mathrm{X}^1\Sigma^+_\mathrm{g})$ - $\mathrm{N_2}$	2.3×10^{29}	-3.5		
Park (1988) [109] ([a])	$\mathrm{N_2}(\mathrm{X}^1\Sigma^+_\mathrm{g})$ - N	3×10^{22}	-1.6	113,200	[6,000; 13,000]
	$\mathrm{N_2}(\mathrm{X}^1\Sigma^+_\mathrm{g})$ - $\mathrm{N_2}$	7×10^{21}	-1.6		

[a] Although the work done by Park is labelled here as an experiment, it is actually a theoretical study involving the other experimental works.

All the experiments previous to the ones done by Hanson and Baganoff [107], and by Kewley and Hornung [108] considered a test gas composed by molecular nitrogen and a diluted inert gas. Such mixture was chosen instead of a pure molecular nitrogen gas, so that dissociation of nitrogen could occur from lower shock speeds. As referred by Park [109]: "this was done because $\mathrm{N_2}$ has a large dissociation energy and hence its dissociation requires a large shock speed, attainable only with a sophisticated facility, unless a large concentration of argon is included". Therefore, at first glance, one one can consider the experiments of Hanson and Baganoff [107] and of Kewley and Hornung [108] to be more reliable than the ones of Cary [104], Byron [105] and Appleton et al. [106]. The study performed by Park [109] wasn't an experiment but a reinterpretation of the previously obtained experimental results. Such reinterpretation accounted the possibility of non-thermal equilibrium between the translational and vibrational modes of the particles, i.e. $T_{\mathrm{tr_h}} \neq T_{\mathrm{vib}}$, during the dissociation of $\mathrm{N_2}$. The results showed by the other authors assumed thermal equilibrium, which may not be reasonable. It's important to mention that the temperature in the modified Arrhenius function (2.88) for the case of thermal dissociation rates of Park is actually an geometrically

averaged temperature $T_a = \sqrt{T_{tr_h} T_{vib}}$. Anyway, in thermal equilibrium one has $T = T_{tr_h} = T_{vib}$, and the averaged temperature match the single-temperature, i.e. $T_a = T$. Due to the thoroughness of Park, his results are currently referred as the state-of-the-art. Jaffe et al. [110] wrote " [...] dissociation rate coefficients from the Park [T_{tr_h} - T_{vib}] hypersonic nonequilibrium chemistry model, which is currently the de facto standard for aerothermodynamic modeling". And Candler and Olejniczak [111] said "[t]he results of Park's two-temperature interpretation of the experimental data are now accepted as the most widely accurate expressions for the equilibrium dissociation rates". These statements were found to be convincing enough to use the Park results for calibration of the ones obtained in this work.

The calibration of the numerical rate coefficients for thermal dissociation in respect of the interactions $N_2(X^1\Sigma_g^+)$ - N_2 and $N_2(X^1\Sigma_g^+)$ - N, i.e. $k^D_{N_2(X^1\Sigma_g^+)\text{ - }N_2}(T)$ and $k^D_{N_2(X^1\Sigma_g^+)\text{ - N}}(T)$, consisted in the minimisation of the *root mean square deviation* (a cost function) between these and Park's rate coefficients by sweeping the difference between the upper bound value for the vibrational energy of the quasi-bound levels and the potential well $G^{D_e}_{v'_u}$. Let $G^{D_e,\text{opt}}_{v'_u,N_2(X^1\Sigma_g^+)\text{ - }N_2}$ and $G^{D_e,\text{opt}}_{v'_u,N_2(X^1\Sigma_g^+)\text{ - N}}$ be the respective optimum values. The root mean square deviations of $k^D_{N_2(X^1\Sigma_g^+)\text{ - }N_2}(T)$ and $k^D_{N_2(X^1\Sigma_g^+)\text{ - N}}(T)$ relatively to the Park's rate coefficients are defined as

$$\Delta_{N_2(X^1\Sigma_g^+)\text{ - }N_2}(G^{D_e}_{v'_u}) = \sqrt{\frac{\sum_n \left[k^D_{N_2(X^1\Sigma_g^+)\text{ - }N_2}(T_n) - k^{D,(\text{Park})}_{N_2(X^1\Sigma_g^+)\text{ - }N_2}(T_n)\right]^2}{N}}\,, \tag{3.11}$$

$$\Delta_{N_2(X^1\Sigma_g^+)\text{ - N}}(G^{D_e}_{v'_u}) = \sqrt{\frac{\sum_n \left[k^D_{N_2(X^1\Sigma_g^+)\text{ - N}}(T_n) - k^{D,(\text{Park})}_{N_2(X^1\Sigma_g^+)\text{ - N}}(T_n)\right]^2}{N}}\,, \tag{3.12}$$

being $k^{D,(\text{Park})}_{N_2(X^1\Sigma_g^+)\text{ - }N_2}(T_n)$ and $k^{D,(\text{Park})}_{N_2(X^1\Sigma_g^+)\text{ - N}}(T_n)$ the Park's rate coefficients, T_n the n-th temperature value at which the rate coefficients are evaluated, and N the number of temperature values for evaluation. Only the experimentally valid range of temperatures was considered for the optimisation process.

The curves $\Delta_{N_2(X^1\Sigma_g^+)\text{ - }N_2}(G^{D_e}_{v'_u})$ and $\Delta_{N_2(X^1\Sigma_g^+)\text{ - N}}(G^{D_e}_{v'_u})$ obtained by the sweeping procedure are represented in Figure 3.4.

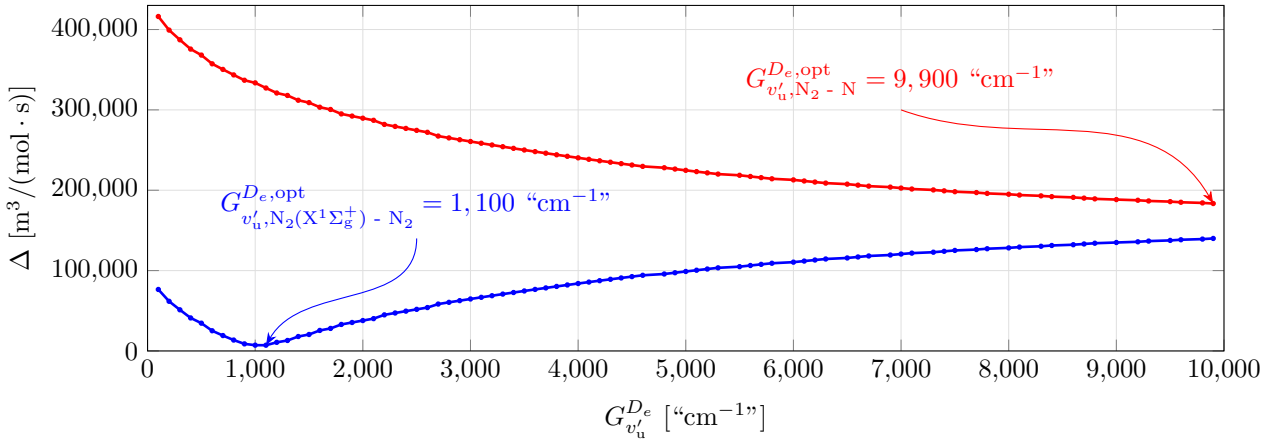

Figure 3.4: Curves of root mean squared deviation $\Delta_{N_2(X^1\Sigma_g^+)\text{ - }N_2}(G^{D_e}_{v'_u})$ (at blue) and $\Delta_{N_2(X^1\Sigma_g^+)\text{ - N}}(G^{D_e}_{v'_u})$ (at red), obtained by a sweeping procedure with $G^{D_e}_{v'_u} \in [0;\, 10,000]$ "cm^{-1}", with an increment step of 100 "cm^{-1}".

For the case of the interaction $N_2(X^1\Sigma_g^+)$ - N_2, a minimum for the root mean squared deviation was found, being the minimiser $G^{D_e,\text{opt}}_{v'_u,N_2(X^1\Sigma_g^+)\text{ - }N_2} = 1,100$ "cm^{-1}". For the case of the interaction $N_2(X^1\Sigma_g^+)$ - N, no minimum was found in the range $G^{D_e}_{v'_u} \in [0; 10,000]$ "cm^{-1}". Only some of the decreasing part of the full curve is supported by that domain. A sweeping procedure for the higher $(G^{D_e}_{v'_u})$ values would be required to obtain the minimum point. However, it was found that an increase of the number of considered quasi-bound vibrational levels would not make a meaningful difference in the root mean squared deviation value, due to the even lower probabilities of transition to the higher quasi-bound vibrational levels. On the other hand, the higher the number of the considered quasi-bound vibrational levels, the higher the the amount of computations for the evaluation of the rate coefficients, making a new sweep not worth it. It was then decided to choose the optimum difference between the upper bound value for the vibrational energy of the quasi-bound levels and the potential well for the $N_2(X^1\Sigma_g^+)$ - N case as the the one that minimises the root mean squared deviation in the range $G^{D_e}_{v'_u} \in [0; 10,000]$ "cm^{-1}", i.e. $G^{D_e,\text{opt}}_{v'_u,N_2(X^1\Sigma_g^+)\text{ - N}} = 9,900$ "cm^{-1}".

Figures 3.5 and 3.6 show the calibrated rate coefficient curves and the experimental ones listed in Table 3.5, for the cases $N_2(X^1\Sigma_g^+)$ - N_2 and $N_2(X^1\Sigma_g^+)$ - N, respectively. These figures also show recent numerical rate coefficient values individually obtained by Bender et al. [112], Macdonald et al. [113], Esposito and Capitelli [114], and Jaffe et al. [115], using the Quasi-Classical Trajectory model (QCT), which is considered to be more sophisticated than the FHO model. In the second subfigure of each figure, the ratio between the FHO rate coefficient values and the ones obtained by Park [109], as well as the ones obtained through the QCT model is depicted.

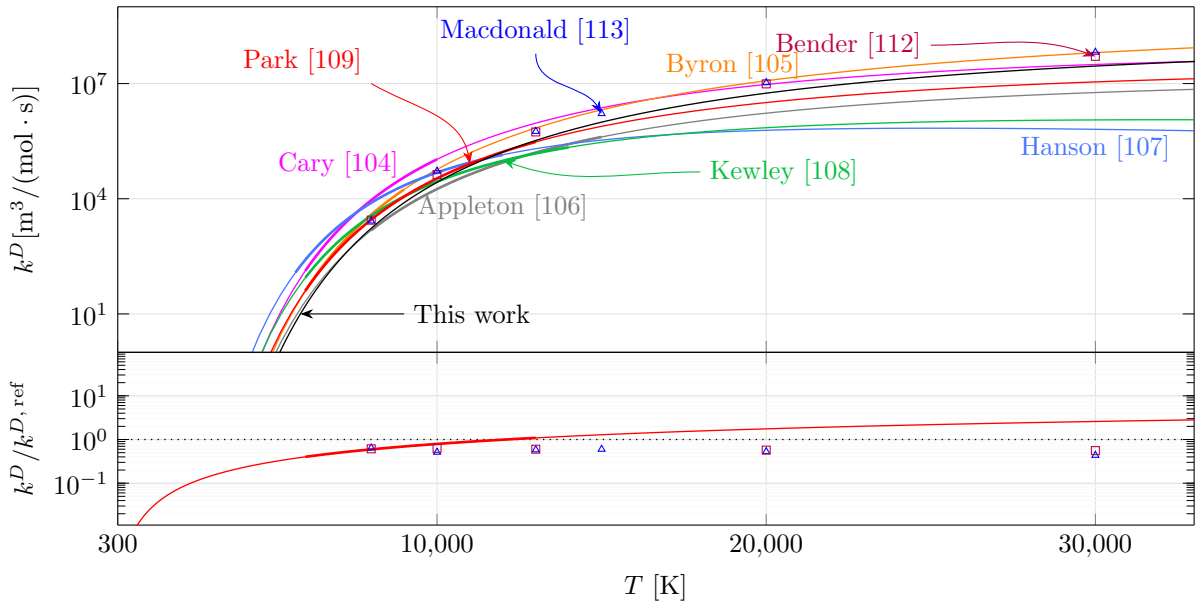

Figure 3.5: Rate coefficient values for thermal dissociation of $N_2(X^1\Sigma_g^+)$ due to the interaction $N_2(X^1\Sigma_g^+)$ - N_2, and ratio between the FHO result and the one obtained by Park [109], as well as the ones obtained by the QCT model (Bender et al. [112], and Macdonald et al. [113]). The thick part of the lines for each of the experiments listed in Table 3.5, is associated to the respective experimentally valid domains.

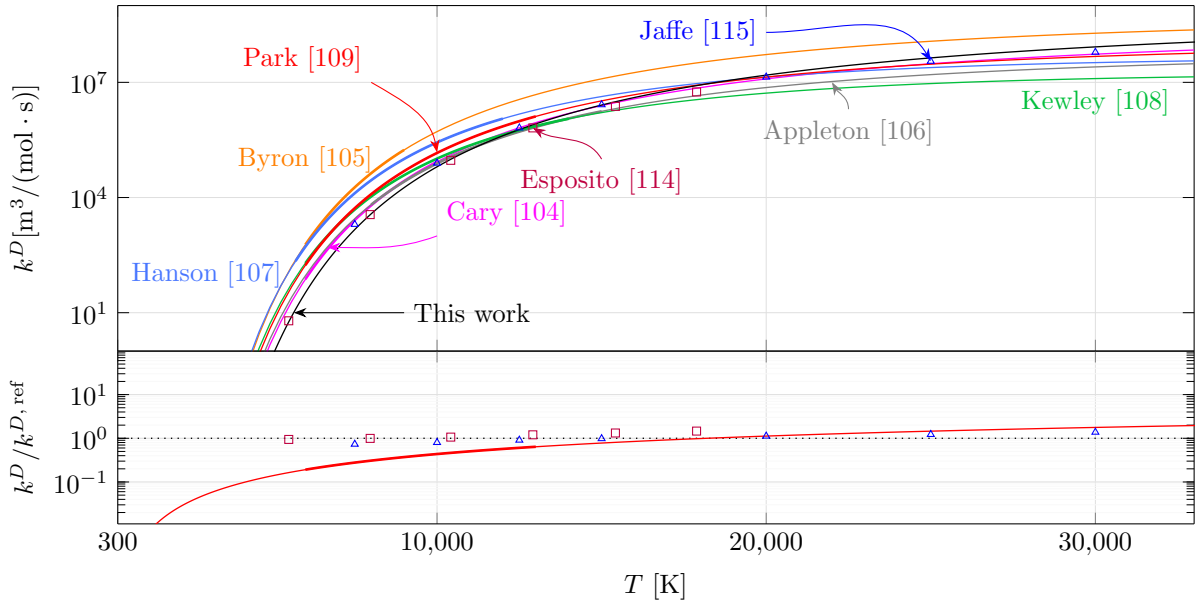

Figure 3.6: Rate coefficient values for thermal dissociation of $N_2(X^1\Sigma_g^+)$ due to the interaction $N_2(X^1\Sigma_g^+)$ - N, and ratio between the FHO result and the one obtained by Park [109], as well as the ones obtained by the QCT model (Esposito and Capitelli [114], and Jaffe et al. [115]). The thick part of the lines for each of the experiments listed in Table 3.5, are associated to the respective experimentally valid domains.

From these two figures, it's possible to observe some overall discrepancies between the experimental results, either in offset and in trend. For both the interactions $N_2(X^1\Sigma_g^+)$ - N_2 and $N_2(X^1\Sigma_g^+)$ - N, it's found an underestimation of the Park [109] results by the FHO model in the low to medium temperatures region, and an overestimation in the high temperatures region. There's a better agreeability between the two results in the experimentally valid region for the former case (a maximum underestimation of 59.9% and overestimation of 8.9% in contrast with a maximum underestimation of 80.9% and minimum underestimation of 36.1% for the latter case). This is expected since it was only in the former case that the optimisation procedure was successful in the minimisation of the cost function. The FHO results underestimate all the QCT results for the case of the interaction $N_2(X^1\Sigma_g^+)$ - N_2, with maximum absolute relative deviations of 44.3% and 56.5% from the values of Bender et al. [112] and Macdonald et al. [113], respectively. For the case of the interaction $N_2(X^1\Sigma_g^+)$ - N, one finds that the FHO results underestimate the QCT results at the lower temperatures and overestimate them at the higher ones, with maximum absolute relative deviations of 46.2% and 37.9% from the values of Esposito and Capitelli [114] and Jaffe et al. [115], respectively.

3.2.2 Vibronic transition of $N_2(A^3\Sigma_u^+, v_1)$ to $N_2(B^3\Pi_g, v_1')$ by collision with $N_2(X^1\Sigma_g^+, v_2)$ and $N(^4S_u)$

Herein the proposed VE-m-h model (2.365) will be implemented for the cases of vibronic transitions of $N_2(A^3\Sigma_u^+, v_1)$ to $N_2(B^3\Pi_g, v_1')$ by collisions of $N_2(A^3\Sigma_u^+, v_1)$ with $N_2(X^1\Sigma_g^+, v_2)$ and $N(^4S_u)$. For that purpose, the average process cross sections experimentally obtained by Bachmann et al. [35] were used.

Bachmann et al. studied intramolecular VE-m-h processes of the form:

$$\mathrm{N_2}(\mathrm{A}^3\Sigma_\mathrm{u}^+, v_1) + \mathrm{M} \longrightarrow \mathrm{N_2}(\mathrm{B}^3\Pi_\mathrm{g}, v_1') + \mathrm{M}\ , \tag{3.13}$$

being M the collision partner which may correspond to an atomic particle, $\mathrm{M} \in \{\mathrm{He}, \mathrm{Ne}, \mathrm{Ar}, \mathrm{Kr}, \mathrm{Xe}\} := \{\mathrm{M_a}\}$, or to a molecular particle, $\mathrm{M} \in \{\mathrm{H_2}, \mathrm{N_2}, \mathrm{NO}\} := \{\mathrm{M_m}\}$ in its ground energy level. The authors, however strongly believed that two intermolecular VE-m-h processes for the case $\mathrm{M} = \mathrm{N_2}$ were found due to their quasi-resonance [35]:

$$\mathrm{N_2}(\mathrm{A}^3\Sigma_\mathrm{u}^+, 15) + \mathrm{N_2}(\mathrm{X}^1\Sigma_\mathrm{g}^+, 0) \longrightarrow \mathrm{N_2}(\mathrm{B}^3\Pi_\mathrm{g}, 4) + \mathrm{N_2}(\mathrm{X}^1\Sigma_\mathrm{g}^+, 1)\ , \tag{3.14}$$

$$\mathrm{N_2}(\mathrm{A}^3\Sigma_\mathrm{u}^+, 17) + \mathrm{N_2}(\mathrm{X}^1\Sigma_\mathrm{g}^+, 0) \longrightarrow \mathrm{N_2}(\mathrm{B}^3\Pi_\mathrm{g}, 5) + \mathrm{N_2}(\mathrm{X}^1\Sigma_\mathrm{g}^+, 1)\ . \tag{3.15}$$

This consideration was also regarded in this work. It's important to point out that the experiment was done at room temperature $T_{\mathrm{tr_h}} = 300\,\mathrm{K} := T_\mathrm{ref}$. Although the work of Bachmann et al. doesn't provide data for the case M = N, a model applied on the available results would allow one to infer values for such case. The final objective would be to obtain rate coefficients through the law (2.365) for the VE-m-h processes represented by the chemical equations

$$\mathrm{N_2}(\mathrm{A}^3\Sigma_\mathrm{u}^+, v_1) + \mathrm{N_2}(\mathrm{X}^1\Sigma_\mathrm{g}^+, v_2) \longrightarrow \mathrm{N_2}(\mathrm{B}^3\Pi_\mathrm{g}, v_1') + \mathrm{N_2}(\mathrm{X}^1\Sigma_\mathrm{g}^+, v_2'), \quad \forall\, v_1,\ v_1',\ v_2,\ \text{and}\ v_2'\ , \tag{3.16}$$

$$\mathrm{N_2}(\mathrm{A}^3\Sigma_\mathrm{u}^+, v_1) + \mathrm{N}(^4\mathrm{S_u}) \longrightarrow \mathrm{N_2}(\mathrm{B}^3\Pi_\mathrm{g}, v_1') + \mathrm{N}(^4\mathrm{S_u}), \quad \forall\, v_1 \text{ and } v_1'\ . \tag{3.17}$$

By fitting the exponential gap law curve (2.363) to the set of points constituted by energy defect absolute values $|\Delta E|$ as abscissas, and average process cross section values $\sigma_{p,\mathrm{av}}$ as ordinates, it's possible to obtain characteristic cross sections σ_0 and energies E_0 for each collisional partner. The resultant exponential gap law curves are depicted by Figures 3.7 and 3.8 for the case of atomic and molecular collision partners, respectively.

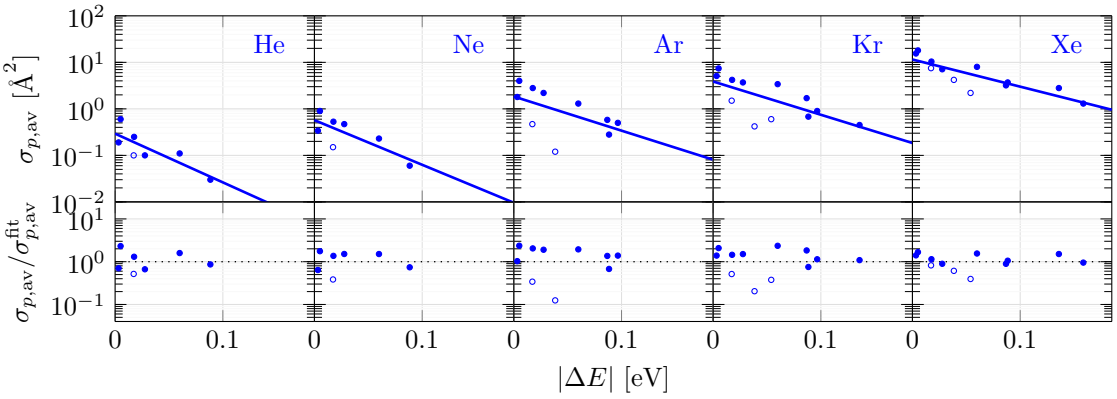

Figure 3.7: Upper plots: data of Bachmann et al. [35] and fitted curves (2.363) for the dependence of the average process cross sections $\sigma_{p,\mathrm{av}}$ on the absolute value of the energy defects $|\Delta E|$, regarding the atomic collision partners He, Ne, Ar, Kr and Xe. Lower plots: values for the ratios between the data and the fitted curves. Intramolecular exothermic processes: ●; intramolecular endothermic processes: ○.

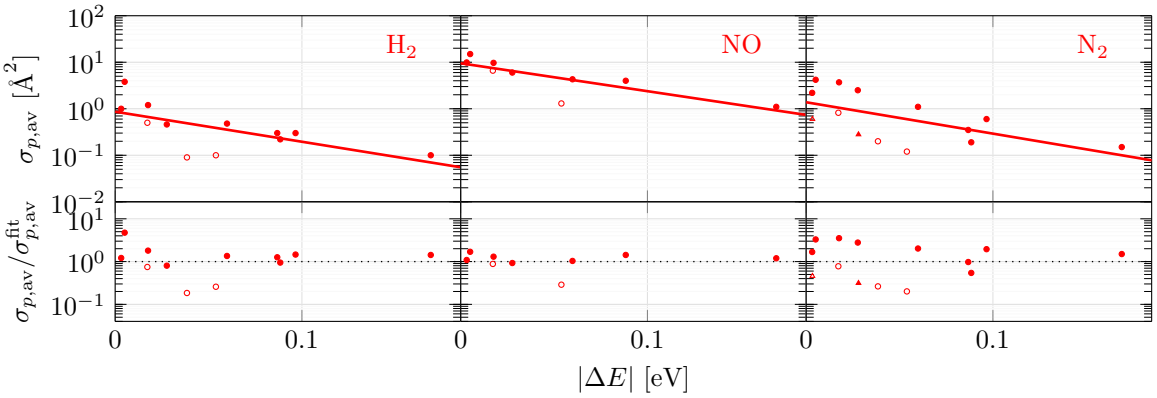

Figure 3.8: Upper plots: data of Bachmann et al. [35] and fitted curves (2.363) for the dependence of the average process cross sections $\sigma_{p,\mathrm{av}}$ on the absolute value of the energy defects $|\Delta E|$, regarding the molecular collision partners H_2, NO and N_2. Lower plots: values for the ratios between the data and the fitted curves. Intramolecular exothermic processes: ●; Intramolecular endothermic processes: ○; intermolecular exothermic processes: ▲; intermolecular endothermic processes: △.

Bachmann et al. refer that the data associated to the endothermic processes appears to follow a law which is distinct from the one associated to the exothermic processes. However, the number of points associated to the endothermic processes is not reasonable enough to properly build a different model for them. It was then decided in this work to fit the data altogether, since obtaining rate coefficients for both exothermic and endothermic processes is of capital importance. In general, the fitted curves underestimate the rate coefficients for the exothermic processes and overestimate the rate coefficients for the endothermic ones. The ratio between the data average process cross sections and the fit ones is as low as 0.1 and as high as 4.7.

By analysing the obtained values for the characteristic cross sections σ_0 and energies E_0 associated to processes involving the atomic collision partners, it was found that these quantities increase exponentially with the hard-sphere diameter d_{M} of the latter. It was then decided to obtain the values of σ_0 and E_0 for the processes involving the collision partner M = N by fitting exponential curves to the data $(d_{\mathrm{M}}, \sigma_0)$ and (d_{M}, E_0), respectively. The values for the hard-sphere diameters d_{M} were taken from the work of Svehla [54]. The results are depicted by Figure 3.9, which additionally reveal that the data $(d_{\mathrm{M}}, \sigma_0)$ and (d_{M}, E_0) for the processes involving molecular particles seems to not follow any evident law (though the number of only three data points for each plot is too small to make a proper judgement). The data σ_0 and E_0 values deviate from the fit ones in an interval between -34.6% and 9.7%, and between -2.6% and 2.7%, respectively, thus showing a much greater agreeability on the latter quantity than on the former.

The computation of the respective rate coefficients through expression (2.365) requires the knowledge of the potential well depths for the interactions between N_2 and the collision partners M, i.e. $\varepsilon := \varepsilon_{\mathrm{N_2\text{ - }M}}$. For that purpose, values of potential well depths associated to Lennard-Jones (12-6) interactions between collision partners of the same species $\varepsilon_{\mathrm{M\text{ - }M}} := E_{\mathrm{LJ,M\text{ - }M}}$ were extracted from the work of Svehla [54]. The quantities ε were then assumed to be equal to the geometric mean of $\varepsilon_{\mathrm{N_2\text{ - }N_2}}$ and $\varepsilon_{\mathrm{M\text{ - }M}}$, i.e. $\varepsilon = \sqrt{\varepsilon_{\mathrm{N_2\text{ - }N_2}} \cdot \varepsilon_{\mathrm{M\text{ - }M}}}$, as suggested by Parmenter et al. [76, 77]. The mass of the collision partners m_{M} which are needed for the computation of the reduced masses $\mu = m_{\mathrm{N_2}} \cdot m_{\mathrm{M}}/(m_{\mathrm{N_2}} + m_{\mathrm{M}})$ present in

expression (2.365) were taken from the work of Meija et al. [116].

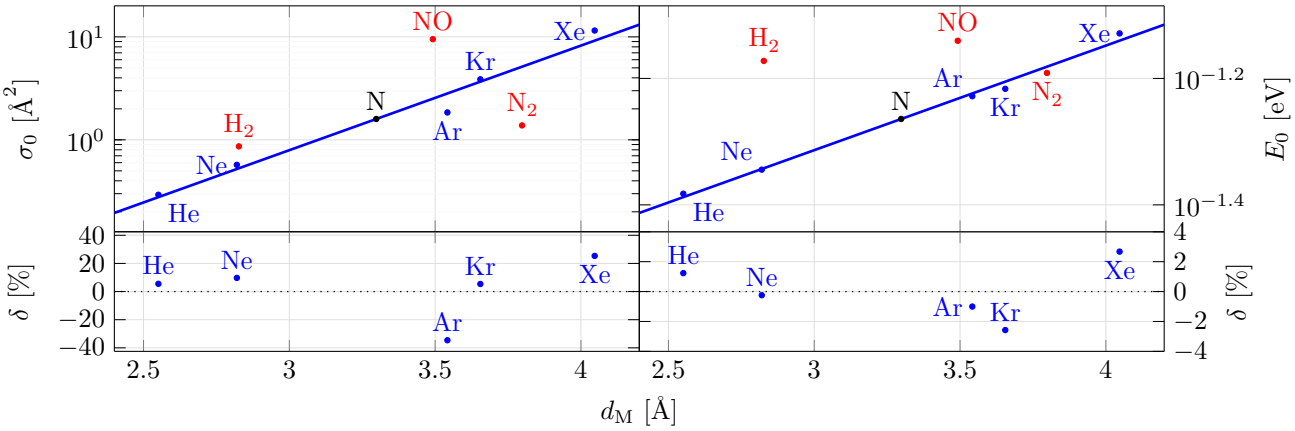

Figure 3.9: Upper plots: exponential curves fitted to the data (d_M, σ_0) (at left) and (d_M, E_0) (at right) for the processes involving the atomic collision partners. Lower plots: relative deviations of the data, $\delta = (\sigma_0 - \sigma_{0,\text{fit}})/\sigma_{0,\text{fit}}$ (at left) and $\delta = (E_0 - E_{0,\text{fit}})/E_{0,\text{fit}}$ (at right). Atomic collision partners: ●; molecular collision partners: ●; nitrogen atom N: ●.

The chemical equation (3.16) represents a large number of different kinetic processes, each one associated to particular set of values of vibrational quantum numbers v_1, v_1', v_2 and v_2'. Since accounting all of these kinetic processes would require too much computational resources for the incoming CFD simulations, it was decided to regard only the most significant ones. The accounted kinetic processes of (3.16) were the ones for which the ratio between the rate coefficient $k_{v_1,v_2}^{v_1',v_2'}$ given by (2.365) and the specific collisional frequency Z given by (2.86) in the limit of the high temperatures (since this will correspond to the simulated regime) was higher or equal to an arbitrated factor of 2×10^{-2}, i.e

$$\lim_{T_{\text{tr}_h} \to +\infty} \frac{k_{v_1,v_2}^{v_1',v_2'}}{Z} = \frac{\sigma_0}{\sigma} e^{-\left(\frac{\varepsilon}{k_B T_{\text{ref}}} + \frac{|\Delta E|}{E_0}\right)} \geq 2 \times 10^{-2} \ ,$$

being $\sigma = \pi d_{N_2}^2$, the respective collisional cross section. This reduces the number of regarded processes from the unbearable $4,059,264$ to the reasonably manageable $7,436$.

A synopsis on the relevant obtained data is issued by Table 3.6.

Table 3.6: Hard-sphere diameters d_M, collisional cross sections σ, interaction potential well depths $\varepsilon_{M\text{ - }M}$ and ε, particle masses m_M, reduced masses μ, characteristic cross sections σ_0 and characteristic energies E_0 associated to the collision partners N and N_2.

M [-]	d_M [Å]	σ [Å^2]	$\varepsilon_{M\text{ - }M}$ [$k_B \cdot$ K]	ε [$k_B \cdot$ K]	m_M [u]	μ [u]	σ_0 [Å^2]	E_0 [eV]
N	3.298	39.547	71.400	71.400	14.007	9.338	1.594	0.054
N_2	3.798	45.317	71.400	71.400	28.014	14.007	1.380	0.064

3.2.3 Vibronic transition of $N_2(W^3\Delta_u, v_1)$ to $N_2(B^3\Pi_g, v_1')$ by collision with $N_2(X^1\Sigma_g^+, v_2)$ and $N(^4S_u)$

In this section, and in similarity to the previous one, the proposed VE-m-h model (2.365) will be implemented for the cases of vibronic transitions of $N_2(W^3\Delta_u, v_1)$ to $N_2(B^3\Pi_g, v_1')$ by collisions of $N_2(W^3\Delta_u, v_1)$ with $N_2(X^1\Sigma_g^+, v_2)$ and $N(^4S_u)$. These are described by the chemical equations

$$N_2(W^3\Delta_u, v_1) + N_2(X^1\Sigma_g^+, v_2) \longrightarrow N_2(B^3\Pi_g, v_1') + N_2(X^1\Sigma_g^+, v_2'), \qquad \forall\, v_1,\ v_1',\ v_2,\ \text{and}\ v_2'\ , \tag{3.18}$$

and

$$N_2(W^3\Delta_u, v_1) + N(^4S_u) \longrightarrow N_2(B^3\Pi_g, v_1') + N(^4S_u), \qquad \forall\, v_1 \text{ and } v_1'\ , \tag{3.19}$$

respectively. Bachmann et al. [34, 35] obtained characteristic cross sections σ_0 and characteristic energies E_0 for the intramolecular endothermic and exothermic vibronic processes regarding atomic collisional partners $M \in \{He, Ne, Ar, Kr, Xe\} := \{M_a\}$ and molecular collisional partners $M \in \{H_2, N_2, NO\} := \{M_m\}$ in their ground energy level, by fitting the exponential gap law curve (2.363) to the set of points constituted by energy defect absolute values $|\Delta E|$ as abscissas, and experimentally obtained average process cross sections $\sigma_{p,\text{av}}$ as ordinates.

Since no data is available for the case M = N, it was decided to make a study about the dependence of the average process cross section on the atomic collision partner - in a similar way to what was done in §3.2.2 - and from it obtain the respective data. It was found that the characteristic cross section σ_0 varies exponentially with the hard-sphere diameter d_M of the atomic collision partners. However, the same can't be said about the characteristic energy E_0, conversely to the result which was obtained in §3.2.2. Figure 3.10 presents exponential curves fitted to the data (d_M, σ_0) and (d_M, E_0) of the atomic collision partners, showing deviations between -8.5% and 6.2% with respect to the former, and between -44.8% and 83.6% with respect to the latter.

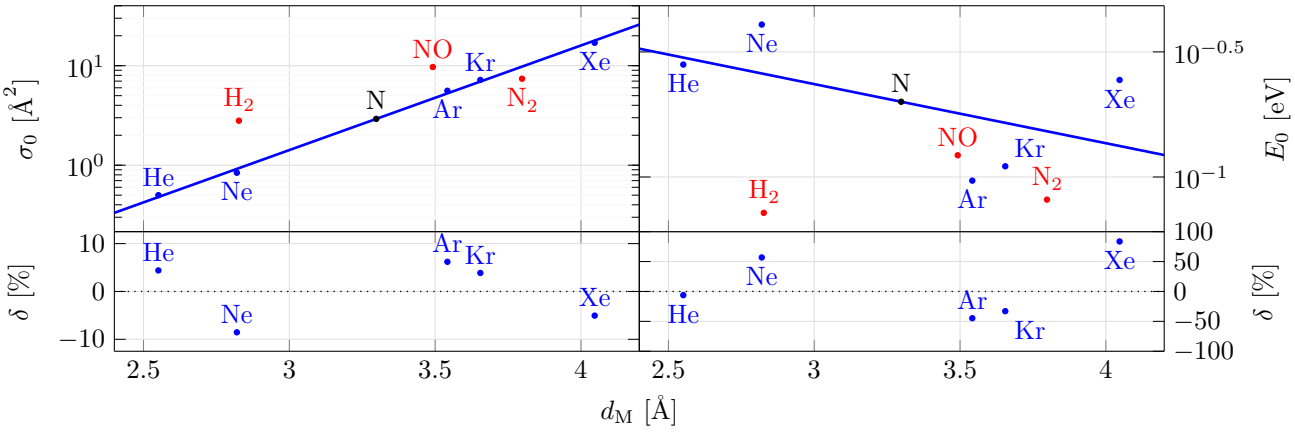

Figure 3.10: Upper plots: exponential curves fitted to the data (d_M, σ_0) (at left) and (d_M, E_0) (at right) for the processes involving the atomic collision partners. Lower plots: relative deviations of the data, $\delta = (\sigma_0 - \sigma_{0,\text{fit}})/\sigma_{0,\text{fit}}$ (at left) and $\delta = (E_0 - E_{0,\text{fit}})/E_{0,\text{fit}}$ (at right). Atomic collision partners: ●; molecular collision partners: ●; nitrogen atom N: ●.

Values of $\sigma_0 = 2.921$ Å^2 and $E_0 = 0.200$ eV were obtained for the case M = N. And values of $\sigma_0 = 7.400$ Å^2 and $E_0 = 0.081$ eV were obtained for the case M = N_2.

The accounted kinetic processes of (3.18) were the ones for which the ratio between the rate coefficient $k_{v_1,v_2}^{v_1',v_2'}$ given by (2.365) and the specific collisional frequency Z given by (2.86) in the limit of the high temperatures was higher or equal to an arbitrated factor of 1.2×10^{-1}. This allowed a reduction on the number of regarded processes from $1,682,816$ to $5,720$.

3.2.4 Vibronic transition of $\mathbf{N_2}(\mathbf{A}^3\Sigma_\mathbf{u}^+, v_1)$ to $\mathbf{N_2}(\mathbf{B}^3\Pi_\mathbf{g}, v_1')$ and $\mathbf{N_2}(\mathbf{C}^3\Pi_\mathbf{u}, v_1')$, by collision with $\mathbf{N_2}(\mathbf{A}^3\Sigma_\mathbf{u}^+, v_2)$, which, in its turn, transits to $\mathbf{N_2}(\mathbf{X}^1\Sigma_\mathbf{g}^+, v_2')$

A nitrogen molecule in the $A^3\Sigma_u^+$ electronic level may transit to $B^3\Pi_g$ and to $C^3\Pi_u$ by colliding with another nitrogen molecule also in the $A^3\Sigma_u^+$ electronic level. Piper [88, 89] studied such processes considering the simultaneous transition of the collision partner to the ground electronic level, i.e

$$N_2(A^3\Sigma_u^+, v_1) + N_2(A^3\Sigma_u^+, v_2) \longrightarrow N_2(B^3\Pi_g, v_1') + N_2(X^1\Sigma_g^+, v_2') \ , \tag{3.20}$$

and

$$N_2(A^3\Sigma_u^+, v_1) + N_2(A^3\Sigma_u^+, v_2) \longrightarrow N_2(C^3\Pi_u, v_1') + N_2(X^1\Sigma_g^+, v_2') \ . \tag{3.21}$$

Piper issues rate coefficients values for (3.20) and (3.21) at room temperature $T_{\mathrm{tr_h}} = 300$ K $:= T\mathrm{ref}$, which are specific to the vibrational levels v_1, v_2 and v_1' but not to v_2', i.e. $k_{v_1,v_2}^{v_1'}(T_{\mathrm{ref}}) := k_{v_1,v_2}^{v_1',\mathrm{ref}}$. Since rate coefficients for the full set of vibrational levels v_1, v_2, v_1' and v_2' and temperatures $T_{\mathrm{tr_h}}$ are wanted, the model (2.365) was considered, allowing one to express a relationship between the non v_2'-specific rate coefficient $k_{v_1,v_2}^{v_1',\mathrm{ref}} = \sum_{v_2'} k_{v_1,v_2}^{v_1',v_2'}(T_{\mathrm{ref}})$ and the v_2'-specific rate coefficients $k_{v_1,v_2}^{v_1',v_2'}(T_{\mathrm{ref}})$ through

$$k_{v_1,v_2}^{v_1',\mathrm{ref}} = \frac{\sigma_0}{1+\delta_{v_1,v_2}} \sqrt{\frac{8k_BT_{\mathrm{ref}}}{\pi\mu}} \left(\sum_{v_2'} e^{-\frac{\left|(\Delta E)_{v_1,v_2}^{v_1',v_2'}\right|}{E_0}} \right) \ . \tag{3.22}$$

By fitting curve (3.22) to the data issued by Piper, values for the characteristic cross section σ_0 and characteristic energy E_0 may be obtained. Figures 3.11 and 3.12 depict such fitted curves, with the absolute value of the partial energy defect $\left|(\Delta E)_{v_1}^{v_1'}\right|$ in the asbcissas axes[5]. This partial energy defect corresponds to the difference between the initial and final internal energies of solely the first collision partner, i.e. $(\Delta E)_{v_1}^{v_1'} = T_{e_1 v_1} - T_{e_1' v_1'}$. Quantities $\sigma_0 = 0.132$ Å^2 and $E_0 = 1.960$ eV, and $\sigma_0 = 0.873$ Å^2 and $E_0 = 1.071$ eV, were obtained for processes (3.20) and (3.21), respectively. The fit points did however depart significantly from the data points, in both value and behaviour. The ratio between the data rate values and the fit rate values was as low as 0.3 and as high as 2.7.

[5]Since the issued rate coefficients $k_{v_1,v_2}^{v_1',\mathrm{ref}}$ are not v_2'-specific the energy defect $(\Delta E)_{v_1,v_2}^{v_1',v_2'}$ can't be used to label the process.

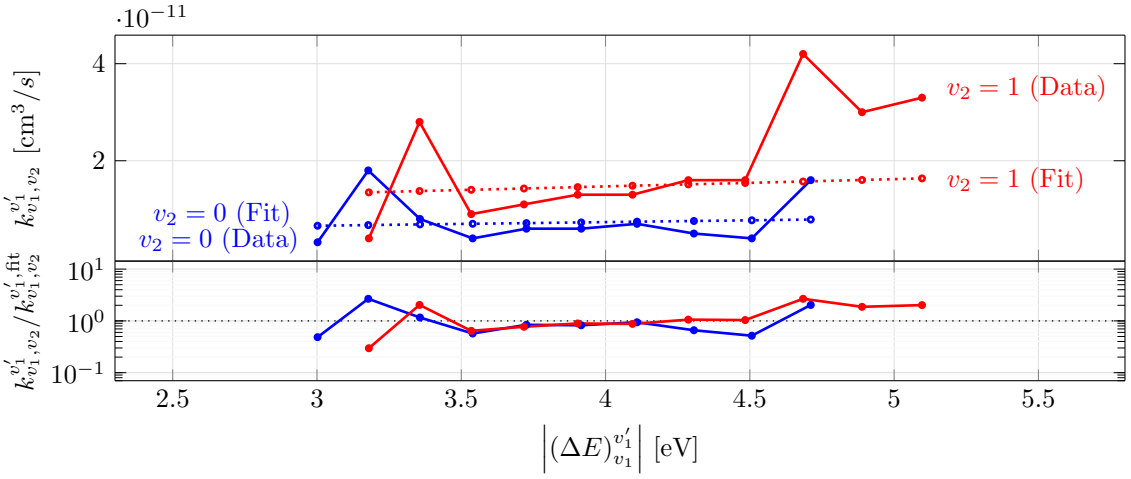

Figure 3.11: Upper plot: points of the fitted curve (3.22) to the data $(\{(\Delta E)^{v_1',v_2'}_{v_1,v_2}\}, k^{v_1'}_{v_1,v_2})$ with the rate coefficients $k^{v_1'}_{v_1,v_2}$ issued by Piper [88] for process (3.20). Lower plot: values of ratios between the data rate coefficients and the fit rate coefficients, $r = k^{v_1'}_{v_1,v_2}/k^{v_1',\mathrm{fit}}_{v_1,v_2}$. The issued data is with respect to $v_1 = 0$, $v_2 = 0$, $v_2 = 1$, and $v_1' \in [1, 11]$.

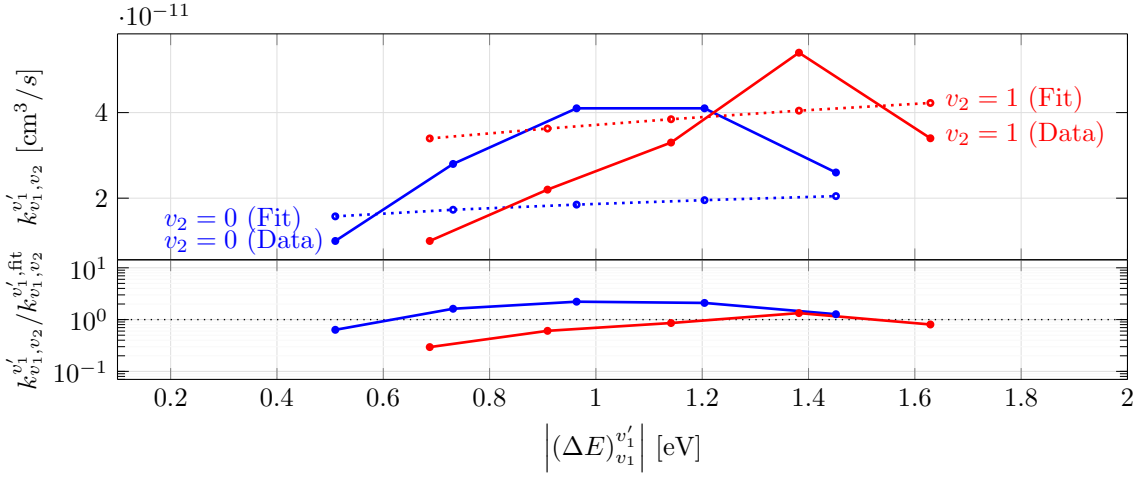

Figure 3.12: Upper plot: points of the fitted curve (3.22) to the data $(\{(\Delta E)^{v_1',v_2'}_{v_1,v_2}\}, k^{v_1'}_{v_1,v_2})$ with the rate coefficients $k^{v_1'}_{v_1,v_2}$ issued by Piper [89] for process (3.21). Lower plot: values of ratios between the data rate coefficients and the fit rate coefficients, $r = k^{v_1'}_{v_1,v_2}/k^{v_1',\mathrm{fit}}_{v_1,v_2}$. The issued data is with respect to $v_1 = 0$, $v_2 = 0$, $v_2 = 1$, and $v_1' \in [1, 11]$.

The rate coefficients $k^{v_1',v_2'}_{v_1,v_2}(T_{\mathrm{tr_h}})$ may be then computed through the law (2.365) constrained to the σ_0 and E_0 obtained values. Since the number of processes described by the chemical equations (3.20) and (3.21) is too large, solely the ones for which the ratio between the rate coefficient and the specific collisional frequency in the limit of the high temperatures was higher or equal to the arbitrated factors 2.28×10^{-3} and 1.3×10^{-2}, respectively, were regarded. This procedure allowed a reduction of the number of accounted processes from $2,095,104$ to $6,067$ for the case of (3.20), and from $317,440$ to $8,135$ for the case of (3.21).

3.2.5 Vibronic transition of $\mathbf{N_2(A^3\Sigma_u^+, v_1)}$ to $\mathbf{N_2(X^1\Sigma_g^+, v_1')}$ by collision with $\mathbf{N_2(X^1\Sigma_g^+, v_2)}$ and $\mathbf{N(^4S_u)}$, which, in its turn, transits to $\mathbf{N(^2P_u)}$

Let's consider the vibronic transition of a nitrogen molecule in the $A^3\Sigma_u^+$ electronic level to the ground electronic level, by collision with a heavy particle:

$$N_2(A^3\Sigma_u^+, v) + M \longrightarrow N_2(X^1\Sigma_g^+, v') + M \ . \tag{3.23}$$

There is some data available in the literature that may be useful in this work. These correspond to experimentally obtained values for the rate coefficient of the process (3.23) at room temperature $T_{\mathrm{tr_h}} = 300\ \mathrm{K} := T_{\mathrm{ref}}$ concerning the particular cases

$$N_2(A^3\Sigma_u^+, v_1) + N_2(X^1\Sigma_g^+, v_2) \longrightarrow N_2(X^1\Sigma_g^+, v_1') + N_2(X^1\Sigma_g^+, v_2') \ , \tag{3.24}$$

and

$$N_2(A^3\Sigma_u^+, v_1) + N(^4S_u) \longrightarrow N_2(X^1\Sigma_g^+, v_1') + N(^2P_u) \ , \tag{3.25}$$

with $v_1 \in \{0, 1\}$ and $v_2 = 0$.

Table 3.7 presents the values obtained in the works of Drewer and Pener [117], Vidaud et al. [118] and Levron and Phelps [87], for the rate coefficient associated to process (3.24). Vidaud et al. didn't treat the vibrational levels $N_2(A^3\Sigma_u^+, 0)$ and $N_2(A^3\Sigma_u^+, 1)$ separately. Their issued rate coefficient value is with respect to these two levels lumped together. The values issued by Levron and Phelps do agree with the one of Vidaud et al. although not as much with the ones of Drewer and Pener. Also, since Vidaud et al. supply a lumped rate coefficient instead of the vibrationally-specific ones of Levron and Phelps, it was decided to regard the results of Levron and Phelps in this work.

Table 3.7: Experimentally obtained values for the rate coefficient of process (3.24) with $v_1 \in \{0, 1\}$ and $v_2 = 0$, at $T_{\mathrm{tr_h}} = 300$ K, i.e. $k_{v_1,0}(T_{\mathrm{ref}}) := k_{v_1,0}^{\mathrm{ref}}$.

$k_{0,0}^{\mathrm{ref}}$[cm^3/s]	$k_{1,0}^{\mathrm{ref}}$[cm^3/s]	Reference
3.7×10^{-16}	3.4×10^{-16}	Drewer and Pener [117]
4.5×10^{-17} [a]		Vidaud et al. [118]
2.6×10^{-18}	3.8×10^{-17}	Levron and Phelps [87]

[a] This value is with respect to $N_2(A^3\Sigma_u^+, 0)$ and $N_2(A^3\Sigma_u^+, 1)$ lumped together.

The process (3.25) not only describes a vibronic transition of $N_2(A^3\Sigma_u^+, v_1)$ to $N_2(X^1\Sigma_g^+, v_1')$ but also an excitation of the collision partner, $N(^4S_u)$ to $N(^2P_u)$. This latter excitation was assumed in accordance with the discussions done by Meyer et al. [119] and Young and Dunn [120]. There was an attempt, performed by Piper [85], to quantify the fraction of ground state nitrogen atoms which are actually excited in the process. Such attempt wasn't however successful, as Piper [121] later showed that electronically excited nitrogen molecules different from $N_2(A^3\Sigma_u^+)$ were present in his experiment, and

by being undetected and unaccounted leaded to wrong results. With only the evidence of Meyer et al. and Young and Dunn available, it was decided to assume that excitation of $N(^4S_u)$ to $N(^2P_u)$ always occurred. Table 3.8 presents experimental values for the rate coefficient of process (3.25) obtained in the works of Wray [122], Young and St. John [123], Meyer et al. [119], Dunn and Young [124], Vidaud et al. [118], and Piper [85]. The results agree reasonably well with each other, being of the same order of magnitude. It was decided to regard the most recent ones, the results of Piper, in this work.

Table 3.8: Experimentally obtained values for the rate coefficient of process (3.25) with $v_1 \in \{0, 1\}$, at $T_{\mathrm{tr_h}} = 300$ K, i.e. $k_{v_1}(T_{\mathrm{ref}}) := k_{v_1}^{\mathrm{ref}}$.

k_0^{ref}[cm^3/s]	k_1^{ref}[cm^3/s]	Reference
5.4×10^{-11}	—	Wray [122]
5×10^{-11}	—	Young and St. John [123]
4.3×10^{-11}	—	Meyer et al. [119]
4.8×10^{-11}	4.8×10^{-11}	Dunn and Young [124]
3.5×10^{-11} [a]		Vidaud et al. [118]
4.0×10^{-11}	4.0×10^{-11}	Piper [85]

[a] This value is with respect to $N_2(A^3\Sigma_u^+, 0)$ and $N_2(A^3\Sigma_u^+, 1)$ lumped together.

Values for the rate coefficient of the process (3.24) for all v_1, v_2, v_1' and v_2', and values for the rate coefficient of the process (3.25) for all v_1, and v_1', in the full set of heavy particle translational temperatures $T_{\mathrm{tr_h}}$, are wanted. It is then necessary to make an assumption regarding both vibrational and temperature dependences of the rate coefficient, since the available data only concerns some few vibrational levels and a room temperature. The VE-m-h model (2.365) may be regarded for that purpose. Let's start by analysing process (3.24). From (2.365), the respective rate coefficient is given by

$$k_{v_1,v_2}^{v_1',v_2'}(T_{\mathrm{tr_h}}) = \sigma_0 \, e^{-\frac{\left|(\Delta E)_{v_1,v_2}^{v_1',v_2'}\right|}{E_0}} \sqrt{\frac{8k_B T_{\mathrm{tr_h}}}{\pi\mu}} e^{\frac{\varepsilon}{k_B}\left(\frac{1}{T_{\mathrm{tr_h}}} - \frac{1}{T_{\mathrm{ref}}}\right)} \, . \tag{3.26}$$

The vibrational dependence of the rate coefficient is dictated by the characteristic energy E_0. It was decided to make the value of this variable to coincide with one of the obtained set for the analogous processes studied in sections §3.2.2, §3.2.3 and §3.2.4. Since the process treated in §3.2.3 regards a single vibronic transition of the collision partners from a higher electronic level to a lower electronic level in similarity with this one and in dissimilarity with the transitions treated in §3.2.2 and §3.2.4, the E_0 value obtained in §3.2.3 was the one chosen, i.e. the value for the vibronic transition of $N_2(W^3\Delta_u, v_1)$ to $N_2(B^3\Pi_g, v_1')$ by impact with $N_2(X^1\Sigma_g^+, v_2)$. The variable σ_0, in its turn, can be computed using either $k_{0,0}^{\mathrm{ref}}$ or $k_{1,0}^{\mathrm{ref}}$. Arbitrarily, it was decided to use $k_{0,0}^{\mathrm{ref}}$ and then to quantify the discrepancy between $k_{1,0}^{\mathrm{ref}}$ and the respective value obtained from the model. The rate coefficient for (3.24) with $v_1 = 0$ and $v_2 = 0$ regardless of the vibrational levels v_1' and v_2', at $T_{\mathrm{tr_h}} = T_{\mathrm{ref}}$, is given by

$$k_{0,0}^{\mathrm{ref}} = \sum_{v_1',v_2'} k_{0,0}^{v_1',v_2'}(T_{\mathrm{ref}}) = \sigma_0 \sqrt{\frac{8k_B T_{\mathrm{ref}}}{\pi\mu}} \left(\sum_{v_1',v_2'} e^{-\frac{\left|(\Delta E)_{0,0}^{v_1',v_2'}\right|}{E_0}} \right) \, . \tag{3.27}$$

By solving (3.27) with respect to σ_0, one may get

$$\sigma_0 = \frac{k_{0,0}^{\mathrm{ref}}}{\sqrt{\frac{8k_B T_{\mathrm{ref}}}{\pi\mu}}\left(\sum_{v_1',v_2'} e^{-\frac{\left|(\Delta E)_{0,0}^{v_1',v_2'}\right|}{E_0}}\right)} \ . \tag{3.28}$$

And by inserting the result (3.28) into (3.26) a general expression for the rate coefficient of process (3.24) may be obtained:

$$k_{v_1,v_2}^{v_1',v_2'}(T_{\mathrm{tr_h}}) = k_{0,0}^{\mathrm{ref}} \frac{e^{-\frac{\left|(\Delta E)_{v_1,v_2}^{v_1',v_2'}\right|}{E_0}}}{\sum_{v_1',v_2'} e^{-\frac{\left|(\Delta E)_{0,0}^{v_1',v_2'}\right|}{E_0}}} \sqrt{\frac{T_{\mathrm{tr_h}}}{T_{\mathrm{ref}}}} e^{\frac{\varepsilon}{k_B}\left(\frac{1}{T_{\mathrm{tr_h}}}-\frac{1}{T_{\mathrm{ref}}}\right)} \ . \tag{3.29}$$

In similarity to what was done in section §3.2.3, it was decided to account only the kinetic processes of (3.24) for which the ratio between the rate coefficient $k_{v_1,v_2}^{v_1',v_2'}$ and the specific collisional frequency Z in the limit of the high temperatures was higher or equal to an arbitrated factor of 3.3×10^{-10}, i.e:

$$\lim_{T_{\mathrm{tr_h}} \to +\infty} \frac{k_{v_1,v_2}^{v_1',v_2'}}{Z} = \frac{k_{0,0}^{\mathrm{ref}}}{\sigma\sqrt{\frac{8k_B T_{\mathrm{ref}}}{\pi\mu}}} \frac{e^{-\frac{\left|(\Delta E)_{v_1,v_2}^{v_1',v_2'}\right|}{E_0}}}{\sum_{v_1',v_2'} e^{-\frac{\left|(\Delta E)_{0,0}^{v_1',v_2'}\right|}{E_0}}} e^{-\frac{\varepsilon}{k_B T_{\mathrm{ref}}}} \geq 3.3 \times 10^{-10} \ .$$

This allows one to reduce the number of regarded processes from 7,626,496 to 7,355. A characteristic cross section $\sigma_0 = 2.04 \times 10^{-8}\,\text{Å}^2$ was obtained. The ratio between the model obtained result $k_{1,0}(T_{\mathrm{ref}})$ and the experimental one $k_{1,0}^{\mathrm{ref}}$ corresponds to $k_{1,0}(T_{\mathrm{ref}})/k_{1,0}^{\mathrm{ref}} = 0.06$, evidencing a significant underestimation of this quantity by the model. This shows how crude the assumption on the vibrational dependency of the rate coefficient may be. For the case of process (3.25), it can be shown that if model (2.365), the result k_0^{ref} and the value obtained E_0 in section §3.2.3 for the vibronic transitions of $\mathrm{N_2}(\mathrm{W}^3\Delta_\mathrm{u}, v_1)$ to $\mathrm{N_2}(\mathrm{B}^3\Pi_\mathrm{g}, v_1')$ by $\mathrm{N}(^4\mathrm{S_u})$ are both regarded, the rate coefficient $k_{v_1}^{v_1'}$ of the process is given by

$$k_{v_1}^{v_1'}(T_{\mathrm{tr_h}}) = k_0^{\mathrm{ref}} \frac{e^{-\frac{\left|(\Delta E)_{v_1}^{v_1'}\right|}{E_0}}}{\sum_{v_1'} e^{-\frac{\left|(\Delta E)_{0}^{v_1'}\right|}{E_0}}} \sqrt{\frac{T_{\mathrm{tr_h}}}{T_{\mathrm{ref}}}} e^{\frac{\varepsilon}{k_B}\left(\frac{1}{T_{\mathrm{tr_h}}}-\frac{1}{T_{\mathrm{ref}}}\right)} \ . \tag{3.30}$$

A characteristic cross section $\sigma_0 = 3.33\,\text{Å}^2$ was obtained. The relative deviation between the model obtained result $k_1(T_{\mathrm{ref}})$ and the experimental one k_1^{ref} corresponds to 10.2%, evidencing an overestimation of this quantity by the model.

3.2.6 Vibronic transition of $\mathbf{N_2}(\mathbf{A'^5\Sigma_g^+}, v)$ to $\mathbf{N_2}(\mathbf{B^3\Pi_g}, v')$ by collision with $\mathbf{N_2}(\mathbf{X^1\Sigma_g^+}, 0)$ and $\mathbf{N}(^4\mathbf{S_u})$

According to the work of Ottinger et al. [86], there's the possibility of occuring intramolecular vibronic transitions from $\mathrm{N_2}(\mathrm{A'}^5\Sigma_\mathrm{g}^+, v, J)$ to $\mathrm{N_2}(\mathrm{B}^3\Pi_\mathrm{g}, v', J')$ by collisions with heavy particles through the so-

called *gateway mechanism* [125–127]:

$$\mathrm{N_2(A'^5\Sigma_g^+, v, J) + M \longrightarrow N_2(B^3\Pi_g, v', J') + M\ .} \tag{3.31}$$

The main route is the one associated to $v = 0$, $J = 12$, $v' = 10$ and $J' = 12$. The authors issue experimental values for average process cross sections $\sigma^{v',J'}_{p,\mathrm{av},v,J}$ associated to this main route considering atomic collision partners, $\mathrm{M} \in \{\mathrm{He, Ne, Ar, Kr, Xe}\} := \{\mathrm{M_a}\}$, as well as molecular collision partners, $\mathrm{M} \in \{\mathrm{H_2, N_2, NO, O_2}\} := \{\mathrm{M_m}\}$ in their ground energy levels. The experiment was done at room temperature $T_{\mathrm{tr_h}} = 300\ \mathrm{K} := T_{\mathrm{ref}}$. In this very work, a vibronic-specific rate coefficient for the process

$$\mathrm{N_2(A'^5\Sigma_g^+, v) + M \longrightarrow N_2(B^3\Pi_g, v') + M\ ,} \tag{3.32}$$

with $\mathrm{M} \in \{\mathrm{N,\ N_2}\}$, $v = 0$ and $v' = 10$ instead of a rovibronic one for process (3.31) is wanted. The rate coefficient for process (3.31) corresponds to $k^{v',J'}_{v,J}$ such that the variation on time of the concentration of $\mathrm{N_2(A'^5\Sigma_g^+}, v, J)$ due to this same process is given by

$$\left(\frac{d[\mathrm{N_2(A'^5\Sigma_g^+}, v, J)]}{dt}\right)^{v',J'}_{v,J} = -k^{v',J'}_{v,J}[\mathrm{N_2(A'^5\Sigma_g^+}, v, J)][\mathrm{M}]\ , \tag{3.33}$$

and, similarly, the rate coefficient for process (3.32) corresponds to $k^{v'}_{v}$ such that the variation on time of the concentration of $\mathrm{N_2(A'^5\Sigma_g^+}, v)$ due to this same process is given by

$$\left(\frac{d[\mathrm{N_2(A'^5\Sigma_g^+}, v)]}{dt}\right)^{v'}_{v} = -k^{v'}_{v}[\mathrm{N_2(A'^5\Sigma_g^+}, v)][\mathrm{M}]\ . \tag{3.34}$$

Rate coefficients $k^{v'}_{v}$ and $k^{v',J'}_{v,J}$ are related to each other since from to the definition of $\left(d[\mathrm{N_2(A'^5\Sigma_g^+}, v)]/dt\right)^{v'}_{v}$ one has

$$\left(\frac{d[\mathrm{N_2(A'^5\Sigma_g^+}, v)]}{dt}\right)^{v'}_{v} = \sum_{J,J'}\left(\frac{d[\mathrm{N_2(A'^5\Sigma_g^+}, v, J)]}{dt}\right)^{v',J'}_{v,J} = -\underbrace{\left(\sum_{J,J'} k^{v',J'}_{v,J}\frac{[\mathrm{N_2(A'^5\Sigma_g^+}, v, J)]}{[\mathrm{N_2(A'^5\Sigma_g^+}, v)]}\right)}_{:=k^{v'}_{v}}[\mathrm{N_2(A'^5\Sigma_g^+}, v)][\mathrm{M}]\ . \tag{3.35}$$

Therefore, rate coefficient $k^{v'}_{v}$ is given by

$$k^{v'}_{v} = \sum_{J,J'} k^{v',J'}_{v,J}\frac{[\mathrm{N_2(A'^5\Sigma_g^+}, v, J)]}{[\mathrm{N_2(A'^5\Sigma_g^+}, v)]}. \tag{3.36}$$

Due to the fact that the population of the rotational levels $\mathrm{N_2(A'^5\Sigma_g^+}, v, J)$ follows the Boltzmann distribution (2.29), and only the rotational quantum numbers $J = 12$ and $J' = 12$ contribute to the gateway process (3.31) for $v = 0$ and $v' = 10$ [86], the rate coefficient k^{10}_{0}, given by relation (3.36), is reduced to

$$k^{10}_{0} = k^{10,12}_{0,12}\frac{g_{\mathrm{N_2,rot,A',0,12}}\cdot e^{-\frac{\epsilon_{\mathrm{N_2,rot,A',0,12}}}{k_B T_{\mathrm{ref}}}}}{Q_{\mathrm{N_2,rot,A',0}}}\ . \tag{3.37}$$

From (2.84) and (3.37), the respective average process cross section $\sigma^{10}_{\mathrm{p,av},0}$ is simply given by

$$\sigma^{10}_{\mathrm{p,av},0} = \sigma^{10,12}_{\mathrm{p,av},0,12} \frac{g_{\mathrm{N_2,rot,A',0,12}} \cdot e^{-\frac{\epsilon_{\mathrm{N_2,rot,A',0,12}}}{k_B T_{\mathrm{ref}}}}}{Q_{\mathrm{N_2,rot,A',0}}} \ . \tag{3.38}$$

The quantity $Q_{\mathrm{N_2,rot,A',0}}$ corresponds to the rotational partition function for $\mathrm{N_2}(\mathrm{A'^5}\Sigma^+_\mathrm{g},0)$, which according to its definition (2.18), is given by

$$Q_{\mathrm{N_2,rot,A',0}} = \sum_{J=0}^{J_{\max}} g_{\mathrm{N_2,rot,A',0},J} \cdot e^{-\frac{\epsilon_{\mathrm{N_2,rot,A',0},J}}{k_B T_{\mathrm{ref}}}} \ , \tag{3.39}$$

being $J_{\max}$ the maximum rotational quantum number that $\mathrm{N_2}(\mathrm{A'^5}\Sigma^+_\mathrm{g})$ may assume. For $J > J_{\max}$ the nuclei are subjected to a purely repulsive potential, which makes them to depart from each other resulting in the dissociation of the diatomic particle. Therefore, $J_{\max}$ corresponds to the maximum rotational quantum number J for which the effective internuclear potential, the so-called *centrifugally corrected potential* $V_J(r) = V(r) + \hbar^2 J(J+1)/(2\mu r^2)$ being r the internuclear distance (see appendix B.2 for more details), remains with a well in its curve. For higher J values the well disappears, and the curve is transformed into another with a slope which is non-positive throughout all of its extension. The internuclear force, which corresponds to the symmetric value of the slope and has a positive conventional signal in the direction of increasing internuclear distances, is in its turn transformed into a non-negative quantity, imposing repulsiveness. One gets $J_{\max} = 115$, being the respective centrifugally corrected potential curve $V_{J_{\max}}(r)$ represented in Figure 3.13.

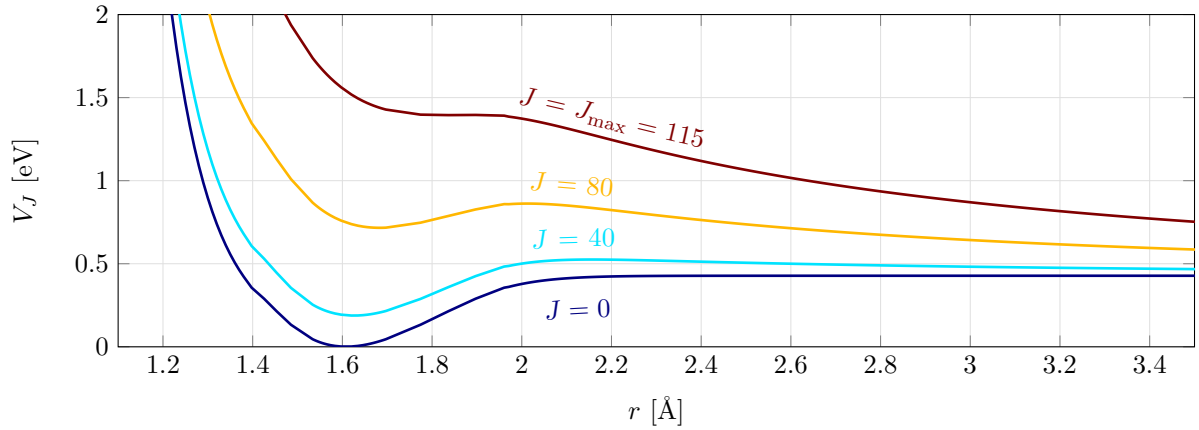

Figure 3.13: Centrifugally corrected potential curves $V_J(r)$ for $J = 0$, 40, 80 and $J_{\max} = 115$ obtained for $\mathrm{N_2}(\mathrm{A'^5}\Sigma^+_\mathrm{g})$.

The sensible rotational energy $\epsilon_{\mathrm{N_2,rot,A',0},J}$ is according to expression (2.21a)

$$\epsilon_{\mathrm{N_2,rot,A',0},J} = B_{\mathrm{N_2,rot,A',0}} J(J+1) \ , \tag{3.40}$$

being $B_{\mathrm{N_2,rot,A',0}}$ the respective rotational energy function given by (B.8).

The rotational degree of degeneracy $g_{\mathrm{N_2,rot,A',0},J}$ can't be computed through expression (2.21b) due to the fact that $\mathrm{N_2}$ isn't a heteronuclear diatomic particle but a homonuclear one. The rotational degree

of degeneracy corresponds to a product between two contributions [128]: one due to the nuclear spin, $g^n_{\mathrm{N_2,rot,A',0,}J}$, and another due to the rotational quantum number, $2J+1$, i.e.

$$g_{\mathrm{N_2,rot,A',0,}J} = g^n_{\mathrm{N_2,rot,A',0,}J} \cdot (2J+1) \ . \tag{3.41}$$

The molecular term symbol $^5\Sigma^+_\mathrm{g}$ associated to the A' electronic level implies that the rotational levels are *symmetric* for even J, and *antisymmetric* for odd J [128]. Additionally, it is known that the nitrogen nuclei follow *Bose-Einstein statistics*. It can then be shown that the contribution of the nuclear spin to the rotational degree of degeneracy of $\mathrm{N_2(A'^5\Sigma^+_g}, v, J)$ corresponds to [128]

$$g^n_{\mathrm{N_2,rot,A',0,}J} = \begin{cases} (2I+1)(I+1), & \text{if } J \text{ is even} \ , \\ (2I+1)I, & \text{if } J \text{ is odd} \ , \end{cases} \tag{3.42}$$

being I the so-called *nuclei spin quantum number*. For the case of the nitrogen nuclei one has $I=1$ [128], meaning that $g^n_{\mathrm{N_2,rot,A',0,}J} = 6$ for even J and $g^n_{\mathrm{N_2,rot,A',0,}J} = 3$ for odd J.

The values of vibronic-specific average process cross sections $\sigma^{10}_{\mathrm{p,av,0}}$ obtained through expression (3.38) are presented in Table 3.9.

Table 3.9: Vibronic-specific average process cross sections $\sigma^{10}_{\mathrm{p,av,0}}$ computed through expression (3.38) using the rovibronic-specific average process cross sections $\sigma^{10,12}_{\mathrm{p,av,0,12}}$ issued by Ottinger et al. [86].

M	He	Ne	Ar	Kr	Xe	H_2	N_2	NO	O_2
$\sigma^{10}_{\mathrm{p,av,0}}[10^{-2}\text{Å}^2]$	2.953	4.430	8.122	11.075	14.767	6.645	5.907	12.552	4.430

Since no data is available for the case M = N, it was decided to make a study about the dependence of the average process cross section on the atomic collision partner - in a similar way to what was done in §3.2.2 - and from it obtain the respective data. It was indeed found that the average process cross section $\sigma^{10}_{\mathrm{p,av,0}}$ increased exponentially with the hard-sphere diameter d_M of the atomic collision partners, although the same can't be said about the molecular collision partners. By fitting an exponential curve to the data points $(d_\mathrm{M}, \sigma^{10}_{\mathrm{p,av,0}})$ for the atomic collision partners, the value of the average process cross section for M = N was obtained. The respective results are depicted by Figure 3.14. The data values for the average process cross sections deviate from the fit ones from -8.6% to 10.6%. A value of $\sigma^{10}_{\mathrm{p,av,0}} = 6.863 \times 10^{-2}\text{Å}^2$ was obtained for the case M = N.

The dependence of the average process cross section $\sigma^{10}_{\mathrm{p,av,0}}$ on the temperature was assumed to be the one referred by Parmenter et al. [76, 77], and therefore, the respective forward rate coefficient may be mathematically expressed by

$$k^{10}_0(T_{\mathrm{tr_h}}) = \sigma'^{\,10,\mathrm{ref}}_{p,\mathrm{av,0}} \sqrt{\frac{8k_B T_{\mathrm{tr_h}}}{\pi\mu}}\, e^{\frac{\varepsilon}{k_B T_{\mathrm{tr_h}}}} \ , \tag{3.43}$$

being $\sigma'^{\,10,\mathrm{ref}}_{p,\mathrm{av,0}} = \sigma^{10,\mathrm{ref}}_{p,\mathrm{av,0}}\, e^{-\frac{\varepsilon}{k_B T_\mathrm{ref}}}$, where $\sigma^{10,\mathrm{ref}}_{p,\mathrm{av,0}}$ is the average process cross section evaluated at the reference temperature T_ref of Ottinger et al. [86] - the object of study considered above, and ambiguously

labelled as $\sigma^{10}_{\mathrm{p,av},0}$. Note that relation (3.43) may be conveniently expressed through a modified Arrhenius function.

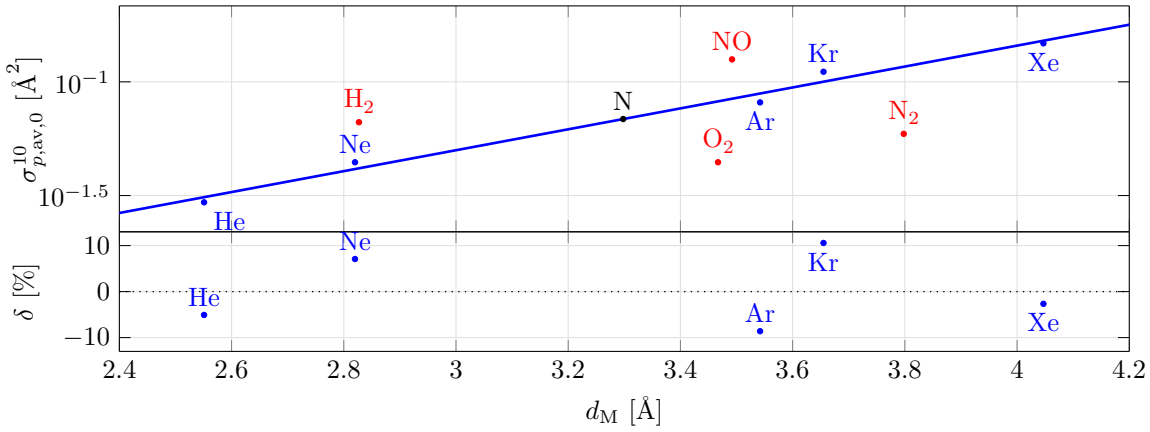

Figure 3.14: Upper plot: exponential curve fitted to the data $(d_{\mathrm{M}}, \sigma^{10}_{\mathrm{p,av},0})$ for process (3.32) involving solely the atomic collision partners. Lower plot: relative deviations of the data, $\delta = \left(\sigma^{10}_{\mathrm{p,av},0} - \sigma^{10,\mathrm{fit}}_{\mathrm{p,av},0}\right)/\sigma^{10,\mathrm{fit}}_{\mathrm{p,av},0}$. Atomic collision partners: ●; molecular collision partners: ●; nitrogen atom N: ●.

3.2.7 Non-dissociative ionisation of N_2 by electron impact

Let's now consider the process of non-dissociative ionisation of the nitrogen molecule N_2 by electron impact, which can be represented by the chemical equation

$$\mathrm{N_2}\left(\mathrm{X^1\Sigma_g^+},\, v\right) + \mathrm{e^-} \longrightarrow \mathrm{N_2^+}\left(e', v'\right) + 2\,\mathrm{e^-}\,. \tag{3.44}$$

Such chemical reaction has a major importance in hypersonic flows since it produces both a molecular ion and an additional free electron from a molecule and a free electron. This additional free electron may in its turn react in the same manner as the previous one, leading to a cascade of reactions. The work of Laricchiuta el al. [101] supplies process cross sections values for (3.44) which can be accessed through the Phys4Entry website [92]. The issued process cross sections are however summed in the electronic levels of N_2^+, $e' \in \{\mathrm{X^2\Sigma_g^+},\, \mathrm{A^2\Pi_u},\, \mathrm{B^2\Sigma_u^+}\}$ as well as in the vibrational levels v' - let these cross sections be denoted by $\sigma_v(E)$, being E the relative translational energy of the collision partners. Also, the data is restricted to $E \in [0, 50]$ eV, and $v \in [0, 40]$ from a database[6] that regards a total of 47 vibrational levels for $\mathrm{N_2}\left(\mathrm{X^1\Sigma_g^+}\right)$. It's worthy to say that Laricchiuta el al. [101] additionally issue values for the process cross sections for each electronic level e' of N_2^+ for the case $v = 0$, i.e. $\sigma_v^{e'}(E)$ with $v = 0$. These data allows one to compute electronically specific *branching ratios* $\mathfrak{BR}_v^{e'}(E) := \sigma_v^{e'}(E)/\sigma_v(E)$ for the case $v = 0$, which are by definition the ratios between the process cross sections for each electronic level e', $\sigma_v^{e'}(E)$, and the sum of all of these, $\sigma_v(E)$. The respective results are depicted by Figure (3.15).

[6] The database for the vibrational levels of $\mathrm{N_2}\left(\mathrm{X^1\Sigma_g^+}\right)$ was directly sent from Dr. Laricchiuta to the author.

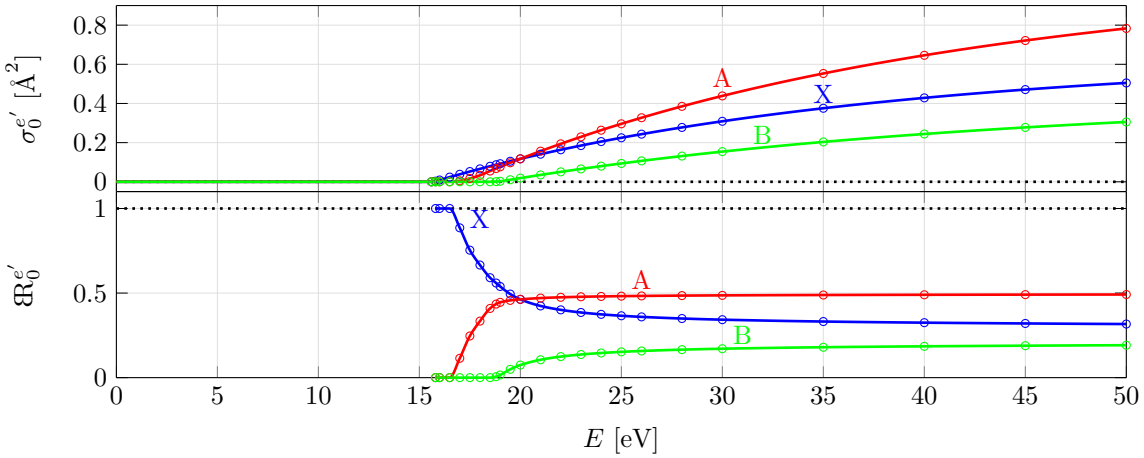

Figure 3.15: Process cross sections $\sigma_v^{e'}(E)$ issued by Laricchiuta el al. [101] and computed branching ratios $\mathfrak{R}_v^{e'}(E)$ for the case $v = 0$, with $e' = \mathrm{X}^2\Sigma_\mathrm{g}^+$, $\mathrm{A}^2\Pi_\mathrm{u}$ and $\mathrm{B}^2\Sigma_\mathrm{u}^+$. The lines correspond to cubic spline interpolated values. Note that branching ratios can't be defined at energy points for which the full cross section values are null.

In order to implement in this work the results of Laricchiuta el al., it was decided to assume that the branching ratios $\mathfrak{R}_v^{e'}(E)$ were the same regardless of the vibrational level v of N_2, implying $\mathfrak{R}_v^{e'}(E) = \mathfrak{R}_0^{e'}(E) \,\forall\, v,\, e'$.

The computation of process rate coefficients $k_v^{e'}(T_{\mathrm{tr_e}})$ involves an improper integral (the upper limit corresponds to infinity), as shown by equation (2.87) in which the distribution of relative speeds of collision, $f(v, T_{\mathrm{tr_e}})$, was considered to be the one in which v is the real relative speed of the colliding particles. Because only finite discrete data points for the process cross section are available, the integration in (2.87) can't be performed in all its domain, and on the other hand, numerical methods are required for its evaluation[7]. When regarding the upper limit of integration, one should first look to the integrand function to know if it's reasonable or not to approximate the improper integral by a proper one. To make the analysis more convenient let's write equation (2.87) in a way so that the integrand function corresponds to a multiplication between the process cross section, $\sigma_v^{e'}$, and a normalised distribution function, say $\tilde{f}$, instead of f which is indeed not normalised. One may obtain

$$k_v^{e'}(T_{\mathrm{tr_e}}) = \sqrt{\frac{8k_B T_{\mathrm{tr_e}}}{\pi m_\mathrm{e}}} \int_0^\infty \sigma_v^{e'}(u)\tilde{f}(u)\, du \;, \tag{3.45}$$

where u is an adimensional variable given by $u = \frac{E}{k_B T_{\mathrm{tr_e}}}$. The normalised distribution function can be shown to be $\tilde{f}(u) = \tilde{f}\left(\frac{E}{k_B T_{\mathrm{tr_e}}}\right) = \frac{E}{k_B T_{\mathrm{tr_e}}} e^{-\frac{E}{k_B T_{\mathrm{tr_e}}}}$. This function goes to zero when $\frac{E}{k_B T_{\mathrm{tr_e}}}$ goes to infinity. And because the variable of dependence is the ratio between E and $k_B T_{\mathrm{tr_e}}$, one can say that the higher the temperature $T_{\mathrm{tr_e}}$, the higher the energy E needed to attain the same small $\tilde{f}$ value. Let's now introduce a new convenient variable: $E_{\max}$, corresponding to the relative kinetic energy value above which there's no process cross section data available. One can say that if $\sigma_v^{e'}(u)$ is a well behaved function (not increasing too much) and $E_{\max}$ is sufficiently large, the contribution of the interval $E \in \,]E_{\max}, +\infty[$ for the integral will be negligible when in comparison with the one associated to the adjunct interval $E \in [0, E_{\max}]$. In

[7] The employed numerical method was the *composite trapezoidal rule*.

such circumstances it would be right to set $E_{\max}$ as the upper limit of the integral.

Figure 3.16 depicts the way that the normalised distribution function $\tilde{f}$ varies with the relative kinetic energy E, for different temperature values, $T_{\mathrm{tr_e}} = 20,000; 40,000; ...; 100,000$ K. Other significant details are present in the figure: the dotted vertical lines correspond to the relative kinetic energy values $E = E_c(T_{\mathrm{tr_e}})$, that if considered as the one in the upper limit of the integration of the normalised distribution function with respect to the variable u, the respective integral would give the value 0.99. Or in mathematical symbolism, $E_c(T_{\mathrm{tr_e}}) = u_{\mathrm{sup}}\, k_B T_{\mathrm{tr_e}} : \int_0^{u_{\mathrm{sup}}} \tilde{f}(u)\, du = 0.99$. These may be interpreted as the cutoff energy values that allows a fulfilment of 99% of the normalised distribution function, for each of the given temperatures. The number 0.99 was chosen by being a number sufficiently near the ideal value: 1. The black solid vertical line in the figure corresponds to the maximum data energy value, $E_{\max} = 50$ eV. And the associated label, $F = 97.945\,\%$, corresponds to the percentage of fulfilment of the distribution function for the temperature $T_{\mathrm{tr_e}} = 100,000$ K by the data energy values. This F value is high, and it is for sure higher for the other temperatures (as said above in other words, the lower the temperature, the higher the percentage of fulfilment of the distribution function, when fixing the energy value in the upper limit of integration).

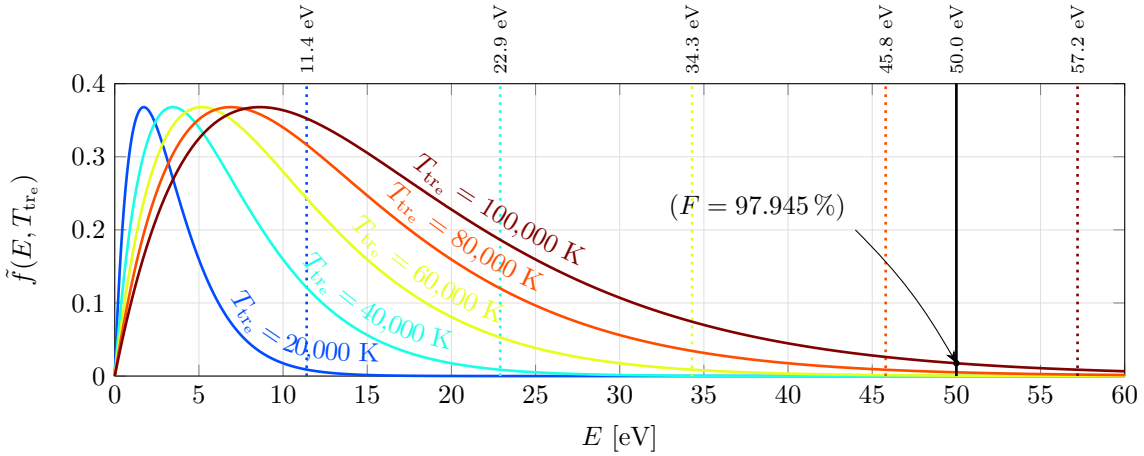

Figure 3.16: Dependence of the normalised distribution function $\tilde{f}\,(E, T_{\mathrm{tr_e}})$, on the relative kinetic energy of collision E, for different temperature values: $T_{\mathrm{tr_e}} = 20,000; 40,000; ...; 100,000$ K. The vertical dotted lines correspond to the cutoff energies associated to a 99 % fulfilment of the distribution function, at the temperature values. The black solid vertical line corresponds to the maximum data energy value $E_{\max}$.

The high F value indicates that the rates $k_v^{e'}(T_{\mathrm{tr_e}})$ can be computed with $E_{\max}$ as the upper limit of integration in equation (3.45), for any temperature $T_{\mathrm{tr_e}} \leq 100,000$ K. If such didn't happened then extrapolation of the rates for the higher temperatures values may be more appropriate than not accounting important contributions of the integral. To have even more confidence about this decision, one can extrapolate the given cross sections to a higher maximum energy $E_{\max}^{\mathrm{extra}} > E_{\max}$ and compute its contribution to the integral $\int_0^{E_{\max}^{\mathrm{extra}}} \sigma_v^{e'}(E)\tilde{f}(E, T_{\mathrm{tr_e}})\, dE = \int_0^{E_{\max}} \sigma_v^{e'}(E)\tilde{f}(E, T_{\mathrm{tr_e}})\, dE + \int_{E_{\max}}^{E_{\max}^{\mathrm{extra}}} \sigma_v^{e',\mathrm{extra}}(E)\tilde{f}(E, T_{\mathrm{tr_e}})\, dE$, being $\sigma_v^{e',\mathrm{extra}}(E)$ the extrapolated cross section function. If $I_{\mathrm{extra}} := \int_{E_{\max}}^{E_{\max}^{\mathrm{extra}}} \sigma_v^{e',\mathrm{extra}}(E)\tilde{f}(E, T_{\mathrm{tr_e}})\, dE$ is negligible when in comparision with $I_{\mathrm{data}} := \int_0^{E_{\max}} \sigma_v^{e'}(E)\tilde{f}(E, T_{\mathrm{tr_e}})\, dE$, then the decision to neglect the former is supported. Although

relying in an analysis that involves extrapolation is risky, it is sometimes the only way to obtain results. Figure 3.17 depicts the case of a linear extrapolation of $\sigma_v^{e'}(E)$ with $v = 0$ and e' =X, showing the two contributions of the integral, I_{data} and I_{extra}, with $T_{\text{tr}_e} = 100,000$ K. Because in this case I_{extra} is one order of magnitude lower than I_{data}, the former may be assumed to be negligible. It was then decided to set $E_{\max}$ as the upper limit of integration in the rates computation formula, for all v and e'.

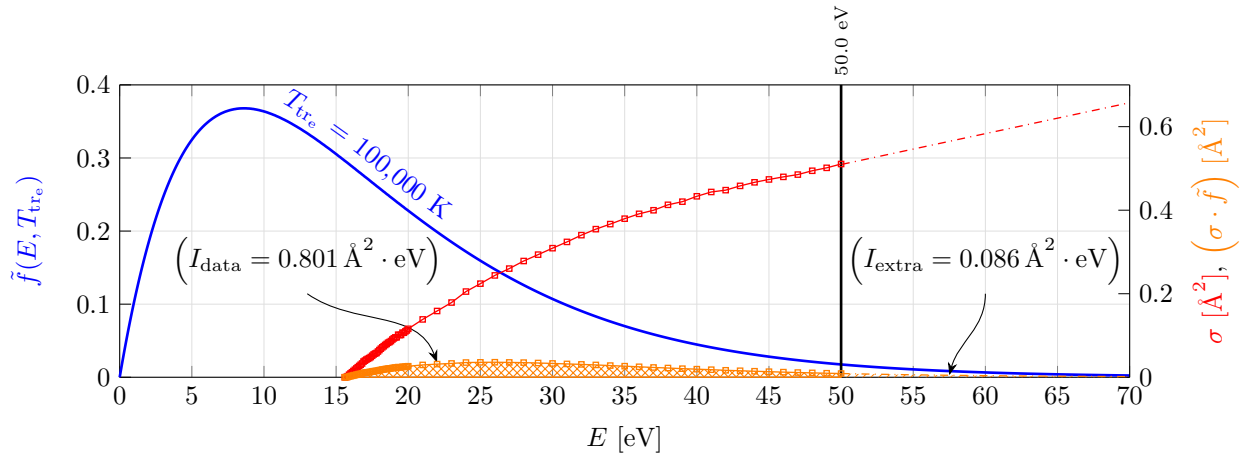

Figure 3.17: A study of the contribution of the data cross section values $\sigma_v^{e'}(E)$ and the extrapolated ones $\sigma_v^{e',\text{extra}}(E)$ to the integral involved in the rates computation formula. The solid curves with squares were generated with the given data and the dashdotted curves were generated with the extrapolated data. The area of the patterned region bellow the $\left(\sigma \cdot \tilde{f}\right)$ curve corresponds to the computed integral. The case depicted here considers $v = 0$, e' =X and $T_{\text{tr}_e} = 100,000$ K.

Figure 3.18 shows the fitted reaction rate curves $k_v^{e',\text{fit}}(T_{\text{tr}_e})$ with the shape of the nine parameters function (2.89), as well as the relative fitting error $\delta_v^{e'}(T_{\text{tr}_e})$, for $v = 0$, 10, 20, 30, 40 and e' =X. The relative fitting error is defined as $\delta_v^{e'}(T_{\text{tr}_e}) := \left[k_v^{e',\text{fit}}(T_{\text{tr}_e}) - k_v^{e'}(T_{\text{tr}_e})\right] / k_v^{e'}(T_{\text{tr}_e})$. The figure shows that the rate coefficients increase with the vibrational quantum number v. Also, the absolute value of the relative error is less than 2%, indicating a good agreement between the fitted curves and the data points.

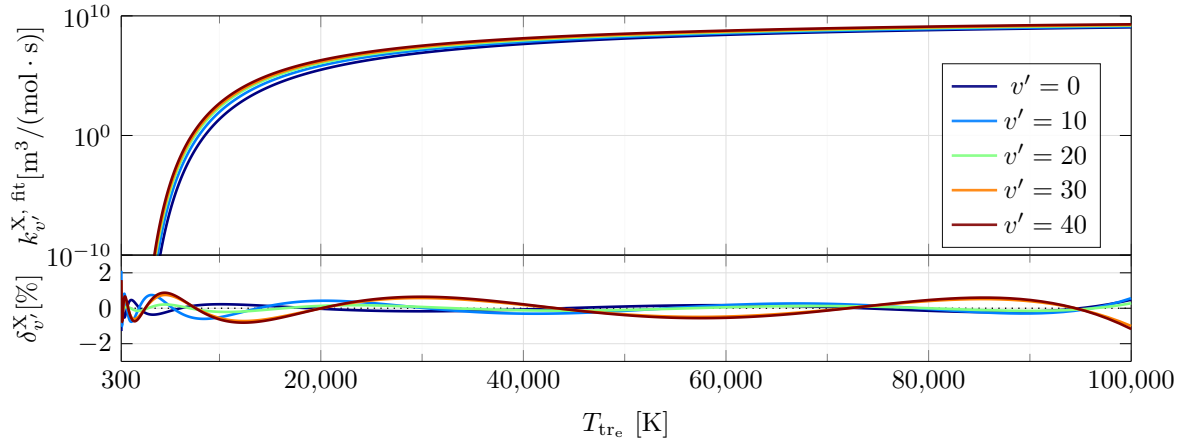

Figure 3.18: Fitted reaction rate curves $k_v^{e',\text{fit}}(T_{\text{tr}_e})$, and relative fitting error $\delta_v^{e'}(T_{\text{tr}_e})$, for $v =$ 0, 10, 20, 30, 40 and $e' = \text{X}^2\Sigma_g^+$.

Note that since the rate coefficients $k_v^{e',\mathrm{fit}}(T_{\mathrm{tr_e}})$ are actually summed on the vibrational level v' of N_2^+, and vibrational-specific rate coefficients were wanted, a vibrational redistribution (VRP) was performed on them.

3.2.8 Dissociative recombination of N_2^+

Dissociative recombination (DR) of molecular nitrogen ions N_2^+ can be represented by the chemical equation

$$N_2^+\left(X^2\Sigma_g^+,\, v\right) + e^- \longrightarrow N\left(e_1'\right) + N\left(e_2'\right)\ , \tag{3.46}$$

being e_1' and e_2' the electronic levels of the produced nitrogen atoms. The reverse of this chemical reaction, i.e. associative ionisation, has a major importance in hypersonic flows since it is one of a few that produce the first free electrons and ions in the matter, transforming the gas into a plasma.

It's important to mention that the chemical equation (3.46) actually solely describes the reactants and final products of a complex reaction, comprising two, three or even four consecutive steps [129]. The two steps process which is termed *direct dissociative recombination* has the form

$$N_2^+\left(X^2\Sigma_g^+,\, v\right) + e^- \longrightarrow N_2\left(e_D',\, v_D'\right) \longrightarrow N\left(e_1'\right) + N\left(e_2'\right)\ . \tag{3.47}$$

In this process, the molecular nitrogen ion N_2^+ captures the electron e^- (hence the designation "recombination"), forming an excited neutral nitrogen molecule N_2 in the electronic level e_D' and vibrational level v_D', which posteriorly dissociates (hence the designation "dissociative") producing two nitrogen atoms in the electronic levels e_1' and e_2'. The three steps process, by the name of *indirect dissociative recombination*, is expressed by the chemical equation

$$N_2^+\left(X^2\Sigma_g^+,\, v\right) + e^- \longrightarrow N_2\left(e_R',\, v_R'\right) \longrightarrow N_2\left(e_D',\, v_D'\right) \longrightarrow N\left(e_1'\right) + N\left(e_2'\right)\ . \tag{3.48}$$

In this process, the transformation of the reactants into the neutral nitrogen molecule in the dissociative state $N_2(e_D',\, v_D')$ is indirect. The recombined neutral nitrogen molecule $N_2(e_R',\, v_R')$ is in a different electronic state called *Rydberg state*, which then transits to the dissociative state. In the four steps process, the transition corresponds to an indirect second-order mechanism: the recombined neutral nitrogen molecule is in a non-Rydberg state $N_2(e',\, v')$, which transits to a Rydberg state $N_2(e_R',\, v_R')$, and in its turn transits to the dissociative state $N_2(e_D',\, v_D')$. The respective chemical equation has the form

$$N_2^+\left(X^2\Sigma_g^+,\, v\right) + e^- \longrightarrow N_2\left(e',\, v'\right) \longrightarrow N_2\left(e_R',\, v_R'\right) \longrightarrow N_2\left(e_D',\, v_D'\right) \longrightarrow N\left(e_1'\right) + N\left(e_2'\right)\ . \tag{3.49}$$

The objective of this section is to assemble rate coefficients $k_v^{e_1',e_2'}(T_{\mathrm{tr_e}})$, each one corresponding to the sum of all of the three possible contributions referred above, in which the molecular nitrogen ion N_2^+ is in the vibrational level v, and the dissociation products are in the electronic levels e_1' and e_2'.

The considered data was the one computed by Guberman [100] which is limited to the ground electronic level of the nitrogen molecular ion N_2^+, to the initial vibrational quantum numbers $v =$

0, 1, 2, 3, and 4 and to a range of free electrons translational temperatures of $T_{\mathrm{tr_e}} \in [100; 3,000]$ K. The considered electronic levels of the dissociative nitrogen molecule N_2 were $e'_D = {}^2\Sigma_g^+$, ${}^{b'1}\Sigma_u^+$, ${}^3\Sigma_u^+$, ${}^1\Pi_u$, ${}^1\Pi_u$, ${}^1\Pi_u$, ${}^3\Pi_u$, ${}^3\Pi_u$, ${}^3\Pi_u$ and ${}^3\Pi_u$. The electronic levels e'_1 and e'_2 for the dissociation products of N_2 in each dissociative state are listed in Table 3.10.

Table 3.10: Electronic levels e'_1 and e'_2 of the dissociation products of the nitrogen molecule N_2 in each considered electronic level e'_D, according to Guberman [100, 130, 131].

e'_D	${}^2\Sigma_g^+$	${}^{b'1}\Sigma_u^+$	${}^3\Sigma_u^+$	${}^1\Pi_u$	${}^1\Pi_u$	${}^1\Pi_u$	${}^3\Pi_u$	${}^3\Pi_u$	${}^3\Pi_u$	${}^3\Pi_u$
e'_1	${}^2D_u$	${}^2D_u$	${}^4S_u$	${}^2D_u$	${}^2D_u$	${}^2D_u$	${}^4S_u$	${}^4S_u$	${}^2D_u$	${}^2D_u$
e'_2	${}^2D_u$	${}^2P_u$	${}^2D_u$	${}^2D_u$	${}^2P_u$	${}^2D_u$	${}^2D_u$	${}^2P_u$	${}^2D_u$	${}^2D_u$

Guberman issues values for the rate coefficients $k_v^{e'_D}(T_{\mathrm{tr_e}})$, i.e. the sum of the contributions (3.47), (3.48), (3.49) for which the molecular nitrogen ion N_2^+ is in the vibrational level v, and the molecular nitrogen N_2 in the dissociative state is in the electronic level e'_D. It can be easily shown that the rate coefficients $k_v^{e'_1,e'_2}(T_{\mathrm{tr_e}})$ correspond to the sum of all rate coefficients $k_v^{e'_D}(T_{\mathrm{tr_e}})$ whose respective electronic levels of the dissociation products associated to the dissociative route e'_D correspond to e'_1 and e'_2: $k_v^{e'_1,e'_2}(T_{\mathrm{tr_e}}) = \sum_{e'_D} k_v^{e'_D}(T_{\mathrm{tr_e}})$. In this very work, Guberman's computed rate coefficients $k_v^{e'_D}(T_{\mathrm{tr_e}})$ were fitted in the domain $T_{\mathrm{tr_e}} \in [300; 3,000]$ K, and the rate coefficients $k_v^{e'_1,e'_2}(T_{\mathrm{tr_e}})$ were then computed by taking into account the respective contributions. These rate coefficients, in their turn, were fitted, being depicted by Figures 3.19, 3.20, 3.21, 3.22 and 3.23, for $v = 0$, 1, 2, 3 and 4, respectively. Modified Arrhenius functions (2.88) were chosen as fitted curves due to their higher stability in the domain not supported by the fitted data (note that in this studied case the non-supported domain $T_{\mathrm{tr_e}} \in [3,000; 100,000]$ K is much bigger than the supported domain $T_{\mathrm{tr_e}} \in [300; 3,000]$ K). However, this decision comes with the drawback of an increase in the values of the relative fitting errors, whose highest absolute value was found to be 16%.

The rate coefficients for the remainder of the vibrational quantum numbers v, i.e. $v = 0$ and $v = 2$ with $(e'_1, e'_2) = ({}^2D_u, {}^2P_u)$, and $v > 4$ with $(e'_1, e'_2) \in \{({}^4S_u, {}^2D_u), ({}^4S_u, {}^2P_u), ({}^2D_u, {}^2D_u), ({}^2D_u, {}^2P_u)\}$, were obtained through a vibrational redistribution procedure based on the rate coefficients for the case $v = 4$.

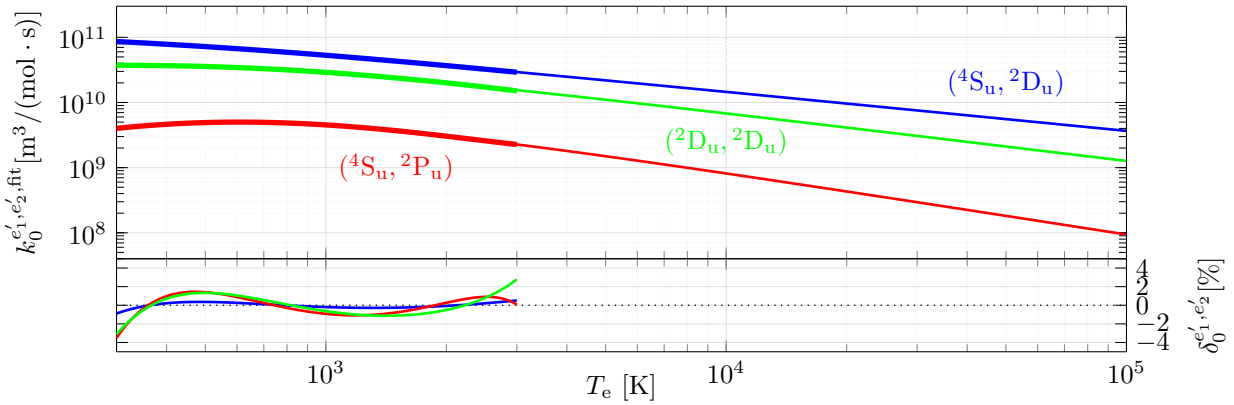

Figure 3.19: Data rate coefficients $k_v^{e_1',e_2'}(T_{\mathrm{tr_e}})$ (thicker lines in the first plot), fitted rate coefficients $k_v^{e_1',e_2',\mathrm{fit}}(T_{\mathrm{tr_e}})$ (thinner lines in the first plot) and relative fitting errors $\delta_v^{e_1',e_2'}(T_{\mathrm{tr_e}})$ (second plot) for $v = 0$ and $(e_1', e_2') \in \{(^4\mathrm{S_u}, ^2\mathrm{D_u}), (^4\mathrm{S_u}, ^2\mathrm{P_u}), (^2\mathrm{D_u}, ^2\mathrm{D_u})\}$.

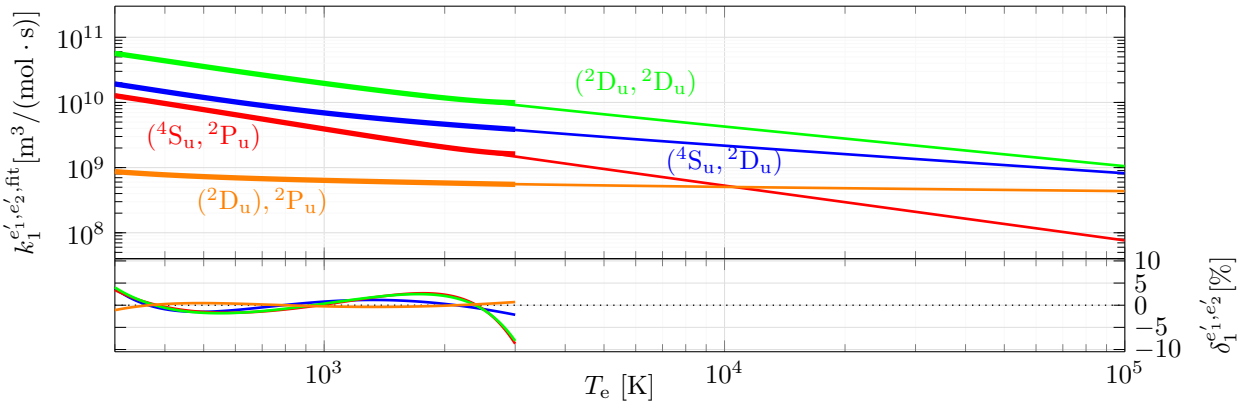

Figure 3.20: Data rate coefficients $k_v^{e_1',e_2'}(T_{\mathrm{tr_e}})$ (thicker lines in the first plot), fitted rate coefficients $k_v^{e_1',e_2',\mathrm{fit}}(T_{\mathrm{tr_e}})$ (thinner lines in the first plot) and relative fitting errors $\delta_v^{e_1',e_2'}(T_{\mathrm{tr_e}})$ (second plot) for $v = 1$ and $(e_1', e_2') \in \{(^4\mathrm{S_u}, ^2\mathrm{D_u}), (^4\mathrm{S_u}, ^2\mathrm{P_u}), (^2\mathrm{D_u}, ^2\mathrm{D_u}), (^2\mathrm{D_u}, ^2\mathrm{P_u})\}$.

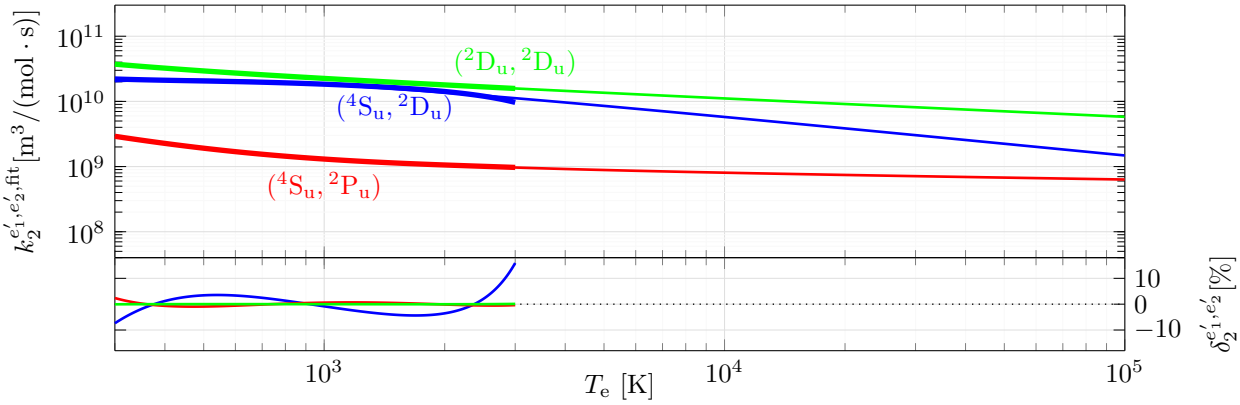

Figure 3.21: Data rate coefficients $k_v^{e_1',e_2'}(T_{\mathrm{tr_e}})$ (thicker lines in the first plot), fitted rate coefficients $k_v^{e_1',e_2',\mathrm{fit}}(T_{\mathrm{tr_e}})$ (thinner lines in the first plot) and relative fitting errors $\delta_v^{e_1',e_2'}(T_{\mathrm{tr_e}})$ (second plot) for $v = 2$ and $(e_1', e_2') \in \{(^4\mathrm{S_u}, ^2\mathrm{D_u}), (^4\mathrm{S_u}, ^2\mathrm{P_u}), (^2\mathrm{D_u}, ^2\mathrm{D_u})\}$.

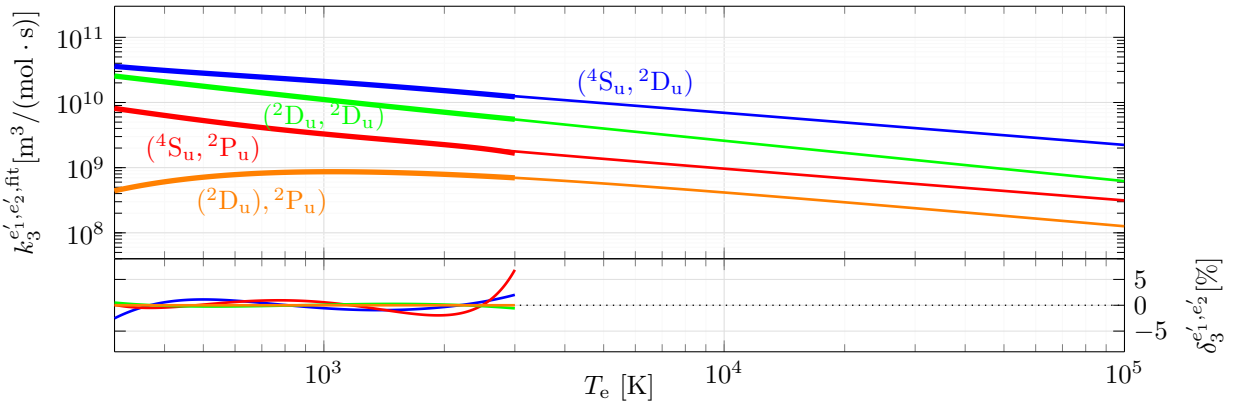

Figure 3.22: Data rate coefficients $k_v^{e'_1,e'_2}(T_{\mathrm{tr_e}})$ (thicker lines in the first plot), fitted rate coefficients $k_v^{e'_1,e'_2,\mathrm{fit}}(T_{\mathrm{tr_e}})$ (thinner lines in the first plot) and relative fitting errors $\delta_v^{e'_1,e'_2}(T_{\mathrm{tr_e}})$ (second plot) for $v = 3$ and $(e'_1, e'_2) \in \{(^4\mathrm{S_u}, {}^2\mathrm{D_u}), (^4\mathrm{S_u}, {}^2\mathrm{P_u}), (^2\mathrm{D_u}, {}^2\mathrm{D_u}), (^2\mathrm{D_u}, {}^2\mathrm{P_u})\}$.

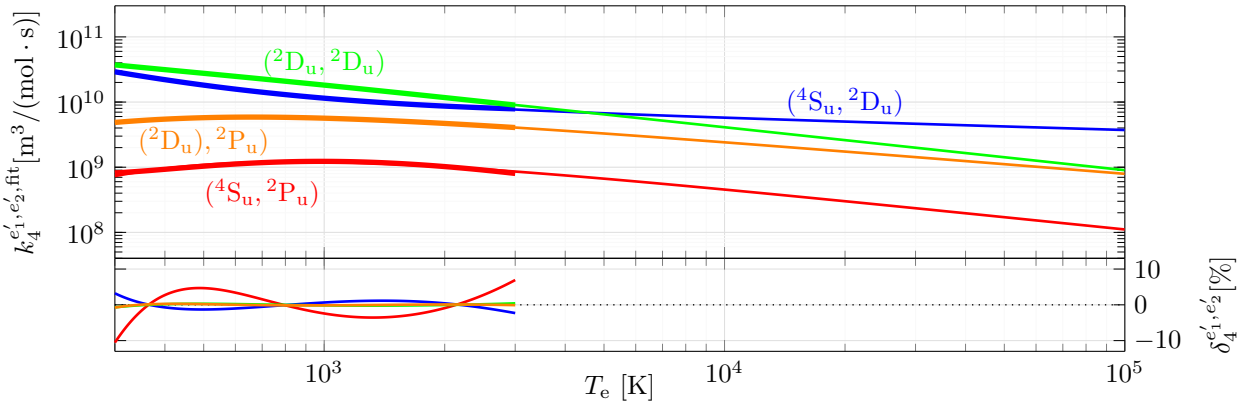

Figure 3.23: Data rate coefficients $k_v^{e'_1,e'_2}(T_{\mathrm{tr_e}})$ (thicker lines in the first plot), fitted rate coefficients $k_v^{e'_1,e'_2,\mathrm{fit}}(T_{\mathrm{tr_e}})$ (thinner lines in the first plot) and relative fitting errors $\delta_v^{e'_1,e'_2}(T_{\mathrm{tr_e}})$ (second plot) for $v = 4$ and $(e'_1, e'_2) \in \{(^4\mathrm{S_u}, {}^2\mathrm{D_u}), (^4\mathrm{S_u}, {}^2\mathrm{P_u}), (^2\mathrm{D_u}, {}^2\mathrm{D_u}), (^2\mathrm{D_u}, {}^2\mathrm{P_u})\}$.

3.2.9 Electronic excitation and ionisation of N and N^+ by electron impact

Rate coefficients for the electronic excitation and ionisation of N and N^+ by electron impact should be obtained through the most accurate data that are currently available, in similarity to the other processes. Therefore, experimental data and results obtained through validated theoretical computations should be preferred to the more simpler semi-empirical correlations. The author considered the theoretical values obtained by Berrington et al. [97] for the process cross sections associated to the excitation of $\mathrm{N}(^4\mathrm{S_u})$ to $\mathrm{N}(^2\mathrm{D_u})$ and $\mathrm{N}(^2\mathrm{P_u})$, as well as the excitation of $\mathrm{N}(^2\mathrm{D_u})$ to $\mathrm{N}(^2\mathrm{P_u})$. The experimental values for the process cross sections obtained by Brook et al. [102] were considered for the ionisation of $\mathrm{N}(^4\mathrm{S_u})$, and the numerical values for the process cross sections computed by Wang et al. [103] were regarded for the ionisation of $\mathrm{N}(^2\mathrm{D_u})$ and $\mathrm{N}(^2\mathrm{P_u})$. Since no experimental or accurate theoretical data were found for the other electronic levels of N, it was necessary to rely on empirical correlations to complete the database. And the same applied for the case electronic excitation of N^+ for all of its electronic levels. Rate coefficients for the excitation and for the ionisation of an atomic particle by electron impact can

be computed through the well-known empirical correlations originally obtained by Drawin [132, 133]. In this work, the Drawin expressions adapted by Panesi et al. [98] were preferred due to their simplicity. The rate coefficient for the electronic excitation of an atomic particle from the e-th electronic level to the e'-th electronic level may then be computed through

$$k_e^{e'}(T_{\mathrm{tr_e}}) = \begin{cases} 4\pi a_0^2 \alpha \sqrt{\frac{8k_B T_{\mathrm{tr_e}}}{\pi m_{\mathrm{e}}}} \left(\frac{\mathrm{Ry}}{k_B T_{\mathrm{tr_e}}}\right)^2 I_1(a_e^{e'}), & \text{if } l_{e'} \neq l_e \ , \\ 4\pi a_0^2 \alpha \sqrt{\frac{8k_B T_{\mathrm{tr_e}}}{\pi m_{\mathrm{e}}}} \left(a_e^{e'}\right)^2 I_2(a_e^{e'}), & \text{if } l_{e'} = l_e \ , \end{cases} \tag{3.50}$$

where a_0 is the *Bohr radius*, $\alpha = 0.05$ is a parameter, Ry is the Rydberg unit of energy, l_e and $l_{e'}$ are the *orbital quantum numbers* of the most energetic electrons in the e and e' electronic levels of the atomic particle, and $a_e^{e'} = (\epsilon_{e'} - \epsilon_e) / (k_B T_{\mathrm{tr_e}})$ is a reduced difference between the final sensible electronic energy $\epsilon_{e'}$ and the initial one ϵ_e. The quantities $I_1(a_e^{e'})$ and $I_2(a_e^{e'})$ are two functions of $a_e^{e'}$ given by

$$I_1(a_e^{e'}) = 0.63255 \left(a_e^{e'}\right)^{-1.6454} e^{-a_e^{e'}} \ , \tag{3.51}$$

$$I_2(a_e^{e'}) = 0.23933 \left(a_e^{e'}\right)^{-1.4933} e^{-a_e^{e'}} \ . \tag{3.52}$$

Also, the rate coefficient for the ionisation of an atomic particle from the e-th electronic may be computed through the expression

$$k_e^{+}(T_{\mathrm{tr_e}}) = 4\pi a_0^2 \alpha^{+} \sqrt{\frac{8k_B T_{\mathrm{tr_e}}}{\pi m_{\mathrm{e}}}} \left(\frac{\mathrm{Ry}}{k_B T_{\mathrm{tr_e}}}\right)^2 I_1(a_e^{+}) \ , \tag{3.53}$$

being $\alpha^{+} = 1$ a parameter, and $a_e^{+} = (\epsilon^{+} - \epsilon_e) / (k_B T_{\mathrm{tr_e}})$ a reduced difference between the *ionisation energy* of the atomic particle from its electronic ground level ϵ^{+} and the initial electronic energy ϵ_e.

One useful property of relations (3.50) and (3.53) is the fact that they can be expressed through a modified Arrhenius function (2.88).

3.2.10 Electronic excitation and ionisation of N and N^+ by heavy particle impact

Due to an overall lack of experimental data for the electronic excitation and ionisation of N and N^+ by heavy particle impact at heavy particle translation temperatures $T_{\mathrm{tr_h}}$ higher than the room one, it was decided to rely on semi-empirical formulae to compute the respective rate coefficients. The relation obtained by Annaloro et al. [84] was regarded:

$$k_f(T_{\mathrm{tr_h}}) = \alpha \sigma_0 \left(\frac{\Delta E}{k_B T_{\mathrm{tr_h}}}\right)^{\beta} \sqrt{\frac{8k_B T_{\mathrm{tr_h}}}{\pi \mu}} e^{-\frac{\Delta E}{k_B T_{\mathrm{tr_h}}}} \ , \tag{3.54}$$

being ΔE the energy defect, i.e. $\Delta E = \epsilon_{e'} - \epsilon_e$ for the case of electronic excitation and $\Delta E = \epsilon^{+} - \epsilon_e$ for the case of ionisation. The variables e, e', ϵ_e, $\epsilon_{e'}$ and ϵ^{+} have the same meaning has the ones declared in previous section §3.2.9. The quantities $\alpha = 0.39534$ and $\beta = 0.3546$ correspond to two convenient parameters, $\sigma_0 = 10^{-20}\,\mathrm{m}^2$ a characteristic cross section, and μ the reduced mass of the collision partners. The collision partners of N and N^+ were considered to be N and N_2 in similarity to the

work of Annaloro et al. [84]. Formula (3.54) is an approximation which is based on a suggestion of Park [134], that tells that the process cross section σ_p depends on the relative kinetic energy of the collision partner E through $\sigma_p(E) = \sigma_0 \ln(E/\Delta E)/(E/\Delta E)$. This suggestion is in its turn based on the empirical correlation established by Lotz [135] for the ionisation of atomic particles by impact with free electrons in the limit $E \gg \Delta E$.

3.3 Radiative processes

3.3.1 Spontaneous emission of the molecular species, N_2 and N_2^+

Level-specific Einstein coefficients for spontaneous emission $A_{e,v}^{e',v'}$ of N_2 and N_2^+ were directly extracted from the literature or were computed through a theoretical expression involving the so-called *sums of the electronic-vibrational transition moments* $\left(\sum R_e^2\right)_{e,v}^{e',v'}$ [136], being these also taken from the literature. Such expression corresponds to [137]

$$A_{e,v}^{e',v'} = \frac{16\pi^3}{3\varepsilon_0 c^3 h} \left(\nu_{e,v}^{e',v'}\right)^3 \frac{\left(\sum R_e^2\right)_{e,v}^{e',v'}}{(2-\delta_{0,\Lambda})\,(2S+1)} \,, \tag{3.55}$$

where $\nu_{e,v}^{e',v'}$ is the frequency of a photon whose energy equals the gap between the initial and final levels, Λ is the initial quantum number for the projection of the total electronic orbital angular momentum vector on the internuclear axis, and S is the initial total spin quantum number as described in §2.8.5.

Table 3.11 assembles all the accounted spontaneous emission processes for the molecular species, listing the name of the *electronic system*[8], the initial and final electronic levels (e and e', respectively), the maximum initial and final vibrational quantum numbers ($v_{\max}$ and $v'_{\max}$, respectively), as well as the reference from which the data were taken from.

[8]The term electronic system is attributed to the set constituted by the initial and the final electronic levels of the particle in the radiative process.

Table 3.11: Molecular spontaneous emission processes for which Einstein coefficients were obtained. The symbol after the reference in the column "Reference" represents the quantity which was extracted from it: Einstein coefficient (if A) or sum of the electronic-vibrational transition moments (if $\sum R_e^2$).

Species	Electronic system	e - e'	$(v_{\max}, v'_{\max})$	Reference
N_2	Vegard-Kaplan	$A^3\Sigma_u^+$ - $X^1\Sigma_g^+$	$(21, 21)$	[138] - A (from [139])
	First positive	$B^3\Pi_g$ - $A^3\Sigma_u^+$	$(21, 21)$	[136] - A
	Wu-Benesch	$W^3\Delta_u$ - $B^3\Pi_g$	$(21, 17)$	[138] - A (from [139])
	IR afterglow	$B'^3\Sigma_u^-$ - $B^3\Pi_g$	$(21, 21)$	[138] - A (from [139])
	Lyman-Birge-Hopfield	$a^1\Pi_g$ - $X^1\Sigma_g^+$	$(21, 21)$	[138] - A (from [139])
	Second positive	$C^3\Pi_u$ - $B^3\Pi_g$	$(4, 21)$	[136] - A
	Birge-Hopfield I	$b^1\Pi_u$ - $X^1\Sigma_g^+$	$(24, 60)$	[140] ([a]) - $\sum R_e^2$
	Worley-Jenkins	${c_3}^1\Pi_u$ - $X^1\Sigma_g^+$	$(11, 60)$	[140] ([a]) - $\sum R_e^2$
	Carroll-Yoshino	$c'_4{}^1\Sigma_g^+$ - $X^1\Sigma_g^+$	$(11, 60)$	[140] ([a]) - $\sum R_e^2$
	Birge-Hopfield II	$b'^1\Sigma_u^+$ - $X^1\Sigma_g^+$	$(46, 60)$	[140] ([a]) - $\sum R_e^2$
	Worley	${o_3}^1\Pi_u$ - $X^1\Sigma_g^+$	$(21, 60)$	[140] ([a]) - $\sum R_e^2$
N_2^+	Meinel	$A^2\Pi_u$ - $X^2\Sigma_g^+$	$(27, 27)$	[138] - A (from [139])
	First negative	$B^2\Sigma_u^+$ - $X^2\Sigma_g^+$	$(12, 21)$	[136] - A
	Second negative	$C^2\Sigma_u^+$ - $X^2\Sigma_g^+$	$(6, 27)$	[138] - A (from [139])

[a] The data were directly sent by Heiko Liebhart to the IPFN group.

3.3.2 Spontaneous emission of the atomic species, N and N^+

For the case of the considered atomic species (N and N^+), level-specific Einstein coefficients for spontaneous emission $A_{s,e^\dagger}^{e^{\dagger\dagger}}$ were extracted from the NIST database [83]. These coefficients are in respect of electronic levels that take into account the fine structure. Since this work considers representative electronic levels computed from the ones with fine structure, it's necessary to compute Einstein coefficients in respect of these representative electronic levels as well. Let's assign the symbol $A_{s,e}^{e'}$ and the name "representative level-specific Einstein coefficient for spontaneous emission" to the resultant Einstein coefficient. The rate of change of the amount concentration of s-th species particles in the representative level e (being this associated to the set of split ones $\{e^\dagger\}$) due to spontaneous emission from that level to the representative level e' (being this associated to the set of split ones $\{e^{\dagger\dagger}\}$) is given by the sum of the rates of change of the amount concentrations of s-th species particles in all the split levels $e^\dagger$ due to spontaneous emission from those levels to all the split levels $e^{\dagger\dagger}$, i.e.

$$\left(\frac{dn_{s,e}}{dt}\right)_{s,e}^{\text{e',se}} = \sum_{e^\dagger,\, e^{\dagger\dagger}} \left(\frac{dn_{s,e^\dagger}}{dt}\right)_{s,e^\dagger}^{e^{\dagger\dagger},\text{se}} , \tag{3.56}$$

which according to (2.93), gives

$$\left(\frac{dn_{s,e}}{dt}\right)_{s,e}^{e',\mathrm{se}} = -\sum_{e^{\dagger},\, e^{\dagger\dagger}} A_{s,e^{\dagger}}^{e^{\dagger\dagger}} n_{s,e^{\dagger}} \ . \tag{3.57}$$

By making the assumption that all states in the set $\{e^{\dagger}\}$ are equiprobable, one gets $n_{s,e^{\dagger}} = (g_{s,e^{\dagger}}/g_{s,e})\, n_{s,e}$, being $g_{s,e^{\dagger}}$ the the degree of degeneracy of the split electronic level $e^{\dagger}$ and $g_{s,e} = \sum_{e^{\dagger}} g_{s,e^{\dagger}}$ the degree of degeneracy of the representative electronic level e. Equation (3.57) is then transformed into

$$\left(\frac{dn_{s,e}}{dt}\right)_{s,e}^{e',\mathrm{se}} = -\left(\sum_{e^{\dagger},\, e^{\dagger\dagger}} \frac{g_{s,e^{\dagger}}}{g_{s,e}} A_{s,e^{\dagger}}^{e^{\dagger\dagger}}\right) n_{s,e} \ , \tag{3.58}$$

Thus, the representative level-specific Einstein coefficient for spontaneous emission is given by

$$A_{s,e}^{e'} = \sum_{e^{\dagger},\, e^{\dagger\dagger}} \frac{g_{s,e^{\dagger}}}{g_{s,e}} A_{s,e^{\dagger}}^{e^{\dagger\dagger}} \ . \tag{3.59}$$

A synopsis on all of the considered atomic spontaneous emission processes is presented in Table 3.12.

Table 3.12: Atomic spontaneous emission processes for which Einstein coefficients were computed.

Species	Number of processes	Reference
N	279 ([a])	NIST[83]
N^{+}	276 ([a])	NIST[83]

[a] As a reminder to the reader: representative Einstein coefficients were computed considering the lumping procedure performed on the split electronic levels.

3.3.3 The line-shape factor

In this work, the line-shape factor $\phi_{\lambda,s,e,v}^{e',v'}$ is considered to be the result of four contributions: Doppler, collisional, Stark, and resonance broadening. One may determine a line-shape factor for each isolated contribution, i.e. $\left(\phi_{\lambda,s,e,v}^{e',v'}\right)_{\mathrm{D}}$, $\left(\phi_{\lambda,s,e,v}^{e',v'}\right)_{\mathrm{col}}$, $\left(\phi_{\lambda,s,e,v}^{e',v'}\right)_{\mathrm{S}}$ and $\left(\phi_{\lambda,s,e,v}^{e',v'}\right)_{\mathrm{res}}$, and then compute the global line-shape factor $\phi_{\lambda,s,e,v}^{e',v'}$ through a triple convolution [47]:

$$\phi_{\lambda,s,e,v}^{e',v'}(\vec{r},t,\lambda) = \int_{-\infty}^{\infty} \left(\phi_{\lambda,s,e,v}^{e',v'}\right)_{\mathrm{D}} (\vec{r},t,\lambda_{s,e,v}^{e',v'}+\lambda') \left\{ \int_{-\infty}^{\infty} \left(\phi_{\lambda,s,e,v}^{e',v'}\right)_{\mathrm{col}} (\vec{r},t,\lambda_{s,e,v}^{e',v'}+\lambda'') \left[\int_{-\infty}^{\infty} \left(\phi_{\lambda,s,e,v}^{e',v'}\right)_{\mathrm{S}} (\vec{r},t,\lambda_{s,e,v}^{e',v'}+\lambda''') \cdot \left(\phi_{\lambda,s,e,v}^{e',v'}\right)_{\mathrm{res}} (\vec{r},t,\lambda-\lambda'-\lambda''-\lambda''')\, d\lambda''' \right] d\lambda'' \right\} d\lambda' \ . \tag{3.60}$$

Let's start by obtaining the line-shape factor for isolated Doppler broadening, $\left(\phi_{\lambda,s,e,v}^{e',v'}\right)_{\mathrm{D}}$. An observer in a referential point which moves with the average speed of the s-th species particles, $\vec{u}_s$, would identify a photon frequency that may be different from the one observed by the s-th species particle that emitted it, due to the relative motion between the two - this phenomenon is termed *Doppler effect*. For convenience, let's consider a reference frame whose origin coincides with the above-mentioned point and whose x axis

has the direction from that point to the emitter. Let's also consider that the radiative process corresponds to a spontaneous emission. The photon frequency observed from the reference point, ν, is related to the photon frequency observed from emitter, $\nu_{s,e,v}^{e',v'}$, through $\nu = \nu_{s,e,v}^{e',v'}(1 - v_x/c)$ [46], being v_x the projection of the relative velocity of the emitter on the x axis. Or, if wavelengths are instead regarded,

$$\lambda = \frac{\lambda_{s,e,v}^{e',v'}}{1 - \frac{v_x}{c}} \ . \tag{3.61}$$

Since the velocity of the heavy particles follows a Maxwell-Boltzmann distribution with a temperature $T_{\mathrm{tr_h}}$, the number density of s-th species particles in the (e, v) vibronic level with a x-component relative velocity $v_x \in [v_x,\, v_x + dv_x]$, per unit of this quantity, is given by

$$\frac{dn_{s,e,v}}{dv_x}(\vec{r}, t, v_x) = n_{s,e,v}(\vec{r}, t)\sqrt{\frac{m_s}{2\pi k_B T_{\mathrm{tr_h}}(\vec{r}, t)}}e^{-\frac{m_s v_x^2}{2k_B T_{\mathrm{tr_h}}(\vec{r},t)}} \ . \tag{3.62}$$

Being the wavelength λ related to the x-component relative velocity v_x through (3.61), one gets $dv_x/d\lambda = c \cdot \lambda_{s,e,v}^{e',v'}/\lambda^2$, and the number density per unit of wavelength of s-th species particles of the (e, v) vibronic level, which if all spontaneously emitted would do it in wavelengths $\lambda \in [\lambda,\, \lambda + d\lambda]$, is

$$\frac{dn_{s,e,v}}{d\lambda}(\vec{r}, t, \lambda) = n_{s,e,v}(\vec{r}, t)\,\frac{\lambda_{s,e,v}^{e',v'}}{\lambda^2}\sqrt{\frac{m_s c^2}{2\pi k_B T_{\mathrm{tr_h}}(\vec{r}, t)}} \cdot e^{-\frac{m_s c^2}{2k_B T_{\mathrm{tr_h}}(\vec{r},t)}\left(\frac{\lambda - \lambda_{s,e,v}^{e',v'}}{\lambda}\right)^2} \ . \tag{3.63}$$

The contribution of the particular spontaneous emission to the emission coefficient corresponds to

$$(j_\lambda)_{s,e,v}^{e',v',\mathrm{se}}(\vec{r}, t, \varphi, \theta, \lambda) = \frac{hc}{\lambda}\frac{A_{s,e,v}^{e',v'}}{4\pi}\frac{dn_{s,e,v}}{d\lambda}(\vec{r}, t, \lambda) = \frac{hc}{\lambda}\frac{A_{s,e,v}^{e',v'}}{4\pi}\left[\frac{\lambda_{s,e,v}^{e',v'}}{\lambda^2}\sqrt{\frac{m_s c^2}{2\pi k_B T_{\mathrm{tr_h}}(\vec{r}, t)}} \cdot e^{-\frac{m_s c^2}{2k_B T_{\mathrm{tr_h}}(\vec{r},t)}\left(\frac{\lambda - \lambda_{s,e,v}^{e',v'}}{\lambda}\right)^2}\right] n_{s,e,v}(\vec{r}, t) \ . \tag{3.64}$$

By comparing (3.64) with the respective term in the global emission coefficient given by (2.107), one may immediately conclude that the line-shape factor for Doppler broadening is given by

$$\left(\phi_{\lambda,s,e,v}^{e',v'}\right)_{\mathrm{D}}(\vec{r}, t, \lambda) = \frac{\lambda_{s,e,v}^{e',v'}}{\lambda^2}\sqrt{\frac{m_s c^2}{2\pi k_B T_{\mathrm{tr_h}}(\vec{r}, t)}} \cdot e^{-\frac{m_s c^2}{2k_B T_{\mathrm{tr_h}}(\vec{r},t)}\left(\frac{\lambda - \lambda_{s,e,v}^{e',v'}}{\lambda}\right)^2} \tag{3.65}$$

It can be shown that the same result holds for the case of induced emission and absorption. Also, it's important to refer here that the relation for the frequency-specific line-shape factor for Doppler broadening $\left(\phi_{\nu,s,e,v}^{e',v'}\right)_{\mathrm{D}} = (\lambda^2/c) \cdot \left(\phi_{\lambda,s,e,v}^{e',v'}\right)_{\mathrm{D}}$ has a well-known form as against the wavelength-specific counterpart:

$$\left(\phi_{\nu,s,e,v}^{e',v'}\right)_{\mathrm{D}}(\vec{r}, t, \nu) = \frac{1}{\nu_{s,e,v}^{e',v'}}\sqrt{\frac{m_s c^2}{2\pi k_B T_{\mathrm{tr_h}}(\vec{r}, t)}} \cdot e^{-\frac{m_s c^2}{2k_B T_{\mathrm{tr_h}}}\left(\frac{\nu - \nu_{s,e,v}^{e',v'}}{\nu_{s,e,v}^{e',v'}}\right)^2} \tag{3.66}$$

Expression (3.66) corresponds to a *Gaussian function* $G(\nu, w_G, \nu_{0G})$ of *half-width at half-maximum*[9]

[9]The half-width at half-maximum of a symmetric function is defined as half of the difference between the two extreme values of the abscissae at which the ordinates are equal to half of their maximum value.

$\left(w_{\nu,s,e,v}^{e',v'}\right)_{\mathrm{D}} = \nu_{s,e,v}^{e',v'}\sqrt{[2\ln 2\, k_B T_{\mathrm{tr_h}}(\vec{r},t)]/(m_s c^2)} := w_G$, centred at $\nu = \nu_{s,e,v}^{e',v'} := \nu_{0G}$ [47]:

$$G(\nu, w_G, \nu_{0G}) = \frac{\sqrt{\ln 2}}{\sqrt{\pi}\cdot w_G}\cdot e^{-\ln 2\left(\frac{\nu-\nu_{0G}}{w_G}\right)^2} \ . \tag{3.67}$$

This function is depicted in Figure 3.24. One may anyway always approximate the wavelength-specific line-shape factor by a Gaussian function [47]. Relation (3.65) may be conveniently expressed through

$$\left(\phi_{\lambda,s,e,v}^{e',v'}\right)_{\mathrm{D}}(\vec{r},t,\lambda) = \frac{\sqrt{\ln 2}}{\sqrt{\pi}\cdot\frac{\left(w_{\nu,s,e,v}^{e',v'}\right)_{\mathrm{D}}\cdot\left(\lambda_{s,e,v}^{e',v'}\right)^2}{c}}\cdot\frac{e^{-\ln 2\left[\frac{\lambda_{s,e,v}^{e',v'}}{\lambda}\cdot\frac{\lambda-\lambda_{s,e,v}^{e',v'}}{\frac{\left(w_{\nu,s,e,v}^{e',v'}\right)_{\mathrm{D}}\cdot\left(\lambda_{s,e,v}^{e',v'}\right)^2}{c}}\right]^2}}{\left(\frac{\lambda}{\lambda_{s,e,v}^{e',v'}}\right)^2} \ , \tag{3.68}$$

which would correspond to a Gaussian function $G(\lambda, \left(w_{\lambda,s,e,v}^{e',v'}\right)_{\mathrm{D}}, \lambda_{s,e,v}^{e',v'})$ of half-width at half-maximum $\left(w_{\lambda,s,e,v}^{e',v'}\right)_{\mathrm{D}} = \left(w_{\nu,s,e,v}^{e',v'}\right)_{\mathrm{D}}\cdot\left(\lambda_{s,e,v}^{e',v'}\right)^2/c = \lambda_{s,e,v}^{e',v'}\sqrt{[2\ln 2\, k_B T_{\mathrm{tr_h}}(\vec{r},t)]/(m_s c^2)}$, centred at $\lambda = \lambda_{s,e,v}^{e',v'}$, if the term $(\lambda/\lambda_{s,e,v}^{e',v'})^2$ in the denominator and the term $\lambda_{s,e,v}^{e',v'}/\lambda$ in the exponent of (3.68) corresponded to 1. Such approximation may indeed be regarded if the condition $[\left(w_{\nu,s,e,v}^{e',v'}\right)_{\mathrm{D}}\cdot\left(\lambda_{s,e,v}^{e',v'}\right)^2/c]/\lambda_{s,e,v}^{e',v'} = \left(w_{\nu,s,e,v}^{e',v'}\right)_{\mathrm{D}}/\nu_{s,e,v}^{e',v'} \ll 1$ holds, i.e. if the half-width at half-maximum of the frequency-specific line-shape factor is much lesser than its centre. It may be shown that this condition is always satisfied.

For the case of collisional broadening, the formula for the frequency-specific line-shape factor based on the *electron theory of Lorentz* and referred by Penner [46], was considered:

$$\left(\phi_{\nu,s,e,v}^{e',v'}\right)_{\mathrm{col}}(\vec{r},t,\nu) = \frac{1}{\pi\frac{Z_{\mathrm{opt},s,e,v}+Z_{\mathrm{opt},s,e',v'}}{2\pi}}\cdot\frac{1}{1+\left(\frac{\nu-\nu_{s,e,v}^{e',v'}}{\frac{Z_{\mathrm{opt},s,e,v}+Z_{\mathrm{opt},s,e',v'}}{2\pi}}\right)^2} \ , \tag{3.69}$$

being $Z_{\mathrm{opt},s,e,v}$ the optical collisional frequency per s-th species particle in (e,v) with the other particles:

$$Z_{\mathrm{opt},s,e,v} = \left(\sum_{q\in\{\mathrm{h}\},e'',v''}\frac{n_{q,e'',v''}\cdot\sigma_{\mathrm{opt},s,e,v}^{q,e'',v''}}{1+\delta_{s,e,v}^{q,e'',v''}}\sqrt{\frac{8k_B T_{\mathrm{tr_h}}}{\pi\,\mu_{s,q}}}\right) + n_{\mathrm{e}}\cdot\sigma_{\mathrm{opt},s,e,v}^{\mathrm{e}}\sqrt{\frac{8k_B T_{\mathrm{tr_e}}}{\pi\, m_{\mathrm{e}}}} \ . \tag{3.70}$$

The sum in (3.70) is done in all the heavy species, their electronic levels and vibrational levels. The quantity $\delta_{s,e,v}^{q,e'',v''}$ is a Kronecker delta giving 1 if $(s,e,v) = (q,e'',v'')$, and 0 if not. The quantity $\sigma_{\mathrm{opt},s,e,v}^{q,e'',v''}$ corresponds to the *optical collisional cross section* for a collision between a particle of the s-th species in (e,v) with a particle of the q-th species in (e'',v''). And the quantity $\sigma_{\mathrm{opt},s,e,v}^{\mathrm{e}}$ corresponds to $\sigma_{\mathrm{opt},s,e,v}^{q,e'',v''}$ for the case of the q-th species being a free electron. Few are the reported values for these optical collisional cross sections, and moreover, there's one for each radiative transition. Penner [46] refers that, according to the available data, such quantities have the same order of magnitude as the respective collisional cross sections $\sigma_{s,e,v}^{q,e'',v''}$. It was decided to consider the approximation $\sigma_{\mathrm{opt},s,e,v}^{q,e'',v''} \approx \sigma_{s,e,v}^{q,e'',v''}$, and to use the data of Svehla [54] to obtain the latter. No data were found for the case of collisions with free electrons, and therefore, its contribution to the optical collisional frequency per particle was disregarded. Note that $Z_{\mathrm{opt},s,e',v'}$ in (3.69) corresponds to the optical collisional frequency per particle of s-th species particles in

(e', v') with the other particles. It is given by (3.70) with e and v substituted by e' and v', respectively. It is worthy to mention that expression (3.69) corresponds to a *Lorentzian function* $L(\nu, w_L, \nu_{0L})$ of half-width at half-maximum $\left(w^{e',v'}_{\nu,s,e,v}\right)_{\text{col}} = (Z_{\text{opt},s,e,v} + Z_{\text{opt},s,e',v'})/(2\pi) := w_L$, centred at $\nu = \nu^{e',v'}_{s,e,v} := \nu_{0L}$ [47], as depicted in Figure 3.24. The function is given by

$$L(\nu, w_L, \nu_{0L}) = \frac{1}{\pi w_L} \cdot \frac{1}{1 + \left(\frac{\nu - \nu_{0L}}{w_L}\right)^2} \ . \tag{3.71}$$

For the case of Stark broadening, it was decided to consider in this work the approach of Johnston [141], which solely accounts the contribution of free electrons. The associated frequency-specific line-shape factor $\left(\phi^{e'v'}_{\nu,s,e,v}\right)_{\text{S}}$ is given by a Lorentzian function $L(\nu, w_L, \nu_{0L})$ of half-width at half-maximum $\left(w^{e',v'}_{\nu,s,e,v}\right)_{\text{S}}$, centred at $\nu = \nu^{e',v'}_{s,e,v}$. By expressing the frequency-specific line-shape factor through

$$\left(\phi^{e'v'}_{\nu,s,e,v}\right)_{\text{S}}(\vec{r}, t, \nu) = \frac{1}{\pi \left(w^{e',v'}_{\nu,s,e,v}\right)_{\text{S}}} \cdot \frac{1}{1 + \left[\frac{\nu - \nu^{e',v'}_{s,e,v}}{\left(w^{e',v'}_{\nu,s,e,v}\right)_{\text{S}}}\right]^2} \ , \tag{3.72}$$

and noting that $d\nu/d\lambda = -c/\lambda^2$, one may show that the wavelength-specific counterpart is given by

$$\left(\phi^{e'v'}_{\lambda,s,e,v}\right)_{\text{S}}(\vec{r}, t, \lambda) = \frac{c}{\lambda^2}\left(\phi^{e'v'}_{\nu,s,e,v}\right)_{\text{S}}(\vec{r}, t, \nu) = \frac{c}{\pi \left(w^{e',v'}_{\nu,s,e,v}\right)_{\text{S}} \left(\lambda^{e',v'}_{s,e,v}\right)^2} \cdot \frac{1}{\left(\frac{\lambda}{\lambda^{e',v'}_{s,e,v}}\right)^2 + \left[\frac{c}{\left(w^{e',v'}_{\nu,s,e,v}\right)_{\text{S}} \lambda^{e',v'}_{s,e,v}} \cdot \frac{\lambda - \lambda^{e',v'}_{s,e,v}}{\lambda^{e',v'}_{s,e,v}}\right]^2} \ . \tag{3.73}$$

If the term $(\lambda/\lambda^{e',v'}_{s,e,v})^2$ in the denominator of (3.73) corresponded to 1, the wavelength-specific line-shape factor would also correspond to a Lorentzian function $L(\lambda, w_L, \lambda_{0L})$, being this of half-width at half-maximum $\left(w^{e',v'}_{\lambda,s,e,v}\right)_{\text{S}} = [(\lambda^{e',v'}_{s,e,v})^2/c] \cdot \left(w^{e',v'}_{\nu,s,e,v}\right)_{\text{S}} := w_L$, centred at $\lambda = \lambda^{e',v'}_{s,e,v} := \lambda_{0L}$. Such function may be indeed regarded as an approximation for (3.73) if the half-width at half-maximum of the frequency-specific line-shape factor is much lesser than its centre [47]. Johnston does consider this approximation, expressing the wavelength-specific line-shape factor as

$$\left(\phi^{e'v'}_{\lambda,s,e,v}\right)_{\text{S}}(\vec{r}, t, \lambda) = \frac{1}{\pi \left(w^{e',v'}_{\lambda,s,e,v}\right)_{\text{S}}} \cdot \frac{1}{1 + \left[\frac{\lambda - \lambda^{e',v'}_{s,e,v}}{\left(w^{e',v'}_{\lambda,s,e,v}\right)_{\text{S}}}\right]^2} \ . \tag{3.74}$$

The half-width at half-maximum regarded by Johnston has a form identical to the one of Park [142]:

$$\left(w^{e',v'}_{\lambda,s,e,v}\right)_{\text{S}} = \left(w^{e',v'}_{\lambda,s,e,v,\text{ref}}\right)_{\text{S}} \left(\frac{T_{\text{tr}_\text{e}}}{T_{\text{tr}_\text{e},\text{ref}}}\right)^n \cdot \left(\frac{n_\text{e}}{n_{\text{e},\text{ref}}}\right) \ , \tag{3.75}$$

where $\left(w^{e',v'}_{\lambda,s,e,v,\text{ref}}\right)_{\text{S}}$ is the half-width at half-maximum at a free electron translational temperature $T_{\text{tr}_\text{e}} = 10,000\,\text{K} := T_{\text{tr}_\text{e},\text{ref}}$ and at a free electron number density $n_\text{e} = 10^{16}\,\text{cm}^{-3} := n_{\text{e},\text{ref}}$. Park assumes a dependence of the half-width at half-maximum on the free electron translational temperature which is of the power type - this is expressed through the exponent n in (3.75). Moreover, relation (3.75) shows a dependence of the half-width at half-maximum on the free electron number density which is linear, being

this behaviour also mentioned by Griem in his work [143]. Park [142] solely treated the case of argon, obtaining the exponent $n = 0.33$ by fitting the curve (3.75) to the values of half-width at half-maximum $\left(w^{e',v'}_{\lambda,s,e,v}\right)_{\mathrm{S}}$ at $n_{\mathrm{e}} = n_{\mathrm{e,ref}}$ for different $T_{\mathrm{tr_e}}$, issued by Griem [143–145]. Johnston considers this exponent value to be also acceptable for the case of the nitrogen and oxygen atoms. In this work, it was decided to take such assumption one step further by regarding this same value for all the considered species. Johnston then considers a model for the reference half-width at half-maximum of the form

$$\left(w^{e',v'}_{\lambda,s,e,v,\mathrm{ref}}\right)_{\mathrm{S}} = \frac{C \cdot \left(\lambda^{e',v'}_{s,e,v}\right)^2}{\left(\epsilon^+_s - \epsilon_{s,e,v}\right)^n} \ , \tag{3.76}$$

being ϵ^+_s the ionisation energy of the a s-th species particle from its ground level, and C and n correspond to some constants. The values for the ionisation energies of all the species considered in this work were taken from the literature, being listed in Table 3.13.

Table 3.13: Ionisation energies from the ground level of N, N^+, N_2 and N_2^+.

s	ϵ^+_s [eV]	Reference
N	14.534	Biémont et al. [146]
N^+	29.601	Biémont et al. [146]
N_2	15.581	Trickl et al. [147]
N_2^+	27.9	Bahati et al. [148]

Model (3.76) is a variant of the one considered by Cowley in its theoretical work [149]. Johnston obtained $C = 1.69 \times 10^{10}\ [(\text{“cm}^{-1}\text{”})^{2.623}/\mathrm{cm}^2] \cdot \mathrm{cm}$ and $n = 2.623$ by fitting the curve (3.76) to the values of $\left(w^{e',v'}_{\lambda,s,e,v,\mathrm{ref}}\right)_{\mathrm{S}}$ for the nitrogen and oxygen atoms, issued by Griem [143] and by Wilson and Nicolet [150]. And by regarding such result in this work, the wavelength and frequency-specific half-widths at half-maxima for Stark broadening are ultimately given by

$$\left(w^{e',v'}_{\lambda,s,e,v}\right)_{\mathrm{S}} = 1.69 \times 10^{10} \frac{\left(\frac{\lambda^{e',v'}_{s,e,v}}{\mathrm{cm}}\right)^2}{\left(\frac{\epsilon^+_s}{\text{“cm}^{-1}\text{”}} - \frac{\epsilon_{s,e,v}}{\text{“cm}^{-1}\text{”}}\right)^{2.623}} \left(\frac{T_{\mathrm{tr_e}}}{10,000\,\mathrm{K}}\right)^{0.33} \cdot \left(\frac{n_{\mathrm{e}}}{10^{16}\,\mathrm{cm}^{-3}}\right) \mathrm{cm} \ , \tag{3.77}$$

and

$$\left(w^{e',v'}_{\nu,s,e,v}\right)_{\mathrm{S}} = \frac{5.066 \times 10^{20}}{\left(\frac{\epsilon^+_s}{\text{“cm}^{-1}\text{”}} - \frac{\epsilon_{s,e,v}}{\text{“cm}^{-1}\text{”}}\right)^{2.623}} \left(\frac{T_{\mathrm{tr_e}}}{10,000\,\mathrm{K}}\right)^{0.33} \cdot \left(\frac{n_{\mathrm{e}}}{10^{16}\,\mathrm{cm}^{-3}}\right) \mathrm{Hz} \ , \tag{3.78}$$

respectively.

For the case of resonance broadening, the theory developed by Griem [145] was considered. The frequency-specific line-shape factor corresponds to a Lorentzian function centred at $\nu = \nu^{e',v'}_{s,e,v}$. Griem issues a very approximate estimate for the half-width at half-maximum of the angular frequency-specific counterpart, which is given by

$$\left(w^{e',v'}_{\omega,s,e,v}\right)_{\mathrm{res}} = 3\pi \sqrt{\frac{g_{s,e',v'}}{g_{s,e,v}}} \frac{\mathrm{e}^2 f^{e,v}_{s,e',v'}}{4\pi\varepsilon_0 m_{\mathrm{e}}\, \omega^{e',v'}_{s,e,v}} n_p \ . \tag{3.79}$$

In (3.79), $\omega_{s,e,v}^{e',v'} = 2\pi\,\nu_{s,e,v}^{e',v'}$ corresponds to the angular frequency of a photon with the same energy as the gap between the initial and final levels, $f_{s,e',v'}^{e,v}$ is the so-called *absorption oscillator strength*, and n_p is the number density of perturbing particles. It was decided in this work to approximate the latter quantity by the number density of particles in the lower level, i.e. $n_p \approx n_{s,e',v'}$, as Potter [151] and Johnston [141] also did. It can be shown that the absorption oscillator strength $f_{s,e',v'}^{e,v}$ and the Einstein coefficient for spontaneous emission $A_{s,e,v}^{e',v'}$ are related to each other through [145]

$$A_{s,e,v}^{e',v'} = \frac{\mathrm{e}^2 \left(\omega_{s,e,v}^{e',v'}\right)^2}{2\pi\varepsilon_0 m_\mathrm{e} c^3} \frac{g_{s,e',v'}}{g_{s,e,v}} f_{s,e',v'}^{e,v} \ . \tag{3.80}$$

And since $\omega = 2\pi\nu$, one has $d\omega/d\nu = 2\pi$, meaning that the frequency-specific line-shape factor $\left(\phi_{\nu,s,e,v}^{e',v'}\right)_\mathrm{res}$ is related to the angular frequency-specific counterpart $\left(\phi_{\omega,s,e,v}^{e',v'}\right)_\mathrm{res}$ simply by $\left(\phi_{\nu,s,e,v}^{e',v'}\right)_\mathrm{res} = 2\pi \left(\phi_{\omega,s,e,v}^{e',v'}\right)_\mathrm{res}$. The half-width at half-maximum of the former is, in its turn, given by

$$\left(w_{\nu,s,e,v}^{e',v'}\right)_\mathrm{res} = \frac{\left(w_{\omega,s,e,v}^{e',v'}\right)_\mathrm{res}}{2\pi} = 3\pi \sqrt{\frac{g_{s,e,v}}{g_{s,e',v'}}} \frac{c^3\, A_{s,e,v}^{e',v'}}{32\pi^4 \left(\nu_{s,e,v}^{e',v'}\right)^3} n_{s,e',v'} \ . \tag{3.81}$$

Being all the broadening mechanisms here described, it is now the time to obtain the global line-shape factor defined by (3.60). By sticking to the assumption that the half-width at half-maximum of the frequency-specific line-shape factor for each isolated line broadening mechanism is much lesser than its centre, one gets

$$\begin{aligned}
\phi_{\lambda,s,e,v}^{e',v'}(\vec{r},t,\lambda) = \int_{-\infty}^{\infty} \left(\phi_{\lambda,s,e,v}^{e',v'}\right)_\mathrm{D} (\vec{r},t,\lambda_{s,e,v}^{e',v'} + \lambda') \left\{ \int_{-\infty}^{\infty} \left(\phi_{\lambda,s,e,v}^{e',v'}\right)_\mathrm{col} (\vec{r},t,\lambda_{s,e,v}^{e',v'} + \lambda'') \left[\right.\right. \\
\left.\left. \int_{-\infty}^{\infty} \left(\phi_{\lambda,s,e,v}^{e',v'}\right)_\mathrm{S} (\vec{r},t,\lambda_{s,e,v}^{e',v'} + \lambda''') \cdot \left(\phi_{\lambda,s,e,v}^{e',v'}\right)_\mathrm{res} (\vec{r},t,\lambda - \lambda' - \lambda'' - \lambda''')\, d\lambda''' \right] d\lambda'' \right\} d\lambda' = \\
= \int_{-\infty}^{\infty} G(\lambda_{s,e,v}^{e',v'} + \lambda', \left(w_{\lambda,s,e,v}^{e',v'}\right)_\mathrm{D}, \lambda_{s,e,v}^{e',v'}) \left\{ \int_{-\infty}^{\infty} L(\lambda_{s,e,v}^{e',v'} + \lambda'', \left(w_{\lambda,s,e,v}^{e',v'}\right)_\mathrm{col}, \lambda_{s,e,v}^{e',v'}) \left[\right.\right. \\
\left.\left. \int_{-\infty}^{\infty} L(\lambda_{s,e,v}^{e',v'} + \lambda''', \left(w_{\lambda,s,e,v}^{e',v'}\right)_\mathrm{S}, \lambda_{s,e,v}^{e',v'}) \cdot L(\lambda - \lambda' - \lambda'' - \lambda''', \left(w_{\lambda,s,e,v}^{e',v'}\right)_\mathrm{res}, \lambda_{s,e,v}^{e',v'})\, d\lambda''' \right] d\lambda'' \right\} d\lambda' \ .
\end{aligned} \tag{3.82}$$

It can be shown that the convolution of two Lorentzian functions is also a Lorentzian function whose half-width at half-maximum and centre are the sum of the respective ones associated to the former. Therefore, (3.82) is transformed into

$$\phi_{\lambda,s,e,v}^{e',v'}(\vec{r},t,\lambda) = \int_{-\infty}^{\infty} G(\lambda_{s,e,v}^{e',v'} + \lambda', \left(w_{\lambda,s,e,v}^{e',v'}\right)_\mathrm{D}, \lambda_{s,e,v}^{e',v'}) \cdot L(\lambda - \lambda', \left(w_{\lambda,s,e,v}^{e',v'}\right)_\mathrm{col} + \left(w_{\lambda,s,e,v}^{e',v'}\right)_\mathrm{S} + \left(w_{\lambda,s,e,v}^{e',v'}\right)_\mathrm{res}, \lambda_{s,e,v}^{e',v'})\, d\lambda' \ . \tag{3.83}$$

The improper integral that appears in (3.83) corresponds to a *Voigt function* of Gaussian and Lorentzian half-widths at half-maxima $w_G = \left(w_{\lambda,s,e,v}^{e',v'}\right)_\mathrm{D}$ and $w_L = \left(w_{\lambda,s,e,v}^{e',v'}\right)_\mathrm{col} + \left(w_{\lambda,s,e,v}^{e',v'}\right)_\mathrm{S} + \left(w_{\lambda,s,e,v}^{e',v'}\right)_\mathrm{res}$, centred

at $\lambda = \lambda_{s,e,v}^{e',v'} := \lambda_{0V}$ [47]:

$$V(\lambda, w_G, w_L, \lambda_{0V}) = \int_{-\infty}^{+\infty} G(\lambda_{0V} + \lambda', w_G, \lambda_{0V}) \cdot L(\lambda - \lambda', w_L, \lambda_{0V})\, d\lambda' \,. \tag{3.84}$$

This function is depicted in Figure 3.24.

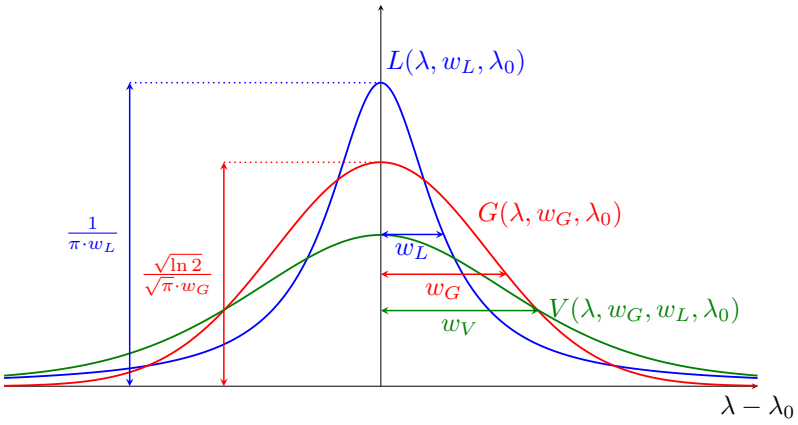

Figure 3.24: Gaussian function $G(\lambda, w_G, \lambda_{0G})$ and Lorentzian function $L(\lambda, w_L, \lambda_{0L})$ for illustrative half-widths at half-maxima w_G and $w_L = (1/2)\, w_G$, and equal centres $\lambda_{0G} = \lambda_{0L} = \lambda_0$, as well as the resultant Voigt function $V(\lambda, w_G, w_L, \lambda_0)$.

The integral in (3.84) is not analytically solvable, and therefore, one should consider a numerical method such as the trapezoidal integral rule, or an empirical approximation such as the formula proposed by Whiting [152] to account it. Although the former may give better results, it requires much more computational resources than the latter. The empirical formula of Whiting was then chosen, which according to his words, matches the exact function within 5 per cent at worst. The approximation consists in a linear combination of both Lorentzian and Gaussian functions with the same half-widths at half-maxima and centres as the resulting ones for the Voigt function, plus a corrective term:

$$\begin{aligned} V(\lambda, w_G, w_L, \lambda_{0V}) \approx \frac{1}{2\, w_V \left[1.065 + 0.447 \frac{w_L}{w_V} + 0.058 \left(\frac{w_L}{w_V}\right)^2\right]} \Bigg\{ \left(1 - \frac{w_L}{w_V}\right) e^{-\ln 2 \left(\frac{\lambda - \lambda_{0V}}{w_V}\right)^2} + \frac{w_L}{w_V} \cdot \frac{1}{1 + \left(\frac{\lambda - \lambda_{0V}}{w_V}\right)^2} \\ + 0.016 \left(1 - \frac{w_L}{w_V}\right) \frac{w_L}{w_V} \left[e^{-0.084 \left| \frac{\lambda - \lambda_{0V}}{w_V} \right|^{2.25}} - \frac{10}{10 + 0.210 \left| \frac{\lambda - \lambda_{0V}}{w_V} \right|^{2.25}} \right] \Bigg\} \,. \end{aligned} \tag{3.85}$$

Although Whiting also issues a formula for the half-width at half-maximum of the Voigt function w_V with an accuracy of about 1 per cent, it was decided to consider here the one obtained by Olivero and Longbothum [153], since it has an even higher accuracy, of about 0.01 per cent. Such formula is expressed by

$$w_V \approx (w_L + w_G) \left\{ 1 - 0.18121 \left[1 - \left(\frac{w_L - w_G}{w_L + w_G} \right)^2 \right] - \left(0.023665\, e^{0.6 \frac{w_L - w_G}{w_L + w_G}} + 0.00418\, e^{-1.9 \frac{w_L - w_G}{w_L + w_G}} \right) \sin\left(\pi \frac{w_L - w_G}{w_L + w_G} \right) \right\} \,. \tag{3.86}$$

One may ultimately write

$$\phi^{e',v'}_{\lambda,s,e,v}(\vec{r},t,\lambda) = V(\lambda, \left(w^{e',v'}_{\lambda,s,e,v}\right)_{\mathrm{D}}, \left(w^{e',v'}_{\lambda,s,e,v}\right)_{\mathrm{col}} + \left(w^{e',v'}_{\lambda,s,e,v}\right)_{\mathrm{S}} + \left(w^{e',v'}_{\lambda,s,e,v}\right)_{\mathrm{res}}, \lambda^{e',v'}_{s,e,v}) \ . \tag{3.87}$$

3.4 Simulations of post-shock flows generated by a shock tube

Herein a detailed description will be made with respect to the implementation of the zero and one-dimensional vibronic-specific state-to-state models (introduced in §2.6.4 and §2.6.5, respectively) in simulations of post-shock flows generated by a shock tube. The studied experiment corresponded to the test 62 of the EAST shock tube done in 2018, being the respective results issued by Brandis and Cruden [43]. For the case of the zero-dimensional model, the fluid flow governing equations to deal with correspond to (2.148), (2.151) and (2.152), which are here rewritten for convenience:

$$\begin{cases} \dfrac{dc_{s,e,v}}{dt} = \dfrac{\dot{\omega}_{s,e,v}}{\rho}, \qquad \forall s,\ v \text{ and } e \ , & \text{(3.88a)} \\ \dfrac{dT_{\mathrm{tr_h}}}{dt} = -\dfrac{\dot{\Omega}_{\mathrm{rad}} + \left(\sum_s \dot{\Omega}^{\mathrm{int}}_{s,\mathrm{e}}\right) + \left(\sum_{s\in\{\mathrm{h}\}} \dot{\omega}_s e_s\right) + \left[\sum_{s\in\{\mathrm{h}\},e,v} \left(\dot{\omega}_{s,e,v} - \frac{c_{s,e,v}}{c_s}\dot{\omega}_s\right) \frac{\epsilon_{s,\text{el-vib},e,v}}{m_s}\right]}{\rho\left(\sum_{s\in\{\mathrm{h}\}} c_s C_{V,s,\text{tr-rot}}\right)} \ , & \text{(3.88b)} \\ \dfrac{dT_{\mathrm{tr_e}}}{dt} = \dfrac{\left(\sum_s \dot{\Omega}^{\mathrm{int}}_{s,\mathrm{e}}\right) - \dot{\omega}_{\mathrm{e}} e_{\mathrm{e}}}{\rho c_{\mathrm{e}} C_{V,\mathrm{e}}} \ . & \text{(3.88c)} \end{cases}$$

And for the case of the one-dimensional model, the fluid flow governing equations to deal with correspond to (2.155), (2.156), (2.159) and (2.160), i.e.

$$\begin{cases} \dfrac{dc_{s,e,v}}{dx} = \dfrac{\dot{\omega}_{s,e,v}}{\rho u}, \qquad \forall s,\ e \text{ and } v \ , & \text{(3.89a)} \\ \left(\dfrac{\rho u^2}{p} - 1\right)\dfrac{du}{dx} + \dfrac{u}{p}\left[\left(\sum_{s\in\{\mathrm{h}\}} \dfrac{p_s}{T_{\mathrm{tr_h}}}\dfrac{dT_{\mathrm{tr_h}}}{dx}\right) + \dfrac{p_{\mathrm{e}}}{T_{\mathrm{tr_e}}}\dfrac{dT_{\mathrm{tr_e}}}{dx}\right] = -\dfrac{1}{p\rho}\left[\left(\sum_{s\in\{\mathrm{h}\}} \dfrac{\dot{\omega}_s p_s}{c_s}\right) + \dfrac{\dot{\omega}_{\mathrm{e}} p_{\mathrm{e}}}{c_{\mathrm{e}}}\right] \ , & \text{(3.89b)} \\ \dfrac{dT_{\mathrm{tr_h}}}{dx} + \dfrac{\left(\sum_{s\in\{\mathrm{h}\}} c_s\right) u}{\sum_{s\in\{\mathrm{h}\}} c_s C_{p,s,\text{tr-rot}}} \cdot \dfrac{du}{dx} = \\ = -\dfrac{\dot{\Omega}_{\mathrm{rad}} + \left(\sum_s \dot{\Omega}^{\mathrm{int}}_{s,\mathrm{e}}\right) + \left[\sum_{s\in\{\mathrm{h}\}} \dot{\omega}_s \left(h_s + \frac{1}{2}u^2\right)\right] + \left[\sum_{s\in\{\mathrm{h}\},e,v} \left(\dot{\omega}_{s,e,v} - \frac{c_{s,e,v}}{c_s}\dot{\omega}_s\right) \frac{\epsilon_{s,\text{el-vib},e,v}}{m_s}\right]}{\rho u\left(\sum_{s\in\{\mathrm{h}\}} c_s C_{p,s,\text{tr-rot}}\right)} \ , & \text{(3.89c)} \\ \dfrac{dT_{\mathrm{tr_e}}}{dx} + \dfrac{u}{C_{p,\mathrm{e}}}\dfrac{du}{dx} = \dfrac{\left(\sum_s \dot{\Omega}^{\mathrm{int}}_{s,\mathrm{e}}\right) - \dot{\omega}_{\mathrm{e}}\left(h_{\mathrm{e}} + \frac{1}{2}u^2\right)}{\rho u c_{\mathrm{e}} C_{p,\mathrm{e}}} \ . & \text{(3.89d)} \end{cases}$$

The unknowns of the equations for the zero-dimensional model are $c_{s,v,e}$ ($\forall s$, v and e), $T_{\mathrm{tr_h}}$ and $T_{\mathrm{tr_e}}$. And the unknowns of the equations for the one-dimensional model are all of these plus the x-component of the flow velocity vector u. Note that in the case of the zero-dimensional model, the mixture mass density ρ is an invariable and its value may be taken as the one attributed with respect to the initial conditions. In the case of the one-dimensional model, ρ is given by equation (2.154).

Initial values need to be assigned to $c_{s,v,e}$, $T_{\mathrm{tr_h}}$, $T_{\mathrm{tr_e}}$, u and ρ. These are associated to the conditions of

the post-shock flow immediately downstream of the shock wave - which will be labelled here by the number "2". As already referred in chapter 1, there are no chemical neither non-chemical processes occurring throughout the thickness of the shock wave - the mixture chemical composition and the distribution of the particles in their internal energy levels stay the same - the mixture is said to be *frozen* while passing through the shock wave. There is however an abrupt increase of the mean collisional frequency as well as the mean relative collisional speed which leads to an almost instantaneous self-equilibration of the translational energy mode of the heavy particles - a value for the heavy particle translational temperature $T_{\mathrm{tr_h},2}$ can be assigned, being higher than the one upstream of the shock wave. The excitation of the rotational energy mode of the particles occurs almost as fast as the excitation of the translational energy mode, and therefore, one may assign a heavy particle translational-rotational temperature $T_{\mathrm{tr_h-rot},2} = T_{\mathrm{tr_h},2} = T_{\mathrm{rot},2}$ instead of solely a heavy particle translational temperature $T_{\mathrm{tr_h},2}$ immediately downstream of the shock wave. From the conditions upstream of the shock wave - which will be labelled here by the symbol "∞" - to the conditions immediately downstream of the shock, no vibrational and electronic excitations of the particles occur, and the values of the vibrational and electronic temperatures in the latter conditions may be setted equal to the ones in the former conditions, i.e. $T_{\mathrm{vib},2} = T_{\mathrm{el},2} = T_{\mathrm{vib},\infty} = T_{\mathrm{el},\infty} = T_\infty$. Particular attention should be given to the free electron translational temperature $T_{\mathrm{tr_e}}$: since the free electrons are much lighter than the heavy particles, the excitation of their translation energy modes occurs in a different way, and it's not certain that an equilibration between them may immediately occur downstream of the shock wave. This topic is vaguely discussed on the literature, and the author is left with no options but to follow the steps done in another works. It was decided to consider the equality $T_{\mathrm{tr_e},2} = T_{\mathrm{tr_h},2}$, as also regarded by Kadochnikov and Arsentiev [154]. Note that the equality is with respect to the conditions immediately downstream of the shock wave and not to the conditions at the further downstream points. The low T_∞ value (of 300 K) allows one to disregard the contribution of the vibrational and electronic energy modes to the particles energy [1] throughout the shock wave. This means that both mixture specific heat at constant volume C_V and mixture specific heat at constant pressure C_p, from the upstream to the immediately downstream conditions, only depend on the translational and rotational energy modes of the particles. These are then given by

$$C_V \approx C_{V,\mathrm{tr_h-rot-tr_e}} := \left(\frac{\partial e_{\mathrm{tr_h}}}{\partial T_{\mathrm{tr_h}}}\right)_V + \left(\frac{\partial e_{\mathrm{rot}}}{\partial T_{\mathrm{rot}}}\right)_V + \left(\frac{\partial e_{\mathrm{tr_e}}}{\partial T_{\mathrm{tr_e}}}\right)_V =$$

$$= \left[\frac{\partial}{\partial T_{\mathrm{tr_h}}}\left(\sum_{s\in\{\mathrm{h}\}} c_s e_{s,\mathrm{tr}}\right)\right]_V + \left[\frac{\partial}{\partial T_{\mathrm{rot}}}\left(\sum_{s\in\{\mathrm{h}\}} c_s e_{s,\mathrm{rot}}\right)\right]_V + \left[\frac{\partial}{\partial T_{\mathrm{tr_e}}}\left(c_{\mathrm{e}} e_{\mathrm{e}}\right)\right]_V =$$

$$= \left[\sum_{s\in\{\mathrm{h}\}} \underbrace{\left(\frac{\partial c_s}{\partial T_{\mathrm{tr_h}}}\right)_V}_{\approx 0} e_{s,\mathrm{tr}} + c_s \underbrace{\left(\frac{\partial e_{s,\mathrm{tr}}}{\partial T_{\mathrm{tr_h}}}\right)_V}_{:=C_{V,s,\mathrm{tr}}}\right] + \left[\sum_{s\in\{\mathrm{h}\}} \underbrace{\left(\frac{\partial c_s}{\partial T_{\mathrm{rot}}}\right)_V}_{\approx 0} e_{s,\mathrm{rot}} + c_s \underbrace{\left(\frac{\partial e_{s,\mathrm{rot}}}{\partial T_{\mathrm{rot}}}\right)_V}_{:=C_{V,s,\mathrm{rot}}}\right] + \underbrace{\left(\frac{\partial c_{\mathrm{e}}}{\partial T_{\mathrm{tr_e}}}\right)_V}_{\approx 0} e_{\mathrm{e}} + c_{\mathrm{e}} \underbrace{\left(\frac{\partial e_{\mathrm{e}}}{\partial T_{\mathrm{tr_e}}}\right)_V}_{:=C_{V,\mathrm{e}}} =$$

$$= \left[\sum_{s\in\{\mathrm{h}\}} c_s \underbrace{\left(C_{V,s,\mathrm{tr}} + C_{V,s,\mathrm{rot}}\right)}_{:=C_{V,s,\mathrm{tr\text{-}rot}}}\right] + c_{\mathrm{e}} C_{V,\mathrm{e}} \Leftrightarrow$$

$$\Leftrightarrow C_V \approx \left(\sum_{s \in \{\mathrm{h}\}} c_s C_{V,s,\text{tr-rot}} \right) + c_\mathrm{e} C_{V,\mathrm{e}} \ , \tag{3.90}$$

and

$$C_p \approx C_{p,\mathrm{tr_h}-\mathrm{rot}-\mathrm{tr_e}} := \left(\frac{\partial h_{\mathrm{tr_h}}}{\partial T_{\mathrm{tr_h}}} \right)_p + \left(\frac{\partial h_\mathrm{rot}}{\partial T_\mathrm{rot}} \right)_p + \left(\frac{\partial h_{\mathrm{tr_e}}}{\partial T_{\mathrm{tr_e}}} \right)_p =$$

$$= \left[\frac{\partial}{\partial T_{\mathrm{tr_h}}} \left(\sum_{s \in \{\mathrm{h}\}} c_s h_{s,\mathrm{tr}} \right) \right]_p + \left[\frac{\partial}{\partial T_\mathrm{rot}} \left(\sum_{s \in \{\mathrm{h}\}} c_s h_{s,\mathrm{rot}} \right) \right]_p + \left[\frac{\partial}{\partial T_{\mathrm{tr_e}}} \left(c_\mathrm{e} h_\mathrm{e} \right) \right]_p =$$

$$= \left[\sum_{s \in \{\mathrm{h}\}} \underbrace{\left(\frac{\partial c_s}{\partial T_{\mathrm{tr_h}}} \right)_p}_{\approx 0} h_{s,\mathrm{tr}} + c_s \underbrace{\left(\frac{\partial h_{s,\mathrm{tr}}}{\partial T_{\mathrm{tr_h}}} \right)_p}_{:= C_{p,s,\mathrm{tr}}} \right] + \left[\sum_{s \in \{\mathrm{h}\}} \underbrace{\left(\frac{\partial c_s}{\partial T_\mathrm{rot}} \right)_p}_{\approx 0} h_{s,\mathrm{rot}} + c_s \underbrace{\left(\frac{\partial h_{s,\mathrm{rot}}}{\partial T_\mathrm{rot}} \right)_p}_{:= C_{p,s,\mathrm{rot}}} \right] + \underbrace{\left(\frac{\partial c_\mathrm{e}}{\partial T_{\mathrm{tr_e}}} \right)_p}_{\approx 0} h_\mathrm{e} + c_\mathrm{e} \underbrace{\left(\frac{\partial h_\mathrm{e}}{\partial T_{\mathrm{tr_e}}} \right)_p}_{:= C_{p,\mathrm{e}}} =$$

$$= \left[\sum_{s \in \{\mathrm{h}\}} c_s \underbrace{\left(C_{p,s,\mathrm{tr}} + C_{p,s,\mathrm{rot}} \right)}_{:= C_{p,s,\text{tr-rot}}} \right] + c_\mathrm{e} C_{p,\mathrm{e}} \Leftrightarrow$$

$$\Leftrightarrow C_p \approx \left(\sum_{s \in \{\mathrm{h}\}} c_s C_{p,s,\text{tr-rot}} \right) + c_\mathrm{e} C_{p,\mathrm{e}} \ , \tag{3.91}$$

respectively. The specific heats correspond to constants, implying that from the conditions upstream of the shock wave to the conditions immediately downstream of it, the mixture is *calorically perfect*. By further neglecting the transport phenomena and the external body forces forces in the fluid flow throughout the shock wave, it's possible to obtain the well-known *Rankine-Hugoniot jump conditions*, which allows one to compute the conditions immediately downstream of the shock wave from the ones upstream of it [3]. These relations can be easily derived by application of the mass, momentum and total energy balance equations to a control volume that encompasses the shock wave (regarded as a simple discontinuity) being fixed relatively to it. For the cases of the mass density ρ_2, the x-component of the flow velocity vector u_2, the heavy particle translational-rotational temperature $T_{\mathrm{tr_h},2}$ and the free electron translational temperature $T_{\mathrm{tr_e},2}$, the respective Rankine-Hugoniot jump conditions give

$$\rho_2 = \frac{(\gamma+1)\, M_\infty^2}{(\gamma-1)\, M_\infty^2 + 2} \rho_\infty \ , \tag{3.92}$$

$$u_2 = \frac{(\gamma-1)\, M_\infty^2 + 2}{(\gamma+1)\, M_\infty^2} u_\infty \ , \tag{3.93}$$

$$T_{\mathrm{tr_h},2} = T_{\mathrm{tr_e},2} = \frac{\left[(\gamma-1)\, M_\infty^2 + 2 \right] \left[2\gamma M_\infty^2 - (\gamma-1) \right]}{(\gamma+1)^2\, M_\infty^2} T_\infty \ , \tag{3.94}$$

being $\gamma = C_p / C_V$ the ratio of specific heats. Since there's no chemical processes neither vibrational and electronic excitation of the particles occurring throughout the shock wave, the vibronic mass fractions $c_{s,v,e}$ immediately downstream of the shock wave are the same as the ones upstream of it, and one can then write $c_{s,v,e,2} = c_{s,v,e,\infty}$. Note that the fluid upstream of the shock wave is found in thermal equilibrium

at a temperature T_∞, and the distribution of the particles in their energy levels follow the law (2.13).

Brandis and Cruden used in their experiment a test gas which is constituted by pure molecular nitrogen N_2 at room temperature $T_\infty = 300$ K and static pressure $p_\infty = 0.2$ Torr. Different shock wave speeds[10] u_s were tested. Since the test gas is initially at rest with respect to the shock tube, it traverses the shock wave with the same speed as the shock wave that moves throughout the shock tube. The upstream flow speed u_∞ - defined in a referential fixed to the shock wave - corresponds then to the herein defined shock wave speed u_s. The upstream Mach number M_∞ is given by $M_\infty = u_\infty / a_\infty$, being $a_\infty = \sqrt{\gamma R T_\infty}$ the upstream speed of sound.

The numerical results obtained from the zero-dimensional simulations may be regarded as the ones that would be obtained from an element of fluid which passes through the shock wave, being immediately constrained to a transparent fixed-volume box, and removed from the flow. Conversely to the actual element of fluid, this hypothetical element of fluid would not be subjected to transport phenomena - mass diffusion, heat conduction and viscosity - mass density change, neither would receive radiative energy from the complementary system. If the above-mention phenomena is found to be negligible, the numerical results of the zero-dimensional simulation may be compared to the experimental one-dimensional results by simply taking into account that the post-shock speed would be near constant, allowing one to write $u \approx u_2$, being u_2 the flow speed immediately downstream of the shock wave in a referential fixed to it. The results of the zero-dimensional simulations depend on the amount of time elapsed after the passage of the element of fluid through the shock wave, t, while the experimental results depend on the distance travelled with respect to the shock wave, x. Being the speed of the post-shock flow nearly constant, one gets $x(t) = u_2 \cdot t$, or equivalently, $t(x) = x/u_2$. With this relation taken into account, it is possible to express the numerical and experimental results through the same variable dependence, either on t or x.

The one-dimensional simulations take into account the effects of momentum transfer in the flow by regarding a momentum balance equation, and therefore, the respective numerical results are expected to agree better with the experimental results than the ones obtained from the zero-dimensional simulations.

Brandis and Cruden measured the post-shock specific radiative intensity I_λ associated to photons propagating in a radial direction of the tube, say $\vec{e}_y$, at the furthest radial point of the plasma, $y = D/2$, being $D = 10.16$ cm the shock tube inner diameter [43]. Figure 3.25 depicts the geometry of the apparatus, emphasising the regarded inertial frame of reference whose origin moves with the shock wave. The x-axis is aligned with the shock tube axis, pointing downstream, the z-axis points upwards, and the y-axis makes a direct dihedral with the other two. The $\vec{e}_y$ direction is represented by the azimuthal angle $\varphi = \pi/2$ and polar angle $\theta = \pi/2$.

[10] Note that the herein defined shock wave speed corresponds to the speed of the shock wave with respect to the shock tube.

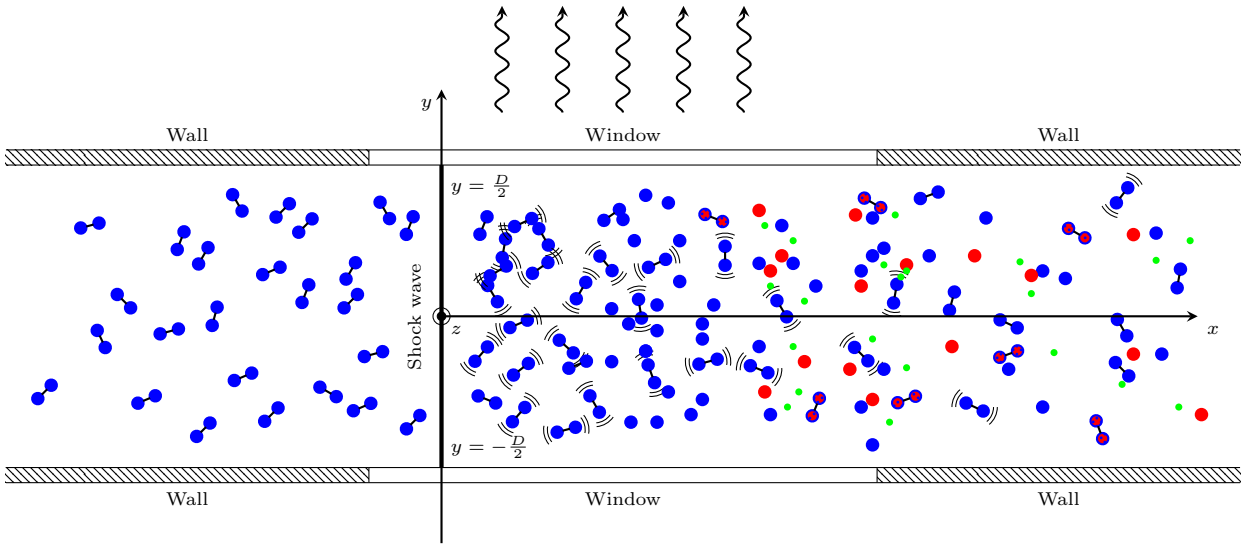

Figure 3.25: Upper view of a longitudinal cross-section of the shock tube, showing the measured radiative field.

One may further describe the measured radiative intensity through the equation of radiative transfer (2.136) for the direction $\vec{e}_s = \vec{e}_y$, disregarding the time-variation term due to the fact that the flow is approximately in a stationary regime when observed from a referential which moves with the shock wave:

$$\frac{\partial I_\lambda}{\partial y}(x, y, 0, \frac{\pi}{2}, \frac{\pi}{2}, \lambda) = j_\lambda(x, y, 0, \frac{\pi}{2}, \frac{\pi}{2}, \lambda) - k_\lambda(x, y, 0, \frac{\pi}{2}, \frac{\pi}{2}, \lambda) \cdot I_\lambda(x, y, 0, \frac{\pi}{2}, \frac{\pi}{2}, \lambda) \ . \tag{3.95}$$

To avoid cumbersome notation the labels $z = 0$, $\varphi = \pi/2$, $\theta = \pi/2$ will be suppressed in the upcoming mathematical manipulations. Equation (3.95) may be simplified by performing the change of variable

$$u(x, y, \lambda) = I_\lambda(x, y, \lambda) e^{\int_{-\frac{D}{2}}^{y} k_\lambda(x, y', \lambda)\, dy'} \ . \tag{3.96}$$

By integrating the resulting equation in y from $y = -D/2$ to $y = D/2$, and acknowledging that the specific radiative intensity at $y = -D/2$ along the direction $\vec{e}_y$ is actually negligible[11], i.e. $I_\lambda(x, -\frac{D}{2}, \lambda) \approx 0$, a general solution is ultimately obtained:

$$I_\lambda(x, \frac{D}{2}, \lambda) = \int_{-\frac{D}{2}}^{\frac{D}{2}} j_\lambda(x, y', \lambda) e^{-\int_{y'}^{\frac{D}{2}} k_\lambda(x, y'', \lambda)\, dy''} \, dy' \ . \tag{3.97}$$

Assuming that the emission and absorption coefficients don't depend on y, the result (3.97) is transformed into

$$I_\lambda(x, \frac{D}{2}, \lambda) = \frac{j_\lambda(x, \lambda)}{k_\lambda(x, \lambda)} \left[1 - e^{-k_\lambda(x, \lambda) D}\right] \ . \tag{3.98}$$

Also, if the plasma is regarded as an optically thin medium, the absorption coefficient may be neglected [3] and (3.98) is reduced to

$$I_\lambda(x, \frac{D}{2}, \lambda) = j_\lambda(x, \lambda) D \ . \tag{3.99}$$

[11] Note that $I_\lambda(x, -\frac{D}{2}, \lambda)$ is generated by the outer medium, being this at room temperature.

By inserting (2.107) into (3.99) and further neglecting induced emission, one obtains

$$I_\lambda(x, \frac{D}{2}, \lambda) = \frac{hcD}{\lambda} \left[\sum_{\text{se}} \frac{A^{e',v'}_{s,e,v}}{4\pi} \phi^{e',v'}_{s,e,v}(\lambda)\, n_{s,e,v}(x) \right] . \tag{3.100}$$

If one instead considers the escape factor introduced in §2.6.4, and simultaneously assumes independence of the involved plasma quantities on the y variable and neglects the induced emission, the solution of the equation of radiative transfer (3.95) may be shown to be simply given by (3.100) with each term in the sum multiplied by the respective escape factor, i.e.

$$I_\lambda(x, \frac{D}{2}, \lambda) = \frac{hcD}{\lambda} \left[\sum_{\text{se}} \Lambda^{e',v'}_{s,e,v} \frac{A^{e',v'}_{s,e,v}}{4\pi} \phi^{e',v'}_{s,e,v}(\lambda)\, n_{s,e,v}(x) \right] . \tag{3.101}$$

To simplify even more the notation, the value $y = D/2$ in the argument of I_λ will be suppressed from now on.

Brandis and Cruden used in their experiment four spectrometers, each one measuring the specific radiative intensity for a particular interval of wavelengths. These intervals of wavelengths are labelled as VUV - from **v**acuum **u**ltra-**v**iolet radiation[12] - "Blue", "Red" and IR - from **i**nfra-**r**ed radiation. Among the issued data (residing in the EAST test data website [156]) there are the *instrumentally resolved radiative intensities* $\hat{I}(x)$ and the *instrumentally resolved non-equilibrium metrics* $\hat{I}^{\text{ne}}_\lambda(\lambda)$ for each of the 42 shots and the four wavelength intervals. The hat denotes instrumentally resolved quantities, in contrast to the real quantities. The former are the ones that are actually obtained in the experiment, being related to the latter through a transformation "applied" by the instruments. The instrumentally resolved radiative intensity associated to the l-th wavelength interval, with $l \in \{\text{VUV, "Blue", "Red", IR}\}$, is given by an integration of the *instrumentally resolved specific radiative intensity* $\hat{I}_\lambda(x, \lambda)$ with respect to the wavelength λ from $\lambda = \lambda^l_{\text{min}}$ to $\lambda = \lambda^l_{\text{max}}$:

$$\hat{I}^l(x) = \int_{\lambda^l_{\text{min}}}^{\lambda^l_{\text{max}}} \hat{I}_\lambda(x, \lambda)\, d\lambda . \tag{3.102}$$

And the instrumentally resolved non-equilibrium metric associated to the l-th wavelength interval is given by an integration of the instrumentally resolved specific radiative intensity $\hat{I}_\lambda(x, \lambda)$ with respect to the position x from $x = x^l_{\text{min}}$ to $x = x^l_{\text{max}}$ - a region characterised by a strong thermodynamic non-equilibrium - divided by the shock tube inner diameter D:

$$\hat{I}^{\text{ne},l}_\lambda(\lambda) = \frac{1}{D} \int_{x^l_{\text{min}}}^{x^l_{\text{max}}} \hat{I}_\lambda(x, \lambda)\, dx . \tag{3.103}$$

One should note here that it is not possible to know the exact position of the shock wave through the spectra obtained in the shock tube experiments done by Brandis and Cruden for multiple reasons: the shock wave isn't a discontinuity and therefore it can't be assigned to a point but to a region, the onset of the radiative field is associated to an increase of the number of excited species (which occurs

[12] Such designation has its historical reasons: ultra-violet radiation of higher energy was found when Victor Schumann placed his spectroscopy apparatus under vacuum instead of air (which absorbs it) [155].

at some distance downstream of the shock wave), and each spectrometer captures the spectra with a different reaction time [157]. The x axis that Brandis and Cruden work with doesn't correspond to the one depicted in Figure 3.25. The issued position values are actually with respect to a particular origin for each shot and wavelength region which doesn't coincide with the shock wave, and therefore they will be denoted here as $\hat{x}$ and termed "relative positions" to distinguish them from the previously introduced ones, x, which are with respect to an origin that hypothetically coincides with the shock wave. The relative position of the shock wave for some shot and the l-th wavelength region, say $\hat{x}^l_{\text{sw}}$, was defined in this work as the point where the instrumentally resolved radiative intensity starts to rise abruptly, as also considered by Cruden in his work [157]. The position x is then given by $x = \hat{x} - \hat{x}^l_{\text{sw}}$.

In this work, only the benchmark data highlighted by Brandis and Cruden were regarded, corresponding to a total of 56 sets of pairs of $\hat{I}^l(x)$ and $\hat{I}^{\text{ne},l}_\lambda(\lambda)$ arrays values. The respective shot number, upstream speed u_∞, wavelength integration limits $[\lambda^l_{\text{min}}, \lambda^l_{\text{max}}]$, and relative position integration limits $[\hat{x}^l_{\text{min}}, \hat{x}^l_{\text{max}}]$ are presented by Table C.1. The estimates for the relative positions of the shock wave $\hat{x}^l_{\text{sw}}$ obtained by the present author are issued in Table C.4

The instrumentally resolved specific radiative intensity $\hat{I}^l_\lambda(x,\lambda)$ departs from the real one, $I^l_\lambda(x,\lambda)$, either spectrally and spatially. The non-ideality of the instrumental apparatus is such that the measured specific radiative intensity $\hat{I}^l_\lambda(x,\lambda)$ associated to some particular wavelength λ and position x is in fact the result of a distribution of the real radiative intensity on intervals of wavelengths and positions around the reference values. Or, mathematically

$$\hat{I}_\lambda(x,\lambda) = \int_{-\infty}^{\infty} \hat{\phi}^{\text{spa}}(x') \left[\int_{-\infty}^{\infty} \hat{\phi}^{\text{spe}}(\lambda') I_\lambda(x-x', \lambda-\lambda')\, d\lambda' \right] dx' \ , \tag{3.104}$$

being $\hat{\phi}^{\text{spe}}(\lambda')$ and $\hat{\phi}^{\text{spa}}(x')$ the so-called *instrument line-shape factor* and *spatial resolution function*, respectively. These are such that $\hat{\phi}^{\text{spa}}(x')\hat{\phi}^{\text{spe}}(\lambda') I_\lambda(x-x', \lambda-\lambda')\, d\lambda'\, dx'$ gives the contribution of the real specific radiative intensity associated to the wavelengths $\lambda' \in [\lambda - \lambda', \lambda - (\lambda' + d\lambda')]$ and positions $x \in [x - x', x - (x' + dx')]$ to the instrumentally resolved specific radiative intensity associated to the wavelength λ and position x. The quantities λ' and x' are regarded as wavelength and position defects with respect to the reference ones.

The instrument line-shape factor and the spatial resolution function are normalised, i.e., they both satisfy

$$\int_{-\infty}^{+\infty} \hat{\phi}^{\text{spe}}(\lambda')\, d\lambda' = 1 \ , \tag{3.105}$$

$$\int_{-\infty}^{+\infty} \hat{\phi}^{\text{spa}}(\lambda')\, d\lambda' = 1 \ . \tag{3.106}$$

According to Brandis and Cruden, the instrument line-shape factor associated to the l-th wavelength interval is given by

$$\hat{\phi}^{\text{spe},l}(\lambda') = \begin{cases} \dfrac{\sqrt{V(\lambda', w^l_G, w^l_L, 0)}}{\int_{-\infty}^{+\infty} \sqrt{V(\lambda', w^l_G, w^l_L, 0)}\, d\lambda'}, & \text{if } l \in \{\text{VUV, "Blue"}\}, \\ \dfrac{G(\lambda', w^l_G, 0) + 10^{r^l} L(\lambda', w^l_L, 0)}{1 + 10^{r^l}}, & \text{if } l \in \{\text{"Red", IR}\}, \end{cases} \tag{3.107}$$

whose involved physical quantities can't be described in a single sentence. The first branch, which is

valid for the VUV and "Blue" wavelength intervals, corresponds to a normalised[13] square root of a Voigt function $V(\lambda', w_G^l, w_L^l, 0)$, being the latter defined by (3.84).

The second branch of (3.107), which is valid for the "Red" and IR wavelength intervals, corresponds to a normalised linear combination of both Gaussian and Lorentzian functions ($G(\lambda', w_G^l, 0)$ and $L(\lambda', w_L^l, 0)$, which are defined by (3.67) and (3.71), respectively) being r^l some constant associated to the l-th wavelength interval. The values for w_G^l, w_L^l and r^l which were obtained by Brandis and Cruden for the benchmark shots considering the four wavelength intervals are presented by Table C.2.

Regarding the spatial resolution function $\hat{\phi}^{\text{spa}}(x')$, it's necessary to account three contributions: one due to the used optics, another due to the spatial resolution of the used *charge-coupled devices* (CCDs) - the "cameras" - and another due to the motion of the flow with respect to these CCDs [157]. For each of three contributions there is a function to ascribe, such that the resultant spatial resolution function $\hat{\phi}^{\text{spa}}(x')$ corresponds to a double convolution of the form

$$\hat{\phi}^{\text{spa}}(x') = \int_{-\infty}^{\infty} \hat{\phi}_{\text{opt}}^{\text{spa}}(x'') \left[\int_{-\infty}^{\infty} \hat{\phi}_{\text{cam}}^{\text{spa}}(x''') \hat{\phi}_{\text{mot}}^{\text{spa}}(x' - x'' - x''') \, dx''' \right] dx'' \, . \tag{3.108}$$

According to Brandis and Cruden, the optics function associated to the l-th wavelength interval $\hat{\phi}_{\text{opt}}^{\text{spa},l}(x'')$ is given by

$$\hat{\phi}_{\text{opt}}^{\text{spa},l}(x'') = \begin{cases} \text{tri}(x'', d_{\text{tri}}^l), & \text{if } l \in \{\text{VUV, "Blue", "Red"}\}, \\ \text{trap}(x'', d_{\text{trap},1}^l, d_{\text{trap},2}^l), & \text{if } l = \text{IR}, \end{cases} \tag{3.109}$$

being $\text{tri}(x'', d_{\text{tri}}^l)$ a normalised *triangular function* of base length d_{tri}^l, and $\text{trap}(x'', d_{\text{trap},1}^l, d_{\text{trap},2}^l)$ a normalised *trapezoidal function* of lower base length $d_{\text{trap},1}^l$ and upper base length $d_{\text{trap},2}^l$. These two functions are expressed by

$$\text{tri}(x'', d_{\text{tri}}^l) = \begin{cases} \frac{2}{d_{\text{tri}}^l} \left(1 - 2 \frac{|x''|}{d_{\text{tri}}^l} \right), & \text{if } |x''| \leq \frac{d_{\text{tri}}^l}{2}, \\ 0, & \text{if } |x''| > \frac{d_{\text{tri}}^l}{2}, \end{cases} \tag{3.110}$$

and

$$\text{trap}(x'', d_{\text{trap},1}^l, d_{\text{trap},2}^l) = \begin{cases} \frac{2}{d_{\text{trap},1}^l + d_{\text{trap},2}^l}, & \text{if } |x''| \leq \frac{d_{\text{trap},2}^l}{2}, \\ \frac{2}{d_{\text{trap},1}^l + d_{\text{trap},2}^l} \cdot \frac{d_{\text{trap},1}^l - 2|x''|}{d_{\text{trap},1}^l - d_{\text{trap},2}^l}, & \text{if } \frac{d_{\text{trap},2}^l}{2} < |x''| \leq \frac{d_{\text{trap},1}^l}{2}, \\ 0, & \text{if } |x''| > \frac{d_{\text{trap},1}^l}{2}, \end{cases} \tag{3.111}$$

respectively, being both represented in Figure 3.26. The camera function associated to the l-th wavelength interval $\hat{\phi}_{\text{cam}}^{\text{spa},l}(x'')$ is in its turn given by

$$\hat{\phi}_{\text{cam}}^{\text{spa},l}(x'') = \begin{cases} \frac{\sqrt{V(x'', w_G^l, w_L^l, 0)}}{\int_{-\infty}^{+\infty} \sqrt{V(x'', w_G^l, w_L^l, 0)} \, d\lambda'}, & \text{if } l \in \{\text{VUV, "Blue", "Red"}\}, \\ G(x'', w_G^l, 0), & \text{if } l = \text{IR}. \end{cases} \tag{3.112}$$

[13] Hence the presence of the denominator.

And the motion function associated to the l-th wavelength interval $\hat{\phi}^{\mathrm{spa},l}_{\mathrm{mot}}(x'')$ corresponds to

$$\hat{\phi}^{\mathrm{spa},l}_{\mathrm{mot}}(x'') = \mathrm{rect}(x'', d^l_{\mathrm{rect}}) \ , \tag{3.113}$$

being $\mathrm{rect}(x'', d^l_{\mathrm{rect}})$ a normalised *rectangular function* of base length d^l_{rect}:

$$\mathrm{rect}(x'', d^l_{\mathrm{rect}}) = \begin{cases} \frac{1}{d^l_{\mathrm{rect}}}, & \text{if } |x''| \leq \frac{d^l_{\mathrm{rect}}}{2}, \\ 0, & \text{if } |x''| > \frac{d^l_{\mathrm{rect}}}{2}, \end{cases} \tag{3.114}$$

This function is depicted in Figure 3.26. Table C.3 presents the base widths d^l_{tri}, $d^l_{\mathrm{trap},1}$, $d^l_{\mathrm{trap},2}$ and d^l_{rect}, as well as the half-widths at half-maxima w^l_G and w^l_L for the spatial resolution function $\hat{\phi}^{\mathrm{spa},l}(x'')$ ascribed to the benchmark shots considering the four wavelength intervals.

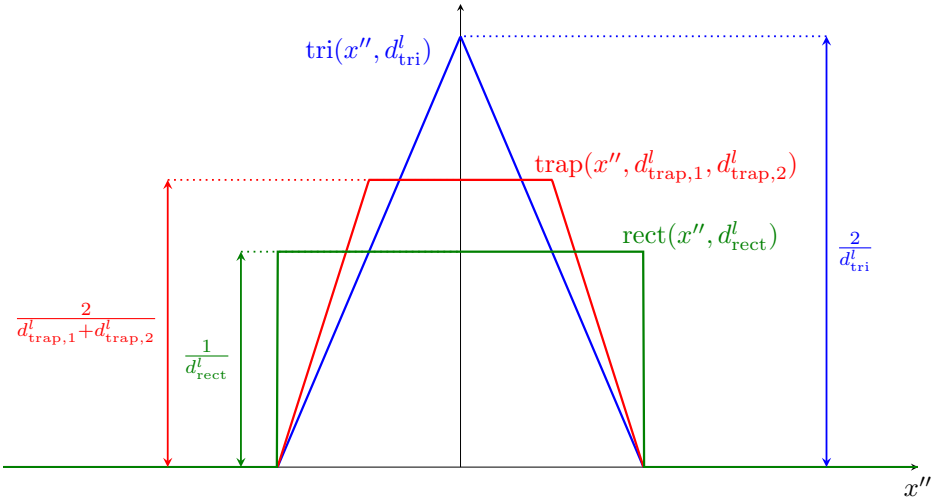

Figure 3.26: Normalised triangular $\mathrm{tri}(x'', d^l_{\mathrm{tri}})$, trapezoidal $\mathrm{trap}(x'', d^l_{\mathrm{trap},1}, d^l_{\mathrm{trap},2})$ and rectangular $\mathrm{rect}(x'', d^l_{\mathrm{rect}})$ functions for illustrative base lengths $d^l_{\mathrm{tri}} = d^l_{\mathrm{trap},1} = d^l_{\mathrm{rect}} = 1$ and $d^l_{\mathrm{trap},2} = d^l_{\mathrm{trap},1}/2$.

The validation of the models employed in this work requires a comparison of the numerically obtained radiative intensities and non-equilibrium metrics with the experimentally obtained ones. For that purpose, it's necessary to impose on the former the same transformations "applied" by the instruments on the latter.

Chapter 4

Results

4.1 The test matrix

Brandis and Cruden [43] issue benchmark data for a total of 17 shock tube shots which may be used for validation of the numerically obtained results. Due to compactness reasons, it was decided to regard solely 3 of these 17 shots, more precisely, shots that spawned conditions of low, medium, and high speed hypersonic flows. In this way, the dependence of the physical quantities on the free stream speed u_∞ may be accessed. Also, greater importance was given to shots whose results were considered to be of benchmark quality in the four wavelength intervals (VUV, "Blue", "Red", and IR), allowing the validation to be performed with respect to the whole spectrum. Under such criteria, the shots 40 (with $u_\infty = 6.88$ m/s), 19 (with $u_\infty = 10.32$ m/s), and 20 (with $u_\infty = 11.16$ m/s) and were taken.

4.2 The analysis methodology

In the following sections, the numerical and experimental results are compared, and possible causes for their discrepancies are enunciated. The tested standard database of kinetic processes corresponds to the set constituted by the collisional processes reported in Table 3.2 and Table 3.3, and the radiative processes reported in Table 3.11. The dependence of the results on different adjustable parameters of the simulations was reported. To properly guide the reader over the extensive set of obtained results, it was decided to treat simultaneously the three shots for each of the four wavelength intervals and to show side-by-side the respective graphs for the two quantities that were measured in the experiments: the instrumentally resolved radiative intensities $\hat{I}^l$ and non-equilibrium metrics $\hat{I}_\lambda^{\mathrm{ne},l}$, with $l \in \{\mathrm{VUV}, \text{"Blue"}, \text{"Red"}, \mathrm{IR}\}$. Further comments on the behaviour of important physical quantities such as temperatures and mole fractions, as well as on the evolution of the system to equilibrium are provided.

4.3 Zero-dimensional simulations of post-shock flows generated by a shock tube

4.3.1 The case of the VUV radiation

The instrumentally resolved radiative intensities $\hat{I}^{\mathrm{VUV}}(x)$ and non-equilibrium metrics $\hat{I}_{\lambda}^{\mathrm{ne,VUV}}(x)$ obtained from the zero-dimensional simulations are depicted in Figure 4.1 and Figure 4.2, respectively. The three graphs appearing in each figure are ordered by increasing free stream speed u_{∞} from top to bottom - the top one is with respect to shot 40, the middle one to 19, and the bottom one to 20. The solid coloured lines represent the numerically obtained contributions of the different systems of spontaneous emission processes to the variables $\hat{I}^{\mathrm{VUV}}(x)$ and $\hat{I}_{\lambda}^{\mathrm{ne,VUV}}(x)$. The solid black lines represent the numerically obtained overall quantities (i.e. the sums of the contributions). And the dotted black lines represent the experimentally obtained overall quantities. The numerical values are quantified in the left y-axis and the experimental ones in the right y-axis. These y-axes are scaled differently in order to make the two sets of values visually comparable. In the case of $\hat{I}^{\mathrm{VUV}}$, the scales are such that the heights of the peaks match each other. And in the case of $\hat{I}_{\lambda}^{\mathrm{ne,VUV}}$, the scales are such that there's a coincidence between the peaks associated to spontaneous emission of N at $\lambda = 149\,\mathrm{nm}$. The necessity of using different scales unveils immediately a significant discrepancy: the numerically obtained values are much lower than the experimental ones. In fact, the heights of the experimental $\hat{I}^{\mathrm{VUV}}$ peaks are 342, 63 and 71 times higher than the numerical ones for the low, medium and high speed shots, respectively. And the heights of the experimental $\hat{I}_{\lambda}^{\mathrm{ne,VUV}}$ peaks at $\lambda = 149\,\mathrm{nm}$ are 455, 641 and 1695 times higher than the numerical ones.

Let's now focus on the relative discrepancies, i.e. the discrepancies between the numerical and experimental results as if they were scaled to the same order of magnitude. Figure 4.1 reveals that the increase of $\hat{I}^{\mathrm{VUV}}$ from nil to peak maximum value and the decrease of $\hat{I}^{\mathrm{VUV}}$ from the peak maximum value to nil are slower (the latter with a much greater significance) than the ones in the experiment, for the case of the low speed shot. This seems to be due to a relative overestimation of the number of spontaneous emissions of the type $\mathrm{N_2^+(C-X)}$, whose contribution to the overall radiative intensity corresponds to a more flattened and delayed peak than the others. In fact, Figure (4.2) shows many $\hat{I}_{\lambda}^{\mathrm{ne,VUV}}$ peaks of considerable heigh assigned to $\mathrm{N_2^+(C-X)}$ which were not actually observed in the experiment. Although the two peaks that appear at $\lambda = 156\,\mathrm{nm}$ and $\lambda = 166\,\mathrm{nm}$ seem to overlap others of $\mathrm{N_2^+(C-X)}$, this should be mere coincidence. The two peaks may be predicted if one considers atomic carbon C - a contaminant species - in the database, as Cruden and Brandis [158] did. Furthermore, according to Cruden and Brandis [158], the experimental peak at $\lambda = 193\,\mathrm{nm}$ - which was not predicted by the database used in this work - should also be due to C. The two most prominent peaks of the experimental $\hat{I}_{\lambda}^{\mathrm{ne,VUV}}$, appearing at $\lambda = 149\,\mathrm{nm}$ and $\lambda = 174\,\mathrm{nm}$, are a result of spontaneous emission of N, being these predicted by the current database. However, the respective features appearing in the obtained numerical spectra stand out as much as the ones for $\mathrm{N_2^+(C-X)}$, showing another evidence of a relative overestimation of the number of spontaneous emissions associated to the latter. Additionally,

one finds the peak at $\lambda = 149\,\text{nm}$ to be higher than the peak at $\lambda = 174\,\text{nm}$ in the numerical spectra, but lower in the experimental one. Such discrepancy may be due to the absorption of radiation associated to the first peak being greater than the one associated to the second peak in the experiment. Meanwhile, in the simulation, absorption was completely disregarded. The discrepancy may also be due to an improper modelling of the rate coefficients which dictate the population of the nitrogen atoms that spontaneously emit radiation at wavelengths $\lambda = 149\,\text{nm}$ and $\lambda = 174\,\text{nm}$. One way of decreasing the height of the first peak and increasing the height of the second in order to make the ratio between the two agreeable with the experimental result, is by decreasing the rate of excitation of atomic nitrogen to the upper level of the system associated to the former and increasing the one associated to the latter. However, for the present case, the upper levels of the system associated to the two peaks are the same, corresponding to the fifth level, say[1] N(4). The first peak is a result of the transitions from the fifth level to the second level, i.e. $\text{N}(4-1)$, and the second peak is a result of the transitions from the fifth level to the third one, i.e. $\text{N}(4-2)$. Therefore, changing the values of the rate coefficients for excitation would not make any difference to the ratio between the heights of the peaks. One should, however, mention here that this inability is in some part due to the lumping procedure performed on the energy levels of N. If split levels were instead regarded, the first peak would actually correspond to a sum of three peaks with their centres very close to each other, and the second peak would correspond to a sum of four peaks. The number of upper energy levels associated to the respective spontaneous emission systems would be two instead of one. By changing the values of the rate coefficients for excitation of the two split levels one could actually obtain the right ratio of heights. Furthermore, it's important to say that the reduction of the number of peaks due to lumping procedure may also affect the numerical spectra obtained for the other wavelength intervals, which, in its turn, may lead to unfair judgments on the structure of the database. Note that this lumping procedure is however virtually unavoidable, since the most part of the processes reported in the literature disregard the fine structure of the particles, and therefore, the application of the respective rate coefficients requires the author to make the same consideration.

The experimental instrumentally resolved radiative intensity $\hat{I}^{\text{VUV}}$ obtained for the case of the medium speed shot has a peak proceeded by a plateau. The shape of the peak is well predicted by the numerical model, but the plateau isn't at all. A transition to nil occurs instead. And for the case of the high speed shot, the experiment didn't produce a sole peak, but a coalescence between a peak and a plateau surpassing it. This feature wasn't also predicted by the numerical model.

[1] The electronic levels of the atomic particles will be labelled here by integer numbers $e = 0, 1, ...$

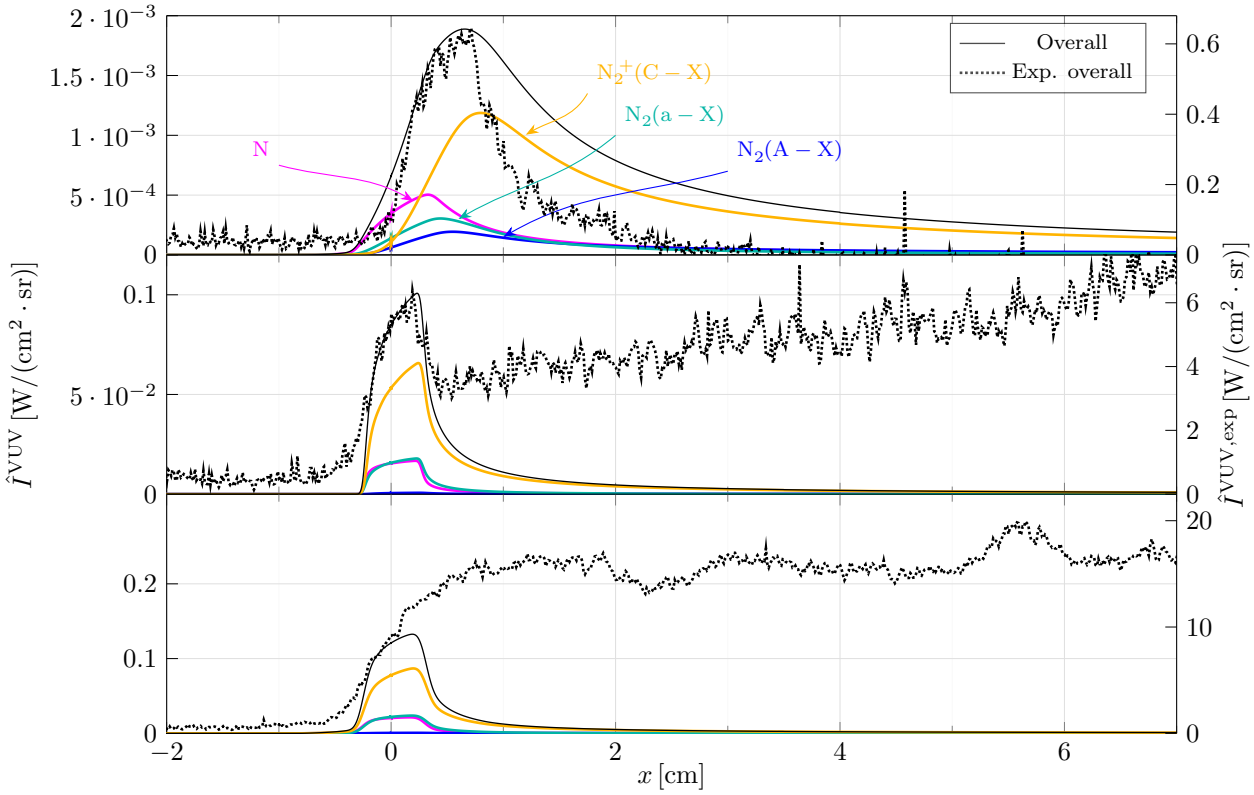

Figure 4.1: Numerical (solid lines) and experimental (dotted lines) instrumentally resolved radiative intensities $\hat{I}^{\mathrm{VUV}}(x)$ obtained for the low, medium and high speed shots.

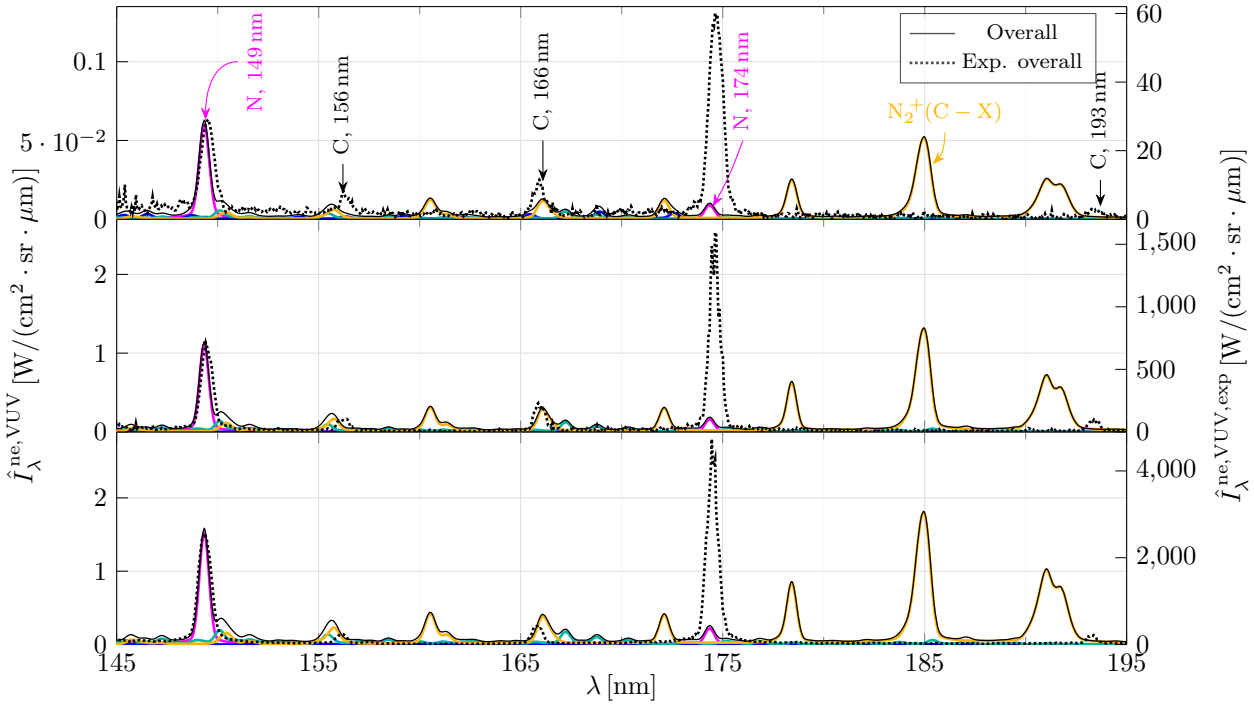

Figure 4.2: Numerical (solid lines) and experimental (dotted lines) instrumentally resolved non-equilibrium metrics $\hat{I}_\lambda^{\mathrm{ne,VUV}}(x)$ obtained for the low, medium and high speed shots.

4.3.2 The case of the "Blue" radiation

The obtained instrumentally resolved radiative intensities $\hat{I}^{\text{Blue}}(x)$ and non-equilibrium metrics $\hat{I}_{\lambda}^{\text{ne,Blue}}(x)$ are depicted in Figure 4.3 and Figure 4.4, respectively. The main contributors to the overall quantities are $N_2(C-B)$ and $N_2^+(B-X)$. And the residual contributors correspond to $N_2(A-X)$ and N for the three shots, and also $N_2^+(A-X)$ for the low speed shot. Meanwhile, Cruden and Brandis [158] showed that $N_2(C-B)$, $N_2^+(B-X)$, N, and the contaminant species CN (cyanogen radical) are enough to describe the experimentally obtained spectrum for the case of the medium speed shot.

As happened for the case of the VUV radiation, the instrumentally resolved radiative intensities and non-equilibrium metrics are underestimated by 2 to 3 orders of magnitude. The scales of the y-axes of the non-equilibrium metrics graphs are such that there's a coincidence between the numerical and experimental peaks associated to spontaneous emission of $N_2^+(B-X)$ at $\lambda = 391\,\text{nm}$. The heights of the experimental $\hat{I}^{\text{Blue}}$ peaks are 730, 68, and 45 times higher than the numerical ones for the low, medium and high speed shots, respectively. And the heights of the experimental $\hat{I}_{\lambda}^{\text{ne,Blue}}$ peaks at $\lambda = 391\,\text{nm}$ are 636, 49 and 66 times higher than the numerical ones. The profile of the numerical radiative intensity $\hat{I}^{\text{Blue}}$ obtained in the low speed shot corresponds to a peak, similar to the experimental one. However, the transitions from nil to the maximum and from the maximum to nil are slower in the former. In the case of the medium and high speed shots, the shape of the peaks are remarkably well predicted, contrary to the plateaus that proceed them: the numerical radiative intensities transit to nil instead of converging to these plateaus. Such behaviour was also obtained in the case of the VUV radiation.

Sets of peaks appearing in the experimental non-equilibrium metrics $\hat{I}_{\lambda}^{\text{ne,Blue}}$ may be discerned, being these in some way predicted by the numerical model. However, the heights of the individual peaks of each set don't agree particularly well with the experimental ones, namely, the ones associated to spontaneous emissions of the types $N_2(C, 0-B, 0)$ and $N_2^+(B, 0-X, 0)$, at $\lambda = 337\,\text{nm}$ and $\lambda = 391\,\text{nm}$, respectively. These were undoubtedly overestimated, prevailing over the others. The discrepancies between the numerical and experimental non-equilibrium metrics may in some part be due to the fact that the regarded spontaneous emissions are vibronic-specific and not rovibronic. If rovibronic-specific spontaneous emissions were instead considered, the peaks associated to the vibronic levels would be divided into several others (each one associated to a rotational level) whose centres may be more or less far from each other, depending on the energy of the rotational levels. The importance of the rotational levels to the spectra should be accessed in the future.

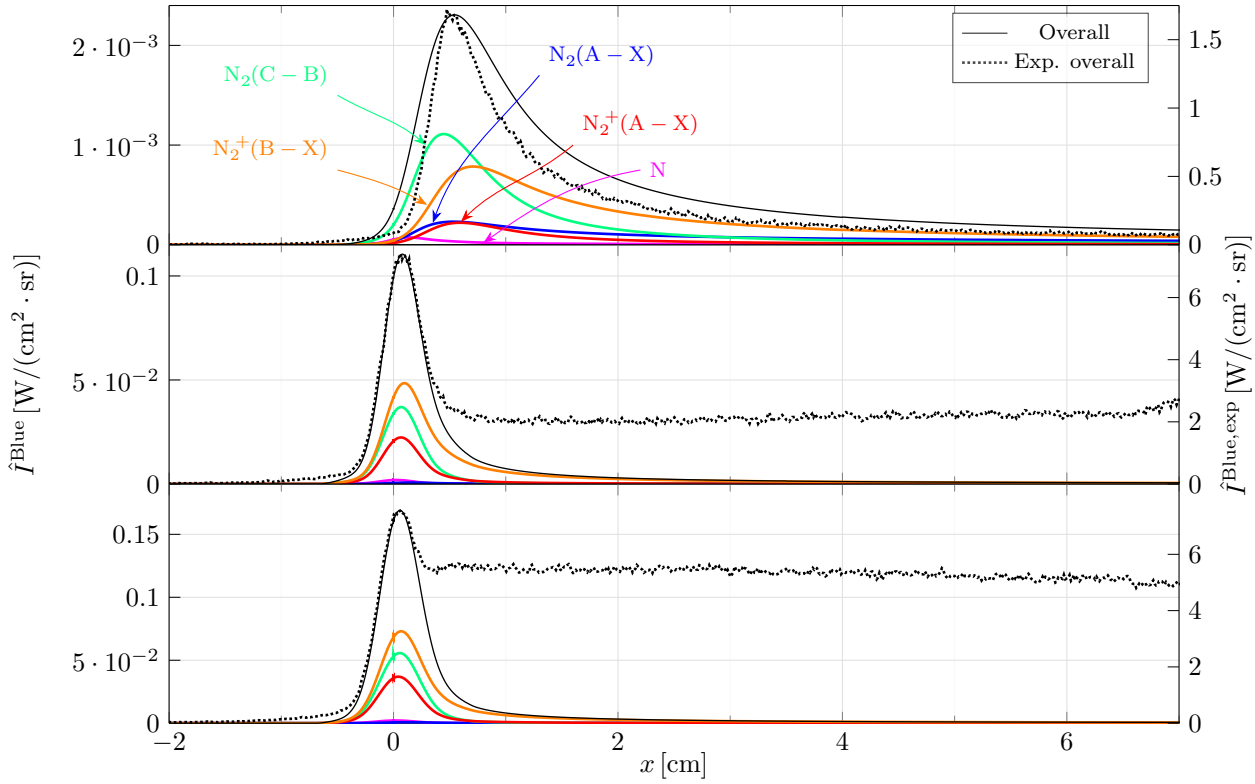

Figure 4.3: Numerical (solid lines) and experimental (dotted lines) instrumentally resolved radiative intensities $\hat{I}^{\mathrm{Blue}}(x)$ obtained for the low, medium and high speed shots.

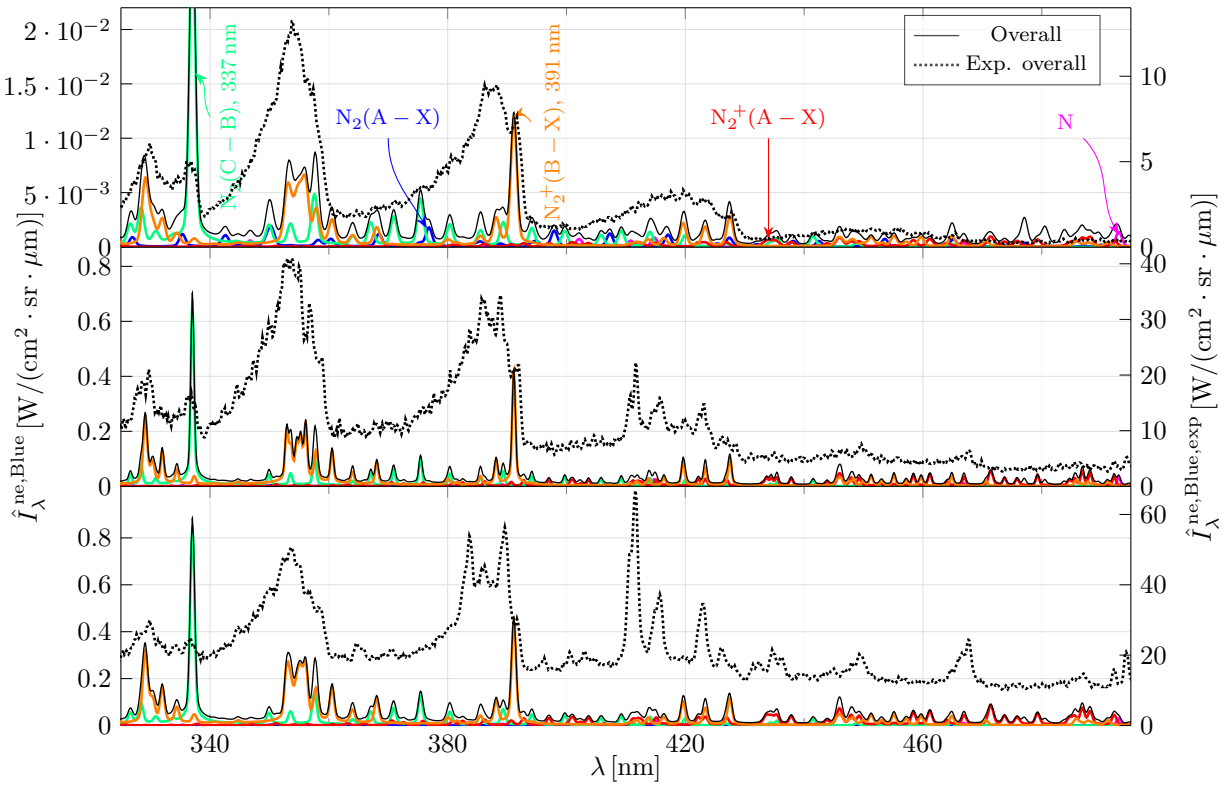

Figure 4.4: Numerical (solid lines) and experimental (dotted lines) instrumentally resolved non-equilibrium metrics $\hat{I}_\lambda^{\mathrm{ne,Blue}}(x)$ obtained for the low, medium and high speed shots.

4.3.3 The case of the "Red" radiation

Figures 4.5 and 4.6 depict the obtained instrumentally resolved radiative intensities $\hat{I}^{\mathrm{Red}}(x)$ and non-equilibrium metrics $\hat{I}_{\lambda}^{\mathrm{ne,Red}}(x)$, respectively. The scales of the $\hat{I}_{\lambda}^{\mathrm{ne,Red}}$ graphs are such that the experimental and numerical peaks at $\lambda = 869\,\mathrm{nm}$ match each other. The experimental $\hat{I}^{\mathrm{Red}}$ peaks are 144, 19, and 30 times higher than the numerical peaks for the low, medium and high speed shots, respectively. And the experimental $\hat{I}_{\lambda}^{\mathrm{ne,Red}}$ peaks at $\lambda = 869\,\mathrm{nm}$ are 167, 430 and 1305 higher than the numerical ones. As happened for the case of the VUV radiation, in the low speed shot, the transition of the numerical radiative intensity $\hat{I}_{\lambda}^{\mathrm{ne,Red}}$ from the peak maximum value to nil was significantly slower than the experimental one. In the medium and high speed shots, plateaus proceeding peaks were obtained from the experiment. These were not predicted by the numerical model.

There is strong evidence of a relative underestimation of spontaneous emissions of N, since the most prominent peaks (such as the ones at $\lambda = 649$, 745, 821, 862 and 869 nm) of the experimental spectra, which are due to N, are surpassed in the numerical spectra by the ones associated to $N_2(B-A)$. Also, spontaneous emissions of the type $N_2^+(A-X)$ should not be as relevant as they were found to be in the numerical spectra. Cruden and Brandis [158] considered in this wavelength interval, for the case of the medium speed shot, solely spontaneous emissions of the type N (the dominant ones), $N_2(B-A)$ and H (atomic hydrogen was found to be a contaminant species).

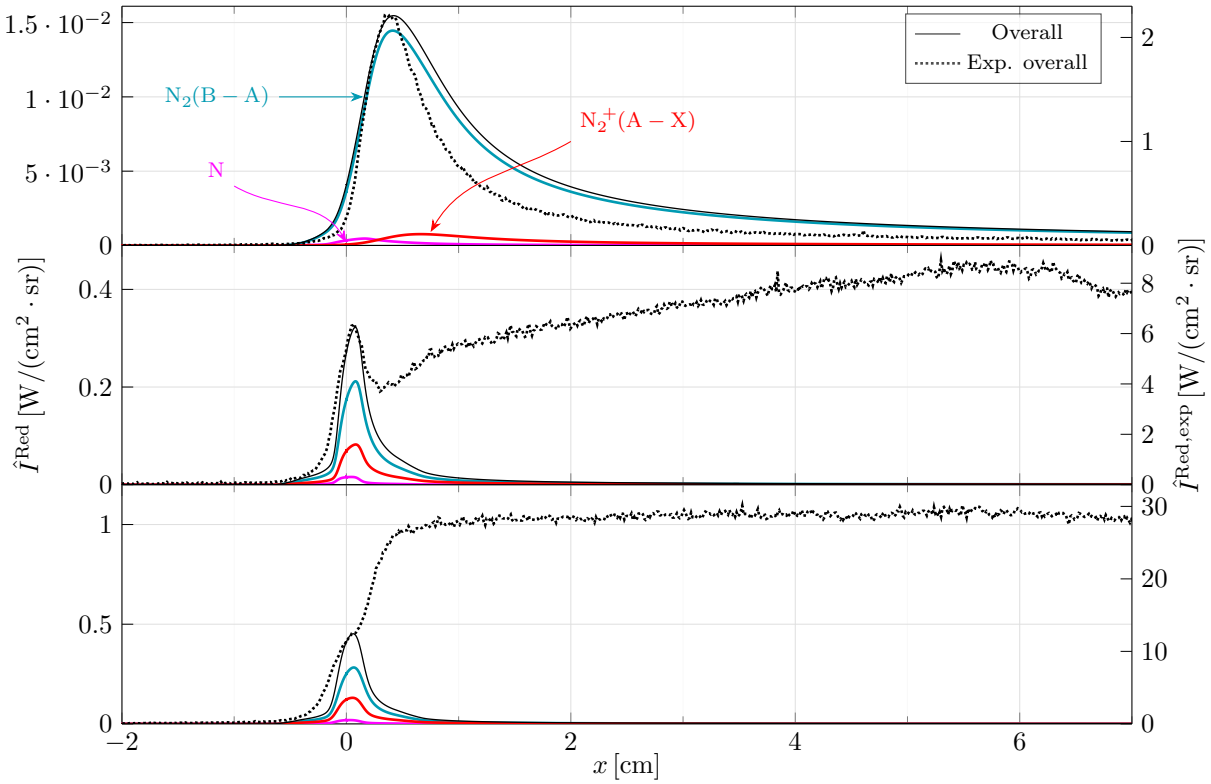

Figure 4.5: Numerical (solid lines) and experimental (dotted lines) instrumentally resolved radiative intensities $\hat{I}^{\mathrm{Red}}(x)$ obtained for the low, medium and high speed shots.

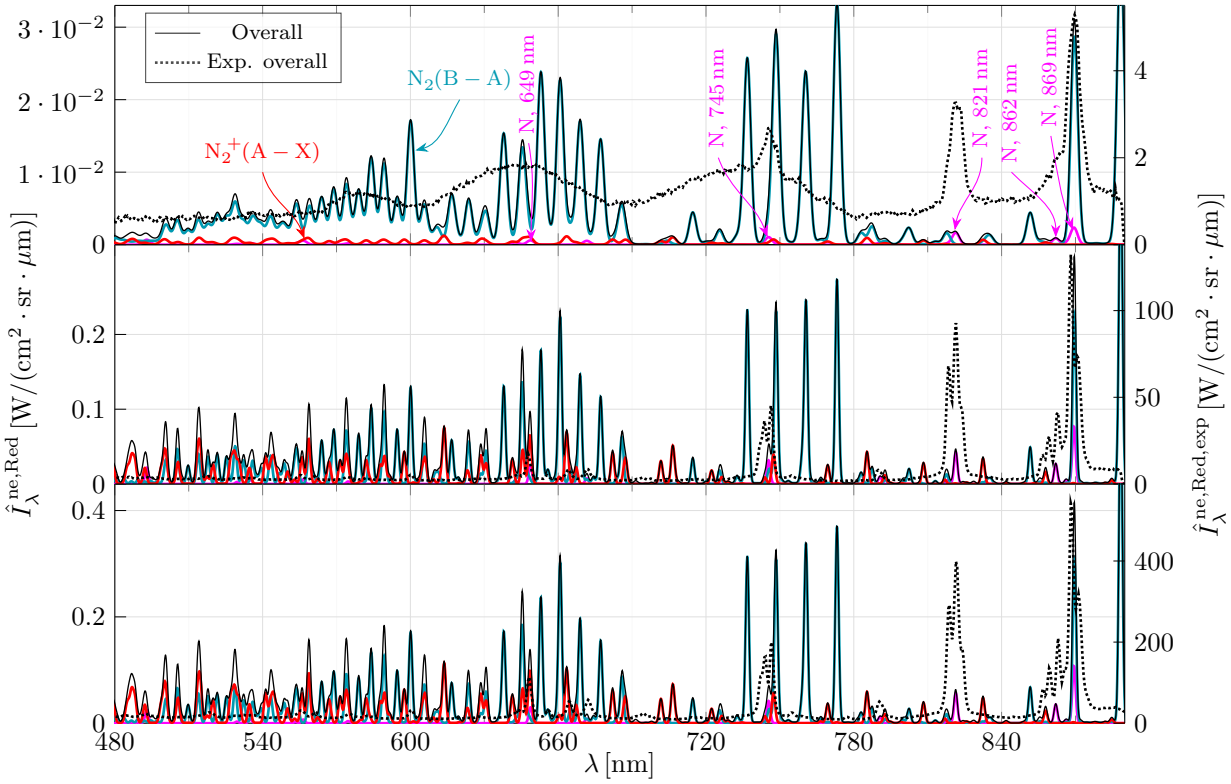

Figure 4.6: Numerical (solid lines) and experimental (dotted lines) instrumentally resolved non-equilibrium metrics $\hat{I}_\lambda^{ne,Red}(x)$ obtained for the low, medium and high speed shots.

4.3.4 The case of the IR radiation

Figures 4.7 and 4.8 depict the obtained instrumentally resolved radiative intensities $\hat{I}^{IR}(x)$ and non-equilibrium metrics $\hat{I}_\lambda^{ne,IR}(x)$, respectively. The scales of the $\hat{I}_\lambda^{ne,IR}$ graphs are such that the experimental and numerical peaks at $\lambda = 940\,nm$ match each other. Unsurprisingly, it was found that the numerical model underestimated the radiative intensities and non-equilibrium metrics by 2 to 3 orders of magnitude, as in the other cases. The experimental $\hat{I}^{IR}$ peaks are 116, 105, and 352 times higher than the numerical peaks for the low, medium and high speed shots, respectively. And the experimental $\hat{I}_\lambda^{ne,IR}$ peaks at $\lambda = 940\,nm$ are 274, 887 and 1784 higher than the numerical ones. In the case of the low speed shot, the numerical $\hat{I}^{IR}$ values rise and fall slightly less abruptly than the experimental values. And in the cases of the medium and high speed shots, sole peaks can't be discerned from the experiment but coalescences between peaks and plateaus occurring above them. Again, such phenomena wasn't predicted by the numerical model.

The obtained non-equilibrium metrics show that spontaneous emissions of the type $N_2(B-A)$ seem to be relatively overestimated, specially the ones at $\lambda = 1047\,nm$ - due to transitions from $v = 0$ to $v' = 0$ - and $\lambda = 1232\,nm$ - due to transitions from $v = 0$ to $v' = 1$ - which prevail over the others. Conversely, the peaks associated to spontaneous emission of N (such as the ones at $\lambda = 905\,nm$, $\lambda = 940\,nm$, $\lambda = 1012\,nm$ and $\lambda = 1053\,nm$) seem to be relatively underestimated, since these predominate in the experimental spectra but not in the numerical spectra.

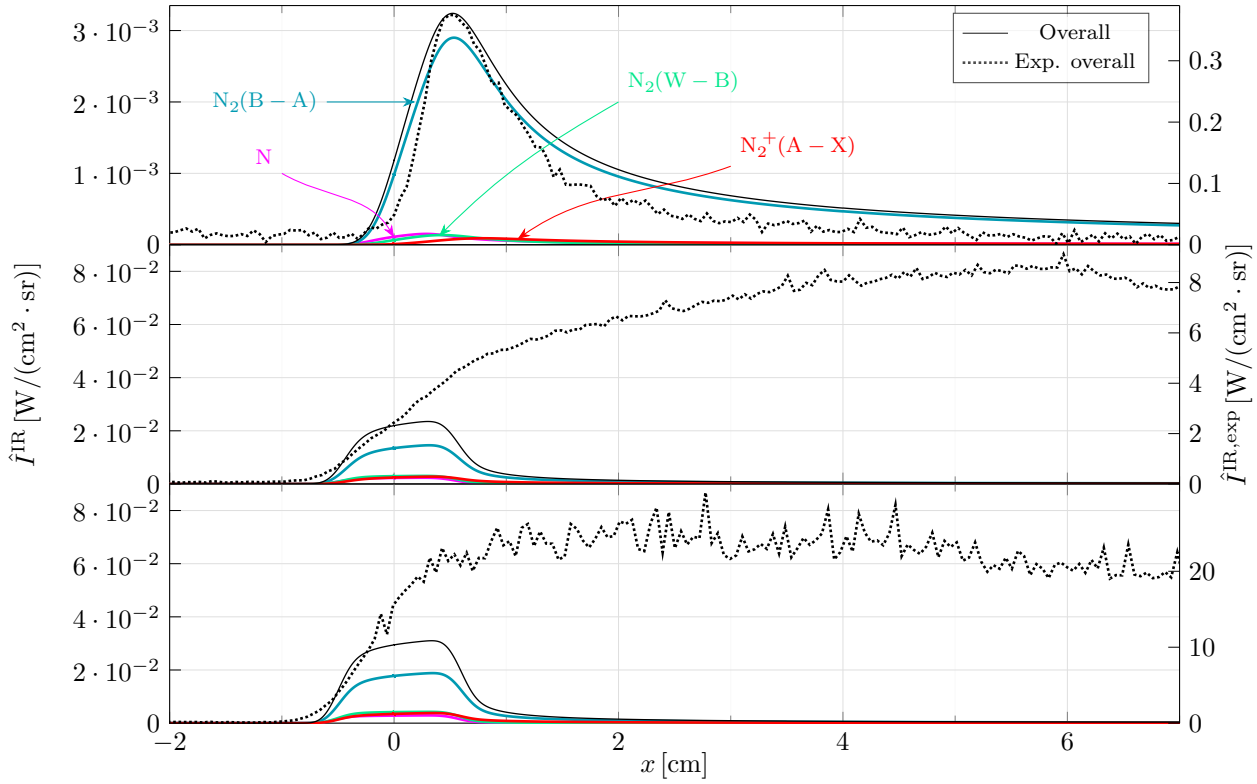

Figure 4.7: Numerical (solid lines) and experimental (dotted lines) instrumentally resolved radiative intensities $\hat{I}^{\mathrm{IR}}(x)$ obtained for the low, medium and high speed shots.

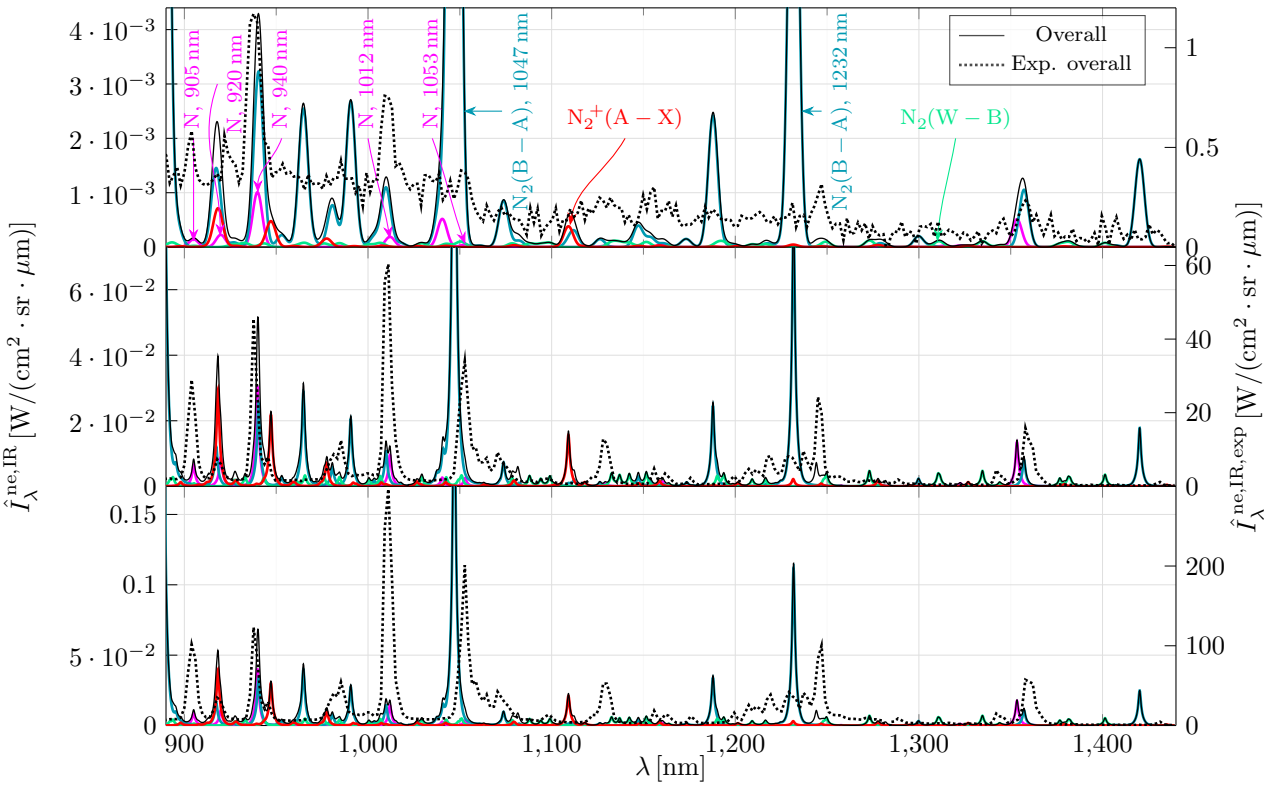

Figure 4.8: Numerical (solid lines) and experimental (dotted lines) instrumentally resolved non-equilibrium metrics $\hat{I}_\lambda^{\mathrm{ne,IR}}(x)$ obtained for the low, medium and high speed shots.

4.4 Euler one-dimensional simulations of post-shock flows generated by a shock tube

The values of the radiation variables obtained from the the Euler one-dimensional simulations are presented by Figures 4.9 to 4.16. The peak values of the instrumentally resolved radiative intensities are still significantly underestimated - by one to two order magnitudes. These peak values are greater than the ones obtained from the zero-dimensional simulations: for the case of the low speed shot, the quintuple was obtained in the VUV and "Blue" wavelength regions, and the triple in the "Red" and IR, and for the case of the medium and high speed shots, the double was obtained. Therefore, the transfer of momentum between elements of fluid should not be neglected. As happened in the zero-dimensional simulations, the plateaus weren't predicted at all. In relative terms, the rises from nil to the peak values and the falls from the peak values to nil of the radiative intensities for the case of the low speed shots were found to be steeper than the ones obtained from the zero-dimensional simulations. The rising parts of the profiles of the numerical peaks now agree relatively well with the experimental ones, but not the falling parts in the "Blue", "Red", and IR wavelength regions which are steeper (being once slighter) than the experimental counterparts.

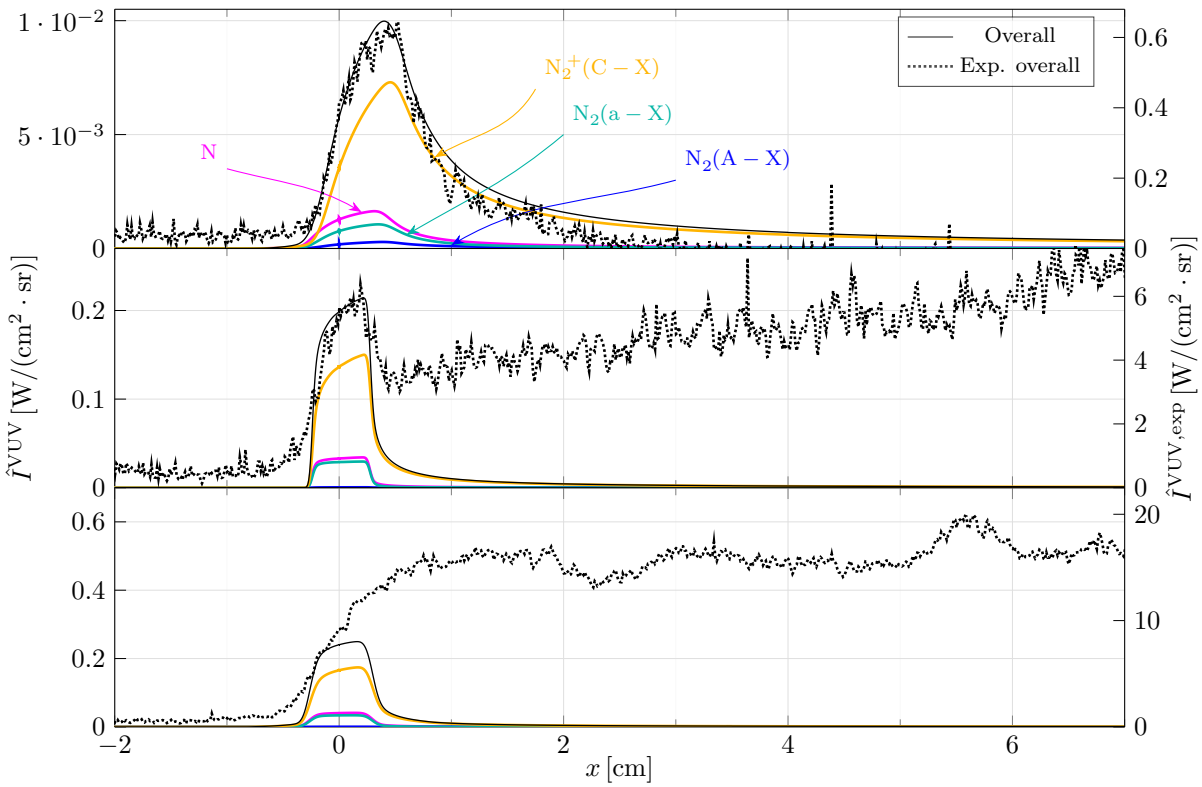

Figure 4.9: Numerical (solid lines) and experimental (dotted lines) instrumentally resolved radiative intensities $\hat{I}^{VUV}(x)$ obtained for the low, medium and high speed shots.

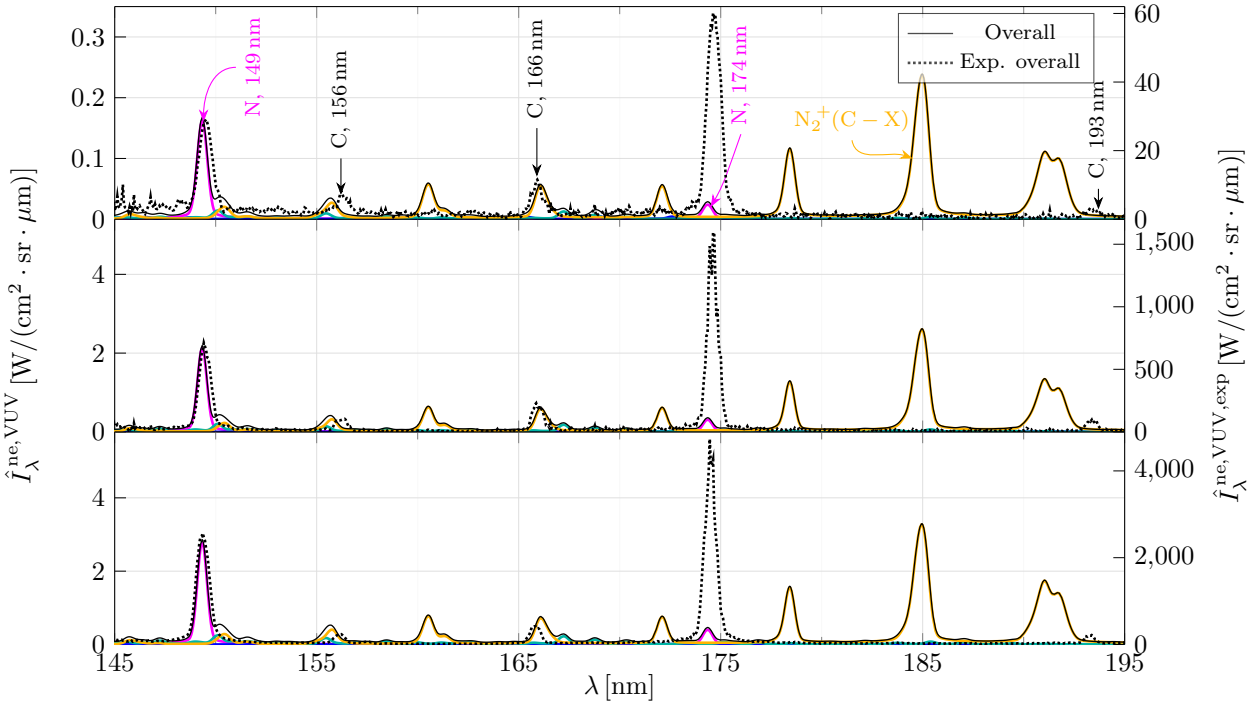

Figure 4.10: Numerical (solid lines) and experimental (dotted lines) instrumentally resolved non-equilibrium metrics $\hat{I}_\lambda^{ne,VUV}(x)$ obtained for the low, medium and high speed shots.

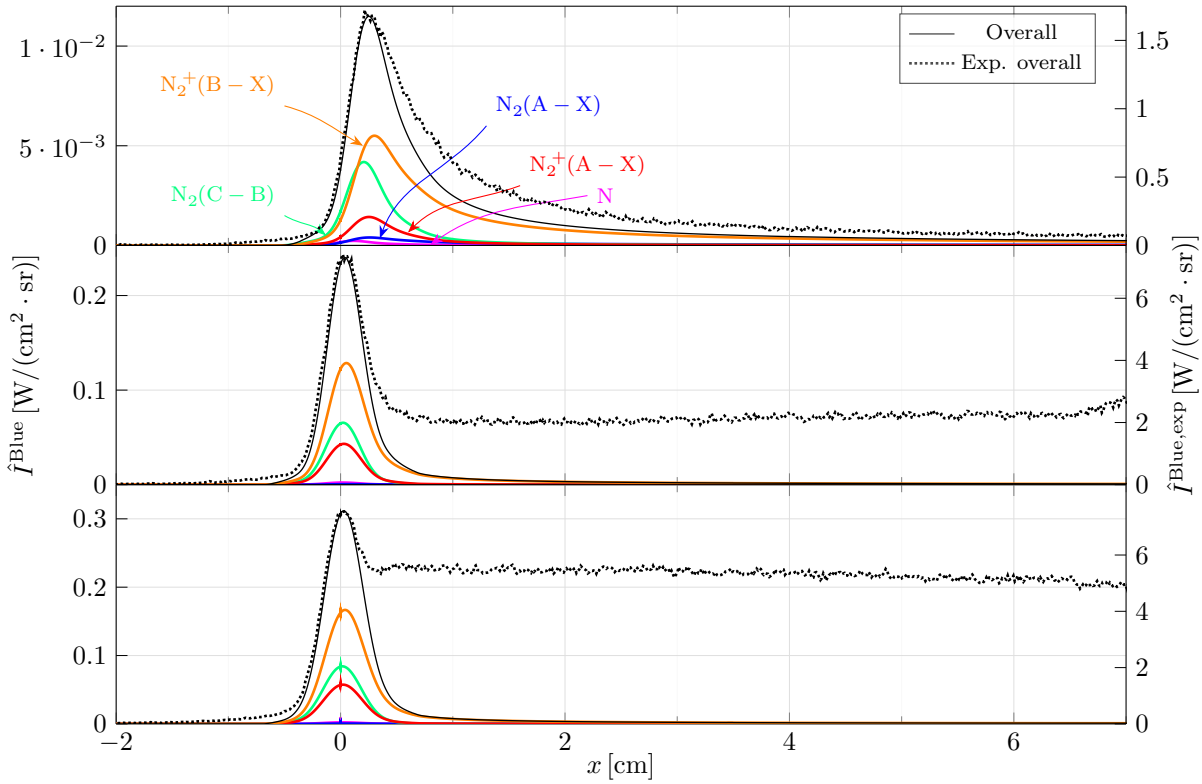

Figure 4.11: Numerical (solid lines) and experimental (dotted lines) instrumentally resolved radiative intensities $\hat{I}^{Blue}(x)$ obtained for the low, medium and high speed shots.

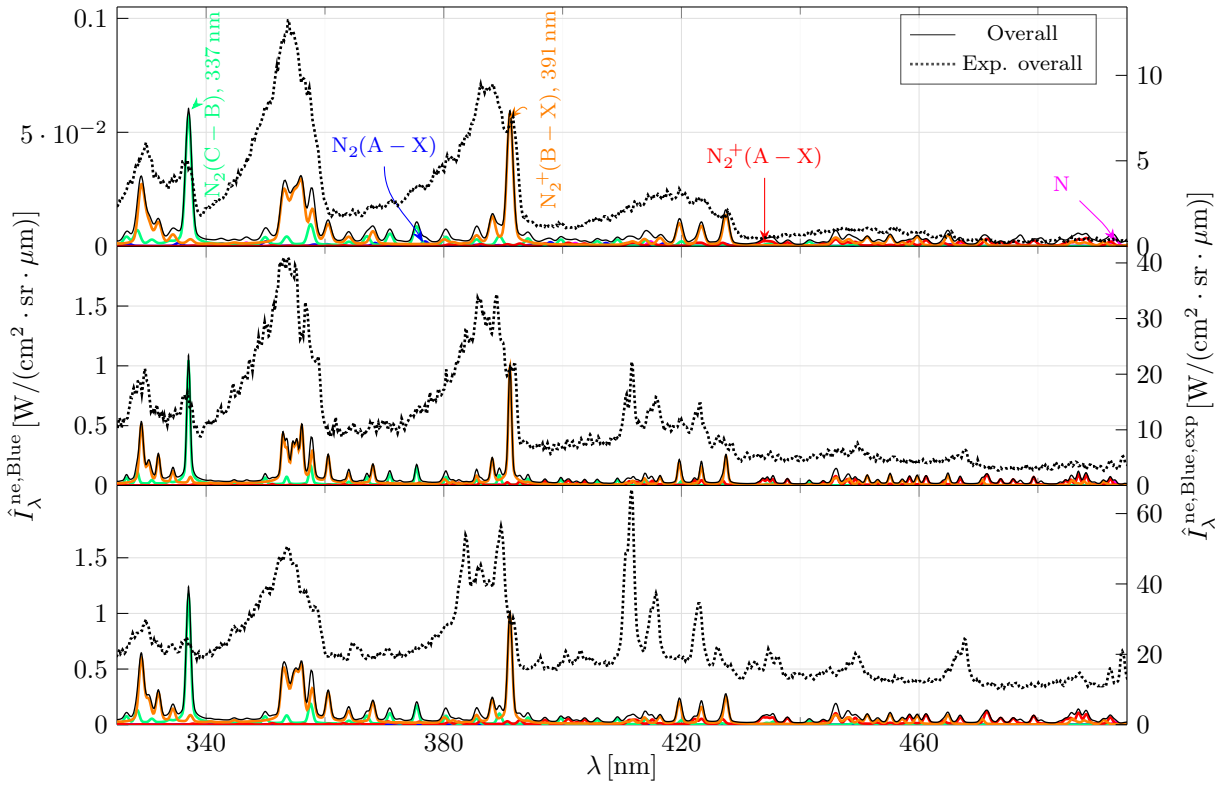

Figure 4.12: Numerical (solid lines) and experimental (dotted lines) instrumentally resolved non-equilibrium metrics $\hat{I}_\lambda^{ne,Blue}(x)$ obtained for the low, medium and high speed shots.

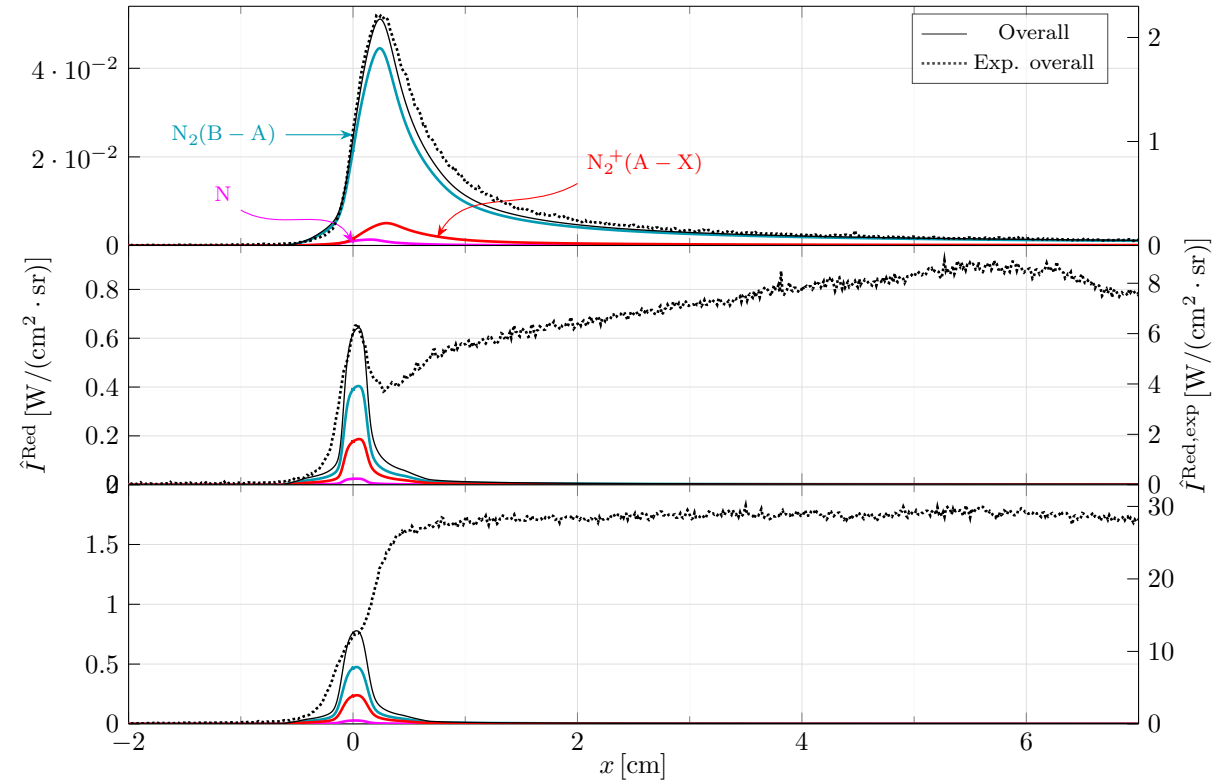

Figure 4.13: Numerical (solid lines) and experimental (dotted lines) instrumentally resolved radiative intensities $\hat{I}^{Red}(x)$ obtained for the low, medium and high speed shots.

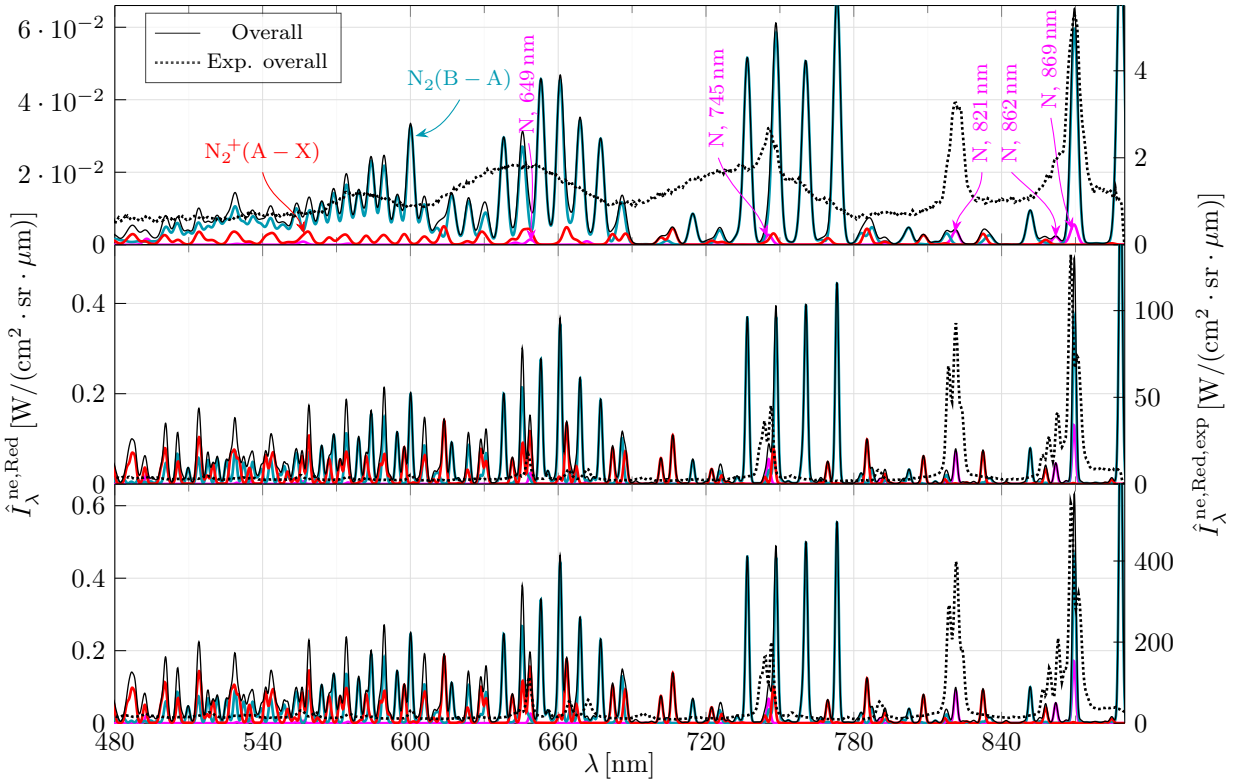

Figure 4.14: Numerical (solid lines) and experimental (dotted lines) instrumentally resolved non-equilibrium metrics $\hat{I}_\lambda^{ne,Red}(x)$ obtained for the low, medium and high speed shots.

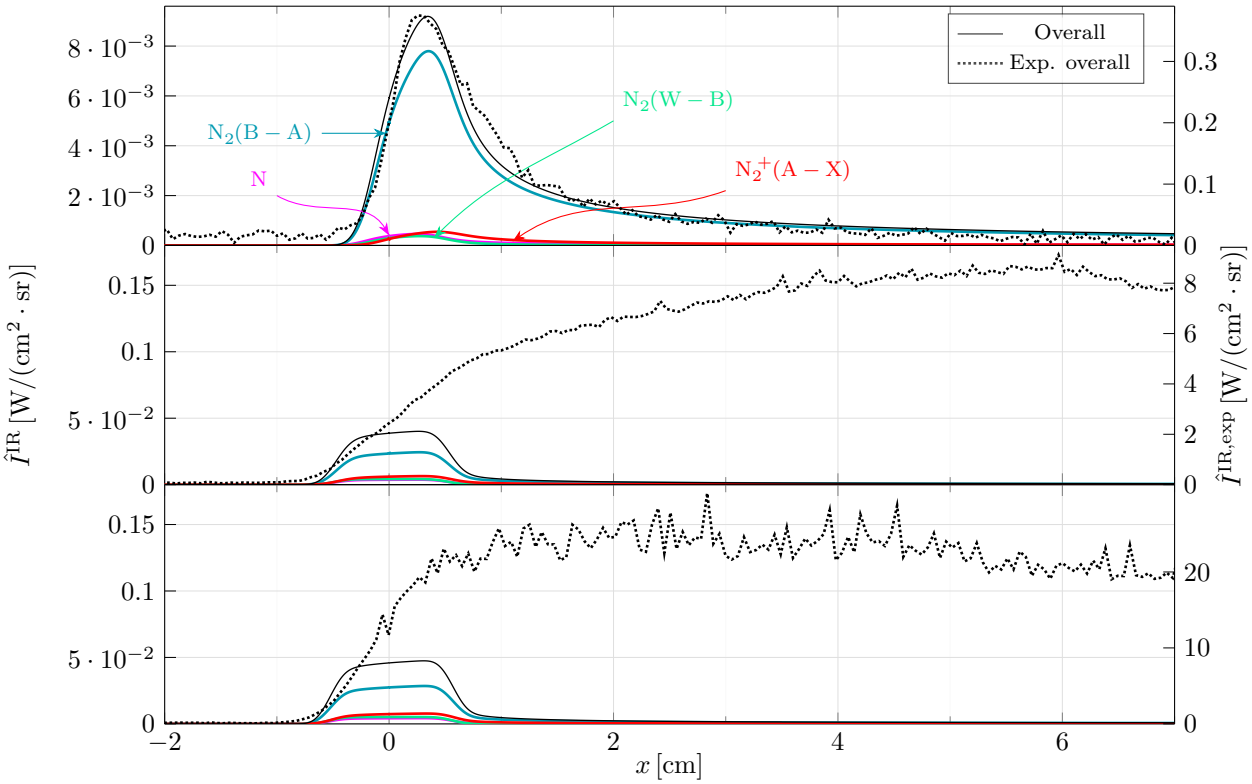

Figure 4.15: Numerical (solid lines) and experimental (dotted lines) instrumentally resolved radiative intensities $\hat{I}^{IR}(x)$ obtained for the low, medium and high speed shots.

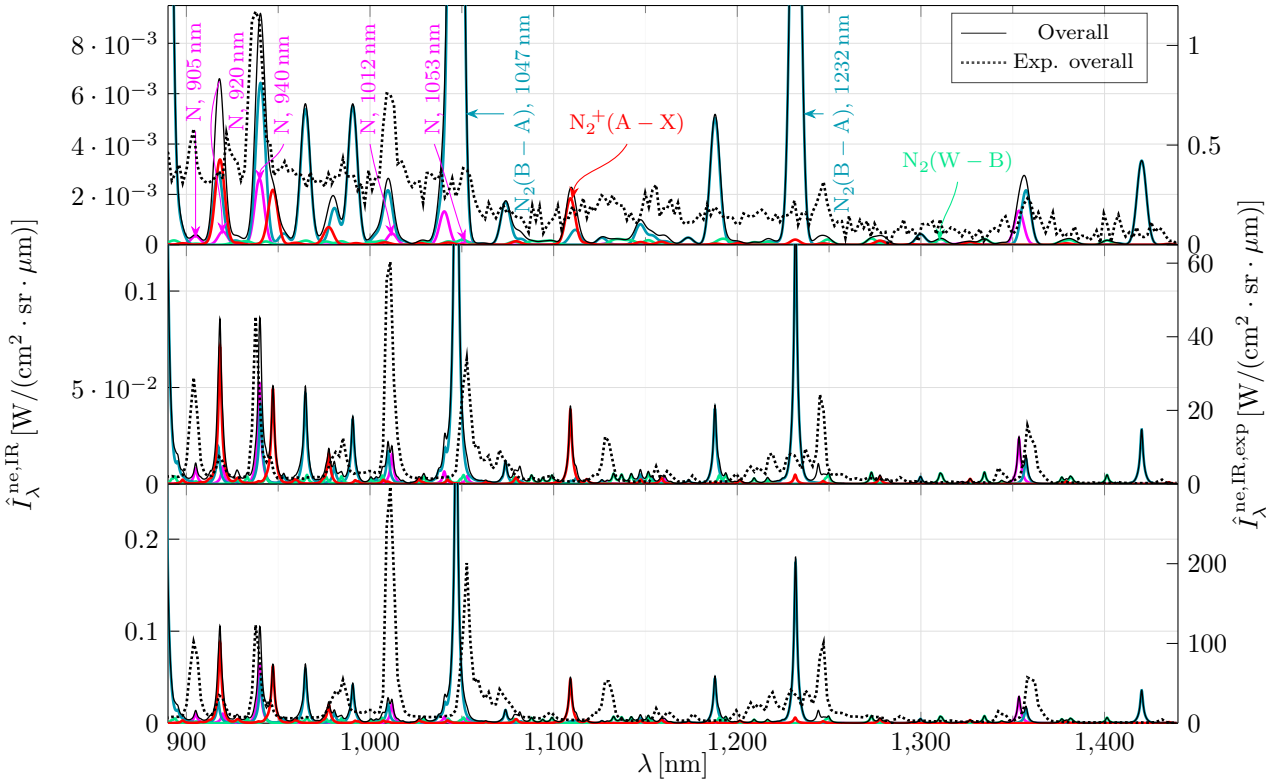

Figure 4.16: Numerical (solid lines) and experimental (dotted lines) instrumentally resolved non-equilibrium metrics $\hat{I}_\lambda^{\mathrm{ne,IR}}(x)$ obtained for the low, medium and high speed shots.

4.4.1 Mole fractions, temperatures, and evolution to equilibrium

Figure 4.17 depicts the obtained heavy particle and free electron translational temperatures, $T_{\mathrm{tr_h}}(x)$ and $T_{\mathrm{tr_e}}(x)$. As according to (3.94), the values of these temperatures, immediately downstream of the shock wave ($x = 0$), correspond to $T_{\mathrm{tr_h},2} = T_{\mathrm{tr_e},2} = 22,434\,\mathrm{K}$, $50,122\,\mathrm{K}$ and $58,565\,\mathrm{K}$ for the low, medium and high speed shots, respectively. As expected, these decrease along x, due to the endothermic processes, to some identical values, and with a rate which is as high as the immediately downstream temperature.

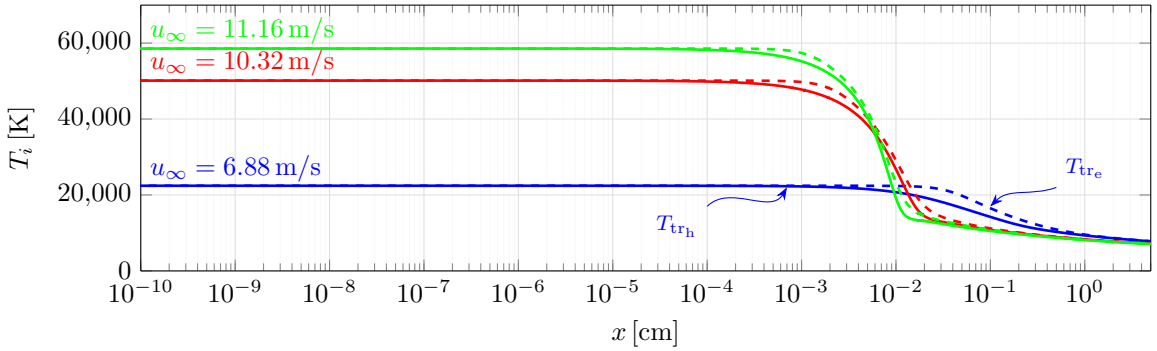

Figure 4.17: Heavy particle (solid lines) and free electron (dashed lines) translational temperatures, $T_{\mathrm{tr_h}}(x)$ and $T_{\mathrm{tr_e}}(x)$, obtained for the low (blue), medium (red) and high (green) speed shots.

Figure 4.18 presents the evolutions of the mole fractions $x_s(x)$ of the five species considered in the simulations - N_2, N, N_2^+, N^+ and e^- - for the low, medium and high speed shots. One finds that an

higher upstream speed implies an earlier dissociation and ionisation of the particles. In the medium and high speed shots, the dissociation is such that the mole fraction of atomic nitrogen N surpasses the mole fraction of molecular nitrogen N_2. There's an increase and posterior decrease of the mole fractions of atomic nitrogen ions N^+, molecular nitrogen ions N_2^+ and free electrons e^-. The former is associated to ionisation and the latter to recombination. The higher the upstream speed, the more abrupt the increases and decreases of the mole fractions of the charged particles are.

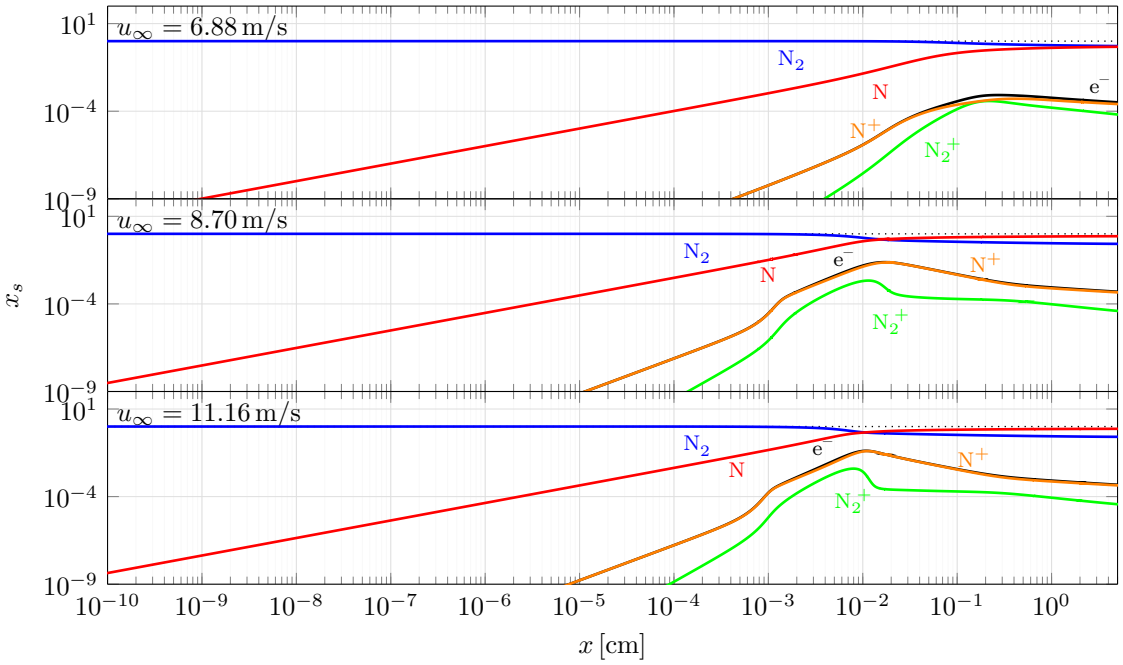

Figure 4.18: Species-specific mole fractions $x_s(x)$ obtained for the low, medium and high speed shots.

Table 4.1 makes a synopsis on the temperatures $T_{\mathrm{tr_h}}$ and $T_{\mathrm{tr_e}}$, and mole fractions x_s, obtained from the simulations of the low, medium and high speed shots, at a far downstream point from the shock wave, $x = 5\,\mathrm{cm}$ - where the radiation intensities were found stagnated. The table also shows the values issued by Cruden and Brandis [158] for the medium speed shot. These were obtained by fitting the conditions of a hypothetical system such that the computed "Blue" and "Red" spectra matched the experimental ones, using the NEQAIR tool [51, 159], at a x position for which the plateaus of radiative intensities occurred. With that objective, a two-temperature model - of temperatures $T_{\mathrm{tr_h-rot}}$ and $T_{\mathrm{vib-el-tr_e}}$ - was assumed and the populations of some particular energy levels were adjusted. Regarding the values of the temperatures at $x = 5\,\mathrm{cm}$ obtained in the present work, one can say that the heavy particle translational temperature departed from the free electron translational temperature by $-18\,\mathrm{K}$ (or $-0.23\,\%$), $-3\,\mathrm{K}$ (or $-0.04\,\%$) and $-1\,\mathrm{K}$ (or $-0.03\,\%$) for the cases of the low, medium and high speed shots. These values are sufficiently small for one to assume that an equilibrium between the respective energy modes was attained. The values of the temperatures obtained by Cruden and Brandis are significantly higher than the ones of this work. The analysis of the "Blue" spectra resulted in a $T_{\mathrm{tr_h}}$ value which is greater by $(1,986 \pm 170)\,\mathrm{K}$ (or $(28 \pm 2)\,\%$) and a $T_{\mathrm{tr_e}}$ value which is greater by $(3,213 \pm 300)\,\mathrm{K}$ (or $(45 \pm 4)\,\%$). The analysis of the "Red" spectra resulted in a $T_{\mathrm{tr_h}}$ value which is greater by $(2,606 \pm 2,490)\,\mathrm{K}$ (or $(36 \pm 35)\,\%$) and a $T_{\mathrm{tr_e}}$ value which is greater by $(2,013 \pm 130)\,\mathrm{K}$ (or $(28 \pm 2)\,\%$). The mole fraction of

N obtained from the simulation of the medium speed shot in the present work, at $x = 5\,\text{cm}$, is almost the double of the one obtained from the simulation of the low speed shot, evidencing a very meaningful augmentation on the dissociation of N_2. The mole fraction of N_2^+ is lower (by 38 %) - due to a much faster recombination - and the one of N^+ is almost the double. The differences between the values of the mole fractions obtained from the simulation of the high speed shot and the ones obtained from the simulation of the medium speed shot aren't significant enough, as also aren't the differences between the upstream speeds. Regarding the results of the work of Cruden and Brandis [158] for the medium speed shot, one can say that not only the differences between the obtained chemical compositions and the one of the present work are staggering but also the difference between the chemical composition resulting from the analysis of the "Blue" spectra and the one resulting from the analysis of the "Red" spectra. The results of the analysis of the "Blue" spectra showed a greater importance of the molecular particles N_2 and N_2^+ and free electrons e^- in the composition, while the results of the analysis of the "Red" spectra showed a greater importance of atomic nitrogen N. In fact, the mole fractions of N_2, N_2^+ and e^- obtained in the the former case are 22, 133 and 30 times greater than the ones obtained in the latter case, and the mole fraction of N is 57 % lower. This incoherence evidences that the models regarded in NEQAIR may not represent sufficiently well the reality. Note that it is true that in the medium speed shot the experimental results showed that the "Blue" spectra was almost completely dominated by radiation of N_2 and N_2^+ while the "Red" spectra was dominated by the radiation of N. However, a valid numerical model should be able to predict both qualities with the same chemical composition of the system, as they were obtained by the same experiment. The results of Cruden and Brandis also evidence a much stronger dissociation of N_2 and ionisation of N than the ones of the present work: the predicted mole fraction of N_2 is at least 9 times lower, and the mole fraction of N^+ is at least 20 times greater. Moreover, this greater dissociation and ionisation are accomplished with a much lower cost of heavy particle and free electron translational temperatures. Such result means that the post-shock elements of fluid simulated in the present work may have lost more energy than they should, or didn't gain as much. Since it was found that the radiation variables were underpredicted by several orders of magnitude, the former hypothesis should be disregarded. Two possible ways of the elements of fluid gaining more energy are by absorption of radiation and conduction of heat, being both not taken into account in the simulations. The former contribution should be more important since it makes the overall system to loose less than before (part of the radiative energy which was once lost is retained) while the latter contribution simply redistributes the energy within it without reducing the losses.

Table 4.1: Temperatures T_{tr_h} and T_{tr_e}, and mole fractions x_s, at $x = 5\,\text{cm}$, obtained from the simulations of the low, medium and high speed shots, as well as the ones obtained by Cruden and Brandis [158].

u_∞[m/s]	Ref.	T_{tr_h}[K]	T_{tr_e}[K]	x_{N_2}	x_N	$x_{N_2^+}$	x_{N^+}	x_{e^-}	x_{CN}	x_H
6.88	This work	$7,793$	$7,811$	0.52	0.48	6.5×10^{-5}	2.6×10^{-4}	3.2×10^{-4}	—	—
10.32	This work	$7,184$	$7,187$	0.27	0.73	4.0×10^{-5}	4.5×10^{-4}	4.9×10^{-4}	—	—
	NEQAIR, "Blue" [158]	$9,170 \pm 170$	$10,400 \pm 300$	0.029	0.42	0.016	0.27	0.27	7.3×10^{-4}	—
	NEQAIR, "Red" [158]	$9,790 \pm 2,490$	$9,200 \pm 130$	0.0013	0.98	1.2×10^{-4}	0.0089	0.0089	—	0.0010
11.16	This work	$7,098$	$7,100$	0.26	0.74	3.7×10^{-5}	4.4×10^{-4}	4.7×10^{-4}	—	—

To ascertain the impact of energy loss by radiation on the developed conditions of the post-shock flow, it was decided to perform simulations disregarding spontaneous emission processes and to compare the respective results with the ones obtained when regarding them. Table 4.2 makes a synopsis on the resultant temperatures $T_{\mathrm{tr_h}}$ and $T_{\mathrm{tr_e}}$, and mole fractions x_s, at $x = 5\,\mathrm{cm}$. All of the temperatures are higher than the respective ones obtained when regarding spontaneous emission processes, and increasing with the upstream speed. While the differences are negligible for the case of the low speed shot - $T_{\mathrm{tr_h}}$ differs by just 266 K (or 3.4 %) - they are meaningful for the case of the medium and high speed shots - $T_{\mathrm{tr_h}}$ differs by 2080 K (or 29 %) and 3,016 K (or 42 %). Meanwhile, a greater dissociation and ionisation had occurred, as evidenced by the lower value for the mole fraction of N_2 and the higher values for the mole fractions of N and N^+. These results show that the energy dumped by spontaneous emission in the highly excited systems has a much higher proportion than in the less excited ones. The more excited the particles are, the higher the number of spontaneous emissions and the higher the energy that is lost through radiation. Surprisingly, the conditions for the medium speed shot disregarding spontaneous emission processes are now coherent with the ones obtained by Cruden and Brandis [158], with the exception of the mole fraction of N_2^+ which is substantiality lower. This result sheds light to the previously enunciated hypothesis of the simulated elements of fluid not receiving the energy that their counterparts seem to receive in the experiment.

Table 4.2: Temperatures $T_{\mathrm{tr_h}}$ and $T_{\mathrm{tr_e}}$, and mole fractions x_s, obtained from the simulations of the low, medium and high speed shots, at $x = 5\,\mathrm{cm}$, disregarding spontaneous emission processes.

u_∞[m/s]	$T_{\mathrm{tr_h}}$[K]	$T_{\mathrm{tr_e}}$[K]	$x_{\mathrm{N_2}}$	x_{N}	$x_{\mathrm{N_2^+}}$	$x_{\mathrm{N^+}}$	$x_{\mathrm{e^-}}$
6.88	8,059	8,076	0.46	0.54	1.0×10^{-4}	4.6×10^{-4}	5.7×10^{-4}
10.32	9,264	9,265	0.022	0.93	3.1×10^{-5}	0.022	0.022
11.16	10,114	10,114	0.0041	0.89	2.4×10^{-5}	0.052	0.052

Another important result that may be ascertained from the numerical simulations is the disparity from thermal equilibrium of the systems conditions. This can be done through computation of *representative temperatures*. A representative temperature with respect to a particular energy mode is quantified by the populations of its energy levels, and solely corresponds to a true temperature if self-equilibrium of the energy mode was attained. In this work, a *representative electronic temperature* was considered for each heavy species, as well as a *representative vibrational temperature* for each electronic level of each molecular species. The way that these variables were defined will be now described.

By invoking the reasoning presented in section §2.2, assuming uncoupling between the rotational and the vibrational energy modes[2], one may infer that if the s-th species particles in the n-th electronic level are at a vibrational temperature $T_{s,\mathrm{vib},n}$, the population of its m-th vibrational level is simply given by

$$N_{s,m,n} = N_{s,n} \frac{g_{s,\mathrm{vib},n,m}\, e^{-\frac{\epsilon_{s,\mathrm{vib},n,m}}{k_B T_{s,\mathrm{vib},n}}}}{Q_{s,\mathrm{vib},n}(T_{s,\mathrm{vib},n})} \ . \tag{4.1}$$

[2]In the SPARK code, the spectroscopic constant α_e was disregarded.

And, by further manipulating (4.1), it's possible to obtain

$$\ln\left(\frac{x_{s,m,n}}{g_{s,\mathrm{el},n}\cdot g_{s,\mathrm{vib},n,m}}\right) = -\frac{1}{k_B T_{s,\mathrm{vib},n}}\epsilon_{s,\mathrm{vib},n,m} + \ln\left(\frac{x_{s,n}}{g_{s,\mathrm{el},n}\cdot Q_{s,\mathrm{vib},n}(T_{s,\mathrm{vib},n})}\right) \ , \tag{4.2}$$

where $x_{s,m,n} = N_{s,m,n}/N$ is the mole fraction of s-th species particles in their n-th electronic level and m-th vibrational level, and $x_{s,n} = N_{s,n}/N$ is the mole fraction of s-th species particles in their n-th electronic level. Equation (4.2) tells that under vibrational self-equilibrium, the natural logarithm of the mole fraction of s-th species particles in a state of the n-th electronic level and m-th vibrational level, i.e. $\ln(x_{s,m,n}/(g_{s,\mathrm{el},n}\cdot g_{s,\mathrm{vib},n,m}))$, decreases linearly with their vibrational energy $\epsilon_{s,\mathrm{vib},n,m}$. A plot of $\ln(x_{s,m,n}/(g_{s,\mathrm{el},n}\cdot g_{s,\mathrm{vib},n,m}))$ against $\epsilon_{s,\mathrm{vib},n,m}$ with s and n fixed, would show points positioned in a line of slope $-1/(k_B T_{s,\mathrm{vib},n})$ and of ordinate of the y-intercept $\ln(x_{s,n}/[g_{s,\mathrm{el},n}\cdot Q_{s,\mathrm{vib},n}(T_{s,\mathrm{vib},n})])$. The representative vibrational temperature associated to the n-th electronic level of the s-th species $T_{s,\mathrm{vib},n}$ which may or may not be in vibrational self-equilibrium is defined in this work as the respective value obtained from a fit of the curve (4.2) to the numerically obtained points of abscissae $\epsilon_{s,\mathrm{vib},n,m}$ and ordinates $\ln(x_{s,m,n}/(g_{s,\mathrm{el},n}\cdot g_{s,\mathrm{vib},n,m}))$. If the s-th species particles are at an electronic temperature $T_{s,\mathrm{el}}$, and uncoupling between the rotational and vibrational energy modes is further assumed as well as between the rotational and the electronic energy modes[3], the population of its n-th electronic level is simply given by

$$N_{s,n} = N_s \frac{g_{s,\mathrm{el},n}\, e^{-\frac{\epsilon_{s,\mathrm{el},n}}{k_B T_{s,\mathrm{el}}}}\, Q_{s,\mathrm{vib},n}(T_{s,\mathrm{vib},n})}{Q_{s,\text{el-vib}}(\{T_{s,\mathrm{vib},n}\}, T_{s,\mathrm{el}})} \ , \tag{4.3}$$

being $Q_{s,\text{el-vib}} = \sum_n g_{s,\mathrm{el},n}\, e^{-\frac{\epsilon_{s,\mathrm{el},n}}{k_B T_{s,\mathrm{el}}}} Q_{s,\mathrm{vib},n}(T_{s,\mathrm{vib},n})$. Expression (4.3) may be conveniently transformed into

$$\ln\left(\frac{x_{s,n}}{g_{s,\mathrm{el},n}}\right) = -\frac{1}{k_B T_{s,\mathrm{el}}}\epsilon_{s,\mathrm{el},n} + \ln\left(\frac{x_s \cdot Q_{s,\mathrm{vib},n}(T_{s,\mathrm{vib},n})}{Q_{s,\text{el-vib}}(\{T_{s,\mathrm{vib},n}\}, T_{s,\mathrm{el}})}\right) \ . \tag{4.4}$$

The representative electronic temperature associated to the s-th species $T_{s,\mathrm{el}}$ which may or may not be in electronic self-equilibrium is defined in this work as the respective value obtained from a fit of the curve (4.4) to the numerically obtained points of abscissae $\epsilon_{s,\mathrm{el},n}$ and ordinates $\ln(x_{s,n}/g_{s,\mathrm{el},n})$. In thermal equilibrium conditions, one has $T_{\mathrm{tr_h}} = T_{\mathrm{tr_e}} = T_{s,\mathrm{vib},n} = T_{s,\mathrm{el}} := T$, $\forall$ s and n. By inserting (4.4) into (4.2) one gets in such conditions

$$\ln\left(\frac{x_{s,m,n}}{g_{s,\mathrm{el},n}\cdot g_{s,\mathrm{vib},n,m}}\right) = -\frac{1}{k_B T}\left(\epsilon_{s,\mathrm{el},n} + \epsilon_{s,\mathrm{vib},n,m}\right) + \ln\left(\frac{x_s}{Q_{s,\text{el-vib}}(T)}\right) \ . \tag{4.5}$$

Therefore, at thermal equilibrium, the points of abscissae $\epsilon_{s,\mathrm{el},n}+\epsilon_{s,\mathrm{vib},n,m}$ and ordinates $\ln(x_{s,m,n}/(g_{s,\mathrm{el},n}\cdot g_{s,\mathrm{vib},n,m}))$, with s fixed, lay in the same curve, being this of slope $-1/(k_B T)$ and of y-intercept $\ln(x_s/Q_{s,\text{el-vib}}(T))$. And if the the vibrational partition function $Q_{s,\mathrm{vib},n}$ doesn't vary too much with the electronic level n such that $Q_{s,\mathrm{vib},n} \approx Q_{s,\mathrm{vib}}$, one may also show from relation (4.4) that in thermal equilibrium the points of abscissae $\epsilon_{s,\mathrm{el},n}$ and ordinates $\ln(x_{s,n}/g_{s,\mathrm{el},n})$, with s fixed, lay in the same curve, being this of slope $-1/(k_B T)$ and of y-intercept $\ln(x_s/Q_{s,\mathrm{el}}(T))$. The representative vibrational and electronic temperatures may in their turn be used to compute *Boltzmann representative vibronic*

[3]In the SPARK code, the spectroscopic constant B_e was approximated by the respective one for the ground electronic level.

mole fractions $x^B_{s,n,m} := x_{s,n,m}(T_{s,\mathrm{vib},n})$ - given by (4.2) - and *Boltzmann representative electronic mole fractions* $x^B_{s,n} := x_{s,n}(T_{s,\mathrm{vib},n}, T_{s,\mathrm{el}})$ - given by (4.4).

Figure 4.19 shows the electronic state-specific mole fractions $x_{s,e}/g_{s,\mathrm{el},e}$ (markers) and respective Boltzmann representatives $x^{\mathrm{B}}_{s,e}/g_{s,\mathrm{el},e}$ (lines) obtained from the simulations of the low, medium and high speed shots, at $x = 5\,\mathrm{cm}$. The markers in the figure sparsely agree with the respective lines. This result shows that self-equilibrium of the electronic energy modes of the different species wasn't attained at $x = 5\,\mathrm{cm}$. Also, one should warn the reader to note that the obtained lines associated to N_2 and N_2^+ aren't straight. As mentioned above, the dependence of the vibrational partition functions on the electronic levels may not be negligible, as it seems not to be for the case of theses species.

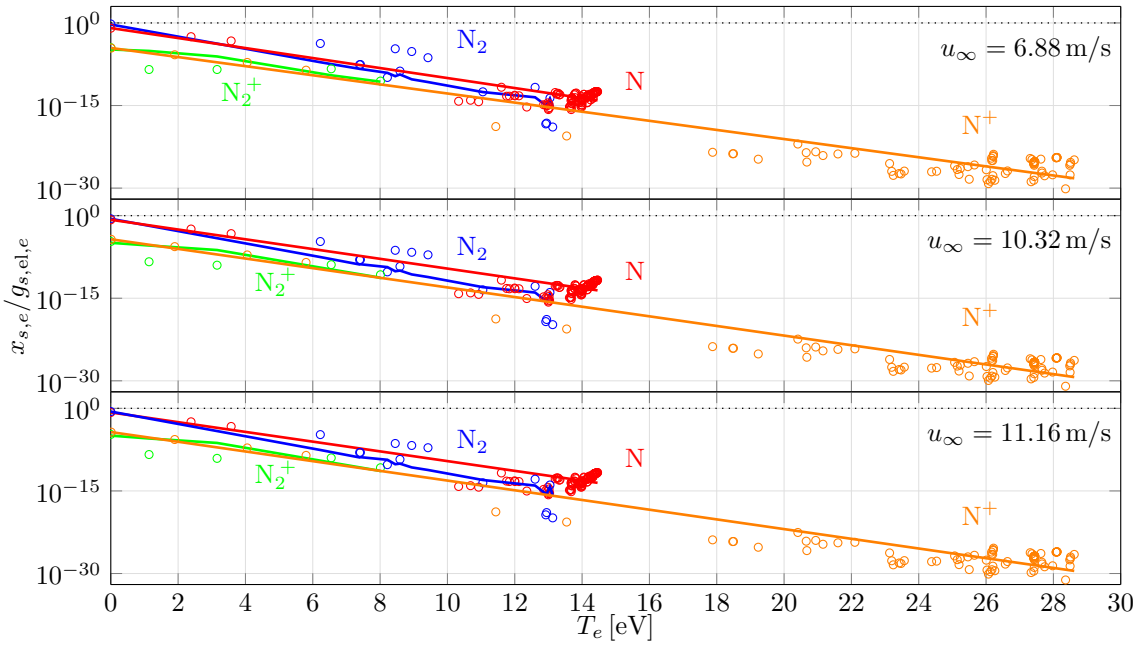

Figure 4.19: Electronic state-specific mole fractions $x_{s,e}/g_{s,\mathrm{el},e}$ (markers) and respective Boltzmann representatives $x^{\mathrm{B}}_{s,e}/g_{s,\mathrm{el},e}$ (lines) as functions of the electronic energies T_e, obtained from the simulations of the low, medium and high speed shots, at $x = 5\,\mathrm{cm}$.

The obtained representative electronic temperatures are presented by Table 4.3. It shows that these temperatures depart from each other and from the obtained heavy particle and free electron translational ones in the order of the thousands of kelvins. In fact, the variables $T_{s,\mathrm{el}}$ are all lower than $T_{\mathrm{tr_h}}$, by amounts from $3,359\,\mathrm{K}$ (or $43.10\,\%$) to $1,407\,\mathrm{K}$ (or $18.05\,\%$), $2,811\,\mathrm{K}$ (or $39.13\,\%$) to $968\,\mathrm{K}$ (or $13.47\,\%$), and $2740\,\mathrm{K}$ (or $38.60\,\%$) to $932\,\mathrm{K}$ (or $13.13\,\%$), for the cases of the low, medium and high speed shots, respectively. Therefore, one cannot state that the electronic and the translational energy modes attained an equilibrium between themselves at $x = 5\,\mathrm{cm}$.

Table 4.3: Heavy particle and free electron translational temperatures $T_{\mathrm{tr_h}}$ and $T_{\mathrm{tr_e}}$, and representative electronic temperatures $T_{s,\mathrm{el}}$ obtained from the simulations of the low, medium and high speed shots, at $x = 5\,\mathrm{cm}$.

u_∞[m/s]	$T_{\mathrm{tr_h}}$[K]	$T_{\mathrm{tr_e}}$[K]	$T_{\mathrm{N_2,el}}$[K]	$T_{\mathrm{N,el}}$[K]	$T_{\mathrm{N_2^+,el}}$[K]	$T_{\mathrm{N^+,el}}$[K]
6.88	7,793	7,811	4,434	5,551	6,386	6,093
10.32	7,184	7,187	4,373	5,682	6,216	5.762
11.16	7,098	7,100	4,358	5,699	6,166	5,719

Figure 4.20 shows the obtained vibronic state-specific mole fractions $x_{s,e,v}/(g_{s,\mathrm{el},e} \cdot g_{s,\mathrm{vib},e,v})$ and respective Boltzmann representatives $x^{\mathrm{B}}_{s,e,v}/(g_{s,\mathrm{el},e} \cdot g_{s,\mathrm{vib},e,v})$ at $x = 5\,\mathrm{cm}$. In this figure, there are markers that agree remarkably well with the respective lines (vibrational self-equilibrium was in those cases achieved), and others (the ones associated to the seemingly horizontal lines) which don't agree at all. It can be shown that the deviations of the latter are due to the non-modelling of the spontaneous emission processes of the higher vibronic levels, implying these to not be depopulated through spontaneous emission in contrast to the lower ones. When fitting the respective vibronic state-specific mole fractions, a nearly horizontal line is obtained, which is associated to a very high representative vibrational temperature. This result is clearly unphysical. To avoid it in the future, one should consider a redistribution procedure on the Einstein coefficients for spontaneous emission to model the vibronic levels whose data aren't available.

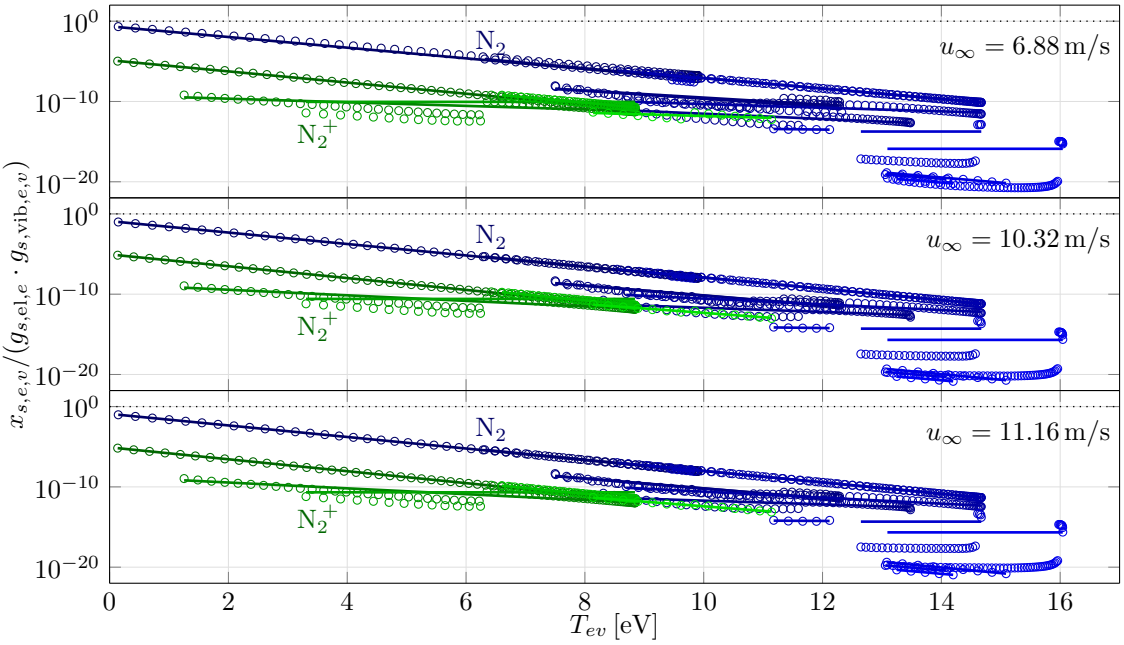

Figure 4.20: Vibronic state-specific mole fractions $x_{s,e,v}/(g_{s,\mathrm{el},e} \cdot g_{s,\mathrm{vib},e,v})$ (markers) and respective Boltzmann representatives $x^{\mathrm{B}}_{s,e,v}/(g_{s,\mathrm{el},e} \cdot g_{s,\mathrm{vib},e,v})$ (lines) as functions of the vibronic energies T_{ev}, obtained from the simulations of the low, medium and high speed shots, at $x = 5\,\mathrm{cm}$.

The non-absurd values of $T_{s,\mathrm{vib},n}$ deviate from $T_{\mathrm{tr_h}}$ by amounts from $-843\,\mathrm{K}$ (or $-10.82\,\%$) to $3,730\,\mathrm{K}$ (or $47.86\,\%$), $-383\,\mathrm{K}$ (or $-5.33\,\%$) to $1,112\,\mathrm{K}$ (or $15.48\,\%$), and $-311\,\mathrm{K}$ (or $-4.38\,\%$) to $1,188\,\mathrm{K}$ (or $16.74\,\%$), for the cases of the low, medium and high speed shots, respectively. These values are too large for one to assume that equilibrium between the vibrational and translational energy modes was

attained for all the considered electronic levels. It's important to note that markers associated to the same species don't lay on the same line, showing that the respective electronic energy mode isn't at self-equilibirum (as also evidenced by the fact that the markers in Figure 4.19 don't coincide with their Boltzmann representatives).

Since no absorption and induced emission processes weren't considered in this work, spontaneous emission occurred without any counterbalance. This may have led to the observed self-non-equilibrium of the electronic energy modes. Figure 4.21 shows the electronic state-specific mole fractions $x_{s,e}/g_{s,\mathrm{el},e}$ and respective Boltzmann representatives $x^{\mathrm{B}}_{s,e}/g_{s,\mathrm{el},e}$ obtained from the simulations of the low, medium and high speed shots, at $x = 5\,\mathrm{cm}$, disregarding spontaneous emission. The markers in this figure agree much more with the respective lines than in Figure 4.19, whose results were obtained assuming spontaneous emission. Self-equilibrium of the electronic energy modes seems to be attained by all species with the exception of N_2 and N in the case of the low speed shot, as the respective markers slightly depart from the lines. Table 4.4 presents the obtained representative electronic temperatures. The variables $T_{s,\mathrm{el}}$ depart from $T_{\mathrm{tr_h}}$, by amounts from $-948\,\mathrm{K}$ (or $-11,76\,\%$) to $432\,\mathrm{K}$ (or $5.36\,\%$), $-83\,\mathrm{K}$ (or $-0.90\,\%$) to $39\,\mathrm{K}$ (or $0.42\,\%$), and $-81\,\mathrm{K}$ (or $-0.80\,\%$) to $11\,\mathrm{K}$ (or $0.11\,\%$), for the cases of the low, medium and high speed shots, respectively. All these values are negligibly small with the exception of the ones of the former case, being the lower limit due to N and the higher limit due to N_2, which, as mentioned above, were also found to not be at electronic self-equilibrium. One can state that the electronic and the translational energy modes of the particles attained an equilibrium between themselves at $x = 5\,\mathrm{cm}$, with the exception of N and N_2 in the case of low speed shot.

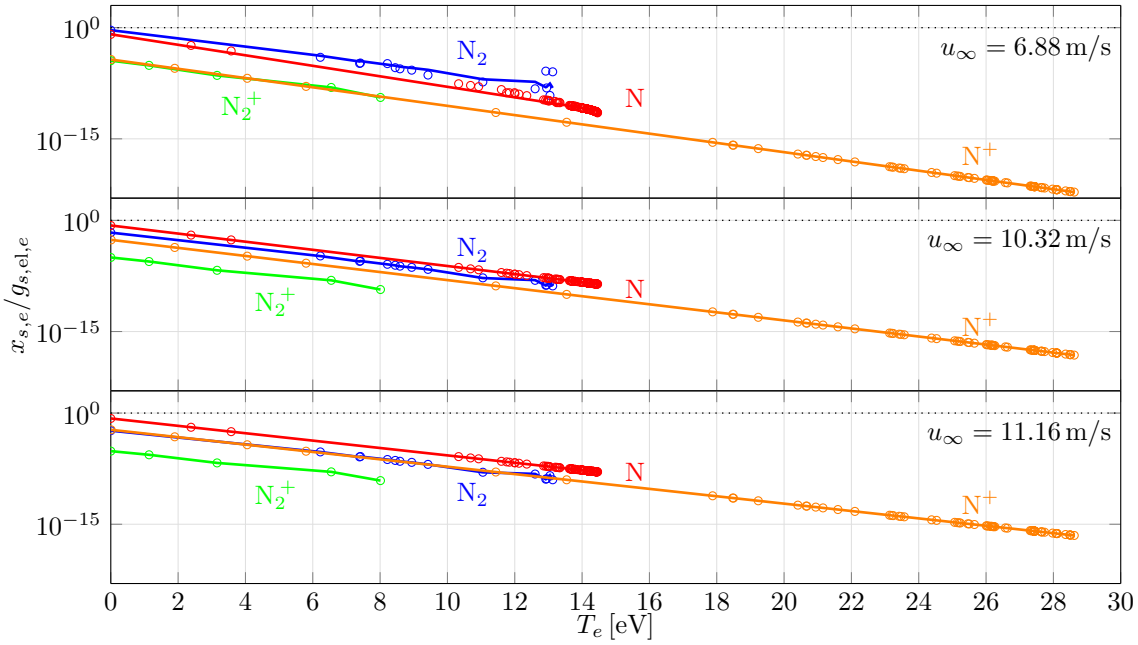

Figure 4.21: Electronic state-specific mole fractions $x_{s,e}/g_{s,\mathrm{el},e}$ (markers) and respective Boltzmann representatives $x^{\mathrm{B}}_{s,e}/g_{s,\mathrm{el},e}$ (lines) as functions of the electronic energies T_e, obtained from the simulations of the low, medium and high speed shots, at $x = 5\,\mathrm{cm}$, disregarding spontaneous emission processes.

Table 4.4: Heavy particle and free electron translational temperatures $T_{\mathrm{tr_h}}$ and $T_{\mathrm{tr_e}}$, and representative electronic temperatures $T_{s,\mathrm{el}}$ obtained from the simulations of the low, medium and high speed shots, at $x = 5\,\mathrm{cm}$, disregarding spontaneous emission.

u_∞[m/s]	$T_{\mathrm{tr_h}}$[K]	$T_{\mathrm{tr_e}}$[K]	$T_{\mathrm{N_2,el}}$[K]	$T_{\mathrm{N,el}}$[K]	$T_{\mathrm{N_2^+,el}}$[K]	$T_{\mathrm{N^+,el}}$[K]
6.88	8,059	8,078	8,491	7,111	8,100	8.063
10.32	9,264	9,271	9,181	9.216	9.303	9.271
11.16	10,114	10,116	10,033	10,113	10,125	10,116

Figure 4.22 shows the vibronic state-specific mole fractions $x_{s,e,v}/(g_{s,\mathrm{el},e} \cdot g_{s,\mathrm{vib},e,v})$ and respective Boltzmann representatives $x^{\mathrm{B}}_{s,e,v}/(g_{s,\mathrm{el},e} \cdot g_{s,\mathrm{vib},e,v})$, obtained from the simulations of the low, medium and high speed shots, at $x = 5\,\mathrm{cm}$, disregarding spontaneous emission. All markers in 4.22 lay in the respective lines, evidencing that vibrational self-equilibrium occurs. However, the lines associated to N_2 for the case of the low speed shot depart slightly from each other. This is a result of an electronic self-non-equilibrium of N_2, which was already mentioned before. The values of $T_{s,\mathrm{vib},n}$ deviate from $T_{\mathrm{tr_h}}$ by amounts from $-1,557\,\mathrm{K}$ (or $-19.32\,\%$) to $46\,\mathrm{K}$ (or $0.57\,\%$), $-1,052\,\mathrm{K}$ (or $-11.36\,\%$) to $42\,\mathrm{K}$ (or $0.45\,\%$), and $-729\,\mathrm{K}$ (or $-7.21\,\%$) to $13\,\mathrm{K}$ (or $0.13\,\%$), for the cases of the low, medium and high speed shots, respectively. The lower limits of the deviations are significant and in the same order of magnitude as the ones obtained when considering spontaneous emission. The upper limits are, however, much smaller. The vibrational and translational energy modes should therefore be closer to an equilibrium between each other when disregarding spontaneous emission than when regarding.

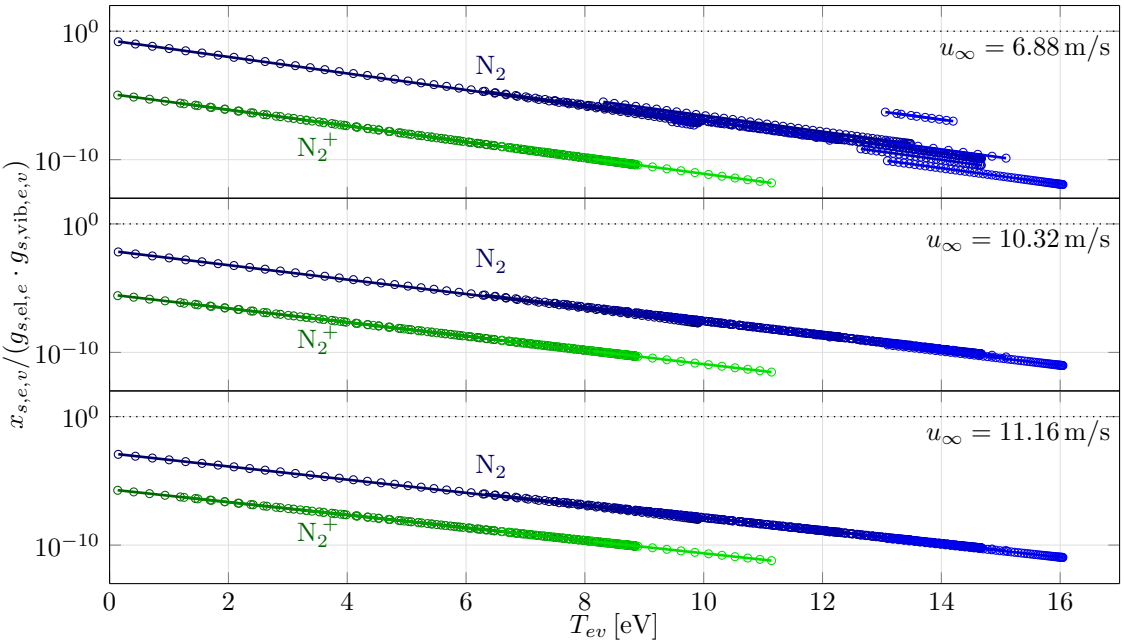

Figure 4.22: Vibronic state-specific mole fractions $x_{s,e,v}/(g_{s,\mathrm{el},e} \cdot g_{s,\mathrm{vib},e,v})$ (markers) and respective Boltzmann representatives $x^{\mathrm{B}}_{s,e,v}/(g_{s,\mathrm{el},e} \cdot g_{s,\mathrm{vib},e,v})$ (lines) as functions of the vibronic energies T_{ev}, obtained from the simulations of the low, medium and high speed shots, at $x = 5\,\mathrm{cm}$, disregarding spontaneous emission processes.

All of the above-mentioned results allow the author to conclude that the spontaneous emission

processes strongly contribute to the observed thermal non-equilibrium conditions of the systems at $x = 5\,\text{cm}$. It should be ascertained in the future if the consideration of absorption and induced emission processes may reduce this thermal non-equilibrium. The results also showed that collisional processes, alone, don't ensure equilibrium between the electronic and translational energy modes of N_2 and N in the case of the low speed shot.

4.4.2 Dependence on the escape factor

It is well known that the emitted VUV radiation is strongly absorbed by the particles in the medium [158] and, therefore, the assumption of it being optically thin may not be valid. By considering an escape factor $\Lambda^{\text{VUV}} < 1$ in the simulations, it's possible to take into account, in a crude way, the effect of auto-absorption (i.e. absorption by the same emitting source) of the VUV radiation on the resultant radiation variables. Part of the energy which was once lost due to emitted VUV radiation escaping from the system may now be used in other processes. More energy becomes available for excitation of the particles, and as a consequence, more energy is radiated in the other wavelength intervals. There's even the possibility of more radiative energy in the VUV wavelength interval escaping from the system, since though a significant fraction of the photons don't escape, the number of emitted photons becomes as high as the number excited particles. Values of $\Lambda^{\text{VUV}} = 0.1$ and 0.01 were tried, and the respective overall radiation variables, are shown in Figures 4.23 to 4.30.

Figure 4.23 shows that by decreasing the escape factor, the peak values of the instrumentally resolved radiative intensities in the VUV wavelength region decreased as much as a half in the three shots. On the other hand, the contributions of N increased significantly becoming now much more dominant than the others (i.e. the ones of $N_2^+(C - X)$, $N_2(a - X)$ and $N_2(A - X)$), as shown in Figure 4.24). The obtained spectra show better agreeability with the experimental result. The radiative intensity profiles show steeper rises and falls, and, in the case of the low speed shot, it got closer to the experimental one. Still, no plateaus were predicted in the cases of the medium and high speed shots. For the case of the "Blue" wavelength region, the decrease in the escape factor made the peak values of the instrumentally resolved radiative intensities to increase with some significance: as much as 10% in the low speed shot, and 40% in the medium and high speed shots. The change on the shape of the peaks isn't noticeable to the eye (see Figure 4.25). Regarding the shape of the instrumentally resolved non-equilibrium metric, Figure 4.26 shows that solely the peak associated to $N_2(C - B)$ at $\lambda = 337\,\text{nm}$ suffered a meaningful change, increasing its height with the decrease in the escape factor value. For the case of the "Red" and IR wavelength regions, the peak values of the instrumentally resolved radiative intensities also increased: as much as 10% in the low speed shot, and 60% (for the case of the former) and 80% (for the case of the latter) in the medium and high speed shots. The shapes of the peaks didn't change significantly. And the contributions of N to the non-equilibrium metrics were preferentially augmented (in particular in the medium and high speed shots), agreeing better with the experimental results.

These results show strong evidence for the studied medium being optically thick in the VUV wavelength region.

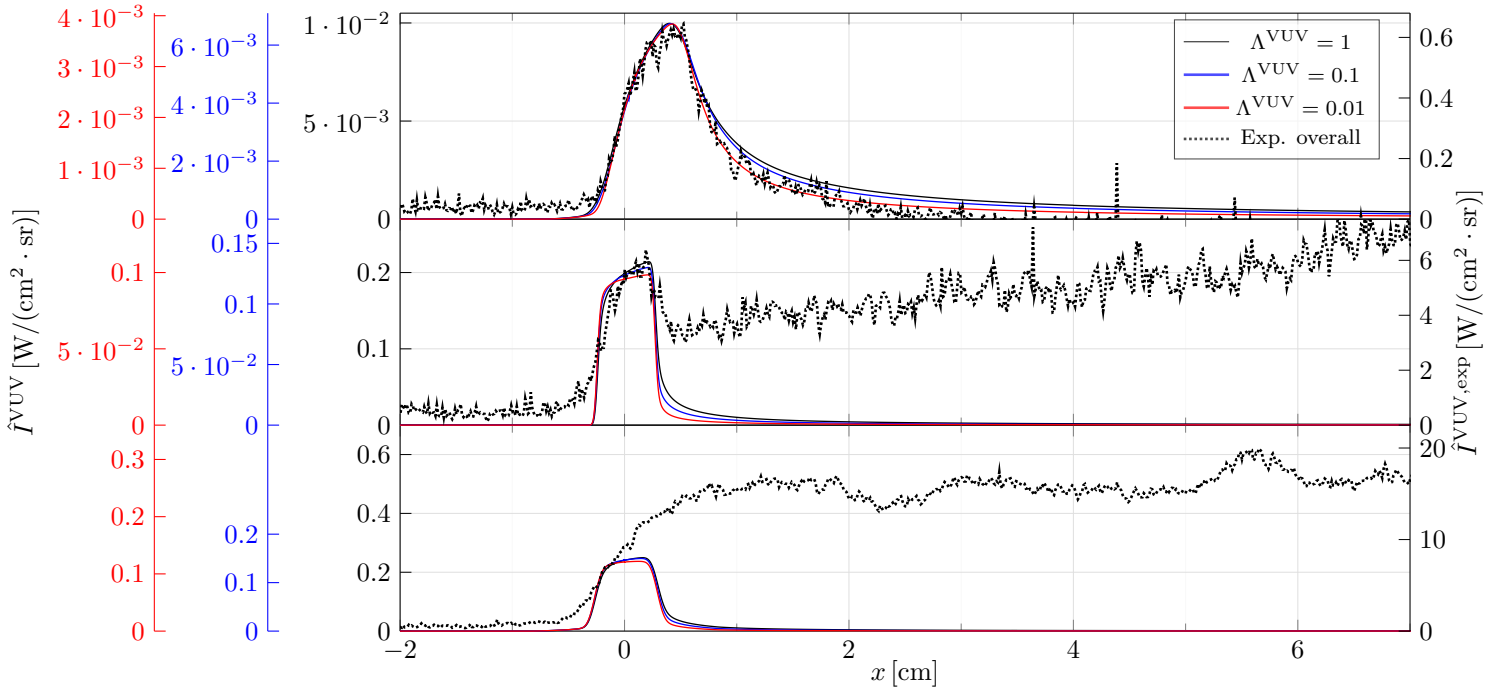

Figure 4.23: Numerical instrumentally resolved radiative intensities $\hat{I}^{\mathrm{VUV}}(x)$, obtained with $\Lambda^{\mathrm{VUV}} = 1$ (solid black lines), $\Lambda^{\mathrm{VUV}} = 0.1$ (solid blue lines), and $\Lambda^{\mathrm{VUV}} = 0.01$ (solid red lines), as well as the respective experimental instrumentally resolved radiative intensities $\hat{I}^{\mathrm{VUV,exp}}(x)$ (dotted black lines).

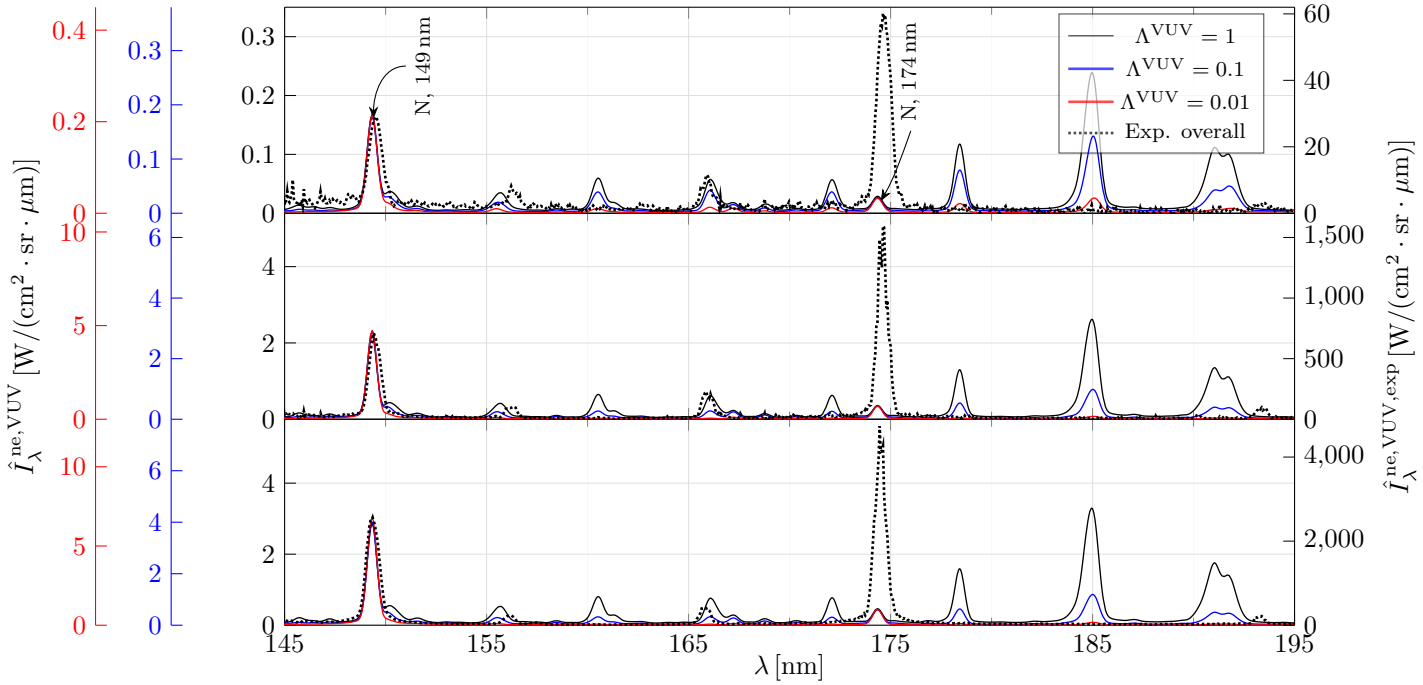

Figure 4.24: Numerical instrumentally resolved non-equilibrium metrics $\hat{I}_\lambda^{\mathrm{ne,VUV}}(x)$, obtained with $\Lambda^{\mathrm{VUV}} = 1$ (solid black lines), $\Lambda^{\mathrm{VUV}} = 0.1$ (solid blue lines), and $\Lambda^{\mathrm{VUV}} = 0.01$ (solid red lines), as well as the respective experimental instrumentally resolved non-equilibrium metrics $\hat{I}_\lambda^{\mathrm{ne,VUV,exp}}(x)$ (dotted black lines).

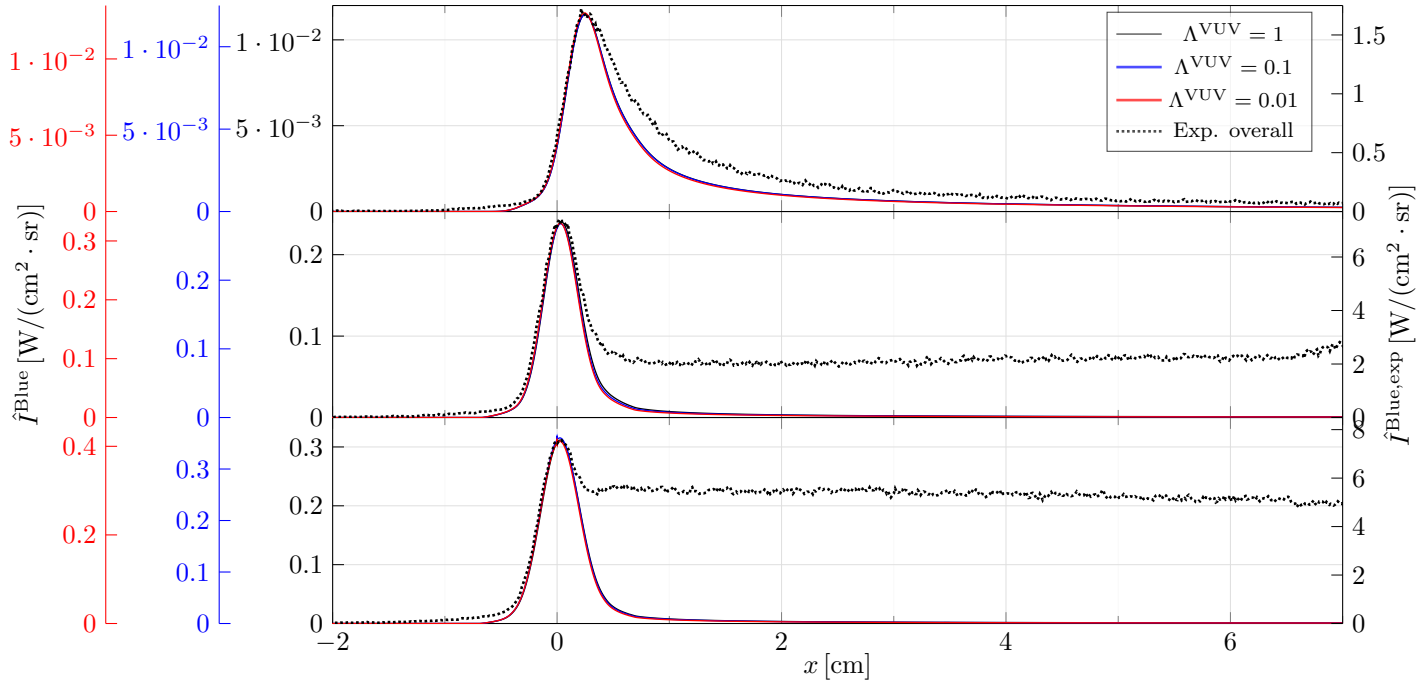

Figure 4.25: Numerical instrumentally resolved radiative intensities $\hat{I}^{\mathrm{Blue}}(x)$, obtained with $\Lambda^{\mathrm{VUV}} = 1$ (solid black lines), $\Lambda^{\mathrm{VUV}} = 0.1$ (solid blue lines), and $\Lambda^{\mathrm{VUV}} = 0.01$ (solid red lines), as well as the respective experimental instrumentally resolved radiative intensities $\hat{I}^{\mathrm{Blue,exp}}(x)$ (dotted black lines).

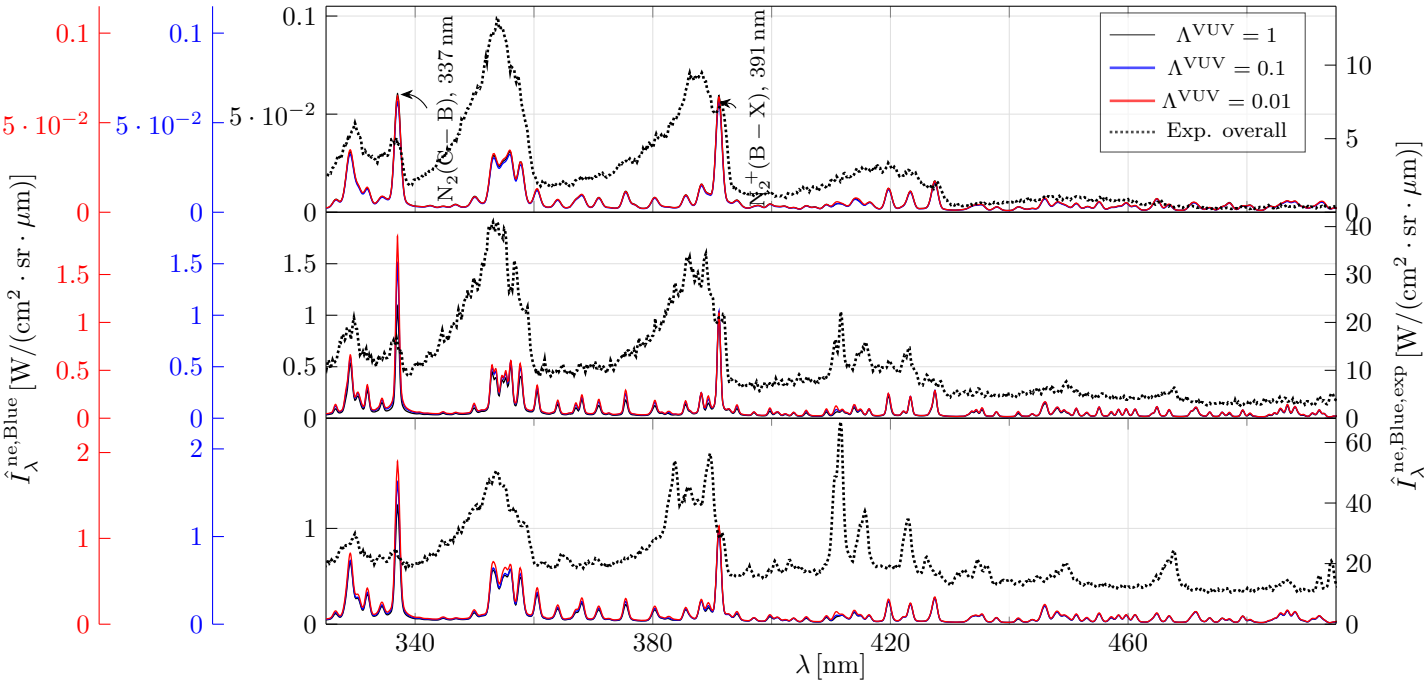

Figure 4.26: Numerical instrumentally resolved non-equilibrium metrics $\hat{I}_\lambda^{\mathrm{ne,Blue}}(x)$, obtained with $\Lambda^{\mathrm{VUV}} = 1$ (solid black lines), $\Lambda^{\mathrm{VUV}} = 0.1$ (solid blue lines), and $\Lambda^{\mathrm{VUV}} = 0.01$ (solid red lines), as well as the respective experimental instrumentally resolved non-equilibrium metrics $\hat{I}_\lambda^{\mathrm{ne,Blue,exp}}(x)$ (dotted black lines).

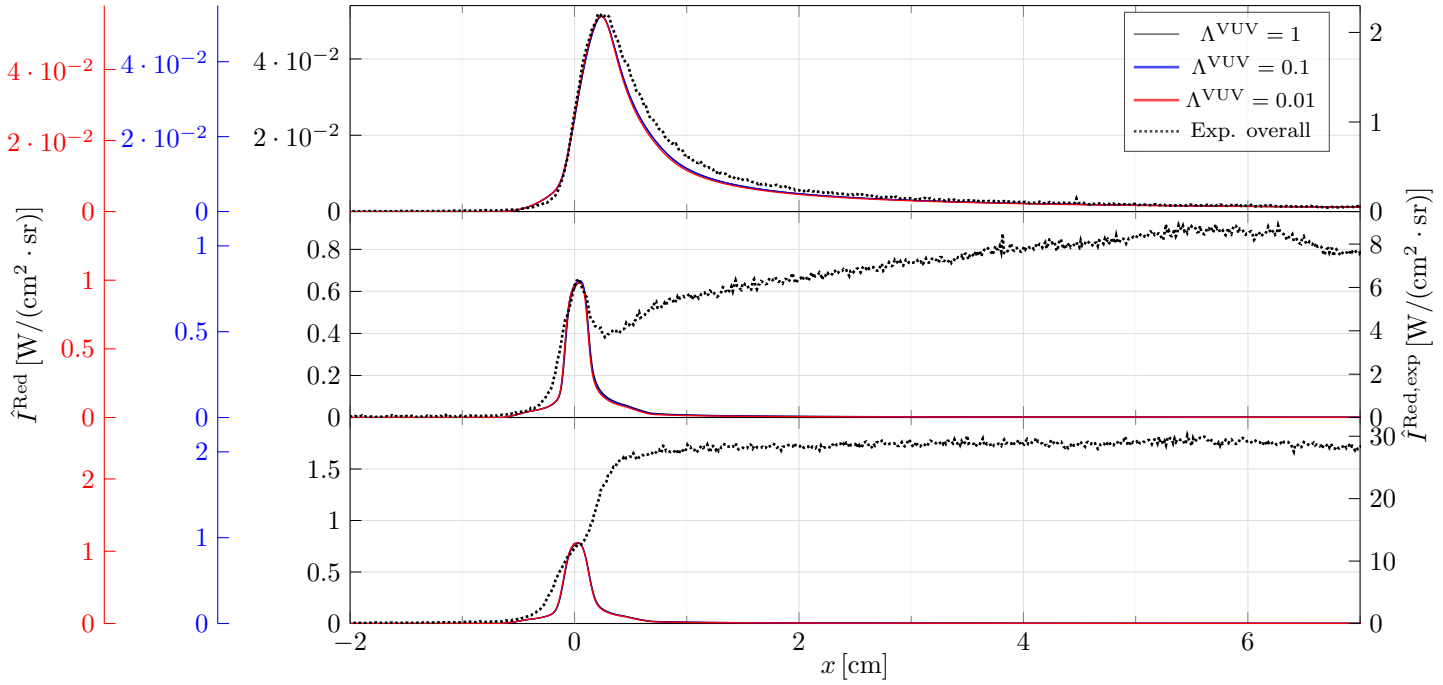

Figure 4.27: Numerical instrumentally resolved radiative intensities $\hat{I}^{\mathrm{Red}}(x)$, obtained with $\Lambda^{\mathrm{VUV}} = 1$ (solid black lines), $\Lambda^{\mathrm{VUV}} = 0.1$ (solid blue lines), and $\Lambda^{\mathrm{VUV}} = 0.01$ (solid red lines), as well as the respective experimental instrumentally resolved radiative intensities $\hat{I}^{\mathrm{Red,exp}}(x)$ (dotted black lines).

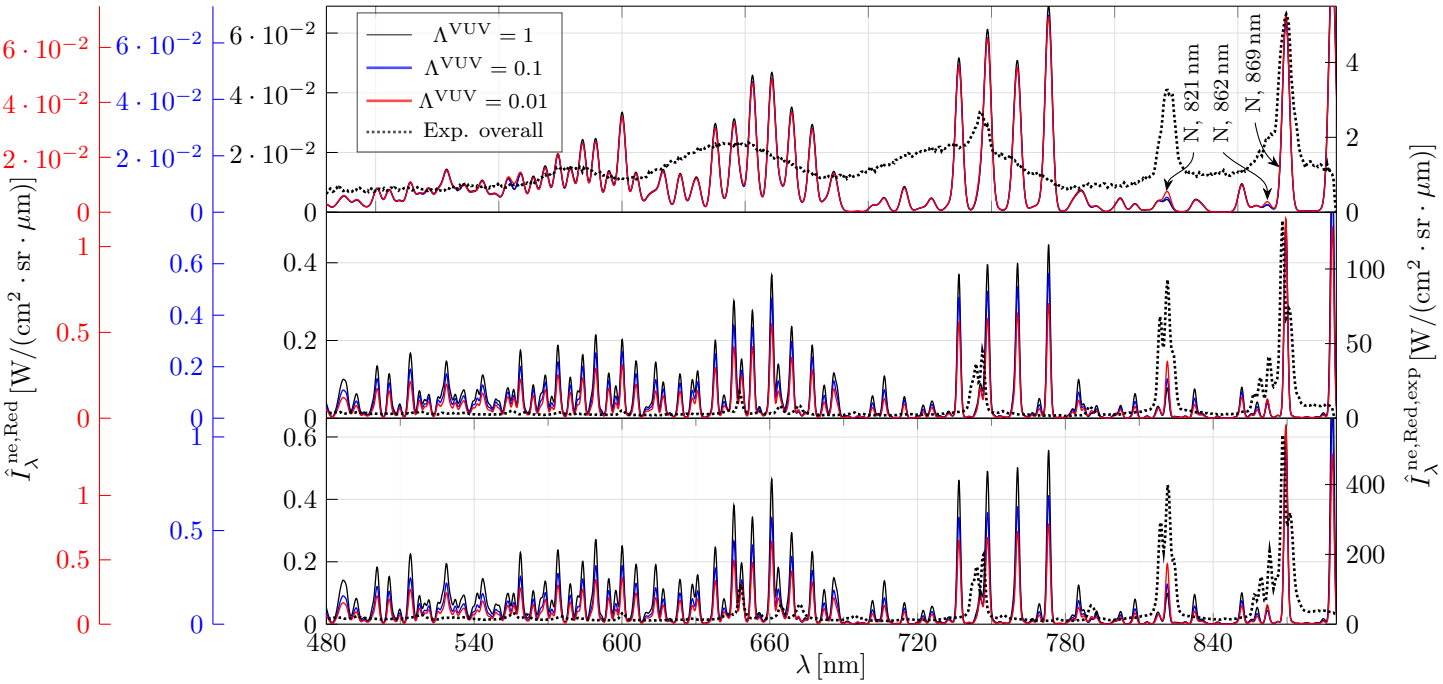

Figure 4.28: Numerical instrumentally resolved non-equilibrium metrics $\hat{I}^{\mathrm{ne,Red}}_{\lambda}(x)$, obtained with $\Lambda^{\mathrm{VUV}} = 1$ (solid black lines), $\Lambda^{\mathrm{VUV}} = 0.1$ (solid blue lines), and $\Lambda^{\mathrm{VUV}} = 0.01$ (solid red lines), as well as the respective experimental instrumentally resolved non-equilibrium metrics $\hat{I}^{\mathrm{ne,Red,exp}}_{\lambda}(x)$ (dotted black lines).

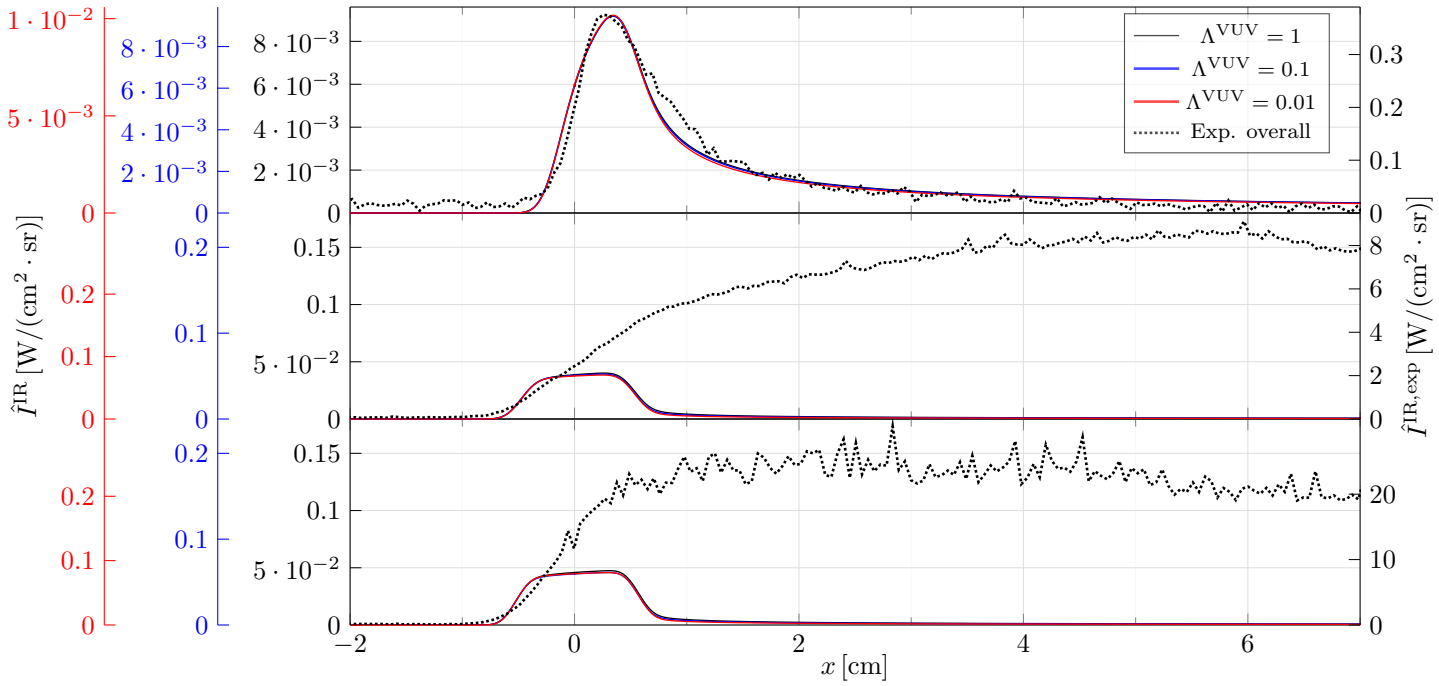

Figure 4.29: Numerical instrumentally resolved radiative intensities $\hat{I}^{\mathrm{IR}}(x)$, obtained with $\Lambda^{\mathrm{VUV}} = 1$ (solid black lines), $\Lambda^{\mathrm{VUV}} = 0.1$ (solid blue lines), and $\Lambda^{\mathrm{VUV}} = 0.01$ (solid red lines), as well as the respective experimental instrumentally resolved radiative intensities $\hat{I}^{\mathrm{IR,exp}}(x)$ (dotted black lines).

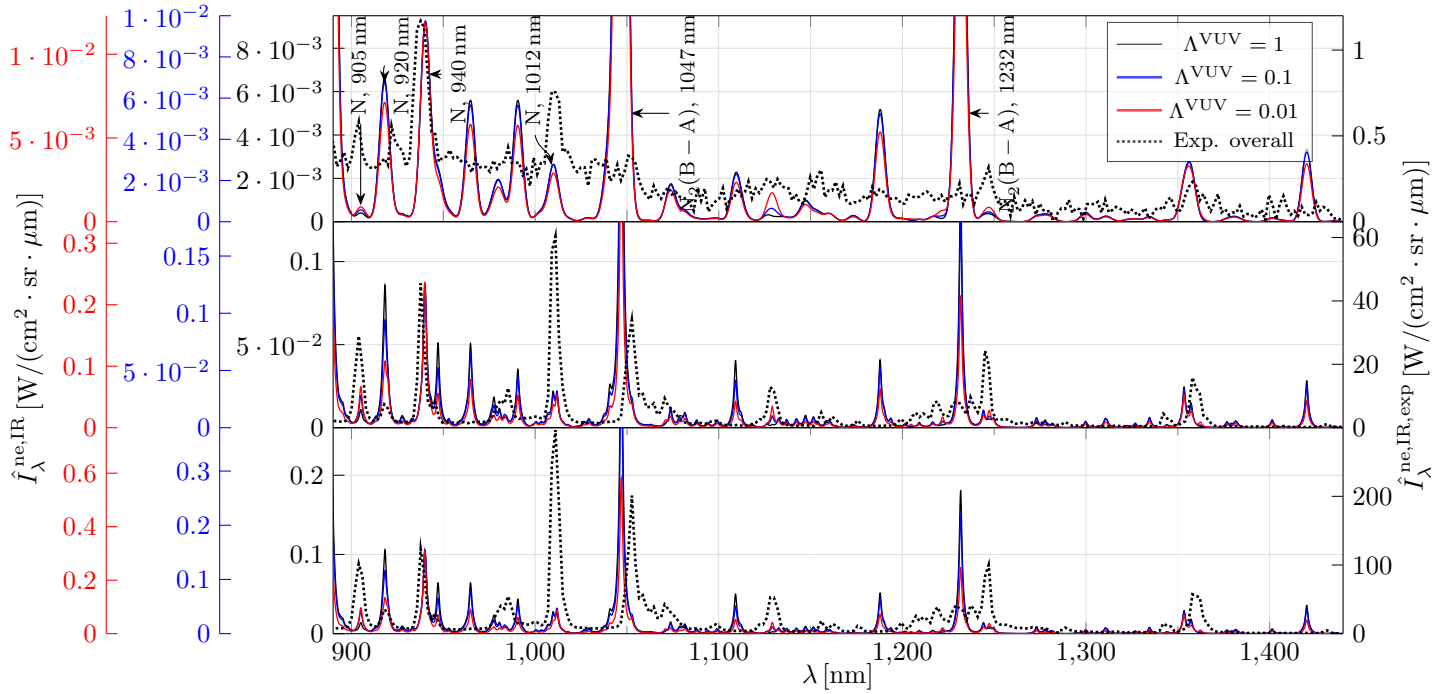

Figure 4.30: Numerical instrumentally resolved non-equilibrium metrics $\hat{I}^{\mathrm{ne,IR}}_{\lambda}(x)$, obtained with $\Lambda^{\mathrm{VUV}} = 1$ (solid black lines), $\Lambda^{\mathrm{VUV}} = 0.1$ (solid blue lines), and $\Lambda^{\mathrm{VUV}} = 0.01$ (solid red lines), as well as the respective experimental instrumentally resolved non-equilibrium metrics $\hat{I}^{\mathrm{ne,IR,exp}}_{\lambda}(x)$ (dotted black lines).

4.4.3 Dependence on the dissociation rates of N_2

The evolution of the post-shock conditions is highly dependent on the dissociation rates of N_2. Greater dissociation rates would imply a production of a greater number of N particles. And, being dissociation an endothermic process, lesser energy would be available for excitation. However, it's hard to say how an increase of the dissociation rates could affect the excitation of the particles to some energy level. Note that being lesser the population of N_2, a lower number of N_2 particles would be left to be excited. Conversely, being greater the population of N, a greater number of N particles would be left to be excited. Therefore, one cannot say, in straight forward manner, if the number of particles in some excited energy level should get lower or higher.

To test the dependence of the numerical results on the dissociation rates of N_2, it was decided to consider dissociation rates of $N_2(X^1\Sigma_g^+)$ (the ground electronic level of molecular nitrogen[4]) scaled by 0.1 and 10, and to keep $\Lambda^{VUV} = 0.01$. The obtained results are shown by Figures 4.31 to 4.38. These figures show that the peak values of the instrumentally resolved radiative intensities increased with a decrease of the rates of dissociation, being this more relevant for the case of all wavelength intervals of the low speed shot and the wavelength intervals "Blue", "Red" and IR of the medium and high speed shots. The increase went from as low as insignificant to as high as the double. And for the case of an increase of the rates of dissociation, the decrease of the peak values went from as low as 20 % to as high as 70 %. The figures for the non-equilibrium metrics show that both contributions of N and N_2 to the radiation variables increased with the decrease of the rates of dissociation, being the effect on the latter contribution much more significant. The energy that was once spent in dissociation was then spent in excitation of N and N_2, and because more N_2 and less N particles were obtained, the effect on N_2 had a greater importance. Note, however, that in order to get a better agreeability with the experimental spectra, the contributions of N should be the ones to get enhanced and not N_2. Also, one should point out that in the case of the low speed shot, the peaks of radiative intensity widened with the decrease of the rates of dissociation, agreeing better with the experimental profiles for all wavelength intervals except for VUV. And in the case of the other shots, the change on the peaks shape wasn't significant. The increase of the rates of dissociation made the peaks to narrow in the case of the low speed shot, agreeing worse with experimental counterparts. Conversely, the increase made the peaks to widen in the case of the "Blue" wavelength interval of the medium and high speed shots, getting closer to the experimental results.

Concluding, a sole decrease or increase of the rates of dissociation of $N_2(X)$ don't unequivocally lead to better results.

[4]The ground electronic level of N_2 is usually more populated than the other ones, being, therefore, more important in what concerns dissociation.

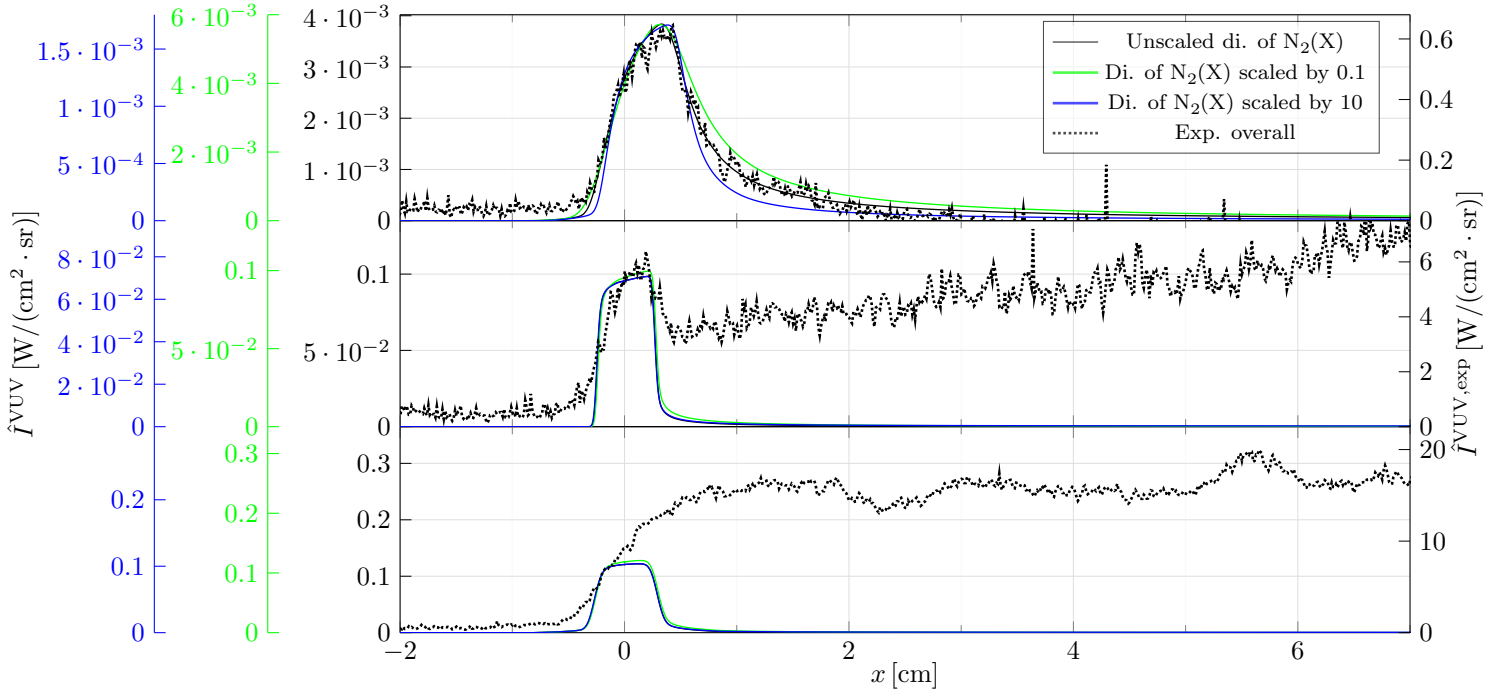

Figure 4.31: Numerical instrumentally resolved radiative intensities $\hat{I}^{\mathrm{VUV}}(x)$, obtained with $\Lambda^{\mathrm{VUV}} = 0.01$, and unscaled dissociation of $N_2(X^1\Sigma_g^+)$ (solid black lines), and scaled by 0.1 (solid green lines), and by 10 (solid blue lines), as well as the respective experimental instrumentally resolved radiative intensities $\hat{I}^{\mathrm{VUV,exp}}(x)$ (dotted black lines).

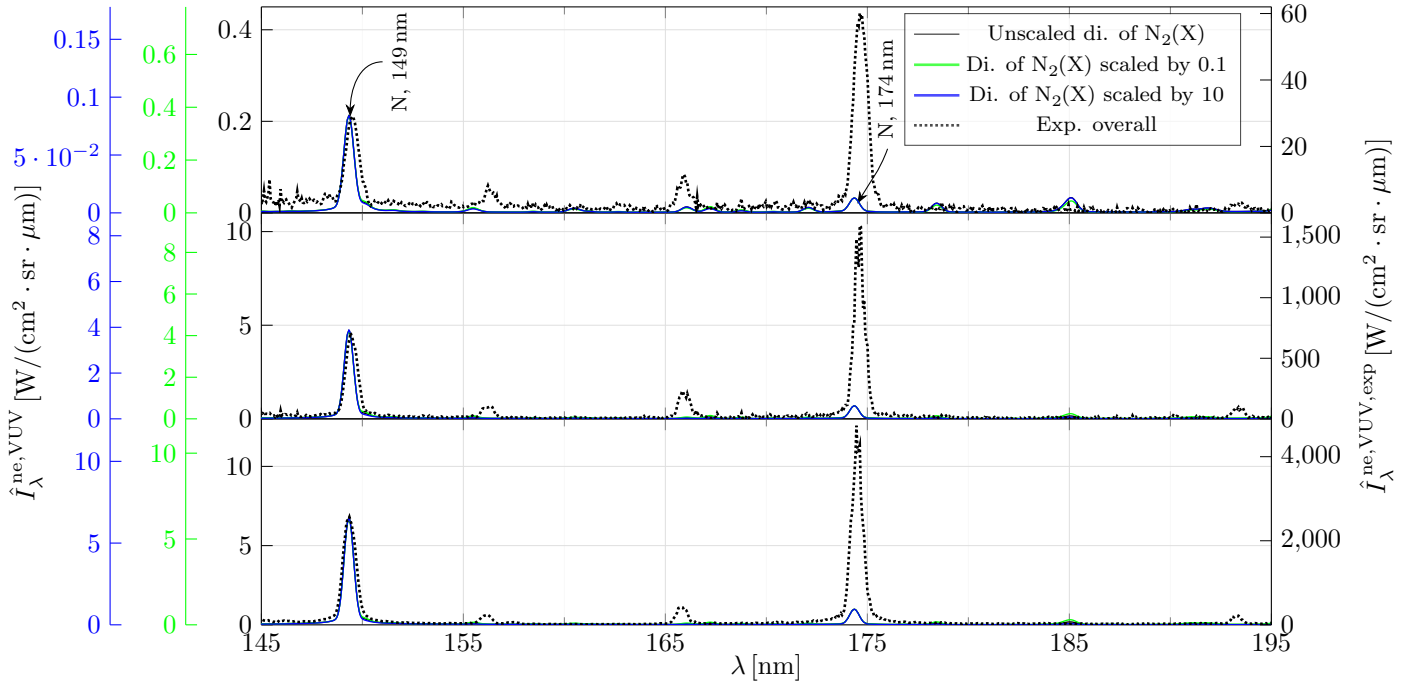

Figure 4.32: Numerical instrumentally resolved non-equilibrium metrics $\hat{I}_\lambda^{\mathrm{ne,VUV}}(x)$, obtained with $\Lambda^{\mathrm{VUV}} = 0.01$, and unscaled dissociation of $N_2(X^1\Sigma_g^+)$ (solid black lines), and scaled by 0.1 (solid green lines), and by 10 (solid blue lines), as well as the respective experimental instrumentally resolved non-equilibrium metrics $\hat{I}_\lambda^{\mathrm{ne,VUV,exp}}(x)$ (dotted black lines).

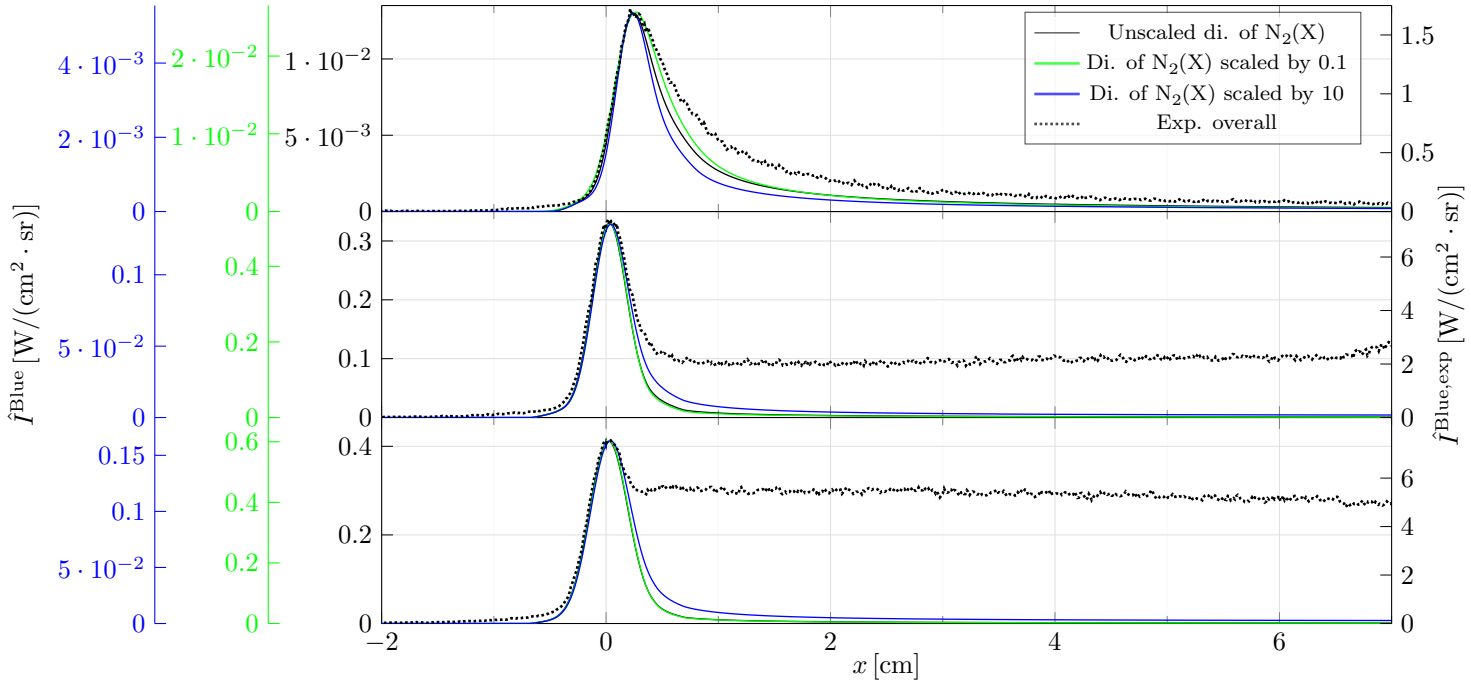

Figure 4.33: Numerical instrumentally resolved radiative intensities $\hat{I}^{\mathrm{Blue}}(x)$, obtained with $\Lambda^{\mathrm{VUV}} = 0.01$, and unscaled dissociation of $N_2(X^1\Sigma_g^+)$ (solid black lines), and scaled by 0.1 (solid green lines), and by 10 (solid blue lines), as well as the respective experimental instrumentally resolved radiative intensities $\hat{I}^{\mathrm{Blue,exp}}(x)$ (dotted black lines).

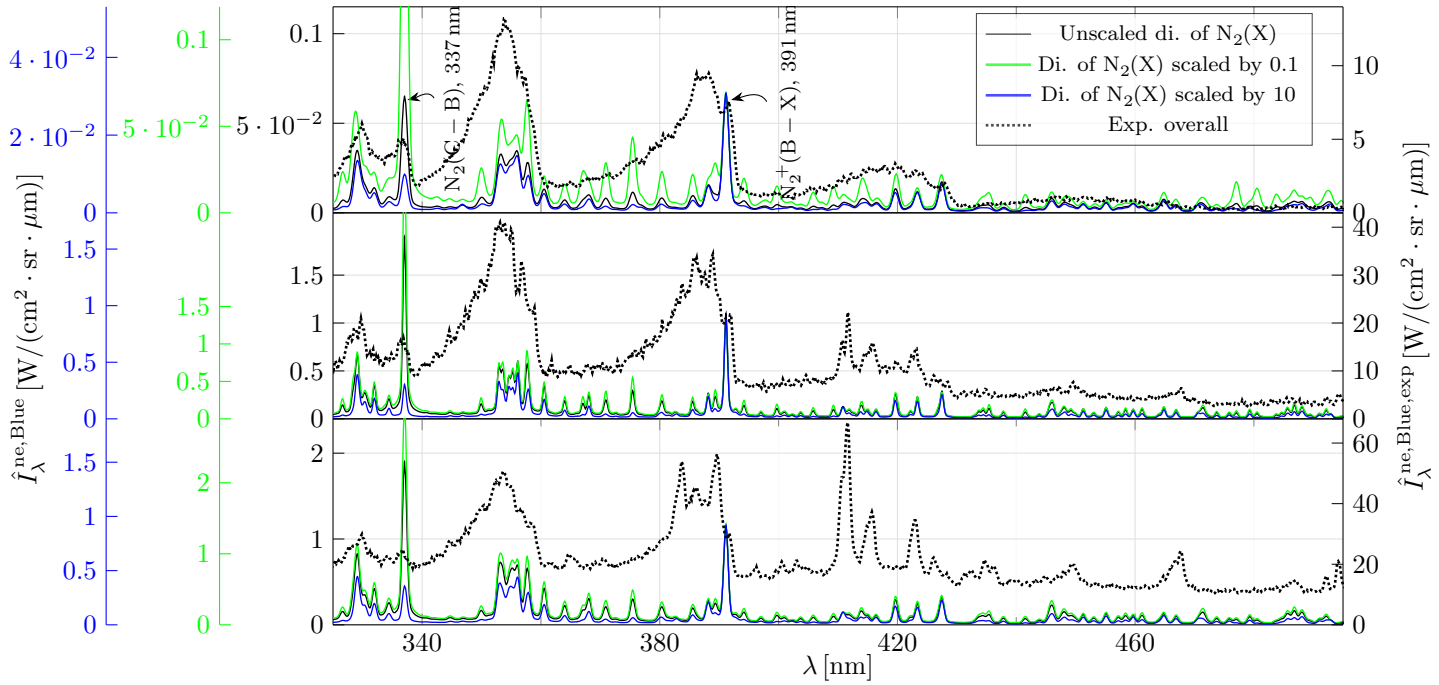

Figure 4.34: Numerical instrumentally resolved non-equilibrium metrics $\hat{I}_\lambda^{\mathrm{ne,Blue}}(x)$, obtained with $\Lambda^{\mathrm{VUV}} = 0.01$, and unscaled dissociation of $N_2(X^1\Sigma_g^+)$ (solid black lines), and scaled by 0.1 (solid green lines), and by 10 (solid blue lines), as well as the respective experimental instrumentally resolved non-equilibrium metrics $\hat{I}_\lambda^{\mathrm{ne,Blue,exp}}(x)$ (dotted black lines).

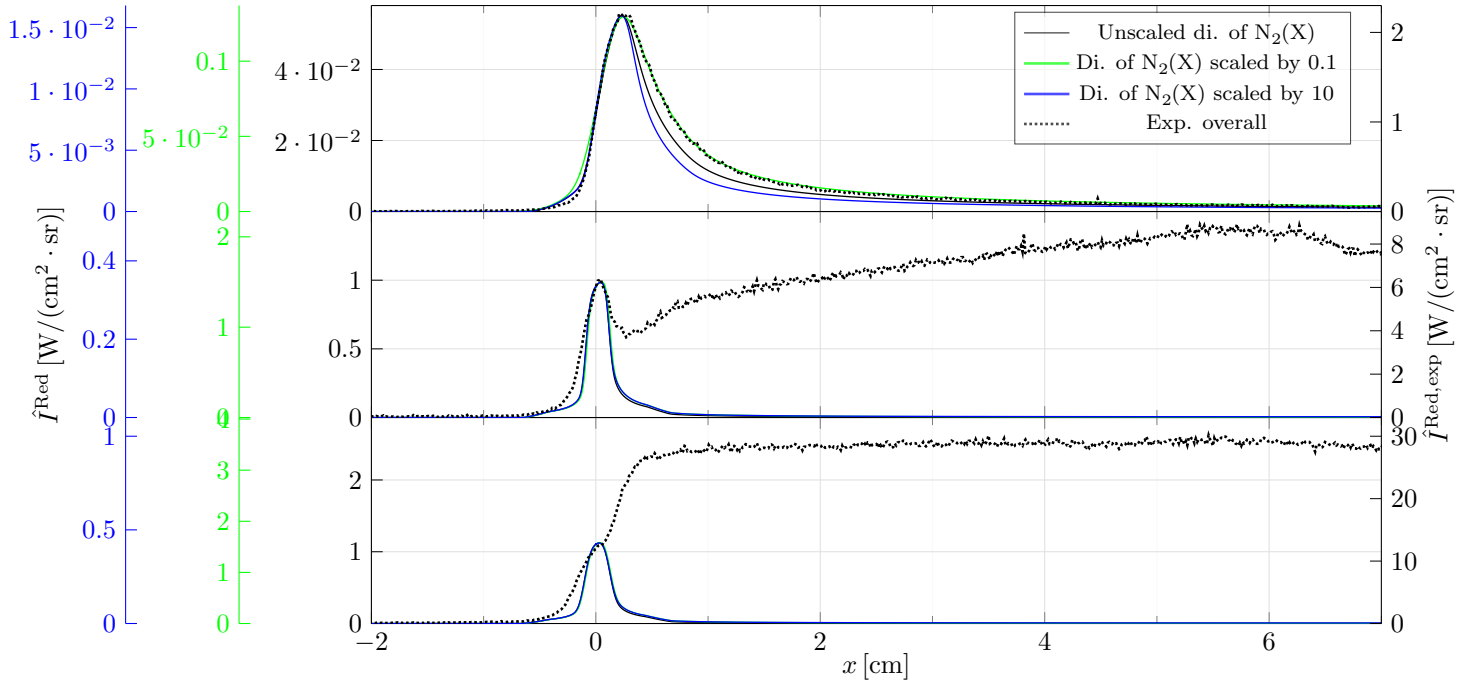

Figure 4.35: Numerical instrumentally resolved radiative intensities $\hat{I}^{\mathrm{Red}}(x)$, obtained with $\Lambda^{\mathrm{VUV}} = 0.01$, and unscaled dissociation of $N_2(X^1\Sigma_g^+)$ (solid black lines), and scaled by 0.1 (solid green lines), and by 10 (solid blue lines), as well as the respective experimental instrumentally resolved radiative intensities $\hat{I}^{\mathrm{Red,exp}}(x)$ (dotted black lines).

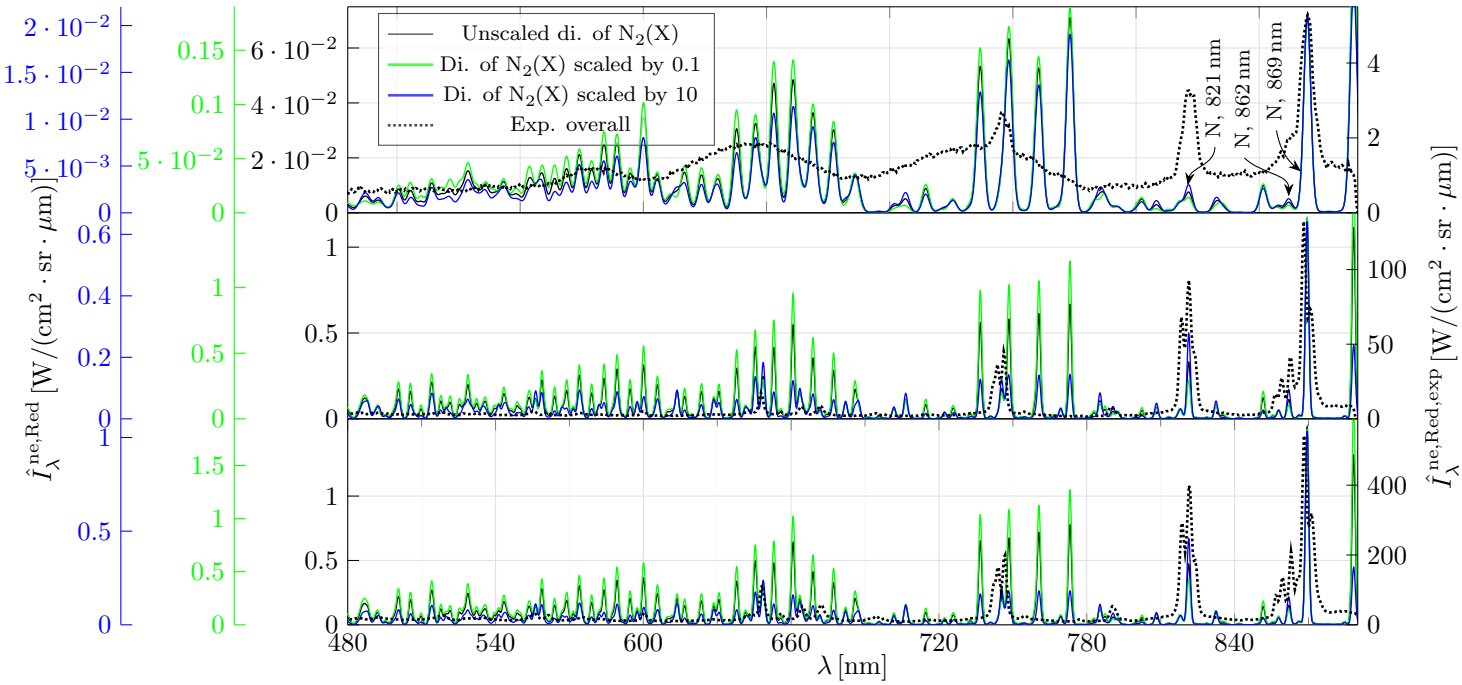

Figure 4.36: Numerical instrumentally resolved non-equilibrium metrics $\hat{I}_{\lambda}^{\mathrm{ne,Red}}(x)$, obtained with $\Lambda^{\mathrm{VUV}} = 0.01$, and unscaled dissociation of $N_2(X^1\Sigma_g^+)$ (solid black lines), and scaled by 0.1 (solid green lines), and by 10 (solid blue lines), as well as the respective experimental instrumentally resolved non-equilibrium metrics $\hat{I}_{\lambda}^{\mathrm{ne,Red,exp}}(x)$ (dotted black lines).

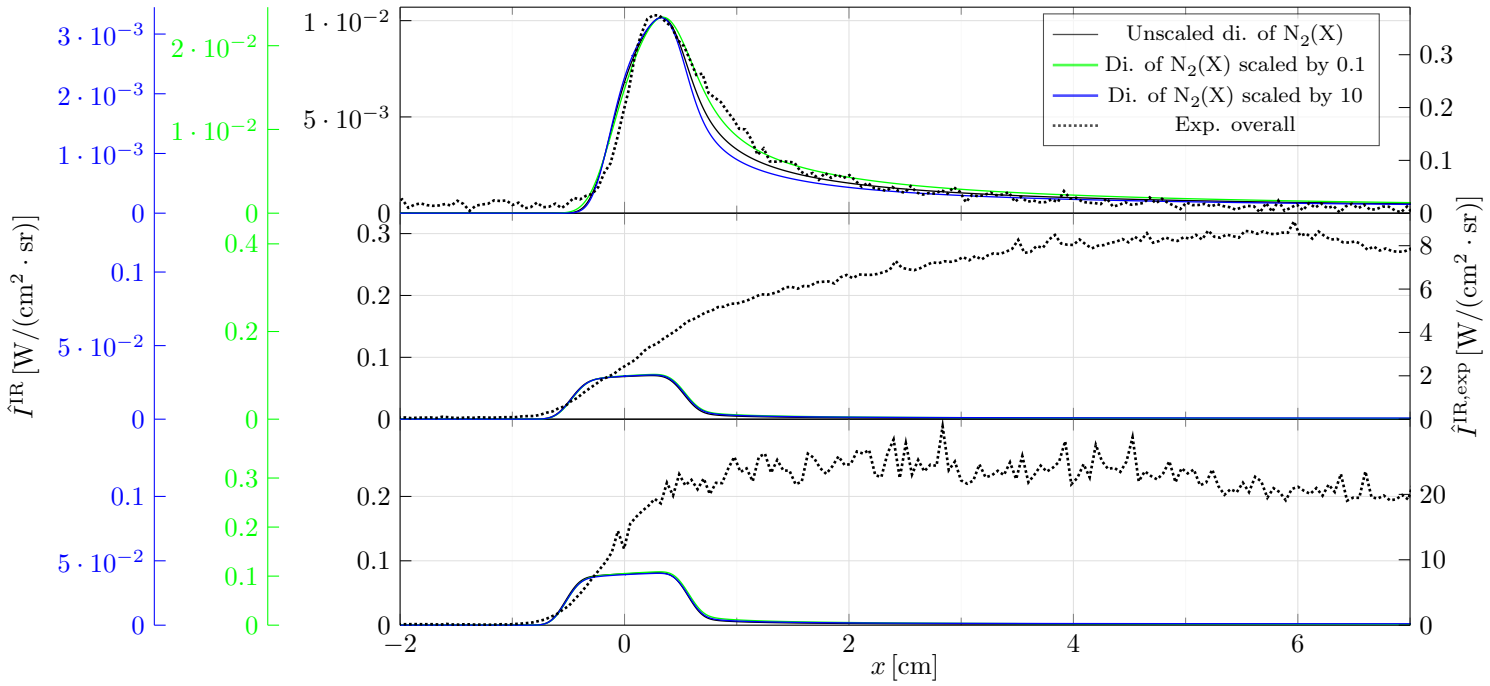

Figure 4.37: Numerical instrumentally resolved radiative intensities $\hat{I}^{\mathrm{IR}}(x)$, obtained with $\Lambda^{\mathrm{VUV}} = 0.01$, and unscaled dissociation of $N_2(X^1\Sigma_g^+)$ (solid black lines), and scaled by 0.1 (solid green lines), and by 10 (solid blue lines), as well as the respective experimental instrumentally resolved radiative intensities $\hat{I}^{\mathrm{IR,exp}}(x)$ (dotted black lines).

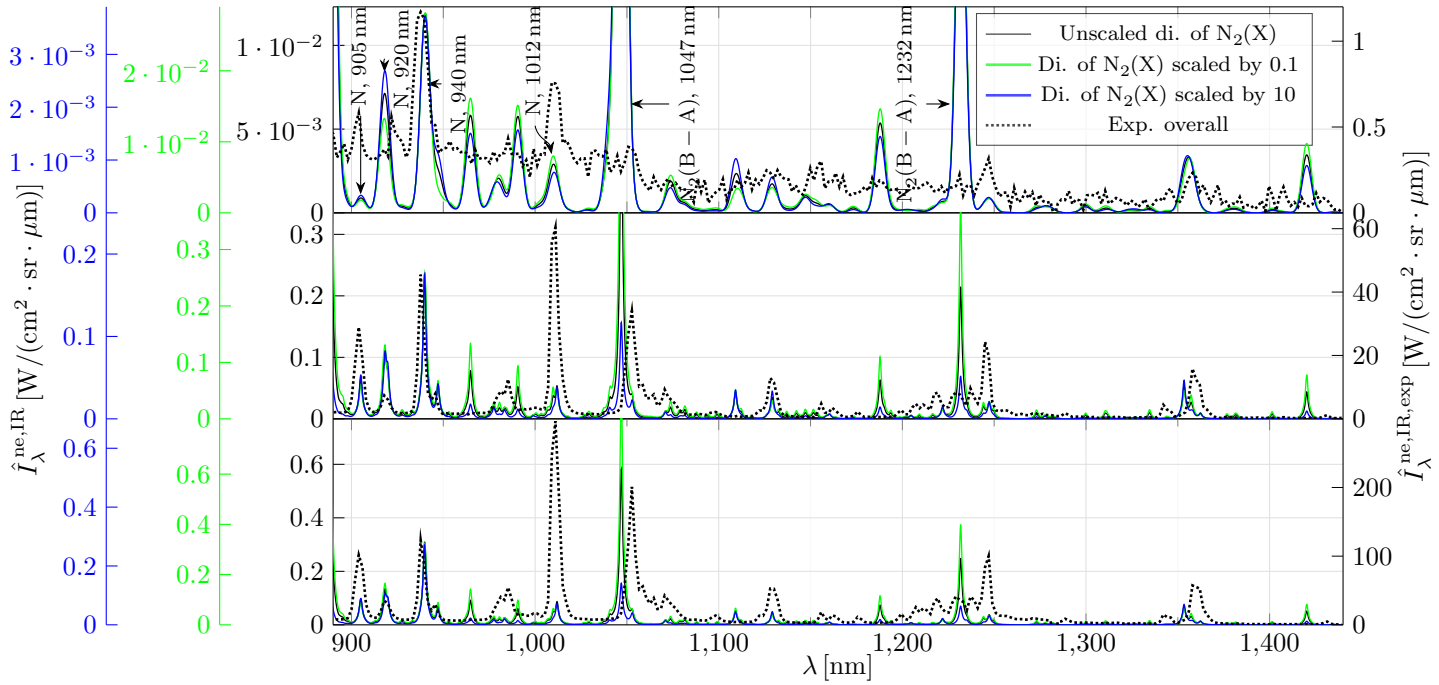

Figure 4.38: Numerical instrumentally resolved non-equilibrium metrics $\hat{I}_\lambda^{\mathrm{ne,IR}}(x)$, obtained with $\Lambda^{\mathrm{VUV}} = 0.01$, and unscaled dissociation of $N_2(X^1\Sigma_g^+)$ (solid black lines), and scaled by 0.1 (solid green lines), and by 10 (solid blue lines), as well as the respective experimental instrumentally resolved non-equilibrium metrics $\hat{I}_\lambda^{\mathrm{ne,IR,exp}}(x)$ (dotted black lines).

4.4.4 Dependence on the excitation rates of N

In §4.4.2 it was found that the contributions of N to the radiation variables were still underestimated when compared with the molecular contributions in the "Red" and IR wavelength intervals. It was then decided to try scaling the excitation rate coefficients of N, keeping $\Lambda^{\mathrm{VUV}} = 0.01$, in order to enhance them. The crude formulae of Annaloro et al. [84] and Panesi et al. [98] employed in this work[5] as models for excitation of N by heavy particle and electron impact, respectively, may indeed accommodate some degree of uncertainty. Their multiplication by 10 and 100 was tried, and solely for the case of low speed shot the numerical simulations converged. This is an indication of the rate coefficients being actually high enough in the conditions of the medium and high speed shots, and by increasing their values, a physical incoherence may have been obtained. The results are shown in Figures 4.39 to 4.46.

With the increase in the rate coefficients for excitation of N, the peaks values of the instrumentally resolved radiative intensities rose as much as to the quintuple in the case of the VUV radiation, the double in the case of the "Blue" and "Red" radiation, and the quadruple in the case of the IR radiation. However, the values are still one to two orders of magnitude lower than the experimental ones. Regarding the shape of the profiles, it was found that the rising and falling parts got steeper deviating significantly from the experimental profiles. This result may be justified by the fact that a greater rate of excitation of N produces a greater rate of emission of radiation, and therefore, the radiative intensity rises faster and higher. As a higher excitation requires more energy, which is then lost in the form of radiation, the system suddenly gets incapable of continually excite the particles, and the radiative intensity falls faster. The Figures 4.40, 4.42, 4.44 and 4.46. show that the contribution of N to the instrumentally resolved non-equilibrium metrics increased in all wavelength regions, agreeing better with the experimental spectra except in the "Blue" wavelength region, for which the contributions of the molecular particles should prevail over the ones of the atomic particles.

Concluding, it can't be said that a sole increase of the rate coefficients for excitation of N unequivocally leads to better results.

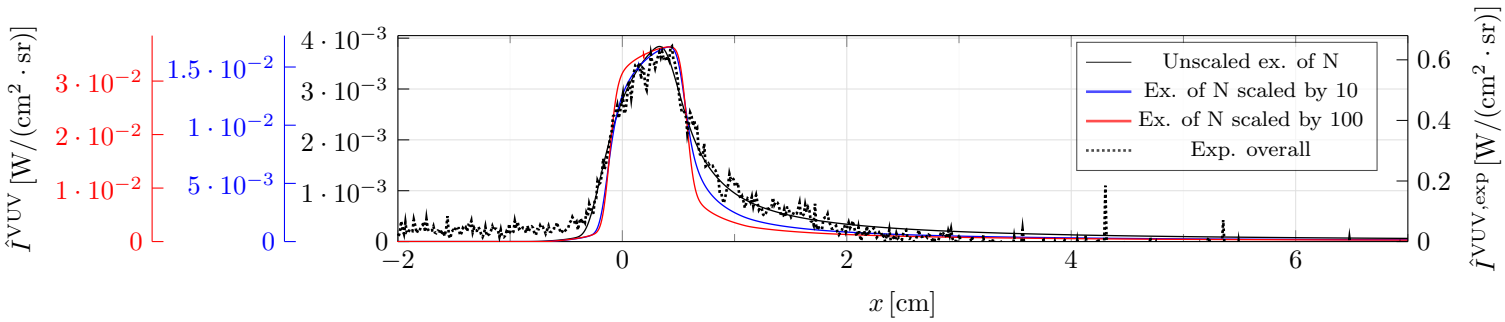

Figure 4.39: Numerical instrumentally resolved radiative intensities $\hat{I}^{\mathrm{VUV}}(x)$, obtained with $\Lambda^{\mathrm{VUV}} = 0.01$, and unscaled excitation of N (solid black lines), and scaled by 10 (solid blue lines), and by 100 (solid red lines), as well as the respective experimental instrumentally resolved radiative intensities $\hat{I}^{\mathrm{VUV,exp}}(x)$ (dotted black lines), for the case of the low speed shot.

[5] See sections §3.2.10 and §3.2.9 for more details.

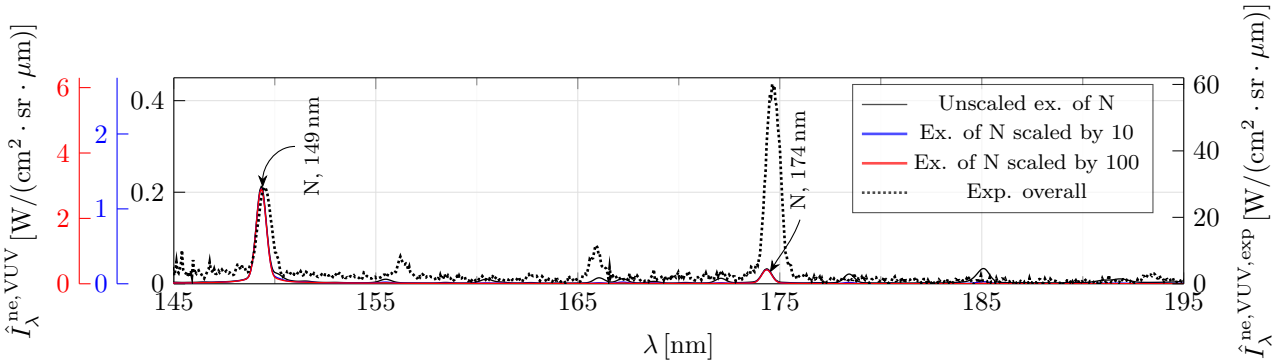

Figure 4.40: Numerical instrumentally resolved non-equilibrium metrics $\hat{I}_\lambda^{\mathrm{ne,VUV}}(x)$, obtained with $\Lambda^{\mathrm{VUV}} = 0.01$, and unscaled excitation of N (solid black lines), and scaled by 10 (solid blue lines), and by 100 (solid red lines), as well as the respective experimental instrumentally resolved non-equilibrium metrics $\hat{I}_\lambda^{\mathrm{ne,VUV,exp}}(x)$ (dotted black lines), for the case of the low speed shot.

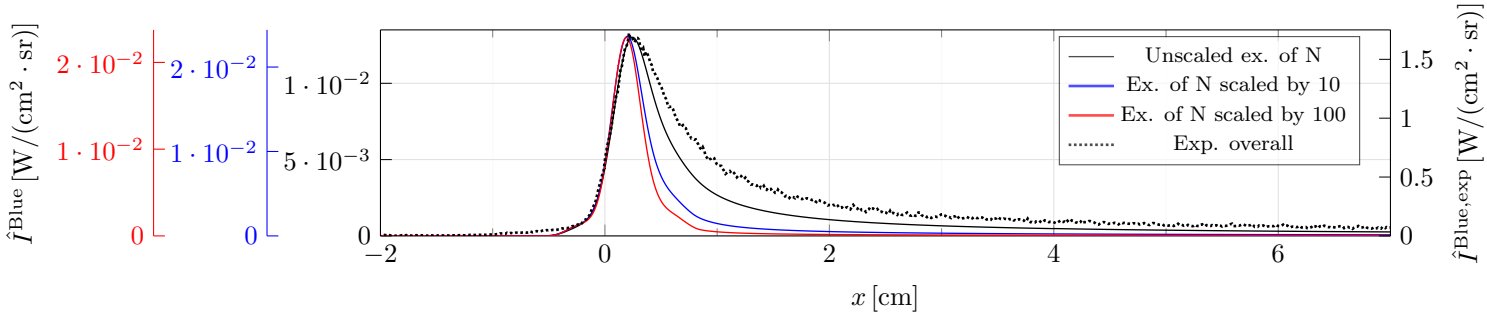

Figure 4.41: Numerical instrumentally resolved radiative intensities $\hat{I}^{\mathrm{Blue}}(x)$, obtained with $\Lambda^{\mathrm{VUV}} = 0.01$, and unscaled excitation of N (solid black lines), and scaled by 10 (solid blue lines), and by 100 (solid red lines), as well as the respective experimental instrumentally resolved radiative intensities $\hat{I}^{\mathrm{Blue,exp}}(x)$ (dotted black lines), for the case of the low speed shot.

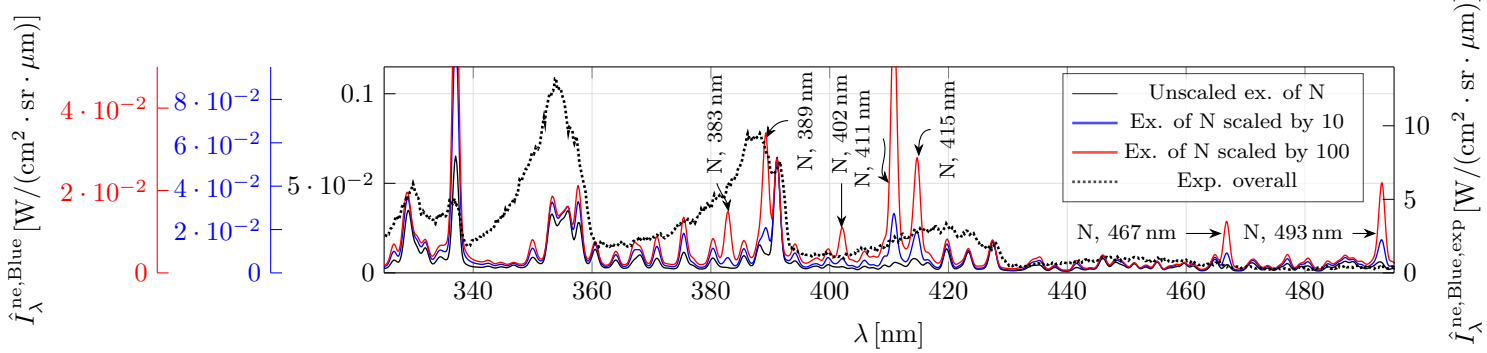

Figure 4.42: Numerical instrumentally resolved non-equilibrium metrics $\hat{I}_\lambda^{\mathrm{ne,Blue}}(x)$, obtained with $\Lambda^{\mathrm{VUV}} = 0.01$, and unscaled excitation of N (solid black lines), and scaled by 10 (solid blue lines), and by 100 (solid red lines), as well as the respective experimental instrumentally resolved non-equilibrium metrics $\hat{I}_\lambda^{\mathrm{ne,Blue,exp}}(x)$ (dotted black lines), for the case of the low speed shot.

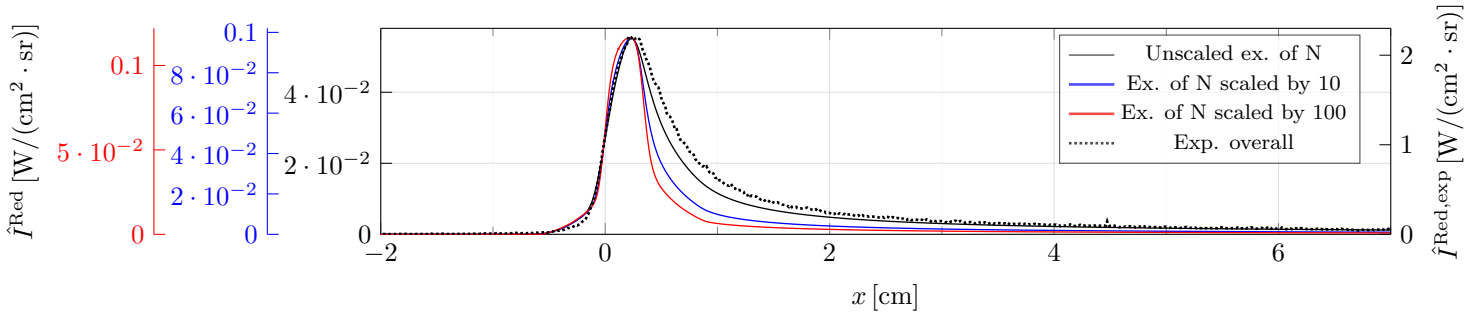

Figure 4.43: Numerical instrumentally resolved radiative intensities $\hat{I}^{\mathrm{Red}}(x)$, obtained with $\Lambda^{\mathrm{VUV}} = 0.01$, and unscaled excitation of N (solid black lines), and scaled by 10 (solid blue lines), and by 100 (solid red lines), as well as the respective experimental instrumentally resolved radiative intensities $\hat{I}^{\mathrm{Red,exp}}(x)$ (dotted black lines), for the case of the low speed shot.

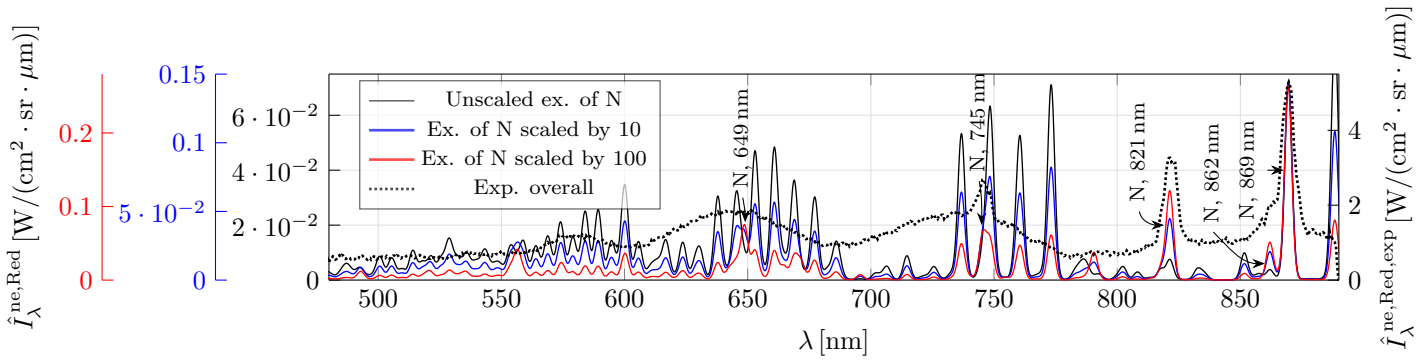

Figure 4.44: Numerical instrumentally resolved non-equilibrium metrics $\hat{I}_\lambda^{\mathrm{ne,Red}}(x)$, obtained with $\Lambda^{\mathrm{VUV}} = 0.01$, and unscaled excitation of N (solid black lines), and scaled by 10 (solid blue lines), and by 100 (solid red lines), as well as the respective experimental instrumentally resolved non-equilibrium metrics $\hat{I}_\lambda^{\mathrm{ne,Red,exp}}(x)$ (dotted black lines), for the case of the low speed shot.

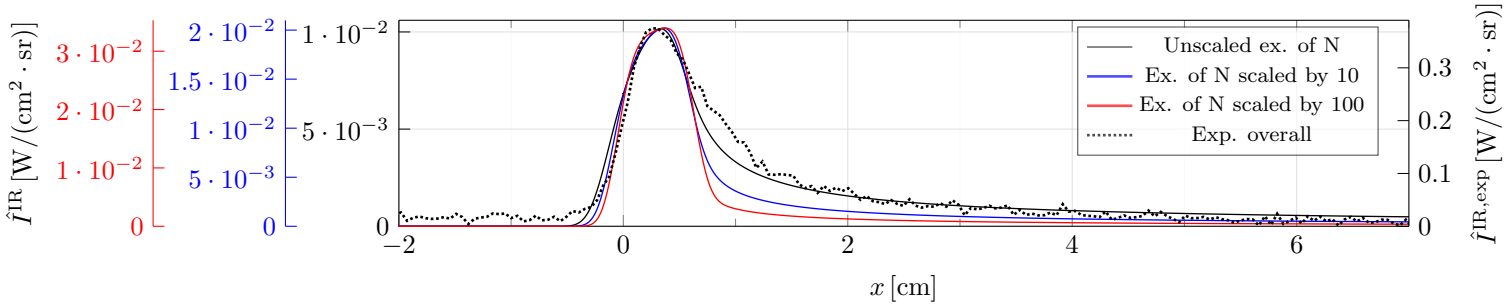

Figure 4.45: Numerical instrumentally resolved radiative intensities $\hat{I}^{\mathrm{IR}}(x)$, obtained with $\Lambda^{\mathrm{VUV}} = 0.01$, and unscaled excitation of N (solid black lines), and scaled by 10 (solid blue lines), and by 100 (solid red lines), as well as the respective experimental instrumentally resolved radiative intensities $\hat{I}^{\mathrm{IR,exp}}(x)$ (dotted black lines), for the case of the low speed shot.

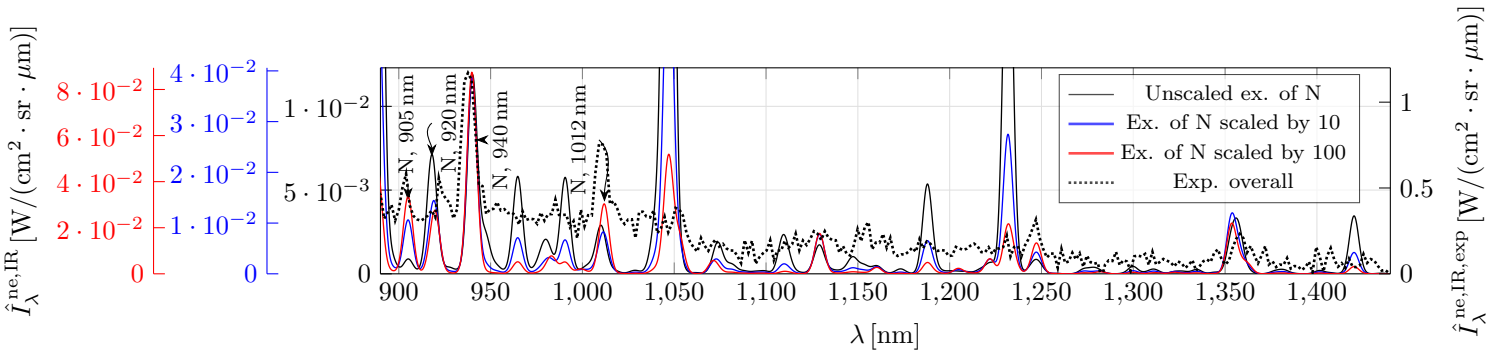

Figure 4.46: Numerical instrumentally resolved non-equilibrium metrics $\hat{I}_\lambda^{\mathrm{ne,IR}}(x)$, obtained with $\Lambda^{\mathrm{VUV}} = 0.01$, and unscaled excitation of N (solid black lines), and scaled by 10 (solid blue lines), and by 100 (solid red lines), as well as the respective experimental instrumentally resolved non-equilibrium metrics $\hat{I}_\lambda^{\mathrm{ne,IR,exp}}(x)$ (dotted black lines), for the case of the low speed shot.

4.4.5 A synopsis about the dependence of the results on the different parameters

Figure 4.47 shows the peak values of the instrumentally resolved radiative intensities $\hat{I}^l_{\mathrm{peak}}$ (with $l \in \{\mathrm{VUV}, \text{“Blue”}, \text{“Red”}, \mathrm{IR}\}$) obtained with the different models and in the experiment for the low, medium and high speed shots. And Figure 4.48 and Figure 4.49 show the temperatures $T_{\mathrm{tr_h}}$ and $T_{\mathrm{tr_e}}$ and mole fractions x_s attained at $x = 5\,\mathrm{cm}$, respectively, which were obtained with the different models of this work and of the work of Cruden and Brandis [158].

As referred before, the peak values of the instrumentally resolved radiative intensities obtained in the zero-dimensional simulation (labelled by “0D” in the figures) are several times lower than the ones obtained in the one-dimensional simulation (labelled by “1D”) and even more lower than the ones of the experiment. On the other hand, the attained temperatures are much greater than the ones of the one-dimensional simulation ($T_{\mathrm{tr_h}}$ differs by 1105 K, 1761 K and 1881 K for the cases of the low, medium and high speed shots), agreeing better with the values of Cruden and Brandis (labelled by “NEQAIR, “Blue”” and “NEQAIR, “Red””). Figure 4.49 shows that dissociation of N_2 is weaker than in the case of the one-dimensional simulation. The attained mole fractions of N_2^+ and N^+ at $x = 5\,\mathrm{cm}$ are higher (with the exception of N^+ in the low speed shot). However, this can be shown to be simply due to a slower recombination. It can be said that in the one-dimension simulation more energy was spent in excitation, dissociation and ionisation of the particles. The results of Cruden and Brandis evidence that these endothermic processes were even more stronger in the experiment.

By considering escape factors $\Lambda^{\mathrm{VUV}} = 0.1$ and $\Lambda^{\mathrm{VUV}} = 0.01$ for the VUV wavelength interval, the peak values of the instrumentally resolved radiative intensities increase for all wavelength intervals except VUV, for which it decreases. The attained temperatures rise just slightly, but the mole fractions of the species don’t change appreciably. Part of the energy which was once lost through VUV radiation is now lost through “Blue”, “Red” and IR radiations.

Decreasing the rates of dissociation of $N_2(X^1\Sigma_g^+)$, keeping $\Lambda^{\mathrm{VUV}} = 0.01$, makes the peak values of the

instrumentally resolved radiative intensities to increase, and increasing the rates of dissociations makes them to decrease. The impact is, however, not so relevant for the case of the VUV wavelength interval of the medium and high speed shots. Figure 4.48 shows that by decreasing the rates of dissociation, less energy is spent on endothermic processes (since higher translational temperatures are attained). Curiously, increasing the rates of dissociation doesn't decrease the attained translational temperatures in the cases of the medium and high speed shots (the translational energy is then redistributed in a different way). It's important to mention here that the values of all of the referred temperatures are still much lower (by several thousands of kelvins) than the ones inferred by Cruden and Brandis. Figure 4.49 shows a tendency for an increase of the attained mole fractions of N and N^+ and decrease of the ones of N_2 and N_2^+ with an increase of the rates of dissociation. The increase on the mole fraction of N^+ and the decrease on the one of N_2^+ can be justified by the fact that a stronger dissociation implies that, in contrast with N_2, more N particles become available to be ionised. The values of the mole fractions obtained by increasing the rate coefficients are actually the ones of all the tried models (regarding spontaneous emission) who better agree with the ones of Cruden and Brandis. Still, their results indicate that the system should have suffered stronger dissociation and ionisation.

By keeping $\Lambda^{\mathrm{VUV}} = 0.01$, and increasing the excitation rates of N (which was only successful for the case of the low speed shot), a meaningful rise of the peak radiation values occurs, in particular the ones of the IR and VUV wavelength intervals. Still, these are one to two orders of magnitude lower than the

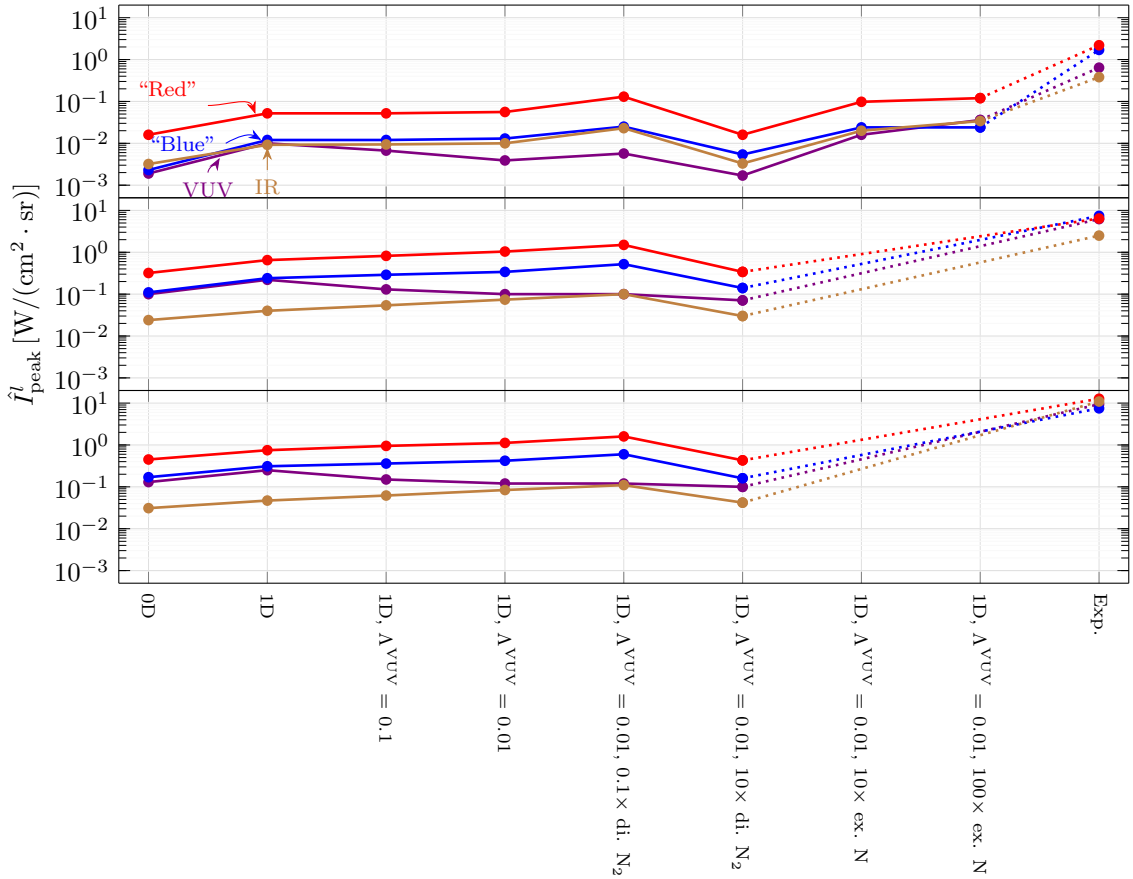

Figure 4.47: Peak values of the instrumentally resolved radiative intensities $\hat{I}^l_{\mathrm{peak}}$ obtained with the different models and in the experiment for the low, medium and high speed shots.

ones obtained in the experiment (labelled by "Exp."). The increase in the radiation variables comes with a cost of the translational temperatures ($T_{\mathrm{tr_h}}$ decreases as much as 698 K) and a weaker dissociation and ionisation of N_2. The mole fraction of N^+ at $x = 5\,\mathrm{cm}$ gets lower due to a faster recombination. The peak value of the mole fraction of N^+ actually increases as the highly excited N particles are more easily ionised. It can be concluded that more energy is used in endothermic processes, being excitation of N the mainly one.

As shown by Figures 4.48 and 4.49, the translational temperatures and the mole fractions of all species except N_2^+ attained in the one-dimension simulations disregarding spontaneous emission (labelled by "1D, no s. emission") agree well with the ones derived by Cruden and Brandis. This endorses the hypothesis of the simulated elements of fluid, when regarding spontaneous emission, not receiving the amount of energy that they should, as only by disregarding spontaneous emission (therefore, retaining a lot more energy) the thermodynamic conditions get reasonably closer to the inferred ones.

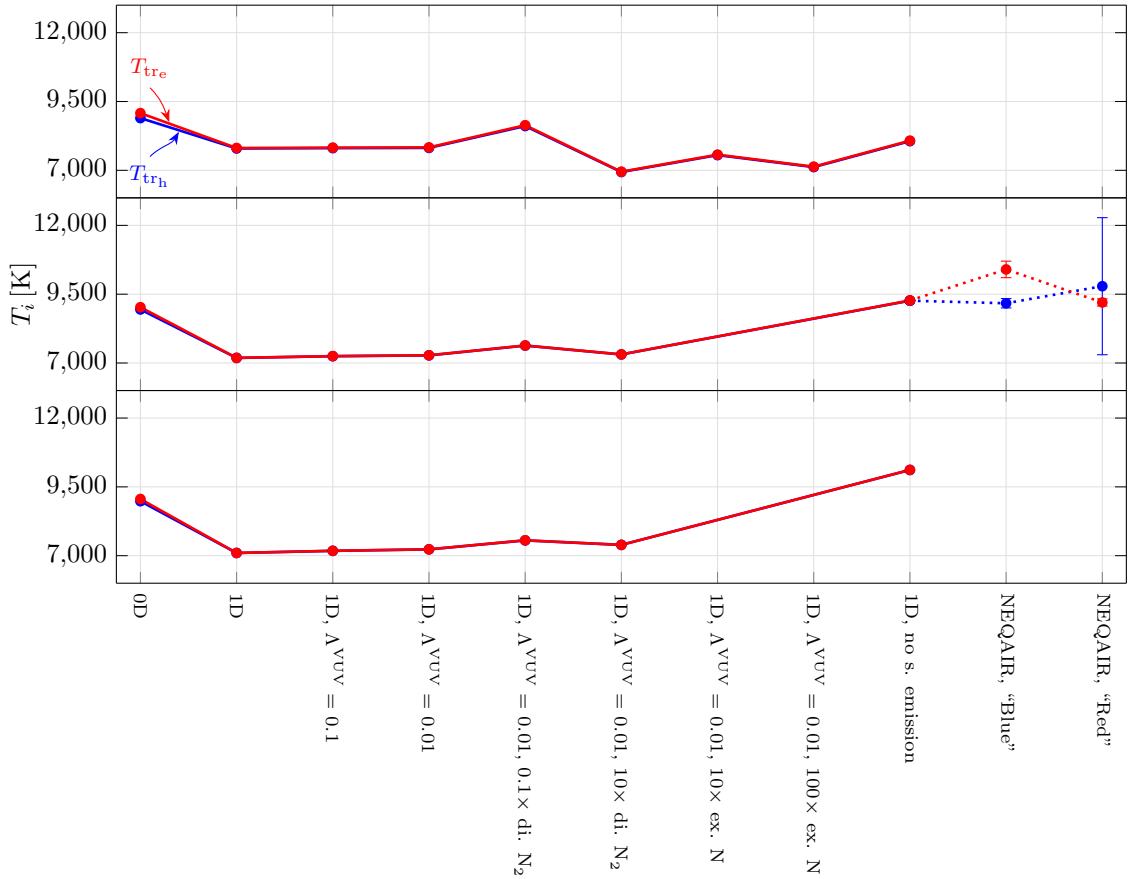

Figure 4.48: Temperatures $T_{\mathrm{tr_h}}$ and $T_{\mathrm{tr_e}}$ at $x = 5\,\mathrm{cm}$ obtained with the different models for the low, medium and high speed shots.

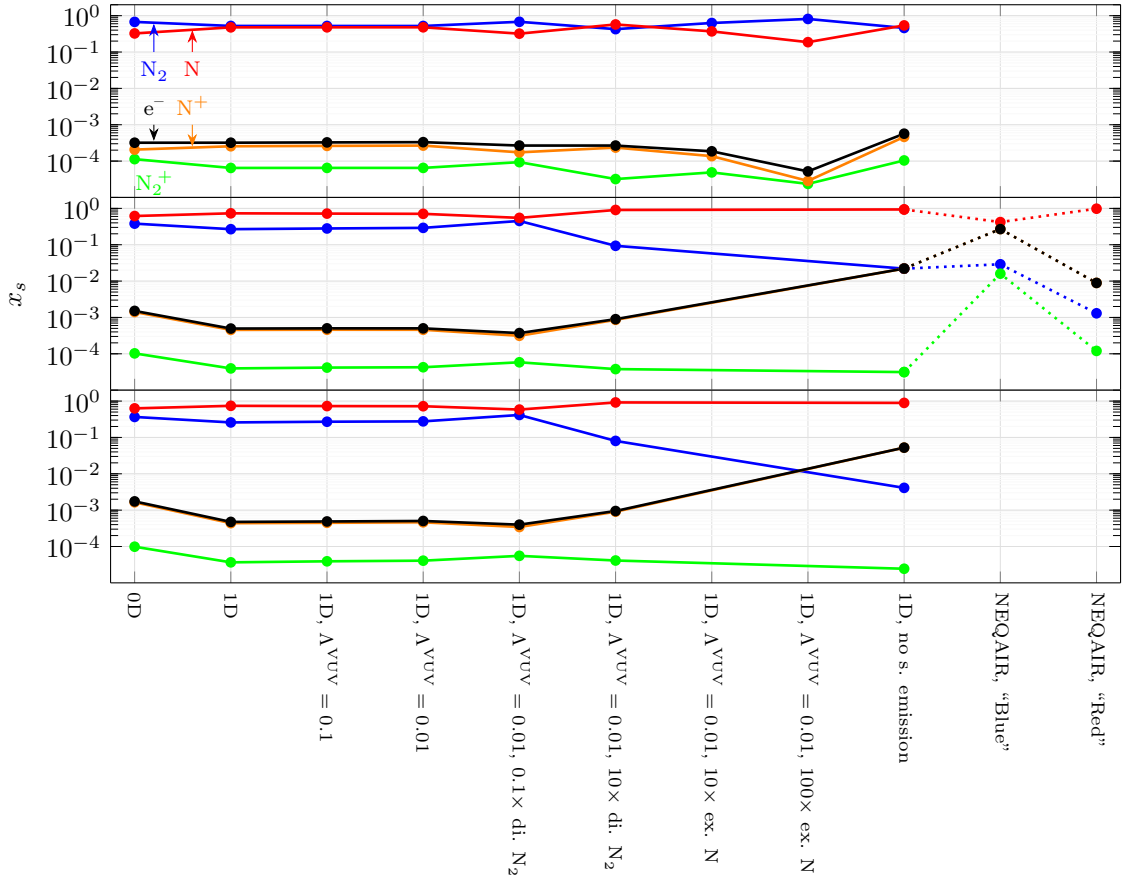

Figure 4.49: Mole fractions x_s at $x = 5\,\text{cm}$ obtained with the different models for the low, medium and high speed shots.

4.4.6 Other possible causes of the significant underestimation of the experimental results by the numerical ones

Several studies in the literature reported the occurrence of analytical and numerical models which significantly underestimated the radiation variables obtained trough shock tube experiments. In fact, these discrepancies had been so recurrently observed that Cruden et al. [160] even used the term "long-standing" to describe the longevity of the problem regarding results obtained from the Japan Aerospace Exploration Agency's High-Enthalpy Shock Tunnel (JAXA-HIEST). Cruden et al. [160] studied the impact that contamination species have on the numerical results, fitting their concentrations in order to match some particular JAXA-HIEST experimental results. They concluded that it may well be possible for contaminants such as Fe (atomic iron) and CN (cyanogen radical) to cause the observed discrepancies. In the case of the experiments that the produced benchmark data regarded in the present work - the EAST test 62 - Cruden and Brandis [158] found evidence for the presence of the contaminants C (atomic carbon), H (atomic hydrogen) and CN. However, it seems improbable that this could explain the deviations in several orders of magnitude on the obtained radiation variables, since the observed spectrum is almost completely dominated by the non-contaminant species (namely N, N_2 and N_2^+). Furthermore, Brandis et al. [161] refer that in the latest EAST campaigns many upgrades to the system have been made in

order to reduce the level of contamination.

A more feasible contribution to the discrepancies between the numerical and experimental results is the non-modelling of the so-called *precursor phenomena*: some of the VUV radiation emitted by highly excited particles in the shock layer is absorbed by others upstream of the shock wave, inducing their excitation, photoionisation and photodissociation. This changes the conditions upstream of the shock wave and, inevitably, also the conditions downstream of it: Nomura et al. [162] refer that the shock layer thickness and the non-equilibrium temperatures are increased, yielding an excess of radiation. Yamada et al. [163] compared experimental results with numerical ones obtained through a model that doesn't account the precursor phenomena, and found that the measured radiation intensities for N_2, N_2^+ and N started to increase upstream of the shock wave. The radiation profiles in the shock layer differed significantly, showing that the precursor phenomena had a great influence on the thermochemical processes that occurred downstream of the shock wave.

Another feasible contribution to the observed discrepancies corresponds to heating of the driven gas due to downstream plasma subjected to a stronger shock wave, and radiative energy transfer from the driver gas and the EAST electric arc. Bogdanoff and Park [164] performed several shock tube experiments and calculations, finding the temperature downstream of the shock wave in the observation point to be three to four times the one obtained through the Rankine-Hugoniot relations. The electric arc of the shock tube increases the temperature of the driver gas to very high values (several tens of thousands of kelvins) which causes it to radiate a lot of energy, some of it to the driven gas upstream and downstream of the shock wave. Also, it is known that the shock wave decelerates through the shock tube, heating more the part of the driven gas near the diaphragm than the part of the driven gas near the observation point. Thus, there's also a transfer of energy from the former to the later while the shock wave moves through the space between them.

Chapter 5

Conclusions

5.1 Achievements

In this work a extensive set of vibronic energy levels for N_2, N_2^+, N and N^+ was built using the most up-to-date data available in the literature. A near complete database of vibronic-specific kinetic processes involving these species was congregated. Special caution was taken to ensure physical consistence up to the highest temperatures. The database comprises chemical processes such as dissociation, ionisation and charge exchange, as well as non-chemical processes, i.e. excitation and de-excitation of the energy levels of the particles. The term "near complete" was herein used to describe it, since it misses transitions between the highest electronic energy levels, as well as bound-free and free-free radiative processes.

Rates for vibrational transition and dissociation of the molecular particles were computed using the FHO model. Thermal dissociation rate coefficients of $N_2(X^1\Sigma_g^+)$ by collisions with N_2 and N were obtained and calibrated using state-of-the-art experimental results, showing an agreeability between -59.9 and $8.9\,\%$, and between -80.9 and $-36.1\,\%$ for the former and latter interactions, respectively. Also, the values were compared with the most recent QCT calculations deviating by a maximum of $56.5\,\%$. Note that although these values seem to be too large, they should be regarded as reasonable, since the deviations are evaluated within an extensive set of temperatures (varying in many thousands of kelvins) for which the rate coefficients suffer changes of several orders of magnitude.

It was ascertained in this work if the well-known Landau-Zener and Rosen-Zener-Demkov models could be extended to vibronic transitions of molecular particles by heavy particle impact beyond electronic transitions of atomic particles by atomic particle impact. As a verdict, it was found impractical, mainly due to a current lack of knowledge about the characteristic constants that describe the models and to the necessity of solving the classical equations of motion of the nuclei. An exponential gap law was then preferred. However, the curve that represents the law was shown to deviate from experimental points by as much as one order magnitude, reducing the confidence on the model.

The developed kinetic database was tested in zero and Euler one-dimensional simulations of the shots 19, 20 and 40 of the test 62 of EAST. The peak values of the radiative intensities obtained from the Euler one-dimensional simulation were found to be between the double and the quintuple of the ones obtained

from the zero-dimensional simulation, showing the hypothesis of the momentum transfer being negligible (which is taken by the latter) to be invalid. Such result discourages the use in future works of the zero-dimensional model as an approximation of the flow generated by shock tubes. Still, the one-dimensional model underpredicted the experimental radiation variables by one to two orders of magnitude. And the sensibility tests performed on the rate coefficients were unsuccessful in getting a reasonable agreeability. The shape of the radiative intensities profiles of the low speed shot was correctly predicted, but not the ones of the medium and high speed shots which revealed non-null plateaus proceeding or coalescing with peaks. These plateaus weren't predicted at all. The analysis of Cruden and Brandis on the spectra obtained in the test 62 of EAST showed that higher values of the radiation variables were attained with a lower cost of translation temperature. There's a strong evidence for the underestimation of the radiation variables observed in this work to result from the non-modelling of heat transfer by radiation within the test gas, and possibly, between the driver gas (as well as the driver arc) and the test gas. The latter hypothesis has been suggested by Bogdanoff and Park as a possible cause for such underestimations also observed in other works.

5.2 Future Work

One of the next steps that should be taken in the future would be to test other kinetic databases reported in the literature and to compare their results with the ones of this work, such that particular qualities which were actually improved or, on the contrary, worsen may be identified. And to quantify the possible divergences between the herein implemented vibronic-specific state-to-state model and the simpler models such as the multi and single-temperature ones, these latter should also be tried.

In order to ascertain the effect of heat transfer within the test gas subjected to strong shock waves generated by shock tubes, higher fidelity one-dimensional simulations should be performed. The crude concept of an escape factor should be disregarded, and an equation of radiative transfer should be solved instead. Also, the transport phenomena should be introduced in the balance equations. It's of capital importance to know if a lack of such complexities in the numerical model was the reason for the significant underestimation of the radiation variables.

The database of radiative processes developed in this work should be extended, accommodating absorption, induced emission, photodissociation, photoassociation, photoionisation, photorecombination and bremsstrahlung, beyond spontaneous emission processes. And these processes should be treated as rovibronic instead of simply vibronic, as the numerical spectra associated to the molecular contributions obtained in this work showed pointier profiles when compared to the ones obtained in the experiments.

An extrapolation of the Einstein coefficients for spontaneous emission to the energy levels whose data aren't available should be performed to avoid getting unphysical populations distributions.

And finally, as more ambitious goals, the impact on the radiation variables of the precursor phenomena, the absorption of radiation emitted by the driver gas and the EAST electric arc, and the conduction of heat from the driver to the test gas should be studied.

Bibliography

[1] John D Anderson Jr. *Hypersonic and high-temperature gas dynamics.* American Institute of Aeronautics and Astronautics, 2nd edition, 2006. doi:10.2514/4.861956.

[2] Chul Park. *Nonequilibrium Hypersonic Aerothermodynamics.* John Wiley and Sons Ltd, New York, United States, April 1990.

[3] W. G. Vincenti and C. H. Kruger. *Introduction to physical gas dynamics.* John Wiley & Sons, 1965.

[4] John J. Bertin. *Hypersonic Aerothermodynamics.* American Institute of Aeronautics and Astronautics, Inc., Washington, DC, 1994.

[5] G. S. R. Sarma. *Relevance of Aerothermochemistry for Hypersonic Technology*, pages 1–20. Springer Netherlands, Dordrecht, 1996. doi:10.1007/978-94-009-0267-1_1.

[6] Stephen Corda. *Introduction to aerospace engineering with a flight test perspective.* John Wiley & Sons, 2017. ISBN:978-1-118-95336-5.

[7] Chul Park. *Modeling of Hypersonic Reacting Flows*, pages 104–127. Birkhäuser Boston, Boston, MA, 1992. doi:10.1007/978-1-4612-0371-1_4, ISBN:978-1-4612-0371-1.

[8] Jong-Hun Lee. Basic governing equations for the flight regimes of aeroassisted orbital transfer vehicles. In *19th Thermophysics Conference*, June 1984. doi:10.2514/6.1984-1729.

[9] Chul Park. Assessment of two-temperature kinetic model for ionizing air. *Journal of Thermophysics and Heat Transfer*, 3(3):233–244, 1989. doi:10.2514/3.28771.

[10] Chul Park. Modeling of hypersonic reacting flows. In Ballmann J. Bertin J.J., Periaux J., editor, *Advances in Hypersonics*, number 8/9 in Progress in Scientific Computing, pages 104–127. Birkhäuser, Boston, MA, 1992. doi:10.1007/978-1-4612-0371-1_4.

[11] Graham Candler. On the computation of shock shapes in nonequilibrium hypersonic flows. In *27th Aerospace Sciences Meeting.* January 1989. doi:10.2514/6.1989-312.

[12] H. G. Hornung. Non-equilibrium dissociating nitrogen flow over spheres and circular cylinders. *Journal of Fluid Mechanics*, 53(1):149–176, 1972. doi:10.1017/S0022112072000084.

[13] R. Kenneth Lobb. Chapter 26 - Experimental Measurement of Shock Detachment Distance on Spheres Fired in Air at Hypervelocities. In Wilbur C. Nelson, editor, *The High Temperature Aspects of Hypersonic Flow*, volume 68 of *AGARDograph*, pages 519–527. Elsevier, 1964. doi:10.1016/B978-1-4831-9828-6.50031-X.

[14] Graham V. Candler, Joseph Olejniczak, and Brent Harrold. Detailed simulation of nitrogen dissociation in stagnation regions. *Physics of Fluids*, 9(7):2108–2117, 1997. doi:10.1063/1.869330.

[15] Alessandro Munafó, Marco Panesi, Richard Jaffe, Thierry Magin, and Andrea Lani. Vibrational State to State Kinetics in Expanding and Compressing Nitrogen Flows. In *10th AIAA/ASME Joint Thermophysics and Heat Transfer Conference*, June 2010. doi:10.2514/6.2010-4335.

[16] Christophe O. Laux, Laurent Pierrot, and Richard J. Gessman. State-to-state modeling of a recombining nitrogen plasma experiment. *Chemical Physics*, 398:46–55, 2012. doi:10.1016/j.chemphys.2011.10.028.

[17] J. Vargas. Improvement of state-resolved kinetic models applied to N2–CH4 hypersonic entry flows. Master's thesis, Instituto Superior Técnico, 2015. url:`https://bibliotecas.utl.pt/cgi-bin/koha/opac-detail.pl?biblionumber=526938`. Accessed: 2020-09-14.

[18] J. Annaloro. *Modèles collisionnels-radiatifs appliqués aux situations d'entrée atmosphérique martienne et terrestre*. PhD thesis, Université de Rouen, 2013. url:`http://www.coria.fr/spip.php?article908&titre_mot=these&lang=en`. Accessed: 2020-09-14.

[19] Igor V Adamovich, Sergey O Macheret, J William Rich, and Charles E Treanor. Vibrational relaxation and dissociation behind shock waves. Part 1 - Kinetic rate models. *AIAA journal*, 33(6):1064–1069, June 1995. doi:10.2514/3.12528.

[20] Igor V Adamovich, Sergey O Macherett, J William Rich, and Charles E Treanor. Vibrational relaxation and dissociation behind shock waves part 2: Master equation modeling. *AIAA journal*, 33(6):1070–1075, June 1995. doi:10.2514/3.48339.

[21] Igor V Adamovich, Sergey O Macheret, J William Rich, and Charles E Treanor. Vibrational energy transfer rates using a forced harmonic oscillator model. *Journal of Thermophysics and Heat Transfer*, 12(1):57–65, January 1998. doi:10.2514/2.6302.

[22] RN Schwartz, ZI Slawsky, and KF Herzfeld. Calculation of vibrational relaxation times in gases. *The Journal of Chemical Physics*, 20(10):1591–1599, May 1952. doi:10.1063/1.1700221.

[23] Don Secrest and B Robert Johnson. Exact Quantum-Mechanical Calculation of a Collinear Collision of a Particle with a Harmonic Oscillator. *The Journal of Chemical Physics*, 45(12):4556–4570, December 1966. doi:10.1063/1.1727537.

[24] GD Billing. Vibration-vibration and vibration-translation energy transfer, including multiquantum transitions in atom-diatom and diatom-diatom collisions. In *Nonequilibrium vibrational kinetics*, pages 85–112. Springer, Berlin, Heidelberg, 1986. doi:10.1007/978-3-642-48615-9_4.

[25] Donald G. Truhlar and James T. Muckerman. Reactive scattering cross sections III: Quasiclassical and semiclassical methods. In *Atom-Molecule Collision Theory*, pages 505–566. Springer, Boston, MA, 1979. doi:10.1007/978-1-4613-2913-8_16.

[26] Edward H Kerner. Note on the forced and damped oscillator in quantum mechanics. *Canadian Journal of Physics*, 36(3):371–377, 1958. doi:10.1139/p58-038.

[27] Charles E Treanor. Vibrational Energy Transfer in High-Energy Collisions. *The Journal of Chemical Physics*, 43(2):532–538, July 1965. doi:10.1063/1.1696777.

[28] Ann Zelechow, Donald Rapp, and Terry E Sharp. Vibrational–vibrational–translational energy transfer between two diatomic molecules. *The Journal of Chemical Physics*, 49(1):286–299, July 1968. doi:10.1063/1.1669823.

[29] M. Lino da Silva, V. Guerra, and J. Loureiro. State-resolved dissociation rates for extremely nonequilibrium atmospheric entries. *Journal of Thermophysics and Heat Transfer*, 21(1):40–49, 2007. doi:10.2514/1.24114.

[30] L. D. Landau. *Phys. Zts. Sov.*, 2(46), 1932.

[31] Clarence Zener and Ralph Howard Fowler. Non-adiabatic crossing of energy levels. *Proceedings of the Royal Society of London. Series A, Containing Papers of a Mathematical and Physical Character*, 137(833):696–702, 1932. doi:10.1098/rspa.1932.0165.

[32] N. Rosen and C. Zener. Double Stern-Gerlach Experiment and Related Collision Phenomena. *Phys. Rev.*, 40:502–507, May 1932. doi:10.1103/PhysRev.40.502.

[33] Yu N Demkov. Charge transfer at small resonance defects. *Sov. Phys. JETP*, 18(1):138–142, 1964.

[34] R. Bachmann, X. Li, Ch. Ottinger, and A. F. Vilesov. Molecular-beam study of the collisional intramolecular coupling of $N_2(B^3\Pi_g)$ with the $N_2(A^3\Sigma_u^+)$ and $N_2(W^3\Delta_u)$ states. *The Journal of Chemical Physics*, 96(7):5151–5164, 1992. doi:10.1063/1.462756.

[35] R. Bachmann, X. Li, Ch. Ottinger, A. F. Vilesov, and V. Wulfmeyer. Vibrational-state-to-state collision-induced intramolecular energy transfer $N_2(A^3\Sigma_u^+, v'' \rightarrow B^3\Pi_g, v')$. *The Journal of Chemical Physics*, 98(11):8606–8625, 1993. doi:10.1063/1.464469.

[36] D. H. Katayama, Terry A. Miller, and V. E. Bondybey. Radiative decay and radiationless deactivation in selectively excited CN. *The Journal of Chemical Physics*, 71(4):1662–1669, 1979. doi:10.1063/1.438504.

[37] D. H. Katayama and J. A. Welsh. The effect of isotopic substitution on the collisional quenching of vibronically excited CO^+. *The Journal of Chemical Physics*, 79(8):3627–3632, 1983. doi:10.1063/1.446299.

[38] D.H. Katayama and J.A. Welsh. The effect of temperature on the collisional deactivation of electronically excited CO^+. *Chemical Physics Letters*, 106(1):74–78, 1984. doi:10.1016/0009-2614(84)87014-1.

[39] D. H. Katayama, A. V. Dentamaro, and J. A. Welsh. State specific electronic quenching rates for $^{14}N_2^+$ and $^{15}N_2^+$. *The Journal of Chemical Physics*, 87(12):6983–6987, 1987. doi:10.1063/1.453394.

[40] Clabon Walter Allen and Arthur N Cox. *Allen's Astrophysical Quantities*. Springer-Verlag New York, 4th edition, 2002. doi:10.1007/978-1-4612-1186-0, ISBN:978-0-387-95189-8.

[41] Julien Annaloro and Arnaud Bultel. Vibrational and electronic collisional-radiative model in air for Earth entry problems. *Physics of Plasmas*, 21(12):123512, 2014. doi:10.1063/1.4904817.

[42] Bruno Lopez and Mário Lino da Silva. SPARK: A Software Package for Aerodynamics, Radiation and Kinetics. In *46th AIAA Thermophysics Conference*, page 4025, June 2016. doi:10.2514/6.2016-4025.

[43] Aaron M Brandis and Brett A Cruden. Shock Tube Radiation Measurements in Nitrogen. In *2018 Joint Thermophysics and Heat Transfer Conference*, 2018. doi:10.2514/6.2018-3437.

[44] Jorge Loureiro and Jayr Amorim. *Kinetics and spectroscopy of low temperature plasmas*. Springer, 2016. doi:10.1007/978-3-319-09253-9, ISBN:978-3-319-09252-2.

[45] A Kuppermann and EF Greene. Chemical reaction cross sections and rate constants. *Journal of Chemical Education*, 45(6):361–369, 1968. doi:10.1021/ed045p361.

[46] S. S. Penner. *Quantitative molecular spectroscopy and gas emissivities*. Addison-Wesley Pub. Co., 1959.

[47] Hans R. Griem. *Principles of Plasma Spectroscopy*. Cambridge Monographs on Plasma Physics. Cambridge University Press, 1997. doi:10.1017/CBO9780511524578.

[48] W. Heitler. *The Quantum Theory of Radiation*. Dover Books on Physics Series. Dover Publications, 1984.

[49] Gerhard Herzberg. *Molecular spectra and molecular structure. Vol. III: Electronic spectra and electronic structure of polyatomic molecules*. Krieger Publishing Company, 1966.

[50] Vincent Giovangigli. *Multicomponent Flow Modeling*. Birkhäuser Basel, 1st edition, 1999. doi:10.1007/978-1-4612-1580-6.

[51] Ellis E. Whiting, Chul Park, Yen Liu, James O. Arnold, and John A. Paterson. NEQAIR96, Nonequilibrium and Equilibrium Radiative Transport and Spectra Program: User's Manual. Technical Report NASA-RP-1389, A-962456, NAS 1.61:1389, NASA Ames Research Center, Moffett Field, CA United States, Dec 1996. url:`https://ntrs.nasa.gov/search.jsp?R=19970004690`. Accessed: 2020-09-14.

[52] Roop N. Gupta, Jerrold M. Yos, Richard A. Thompson, and Kam-Pui Lee. A review of reaction rates and thermodynamic and transport properties for an 11-species air model for chemical and thermal nonequilibrium calculations to 30000 K. Technical Report NASA-RP-1232, L-16634, NAS 1.61:1232, NASA Langley Research Center, Hampton, VA, United States, Aug 1990. url:`https://ntrs.nasa.gov/search.jsp?R=19900017748`. Accessed: 2020-09-14.

[53] Donald Rapp and Thomas Kassal. Theory of vibrational energy transfer between simple molecules in nonreactive collisions. *Chemical Reviews*, 69(1):61–102, February 1969. doi:10.1021/cr60257a003.

[54] Roger A. Svehla. *Estimated viscosities and thermal conductivities of gases at high temperatures.* NASA Lewis Research Center, January 1962. url:`https://ntrs.nasa.gov/archive/nasa/casi.ntrs.nasa.gov/19630012982.pdf`. Accessed: 2020-09-14.

[55] T. L. Cottrell and J. C. McCoubrey. *Molecular energy transfer in gases.* London Butterworths, 1st edition, 1961.

[56] TL Cottrell and N Ream. Transition probability in molecular encounters. Part 1. The evaluation of perturbation integrals. *Transactions of the Faraday Society*, 51:159–171, 1955. doi:10.1039/TF9555100159.

[57] Sergey O. Macheret and Igor V. Adamovich. Semiclassical modeling of state-specific dissociation rates in diatomic gases. *The Journal of Chemical Physics*, 113(17):7351–7361, 2000. doi:10.1063/1.1313386.

[58] Gert Due Billing and Edward R. Fisher. VV and VT rate coefficients in H_2 by a quantum-classical model. *Chemical Physics*, 18(1):225–232, 1976. doi:10.1016/0301-0104(76)87049-8.

[59] Gert Due Billing. WKB approximations in inelastic collision theory. *The Journal of Chemical Physics*, 59(11):6147–6152, 1973. doi:10.1063/1.1679983.

[60] Gert Due Billing and E.R. Fisher. VV and VT rate coefficients in N_2 by a quantum-classical model. *Chemical Physics*, 43(3):395–401, 1979. doi:10.1016/0301-0104(79)85207-6.

[61] Evgeny E. Nikitin. *Theory of elementary atomic and molecular processes in gases.* Clarendon Press, Oxford, 1974.

[62] L. D. Landau and E. M. Lifshitz. *Quantum Mechanics.* Pergamon, 3rd edition, 1977. doi:10.1016/C2013-0-02793-4.

[63] Evgueni Nikitin. *Adiabatic and Diabatic Collision Processes at Low Energies*, pages 741–752. Springer New York, New York, NY, 2006. doi:10.1007/978-0-387-26308-3_49.

[64] V. I. Osherov and A. I. Voronin. Exact analytical solution of the quantum Rosen-Zener-Demkov model. *Phys. Rev. A*, 49:265–271, Jan 1994. doi:10.1103/PhysRevA.49.265.

[65] R. T. Robiscoe. Extension of the rosen-zener solution to the two-level problem. *Phys. Rev. A*, 17:247–260, Jan 1978. doi:10.1103/PhysRevA.17.247.

[66] Hiroki Nakamura. *Nonadiabatic Transition*. World Scientific, 2nd edition, 2012. doi:10.1142/8009.

[67] Gianni L. Bendazzoli, Mario Raimondi, Bruce A. Garetz, Thomas F. George, and Keiji Morokuma. Semiclassical study of collision-induced predissociation: Comparison of the Landau-Zener model with the method of analytic continuation. *Theoretica chimica acta*, 44:341–350, December 1977. doi:10.1007/BF00547828.

[68] John C. Tully and Richard K. Preston. Trajectory Surface Hopping Approach to Nonadiabatic Molecular Collisions: The Reaction of H+ with D2. *The Journal of Chemical Physics*, 55(2):562–572, 1971. doi:10.1063/1.1675788.

[69] M. Capitelli, C.M. Ferreira, B.F. Gordiets, and A.I. Osipov. *Plasma Kinetics in Atmospheric Gases*. Springer-Verlag Berlin Heidelberg, 1st edition, 2000. doi:10.1007/978-3-662-04158-1.

[70] A.S. Kirillov. Application of Landau–Zener and Rosen–Zener approximations to calculate rates of electron energy transfer processes. *Advances in Space Research*, 33(6):993–997, 2004. doi:10.1016/j.asr.2003.06.009.

[71] A.S. Kirillov. Calculation of rate coefficients of electron energy transfer processes for molecular nitrogen and molecular oxygen. *Advances in Space Research*, 33(6):998–1004, 2004. doi:10.1016/j.asr.2003.06.014.

[72] V. E. Bondybey and Terry A. Miller. Radiative and radiationless vibronic deactivation rates in selectively excited CO^+. *The Journal of Chemical Physics*, 69(8):3597–3602, 1978. doi:10.1063/1.437066.

[73] Anthony V. Dentamaro and Daniel H. Katayama. Collision induced transitions between the $A^2\Pi_i(v = 0)$ and $X^2\Sigma^+(v = 10)$ states of CO^+. *The Journal of Chemical Physics*, 90(1):91–95, 1989. doi:10.1063/1.456473.

[74] Guo Jihua, Ashraf Ali, and Paul J. Dagdigian. State-to-state collisional interelectronic and intraelectronic energy transfer involving CN $A^2\Pi$ $v = 3$ and $X^2\Sigma^+$ $v = 7$ rotational levels. *The Journal of Chemical Physics*, 85(12):7098–7105, 1986. doi:10.1063/1.451396.

[75] Lawrence G. Piper. State-to-state $N_2(A^3\Sigma^+u)$ energy pooling reactions. II. The formation and quenching of $N_2(B^3\Pi_g, v' = 1 - 12)$. *The Journal of Chemical Physics*, 88(11):6911–6921, 1988. doi:10.1063/1.454388.

[76] Charles S. Parmenter and Mark Seaver. A method to estimate intermolecular potential well depths for species in both ground and excited electronic states. *The Journal of Chemical Physics*, 70(12):5458–5462, 1979. doi:10.1063/1.437457.

[77] H.-M. Lin, Mark Seaver, K. Y. Tang, Alan E. W. Knight, and Charles S. Parmenter. The role of intermolecular potential well depths in collision-induced state changes. *The Journal of Chemical Physics*, 70(12):5442–5457, 1979. doi:10.1063/1.437456.

[78] C. Clay Marston and Gabriel G. Balint-Kurti. The Fourier grid Hamiltonian method for bound state eigenvalues and eigenfunctions. *The Journal of Chemical Physics*, 91(6):3571–3576, 1989. doi:10.1063/1.456888.

[79] Ragnar Rydberg. Graphische Darstellung einiger bandenspektroskopischer Ergebnisse. *Zeitschrift für Physik*, 73(5):376–385, May 1932. doi:10.1007/BF01341146.

[80] Ragnar Rydberg. Über einige Potentialkurven des Quecksilberhydrids. *Zeitschrift für Physik*, 80(7):514–524, Feb 1933. doi:10.1007/BF02057312.

[81] O. Klein. Zur Berechnung von Potentialkurven für zweiatomige Moleküle mit Hilfe von Spektraltermen. *Zeitschrift für Physik*, 76(3):226–235, Mar 1932. doi:10.1007/BF01341814.

[82] A. L. G. Rees. The calculation of potential-energy curves from band-spectroscopic data. *Proceedings of the Physical Society*, 59(6):998–1008, nov 1947. doi:10.1088/0959-5309/59/6/310.

[83] Alexander Kramida, Yuri Ralchenko, Joseph Reader, et al. NIST Atomic Spectra Database (version 5.7), October 2019. url:`https://www.nist.gov/pml/atomic-spectra-database`. Accessed: 2019-12-15.

[84] Julien Annaloro, Arnaud Bultel, and Pierre Omaly. Collisional-Radiative Modeling Behind Shock Waves in Nitrogen. *Journal of Thermophysics and Heat Transfer*, 28(4):608–622, 2014. doi:10.2514/1.T4263.

[85] Lawrence G. Piper. The excitation of $N(^2P)$ by $N_2(A^3\Sigma_u^+, v' = 0, 1)$. *The Journal of Chemical Physics*, 90(12):7087–7095, 1989. doi:10.1063/1.456237.

[86] Ch. Ottinger, L. G. Smirnova, and A. F. Vilesov. Collision-induced transitions from $N_2(A'^5\Sigma_g^+)$ to $N_2(B^3\Pi_g)$ via the gateway mechanism. *The Journal of Chemical Physics*, 100(7):4848–4861, 1994. doi:10.1063/1.467205.

[87] D. Levron and A. V. Phelps. Quenching of $N_2(A^3\Sigma_u^+, v = 0, 1)$ by N_2, Ar, and H_2. *The Journal of Chemical Physics*, 69(5):2260–2262, 1978. doi:10.1063/1.436788.

[88] Lawrence G. Piper. State-to-state $N_2(A^3\Sigma_u^+)$ energy pooling reactions. II. The formation and quenching of $N_2(B^3\Pi_g, v' = 1–12)$. *The Journal of Chemical Physics*, 88(11):6911–6921, 1988. doi:10.1063/1.454388.

[89] Lawrence G. Piper. State-to-state $N_2(A^3\Sigma_u^+)$ energy-pooling reactions. I. The formation of $N_2(C^3\Pi_u)$ and the Herman infrared system. *The Journal of Chemical Physics*, 88(1):231–239, 1988. doi:10.1063/1.454649.

[90] W. Freysinger, F. A. Khan, P. B. Armentrout, P. Tosi, O. Dmitriev, and D. Bassi. Charge-transfer reaction of $^{14.15}N^+(^3P_J) + N_2(^1\Sigma_g^+)$ from thermal to 100 eV. Crossed-beam and scattering-cell guided-ion beam experiments. *The Journal of Chemical Physics*, 101(5):3688–3695, 1994. doi:10.1063/1.467553.

[91] V. Laporta, D. A. Little, R. Celiberto, and J. Tennyson. Electron-impact resonant vibrational excitation and dissociation processes involving vibrationally excited N_2 molecules. *Plasma Sources Science and Technology*, 23(6):065002, aug 2014. doi:10.1088/0963-0252/23/6/065002.

[92] Phys4Entry - Planetary Entry Integrated Models - Seventh Framework Programme. url:`http://phys4entrydb.ba.imip.cnr.it/Phys4EntryDB/`. Accessed: 2019-12-15.

[93] M. Brunger, S. J. Buckman, and M. T. Elford. *6.4 Excitation cross sections*, volume 17C, chapter 6 Cross sections for scattering- and excitation-processes in electron-molecule collisions. Springer-Verlag Berlin Heidelberg, 2003. doi:10.1007/10874891_7.

[94] Charles P. Malone, Paul V. Johnson, Xianming Liu, Bahar Ajdari, Isik Kanik, and Murtadha A. Khakoo. Integral cross sections for the electron-impact excitation of the $b^1\Pi_u$, $c_3{}^1\Pi_u$, $o_3{}^1\Pi_u$, $b'^1\Sigma_u^+$, $c_4'^1\Sigma_u^+$, $G^3\Pi_u$ and $F^3\Pi_u$ states of N_2. *Phys. Rev. A*, 85:062704, Jun 2012. doi:10.1103/PhysRevA.85.062704.

[95] Yukikazu Itikawa. Cross Sections for Electron Collisions with Nitrogen Molecules. *Journal of Physical and Chemical Reference Data*, 35(1):31–53, 2006. doi:10.1063/1.1937426.

[96] D. H. Crandall, W. E. Kauppila, R. A. Phaneuf, Paul O. Taylor, and Gordon H. Dunn. Absolute cross sections for electron-impact excitation of N_2^+. *Phys. Rev. A*, 9:2545–2551, Jun 1974. doi:10.1103/PhysRevA.9.2545.

[97] K. A. Berrington, P. G. Burke, and W. D. Robb. The scattering of electrons by atomic nitrogen. *Journal of Physics B: Atomic and Molecular Physics*, 8(15):2500–2511, Oct 1975. doi:10.1088/0022-3700/8/15/012.

[98] Marco Panesi, Thierry Magin, Anne Bourdon, Arnaud Bultel, and O. Chazot. Fire II Flight Experiment Analysis by Means of a Collisional-Radiative Model. *Journal of Thermophysics and Heat Transfer*, 23(2):236–248, 2009. doi:10.2514/1.39034.

[99] M. Capitelli, R. Celiberto, A. Eletskii, and A. Laricchiuta. Electron-molecule dissociation cross-sections of H_2, N_2 and O_2 in different vibrational levels. In *Atomic and Plasma-material Interaction Data for Fusion (IAEA)*, number 9, pages 47–64. International Atomic Energy Agency, Vienna, 2001. url:`https://www.iaea.org/publications/6321/atomic-and-plasma-material-interaction-data-for-fusion`. Accessed: 2020-09-14.

[100] Steven L. Guberman. The vibrational dependence of dissociative recombination: Rate constants for N_2^+. *The Journal of Chemical Physics*, 141(20):204307, 2014. doi:10.1063/1.4901892.

[101] Annarita Laricchiuta, Mario Capitelli, Roberto Celiberto, and Gianpiero Colonna. *Dissociation and Ionization Cross Sections and Rate Coefficients of Air Molecules by Electron Impact: the Role of Vibrational Energy.* doi:10.2514/6.2006-2898.

[102] E. Brook, M. F. A. Harrison, and A. C. H. Smith. Measurements of the electron impact ionisation cross sections of He, C, O and N atoms. *Journal of Physics B: Atomic and Molecular Physics*, 11(17):3115–3132, Sep 1978. doi:10.1088/0022-3700/11/17/021.

[103] Yang Wang, Oleg Zatsarinny, and Klaus Bartschat. B-spline R-matrix-with-pseudostates calculations for electron-impact excitation and ionization of nitrogen. *Phys. Rev. A*, 89:062714, Jun 2014. doi:10.1103/PhysRevA.89.062714.

[104] Boyd Cary. Shock-Tube Study of the Termal Dissociation of Nitrogen. *The Physics of Fluids*, 8(1):26–35, 1965. doi:10.1063/1.1761099.

[105] Stanley Byron. Shock-Tube Measurement of the Rate of Dissociation of Nitrogen. *The Journal of Chemical Physics*, 44(4):1378–1388, 1966. doi:10.1063/1.1726870.

[106] J. P. Appleton, M. Steinberg, and D. J. Liquornik. Shock-Tube Study of Nitrogen Dissociation using Vacuum-Ultraviolet Light Absorption. *The Journal of Chemical Physics*, 48(2):599–608, 1968. doi:10.1063/1.1668690.

[107] Ronald K. Hanson and Donald Baganoff. Shock-Tube Study of Nitrogen Dissociation Rates Using Pressure Measurements. *AIAA Journal*, 10(2):211–215, 1972. doi:10.2514/3.50082.

[108] D.J. Kewley and H.G. Hornung. Free-piston shock-tube study of nitrogen dissociation. *Chemical Physics Letters*, 25(4):531–536, 1974. doi:10.1016/0009-2614(74)85360-1.

[109] Chul Park. Two-temperature interpretation of dissociation rate data for N_2 and O_2. In *26th Aerospace Sciences Meeting*, January 1988. doi:10.2514/6.1988-458.

[110] Richard L. Jaffe, Maninder Grover, Simone Venturi, David. W. Schwenke, Paolo Valentini, Thomas E. Schwartzentruber, and Marco Panesi. Comparison of potential energy surface and computed rate coefficients for n2 dissociation. *Journal of Thermophysics and Heat Transfer*, 32(4):869–881, 2018. doi:10.2514/1.T5417.

[111] Graham Candler and Joseph Olejniczak. Nitrogen dissociation rates in complex hypersonic flows. In *32nd Thermophysics Conference*, 1997. doi:10.2514/6.1997-2500.

[112] Jason D. Bender, Paolo Valentini, Ioannis Nompelis, Yuliya Paukku, Zoltan Varga, Donald G. Truhlar, Thomas Schwartzentruber, and Graham V. Candler. An improved potential energy surface and multi-temperature quasiclassical trajectory calculations of $N_2 + N_2$ dissociation reactions. *The Journal of Chemical Physics*, 143(5):054304, 2015. doi:10.1063/1.4927571.

[113] R. L. Macdonald, R. L. Jaffe, D. W. Schwenke, and M. Panesi. Construction of a coarse-grain quasi-classical trajectory method. I. Theory and application to N_2 - N_2 system. *The Journal of Chemical Physics*, 148(5):054309, 2018. doi:10.1063/1.5011331.

[114] F. Esposito and M. Capitelli. Quasiclassical molecular dynamic calculations of vibrationally and rotationally state selected dissociation cross-sections: $N + N_2(v, J) \longrightarrow 3\,N$. *Chemical Physics Letters*, 302(1):49–54, 1999. doi:10.1016/S0009-2614(99)00099-8.

[115] Richard Jaffe, David Schwenke, and Galina Chaban. Vibration-Rotation Excitation and Dissociation in N_2 - N_2 Collisions from Accurate Theoretical Calculations. In *10th AIAA/ASME Joint Thermophysics and Heat Transfer Conference*, 2010. doi:10.2514/6.2010-4517.

[116] Juris Meija, Tyler B. Coplen, Michael Berglund, Willi A. Brand, Paul De Bièvre, Manfred Gröning, Norman E. Holden, Johanna Irrgeher, Robert D. Loss, Thomas Walczyk, and Thomas Prohaska. Atomic weights of the elements 2013 (IUPAC Technical Report). *Pure and Applied Chemistry*, 88(3):265–291, 2016. doi:10.1515/pac-2015-0305.

[117] J. W. Dreyer and D. Perner. Deactivation of $N_2(A^3\Sigma_u^+, v = 0–7)$ by ground state nitrogen, ethane, and ethylene measured by kinetic absorption spectroscopy. *The Journal of Chemical Physics*, 58(3):1195–1201, 1973. doi:10.1063/1.1679301.

[118] P. H. Vidaud, R. P. Wayne, M. Yaron, and A. von Engel. Collisional quenching of $N_2(A^3\Sigma_u^+, v = 0, 1)$ by N atoms, ground state N_2 and a pyrex surface. *J. Chem. Soc., Faraday Trans. 2*, 72:1185–1193, 1976. doi:10.1039/F29767201185.

[119] Jeffrey Alan Meyer, Donald W. Setser, and Donald H. Stedman. Energy transfer reactions of $N_2(A^3\Sigma_u^+)$. II. Quenching and emission by oxygen and nitrogen atoms. *The Journal of Physical Chemistry*, 74(10):2238–2240, 1970. doi:10.1021/j100909a041.

[120] R. A. Young and O. J. Dunn. The excitation and quenching of $N(^2P)$. *The Journal of Chemical Physics*, 63(3):1150–1153, 1975. doi:10.1063/1.431441.

[121] Experimental determination of the Einstein coefficient for the $N(^2P–^4S)$ transition. *Chemical Physics Letters*, 296(3):397–402, 1998. doi:10.1016/S0009-2614(98)01043-4.

[122] Kurt L. Wray. Excitation studies on the $N_2(1+)$ and $N_2^+(1-)$ systems in shock-heated N–N_2 mixtures. *The Journal of Chemical Physics*, 44(2):623–632, 1966. doi:10.1063/1.1726735.

[123] Robert A. Young and Gilbert A. St. John. Experiments on $N_2(A^3\Sigma_u^+)$. I. Reaction with N. *The Journal of Chemical Physics*, 48(2):895–897, 1968. doi:10.1063/1.1668731.

[124] O. J. Dunn and R. A. Young. Quenching of $N_2(A^3\Sigma_u^+)$ by O_2, O, N, and H. *International Journal of Chemical Kinetics*, 8(2):161–172, 1976. doi:10.1002/kin.550080202.

[125] William M. Gelbart and Karl F. Freed. Intramolecular perturbations and the quenching of luminescence in small molecules. *Chemical Physics Letters*, 18(4):470–475, 1973. doi:10.1016/0009-2614(73)80445-2.

[126] Karl F. Freed. *Collision-Induced Intersystem Crossing*, pages 291–336. John Wiley & Sons, Ltd, 2007. doi:10.1002/9780470142660.ch10.

[127] A. Tramer and A. Nitzan. *Collisional Effects in Electronic Relaxation*, pages 337–380. John Wiley & Sons, Ltd, 2007. doi:10.1002/9780470142660.ch11.

[128] G. Herzberg and K.P. Huber. *Molecular Spectra and Molecular Structure: Spectra of diatomic molecules*. Molecular Spectra and Molecular Structure. Van Nostrand, 1950.

[129] Steven L. Guberman. Role of Excited Core Rydberg States in Dissociative Recombination. *The Journal of Physical Chemistry A*, 111(44):11254–11260, 2007. doi:10.1021/jp070892q.

[130] Steven L. Guberman. Spectroscopy above the ionization threshold: Dissociative recombination of the ground vibrational level of N_2^+. *The Journal of Chemical Physics*, 137(7):074309, 2012. doi:10.1063/1.4739472.

[131] Steven L. Guberman. The vibrational dependence of dissociative recombination: Cross sections for N_2^+. *The Journal of Chemical Physics*, 139(12):124318, 2013. doi:10.1063/1.4821595.

[132] HW Drawin. Atomic cross-sections for inelastic electronic collisions. *Report EURCEA-FC*, 1963.

[133] Hans-Werner Drawin. Zur formelmäßigen Darstellung des Ionisierungsquerschnitts für den Atom-Atomstoß und über die Ionen-Elektronen-Rekombination im dichten Neutralgas. *Zeitschrift für Physik A Hadrons and nuclei*, 211(2):404–4017, 1963. doi:10.1007/BF01379963.

[134] Chul Park. Assessment of a two-temperature kinetic model for dissociating and weakly ionizing nitrogen. *Journal of Thermophysics and Heat Transfer*, 2(1):8–16, 1988. doi:10.2514/3.55.

[135] Wolfgang Lotz. Electron-impact ionization cross-sections and ionization rate coefficients for atoms and ions from hydrogen to calcium. *Zeitschrift für Physik*, 216:241–247, 6 1988. doi:10.1007/BF01392963.

[136] Christophe O. Laux and Charles H. Kruger. Arrays of radiative transition probabilities for the N_2 first and second positive, no beta and gamma, N_2^+ first negative, and O_2 Schumann-Runge band systems. *Journal of Quantitative Spectroscopy and Radiative Transfer*, 48(1):9–24, 1992. doi:10.1016/0022-4073(92)90003-M.

[137] Ellis E. Whiting and Ralph W. Nicholls. Reinvestigation of Rotational-Line Intensity Factors in Diatomic Spectra. *The Astrophysical Journal Supplement Series*, 27:1, Jan 1974. doi:10.1086/190286.

[138] Z. Qin, J.M. Zhao, and L.H. Liu. Radiative transition probabilities for the main diatomic electronic systems of N_2, N_2^+, NO, O_2, CO, CO^+, CN, C_2 and H_2 produced in plasma of atmospheric entry. *Journal of Quantitative Spectroscopy and Radiative Transfer*, 202:286–301, 2017. doi:10.1016/j.jqsrt.2017.08.010.

[139] Z. Qin, J.M. Zhao, and L.H. Liu. Supplemental data of our research paper "Radiative transition probabilities for the main diatomic electronic systems of N_2, N_2^+, NO, O_2, CO, CO^+, CN, C_2 and H_2 produced in plasma of atmospheric entry". url:`https://www.researchgate.net/publication/337928363_Supplemental_datarar`. Accessed: 2020-04-01.

[140] Heiko Liebhart, Markus Fertig, Georg Herdrich, and Hans-Peter Röser. *Contribution of Vacuum-Ultraviolet Transitions of Molecular Nitrogen to Radiation During Atmospheric Reentry.* 2010. doi:10.2514/6.2010-4774.

[141] Christopher Owen Johnston. *Nonequilibrium shock-layer radiative heating for Earth and Titan entry.* PhD thesis, Virginia Tech, 2006. url:`https://vtechworks.lib.vt.edu/handle/10919/29769`. Accessed: 2020-11-01.

[142] Chul Park. Calculation of radiation from argon shock layers. *Journal of Quantitative Spectroscopy and Radiative Transfer*, 28(1):29–40, 1982. doi:10.1016/0022-4073(82)90094-2.

[143] Hans R. Griem. *Spectral Line Broadening by Plasmas.* Academic Press, 1st edition, January 1974.

[144] Hans R. Griem. Stark Broadening of Isolated Spectral Lines from Heavy Elements in a Plasma. *Phys. Rev.*, 128:515–523, Oct 1962. doi:10.1103/PhysRev.128.515.

[145] Hans R. Griem. *Spectral Line Broadening by Plasmas.* McGraw-Hill, 1964.

[146] E. Biémont, Y. Frémat, and P. Quinet. Ionization Potentials of Atoms and Ions from Lithium to Tin ($Z = 50$). *Atomic Data and Nuclear Data Tables*, 71(1):117–146, 1999. doi:10.1006/adnd.1998.0803.

[147] T. Trickl, E. F. Cromwell, Y. T. Lee, and A. H. Kung. State-selective ionization of nitrogen in the $X^2\Sigma_g^+$ $v_+ = 0$ and $v_+ = 1$ states by two-color $(1+1)$ photon excitation near threshold. *The Journal of Chemical Physics*, 91(10):6006–6012, 1989. doi:10.1063/1.457417.

[148] E. M. Bahati, J. J. Jureta, D. S. Belic, H. Cherkani-Hassani, M. O. Abdellahi, and P. Defrance. Electron impact dissociation and ionization of N_2^+. *Journal of Physics B: Atomic, Molecular and Optical Physics*, 34(15):2963–2973, jul 2001. doi:10.1088/0953-4075/34/15/303.

[149] C. R. Cowley. An approximate Stark broadening formula for use in spectrum synthesis. *The Observatory*, 91:139–140, Aug 1971. `https://ui.adsabs.harvard.edu/abs/1971Obs....91..139C/abstract`.

[150] K.H. Wilson and W.E. Nicolet. Spectral absorption coefficients of carbon, nitrogen and oxygen atoms. *Journal of Quantitative Spectroscopy and Radiative Transfer*, 7(6):891–941, 1967. doi:10.1016/0022-4073(67)90005-2.

[151] Daniel Potter. *Modelling of radiating shock layers for atmospheric entry at Earth and Mars.* PhD thesis, The University of Queensland, 2011. url:`https://espace.library.uq.edu.au/view/UQ:242003`. Accessed: 2020-11-03.

[152] E.E. Whiting. An empirical approximation to the Voigt profile. *Journal of Quantitative Spectroscopy and Radiative Transfer*, 8(6):1379–1384, 1968. doi:10.1016/0022-4073(68)90081-2.

[153] J.J. Olivero and R.L. Longbothum. Empirical fits to the Voigt line width: A brief review. *Journal of Quantitative Spectroscopy and Radiative Transfer*, 17(2):233–236, 1977. doi:10.1016/0022-4073(77)90161-3.

[154] I. N. Kadochnikov and I. V. Arsentiev. Modelling of vibrational nonequilibrium effects on the H_2-air mixture ignition under shock wave conditions in the state-to-state and mode approximations. *Shock Waves*, 30:491–504, 7 2020. doi:10.1007/s00193-020-00961-0.

[155] Theodore Lyman. Victor Schumann. *The Astrophysical Journal*, 38:1, January 1914. doi:10.1086/142050.

[156] NASA's Data Portal - Electric Arc Shock Tube (EAST) Test Data. url:`https://data.nasa.gov/docs/datasets/aerothermodynamics/EAST/index.html`. Accessed: 2020-10-07.

[157] Brett A. Cruden. Recent Progress in Entry Radiation Measurements in the NASA Ames Electric ARC Shock Tube Facility. In 5^{th} *International Workshop on Radiation of High Temperature Gases in Atmospheric Entry Workshop*, Barcelona, October 2012. url:`https://ntrs.nasa.gov/search.jsp?R=20130001599`.

[158] Brett A. Cruden and Aaron M. Brandis. *Analysis of Shockwave Radiation Data in Nitrogen.* Jun 2019. doi:10.2514/6.2019-3359.

[159] Brett A Cruden and Aaron M Brandis. Updates to the neqair radiation solver. *Radiation in High Temperature Gases*, 2014. `https://ntrs.nasa.gov/api/citations/20150022164/downloads/20150022164.pdf`.

[160] Brett A. Cruden, Aaron M. Brandis, Jay H. Grinstead, Joseph Olejniczak, Lindsay Kirk, Randolph P. Lillard, Hideyuki Tanno, and Tomoyuki Komuro. *Measurement of Ultraviolet Radiative Heating Augmentation in HIEST Reflected Shock Tunnel.* Jun 2015. doi:10.2514/6.2015-2512.

[161] Aaron Brandis, Brett Cruden, Dinesh Prabhu, Deepak Bose, Matthew McGilvray, Richard Morgan, and Richard Morgan. *Analysis of Air Radiation Measurements Obtained in the EAST and X2 Shocktube Facilities.* Jun 2010. doi:10.2514/6.2010-4510.

[162] Satoshi Nomura, Taito Kawakami, and Kazuhisa Fujita. Nonequilibrium Effects in Precursor Electrons Ahead of Shock Waves. *Journal of Thermophysics and Heat Transfer*, 0(0):1–6, 2020. doi:10.2514/1.T6057.

[163] Gouji Yamada, Mizuki Kajino, and Kiyonobu Ohtani. Experimental and numerical study on radiating shock tube flows for spacecraft reentry flights. *Journal of Fluid Science and Technology*, 14(3):JFST0022–JFST0022, 2019. doi:10.1299/jfst.2019jfst0022.

[164] D.W. Bogdanoff and C. Park. Radiative interaction between driver and driven gases in an arc-driven shock tube. *Shock Waves*, 12:205–214, Nov 2002. doi:10.1007/s00193-002-0157-y.

[165] Christophe O Laux. Radiation and nonequilibrium collisional-radiative models. *von Karman Institute Lecture Series*, 7, 2002.

[166] K. P. Huber and G. Herzbeg. *Molecular Spectra and Molecular Structure: IV. Constants of Diatomic Molecules.* Van Nostrand Reinhold Company, New York, 1979. doi:10.1007/978-1-4757-0961-2.

[167] J. L. Dunham. The Energy Levels of a Rotating Vibrator. *Phys. Rev.*, 41:721–731, Sep 1932. doi:10.1103/PhysRev.41.721.

[168] Mark S Child. *Semiclassical mechanics with molecular applications*. Oxford University Press, USA, 2014. doi:10.1093/acprof:oso/9780199672981.001.0001.

[169] Hugh M. Hulburt and Joseph O. Hirschfelder. Potential Energy Functions for Diatomic Molecules. *The Journal of Chemical Physics*, 9(1):61–69, 1941. doi:10.1063/1.1750827.

[170] Philip Huxley and John N. Murrell. Ground-state diatomic potentials. *J. Chem. Soc., Faraday Trans. 2*, 79:323–328, 1983. doi:10.1039/F29837900323.

[171] F. Gilmore. Potential energy curves for N_2, NO, O_2 and corresponding ions. *Journal of Quantitative Spectroscopy and Radiative Transfe*, 5:369–389, April 1965. doi:10.1016/0022-4073(65)90072-5.

[172] M. Hochlaf, H. Ndome, D. Hammoutène, and M. Vervloet. Valence–Rydberg electronic states of N_2: spectroscopy and spin–orbit couplings. *Journal of Physics B: Atomic, Molecular and Optical Physics*, 43(24):245101, nov 2010. doi:10.1088/0953-4075/43/24/245101.

[173] Alf Lofthus and Paul H. Krupenie. The Spectrum of Molecular Nitrogen. *Journal of Physical and Chemical Reference Data*, 6(1):113–307, 1977. doi:10.1063/1.555546.

[174] Harry Partridge, Stephen R. Langhoff, Charles W. Bauschlicher, and David W. Schwenke. Theoretical study of the $A'^5\Sigma_g^+$ and $C''^5\Pi_u$ states of N_2: Implications for the N_2 afterglow. *The Journal of Chemical Physics*, 88(5):3174–3186, 1988. doi:10.1063/1.453962.

[175] Sophie Chauveau. *Constitution de bases de données spectroscopiques relatives à un plasma d'air : application au calcul de transferts radiatifs*. PhD thesis, École centrale de Paris, 2001. Thèse de doctorat dirigée par Perrin, Marie-Yvonne Energétique Châtenay-Malabry, url:`http://www.theses.fr/2001ECAP0697`. Accessed: 2020-09-14.

[176] Russ R. Laher and Forrest R. Gilmore. Improved Fits for the Vibrational and Rotational Constants of Many States of Nitrogen and Oxygen. *Journal of Physical and Chemical Reference Data*, 20(4):685–712, 1991. doi:10.1063/1.555892.

[177] Ch. Ottinger and A. F. Vilesov. Laser spectroscopy of perturbed levels in $N_2(B^3\Pi_g, v = 10)$ and the first experimental determination of the $N_2(A'^5\Sigma_g^+)$ term energy. *The Journal of Chemical Physics*, 100(7):4862–4869, 1994. doi:10.1063/1.467206.

[178] J.W. McGowan. *The Excited State in Chemical Physics, Part 2*, volume 45 of *Advances in Chemical Physics*. Wiley, 2009. url:`https://www.wiley.com/en-us/Excited+State+in+Chemical+Physics%2C+Part+2%2C+Volume+45-p-9780470143100`.

[179] M. Hochlaf, H. Ndome, and D. Hammoutène. Quintet electronic states of N_2. *The Journal of Chemical Physics*, 132(10):104310, 2010. doi:10.1063/1.3359000.

[180] K. P. Huber and M. Vervloet. High-Resolution Fourier Transform Spectroscopy of Supersonic Jets. The $C''^5\Pi_u \rightarrow A'^5\Sigma_g^+$ Herman Infrared Bands of $^{14}N_2$. *Journal of Molecular Spectroscopy*, 153(1):17–25, 1992. doi:10.1016/0022-2852(92)90453-U.

Appendix A

The quantum free harmonic oscillator

The quantum free harmonic oscillator is exactly solvable, and it proves to be useful in this work when dealing with the vibration modes of molecular particles. The classical picture of a free harmonic oscillator, illustrated by Figure A.1, consists of a rigid mass, m, connected to a wall through a spring of stiffness f (also referred as a "force constant"). The "free" label emphasises the fact that no external forces act on the system. And the "harmonic" label is due to the assumed law which the spring follows: the *Hooke's law*.

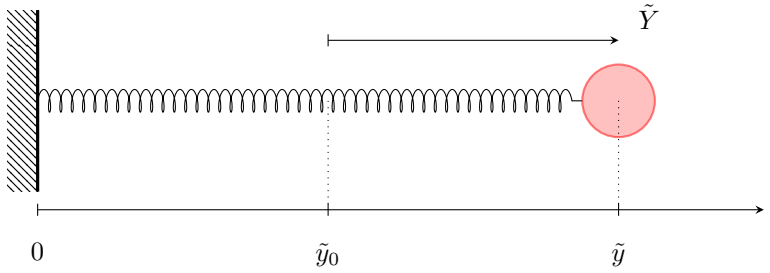

Figure A.1: Classical picture of the free harmonic oscillator.

Let $\tilde{y}$ and $\tilde{y}_0$ be the instantaneous and equilibrium body positions, respectively. Let also $\tilde{Y} = \tilde{y} - \tilde{y_0}$ be the body displacement. The *Schrödinger equation* for this system is expressed by

$$\left(-\frac{\hbar^2}{2m}\frac{\partial^2}{\partial \tilde{Y}^2} + \frac{1}{2}f\tilde{Y}^2\right)\Psi(t,\tilde{Y}) = i\hbar\frac{\partial \Psi}{\partial t}(t,\tilde{Y})\ . \tag{A.1}$$

Since the potential $V(\tilde{Y}) = \frac{1}{2}f\tilde{Y}^2$ doesn't depend explicitly on time, the *wave function* is separable, i.e. $\Psi(t,\tilde{Y}) = T(t)\psi(\tilde{Y})$, where $T(t)$ and $\psi(\tilde{Y})$ are functions of time and the oscillator displacement, respectively. By using the method of separation of variables, one can show (the involved steps will not

be shown here for compactness reasons) that the solution of the Schrödinger equation is given by

$$\Psi(t,\tilde{Y}) = \sum_{n=0}^{\infty} c_n H_n(\tilde{Y}) e^{-i\frac{E_n}{\hbar}t} \ , \tag{A.2}$$

where c_n, with $n = 0,\ 1,\ 2,\ ...$, are some constants. The quantities $H_n\left(\tilde{Y}\right)$ and E_n, are the *eigenfunctions* and *eigenenergies* of the system, respectively. These are expressed by

$$H_n\left(\tilde{Y}\right) = \left(\frac{m\omega}{\pi\hbar}\right)^{\frac{1}{4}} \left(2^n n!\right)^{-\frac{1}{2}} \mathscr{H}_n\left(\frac{\tilde{Y}}{\sqrt{\frac{\hbar}{m\omega}}}\right) e^{-\frac{m\omega}{2\hbar}\tilde{Y}^2} \ , \qquad E_n = \left(n+\frac{1}{2}\right)\hbar\omega \ , \tag{A.4}$$

(A.3)

respectively, where $\omega = \sqrt{\frac{f}{m}}$ is the natural angular frequency of the harmonic oscillator and $\mathscr{H}_n(x)$ are the *physicists' Hermite polynomials*, of variable $x = \frac{\tilde{Y}}{\sqrt{\frac{\hbar}{m\omega}}}$, which are given by

$$\mathscr{H}_n(x) = (-1)^n e^{x^2} \frac{d^n}{dx^n}\left(e^{-x^2}\right) \ . \tag{A.5}$$

By definition, the eigenfunctions and eigenenergies of the system satisfy the *time-independent Schrödinger equation*:

$$\left(-\frac{\hbar^2}{2m}\frac{\partial^2}{\partial\tilde{Y}^2} + \frac{1}{2}f\tilde{Y}^2\right) H_n\left(\tilde{Y}\right) = E_n H_n\left(\tilde{Y}\right) \ . \tag{A.6}$$

Appendix B

Spectroscopy: the internal energy of a diatomic molecular particle

The internal energy of a diatomic molecular particle is the one resultant from the movement of its internal structure: nuclei and electrons. There are therefore three contributions to the internal energy: vibrational energy G_v, rotational energy F_{vJ}, and electronic sensible energy T_e [165]. The letters v and J subscripted in the symbols G_v and F_{vJ}, denote the vibrational and rotational quantum numbers of the molecule, respectively (v = 0, 1, 2, ... and J = 0, 1, 2, ...). The letter e subscripted in the symbol T_e denotes the electronic level per se, and not an electronic quantum number. Although coupling exists between vibration and rotation, only rotation expresses some of this coumpling (hence the letter v in F_{vJ} besides J) since the motion associated to the latter is usually much faster than the one associated to the former [44]. The coupling between the electronic motion and the vibrational and rotation motions is also considered by both vibrational energy G_v and rotational energy F_{vJ} (the label for the electronic level e doesn't however appear in these symbols for simplicity reasons).

The sum of the vibrational and rotational energies, also denominated *rovibrational energy*, can be denoted by the symbol T_{vJ} [166]. And in a similar way, the sum of the electronic and vibrational energies - the *vibronic energy* - can be denoted by the symbol T_{ev} (instead of T_{ev}, the symbol T_v usually appears in the literature [165], but the latter may induce ambiguity problems). The symbol T_{evJ} is attributed to the sum of all of the three contributions to the internal energy of the particle - the *rovibronic energy*. One should then write

$$T_{vJ} = G_v + F_{vJ} \ , \qquad \text{(B.1)} \qquad T_{ev} = T_e + G_v \ , \qquad \text{(B.2)} \qquad T_{evJ} = T_e + G_v + F_{vJ} \ . \qquad \text{(B.3)}$$

The following section will focus only on the rovibrational energy.

B.1 The Dunham expansion

The rovibrational energy of a diatomic molecule in the e-th electronic energy level can be expressed through an infinite series known as *Dunham expansion* [167]:

$$T_{vJ} = \sum_{i,j=0}^{\infty} Y_{ij} \left(v + \frac{1}{2}\right)^i \left[J\left(J+1\right)\right]^j \ . \tag{B.4}$$

The constant coefficients Y_{ij} are called *Dunham parameters*, and they are specific to the electronic level of the molecule (i.e. there is a set of Dunham parameters for each electronic level e). It's easy to conclude from equation (B.4) that, if the quantum numbers are treated as continuous variables, the Dunham expansion is actually a Taylor series expansion of the function T_{vJ} in the $v+\frac{1}{2}$ and $J\left(J+1\right)$ variables around $v+\frac{1}{2}=0$ and $J\left(J+1\right)=0$. Therefore, in such conditions, the Dunham parameters are the coefficients of that Taylor series, which are ultimately defined by

$$Y_{ij} = \frac{1}{i!j!} \left\{ \frac{\partial^{i+j} T_{vJ}}{\partial \left(v+\frac{1}{2}\right)^i \partial \left[J\left(J+1\right)\right]^j} \right\} \Bigg|_{v+\frac{1}{2}=0,\, J(J+1)=0} \ . \tag{B.5}$$

When $J=0$ there's no rotation and the rovibrational energy T_{vJ} is purely vibrational. When $J\neq 0$ new terms in the Dunham expansion appear, whose contribution corresponds to the rotational energy. Therefore vibrational and rotational energies can be defined as $G_v = T_{v0}$ and $F_{vJ} = T_{vJ} - G_v$, respectively. And by invoking the Dunham expansion (B.4), these quantities are expressed through

$$G_v = \sum_{i=0}^{\infty} Y_{i0} \left(v+\frac{1}{2}\right)^i = Y_{00} + \omega_e \left(v+\frac{1}{2}\right) - \omega_e x_e \left(v+\frac{1}{2}\right)^2 + \omega_e y_e \left(v+\frac{1}{2}\right)^3 + \omega_e z_e \left(v+\frac{1}{2}\right)^4 + \omega_e a_e \left(v+\frac{1}{2}\right)^5 + \omega_e b_e \left(v+\frac{1}{2}\right)^6 + \omega_e c_e \left(v+\frac{1}{2}\right)^7 + \dots \ , \tag{B.6}$$

$$F_{vJ} = \sum_{\substack{i=0 \\ j=1}}^{\infty} Y_{ij} \left(v+\frac{1}{2}\right)^i \left[J\left(J+1\right)\right]^j = B_v J\left(J+1\right) - D_v \left[J\left(J+1\right)\right]^2 + H_v \left[J\left(J+1\right)\right]^3 + L_v \left[J\left(J+1\right)\right]^4 + \dots \ , \tag{B.7}$$

being the functions B_v, D_v, H_v and L_v introduced in (B.7) given by:

$$B_v = \sum_{i=0}^{\infty} Y_{i1} \left(v+\frac{1}{2}\right)^i = B_e - \alpha_e \left(v+\frac{1}{2}\right) + \gamma_e \left(v+\frac{1}{2}\right)^2 + \delta_e \left(v+\frac{1}{2}\right)^3 + \eta_e \left(v+\frac{1}{2}\right)^4 + \dots \ , \tag{B.8}$$

$$D_v = -\sum_{i=0}^{\infty} Y_{i2} \left(v+\frac{1}{2}\right)^i = D_e + \beta_e \left(v+\frac{1}{2}\right) + \dots \ , \tag{B.9}$$

$$H_v = \sum_{i=0}^{\infty} Y_{i3} \left(v+\frac{1}{2}\right)^i = H_e + \dots \ , \tag{B.10}$$

$$L_v = \sum_{i=0}^{\infty} Y_{i4} \left(v + \frac{1}{2} \right)^i = L_e + \ldots \, . \tag{B.11}$$

The constants involved in the expression for the vibrational energy (B.6) - Y_{00}, ω_e, $\omega_e x_e$, $\omega_e y_e$, $\omega_e z_e$, $\omega_e a_e$, $\omega_e b_e$ and $\omega_e c_e$ - are called *vibrational constants*, and the constants involved in the expression for the rotational energy (B.7) - B_e, D_e, H_e, L_e, α_e, β_e, γ_e, δ_e, η_e - are called *rotational constants*. All of these quantities are denominated *spectroscopic constants*, corresponding apart from sign to Dunham parameters Y_{ij} as shown in Table B.1.

Table B.1: Relation between Dunham parameters and the spectroscopic constants.

$i \backslash Y_{ij}$	Y_{i0}	Y_{i1}	Y_{i2}	Y_{i3}	Y_{i4}
0	Y_{00}	B_e	$-D_e$	H_e	L_e
1	ω_e	$-\alpha_e$	$-\beta_e$		
2	$-\omega_e x_e$	γ_e			
3	$\omega_e y_e$	δ_e			
4	$\omega_e z_e$	η_e			
5	$\omega_e a_e$				
6	$\omega_e b_e$				
7	$\omega_e c_e$				

The Dunham parameter Y_{00} may be approximated by [168]

$$Y_{00} \approx \frac{B_e}{4} + \frac{\alpha_e \omega_e}{12 B_e} + \frac{(\alpha_e \omega_e)^2}{144 B_e^3} - \frac{\omega_e x_e}{4} \, . \tag{B.12}$$

It can be easily seen that functions G_v, B_v, D_v, H_v and L_v correspond apart of sign to the first five coefficients of a Taylor expansion of T_{vJ} in $J(J+1)$ around $J(J+1) = 0$:

$$G_v = T_{v0} \, , \tag{B.13}$$

$$B_v = \left\{ \frac{\partial T_{vJ}}{\partial \left[J(J+1) \right]} \right\} \Bigg|_{J(J+1)=0} \, , \tag{B.14}$$

$$D_v = -\frac{1}{2} \left\{ \frac{\partial^2 T_{vJ}}{\partial \left[J(J+1) \right]^2} \right\} \Bigg|_{J(J+1)=0} \, , \tag{B.15}$$

$$H_v = \frac{1}{6} \left\{ \frac{\partial^3 T_{vJ}}{\partial \left[J(J+1) \right]^3} \right\} \Bigg|_{J(J+1)=0} \, , \tag{B.16}$$

$$L_v = \frac{1}{24} \left\{ \frac{\partial^4 T_{vJ}}{\partial \left[J(J+1) \right]^4} \right\} \Bigg|_{J(J+1)=0} \, . \tag{B.17}$$

B.2 The Fourier Grid Hamiltonian method

If all of the Dunham parameters (which correspond to an infinite set) in equation (B.4) were known, the rovibrational energy T_{vJ} would be well defined for all vibrational and rotational quantum numbers. But the truth is that only a finite set of Dunham parameters can be obtained from experiment. This finite set

usually correspond to the first Dunham parameters, making the Dunham expansion only valid for the first quantum numbers. Note that the highest terms in the Dunham expansion become more important with the increase in the quantum numbers values - the higher the order of the terms the higher the exponent in v and $J\left(J+1\right)$. Therefore, the higher the values of the quantum numbers the more imprecise is the Dunham expansion in estimating the respective rovibrational energy.

To obtain the rovibrational energies for all of the allowable vibrational and rotational quantum numbers, from the lowest to the highest ones, a more reliable method should be considered, as is example the Fourier Grid Hamiltonian method (FGH) [78]. This method consists in a numerical algorithm that determines the eigenenergies and eigenfunctions of a quantum system by solving its Schrödinger equation. Because the desired eigenvalues correspond to the rovibrational energies T_{vJ}, the Schrödinger equation to be solved should the radial Schrödinger equation (2.307) with the energy relatively to the centre of mass of the system E' subtracted by the electronic sensible energy T_e (giving $T_{vJ} := E' - T_e$), and the centrifugally corrected internuclear potential energy $U_{n,l}(R)$ (expressed by (2.309)) also subtracted by the electronic sensible energy T_e (giving $V_J(r) := U_{n,l}(R) - T_e$):

$$\left[-\frac{\hbar^2}{2\mu}\frac{\partial^2}{\partial r^2} + V_J(r)\right]\psi_{v,J}(r) = T_{v,J}\psi_{v,J}(r) \ , \tag{B.18}$$

where μ is the reduced mass of the diatomic molecule, r is the internuclear distance (expressed by R in (2.307)), J is the already mentioned rotational quantum number (expressed by l in (2.307)) and $\psi_{v,J}$ is the (v,J)-th eigenfunction of the system (expressed by $x_{n,l,m}(R)$ in (2.307)). Note also that the label n for the electronic level as well as the quantum number for the z-component of the angular momentum m in (2.307) were occulted in (B.18).

To simplify the nomenclature, $V_J(r) = V(r) + \hbar^2 J\left(J+1\right)/\left(2\mu r^2\right)$ will be called the "centrifugally corrected internuclear potential energy" and $V(r)$ will be called the "internuclear potential energy" until the end of this appendix, although these terms were already attributed before to $U_{n,l}(R)$ and $U_n(R)$, respectively.

B.3 The Rydberg-Klein-Rees method

The Rydberg [79, 80]–Klein [81]–Rees [82] method (RKR), which is based on Semiclassical Mechanics, allows the determination of the internuclear potential energy function $V(r)$ for a diatomic molecule, requiring only the knowledge of its spectroscopic constants. The book of Child [168] explains the foundations of the method within a great detail. A derivation of this method can be developed by departing from the *Bohr-Sommerfeld quantisation condition*:

$$v_J(E) + \frac{1}{2} = \frac{1}{\pi}\sqrt{\frac{2\mu}{\hbar^2}}\int_{a_J(E)}^{b_J(E)}\left[E - V_J(r)\right]^{\frac{1}{2}}\,dr \ , \tag{B.19}$$

being $v_J(E)$ the vibrational quantum number associated to the rovibrational energy E and rotational quantum number J, $a_J(E)$ the respective lower classical turning point, and $b_J(E)$ the respective upper classical turning point. Note that, from a quantum perspective, energy E is equivalent to the previously

stated energy T_{vJ}, but from a classical perspective, it corresponds to the total relative energy $\frac{1}{2}\mu\dot{r}^2+V_J(r)$. Since the RKR method is semiclassical, it embodies concepts of both Quantum and Classical Mechanics. To understand the classical view of the nuclei motion, one should first look to a typical potential curve $V_J(r)$ as the one depicted in Figure B.1.

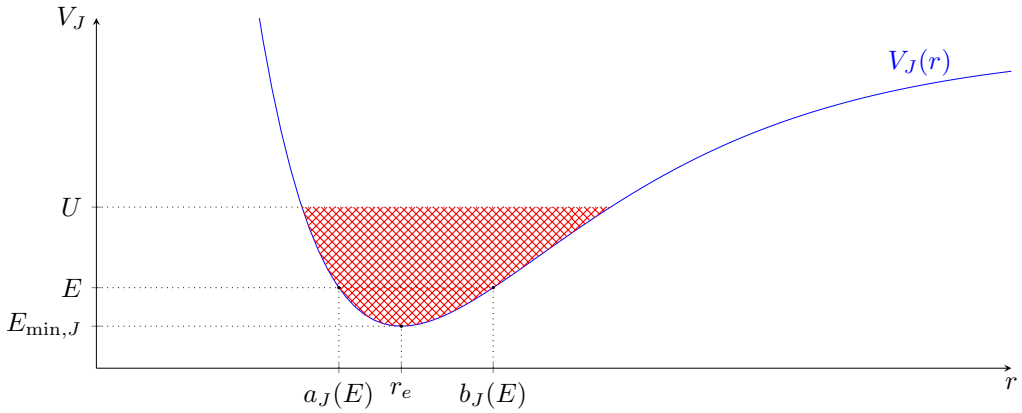

Figure B.1: Centrifugally corrected internuclear potential energy $V_J(r)$, and the classical turning points $a_J(E)$ and $b_J(E)$ for a given energy E. The figure also depicts the potential minimum $E_{\min,J}$, the energy value U, and the integration domain, filled in red, both considered in equation (B.21).

Classically, if $E = V_J(r)$ then $\dot{r} = 0$, stating a null relative speed of the nuclei. Due to the concavity of the potential $V_J(r)$, there are two points for each E value at which such condition is satisfied[1]: $a_J(E)$ and $b_J(E)$. Because $V_J(r)$ needs to be lower or equal to E (or $\dot{r}$ would be imaginary) the internuclear distance should always be in the interval $[a_J(E),\, b_J(E)]$. The point $(r, V_J) = (r_e, E_{\min,J})$ corresponds to a minimum, in which the curve has no slope (i.e. $\frac{dV_J}{dr}(r_e) = 0$) and therefore the internuclear force F at that point is null as well as the relative acceleration $\ddot{r}$ (note that $F = \mu\ddot{r} = -\frac{dV_J(r)}{dr}$). A diatomic molecule at $r = r_e$ with $\dot{r} = 0$ would have its nuclei permanently stationary in relation to each other. And if instead the molecule had $\dot{r} > 0$, the internuclear distance r would increase, passing to the interval $]r_e,\, b_J(E)]$. Due to the positive slope of the curve $V_J(r)$ in $]r_e, b_J(E)]$, the relative acceleration $\ddot{r}$ would be negative, which implies a reduction of the relative velocity $\dot{r}$ to a null value, at $r = b_J(E)$, and to a negative one after that, meaning an inversion of the relative trajectory of the nuclei. If instead the molecule had $\dot{r} > 0$ at $r = r_e$, the analogous would happen, but with a symmetric signal in $\dot{r}$ and $\ddot{r}$, being $a_J(E)$ the internuclear distance r at which the relative velocity becomes null. Due to the fact that this behaviour of the molecule is only supported in a classical world, $a_J(E)$ and $b_J(E)$ are called classical turning points of the trajectory.

To obtain the potential curve $V_J(r)$, one can compute the classical turning points $a_J(E)$ and $b_J(E)$ for known rovibrational energy values $E = T_{vJ}$, resulting in a set of points $(r, V_J) = (a_J(E), E)$ and $(r, V_J) = (b_J(E), E)$ (note that $V_J = E$ in $r = a_J(E)$ and $r = b_J(E)$, by definition of classical turning point). This procedure would recreate only the part of the potential supported by the domain of the known rovibrational energies. Another procedure would be needed to attain the remaining parts of the

[1]There's an exception to this proposition: at the minimum of the potential $V_J(r)$, the equality $E = V_J(r)$ only occurs for one point. Such case depicts a molecule whose nuclei are perpetually at rest in relation to each other.

potential, a problem that will be addressed in the following section. But before that, expressions to compute $a_J(E)$ and $b_J(E)$ should be found. Let's start by considering the function

$$A_J(U) = \pi \int_{E_{\min,J}}^{U} \frac{v_J(E) + \frac{1}{2}}{(U-E)^{\frac{1}{2}}}\, dE \ . \tag{B.20}$$

By substituting (B.19) in (B.20) one can obtain

$$A_J(U) = \sqrt{\frac{2\mu}{\hbar^2}} \int_{E_{\min,J}}^{U} \left\{ \int_{a_J(E)}^{b_J(E)} \left[\frac{E - V_J(r)}{U-E} \right]^{\frac{1}{2}} dr \right\} dE \ . \tag{B.21}$$

And by considering the integration domain represented in Figure B.1, a change in the order of integration in (B.21) can be easily performed, giving

$$A_J(U) = \sqrt{\frac{2\mu}{\hbar^2}} \int_{a_J(U)}^{b_J(U)} \int_{V_J(r)}^{U} \left[\frac{E - V_J(r)}{U-E} \right]^{\frac{1}{2}} dE\, dr = \frac{\pi}{2} \sqrt{\frac{2\mu}{\hbar^2}} \int_{a_J(U)}^{b_J(U)} \left[U - V_J(r) \right] dr \ . \tag{B.22}$$

On the other hand, by picking equation (B.20), performing an integration by parts and making a change in the integration variable,the following relation can be obtained:

$$A_J(U) = 2\pi \int_{v_{\min,J}}^{v_J(U)} \left[U - E_J(v) \right]^{\frac{1}{2}} dv \ , \tag{B.23}$$

where $E_J(v)$ corresponds to the rovibrational energy E associated to the quantum numbers v and J, and $v_{\min,J}$ is the vibrational quantum number v for which the respective rovibrational energy coincides with its minimum value, i.e. $v_{\min,J} = v : E_J(v) = E_{\min,J}$. From a quantum view, the rovibrational energy corresponds to $E_J(v) = T_{vJ} = G_v + F_{vJ}$, whose minimum occurs for $v = -\frac{1}{2}$, if $Y_{00} \approx 0$. This assumption will be considered from now on, and therefore $v_{\min,J}$ will be substituted by $-\frac{1}{2}$ in the following mathematical manipulations.

From (B.22) and (B.23), one has the equality

$$\int_{-\frac{1}{2}}^{v_J(U)} \left[U - E_J(v) \right]^{\frac{1}{2}} dv = \frac{1}{4} \sqrt{\frac{2\mu}{\hbar^2}} \int_{a_J(U)}^{b_J(U)} \left[U - V_J(r) \right] dr \ . \tag{B.24}$$

By differentiating[2] equation (B.24) in U, one can obtain

$$b_J(U) - a_J(U) = 2\sqrt{\frac{\hbar^2}{2\mu}} \int_{-\frac{1}{2}}^{v_J(U)} \frac{1}{\left[U - E_J(v) \right]^{\frac{1}{2}}}\, dv := f_J(U) \ . \tag{B.25}$$

And by differentiating[3] equation (B.24) in J, one can get

$$\frac{1}{a_J(U)} - \frac{1}{b_J(U)} = 2\sqrt{\frac{2\mu}{\hbar^2}} \int_{-\frac{1}{2}}^{v_J(U)} \frac{B_J(v)}{\left[U - E_J(v) \right]^{\frac{1}{2}}}\, dv := g_J(U) \ , \tag{B.26}$$

[2] Which requires the use of the Leibniz integral rule, since there are limits of integration in equation (B.24) that depend on U.

[3] In a similar way to the previous case, such derivation requires the use of the Leibniz integral rule, since there are limits of integration in equation (B.24) that depend on J.

where $B_J(v) = \frac{\partial[E_v(J)]}{\partial[J(J+1)]}$. Note that $B_0(v) = B_v$, being B_v the previously introduced function given by expressions (B.8) and (B.14).

From equations (B.25) and (B.26) one can obtain the classical turning points $a_J(U)$ and $b_J(U)$:

$$\begin{cases} a_J(U) = \frac{1}{2}\left[\sqrt{f_J^2(U) + 4\frac{f_J(U)}{g_J(U)}} - f_J(U)\right] , & \text{(B.27a)} \\ b_J(U) = \frac{1}{2}\left[\sqrt{f_J^2(U) + 4\frac{f_J(U)}{g_J(U)}} + f_J(U)\right] , & \text{(B.27b)} \end{cases}$$

being $f_J(U)$ and $g_J(U)$ given by (B.25) and (B.26), respectively. Because only the non centrifugally corrected potential $V(r)$ needs to be determined (the correction term is known), and $V_J(r) = V(r)$ if $J = 0$, solely the classical turning points $a_0(U)$ and $b_0(U)$ are required. Also, one only needs to consider the $J = 0$ associated energies, i.e. $E_J(v) = E_0(v) = G_v$ and $B_J(v) = B_0(v) = B_v$.

B.4 Extrapolation of the RKR resultant potential

The non-experimentally supported parts of the potential $V(r)$ can be obtained through extrapolation. The part of the potential obtained through the RKR method, i.e. the experimentally supported part, corresponds to the middle of the desired full curve (since the experimental energies are usually the lower ones and the middle of the curve corresponds to the bottom of the well). Let this middle part be $V_{\mathrm{RKR}}(r)$. Therefore, not one but two extrapolations are actually required: one for the short-range (left) part and another for the long-range (right) part of the potential. Let $V_{\mathrm{sr}}(r)$ be the former and $V_{\mathrm{lr}}(r)$ the latter.

The short-range part of the potential was assumed to have the form

$$V_{\mathrm{sr}}(r) = \alpha r^{-\beta} , \tag{B.28}$$

where α and β are positive constants. These constants can be determined by fitting the curve $V_{sr}(r)$ to the repulsive part of $V_{\mathrm{RKR}}(r)$. In this work, the three leftest points of $V_{\mathrm{RKR}}(r)$ were chosen as the fitting data.

The long-range part of the potential was assumed to have one of two possible forms:

$$V_{\mathrm{HH}}(r) = D_e\left\{\left[1 - e^{-\gamma(r-r_e)}\right]^2 + \delta\gamma^3\left(r - r_e\right)^3 e^{-2\gamma(r-r_e)}\left[1 + \zeta\gamma\left(r - r_e\right)\right]\right\} , \tag{B.29}$$

$$V_{\mathrm{ER}}(r) = D_e - D_e\left[1 + \gamma\left(r - r_e\right) + \delta\left(r - r_e\right)^2 + \zeta\left(r - r_e\right)^3\right] e^{-\gamma(r-r_e)} , \tag{B.30}$$

where r_e is the equilibrium internuclear distance, and D_e is the depth of the potential well. These are *a priori* known. The constants γ, δ and ζ are three fittable parameters. In this work, they were obtained by fitting the respective curve to the three rightest points of $V_{\mathrm{RKR}}(r)$. Equation (B.29) represents a *Hulburt-Hirschfelder potential* [169] and equation (B.30) represents an *Extended Rydberg potential* [170]. In contrast with the Extended Rydberg potential, the fit resultant Hulburt-Hirschfelder potential may

express an upward "bump" at the right of the potential well[4], which may or may not exist in reality. If it is known that such "bump" doesn't exist in reality[5], then the Extended Rydberg potential should be considered instead. As an illustrative example, Figure B.2 depicts the full reconstructed potential curve $V(r)$ for the electronic level $B^3\Pi_g$ of the nitrogen molecule N_2. Two different cases are shown: one in which the the long-range part of the potential is obtained through an extrapolation using the Hulburt-Hirschfelder shape, and another in which the Extended Rydberg shape is employed instead. A "bump" appears for the Hulburt-Hirschfelder case, which isn't real (one can compare the obtained curve with the ones in references [171] and [172]), and therefore the Extended Rydberg shape should be the one to consider.

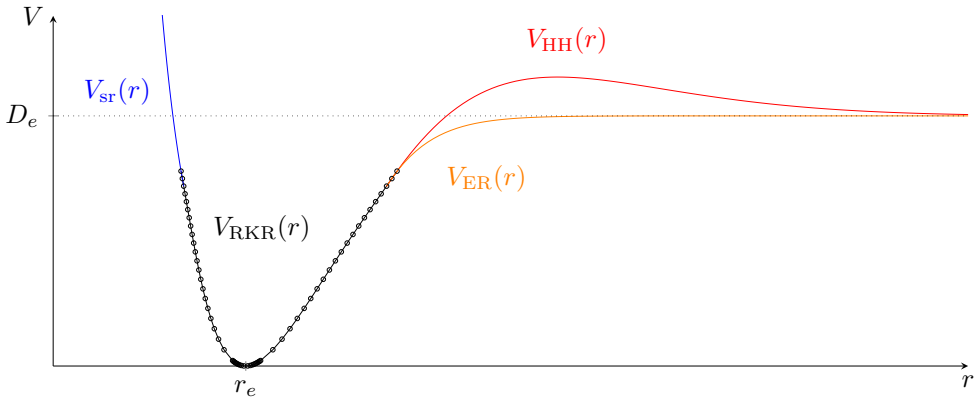

Figure B.2: Full reconstructed potential curve $V(r)$ for the case of the electronic level $B^3\Pi_g$ of the nitrogen molecule N_2, considering either a Hulbuth-Hirschfelder or an Extended Rydberg shape for the extrapolated long-range part.

B.5 Potential curves for N_2 in its different electronic levels

Potential curves $V(r)$ for the electronic levels $X^1\Sigma_g^+$, $A^3\Sigma_u^+$, $B^3\Pi_g$, $W^3\Delta_u$, $B'^3\Sigma_u^-$, $a'^1\Sigma_u^-$, $a^1\Pi_g$, $w^1\Delta_u$, $A'^5\Sigma_g^+$, $C^3\Pi_u$, $b^1\Pi_u$, $c_3{}^1\Pi_u$, $c_4'{}^1\Sigma_u^+$, $b'^1\Sigma_u^+$ and $o_3{}^1\Pi_u$ of the nitrogen molecule N_2 were obtained. All curves were constructed by application of the RKR method and posterior extrapolation. Values for the Dunham parameters which are the input variables of the RKR method, were required. Table B.2 shows such values, being taken from the literature. The potential curves $V_e(r) = V(r) + T_e$ obtained for each of the electronic levels of molecular nitrogen N_2, are depicted in Figure B.3. All of the dissociation products shown in Figure B.3 were taken from reference [173] with the exception of the one associated to the electronic level $A'^5\Sigma_g^+$, which was taken from reference [174].

[4]The states of the molecule associated to this "bump" are called *quasi-bound states*.

[5]To verify if the molecule assumes, or not, quasi-bound states, accurate potentials in the literature, which correspond the curves that the author intend to reconstruct, were reviewed.

Table B.2: Spectroscopic constants T_e, D_e and r_e, maximum vibrational quantum number $v_{\max}$ for which the respective Dunham expansion is valid, Dunham parameters Y_{i0} with $i = 0, 1, ..., 6$ and Y_{i1} with $i = 0, 1, ..., 4$ and the shape of the extrapolated long-range part of the potential V_{lr} of the different electronic levels of molecular nitrogen N_2.

e	$X^1\Sigma_g^+$	$A^3\Sigma_u^+$	$B^3\Pi_g$	$W^3\Delta_u$	$B'^3\Sigma_u^-$	$a'^1\Sigma_u^-$	$a^1\Pi_g$	$w^1\Delta_u$	$A'^5\Sigma_g^+$	$C^3\Pi_u$	$b^1\Pi_u$	$c_3{}^1\Pi_u$	$c_4'{}^1\Sigma_u^+$	$b'^1\Sigma_u^+$	$o_3{}^1\Pi_u$
Ref. for T_e	[175] ([a])	[175] ([a])	[175] ([a])	[176] ([a])	[176] ([a])	[176] ([a])	[176] ([a])	[176] ([a])	[177]	[175] ([a])	[175] ([a])	[175] ([a])	[175] ([a])	[175] ([a])	[175] ([a])
T_e [“cm^{-1}”]	0.00	50203.66	59618.77	59805.85	66271.53	68152.79	69283.34	72097.31	75990.03	89137.92	101660.02	104217.77	104418.37	105215.38	105873.81
Ref. for D_e	[175] ([b])	[175] ([b])	[175] ([b])	[173] ([b])	[173] ([b])	[173] ([b])	[173] ([b])	[173] ([b])	[174]	[175] ([b])	[175] ([b])	[175] ([b])	[175] ([b])	[175] ([b])	[175] ([b])
D_e [“cm^{-1}”]	79886.67	29686.89	39499.33	39308.13	42456.54	50186.28	49055.63	46241.86	3450.00	9980.02	16677.65	47196.90	87946.60	24185.10	88858.57
Ref. for r_e	[166]	[166]	[166]	[178]	[173]	[173]	[173]	[173]	[179]	[166]	[166]	[166]	[166]	[166]	[166]
r_e [Å]	1.09768	1.28660	1.21260	1.28	1.27838	1.27542	1.22025	1.26883	1.60840	1.14860	1.28400	1.11630	1.10800	1.44390	1.17840
Ref. for $v_{\max}$	[175]	[175]	[175]	[176]	[176]	[176]	[176]	[176]	This work ([c])	[175]	[175]	[175]	[175]	[175]	[175]
$v_{\max}$	15	16	21	11	17	18	14	5	5	4	19	4	8	28	4
Ref. for Y_{i0}	[175]	[175]	[175]	[176]	[176]	[176]	[176]	[176]	([c])	[175]	[175]	[175]	[175]	[175]	[175]
Y_{00} [“cm^{-1}”]	7.30(−2)	−1.89(−1)	−8.30(−2)	—	1.38(−1)	1.67(−1)	1.20(−2)	1.05(−1)	−2.50(−2)	−1.79(0)	6.53(0)	3.90(0)	7.27(−1)	2.89(−1)	4.24(0)
Y_{10} [“cm^{-1}”]	2.36(3)	1.46(3)	1.73(3)	1.51(3)	1.52(3)	1.53(3)	1.69(3)	1.56(3)	7.31(2)	2.05(3)	6.42(2)	2.20(3)	2.17(3)	7.59(2)	1.97(3)
Y_{20} [“cm^{-1}”]	−1.43(1)	−1.40(1)	−1.44(1)	−1.26(1)	−1.22(1)	−1.21(1)	−1.39(1)	−1.20(1)	−1.09(1)	−2.89(1)	2.17(1)	−2.56(1)	−1.33(1)	−3.40(0)	−1.09(1)
Y_{30} [“cm^{-1}”]	−3.31(−3)	2.40(−2)	−3.30(−3)	3.09(−2)	4.19(−2)	4.13(−2)	7.94(−3)	4.54(−2)	−2.25(0)	2.25(0)	−1.41(0)	—	−2.94(−1)	1.78(−2)	—
Y_{40} [“cm^{-1}”]	−1.95(−4)	2.56(−3)	−7.90(−4)	−7.10(−4)	−7.30(−4)	−2.9(−4)	2.9(−4)	—	—	−5.51(−1)	2.29(−2)	—	—	−1.78(−3)	—
Y_{50} [“cm^{-1}”]	—	—	4.20(−5)	—	—	—	—	—	—	—	—	—	—	—	—
Y_{60} [“cm^{-1}”]	—	—	1.68(−6)	—	—	—	—	—	—	—	—	—	—	—	—
Ref. for Y_{i1}	[175]	[175]	[175]	[176]	[176]	[176]	[176]	[176]	[179]	[175]	[175]	[175]	[175]	[175]	[175]
Y_{01} [“cm^{-1}”]	2.00(0)	1.45(0)	1.64(0)	1.47(0)	1.47(0)	1.48(0)	1.62(0)	1.50(0)	9.31(−1)	1.83(0)	1.39(0)	1.98(0)	1.93(0)	1.16(0)	1.73(0)
Y_{11} [“cm^{-1}”]	−1.73(−2)	−1.75(−2)	−1.79(−2)	−1.70(−2)	−1.67(−2)	−1.66(−2)	−1.79(−2)	−1.63(−2)	−1.71(−2)	−2.40(−2)	−1.42(−2)	−3.80(−2)	−1.96(−2)	−1.04(−2)	−2.75(−2)
Y_{21} [“cm^{-1}”]	−3.01(−5)	−1.40(−4)	−1.00(−4)	−1.01(−5)	1.84(−5)	2.41(−5)	−2.93(−5)	—	—	1.90(−3)	−5.21(−4)	—	—	3.90(−4)	—
Y_{31} [“cm^{-1}”]	−6.93(−8)	—	5.00(−6)	3.30(−7)	−4.50(−7)	—	—	—	—	−6.00(−4)	—	—	—	−1.73(−5)	—
Y_{41} [“cm^{-1}”]	—	—	2.10(−7)	—	—	—	—	—	—	—	—	—	—	—	—
V_{lr}	V_{HH}	V_{ER}	V_{ER}	V_{ER}	V_{ER}	V_{ER}	V_{ER}	V_{ER}	V_{HH}	V_{HH}	V_{ER}	([d])	([d])	V_{ER}	([d])

The number between parenthesis in the Y_{i0} and Y_{i1} cells correspond to the orders of magnitude of these quantities.

[a] This reference only reports the value for $\Delta T_{e0} := T_{e0} - T_{X0}$, in which T_{e0} is the quantity $T_{ev} = T_e + G_v$ with $v = 0$ for the electronic level e, and T_{X0} is the homologous quantity for the ground electronic level X. Therefore, and sticking with the introduced notation, one can obtain T_e by using the relation $T_e = \Delta T_{e0} + G_0^X - G_0^e$.

[b] This reference only reports the value for the dissociation energy $D_0 := D_e - G_0$, and therefore the potential well depth needs to be computed using the relation $D_e = D_0 + G_0$.

[c] The values for Y_{i0}, with $i = 0, 1, ..., 3$ for the case $e = A'^5\Sigma_g^+$ were obtained by fitting the vibrational energies values G_v, with $v = 0, 1, ..., 5$, taken from the literature, considering as fitting function a Dunham expansion of third order, i.e. $G_v = \sum_{i=0}^{3} Y_{i0} \left(v + \frac{1}{2}\right)^i$, with Y_{00} given by equation (B.12). The G_0 value was taken from [180], and the others G_v values were taken from [179] (note that in the article these appear subtracted by G_0).

[d] Since it is known that the potential curve for this electronic level doesn't have a conventional shape like the $V_{\mathrm{HH}}(r)$ or $V_{\mathrm{ER}}(r)$ curves, and its dissociation products weren't already determined, no attempt to extrapolate the RKR potential was performed. Therefore, it was assumed that the dissociation of the molecule in this electronic level doesn't occur, and only the vibrational levels restrained to RKR determined part may be accessed.

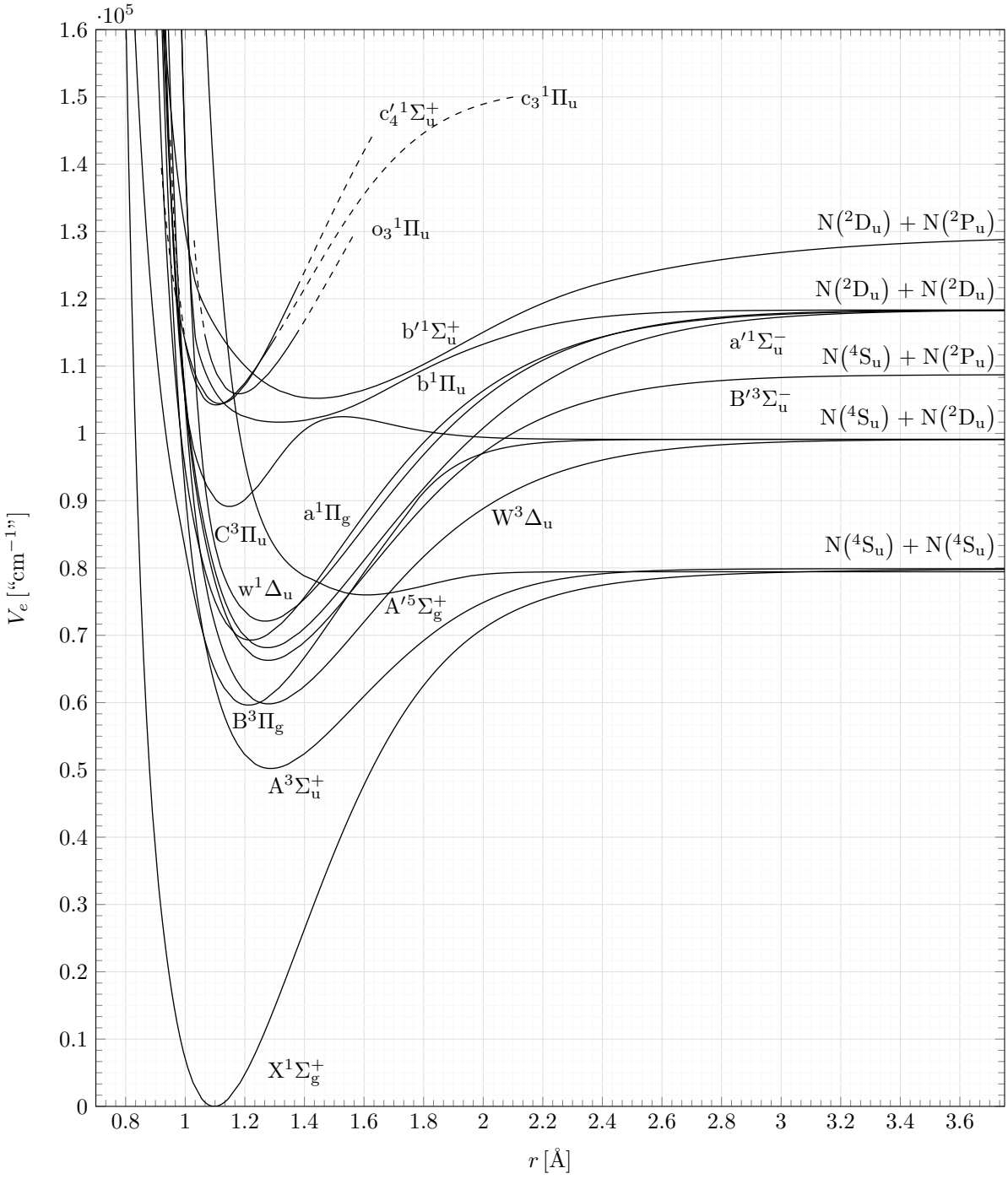

Figure B.3: Full reconstructed potential curves $V_e(r) = T_e + V(r)$ for the different electronic levels of the nitrogen molecule N_2. The terms $N(^4S_u) + N(^4S_u)$, $N(^4S_u) + N(^2D_u)$, $N(^4S_u) + N(^2P_u)$, $N(^2D_u) + N(^2D_u)$ and $N(^2D_u) + N(^2P_u)$ represent the dissociation products of the nitrogen molecule in the electronic levels associated to the immediately below potential curves.

B.6 Potential curves for N_2^+ in its different electronic levels

All the data required to obtain the potential curves $V(r)$ for the different electronic levels of the nitrogen molecular ion N_2^+, is found in Table B.3. The considered electronic levels for this species were $X^2\Sigma_g^+$, $A^2\Pi_u$, $B^2\Sigma_u^+$, $D^2\Pi_g$ and $C^2\Sigma_u^+$. The resultant potential curves $V_e(r) = V(r) + T_e$, are depicted in Figure B.4. All of the dissociation products shown in Figure B.4 were taken from reference [173].

Table B.3: Spectroscopic constants T_e, D_e and r_e, maximum vibrational quantum number $v_{\max}$ for which the respective Dunham expansion is valid, Dunham parameters Y_{i0} with $i = 0, 1, ..., 7$ and Y_{i1} with $i = 0, 1, ..., 3$ and the shape of the extrapolated long-range part of the potential $V_{\rm lr}$ of the different electronic levels of nitrogen molecular ion N_2^+.

e	$X^2\Sigma_g^+$	$A^2\Pi_u$	$B^2\Sigma_u^+$	$D^2\Pi_g$	$C^2\Sigma_u^+$
Ref. for T_e	[175] ([a])	[175] ([a])	[175] ([a])	[173] ([a])	[175] ([a])
T_e ["cm^{-1}"]	0.00	9167.34	25462.43	52814.06	64610.79
Ref. for D_e	[175] ([b])	[175] ([b])	[175] ([b])	[173] ([b])	[175] ([b])
D_e ["cm^{-1}"]	71368.43	62201.49	45903.08	18557.87	25988.34
Ref. for r_e	[166]	[166]	[166]	[173]	[166]
r_e [Å]	1.11642	1.17490	1.07400	1.47082	1.26200
Ref. for $v_{\max}$	[175]	[175]	[175]	—	[175]
$v_{\max}$	21	27	8	5	6
Ref. for Y_{i0}	[175]	[175]	[175]	[173]	[175]
Y_{00} ["cm^{-1}"]	$-1.20(-1)$	$1.70(-2)$	$-1.43(0)$	$1.67(-1)$	$-1.80(0)$
Y_{10} ["cm^{-1}"]	2.21(3)	1.90(3)	2.42(3)	9.12(2)	2.07(3)
Y_{20} ["cm^{-1}"]	$-1.62(1)$	$-1.51(1)$	$-2.41(1)$	$-1.26(1)$	$-8.30(0)$
Y_{30} ["cm^{-1}"]	$4.00(-3)$	$1.12(-2)$	$-3.00(-1)$	$5.55(-2)$	$-6.30(-1)$
Y_{40} ["cm^{-1}"]	$-6.10(-3)$	$-2.70(-4)$	$-6.67(-2)$	—	$1.30(-2)$
Y_{50} ["cm^{-1}"]	$3.90(-4)$	—	—	—	—
Y_{60} ["cm^{-1}"]	$-1.40(-5)$	—	—	—	—
Y_{70} ["cm^{-1}"]	$2.00(-7)$	—	—	—	—
Ref. for Y_{i1}	[175]	[175]	[175]	[173]	[175]
Y_{01} ["cm^{-1}"]	1.93(0)	1.74(0)	2.09(0)	1.11(0)	1.51(0)
Y_{11} ["cm^{-1}"]	$-1.88(-2)$	$-1.87(-2)$	$-2.12(-2)$	$-2.00(-2)$	$1.00(-3)$
Y_{21} ["cm^{-1}"]	$-6.77(-5)$	$-6.00(-5)$	$-5.00(-4)$	—	$-1.50(-3)$
Y_{31} ["cm^{-1}"]	$-2.32(-6)$	$-1.10(-6)$	$-8.80(-5)$	—	$6.00(-5)$
$V_{\rm lr}$	$V_{\rm ER}$	$V_{\rm ER}$	$V_{\rm ER}$	$V_{\rm ER}$	$V_{\rm HH}$

The number between parenthesis in the Y_{i0} and Y_{i1} cells correspond to the orders of magnitude of these quantities.

[a] This reference only reports the value for $\Delta T_{e0} := T_{e0} - T_{\rm X0}$, in which T_{e0} is the quantity $T_{ev} = T_e + G_v$ with $v = 0$ for the electronic level e, and $T_{\rm X0}$ is the homologous quantity for the ground electronic level X. Therefore, and sticking with the introduced notation, one can obtain T_e by using the relation $T_e = \Delta T_{e0} + G_0^X - G_0^e$.

[b] This reference only reports the value for the dissociation energy $D_0 := D_e - G_0$, and therefore the potential well depth needs to be computed using the relation $D_e = D_0 + G_0$.

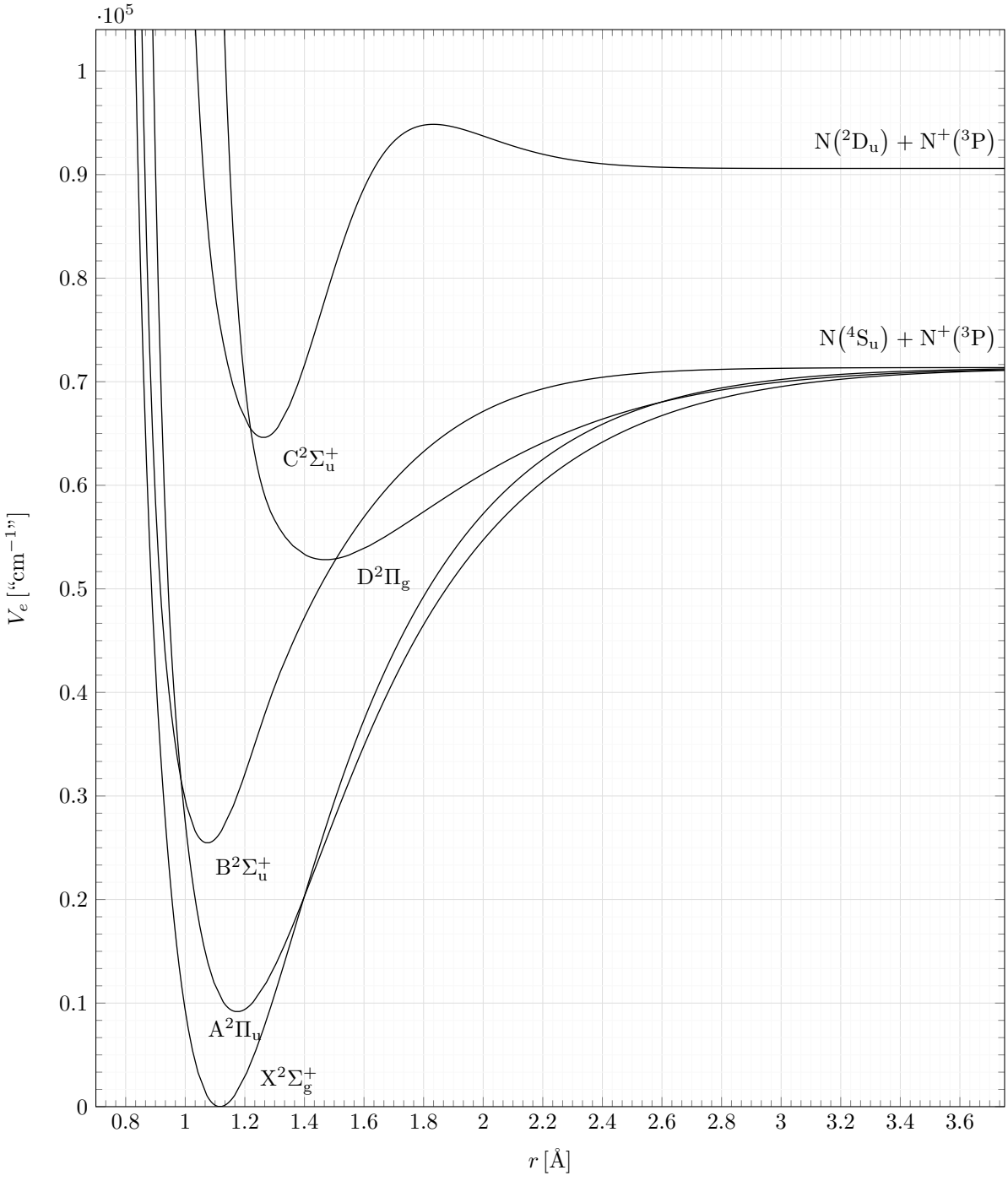

Figure B.4: Full reconstructed potential curves $V_e(r) = T_e + V(r)$ for the different electronic levels of the nitrogen molecular ion N_2^+. The terms $\mathrm{N}(^4\mathrm{S_u}) + \mathrm{N}^+(^3\mathrm{P})$ and $\mathrm{N}(^2\mathrm{D_u}) + \mathrm{N}^+(^3\mathrm{P})$ represent the dissociation products of the nitrogen molecular ion in the electronic levels associated to the immediatly below potential curves.

Appendix C

Auxiliary data from test 62 of the EAST shock tube

In this chapter, auxiliary data from test 62 of the EAST shock tube issued by Brandis and Cruden [43] via NASA's repository website [156] is presented. The auxiliary data is grouped into three tables. Table C.1 issues the upstream speeds u_∞, wavelength integration limits $[\lambda^l_{\text{min}}, \lambda^l_{\text{max}}]$ for the instrumentally resolved specific radiative intensities $\hat{I}^l(x)$ - defined by (3.102) - and relative position integration limits $[\hat{x}^l_{\text{min}}, \hat{x}^l_{\text{max}}]$ for the instrumentally resolved non-equilibrium metrics $\hat{I}^{\text{ne},l}_\lambda(\lambda)$ - defined by (3.103) - with respect to the benchmark shots considering the four wavelength intervals. Table C.2 issues the half-widths at half-maxima w^l_G and w^l_L as well as the exponents r^l for the instrument line-shape factors $\hat{\phi}^{\text{spe},l}(\lambda')$ - given by (3.107). Table C.3 issues the base widths d^l_{tri}, $d^l_{\text{trap},1}$, $d^l_{\text{trap},2}$ and d^l_{rect}, as well the as half-widths at half-maxima w^l_G and w^l_L for the spatial resolution function $\hat{\phi}^{\text{spa},l}(x'')$ - given by (3.108).

Also, estimates for the relative position of the shock wave associated to the benchmark data and the respective wavelength intervals $\hat{x}^l_{\text{sw}}$ (which were inferred by the present author) are issued in table C.4.

Table C.1: Shot numbers, upstream speeds u_∞, wavelength integration limits $[\lambda^l_{\min}, \lambda^l_{\max}]$, and relative position integration limits $[\hat{x}^l_{\min}, \hat{x}^l_{\max}]$ associated to the benchmark data issued by Brandis and Cruden [43].

Shot	u_∞ [km/s]	$[\lambda^{\text{VUV}}_{\min}, \lambda^{\text{VUV}}_{\max}]$ [nm]	$[\hat{x}^{\text{VUV}}_{\min}, \hat{x}^{\text{VUV}}_{\max}]$ [cm]	$[\lambda^{\text{Blue}}_{\min}, \lambda^{\text{Blue}}_{\max}]$ [nm]	$[\hat{x}^{\text{Blue}}_{\min}, \hat{x}^{\text{Blue}}_{\max}]$ [cm]	$[\lambda^{\text{Red}}_{\min}, \lambda^{\text{Red}}_{\max}]$ [nm]	$[\hat{x}^{\text{Red}}_{\min}, \hat{x}^{\text{Red}}_{\max}]$ [cm]	$[\lambda^{\text{IR}}_{\min}, \lambda^{\text{IR}}_{\max}]$ [nm]	$[\hat{x}^{\text{IR}}_{\min}, \hat{x}^{\text{IR}}_{\max}]$ [cm]
2	10.04	[145, 195]	[1.34, 5.34]	[330, 480]	[1.81, 5.81]	—	—	—	—
4	9.88	[120, 170]	[0.87, 4.87]	[190, 330]	[1.14, 5.14]	—	—	—	—
5	9.63	[145, 195]	[1.05, 5.05]	[330, 480]	[1.53, 5.53]	[480, 890]	[0.97, 4.97]	[890, 1400]	[1.05, 5.05]
6	8.70	[145, 195]	[1.10, 5.10]	[330, 480]	[1.57, 5.57]	[480, 890]	[0.95, 4.95]	[890, 1400]	[2.13, 6.13]
9	8.98	[120, 170]	[1.15, 5.15]	[190, 330]	[1.53, 5.53]	—	—	[1130, 1650]	[1.96, 5.96]
13	8.12	[145, 195]	[1.11, 5.11]	[330, 480]	[1.54, 5.54]	[480, 890]	[0.97, 4.97]	[890, 1400]	[1.54, 5.54]
15	8.19	[120, 170]	[1.15, 5.15]	[190, 330]	[1.41, 5.41]	—	—	[1130, 1650]	[1.44, 5.44]
16	7.70	[120, 170]	[0.98, 4.97]	[190, 330]	[1.38, 5.38]	—	—	[1130, 1650]	[2.31, 6.31]
19	10.32	[145, 195]	[1.57, 5.57]	[330, 480]	[2.16, 6.16]	[480, 890]	[1.45, 5.45]	[890, 1450]	[2.75, 6.75]
20	11.16	[145, 195]	[1.82, 5.82]	[330, 480]	[2.46, 6.46]	[480, 890]	[1.87, 5.87]	[890, 1450]	[2.35, 6.35]
21	10.72	[145, 195]	[1.37, 5.37]	[330, 480]	[1.72, 5.72]	[480, 890]	[0.97, 4.97]	[890, 1450]	[2.49, 6.49]
23	10.74	[120, 170]	[1.11, 5.11]	[190, 330]	[1.32, 5.32]	[654, 658]	[0.37, 4.37]	[890, 1450]	[2.36, 6.36]
29	10.34	[120, 170]	[0.87, 4.87]	[190, 330]	[1.54, 5.54]	[654, 658]	[0.01, 4.01]	[1130, 1650]	[1.38, 5.38]
37	7.15	—	—	[190, 330]	[1.68, 5.68]	—	—	[1130, 1650]	[1.77, 5.77]
40	6.88	[145, 195]	[1.44, 5.44]	[330, 480]	[1.82, 5.82]	[480, 890]	[1.13, 5.13]	[890, 1400]	[2.20, 6.20]
41	6.20	—	—	[330, 480]	[1.81, 5.81]	[480, 890]	[1.19, 5.19]	[890, 1400]	[3.51, 7.51]
42	5.94	—	—	[190, 330]	[1.44, 5.44]	[480, 890]	[1.04, 5.04]	—	—

Table C.2: Half-widths at half-maxima w^l_G and w^l_L, and exponents r^l for the instrument line-shape factors $\hat{\phi}^{\text{spe},l}(\lambda')$ associated to the benchmark data issued by Brandis and Cruden [43].

Shot	w^{VUV}_G [nm]	w^{VUV}_L [nm]	w^{Blue}_G [nm]	w^{Blue}_L [nm]	w^{Red}_G [nm]	w^{Red}_L [nm]	r^{Red}	w^{IR}_G [nm]	w^{IR}_L [nm]	r^{IR}
2	0.198	0.006	0.222	0.024	—	—	—	—	—	—
4	0.198	0.006	0.307	0.024	—	—	—	—	—	—
5	0.198	0.006	0.307	0.024	1.121	9.469	−1.498	2.335	0.868	0.425
6	0.198	0.006	0.307	0.024	1.121	9.469	−1.498	2.335	0.868	0.425
9	0.198	0.006	0.307	0.024	—	—	—	2.335	0.868	0.425
13	0.207	0.007	0.422	0.022	1.690	13.838	−1.529	3.034	—	−∞ [a]
15	0.207	0.007	0.422	0.022	—	—	—	3.034	—	−∞ [a]
16	0.207	0.007	0.422	0.022	—	—	—	3.034	—	−∞ [a]
19	0.192	0.006	0.222	0.024	0.811	6.009	−1.387	2.335	0.868	0.425
20	0.198	0.006	0.307	0.024	0.811	6.009	−1.387	2.335	0.868	0.425
21	0.198	0.006	0.307	0.024	0.811	6.009	−1.387	2.316	0.789	0.469
23	0.198	0.006	0.307	0.024	0.012	0.046	−0.815	2.316	0.789	0.469
29	0.198	0.006	0.307	0.024	0.012	0.046	−0.815	2.335	0.868	0.425
37	—	—	0.422	0.022	—	—	—	3.034	—	−∞ [a]
40	0.207	0.007	0.422	0.022	1.690	13.838	−1.529	3.034	—	−∞ [a]
41	—	—	0.422	0.022	1.690	13.838	−1.529	3.034	—	−∞ [a]
42	—	—	0.422	0.022	1.690	13.838	−1.529	—	—	—

[a] For this case, the second branch of the instrument line-shape factor given by (3.107) is regarded to be purely gaussian, hence the value $-\infty$ for r^{IR} and the empty one for w^{IR}_L.

Table C.3: Base widths d^l_{tri}, $d^l_{\mathrm{trap},1}$, $d^l_{\mathrm{trap},2}$ and d^l_{rect}, as well as half-widths at half-maxima w^l_G and w^l_L for the spatial resolution function $\hat{\phi}^{\mathrm{spa},l}(x'')$ associated to the benchmark data issued by Brandis and Cruden [43].

Shot	$d^{\mathrm{VUV}}_{\mathrm{tri}}$ [cm]	w^{VUV}_G [cm]	w^{VUV}_L [10^{-4}cm]	$d^{\mathrm{VUV}}_{\mathrm{rect}}$ [cm]	$d^{\mathrm{Blue}}_{\mathrm{tri}}$ [cm]	w^{Blue}_G [cm]	w^{Blue}_L [10^{-4}cm]	$d^{\mathrm{Blue}}_{\mathrm{rect}}$ [cm]	$d^{\mathrm{Red}}_{\mathrm{tri}}$ [cm]	w^{Red}_G [cm]	w^{Red}_L [10^{-4}cm]	$d^{\mathrm{Red}}_{\mathrm{rect}}$ [cm]	$d^{\mathrm{IR}}_{\mathrm{trap},1}$ [cm]	$d^{\mathrm{IR}}_{\mathrm{trap},2}$ [cm]	w^{IR}_G [cm]	$d^{\mathrm{IR}}_{\mathrm{rect}}$ [cm]
2	0.041	0.039	5.52	0.502	0.041	0.111	15.9	0.251	—	—	—	—	—	—	—	—
4	0.041	0.043	7.72	0.494	0.041	0.111	15.9	0.247	—	—	—	—	—	—	—	—
5	0.041	0.048	4.02	0.481	0.041	0.122	17.4	0.241	0.041	0.033	49.6	0.193	0.313	0.128	0.088	0.944
6	0.041	0.035	15.7	0.435	0.041	0.111	12.6	0.218	0.041	0.048	59.8	0.174	0.313	0.128	0.092	0.853
9	0.041	0.046	5.87	0.449	0.041	0.112	15.5	0.225	—	—	—	—	0.313	0.128	0.080	0.880
13	0.041	0.046	4.32	0.406	0.041	0.110	21.6	0.203	0.041	0.032	45.2	0.162	0.313	0.128	0.076	0.795
15	0.041	0.046	4.32	0.819	0.041	0.110	21.6	0.410	—	—	—	—	0.313	0.128	0.079	0.803
16	0.041	0.046	5.31	0.770	0.041	0.101	5.75	0.385	—	—	—	—	0.313	0.128	0.079	0.754
19	0.041	0.015	1.47×10^{-6}	0.516	0.041	0.104	22.2	0.258	0.041	0.019	30.3	0.206	0.313	0.128	0.094	1.011
20	0.041	0.041	3.79	0.558	0.041	0.120	15.3	0.279	0.041	0.034	47	0.223	0.313	0.128	0.081	1.094
21	0.041	0.037	1.71	0.268	0.041	0.117	18.3	0.268	0.041	0.032	46.7	0.214	0.313	0.128	0.090	1.050
23	0.041	0.039	3.28	0.268	0.041	0.091	23.6	0.268	0.041	0.024	56.8	1.074	0.313	0.128	0.111	1.052
29	0.041	0.037	4.94	0.517	0.041	0.087	58.7	0.258	0.041	0.024	56.5	1.034	0.313	0.128	0.086	1.013
37	—	—	—	—	0.041	0.087	58.7	0.357	—	—	—	—	0.313	0.128	0.086	0.700
40	0.041	0.037	4.94	0.688	0.041	0.087	58.7	0.172	0.041	0.024	56.5	0.344	0.313	0.128	0.086	0.674
41	—	—	—	—	0.041	0.087	58.7	0.155	0.041	0.024	56.5	0.310	0.313	0.128	0.086	0.607
42	—	—	—	—	0.041	0.087	58.7	0.297	0.041	0.024	56.5	0.594	—	—	—	—

Table C.4: Relative positions of the shock wave $\hat{x}^l_{\mathrm{sw}}$ associated to the benchmark data issued by Brandis and Cruden [43], being these inferred by the present author.

Shot	$\hat{x}^{\mathrm{VUV}}_{\mathrm{sw}}$ [cm]	$\hat{x}^{\mathrm{Blue}}_{\mathrm{sw}}$ [cm]	$\hat{x}^{\mathrm{Red}}_{\mathrm{sw}}$ [cm]	$\hat{x}^{\mathrm{IR}}_{\mathrm{sw}}$ [cm]
2	2.880	3.250	—	—
4	2.400	2.850	—	—
5	2.630	2.950	2.550	2.500
6	2.660	3.160	2.620	3.370
9	2.680	3.050	—	3.440
13	2.690	3.120	2.580	2.940
15	2.230	2.830	—	2.840
16	2.330	2.860	—	3.770
19	3.260	3.730	3.250	4.310
20	3.360	3.910	3.380	3.990
21	2.960	3.240	2.710	3.930
23	2.790	3.020	1.730	4.040
29	2.350	3.070	1.810	3.000
37	—	3.140	—	3.220
40	2.660	3.390	2.700	3.710
41	—	3.170	2.660	4.910
42	—	2.900	2.220	—